

OPTICAL SCIENCES

André Moliton

# Optoelectronics of Molecules and Polymers

 Springer

*Founded by H.K.V. Lotsch*

Editor-in-Chief: W.T. Rhodes, Atlanta

Editorial Board: T. Asakura, Sapporo  
T.W. Hänsch, Garching  
T. Kamiya, Tokyo  
F. Krausz, Garching  
B. Monemar, Linköping  
H. Venghaus, Berlin  
H. Weber, Berlin  
H. Weinfurter, München

# Springer Series in OPTICAL SCIENCES

---

The Springer Series in Optical Sciences, under the leadership of Editor-in-Chief *William T. Rhodes*, Georgia Institute of Technology, USA, provides an expanding selection of research monographs in all major areas of optics: lasers and quantum optics, ultrafast phenomena, optical spectroscopy techniques, optoelectronics, quantum information, information optics, applied laser technology, industrial applications, and other topics of contemporary interest.

With this broad coverage of topics, the series is of use to all research scientists and engineers who need up-to-date reference books.

The editors encourage prospective authors to correspond with them in advance of submitting a manuscript. Submission of manuscripts should be made to the Editor-in-Chief or one of the Editors.

See also [www.springeronline.com/series/624](http://www.springeronline.com/series/624)

## *Editor-in-Chief*

**William T. Rhodes**  
Georgia Institute of Technology  
School of Electrical and Computer Engineering  
Atlanta, GA 30332-0250, USA  
E-mail: [bill.rhodes@ece.gatech.edu](mailto:bill.rhodes@ece.gatech.edu)

## *Editorial Board*

**Toshimitsu Asakura**  
Hokkai-Gakuen University  
Faculty of Engineering  
1-1, Minami-26, Nishi 11, Chuo-ku  
Sapporo, Hokkaido 064-0926, Japan  
E-mail: [asakura@eli.hokkai-s-u.ac.jp](mailto:asakura@eli.hokkai-s-u.ac.jp)

**Theodor W. Hänsch**  
Max-Planck-Institut für Quantenoptik  
Hans-Kopfermann-Straße 1  
85748 Garching, Germany  
E-mail: [t.w.haensch@physik.uni-muenchen.de](mailto:t.w.haensch@physik.uni-muenchen.de)

**Takeshi Kamiya**  
Ministry of Education, Culture, Sports  
Science and Technology  
National Institution for Academic Degrees  
3-29-1 Otsuka, Bunkyo-ku  
Tokyo 112-0012, Japan  
E-mail: [kamiyatk@niad.ac.jp](mailto:kamiyatk@niad.ac.jp)

**Ferenc Krausz**  
Ludwig-Maximilians-Universität München  
Lehrstuhl für Experimentelle Physik  
Am Coulombwall 1  
85748 Garching, Germany  
and  
Max-Planck-Institut für Quantenoptik  
Hans-Kopfermann-Straße 1  
85748 Garching, Germany  
E-mail: [ferenc.krausz@mpq.mpg.de](mailto:ferenc.krausz@mpq.mpg.de)

**Bo Monemar**  
Department of Physics  
and Measurement Technology  
Materials Science Division  
Linköping University  
58183 Linköping, Sweden  
E-mail: [bom@ifm.liu.se](mailto:bom@ifm.liu.se)

**Herbert Venghaus**  
Heinrich-Hertz-Institut  
für Nachrichtentechnik Berlin GmbH  
Einsteinufer 37  
10587 Berlin, Germany  
E-mail: [venghaus@hhi.de](mailto:venghaus@hhi.de)

**Horst Weber**  
Technische Universität Berlin  
Optisches Institut  
Straße des 17. Juni 135  
10623 Berlin, Germany  
E-mail: [weber@physik.tu-berlin.de](mailto:weber@physik.tu-berlin.de)

**Harald Weinfurter**  
Ludwig-Maximilians-Universität München  
Sektion Physik  
Schellingstraße 4/III  
80799 München, Germany  
E-mail: [harald.weinfurter@physik.uni-muenchen.de](mailto:harald.weinfurter@physik.uni-muenchen.de)

André Moliton

# Optoelectronics of Molecules and Polymers

With 229 Illustrations

 Springer

André Moliton  
Unité de Microélectronique,  
Optoélectronique et Polymères,  
Université de Limoges  
France  
amoliton@unilim.fr

Roger C. Hiorns  
(Translator)  
Laboratoire de Physico-Chimie des Polymères,  
Université de Pau et des Pays de l'Adour,  
France  
roger.hiorns@univ-pau.fr

Library of Congress Control Number: 2005925187

ISBN-10: 0-387-23710-0

e-ISBN: 0-387-25103-0

ISBN-13: 978-0387-23710-7

Printed on acid-free paper.

© 2006 Springer Science+Business Media, Inc.

All rights reserved. This work may not be translated or copied in whole or in part without the written permission of the publisher (Springer Science+Business Media, Inc., 233 Spring Street, New York, NY 10013, USA), except for brief excerpts in connection with reviews or scholarly analysis. Use in connection with any form of information storage and retrieval, electronic adaptation, computer software, or by similar or dissimilar methodology now known or hereafter developed is forbidden.

The use in this publication of trade names, trademarks, service marks, and similar terms, even if they are not identified as such, is not to be taken as an expression of opinion as to whether or not they are subject to proprietary rights.

Printed in the United States of America. (Techset/EB)

9 8 7 6 5 4 3 2 1

springeronline.com

To Colette,  
Céline and Vivien

To the memory of my mother and father

---

## Preface

Molecular materials have been known since the 1960's to show semiconducting properties, but the past decade has seen an unprecedented level of activity. This has been driven both by scientific advance, and also by the prospects for new technologies based on large-area deposition of thin-film organic semiconductors. Molecular semiconductors have come of age, and those active in the field now need access to a modern account of the semiconductor physics and engineering that underpins the emerging applications of these materials including light-emitting diodes for displays, photovoltaic diodes, and electro-optical modulators.

The necessity of bringing together realisable technology, which is primarily the process of thin-film deposition of semiconductor films, with useful semiconductor properties still intact often produces a complex physical system. In particular, disorder is inevitably present in these structures, and one of the central issues, which must determine the limitations for useful applications, is the way in which disorder modifies electronic structure. At its most simple, disorder in molecular materials is much less damaging to semiconducting properties than is the case in inorganic semiconductors. Deviation from perfect crystalline order in inorganic semiconductors generally produces broken chemical bonds which produce 'non-bonding' energy levels within the semiconductor gap, and this is particularly important at interfaces. However, disorder in molecular materials can often be accommodated without the breaking of chemical bonds, so that surfaces or interfaces can also, in this sense, remain chemically intact. In this situation, working semiconductor devices, such as LEDs, can operate when made from very disordered layers of molecular semiconductor. However, more careful examination of the role of disorder is required, because it affects electronic charge transport very strongly, and the understanding of how this controls device operation is of great importance.

André Moliton has written the book that provides students and researchers in this field with the broad perspective that is now needed. He provides a very clear picture of the way in which molecular semiconductors derive their semiconducting properties, and he develops the description of their electronic transport and optical properties which derive from the molecular characteristics of these materials, such as weak delocalisation of electron states, and local vibration coupling, leading to polaron

formation. His account is particularly useful in bringing his knowledge from the field of inorganic disordered semiconductors, such as amorphous silicon, to provide a useful model for understanding of the role of disorder here. The integration of this with the operation of semiconductor device structures provides the main theme for the later part of this book, and many students will find this particularly useful.

In summary, I commend this book for bringing together with great clarity: the framework of traditional semiconductor science, the new physics which comes with molecular semiconductors, and the complexities associated with real semiconductor device fabrication, particularly disorder. It will be much appreciated by both experts and students alike.

Sir Richard Friend  
Cavendish Professor of Physics  
Cambridge  
November 2002



---

## Abbreviations

Alq3	tris(8-hydroxyquinoline) aluminium
CB	conduction band
CP	conducting polymer
CuPc	copper phtalocyanine
$\epsilon_r$	relative dielectric permittivity
EL	electroluminescence
ET	electronic transverse mode
FB	forbidden band
FET	field effect transistor
HOMO	highest occupied molecular orbital
I	insulator
ITO	indium tin oxide
$J_s$	saturation current
$J_{sp}$	saturation current in the presence of traps
LED	light emitting diode
LPPP	ladder poly( <i>para</i> -phenylene)
LUMO	lowest unoccupied molecular orbital
M	metal
MIM	metal-insulator-metal
MIS	metal-insulator-semiconductor
MT	magnetic transverse mode
OLED	organic light emitting diode
PEDOT	poly(3,4-ethylenedioxythiophene)
PLED	polymer light emitting diode
PMMA	poly(methyl methacrylate)
PPP	poly( <i>para</i> -phenylene)
PPV	poly( <i>para</i> -phenylene vinylene)
PVK	polyvinylcarbazole
SC	semiconductor
SCLC	space charge limited current
TEP	thermoelectric power
TFL	trap-filled-limit
VB	valence band
$V_{TFL}$	tension at which all traps are filled

---

## **Introduction: the origin and applications of optoelectronic properties of molecules and polymers**

During the second half of the twentieth century, an upheaval in industrialised societies has been brought about by the application of the properties of certain solids to electronic and optical fields. Solids recognised as semiconductors have caused the greater part of this change. Even while the band theory for silicon was incomplete [fis 88], radio valves were being replaced by transistors at the end of the 1950s. The electronic industry then benefited from developments in solid state theories, which yielded a more thorough understanding of properties specific to semiconductors. Simultaneously, innovative techniques, such as wafer technology, permitted miniaturisation of electronic components. Their 'integration' into circuits gave the computer revolution, which we are still witnessing. Central to this technology is the mobility that electrons display in perfect crystals—around  $10^4 \text{ cm}^2 \text{ V}^{-1} \text{ s}^{-1}$ .

There remains a large number of devices for which this rate of commutation and response time is no where as near important. This can be found in a wide range of display technologies, for example in standard video technology where an image is replaced once every 1/25th of a second, and also in photovoltaic systems, in which the goal is to separate and collect photogenerated charges without paying any particular attention to the duration of processes brought into play. In such systems, the desire for the properties which crystalline semiconductors do not have is very much in evidence. It includes the need for mechanical flexibility and low cost fabrication of devices covering large surface areas. After having equipped the American satellite Vanguard with solar cells made from crystalline silicon to provide power for its radio, research was initiated into amorphous silicon to fulfil these design requirements. The initial conquest of space was then followed by the use of satellites which, with their total of hundreds of thousands of solar cells, now allow communication by telephone and television between continents.

In reality, the development of amorphous silicon was troubled by the long thought theory that amorphous semiconductors could not be doped. The theory at the time was based on the '8-N' rule (N is the number of electrons in the outer layer of a given atom), which was applied to glass-like materials and supposed that each atom was surrounded by 8-N close neighbours. All electrons could then be thought of being 'engaged' either in bonds between neighbouring atoms, or in 'isolated pair' orbitals.

This would disallow the possibility of having free carriers coming from incomplete bonds. However, amorphous silicon is not a glass in proper terms and it does not always follow the 8-N rule. For example, phosphorus atoms which often exhibit a co-ordination number of 3, and are thus not electronically active as ascribed by the 8-N rule, can take on a co-ordination number of 4, just as in the crystalline form. The 5th phosphorus electron does not therefore remain on the phosphorus atom, but falls into a dangling silicon bond site—a bond characteristic of the amorphous state and associated with a state localised within the so-called mobility gap. The Fermi level, initially situated more or less at the centre of the gap is displaced towards the bottom of the conduction band ( $E_C$ ) by a quantity  $\Delta E_F$ , which is of the order of  $N_D/N(E_F)$  where  $N_D$  denotes the electron density coming from the donor phosphorus atoms and  $N(E_F)$  represents the state density function for states close to the Fermi level. With a low value of  $N(E_F)$ , which can be realised by saturating the dangling silicon bonds with hydrogen, the displacement of the Fermi level can become significant and, in consequence, the doping effect becomes all important.

Even though the properties of amorphous semiconductors such as hydrogenated silicon (a-Si:H) are well understood [com 85], their use remains relatively limited. This is because of two factors. The first is that the properties of these materials are inferior to those of crystalline silicon—for examples, they exhibit mobilities of the order of  $1 \text{ cm}^2 \text{ V}^{-1} \text{ s}^{-1}$  and, in photovoltaic cells, have efficiencies of around 14 % against 24 % for the crystalline material. Secondly, their manufacture remains difficult and expensive, as they require techniques involving deposition under vacuum or chemical reactions in the vapour phase and the use of high temperatures. In 1999, photovoltaic cells fabricated using amorphous silicon accounted for only 12 % of total production. All things are not bright for crystalline silicon though. This material remains expensive, and the photovoltaic industry requires cheaper material from a pathway which does not involve the costly wastes associated with selecting the best parts of silicon ingots usually fabricated for the electronics industry.

Against this background, the possibility that organic materials, which might be facile to manipulate and relatively cheap to obtain, has always held a certain interest. A serious brake on their use though has been the poor understanding of the origins of their electronic and optical properties. In addition, as much as for amorphous inorganic semiconductors, it has taken considerable time to master their n- and p-type doping, an absolute necessity for their use in devices. In contrast to inorganic semiconductors, organic semiconductors are not atomic solids: they are  $\pi$ -conjugated materials in which the transport mechanisms vary considerably from those classically derived for solids. And even more so than in inorganic materials, the roles of defaults such as traps and structural inhomogeneities play an essential role in determining the transport and interstitial and non-substitutional doping phenomena.

Polymers which have conjugated double bonds yielding  $\pi$ -conjugation present two particular advantages. They exhibit good electronic transport properties—with a facile delocalisation of electrons—and good optical properties. The energy separation between  $\pi$ - and  $\pi^*$ -bands (which resemble, respectively, valence and conduction bands for solid state physicists), is typically around 1.5 to 3 eV, a value ideal for the optical domain. It is worth noting that polymers such as polyethylene, which contain

only single  $\sigma$ -bonds, exhibit high resistivities due to the localisation of electrons around  $\sigma$ -bonds. Due to transitions between  $\sigma$ - and  $\sigma^*$ -bands of the order of 5 eV, the properties of these materials lie beyond the optical domain.

Certain  $\pi$ -conjugated materials have been studied throughout the 20th century. Anthracene is a particularly good example [pop 82], as quantum theories developed for this material allowed an interpretation of its numerous physical properties. The large size of the crystals obtained necessitated extremely elevated tensions to study their electroluminescence, arresting initial developments. Similarly, linear polyacetylenes, first prepared in 1968 [ber 68], were only available as black powders, a near impractical form for characterising. The fabrication of organic materials in thin films permitted a development of the number of derived applications. Over the last few decades, decisive developments have occurred: the preparation of polyacetylene in film form, realised in 1977 by A. MacDiarmid and H. Shirakawa which gained them and the physicist A. Heeger the Noble prize for chemistry in 2000; and the improved understanding of transport and doping properties of  $\pi$ -conjugated materials [su 79 and bré 82b]. The insertion of these materials into devices such as electroluminescent diodes made sure of their important position in the optoelectronics industry of the 21st century. There are notable articles which come from this period and include for 'small molecules' that published in 1987 on Alq3 [tan 87], and for  $\pi$ -conjugated polymers that published in 1990 on poly(phenylene vinylene) (PPV) [bur 01].

Nearly a century after the initial discovery of photoconductivity in anthracene in 1906 by Pochettino, we have realised the 'dream' of optoelectronic and electronic technology based on thousands and even millions [pop 82] of organic molecules and polymers. All this has been made possible by synthetic organic chemistry. As will be detailed in this book, it is now possible to adjust the optical gap and thus the absorption and emission wavelengths of materials simply, for example, by adjusting organic, molecular chain lengths. These organic materials have exhibited not only photoconductivity and electroluminescence but also triboelectric properties, metal-like conductivity, superconductivity, photovoltaic effects, optical and non-linear effects and even charge stocking and emission.

Elaborated theories have demonstrated that the electronic and optical properties of organic solids are intimately tied, just as for inorganic materials. These theories are based on interpretations of the quantum mechanics and the macroscopic environment, including effects caused by impurities and defects, of the molecules. Quasi-particles, such as polarons and excitons, introduced through the understanding of inorganic structures, are also useful in explaining electronic and optical behaviours of organic materials, although they present particularities specific to the organic media such as non-negligible electron-lattice interactions.

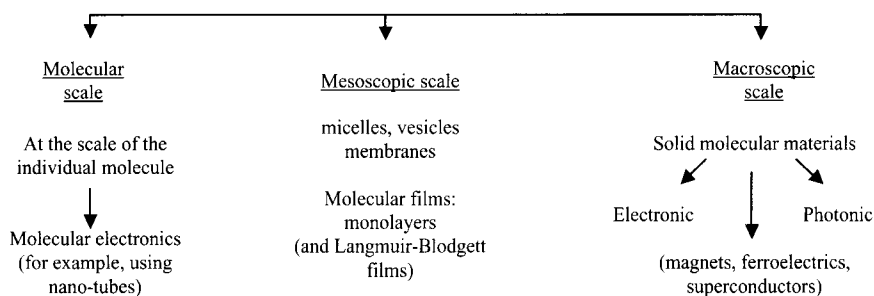
This book aims to bring together the practically indispensable knowledge required to understand the properties specific to organic devices which chemists, physicists and specialists in electronics are now proposing. Accordingly, after discussing concepts used for well organised solids, notably for one-dimensional systems, we detail the concepts used for localised levels in disordered materials (initially developed for amorphous inorganic solids). The first approximations to real organic materials are then made [mol 91 and mol 96], which have recently been further developed by

Reghu Menon, Yoon, Moses and Heeger [men 98]. After having passed by the requisite step of determining energy levels in 'perfect' molecular and macromolecular systems, the effect of quasi-particles are introduced. The importance of the latter type of particles is stressed, as their role in the interpretation of transport or doping mechanisms and in optical processes is singularly important. The role of excitons—here an electronic excitation in an organic solid—is detailed, and thus the transfer mechanism of an excitation between two interfaces is studied. The role of aggregates in solid matrices is also explored with respect to understanding charge injection, resistive media and the problems encountered at interfaces.

Technological developments are discussed in the second part of this book. The practicalities of fabricating devices using dry etching techniques with ion beams for example are presented. This information is supplemented by descriptions of the opto-electronic characterisations which can be performed. With the exception of the brief Appendix A-11, which is more a catalogue of the most important organic materials, the organic synthesis of these materials is not touched upon, and the reader in search of this information can look to some excellent reviews such as [bar 00a, den 00 and kra 98]. Another reason is of course that organic synthesis does not make up part of the competencies of the author!

The devices based on organic materials that are covered are those which, for the present time, monopolise the attention of many researchers in the fields of their application. Included are the domains of visualisation, photon-electron conversion (photovoltaics) and electro-optical modulation which essentially concerns communications. These domains are often interdependent: we have already mentioned that communication satellites often require the use of photovoltaic cells. Indeed the insertion of such cells into portable telephones and computers would often resolve problems associated with the lifetimes of batteries.

We can imagine that the properties of these materials has been treated at different scales:



The macroscopic scale is the oldest area of study and the closest to the realm of applications. And it is in this area that this book attempts to place active,  $\pi$ -conjugated materials which can serve as:

- conductors or semiconductors of electricity;
- electroluminescent emitters;
- 'converters' of light into electricity; and
- optically active devices, and in particular, second-order non-linear devices.

More precisely, we will encounter the use of organic materials in the following components:

- light emitting devices, or rather, organic light emitting devices (OLEDs) or polymer light emitting devices (PLEDs). The whole of Chapter 10 is dedicated to the various uses of these LEDs in displays and includes details on one of the first organic screens developed for commercial use in portable telephones. Many industrial groups own prototypes of this sort of component (see the conclusion of Chapter 10). Lasing diodes, diodes which emit white light or infra-red are also presented along with their applications;
- photovoltaic cells, where we will detail the originality of the organic based structures currently under development and based on interpenetrating networks of donor and acceptor molecules. While organic materials possess the advantage of increasing electron mobilities with temperature, they present—for the meantime—problems of stability; and
- electro-optical modulators (of phase or amplitude) where the problems of handling and fabrication into devices and the choice of appropriate materials is discussed. The high resistance of certain polymers, such as polyimides, to oxygen and humidity does leave open the possibility of fabricating low cost devices which could be installed without precaution, perhaps underground, in both commercial and domestic environments.

This book was written with the desire to make it ‘self-supporting’ so that the reader would not find it necessary to turn to numerous, specialised publications and manuals. Appendices which give further details have been added and consist of ‘*aide-mémoires*’ and supplementary information, and can give answers to albeit less fundamental but just as important questions. These Appendices may be of particular use to readers more used to books on physics, electronics, physical-chemistry and chemistry.

This manual is destined to be used by students following their first degree, but was especially written for Masters and PhD students. It should give a solid introduction to the optoelectronics of organic solids to researchers and engineers who wish to be more involved in the field, and I have no doubt that they will be passionate followers of a technology undergoing full expansion.

---

# Contents

<b>Preface by Richard H. Friend</b> .....	vii
<b>List of abbreviations</b> .....	ix
<b>Introduction</b> .....	xi

---

## **Part One: Concepts: Electronic and optical processes in organic solids**

---

<b>Chapter I: Band and electronic structures in regular 1-dimensional media</b> .....	3
I An introduction to approximations of weak and strong bonds .....	3
1 Materials with weak bonds .....	3
2 Materials with strong bonds .....	4
II Band Structure in weak bonds .....	6
1 Prior result for zero order approximation .....	6
2 Physical origin of forbidden bands .....	6
3 Simple estimation of the size of the forbidden band .....	8
III Floquet's theorem: wavefunctions for strong bonds .....	9
1 Form of the resulting potential .....	9
2 The form of the wavefunction .....	10
3 Floquet's theorem: effect of potential periodicity on wavefunction form .....	11
IV A study on energy .....	12
1 Defining equations (with $x \equiv r: 1 - D$ ) .....	12
2 Calculation of energy for a chain of N atoms .....	13
3 Additional comments: physical significance of terms ( $E_0 - \alpha$ ) and $\beta$ ; simple calculation of E; and the appearance of allowed and forbidden bands in strong bonds .....	16

V	1-D crystal and the distorted chain	19
	1 AB type crystal	19
	2 The distorted chain	20
VI	Density function and its application, the metal insulator transition and calculation of $E_{\text{relax}}$	22
	1 State density functions	22
	2 Filling up zones and Peierls insulator-metal transition	24
	3 Principle of the calculation of $E_{\text{relax}}$ for a distorted chain	25
VII	Practical example: calculation of wavefunction energy levels, orbital density function and band filling for a regular chain of atoms	26
	1 Limits of variation in $k$	26
	2 Representation of energy and the orbital density function using $N = 8$	26
	3 Wavefunction forms for bonding and antibonding states	27
	4 Generalisation regarding atomic chain states	30
VIII	Conclusion	30

<b>Chapter II:</b>	<b>Electron and band structure</b>	33
I	Introduction	33
II	Going from 1-D to 3-D	34
	1 3-D General expression of permitted energy	34
	2 Expressions for effective mass, band size and mobility	35
III	3-D covalent crystal from a molecular model: $sp^3$ hybrid states at nodal atoms	36
	1 General notes	36
	2 Independent bonds: formation of molecular orbitals	38
	3 Coupling of molecular orbitals and band formation	40
IV	Band theory limits and the origin of levels and bands from localised states	41
	1 Influence of defects on evolution of band structure and the introduction of 'localised levels'	41
	2 The effects of electronic repulsions, Hubbard's bands and the insulator-metal transition	43
	3 Effect of geometrical disorder and Anderson localisation	47
V	Conclusion	57



<b>Chapter III:</b>	<b>Electron and band structures of ‘perfect’ organic solids . . .</b>	<b>59</b>
I	Introduction: organic solids . . . . .	59
1	Context . . . . .	59
2	Generalities . . . . .	59
3	Definition of conjugated materials; an <i>aide-mémoire</i> for physicians and electricians . . . . .	62
II	Electronic structure of organic intrinsic solids: $\pi$ -conjugated polymers . . . . .	63
1	Degenerate $\pi$ -conjugated polymers . . . . .	63
2	Band scheme for a non-degenerate $\pi$ -conjugated polymer: poly( <i>para</i> -phenylene) . . . . .	65
III	Electronic structure of organic intrinsic solids: small molecules . . . . .	68
1	Evolution of energy levels in going from an isolated chain to a system of solid state condensed molecules . . . . .	68
2	Energy level distribution in Alq3 . . . . .	69
3	Fullerene electronic levels and states . . . . .	70
IV	Conclusion: energy levels and electron transport . . . . .	74
<b>Chapter IV:</b>	<b>Electron and band structures of ‘real’ organic solids . . . . .</b>	<b>77</b>
I	Introduction: ‘real’ organic solids . . . . .	77
II	Lattice-charge coupling—polarons . . . . .	77
1	Introduction . . . . .	77
2	Polarons . . . . .	78
3	Model of molecular crystals . . . . .	79
4	Energy spectrum of small polaron . . . . .	83
5	Polarons in $\pi$ -conjugated polymers . . . . .	85
6	How do we cross from polaron-exciton to polaron? . . . . .	87
7	Degenerate $\pi$ -conjugated polymers and solitons . . . . .	88
III	Towards a complete band scheme . . . . .	90
1	Which effects can intervene? . . . . .	90
2	Complete band scheme accumulating different possible effects . . . . .	91
3	Alq3 and molecular crystals . . . . .	93
IV	Conclusion . . . . .	95
<b>Chapter V:</b>	<b>Conduction in delocalised, localised and polaronic states . .</b>	<b>99</b>
I	Introduction . . . . .	99
II	General theories of conduction in delocalised states . . . . .	100
1	General results of conductivity in a real crystal: limits of classical theories . . . . .	100

	2	Electrical conduction in terms of mobilities and the Kubo–Greenwood relationship: reasoning in reciprocal space and energy space for delocalised states . . . . .	101
III		Conduction in delocalised band states: degenerate and non-degenerate organic solids . . . . .	103
	1	Degenerate systems . . . . .	103
	2	Non-degenerate systems: limits of applicability of the conduction theory in bands of delocalised states for systems with large or narrow bands (mobility condition) . . . . .	105
IV		Conduction in localised state bands . . . . .	109
	1	System 1: Non-degenerated regime; conductivity in the tail band . . . . .	110
	2	System 2: degenerate regime; conductivity in deep localised states . . . . .	111
V		Transport mechanisms with polarons . . . . .	116
	1	Displacements in small polaron bands and displacements by hopping . . . . .	116
	2	Characteristics of hopping by small polarons . . . . .	117
	3	Precisions for the ‘semi-classical’ theory: transition probabilities . . . . .	120
	4	Relationships for continuous conductivity through polaron transport . . . . .	122
	5	Conduction in 3D in $\pi$ -conjugated polymers . . . . .	124
VI		Other envisaged transport mechanisms . . . . .	128
	1	Sheng’s granular metal model . . . . .	128
	2	Efros—Shklovskii’s model from Coulombic effects . . . . .	128
	3	Conduction by hopping from site to site in a percolation pathway . . . . .	128
	4	Kaiser’s model for conduction in a heterogeneous structure . . . . .	129
VII		Conclusion: real behaviour . . . . .	129
	1	A practical guide to conducting polymers . . . . .	129
	2	Temperature dependence analysed using the parameter $w = -[(\partial \ln \rho) / \partial \ln T]$ . . . . .	131
<b>Chapter VI:</b>		<b>Electron transport properties . . . . .</b>	<b>133</b>
I		Introduction . . . . .	133
II		Basic mechanisms . . . . .	133
	1	Injection levels . . . . .	133
	2	Three basic mechanisms . . . . .	134
III		Process A: various (emission) currents produced by electrodes . . . . .	135

	1	Rectifying contact (blocking metal $\rightarrow$ insulator) ..	135
	2	Thermoelectronic emission ( $T \neq 0$ ; $E_a = 0$ ) .....	136
	3	Field effect emission (Schottky): $E_a$ is 'medium intense' .....	136
	4	Tunnelling effect emissions and Fowler–Nordheim's equation .....	137
IV		Process B (simple injection): ohmic contact and current limited by space charge .....	138
	1	Ohmic contact (electron injection) .....	138
	2	The space charge limited current law and saturation current ( $J_s$ ) for simple injection in insulator without traps .....	139
	3	Transitions between regimes .....	143
	4	Insulators with traps and characteristics of trap levels .....	144
	5	Expression for current density due to one carrier type ( $J_{sp}$ ) with traps at one discrete level ( $E_t$ ); effective mobility .....	147
	6	Deep level traps distributed according to Gaussian or exponential laws .....	151
V		Double injection and volume controlled current: mechanism C in Figure VI-2 .....	154
	1	Introduction: differences in properties of organic and inorganic solids .....	154
	2	Fundamental equations for planar double injection (two carrier types) when both currents are limited by space charge: form of resulting current $J_{VCC}$ (no trap nor recombination centres) .	155
	3	Applications .....	157
VI		The particular case of conduction by the Poole–Frenkel effect .....	159
	1	Coulombic traps .....	160
	2	Conduction due to Poole-Frenkel effect (as opposed to Schottky effect).....	160

**Chapter VII: Optical processes in molecular and macromolecular solids** 163

I		Introduction .....	163
II		Matrix effects due to insertion of atoms with incomplete internal electronic levels .....	164
	1	Electronic configuration of transition elements and rare earths .....	164
	2	Incorporation of transition metals and rare earths into dielectric or a semiconductor matrix: effects on energy levels .....	165

	3	Transitions studied for atoms with incomplete layers inserted in a matrix	167
III		Classic optical applications using transition and rare earth elements	171
	1	Electroluminescence in passive matrices	171
	2	Insertion into semiconductor matrix	172
	3	Light amplification: erbium lasers	173
IV		Molecular edifices and their general properties	174
	1	Aide mémoire: basic properties	174
	2	Selection rule with respect to orbital parities for systems with centre of symmetry	176
	3	More complicated molecules: classical examples of existing chromophores	177
V		Detailed description of the absorption and emission processes in molecular solids	179
	1	Electron-lattice coupling effects during electron transitions	179
	2	Selection rules and allowed transitions	180
	3	Modified Jablonsky diagram and modification of selection rules: fluorescence and phosphorescence	181
	4	Experimental results: discussion	183
VI		Excitons	185
	1	Introduction	185
	2	Wannier and charge transfer excitons	186
	3	Frenkel excitons	188
	4	States, energy levels and transitions in physical dimers	189
	5	System containing an infinite number of interacting molecules and exciton band: Davydov displacement and breakdown	192
	6	Aggregates	194
	7	Förster and Dexter mechanisms for transfer of electron excitation energy	195

---

## Part Two: Components: OLEDs, photovoltaic cells and electro-optical modulators

---

		<b>Chapter VIII: Fabrication and characterisation of molecular and macromolecular optoelectronic components</b>	201
	I	Deposition methods	201
		1 Spin coating	201
		2 Vapour phase deposition	202

	3	Polymerisation in the vapour phase (VDP method) . . . . .	203
	4	Film growth during vapour deposition: benefits due to deposition assisted by ion beams . . . . .	204
	5	Comment: substrate temperature effects . . . . .	209
II		Fabrication methods: OLEDs and optical guides for modulator arms . . . . .	210
	1	OLED fabrication . . . . .	210
	2	Fabrication of modulator guides/arms from polymers . . . . .	212
III		Photometric characterisation of organic LEDs (OLEDs or PLEDs) . . . . .	217
	1	General definitions . . . . .	217
	2	Internal and external fluxes and quantum yields: emissions inside and outside of components . . . . .	221
	3	Measuring luminance and yields with a photodiode . . . . .	226
IV		Characterisation of polymer based linear wave guides . .	232
	1	Measuring transversally diffused light . . . . .	232
	2	Loss analyses using 'Cut – Back' and 'Endface Coupling' methods . . . . .	233

## **Chapter IX: Organic structures and materials in optoelectronic**

		<b>emitters</b> . . . . .	235
I		Introduction . . . . .	235
II		How CRTs work . . . . .	235
III		Electroluminescent inorganic diodes . . . . .	236
	1	How they work . . . . .	236
	2	Display applications . . . . .	237
	3	Characteristic parameters . . . . .	237
	4	In practical terms . . . . .	238
IV		Screens based on liquid crystals . . . . .	239
	1	General points . . . . .	239
	2	How liquid crystal displays work . . . . .	240
	3	LCD screen structure and the role of polymers . . .	242
	4	Addressing in LCD displays . . . . .	243
	5	Conclusion . . . . .	244
V		Plasma screens . . . . .	244
VI		Micro-point screens (field emission displays (FED)) . . .	245
VII		Electroluminescent screens . . . . .	246
	1	General mechanism . . . . .	246
	2	Available transitions in an inorganic phosphor . . . .	247
	3	Characteristics of inorganic phosphors from groups II–VI . . . . .	249

	4	Electroluminescent thin film displays: how they work with alternating currents	250
	5	Electroluminescent devices operating under direct current conditions	251
VIII		Organic (OLED) and polymer (PLED) electroluminescent diodes	253
	1	Brief history and résumé	253
	2	The two main developmental routes	253
	3	How OLEDs function and their interest	254
<b>Chapter X:</b>		<b>Electroluminescent organic diodes</b>	<b>257</b>
I		Introduction	257
II		Comparing electronic injection and transport models with experimental results	258
	1	General points: properties and methods applied to their study	258
	2	Small molecules (Alq <sub>3</sub> )	259
	3	Polymers	267
III		Strategies for improving organic LEDs and yields	272
	1	Scheme of above detailed processes	272
	2	Different types of yields	273
	3	Various possible strategies to improve organic LED performances	274
IV		Adjusting electronic properties of organic solids for electroluminescent applications	276
	1	A brief justification of n- and p-type organic conductivity	276
	2	The problem of equilibrating electron and hole injection currents	277
	3	Choosing materials for electrodes and problems encountered with interfaces	277
	4	Confinement layers and their interest	279
V		Examples of organic multi-layer structures	279
	1	Mono-layer structures and the origin of their poor performance	279
	2	The nature of supplementary layers	280
	3	Classic examples of the effects of specific organic layers	280
	4	Treatment of the emitting zone in contact with the anode	284
VI		Modification of optical properties of organic solids for applications	285
	1	Adjusting the emitted wavelength	285
	2	Excitation energy transfer mechanisms in films doped with fluorescent or phosphorescent dyes	286

	3	Circumnavigating selection rules: recuperation of non-radiative triplet excitons	288
	4	Energy transfer with rare earths and infrared LEDs	290
	5	Microcavities	292
	6	Electron pumping and the laser effect	292
VII		Applications in the field of displays: flexible screens	294
	1	The advantages	294
	2	The problem of ageing	294
	3	The specific case of white diodes	296
	4	The structure of organic screens	296
	5	A description of the fabrication processes used for organic RGB pixels	298
	6	Emerging organic-based technologies: flexible electronic 'pages'	304
VIII		The prospective and actual production at 2002	306
IX		Conclusion	309
X		Actual state-of-the-art and prospectives	310
<b>Chapter XI:</b>		<b>Organic photovoltaic devices</b>	<b>313</b>
I		Principles and history of organic based photovoltaics	313
	1	General points: the photovoltaic effect	313
	2	Initial attempts using organic materials: the phthalocyanines	316
	3	Solar cells based on pentacene doped with iodine	318
	4	The general principle of Graetzel and current organic solar cells	320
II		$\pi$ -Conjugated materials under development for the conversion of solar energy	321
	1	Metal-Insulator-Metal structures	321
	2	How bilayer hetero-structures work and their limits	322
	3	Volume heterojunctions	325
III		Additional informations about photovoltaic cells and organic components	328
	1	Discussion about mechanisms leading to the generation of charge carriers in organics	328
	2	Electric circuit based on an irradiated pn-junction; photovoltaic parameters	330
	3	Circuit equivalent to a solar cell	334
	4	Possible limits	336
	5	Examples; routes under study and the role of various parameters	337
	6	Conclusion	339

<b>Chapter XII: The origin of non-linear optical properties</b> .....	341
I Introduction: basic equations for electro-optical effects .....	341
1 Context .....	341
2 Basic equations used in non-linear optics .....	341
II The principle of phase modulators and organic materials .....	343
1 Phase modulator .....	343
2 The advantages of organic materials .....	345
3 Examples of organic donor-acceptor non-linear optical systems .....	346
4 General structure of molecules used in non-linear optics .....	348
III The molecular optical diode .....	349
1 The centrosymmetric molecule .....	349
2 Non-centrosymmetric molecules .....	350
3 Conclusion .....	351
IV Phenomenological study of the Pockels effect in donor-spacer-acceptor systems .....	353
1 Basic configuration .....	353
2 Fundamental equation for a dynamic system .....	355
3 Expressions for polarisability and susceptibility ..	355
4 Expression for the indice—and the insertion of the electro-optical coefficient $r$ .....	356
V Organic electro-optical modulators and their basic design .....	358
1 The principal types of electro-optical modulators ..	358
2 Figures of merit .....	359
3 The various organic systems available for use in electro-optical modulators .....	361
VI Techniques such as etching and polyimide polymer structural characteristics .....	363
1 Paired materials: polyimide/DR1 .....	363
2 Device dimensions—resorting to lithography .....	364
3 Etching .....	365
4 Examples of polymer based structures .....	367
VII Conclusion .....	368

---

## Appendices

---

<b>Appendix A-1: Atomic and molecular orbitals</b> .....	373
I Atomic and molecular orbitals .....	373
1 Atomic s- and p-orbitals .....	373
2 Molecular orbitals .....	376



	3	$\sigma$ - and $\pi$ -bonds . . . . .	380
II		The covalent bond and its hybridisation . . . . .	381
	1	Hybridisation of atomic orbitals . . . . .	381
	2	$sp^3$ Hybridisation . . . . .	383
<b>Appendix A-2: Representation of states in a chain of atoms . . . . . 389</b>			
I		A chain of atoms exhibiting $\sigma$ -orbital overlapping . . . . .	389
	1	$\sigma$ -orbitals and a compliment to the example of 8 atoms in a chain . . . . .	389
	2	General representation of states in a chain of overlapping $\sigma$ s-orbitals . . . . .	391
	3	General representation of states in a chain of overlapping $\sigma$ p-orbitals . . . . .	393
II		$\pi$ Type overlapping of p-orbitals in a chain of atoms: $\pi$ -p- and $\pi^*$ -p-orbitals . . . . .	393
III		$\sigma$ -s- and $\sigma$ -p-bonds in chains of atoms . . . . .	394
IV		Comments . . . . .	395
	1	The Bloch function . . . . .	395
	2	Expression for the effective mass ( $m^*$ ) . . . . .	396
<b>Appendix A-3: Electronic and optical properties of fullerene-C60 in the solid (film) state . . . . . 397</b>			
I		Electronic properties of fullerene-C60 . . . . .	397
II		Optical properties and observed transitions . . . . .	401
<b>Appendix A-4: General theory of conductivity for a regular lattice . . . . . 403</b>			
I		Electron transport effected by an external force and its study . . . . .	403
	1	Effect of force on electron movement and reasoning within reciprocal space . . . . .	403
	2	Boltzmann's transport equation . . . . .	404
II		State density function, carrier flux and current density in the reciprocal space . . . . .	406
	1	General expressions for fluxes of particles . . . . .	406
	2	Expressions for the state density function . . . . .	406
	3	Expression for flux . . . . .	408
	4	Expression for current density in reciprocal space . . . . .	408
III		Different expressions for the current density . . . . .	409
	1	Usual expression for current density in energy space . . . . .	409
	2	Studies using various examples . . . . .	410
	3	Expressions for mobility . . . . .	412
	4	The Kubo – Greenwood expression for conductivity . . . . .	413

IV	Complementary comments	414
	1 Concerning the approximation of the effective mass and isotropic diffusions	414
	2 General laws for changes in mobility with temperature	415
<b>Appendix A-5: General theory of conductivity in localised states</b>		417
I	Expression for current intensity associated with hopping transport	417
	1 Transcribing transport phenomena into equations	417
	2 Calculating the current intensity due to hopping mechanisms	419
II	Expression for current density and thermally activated mobility	419
	1 Expression for current density relative to transport at a particular energy level	419
	2 Generalisation of the form of Kubo–Greenwood conductivity	420
	3 Thermally activated mobility	420
III	Approximations for localised and degenerate states	421
<b>Appendix A-6: Expressions for thermoelectric power in solids: conducting polymers</b>		423
I	Definition and reasons for use	423
	1 Definition	423
	2 Reasons for use	423
II	TEP of metals ( $E_F$ within a band of delocalised states)	424
III	TEP of semiconductors (SC) ( $E_F$ in the gap)	424
	1 Preliminary remark	425
	2 An ideal n-type semiconductor	425
	3 An ideal n-type semiconductor	426
	4 Comment on amorphous semi-conductors	426
	5 A non-ideal amorphous semiconductor with $E_F$ below its states in the band tails	426
IV	TEP under a polaronic regime	427
	1 High temperature regime	427
	2 Intermediate temperature regime	427
	3 Other regimes	427
V	The TEP for a high density of localised states around $E_F$	427
	1 Initial hypothesis	427
	2 The result in VRH	428

VI	General representation .....	429
VII	Real behaviour .....	429
	1 General laws .....	429
	2 Behaviour as a function of doping levels .....	430
	3 Representational graph .....	431
	4 An example result .....	431

**Appendix A-7: Stages leading to emission and injection laws at**

	<b>interfaces</b> .....	433
I	Thermoelectric emission and the Dushman–Richardson law .....	433
II	Schottky injection (field effect emissions) .....	434
	1 The potential barrier at the atomic scale .....	435
	2 Emission conditions: Schottky emission law and the decrease in the potential barrier by field effect .....	435
III	Injection through tunnelling effect and the Fowler–Nordheim equation .....	437
	1 The problem .....	437
	2 Form of the transparency (T) of a triangular barrier .....	438
	3 The Fowler–Nordheim equation .....	440

**Appendix A-8: Energy levels and permitted transitions (and selection rules) in isolated atoms** .....

I	Spherical atoms with an external electron .....	443
	1 Energy levels and electron configuration .....	443
	2 Selection rules .....	444
II	An atom with more than one peripheral electron .....	445
	1 First effect produced from the perturbation $H_{ee}$ due to exact electronic interactions .....	445
	2 Perturbation involving the coupling energy between different magnetic moments exactly tied to kinetic moments .....	446
	3 Selection rules .....	447

**Appendix A-9: Etching polymers with ion beams: characteristics and results** .....

I	Level of pulverisation (Y) .....	449
	1 Definition .....	449
	2 The result $Y_{\text{physical}} = f(E)$ : 3 zones .....	450
	3 Level of chemical pulverisation .....	451
II	The relationship between etching speed and degree of pulverisation .....	451
	1 At normal incidence .....	451
	2 At oblique incidence .....	452

III	Speed of reactive etching (IBAE Ar <sup>+</sup> /O <sub>2</sub> or O <sup>+</sup> /O <sub>2</sub> ) . . .	452
IV	Preliminary modelling of Y <sub>physical</sub> for PI 2566 . . . . .	454
	1 Levels of carbon pulverisation using O <sup>+</sup> ions . . . .	454
	2 Comparing simulations of Y <sub>physical</sub> (θ) = f(θ) and the Thompson and Sigmund models . . . . .	454
V	Results from etching of polyimides . . . . .	455
	1 Self-supporting polyimide: UPILEX . . . . .	455
	2 A study of the etching of PI 2566 . . . . .	456
<b>Appendix A-10: An aide-mémoire on dielectrics . . . . .</b>		<b>459</b>
I	Definitions of various dielectric permittivities . . . . .	459
	1 Absolute permittivity . . . . .	459
	2 Relative permittivity . . . . .	459
	3 Complex relative permittivity . . . . .	460
	4 Limited permittivities . . . . .	460
	5 Dielectric conductivity . . . . .	461
	6 Classification of diverse dielectric phenomena . . . .	461
II	Relaxation of a charge occupying two position separated by a potential barrier . . . . .	463
	1 <i>Aide-mémoire</i> . . . . .	463
	2 Transportation in a dielectric with trapping levels, and the effect of an electric field on transitions between trap levels . . . . .	464
	3 Expression for the polarisation at an instant t following the displacement of electrons . . . . .	466
	4 Practical determination of potential well depths . . .	467
<b>Appendix A-11: The principal small molecules and polymers used in organic optoelectronics . . . . .</b>		<b>471</b>
I	Chemical groups and electron transport . . . . .	471
II	Examples of polymers used for their electroluminescence . . . . .	471
	1 The principal emitting polymers . . . . .	471
	2 'The' polymer for hole injection layers (HIL) . . . .	472
	3 Example of a polymer used in hole transport layers (HTL) . . . . .	473
	4 Example of a polymer used in electron transport layer (ETL) . . . . .	473
III	Small molecules . . . . .	473
	1 The principal green light emitting ligands . . . . .	473
	2 Principal electron transporting small molecules emitting green light . . . . .	474
	3 Example electron transporting small molecules emitting blue light . . . . .	474
	4 Example small molecules which emit red light . . .	474

- 5 Examples of small molecules which serve principally as hole injection layers (HIL) ..... 475
- 6 Examples of small molecules serving principally in hole transport layers (HTL) ..... 475
- 7 Example of a small molecule serving principally to confine holes in ‘hole blocking layers’ (HBL) .. 476

**Appendix A-12: Mechanical generation of the second harmonic and the Pockels effect** ..... 477

- I Mechanical generation of the second harmonic (in one-dimension) ..... 477
  - 1 Preliminary remark: the effect of an intense optical field ( $E^\omega$ ) ..... 477
  - 2 Placing the problem into equations ..... 477
  - 3 Solving the problem ..... 480
- II Excitation using two pulses and the Pockels effect ... 481
  - 1 Excitation from two pulses ..... 481
  - 2 The Pockels Effect ..... 482

**Bibliography** ..... 485

**Index** ..... 495

## **Part One**

---

**Concepts: electronic and optical processes in  
organic solids**

# I

---

## **Band and electronic structures in regular 1-dimensional media**

### **I An introduction to approximations of weak and strong bonds**

Historically, the relatively simple theory of free electrons moving within the confines of a flat-bottomed well, the walls coinciding with physical limits, has been used to understand the conduction of electrons in metals. Classically, in a 3 dimensional system a potential box is used as detailed in [kit 96] or [ash 76].

To more fully describe the electrical properties of metals, semiconductors and insulators, however, increasingly elaborate models are required which take into account precise interactions between electrons and their environments.

Depending on the nature of the bonding in the solid, two different approaches may be used.

#### **1 Materials with weak bonds**

The potential box model can be refined by imposing on electrons a potential generated by a regularly spaced crystal lattice, in which the Coulombic potential varies inversely to the radius ( $1/r$ ) of each electron from an ion at any lattice node. In Figure I-1, the row of atoms along axis Ox with periodic spacing  $a$ , the lattice constant, has electrons in an orbitals radius  $R$  (Figure I-1-a). A 1-dimensional representation of the potential energy of electrons is given in Figure I-1-b, with the condition that  $a < 2R$ . Admittedly, in using the term 'potential energy' rather than 'potential', we fall into a slight linguistic error, however the term 'potential energy' is widely used in material physics and quantum mechanics.

When an electron moves towards any nucleus in the lattice, the potential it undergoes varies according to the direction defined by line Ox, which runs through the nuclei. Changes in potential with respect to Ox have no actual physical meaning as conducting electrons are actually situated on the outer layers of atoms. In using line D, however, which does not pass through lattice nuclei, the electron to nucleus distance no longer tends to zero and potentials going to finite values can be resolved. In addition, with the superposition of two potential curves, due to a  $a < 2R$ , the barrier

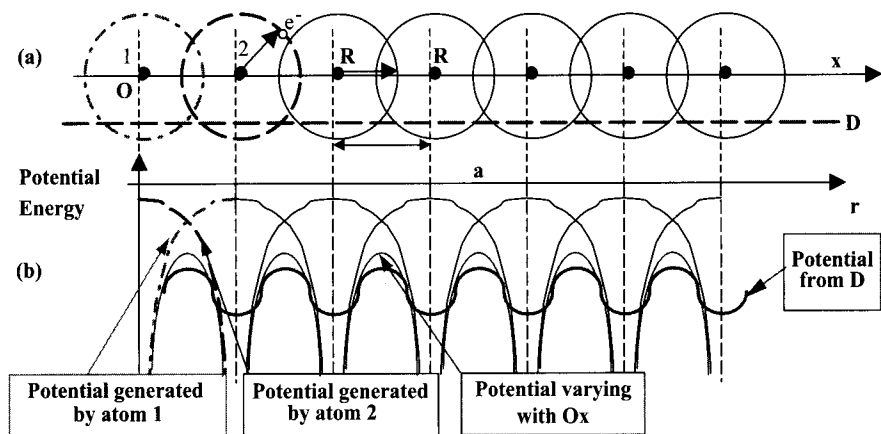


**Figure I-1.** Weak bonds: (a) atomic orbitals (s type with radius  $R$ ) in a regular lattice of periodicity  $a$  obeying the condition  $a < 2R$ ; and (b) 1-dimensional representation of the resulting potential energy (thick line) observed by electrons.

which exists mid-way between two adjacent nodes is lowered, and thus, for a solid, a potential with periodic fluctuations can be resolved. The initial representation using a flat-bottomed well—which implied that electrons are free electrons—is now replaced by a wavy-bottomed well and to a first approximation in 1-dimension (i.e.  $r \equiv x$ ), the potential is now defined by  $V(x) = w_0 \cos \frac{2\pi}{a} x$ . As  $a$  decreases below  $2R$ ,  $w_0$  also decreases and with it perturbations due to the crystal lattice. In reality, treatment of this problem by the method of perturbation becomes increasingly plausible as the value of  $a$  decreases with respect to  $2R$ . An approximation for a half-free electron, according to the Hamiltonian 1<sup>st</sup> order of approximation,  $H^{(1)} = w_0 \cos \frac{2\pi}{a} x$ , is an improvement upon that of a free electron (which ignores  $H^{(1)}$ ). As an electron delocalised within a metallic lattice has a low value of  $w_0$ , the theory developed for weak bonds can also be applied to bonds within metals.

## 2 Materials with strong bonds

The way in which strong bonds are treated closely resembles a chemist's point of view, as the properties of a solid are derived from orbitals of constituent atoms and the chemical bonding can be specified using a linear combination of atomic orbitals. This reasoning is moreover acceptable when the electrons under consideration are attached closely to bonding atoms, as approximations of strong bonds are justifiable when  $a > 2R$  is obeyed (Figure I-2-a).

An approximation can therefore be made for covalent solids in which valence electrons ensuring bonding are localised between two atoms (for bonding states in more detail, see Appendix A). However, if we study potential curves using  $Ox$ , we obtain a function which diverges when electrons are close to nuclei. While discontinuity



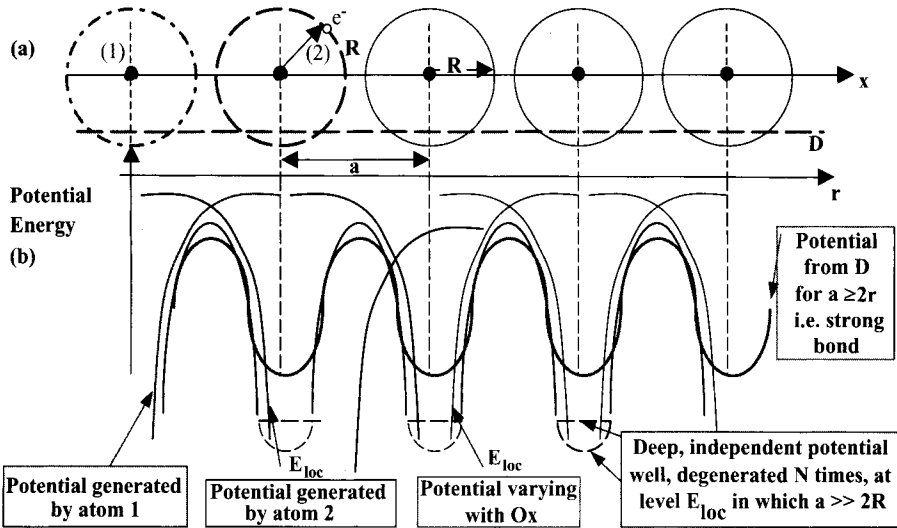


**Figure I-2.** Strong bonds: (a) atomic orbitals (s type with radius  $R$ ) in a regular lattice (lattice constant  $a$ ) obeying the condition  $a \geq 2R$ ; and (b) 1-dimensional representation of the resulting potential energy (thick line) observed by electrons.

is removed when line  $D$  is used relative to valence electrons, two scenarios may be envisaged:

- If  $a \gg 2R$ , very deep potential wells appear because there is practically no overlap between potentials generated by adjacent nuclei. Taking this argument to its limit, if a chain of  $N$  atoms and  $N$  valence electrons is formed with sufficiently long bonds to make  $N$  electrons independent in  $N$  deep, independent potential wells, the energy levels ( $E_{loc}$  in Figure I-2) are degenerated  $N$  times, are all identical and therefore indiscernible from one another.
- If  $a \geq 2R$ , the decreasing gap between atoms induces a slight overlap of potentials, generated by adjacent nuclei, and potential wells, therefore, are no longer independent. Subsequently, degeneration occurs in which the electrons of one bond interact with those of neighbouring bonds to break-up energy level bands. It should be noted though that the potential wells are, however, considerably deeper than those found for weak bonds ( $a < 2R$ ), so much so that electrons remain considerably more in the locality of each atom to which they are attached. We should also note that, unlike for weak bonds, simple treatment using the perturbation method is no longer possible due to the considerable depth of the wells.

Most of the remainder of this chapter will detail the determination of energy levels and bands in 1-D for strong bonds. Beforehand though, and by way of comparison, we will consider the origin of energy bands due to weak bonds.

## II Band Structure in weak bonds

### 1 Prior result for zero order approximation

While the description of weak bonds corresponds essentially to that of metallic bonds, it would be more appropriate to outline reasons for the origin of potential bands in which electrons are found, as represented in Figure I-3 which follows on from Figure I-1.

Initially we should remember that for free electrons (zero order approximation) potentials correspond to that of a flat-bottomed well (horizontal line joining nodes in Figure I-3). For this system where the potential (or potential energy)  $V = V^0 = 0$ , the amplitude in Schrödinger's wave equation is expressed as  $\Delta\psi^0 + \frac{2m}{\hbar^2}E\psi^0 = 0$ . By favouring real solutions and assuring the propagation of a wave associated with an electron by using  $k^2 = \frac{2m}{\hbar^2}E$ , we have  $\psi^0 = Ae^{\pm ikx}$ ; elsewhere, the curve  $E = f(k)$  is obtained from  $E = E^0 = \frac{\hbar^2}{2m}k^2$ .

We have seen that lattice effects result in a perturbed periodic potential. From this the first term of a developing Fourier series allows an approximation to be made:

$$V \approx V^{(1)} = w(x) = w_0 \cos \frac{2\pi}{a}x.$$

The function of the wave is itself perturbed and takes on the form of a Bloch function i.e.  $\psi_k(x) = \psi^0 u(x) = e^{ikx} u(x)$ , in which  $u(x)$  is a periodic function based on the lattice constant  $a$ . The reason for this is that the wavefunction must remain unchanged while undergoing translations of modulus  $a$  ( $T_a$ ) which imposes  $u(x) = u(x + a)$ : cf. remarks in Appendix A-2, Part IV.

### 2 Physical origin of forbidden bands

Figure I-4 shows a regular chain of atoms and two incident rays. Incident rays are reflected by lattice atoms and constructive interference occurs when the difference in step ( $\Delta$ ) between two waves is equal to the ray wavelength multiplied by a whole number.

In a 1-D system, the difference  $\Delta$  of parallel waves 1 and 2 after reflection is  $\Delta = 2a$ , however, incident waves undergoing maximum reflection will have wavelength  $\lambda_n$  such that  $\Delta = 2a = n \lambda_n$ . In addition, we should note that if the vector modulus

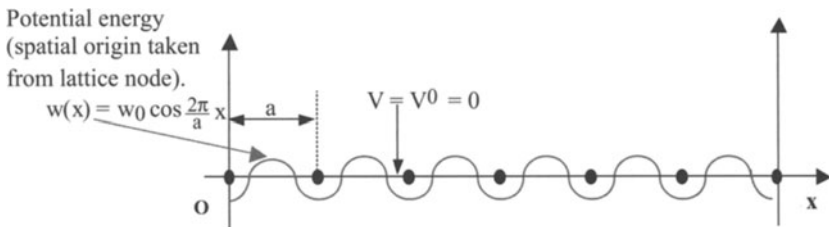


Figure I-3. Potential energy curve  $w(x) = w_0 \cos \frac{2\pi}{a}x$  showing  $w_0 < 0$ .

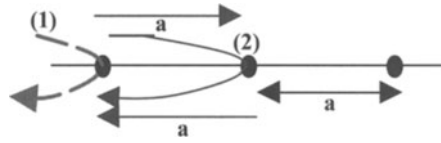


Figure I-4. Bragg reflection for a 1-D.

of a wave is  $k = \frac{2\pi}{\lambda}$ , incident waves with  $k = k_n = \frac{2\pi}{\lambda_n} = n\frac{\pi}{a}$  undergo the maximum reflection, according to Bragg's condition.

Using the zero order approximation, the amplitude of an incident wave associated with an electron in a weak bond is only slightly perturbed such that  $\psi_k^0 = Ae^{ikx}$ .

The time dependent incident wave is therefore written as  $[\Psi_k^0(x, t)]_{inc.} = Ae^{i(kx - \omega t)}$  and is expressed as an incident wave progressing in the direction  $x > 0$ .

When  $k = k_n$  exactly, the reflected wave tends towards  $x < 0$  and  $[\Psi_{k_n}^0(x, t)]_{refl.} = Ae^{i(k_n x + \omega t)}$ .

When stationary waves are formed from the superposition of incident and reflected waves, for which  $k = k_n = n\frac{\pi}{a}$ , both symmetric and asymmetric solutions are formed i.e.  $\Psi^+ \pi \cos(\frac{n\pi}{a}x)e^{-i\omega t}$  and  $\Psi^- \pi \sin(\frac{n\pi}{a}x)e^{-i\omega t}$ , respectively. Concerning electrons fulfilling  $k = k_n = n\frac{\pi}{a}$  for these two wavefunctions there are two corresponding probable electron densities:  $\rho^+ = \Psi^+ \Psi^{+*} \pi \cos(\frac{n\pi}{a}x)$  and  $\rho^- = \Psi^- \Psi^{-*} \pi \sin^2(\frac{n\pi}{a}x)$ .

For any single given value of  $k_n$ , the probable electron densities  $\rho^+$ ,  $\rho^-$ , and  $\rho$  for electrons respectively described by stationary waves  $\Psi^+$  and  $\Psi^-$  and the progressive wave  $[\Psi_{k_n}(x, t)] = Ae^{i(k_n x - \omega t)}$  are shown in Figure I-5. The progressive wave corresponds to  $\rho = \text{constant}$ , and when  $k = k_n$ , can only exist by neglecting any reflections due to the lattice with spatial period  $a$ . With the zero order approximation,  $V = V^0 = 0$ ; when  $V \neq V_0$ , this type of wave can only exist when  $k \neq k_n$ .

In Figure I-5, we can see that:

- $\rho^+$  displays the highest concentration of electrons close to nuclei in a configuration which corresponds to the lowest average energy  $w^+$  (the small distance between electron and nuclei results in a high modulus of negative Coulombic energy);

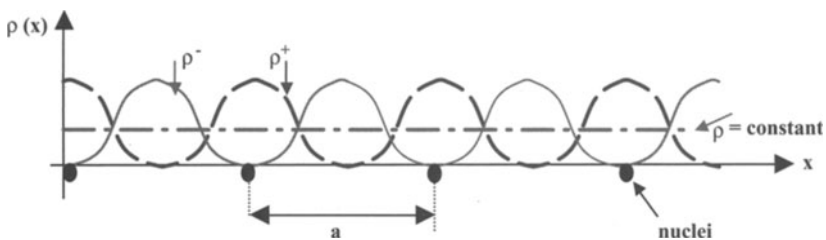


Figure I-5. Electron densities  $\rho^+$ ,  $\rho^-$  and  $\rho$  associated, respectively, with stationary waves  $\Psi^+$ ,  $\Psi^-$  and a progressive wave.

- $\rho^-$  shows a maximum concentration of electrons mid-way between nuclei in a configuration associated with the highest energy  $w^-$  (high average electron-nucleus distances result in low Coulombic potential moduli);
- at  $\rho = \text{constant}$ , where there is an equal distribution of electrons associated with an intermediate electron-nucleus distance, the configuration corresponds to an intermediate energy, which approximates to that of a free electron.

Finally, two different energy values are generated by two physical solutions,  $\Psi^+$  and  $\Psi^-$ , for the same value  $k_n$  of  $k$  ( $k = k_n = n\frac{\pi}{a}$ ), and this dispersion, or degeneration, of energy values is represented in Figure I-6, in which  $E = f(k)$ . The ‘gap’  $E_G = w^- - w^+$  is a forbidden band because, at the same value of  $k = k_n$ , there is a discontinuous change from values of energy  $w^+$  to  $w^-$ .

### 3 Simple estimation of the size of the forbidden band

The wavefunctions  $\Psi^+$  and  $\Psi^-$ , normalised for a segment  $L = Na$ , corresponding to a 1-D chain of  $N + 1 \approx N$  atoms, are such that:

$$\int_0^{L=Na} |\Psi^+(x)|^2 dx = 1 \quad \text{or} \quad \Psi^+(x) = \sqrt{\frac{2}{L}} \cos\left(\frac{\pi x}{a}\right),$$

$$\int_0^{L=Na} |\Psi^-(x)|^2 dx = 1 \quad \text{or} \quad \Psi^-(x) = \sqrt{\frac{2}{L}} \sin\left(\frac{\pi x}{a}\right).$$

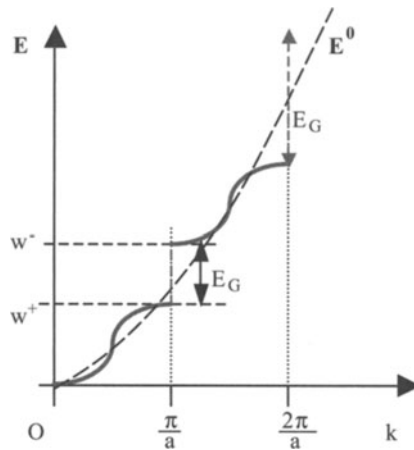


**Figure I-6.** Curve  $E = f(k)$ . The zero order approximation, corresponding to perturbation potential  $w(x) = 0$ , results in energy  $E^0 = \frac{\hbar^2 k^2}{2m}$ . Thus lattice-electron interaction is considered negligible, just as for a flat-bottomed well.

Through waves associated with electrons at atoms in a regular chain, the lattice results in two solutions for energy for each value  $k = k_n = n\frac{\pi}{a}$ , with  $w^+ < w^-$  as detailed in Section II-2.

The gap in energy, equal to  $E_G = w^- - w^+ = -(w^+ - w^-)$  gives us:

$$\begin{aligned} E_G &= -(\langle \Psi^+ | w(x) | \Psi^+ \rangle - \langle \Psi^- | w(x) | \Psi^- \rangle) \\ &= -\frac{2w_0}{L} \int_0^L \cos\left(\frac{2\pi}{a}x\right) \left[ \cos^2\frac{\pi}{a}x - \sin^2\frac{\pi}{a}x \right] dx \\ &= -\frac{2w_0}{L} \int_0^L \cos^2\left(\frac{2\pi}{a}x\right) dx. \end{aligned}$$

As  $w_0$  must remain negative, the potential energy curve goes through a minimum at the nuclei where the origin is placed, as shown in Figure I-3, and we obtain a positive value for  $E_G = -w_0$ .

As  $E_G = |w_0|$ , stronger electron-lattice interactions, and an increasing  $w_0$ , result in a larger forbidden band.

### III Floquet's theorem: wavefunctions for strong bonds

#### 1 Form of the resulting potential

Figure I-7 represents an infinite chain of atoms spaced distance  $a$  apart with  $a > 2R$ .

As the atoms are numbered  $\dots (0), (1), (2), \dots (s-1)$  and the origin is at the nucleus (0), the distance between the nucleus of atom  $s$  from the origin is  $r_s = s.a$ .

Using the layout shown above, the potential generated by atom (s) at a point in space located by  $\vec{r}$ , or  $v_s(\vec{r})$ , is the same as that generated by atom (0) at point  $\vec{r}'$ , similarly denoted  $v_0(\vec{r}')$ . In giving  $\vec{r}_s = s\vec{a}$ , and using  $\vec{r}_s + \vec{r}' = \vec{r}$ , we obtain  $v_s(\vec{r}) = v_0(\vec{r}') = v_0(\vec{r} - \vec{r}_s)$ . In addition to the potential generated by atom (s), any electron placed at  $\vec{r}$  will undergo a potential  $v_{s-1}(\vec{r}) = v_0(\vec{r} - \vec{r}_{s-1})$  resulting from neighbouring atoms (s-1), and so on for other atoms. We can therefore sum the resulting potential in terms of  $\vec{r}$  over an infinite chain:

$$V(\vec{r}) = \sum_{s=-\infty}^{s=+\infty} v_s(\vec{r}) = \sum_{s=-\infty}^{s=+\infty} v_0(\vec{r} - \vec{r}_s). \quad (1)$$

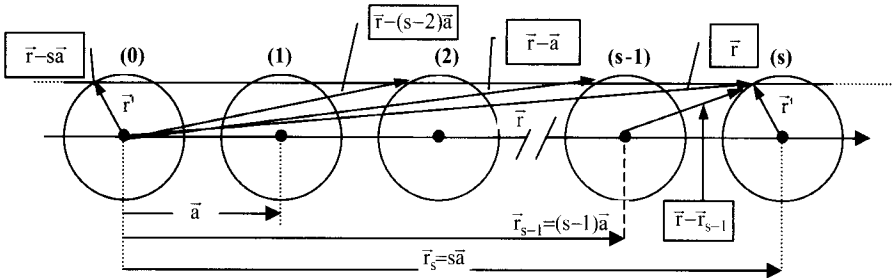


Figure I-7. Atoms in a 1-D infinite chain.

We can now note that the resulting potential,  $V(\vec{r})$ , is periodic with respect to  $\vec{a}$ , and that symmetry imposed by an infinite chain results in a potential in  $\vec{r}$  which is the same if calculated using  $\vec{r} - \vec{a}, \dots, \vec{r} - s\vec{a}, \dots$  and so on. We can therefore write, independent of  $s$  being positive or negative

$$V(\vec{r}) = V(\vec{r} - \vec{a}) = V(\vec{r} - s\vec{a}). \quad (2)$$

As the potential  $V(\vec{r})$ , in which is placed each electron, is a periodic function, the corresponding wavefunction is a Bloch function. We shall use these results to establish Floquet's theorem in Section 3.

## 2 The form of the wavefunction

As shown in Figure I-8, if a valence electron on a nucleus  $s$  is not influenced by the presence of neighbouring nuclei, as the atoms are far apart, then the potential at an electron at  $\vec{r}$  is reduced to  $v_s(\vec{r}) = v_0(\vec{r} - \vec{r}_s)$ , and therefore  $V(\vec{r}) \approx v_0(\vec{r} - \vec{r}_s)$ . Subsequently, the obtained wavefunction corresponds to that of a lone atom  $s$  with atomic wavefunction  $\psi_s(\vec{r})$ .

If the atoms are moved close enough together, an electron placed in  $\vec{r}$  will be influenced by more than one and its wavefunction corresponds to a molecular orbital derived using the LCAO method (see Appendix A-1). That is:

$$\psi(\vec{r}) = \sum_s c_s \psi_s(\vec{r}),$$

in which  $\psi_s(\vec{r})$  is the wavefunction of an electron from atom  $s$  at  $\vec{r}$ .

We can thus see that the form of the solution chosen for a wavefunction is identical to that followed by the potential in which an electron is placed.

By the reasoning developed above for an electron and the potential to which it is subject, the wavefunction  $\psi_s(\vec{r})$  relative to an electron positioned at  $\vec{r}$  from an atom  $s$  is identical to that of the same electron placed at  $\vec{r}'$  on an atom (0):

$$\psi_s(\vec{r}) = \psi_0(\vec{r}'), \quad \text{or with } \vec{r} = \vec{r}_s + \vec{r}', \quad \psi_s(\vec{r}) = \psi_0(\vec{r} - \vec{r}_s).$$

We can thus write, in a manner similar to that for the potential:

$$\psi(\vec{r}) = \sum_{s=-\infty}^{+\infty} c_s \psi_0(\vec{r} - \vec{r}_s) \quad (3)$$

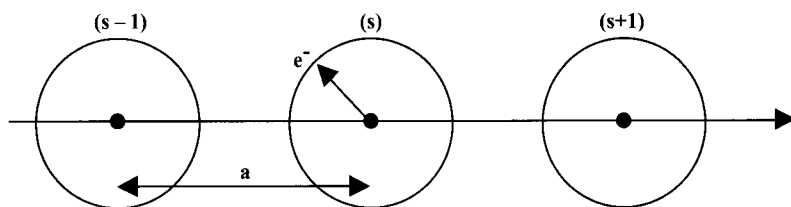


Figure I-8. System of effectively independent atoms.

### 3 Floquet's theorem: effect of potential periodicity on wavefunction form

For an electron at  $\vec{r}$  belonging to an infinite, regular chain, the wavefunction can be written:

— in the form of a linear combination,

$$\psi(\vec{r}) = \sum_{s=-\infty}^{+\infty} c_s \psi_0(\vec{r} - \vec{r}_s), \quad (3)$$

corresponding to Hückel's wavefunction representation;

— or in the form of a Bloch function, under which the electron is subject to a periodic potential (see Part II-1), and

$$\psi_{\mathbf{k}}(r) = e^{i\mathbf{k}r} u(r) \quad \text{with} \quad u(r) = u(r + a). \quad (4)$$

Initially, the Bloch form applied to a wavefunction calculated in  $\vec{r} + \vec{a}$  results in:

$$\psi_{\mathbf{k}}(\vec{r} + \vec{a}) = e^{i\vec{k}(\vec{r}+\vec{a})} u(\vec{r} + \vec{a}) = e^{i\vec{k}\vec{a}} e^{i\vec{k}\vec{r}} u(\vec{r}) = e^{i\vec{k}\vec{a}} \psi_{\mathbf{k}}(\vec{r}) \quad (5)$$

Using Hückel's expression (3) to develop  $\psi_{\mathbf{k}}(\vec{r})$  as described in eqn (5), we obtain a first expression for  $\psi_{\mathbf{k}}(\vec{r} + \vec{a})$ :

$$\psi_{\mathbf{k}}(\vec{r} + \vec{a}) = e^{i\vec{k}\vec{a}} [c_0 \psi_0(\vec{r}) + c_1 \psi_0(\vec{r} - \vec{a}) + \dots + c_s \psi_0(\vec{r} - s\vec{a})]. \quad (6)$$

Directly performing a Hückel type representation of  $\psi_{\mathbf{k}}(\vec{r} + \vec{a})$  yields:

$$\begin{aligned} \psi_{\mathbf{k}}(\vec{r} + \vec{a}) &= c_0 \psi_0(\vec{r} + \vec{a}) + c_1 \psi_0(\vec{r} + \vec{a} - \vec{a}) + \dots + c_s \psi_0(\vec{r} + \vec{a} - s\vec{a}) \\ &\quad + c_{s+1} \psi_0(\vec{r} + \vec{a} - [s+1]\vec{a}) + \dots \end{aligned} \quad (7)$$

If we identify term by term through (6) and (7) we obtain:

$$\begin{aligned} e^{i\vec{k}\vec{a}} c_0 \psi_0(\vec{r}) &= c_1 \psi_0(\vec{r}), \quad \text{or} \quad c_1 = c_0 e^{i\vec{k}\cdot\vec{a}} \\ e^{i\vec{k}\vec{a}} c_1 \psi_0(\vec{r} - \vec{a}) &= c_2 \psi_0(\vec{r} + \vec{a} - 2\vec{a}), \quad \text{or} \quad c_2 = c_1 e^{i\vec{k}\vec{a}} \\ e^{i\vec{k}\vec{a}} c_s \psi_0(\vec{r} - s\vec{a}) &= c_{s+1} \psi_0(\vec{r} + \vec{a} - [s+1]\vec{a}), \quad \text{or} \quad c_{s+1} = c_s e^{i\vec{k}\vec{a}} \end{aligned}$$

We therefore have, as a general rule:

$$c_s = c_{s-1} e^{i\vec{k}\vec{a}} = c_{s-2} e^{i\vec{k}\cdot 2\vec{a}} = \dots = c_0 e^{i\vec{k}\cdot s\vec{a}} = c_0 e^{i\vec{k}\cdot\vec{r}_s} \quad (8)$$

We are thus brought to the final form of the wavefunction, or Floquet's theorem, which can be written in two equivalent ways (using the notation  $\psi(\vec{r}) \equiv \psi_{\mathbf{k}}(\vec{r})$ ):

$$\psi(\vec{r}) = \sum_s c_s \psi_s(\vec{r}), \quad \text{with} \quad c_s = c_0 e^{i\vec{k}\cdot\vec{r}_s}, \quad \psi(\vec{r}) = \psi_{\mathbf{k}}(\vec{r}) = c_0 \sum_s e^{i\vec{k}\cdot\vec{r}_s} \psi_s(\vec{r}); \quad (9)$$

or:

$$\psi_{\mathbf{k}}(\vec{r}) = \sum_{s=-\infty}^{+\infty} c_s \psi_0(\vec{r} - \vec{r}_s) = c_0 \sum_{s=-\infty}^{+\infty} e^{i\vec{k}\cdot\vec{r}_s} \psi_0(\vec{r} - \vec{r}_s), \quad \text{with} \quad \vec{r}_s = s\vec{a}. \quad (10)$$

## IV A study on energy

### 1 Defining equations (with $x \equiv r: 1 - D$ )

We shall consider a specific atom  $s$  and its neighbours. The resulting potential, around this atom, is  $V(x)$  as described by the dotted curve in Figure I-9. Alternatively, if the atoms are sufficiently spaced out to be considered independent, the equivalent potential would be  $U_0(x)$ . Figure I-9 represents  $U_0(x)$ , generated in terms of  $x$  by atom  $s$ , which is the same potential  $U_0(x + a)$  generated by atom  $(s + 1)$  at  $(x + a)$ . This results in  $U_0(x) = U_0(x + a)$ , in which  $U_0$  is periodic due to there being isolated atoms in the chain.

Equally, we can see that for  $x \in ]r_s - \frac{a}{2}, r_s + \frac{a}{2}[$  we have  $V(x) \approx U_0(x)$ .

When  $W(x) = V(x) - U_0(x)$ , for  $r_s - \frac{a}{2} < x < r_s + \frac{a}{2}$ ,  $W(x)$  is small; in addition, as  $V(x) < U_0(x)$  and now  $W(x) < 0$ .

Detailing the Schrödinger wave equation:

- for an electron described by the wavefunction  $\Psi_k(x)$  and placed in the resulting potential  $V(x)$ , in which  $\Psi_k(x)$  and  $V(x)$  take into account effects from neighbouring atoms:

$$E\Psi_k(x) = -\frac{\hbar^2}{2m}\Delta\Psi_k(x) + V(x)\Psi_k(x); \quad (11)$$

- or for an electron belonging to an isolated atom  $s$ : the wavefunction of an electron positioned in terms of  $x$  from the isolated atom is  $\Psi_s(x) = \Psi_0(x - sa)$ , while the

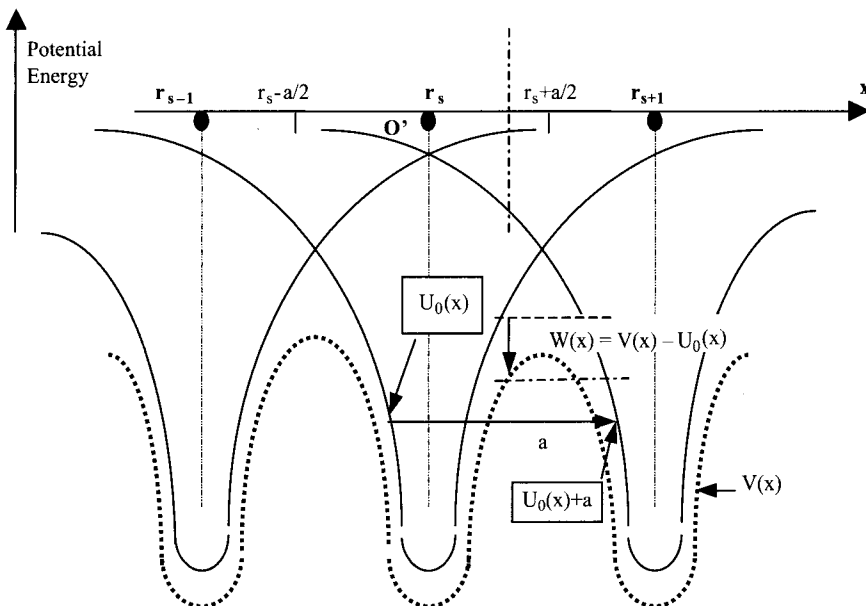


Figure I-9. The function  $W(x) = V(x) - U_0(x)$ .



potential is  $U_0(x) = U_0(x - sa)$ . Noting that its energy is  $E_0$ , we now have

$$E_0\psi_0(x - sa) = -\frac{\hbar^2}{2m}\Delta\psi_0(x - sa) + U_0(x)\psi_0(x - sa). \quad (12)$$

Multiplying the two parts of eqn (12) by  $c_0e^{ikr_s}$  (with  $r_s = sa$ ), and integrating over  $s$ :

$$E_0 \sum_s c_0 e^{ikr_s} \psi_0(x - r_s) = -\frac{\hbar^2}{2m} \Delta \left[ \sum_s c_0 e^{ikr_s} \psi_0(x - r_s) \right] + U_0(x) \sum_s e^{ikr_s} \psi_0(x - r_s).$$

Taking into account eqn (10), this can be rewritten as:

$$E_0\Psi_k(x) = -\frac{\hbar^2}{2m}\Delta\Psi_k(x) + U_0(x)\Psi_k(x). \quad (13)$$

In taking the difference [eqn (11) – eqn (13)], we obtain:

$$(E - E_0)\Psi_k(x) = [V(x) - U_0(x)]\Psi_k(x) \quad (14)$$

And the potential,  $V(x)$ , if periodic, gives  $V(x) = V(x - r_s)$  and thus:

$$W(x) = [V(x) - U_0(x)] = [V(x - r_s) - U_0(x - r_s)] = W(x - r_s). \quad (15)$$

We should note that  $W(x - r_s)$  is a function with period  $a$ , and is consequently independent of  $s$  even though the parameter can be brought into or taken out of the integral sum.

Developing eqn (14) gives  $\Psi_k(x)$  according to Floquet's eqn (10):

$$(E - E_0)\Psi_k(x) = c_0 \sum_s e^{ikr_s} W(x - r_s) \psi_0(x - r_s). \quad (16)$$

## 2 Calculation of energy for a chain of N atoms

We can directly obtain the following equation by multiplying eqn (16) by  $\Psi_k^*(x)$  and integrating over a range of N atoms from 0 to  $(N - 1)$ :

$$(E - E_0)\langle\Psi_k(x)|\Psi_k(x)\rangle = c_0 \sum_s e^{ikr_s} \int \Psi_k^*(x) W(x - r_s) \psi_0(x - r_s) dx. \quad (17)$$

With eqn (10), we obtain

$$\langle\Psi_k(x)|\Psi_k(x)\rangle = |c_0|^2 \sum_{s=0}^{s=N-1} \sum_{t=0}^{t=N-1} e^{i(ks-kt)a} \langle\psi_0(x - r_s)|\psi_0(x - r_t)\rangle.$$

As  $\langle \psi_0(x-r_s) | \psi_0(x-r_t) \rangle = \delta_s^t$  (with  $\delta_s^t = 1$  if  $s = t$ ,  $\delta_s^t = 0$  if  $s \neq t$ ),

$$\langle \Psi_k(x) | \Psi_k(x) \rangle = |c_0|^2 \sum_{s=0}^{s=N-1} \sum_{t=0}^{t=N-1} e^{i(ks-kt)a} \delta_s^t = |c_0|^2 \sum_{s=0}^{s=N-1} e^{i(ks-ks)a} = |c_0|^2 \cdot N$$

Normalisation of the function  $\Psi_k(x)$ :  $\langle \Psi_k(x) | \Psi_k(x) \rangle = 1 = |c_0|^2 \cdot N$ , gives

$$c_0 = \frac{1}{\sqrt{N}}. \quad (18)$$

From eqn (17) we can deduce that with  $\Psi_k^*(x) = c_0^* \sum_t e^{-ikr_t} \psi_0^*(x-r_t)$ ,

$$(E - E_0) = |c_0|^2 \sum_s e^{ikr_s} \sum_t e^{-ikr_t} \int \psi_0^*(x-r_t) W(x-r_s) \psi_0(x-r_s) dx,$$

and through eqn (18),

$$E - E_0 = \frac{1}{N} \sum_{s,t} e^{ik(s-t)a} \int \psi_0^*(x-ta) W(x-sa) \psi_0(x-sa) dx.$$

The latter can also be written:

$$E = E_0 + \frac{1}{N} \sum_{s,t} e^{ik(s-t)a} \langle \psi_0(x-ta) | W(x-sa) | \psi_0(x-sa) \rangle. \quad (19)$$

Using Hückel's approximations, which assume couplings only with first neighbours:

$$\begin{aligned} \langle \psi_0(x-ta) | W(x-sa) | \psi_0(x-sa) \rangle &= \langle \psi_t | W | \psi_s \rangle \\ &= \begin{cases} -\alpha & \text{for } s = t \text{ (with } \alpha > 0 \text{ as } W < 0) \\ -\beta & \text{for } s = t \pm 1 \\ 0 & \text{for all others.} \end{cases} \end{aligned} \quad (20)$$

(As  $W < 0$ , we also have  $\beta > 0$ , if orbitals  $\Psi_t$  and  $\Psi_s$  are of the same sign: cf. Appendix 1, Section IV).

Given the approximation, the integration of energy in eqn (19) over  $s$  from  $s_0 = 0$  to  $s_{N-1} = N - 1$  yields:

$$\begin{aligned} E = E_0 + \frac{1}{N} \left[ \sum_t e^{ik(s_0-t)a} \langle \psi_t | W | \psi_{s_0} \rangle + \sum_t e^{ik(s_1-t)a} \langle \psi_t | W | \psi_{s_1} \rangle \right. \\ \left. + \dots + \sum_t e^{ik(s_{N-1}-t)a} \langle \psi_t | W | \psi_{s_{N-1}} \rangle \right] \end{aligned} \quad (21)$$

Each term between the square brackets has N terms, as s takes on N values, and therefore each term yields the same contribution, in the form:

$$\begin{aligned} \sum_t e^{ik(s_j-t)a} \langle \psi_t | W | \psi_{s_j} \rangle &= \underbrace{e^{ik(0)a}(-\alpha)}_{s_j=t} + \underbrace{e^{ik(-1)a}(-\beta)}_{s_j=t-1} + \underbrace{e^{ik(+1)a}(-\beta)}_{s_j=t+1} \\ &= -\alpha - \beta e^{-ika} - \beta e^{ika} \end{aligned}$$

Finally, the term inside the square brackets of eqn (21) is equal to  $N[-\alpha - \beta e^{-ika} - \beta e^{ika}]$ , and thus E can be expressed as:

$$\begin{aligned} E &= E_0 - \alpha - \beta e^{-ika} - \beta e^{ika} = E_0 - \left[ \alpha + 2\beta \left( \frac{e^{ika} + e^{-ika}}{2} \right) \right] \\ &= E_0 - [\alpha + 2\beta \cos ka]. \end{aligned}$$

This can be rewritten as:

$$\boxed{E = E_0 - \alpha - 2\beta \cos ka} \tag{22}$$

Figure I-10 shows a graphical representation of the energy dispersion curve  $E = f(k)$ . The amplitude of variation in E, with respect to k, is equal to  $4\beta$ . Appropriately, allowed bands increase in size with higher values of  $\beta$  due to strong interactions between electrons on neighbouring atoms.

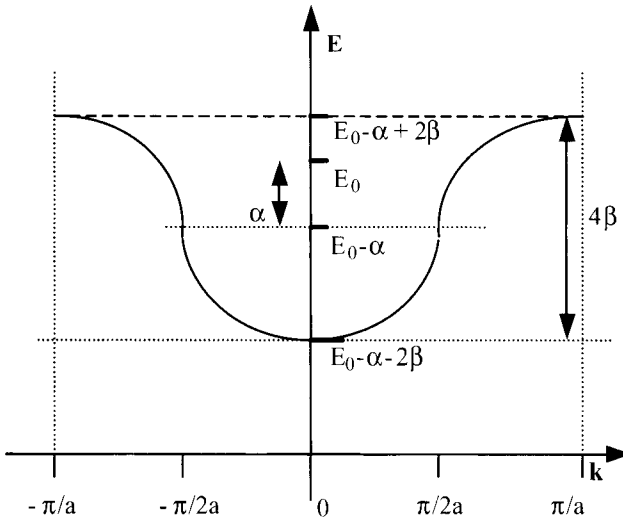


**Figure I-10.** Energy dispersion curve for  $E = f(k)$ , within Hückel and strong bond approximations.

### 3 Additional comments: physical significance of terms $(E_0 - \alpha)$ and $\beta$ ; simple calculation of $E$ ; and the appearance of allowed and forbidden bands in strong bonds.

#### a Physical significance of terms $(E_0 - \alpha)$ and $\beta$

From eqn (12),  $E_0 \Psi_0(x - sa) = -\frac{\hbar^2}{2m} \Delta \Psi_0(x - sa) + U_0(x) \Psi_0(x - sa)$ , and with eqn (20) we obtain:

$$\begin{cases} E_0 = \langle \Psi_0(x - sa) | -\frac{\hbar^2}{2m} \Delta + U_0(x) | \Psi_0(x - sa) \rangle (12') \\ -\alpha = \langle \Psi_0(x - sa) | W(x - sa) | \Psi_0(x - sa) \rangle \text{ (one of Hückel conditions in eqn (20))} \end{cases}$$

so with  $W(x - sa) = W(x)$  (eqn (15) gives periodicity  $W$ ):

$$\begin{aligned} E_0 - \alpha &= \left\langle \Psi_0(x - sa) \left| -\frac{\hbar^2}{2m} \Delta + U_0(x) + W(x) \right| \Psi_0(x - sa) \right\rangle \\ &= \left\langle \Psi_s(x) \left| -\frac{\hbar^2}{2m} \Delta + U_0(x) + W(x) \right| \Psi_s(x) \right\rangle, \text{ or:} \\ (E_0 - \alpha) &= \left\langle \Psi_s(x) \left| -\frac{\hbar^2}{2m} \Delta + V(x) \right| \Psi_s(x) \right\rangle, \text{ as } V(x) = U_0(x) + W(x). \quad (23) \end{aligned}$$

From the terms within brackets we can now say that:

- $E_0$  represents the energy of an electron situated on a given atom  $s$  subject to a potential,  $U_0(x)$ , resulting from the given atom;
- and  $-\alpha$  represents the energy of an electron situated on a given atom  $s$  subject to a potential,  $W(x)$ , resulting from that given atom and its neighbours;
- the term  $(E_0 - \alpha) = E'_0$  represents the energy of an electron situated on a given atom  $s$  subject to a general potential,  $U_0(x)$  and  $W(x)$ , resulting, respectively, from that given atom and its neighbours, as shown in Figure I-11.

From eqn (20) we have seen that  $-\beta = \langle \Psi_0(x - ta) | W(x - sa) | \Psi_0(x - sa) \rangle = \langle \Psi_t | W | \Psi_s \rangle$ , with  $s = t \pm 1$ . This term corresponds to the coupling energy of an electron, at given atom  $s$ , with electrons at adjacent atoms ( $t$ ) and such that  $t = s \pm 1$ , which are in the same orbital. This coupling is brought about by the intermediate perturbation potential ( $W(x)$ ) resulting from neighbouring atoms which gives rise to an increase in degeneration, shown in zone II of Figure I-11, corresponding to the allowed energy bands in Figure I-10.

As lattice atoms are brought together and  $a$  decreases the perturbation  $W$  increases and the permitted band increases in size as shown in zone II of Figure I-12.

Elsewhere [Ngu 94], the term  $-\beta$  can be seen as the energy of the electron population associated with the covering integral  $\langle \Psi_0(x - ta) | \Psi_0(x - sa) \rangle$ .

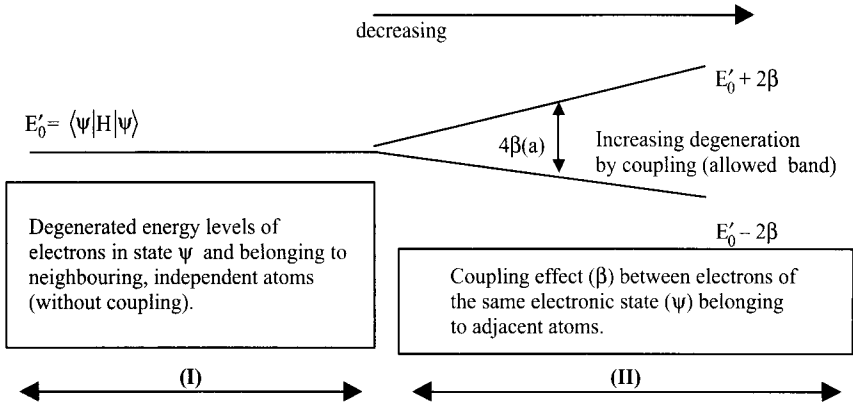


**Figure I-11.** Scheme of coupling effect between electrons in the same electronic state. In zone II, the interaction between atoms increases, and a decreases, with  $\beta(a)$ .

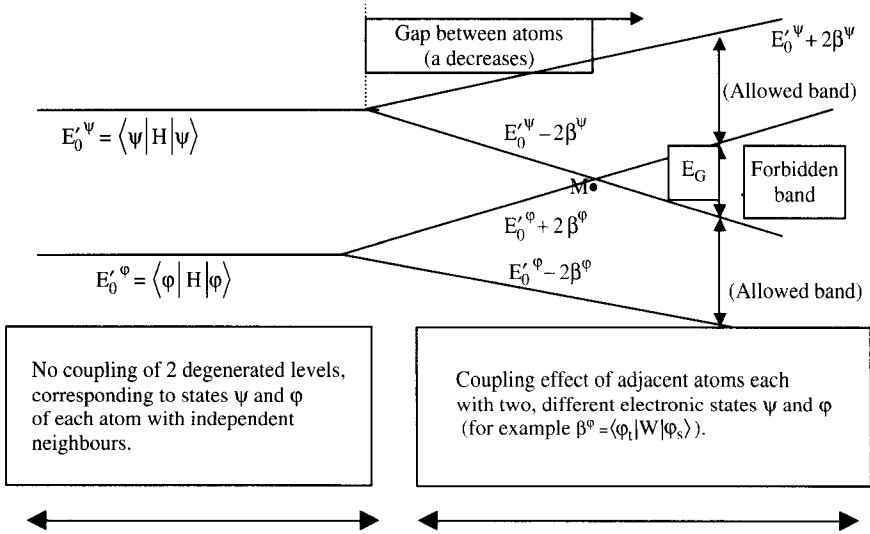


**Figure I-12.** Scheme to first approximation of formation of a forbidden band from electrons with different states of  $\psi$  and  $\phi$ .

**b Comment on simplified energy calculation**

With  $H = -\frac{\hbar^2}{2m} \Delta + V(x)$  we have following eqn (23)

$$(E_0 - \alpha) = E'_0 = \langle \psi_s(x) | H | \psi_s(x) \rangle.$$

Often the term  $(E_0 - \alpha) = E'_0$  is noted as  $-\alpha$  as it can be obtained by a more direct calculation, which inconveniently also hides certain physical realities.

Thus, the following can be written:

$$E = E(k) = \frac{\langle \psi_k | H | \psi_k \rangle}{\langle \psi_k | \psi_k \rangle} = \frac{\sum_s \sum_t e^{ik(s-t)a} \langle \psi_s | H | \psi_t \rangle}{\sum_s \sum_t e^{ik(s-t)a} \langle \psi_s | \psi_t \rangle}.$$

By using the relationship  $\langle \psi_s | \psi_t \rangle = \delta_{st}$  and considering that Hückel approximations can be given as

$H_{ss} = \langle \psi_s | H | \psi_s \rangle = -\alpha =$  Coulomb integral = negative constant, given the origin to be the energies of an electron at infinity (cf. p. 58 of [Ngu 54]);

$H_{st} = \langle \psi_s | H | \psi_t \rangle = -\beta$  for  $s \neq t$  with  $s$  and  $t$  as adjacent neighbours ( $-\beta < 0$ , is the resonance integral between electrons  $s$  and  $t$ ); and as the double integration is equivalent it can be ignored, saving a not inconsiderable amount of time and tedium, we can directly derive

$$E = E(k) = -\alpha - \beta e^{ika} - \beta e^{-ika} = -\alpha - 2\beta \cos(k.a).$$

In this latest Hückel approximation:

- first, the term  $H_{ss} = -\alpha$  is identical to the term  $E'_0 = E_0 - \alpha$  of Part IV-2
- second, the term  $H_{st} = -\beta$  for  $s = t \pm 1$ , can be written as:

$$\begin{aligned} H_{st} &= \langle \psi_s | H | \psi_t \rangle = \left\langle \psi_s \left| -\frac{\hbar^2}{2m} \Delta + V(x) \right| \psi_t \right\rangle \\ &= \left\langle \psi_s \left| -\frac{\hbar^2}{2m} \Delta + U_0(x) + W(x) \right| \psi_t \right\rangle \\ &= E_0 \langle \psi_s | \psi_t \rangle + \langle \psi_s | W | \psi_t \rangle = \langle \psi_s | W | \psi_t \rangle. \end{aligned}$$

in which the initial value of  $-\beta$  is found, as proposed in Section IV-2.

### c Conditions for the appearance of allowed and forbidden bands

For a forbidden band to appear within a system (zone II of Figure I-12), at least two distinct band levels (zone I of Figure I-11), need to disintegrate. It is here that we realise that each atom in a chain presents two distinct orbitals,  $\psi$  and  $\varphi$ , such that  $E_0^\psi = \langle \psi | H | \psi \rangle$  and  $E_0^\varphi = \langle \varphi | H | \varphi \rangle$  (see Figure I-12). For crystals in which electrons from different states, type  $p$  or  $s$  for example, are made to interact, or for crystals made up of different types of atoms (see Section V-1 below), or even crystals which exhibit dissymmetry (see Section V-2 below), a band gap ( $E_G$ ) may appear.

As schematised in Zone II of Figure I-12, when atoms move closer, the degeneration of each level initially results in allowed bands which remain close to the original band level. As  $a$  becomes sufficiently small, and breakdown increases, the degenerate levels mix (shown at point M in Figure I-12) and a forbidden band results. This phenomenon will be detailed further in Chapter 2 using the example of carbon in 3-dimensions.

## V 1-D crystal and the distorted chain

### 1 AB type crystal

Taking a 1-D crystal formed of alternating A and B type atoms, separated by distance  $a$ , with a total of  $2n = N$  A or B atoms as described in Figure I-13, we can easily see that the repeat unit is  $2a$ .

For electrons on atoms A and B, with corresponding wavefunctions  $\varphi_A$  et  $\varphi_B$ , we shall call their respective energy levels  $E_A$  and  $E_B$ . This scenario can be equated in a manner similar to that shown in eqn (11), with the exception that here there are two equations, each specific to atom A or B. By using a linear combination of atomic orbitals, with  $N$  pairs of A and B atoms, the proper states can be determined using

$$|\psi_k\rangle = \sum_{j=1}^{N/2} (v_{kj}|\varphi_{Aj}\rangle + \eta_{kj}|\varphi_{Bj}\rangle),$$

and by following Floquet's theorem,  $v_{kj} = a_k \exp(ik2ja)$  and  $\eta_{kj} = b_k \exp(ik2ja)$ .

In going further with the hypothesis that there is a slight superposition of adjacent neighbouring orbitals,

$$\langle\varphi_{Ai}|\varphi_{Aj}\rangle = \delta_{ij} = \langle\varphi_{Bi}|\varphi_{Bj}\rangle \quad \text{and} \quad \langle\varphi_{Ai}|\varphi_{Bj}\rangle = 0$$

and we obtain a wavefunction for which normalisation can be performed using  $|a_k|^2 + |b_k|^2 = 1$ ):

$$|\psi_k\rangle = N^{-1/2} \sum_{j=1}^{N/2} \exp(ik2ja)[a_k|\varphi_{Aj}\rangle + b_k|\varphi_{Bj}\rangle].$$

The equation, in proper values, is  $H|\psi_k\rangle = E_k|\psi_k\rangle$ , with

$$H = -\frac{\hbar^2}{2m} \Delta + \sum_j V_{Aj} + \sum_j V_{Bj},$$

in which the potentials  $V_{Aj}$  and  $V_{Bj}$  are defined for a lone atom. Multiplication of the last equation by  $|\varphi_{Aj}\rangle$  and then by  $|\varphi_{Bj}\rangle$ , gives rise to two types of equations which can be made compatible by use of a second degree equation (see [Sap 90] for further details of this procedure). From these, we obtain two solutions for the energy,  $E^-$  and  $E^+$ , of which the difference  $\Delta E = E^+ - E^-$  corresponds to the forbidden band and the result is shown schematically in Figure I-14. When  $k = 0$ , the curve  $E^-$  corresponding to the lowest energy band represents the bonding orbital  $\Psi_L$ , while the highest energy band represents the anti-bonding orbital  $\Psi_A$  and is shown by curve  $E^+$ .

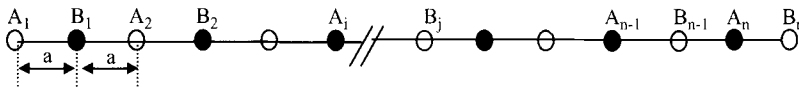


**Figure I-13.** Alternating chain of  $n$  pairs of A and B atoms, with  $n$  varying from 1 to  $N/2$ .

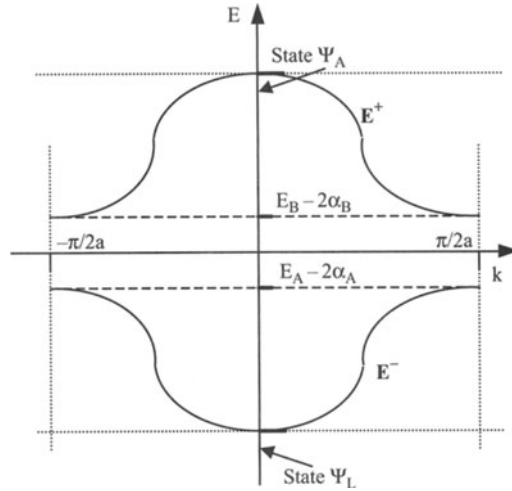


**Figure I-14.** Dispersion curve  $E = f(k)$  of diatomic system AB.

## 2 The distorted chain

### a Representation

In contrast to an alternating chain, in a distorted chain each atom (A) is  $u = \pm \frac{a_1}{2}$  apart, resulting in the distribution shown in Figure I-15.

While the repeat unit is  $2a$ , as A and A' are identical,  $E_A = E_{A'}$ . Figure I-16 details the bands obtained. For comparison, the dashed line describes  $E(k)$  for an undistorted chain with repeat unit length  $a$ , while the continuous line describes  $E(k)$  for the distorted chain with repeat unit length  $2a$ . The distortion provokes a gap  $E_G$  with  $k = \pm \pi/2a$ .

### b Conditions required for calculating a distorted chain

Only by considering the energies  $E_{\text{deform}}$  and  $E_{\text{relax}}$  can it be seen if a chain will undergo deformation. The former term is the energy necessary to produce a deformation between two atoms, and the latter the relaxation energy gained following the opening of a band gap.

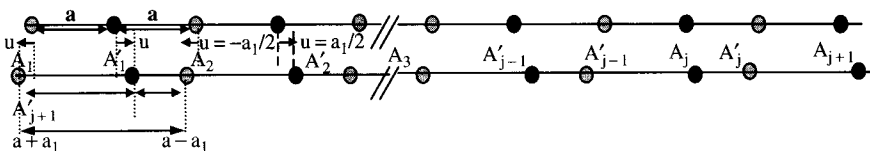


**Figure I-15.** Distorted chain of identical atoms A and A' separated by alternating short and long bonds.



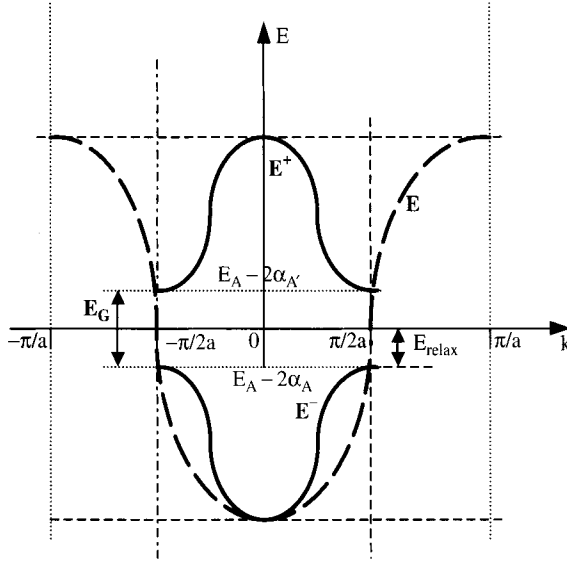


**Figure I-16.** Dispersion curves  $E = f(k)$  for a distorted crystal (continuous line) and undistorted (dashed line). In supposing:  $\langle \varphi_{A'_{j-1}} | H | \varphi_{A_j} \rangle = -\beta_1$  and  $\langle \varphi_{A_j} | H | \varphi_{A'_j} \rangle = -\beta_2$ , we obtain [Ben 91]:  $\Delta E_{(k=\pi/2a)} = E_G = 2(\beta_1 - \beta_2)$ . In addition, supposing that  $\beta_1$  and  $\beta_2$  are of the form  $-\beta_1 = -\beta + \alpha u$  and  $-\beta_2 = -\beta - \alpha u$  (with  $\alpha > 0$  [Caz 96]), we finally obtain  $E_g \approx 4\alpha |u|$ .

- $E_{\text{defor}}$  - this is the energy due to changing from a structure with regular spacing ( $a$ ) to a structure with repetition unit of  $2a$ , consisting of alternating long ( $a + a_1$ ) and short links ( $a - a_1$ ).  $E_{\text{defor}}$  can be described by  $E_{\text{defor}} = \frac{1}{2} N k_e |2u|^2 = 2k_e N u^2$ , in which  $N$  is the number of atoms of type  $A$  or  $A'$  and  $|2u|$  is the stretching or contraction modulus of the 'spring' which mechanically joins two atoms together. In addition, we can note that for two atoms harmonically coupled by an elastic force  $f_e$  of constant  $k_e$ ,  $f_e = -k_e(2u)$ ; if  $2u > 0$ ,  $f_e < 0$  and is therefore an attractive force.
- $E_{\text{relax}}$  corresponds to the reduction in the electronic energy of a system going from the filled energy band of a system with period  $a$  (of energy  $E$ ) to that with period  $2a$  (denoted  $E^-$ ). Figure I-16 shows the approximate value of  $E_{\text{relax}}$ , corresponding to the reduction in energy of the most energetic electrons which are susceptible to participating in conduction bands. Section VI-3 details a more rigorous determination of  $E_{\text{relax}}$ .

If  $\Delta E = E_{\text{defor}} - E_{\text{relax}} < 0$ , i.e. the energy gained by relaxation is greater than that required for deformation, there is a reduction in energy and the system is stable when the value of deformation,  $u_0$ , is such that  $\left[ \frac{\partial(\Delta E)}{\partial u} \right]_{u=u_0} = 0$ . Following dimerisation, or rather the generation of alternating bond lengths, a gap is formed with  $= \pm\pi/2a$  which is termed the Peierls metal-insulator transition.

## VI Density function and its application, the metal insulator transition and calculation of $E_{\text{relax}}$

### 1 State density functions

The density function of each state can be calculated with respect to the dimension of energy, or the dimension of the space reciprocal ( $k$ ).

#### a Definition of state density functions

The state density function within energy space, denoted as  $Z(E)$ , is such that  $Z(E) dE$  represents the number of electronic states within a unit volume, each described by a wavefunction and having energy between  $E$  and  $E + dE$ . For a 1-D system,  $L = 1$ . In the same manner, when considering a unit volume defined by  $k$ , the state density function is described by  $n(k)$  such that  $n(k) dk$  represents the number of electronic states for which the vector  $\vec{k}$  is between  $\vec{k}$  and  $\vec{k} + d\vec{k}$ . The corresponding Figure I-17 shows that  $k$ , which can be negative or positive (privileged solutions for wavefunctions may equally propagate in negative or positive values of  $k$ ), in 1-D, should give:

$$Z(E) dE = 2n(k) dk$$

By way of explication, in terms of space energy the interval  $dE$  corresponds, in  $k$  space, to an interval of  $2 \cdot dk$  which is situated between  $\vec{k}$  and  $\vec{k} + d\vec{k}$ . This correspondence can be seen more clearly though using Figure I-17-b by reducing the 2D model to the 1D model; once the  $k_x$  axis is considered only, we can see that there are two intervals  $dk$  (dotted line with  $k_x$ ).

#### b Determining state density functions

In evaluating  $n(k)$  we note that in reciprocal space, electrons are divided between cells of size  $\Delta k = \frac{2\pi}{L}$  which corresponds to the quantification of space in  $k$  obtained

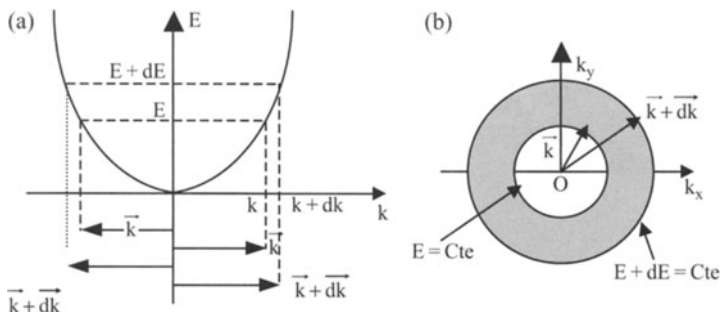


**Figure I-17.** Relationship between energy space  $E$  and space  $k$  with  $E = \hbar^2 k^2 / 2m$ : (a) 1D; and (b) 2D.

from the periodic limit condition (PLC), or Born-Von Karman condition, which is such that for a network of length  $L = Na$ ,  $\psi_k(x) = \psi_k(x + L)$ . With

$$\left. \begin{aligned} \psi_k(x) &= e^{ikx}u(x) \\ &= \psi_k(x + L) \\ &= e^{ik(x+L)}u(x + L) \end{aligned} \right\} \begin{aligned} &\text{as } u(x) = u(x + a) = u(x + 2a) = \dots u(x + L), \\ &\Rightarrow e^{ikL} = 1, \text{ or } kL = 2\pi n, \text{ with whole values of } n. \end{aligned}$$

The difference between two consecutive values of  $k$  obtained for  $\Delta n = 1$  is thus  $\Delta k = \frac{2\pi}{L}$  as detailed in Figure I-18-a. This interval corresponds, on average, to the electronic function  $\psi_k(x)$ , in other terms an actual state. We should note, however, that there are two functions corresponding to two values of  $k$  taken at the extremities of the interval, but each of these functions is shared with this adjacent interval, giving on average one function per  $\Delta k$ . Interestingly enough though, on taking electron spin into account, which allows two functions  $\psi_k^+(x)$  and  $\psi_k^-(x)$  for the same state  $k$ , over an interval  $\Delta k$ , we can place two electronic states, i.e.:  $n(k) \cdot \Delta k = n(k) \cdot (\frac{2\pi}{L})_{L=1} = 2, \Rightarrow n(k) = \frac{1}{\pi}$ ; (for  $L \neq 1$ , the number of orbitals is  $N(k) = L \cdot n(k) = \frac{L}{\pi}$ ).

From  $Z(E) dE = 2n(k) dk$ , we can deduce that  $Z(E) = \frac{2}{\pi} \frac{1}{\frac{dE}{dk}}$ .

When considering a linear chain of  $N$  atoms, we can use eqn (22) of Section IV:

$$E = E_0 - \alpha - 2\beta \cos ka, \text{ or } \frac{dE}{dk} = 2\beta a \sin ka, \text{ in which: } Z(E) = \frac{1}{\pi\beta a} \frac{1}{\sin ka}.$$

With

$$\sin^2(ka) = 1 - \cos^2(ka) = 1 - \left( \frac{E - E_0 + \alpha}{2\beta} \right)^2,$$

we obtain:

$$Z(E) = \frac{1}{\pi\beta a} \times \frac{1}{\sqrt{1 - \left( \frac{E + \alpha - E_0}{2\beta} \right)^2}}.$$

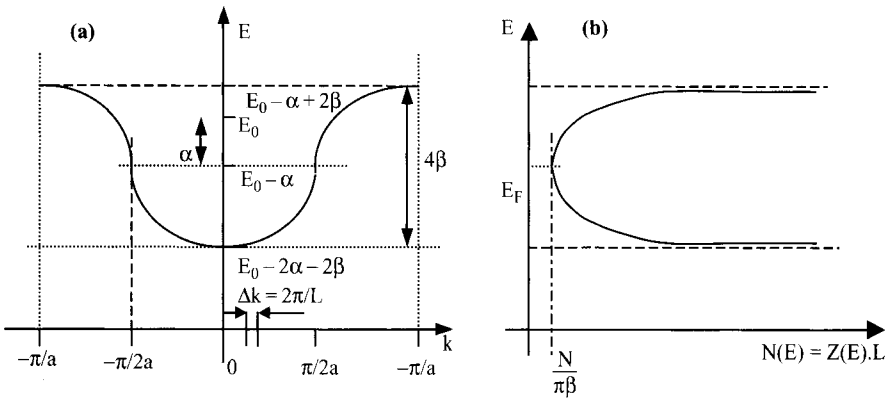


**Figure I-18.** (a) Dispersion curve  $E = f(k)$ ; and (b) density curve of states for a chain of  $N$  atoms.

For a complete chain, or length  $L = Na$ , the number of orbitals is defined by

$$N(E) = LZ(E) = NaZ(E) = \frac{N}{\pi\beta} \times \frac{1}{\sqrt{1 - \left(\frac{E + \alpha - E_0}{2\beta}\right)^2}}$$

$$= \frac{2N}{\pi} \frac{1}{\sqrt{(2\beta)^2 - (E + \alpha - E_0)^2}};$$

a graphical representation is shown in Figure I-18.

## 2 Filling up zones and the Peierls insulator-metal transition

### a Filling up an undistorted zone

For an undistorted chain of  $N$  atoms of length  $L = Na$  and  $N$  electrons in a single quantum orbital, the number of unit cells of dimension  $2\pi/L = 2\pi/Na$  that we can fit into a Brillouin zone, of size  $2\pi/a$ , is  $\frac{2\pi/a}{2\pi/Na} = N$  (situated between  $k = -\pi/a$  and  $k = \pi/a$ ). However, on taking spin into account, 2 electrons can be placed into each cell and therefore, over the whole zone or chain we can place  $2N$  electrons. As the system liberates only  $N$  electrons, the zone shown by the dashed line in Figure I-16 is half full and electrons there can move easily: the system is metallic in nature.

### b The insulator—metal transition

When distortion is energetically favoured, as detailed by the curve  $E = f(k)$  in Figure I-16 which corresponds to a distorted crystal, the zone has the dimension  $\pi/a$  (as it cannot go beyond  $k = -\pi/2a$  and  $k = \pi/2a$ ). For the distributed  $N$  electrons there are only  $N/2$  cells available. In other words, the zone has been completely filled, and because there are no free places electrons cannot move about, as detailed by the interior of the curve  $E^- = f(k)$  in Figure I-16. This change of state, from metallic to insulator, is known as the Peierls transition.

### c Fermi level wave vector and the position of $E_F$

If each atom liberates a single electron into a particular state on a chain of  $N$  atoms separated by period  $a$ , we can determine the wave vector  $k_f$  at absolute zero for electrons at the highest energy level, otherwise called the Fermi level, which divides filled from empty states.

At absolute zero, the Fermi-Dirac splitting function  $F(E) = 1$  while  $E < E_F$  (and  $F(E) = 0$  while  $E > E_F$ ) and the number of electrons ( $N$ ) for a chain of atoms of a certain length ( $L$ ) can be calculated by utilising the functions of orbital density  $Z(E)$

or  $n(k)$  which are such that:

$$\begin{aligned} N &= \int_{E_{\min}}^{+\infty} F(E)N(E) dE = \int_{E_{\min}}^{E_F} N(E) dE = \int_{E_{\min}}^{E_F} L.Z(E) dE \\ N &= \int_{-\infty}^{+\infty} N(k)F(k) dk = \int_{-k_F}^{+k_F} N(k) dk = \int_{-k_F}^{+k_F} L.n(k).dk \\ &= \int_{-k_F}^{+k_F} Na. \frac{1}{\pi} dk = \frac{Na}{\pi} .(2k_F), \text{ in which } k_F = \frac{\pi}{2a}. \end{aligned}$$

Figure I-18-a shows that, for the undistorted chain, the energy  $E_F$ , for  $k_F = \frac{\pi}{2a}$  is such that  $E_F = E_0 - \alpha$ . For a distorted chain, in which there are always  $N$  electrons freed by  $N$  atoms,  $k_F = \frac{\pi}{2a}$  is retained; the Fermi level and midway between occupied and empty levels at 0 K is thus situated in the middle of the gap  $E_G$ , as shown in Figure I-16.

### 3 Principle of the calculation of $E_{\text{relax}}$ for a distorted chain

In Section V-2-b, it was shown how  $E_{\text{relax}}$  corresponded to the difference in energy of  $N$  electrons on to an undistorted chain ( $E_{\text{nd}}$ ) and the energy of the same electrons on a distorted chain ( $E_d$ ) i.e.  $E_{\text{relax}} = E_{\text{nd}} - E_d$ .

Figure I-16 shows the approximate estimation of  $E_{\text{relax}}$  determined by realising that:

- the undistorted chain, as described by the dashed curve  $E = f(k)$  in Figure I-16, electrons participating in conduction are the most energetic and are within  $E_F$  for  $k = k_F = \frac{\pi}{2a}$  situated at the intersection of the energy and  $O k$  axes; and
- for the distorted chain, the zone between  $-\frac{\pi}{2a}$  and  $\frac{\pi}{2a}$  is only just full so that the most energetic electrons, which participate in conduction, are at the highest point of the band indicated by  $E^-$ , otherwise written  $E_A - 2\alpha_A$ .

$E_{\text{relax}}$  as shown in Figure I-16 therefore shows the difference in energy of conducting electrons in undistorted and deformed chains. In going further, a more rigorous estimation than  $E_{\text{relax}} = E_{\text{nd}} - E_d$  can be made using electrons in both calculations (of  $E_{\text{nd}}$  and  $E_d$ ) which fill cells between  $-k_F$  and  $+k_F$  in  $k$  space. Thus:

$$E_{\text{nd}} = \int_{-k_F}^{+k_F} E(k)N(k)dk = \int_{-\pi/2a}^{+\pi/2a} E(k) \frac{L}{\pi} dk,$$

with  $E(k) = E_0 - \alpha - 2\beta \cos ka$  ( $E(k)$  for undistorted chain).

Again, the energy  $E_d$  of a distorted system is given by  $E_d = \int_{-\pi/2a}^{+\pi/2a} E^-(k) \frac{L}{\pi} dk$ , in which  $E^-(k)$  is the energy function of a distorted system, as traced in Figure I-16. More detailed calculations can be found elsewhere [pei 55].

## VII Practical example: calculation of wavefunction energy levels, orbital density function and band filling for a regular chain of atoms

Here the example is of a chain in 1-D (along  $x$ ) consisting of  $N$  atoms regularly spaced by distance  $a$  and of length  $L$ , such that  $L = Na$ . Specifically, we will be looking at a closed or cyclic chain which has  $N = 8$  (Figure I-19).

### 1 Limits of variation in $k$

The domain in which  $k$  can vary can be obtained by periodic limit conditions (PLC), otherwise known as the Born-Von Karmen conditions. These conditions indicate that for a cyclic chain the probability of finding an electron at a co-ordinate point  $x$  is unique and does not depend on the number of times the electron has gone around the chain. This can be expressed as  $\psi(x) = \psi(x + L)$ . Given that the chain is periodic, the wavefunction can be written as a Bloch function in the form  $\psi_k(x) = e^{ikx}u(x)$  with  $u(x)$  such that  $u(x) = u(x + L)$ . The PLCs applied to the Bloch function brings us, as shown in Part V I-1-b, to  $e^{ikL} = 1$ . As  $1 = e^{i2p\pi}$  and  $L = Na$ , we now have:  $k = k_p = 2\pi \frac{p}{Na}$  (with  $p$  equal to zero or a positive or negative integers:  $p = 0, \pm 1, \pm 2, \pm 3, \dots$ ). Note that by using eqn (22),  $E = E_0 - \alpha - 2\beta \cos ka = E_0 - \alpha - 2\beta \cos k_p a$ .

The representation can be restricted to a single period as the curve  $E(k)$  is periodic. Identical solutions for energy would result from other periods. We obtain the so-called reduced zones for  $E$  ( $k$  has period such that  $-\pi < ka < \pi$ ; with  $k = k_p$ ,  $-\frac{\pi}{a} \leq k_p \leq \frac{\pi}{a}$  (a reduction of Brillouin's first zone). As  $k_p = 2\pi \frac{p}{Na}$ ,  $-\frac{N}{2} \leq p \leq \frac{N}{2}$  as  $N$  takes on successive integer values.

### 2 Representation of energy and the orbital density function using $N = 8$

We have just seen that the limits in variation of  $k_p = 2\pi \frac{p}{Na}$  can be reduced to  $-\frac{\pi}{a} \leq k_p \leq \frac{\pi}{a}$ .

As  $N = 8$  and  $k_p = \frac{\pi}{4a}p$ , the successive values of  $k_p$  (with  $-\frac{N}{2} \leq p \leq \frac{N}{2}$ , or  $p \in [-4, -3, \dots, 0, \dots, 3, 4]$ ) are thus:

$$k_p = -\frac{\pi}{a}, -\frac{3\pi}{4a}, -\frac{\pi}{2a}, -\frac{\pi}{4a}, 0, \frac{\pi}{4a}, \frac{\pi}{2a}, \frac{3\pi}{4a}, \frac{\pi}{a}.$$

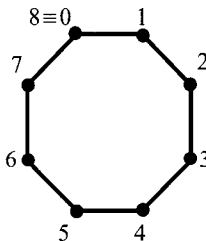
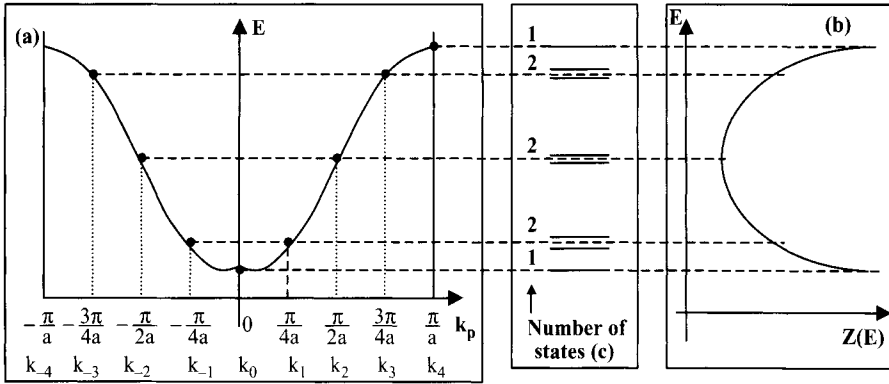


Figure I-19. Representation of a cyclic chain with  $N = 8$ .



**Figure I-20.** Representation for  $N = 8$  of: (a)  $E = f(k_p)$ ; (b)  $Z(E)$ ; and (c) number of states.

The expression for energy from eqn (22) is now  $E = E_0 - \alpha - 2\beta \cos k_p a = E_0 - \alpha - 2\beta \cos \frac{\pi}{4} p$ .

$E = f(k_p)$  and  $Z(E) = g(E)$  are represented in Figures I-20-a and I-20-b.

Only one of the shared and adjacent states in  $k_{-4} = -\frac{\pi}{a}$  and  $k_4 = \frac{\pi}{a}$  needs to be compatibilised. It is also important to note that, in contrast to the middle bands ( $k_{-2}$  and  $k_2$ ), the highest ( $k_{-3}, k_3, k_4$ ) and the lowest ( $k_{-1}, k_1, k_0$ ) bands are well ‘packed’ due to the cosine form of the energy curve—flattened at top and bottom and near-vertical around the ‘waist’—from which they are derived. With increasing  $N$ , the phenomenon becomes ever more exaggerated, to the extent that Figure I-20 would become overly complex; with an increasing value of  $N$ , and therefore also  $k_p$ , the resulting energy levels would be very tight in both the highest and lowest part of the band. This qualitatively explains the form of  $Z(E)$ . In addition, the peak limit can be drawn for this function from the point at which the curve  $E = f(k)$  reaches a tangential horizontal. As Figure I-20-b shows, the orbital density is highest at the extremes and least dense in the middle of the band. Thankfully, while with increasing  $N$  the diagrams and functions become more and more complicated, the system shown here is a sufficiently simple example!

### 3 Wavefunction forms for bonding and antibonding states

With  $k = k_p$  and  $N = 8$ , the wavefunction of eqn (10) can be written:

$$\psi_{k_p}(x) = c_0 \sum_{t=0}^8 \exp(ik_p t a) \psi_0(x - ta), \text{ with } c_0 = 1/\sqrt{N} \text{ following normalisation.}$$

We can look at a representation of the function  $\psi_0(x - ta) = \psi_t(x)$  for  $s$  states (in which the wavefunctions  $\varphi_s$  have quantum number  $l = 0$ , such that  $\psi_0(x - ta) = \psi_t(x)$  can be written as  $\psi_t(x) = \varphi_{st}(x)$  given that  $\varphi_{st} = AR_{n,l=0}(x) = Ce^{-\alpha x}$ ; cf. Section I of Appendix A-1).

Comment: in eqn (10) we could have summed over index  $t$ , which counts the number of atoms in a chain, in place of  $s$  which is reserved for type  $\varphi_s$  orbitals *i.e.* for

the state  $s$  characterised by  $1 = 0$ . Also,  $t = 0 \equiv 8$  as these two values of  $t$  represent ring closure, as detailed in Figure I-19.

**a Atoms without interaction (for  $N = 8$ ).**

By way of introduction, Figure I-21 shows the general form of the wavefunction relative to the  $s$  states of a chain of 8 non-interacting atoms.

**b Representation of the function  $\psi_{k_p}$  (with  $N = 8$ ) for low (bonding) and high (antibonding) bands**

*$\alpha$ -Low band states:*  $p = 0$

When  $p = 0$ ,  $k_p = 0$  and  $\exp(i k_p t a) = 1$ , whatever value taken by  $t$ , we have (to the order of coefficient  $c_0$ ):

$$\psi_{k_0} = \varphi_{s1} + \varphi_{s2} + \varphi_{s3} + \varphi_{s4} + \varphi_{s5} + \varphi_{s6} + \varphi_{s7} + \varphi_{s8=0}$$

A representation is shown in Figure I-22.

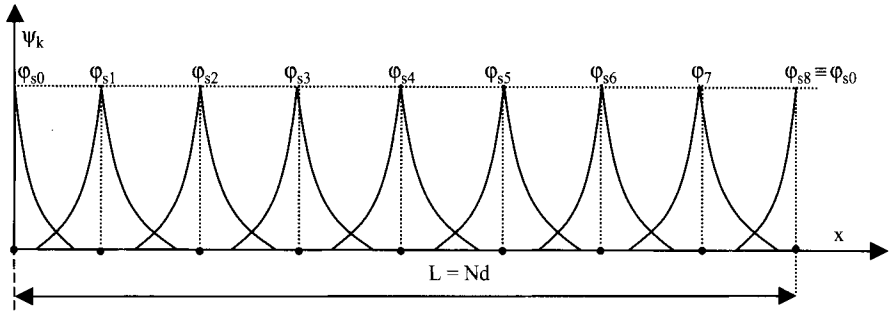


**Figure I-21.** Wavefunction of the  $s$  state for a chain of non-interacting atoms ( $N = 8$ ).

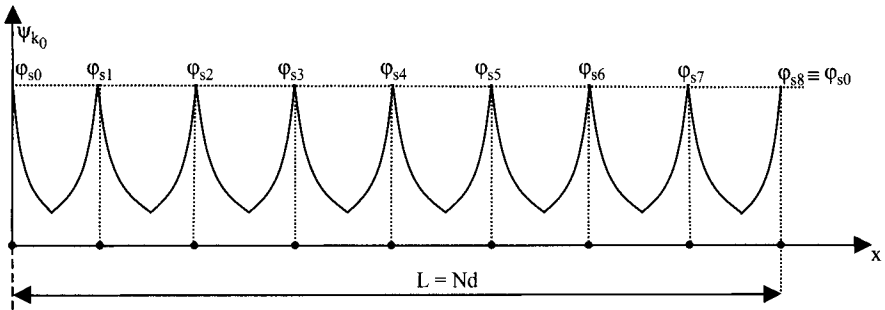


**Figure I-22.** Representation of  $\psi_{k_0}$ .



$\beta$ -High band states:  $p = 4$ .

As  $k_4 = \frac{\pi}{a}$ , successive values of  $t$  through  $k_4ta = \pi t$  and  $\exp(j\pi t) = \cos(\pi t)$  are given in the table below:

$t$	$0 \equiv 8$	1	2	3	4	5	6	7
$k_4ta = \pi t$	$0 \equiv 4\pi$	$\pi$	$2\pi$	$3\pi$	$4\pi$	$5\pi$	$6\pi$	$7\pi$
$\cos(\pi t)$	1	-1	1	-1	1	-1	1	-1

Also  $\lambda_4 = \frac{2\pi}{k_4} = 2a$  and the representation of  $\psi_{k_4}$  are presented in Figure I-23.

**c Bonding and anti-bonding states**

All atoms are in phase and all coefficients  $\exp(i k_0ta)$  are equal to 1 for the lowest band states, as shown in Figure I-22. The resulting wavefunction  $\Psi_{k_0}$  exhibits no nodes as the probable electron density is the same between all atoms, explaining why this state gives rise to the strongest bonding. As energy increases,  $k_p$  increases and the number of nodes in the wavefunction also increase. This can be seen in Figure 2 in Appendix A-2, in which the real part of the wavefunction  $\psi_{k_1}$  corresponding to  $k_1$  is shown. In the middle of the band, at which  $k_2 = \frac{\pi}{2a}$ , the states are neither bonding nor anti-bonding. This is shown in detail in Appendix A-2, Figure 3 for the real part of  $\psi_{k_2}$ . However, for the highest level states, at the highest part of the band ( $k_4 = \frac{\pi}{a}$  and  $k_4a = \pi$ ), successive values of  $\exp(j\pi t) = \cos(\pi t)$  alternate between  $-1$  and  $1$  creating nodes midway between atoms (Figure I-23). At these points the probability of electron presence is zero as they are distributed in an anti-bonding combination giving rise to an anti-bonding bond.

As shown in Figure I-24, the bonding states ( $\Psi_{k_0}, \Psi_{k_1}, \Psi_{k_{-1}}$ ) are lower in energy and more stable than the anti-bonding states ( $\Psi_{k_4}, \Psi_{k_3}, \Psi_{k_{-3}}$ ). However, the energy levels corresponding to  $\Psi_{k_p}$  and  $\Psi_{k_{-p}}$  are identical (as  $k_p = -k_{-p}$ , we have  $\cos k_p a = \cos[k_{-p}a]$ , as  $E_{k_p} = E_{k_{-p}}$ ); these two functions are indeed associated in both senses of wave propagation due to the chain of atoms being a closed

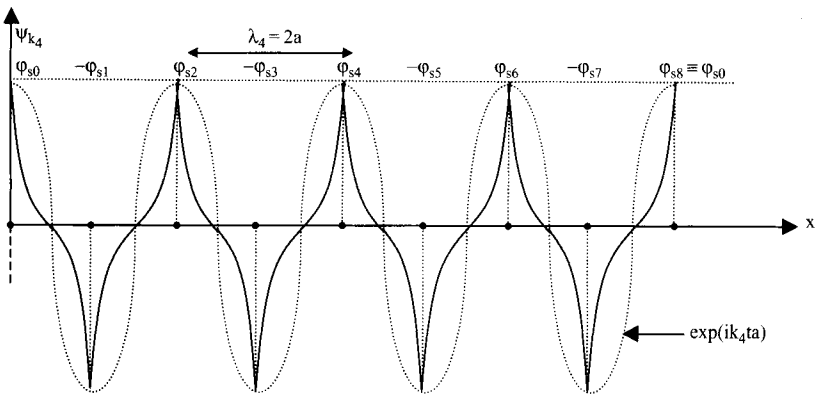
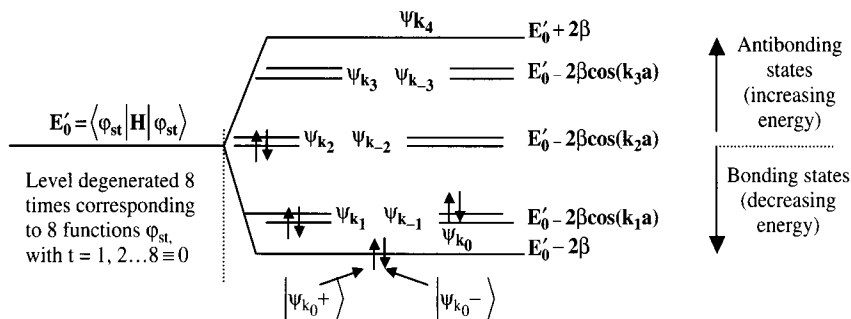


Figure I-23. Representation of  $\psi_{k_4}$ .



**Figure I-24.** Levels and states of energy for a chain of 8 atoms.

ring. Just as for a free electron, we can make an appeal to physical solutions using cosines ( $\text{Re}\{\exp[ik_p a]\}$ )—shown in Figures 2 and 3 of Appendix A-2—and using sine ( $\text{Im}\{\exp[ik_p a]\}$ ). These two types of solutions can be derived by using linear combinations (respectively, addition and subtraction) of  $\Psi_{k_p}$  and  $\Psi_{k_{-p}}$ .

If, unlike in this example, the chain is not cyclic, then solutions of the form  $\sin(\frac{p\pi}{N+1})$  can be obtained and used as coefficients for developing linear combinations of atomic orbitals (see, for example p. 41 of reference [Sut 93]). And indeed, we can see in this example that the interaction of neighbouring atoms results in an increased degeneration, giving 8 levels, each associated with a function of  $\Psi_{k_p}$ . The degeneration is only partial as the two functions  $\Psi_{k_p}$  and  $\Psi_{k_{-p}}$  correspond to the same energy level. It is worth realising though that each function of  $\Psi_{k_p}$  gives rise to two additional functions,  $\Psi_{k_p^+}$  and  $\Psi_{k_p^-}$ . If each atom contributes only one electron to a bond, and for  $N$  atoms there are  $N$  electrons, then for our 8 atoms there are 8 electrons contributed which are spread throughout the available energy levels. And it is for this reason that only the 8 lowest states permitted are occupied, as shown in Figure I-24. As the permitted band is only half-full, a conducting state is obtained if the span between the highest bonding level and the lowest anti-bonding level is small (i.e.  $N$  is large). As we have seen, following Peierls transition, transitions from metallic to insulating states can occur.

#### 4 Generalisation regarding atomic chain states

In this Section VII, we have taken as example the  $s$  states, envisaging that they alone interact in a chain of atoms. In fact, the results we have obtained here can be extended to other states (most notably  $p$  states). Further details on the more common systems are shown in Appendix A-2.

### VIII Conclusion

The energy levels in a periodic network are determined by the extent to which the orbitals overlap, which is in turn controlled by the lattice constant  $a$ , on which the potential due to atoms is dependent, and the radius ( $R$ ) of the outer atomic orbitals.

When orbitals overlap sufficiently, such that they lose their individual identities (weak bonds with  $a < 2R$ ), the semi-free model of electrons is particularly appropriate. To a zero order approximation, which assumes that the electron cloud is delocalised throughout a network, solutions for the wavefunction of form  $\psi = A e^{\pm ikx}$  are obtained, the  $\pm$  appearing because of degeneration caused by the electronic wave being directed in one sense or the other. Alternatively, solutions of the form  $\psi_c = \cos(kx)$  or  $\psi_s = \sin(kx)$ , obtained from linear combination of the two exponential solutions, can be used.

For an electronic wave with a large wavelength, or in other terms  $k = 2\pi/\lambda$  is low, electrons are only weakly effected by the potential ( $V$ ) generated by a chain of nuclei. In Figure I-25 we can see that changes in  $V$  provoke negligible change in the evolution of the wavefunctions which have energy closely approximating to that of a free electron ( $E = \hbar^2 k^2 / 2m$ ) and the probabilities of electron presence can, at the very limit ( $\lambda \rightarrow \infty$ ), be considered a constant throughout the network (i.e. density  $\rho = \text{constant}$  in Figure I-5). However, when  $\lambda$  is small,  $k$  comes close to the values expressed by  $k = \pm\pi/a$  and the functions  $\psi_c$  and  $\psi_s$  tend towards functions  $\psi^+$  and  $\psi^-$  (Section II-2), which exhibit an evolution closely following changes in  $V$  and the probable electron presence becomes centred between or on atoms (Figure I-5). The two functions are very different, as indicated by the resulting presence probabilities, and correspond to two different energy levels which are separated by a "band gap" of energy  $\Delta E = E_G$  (see Figure I-6).

A more 'chemical' representation can be given for strong bonds which are constructed from linear combination of atomic orbitals (LCAO), however, the space between the atoms remains important, in that each component orbital has an individual identity resulting from local variations in the periodic potential. If combining orbitals are all of one type, the resulting energy develops in the form of a permitted band of height  $4\beta$  where  $\beta$  represents the coupling between adjacent atoms.

If only s orbitals are considered, the lowest band states correspond to bonds formed of bonding atomic orbitals, while the highest to anti-bonding orbitals (see Figure I-26 in which there is one s electron per atom). The resulting amplitude of the wavefunction is modulated by the exponential term  $\exp(ik_p ta)$ ; when  $p = 0$ , the wavelength tends towards infinity (and therefore there are no nodal points within the bonding state).

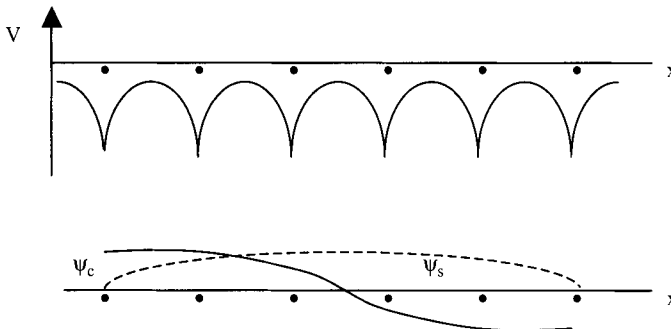
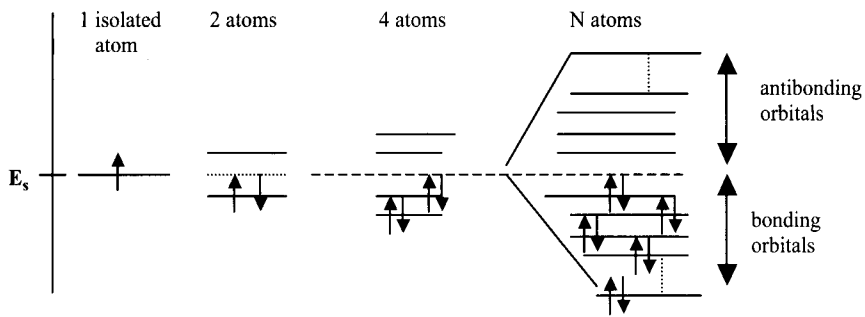


Figure I-25. Wave functions  $\psi_c$  and  $\psi_s$  for large  $\lambda$ .



**Figure I-26.** Energy levels, without a band gap, formed by  $s$  electrons given by atoms in a chain.

However, when  $k = \pi/a$ , we have  $\lambda = 2a$  and the atomic orbitals of two adjacent atoms are of opposite phase and the nodal points between them exhibit antibonding behaviour. This can be compared with Appendix A-2 (Parts I and II, respectively) in which the characteristic behaviour of  $\sigma$ - $s$  bonds and  $\pi$ - $p$  bonds are discussed.

For  $N$  atoms,  $N$  levels are realised, including  $N/2$  bonding levels. As 2 electrons can be placed into each level (taking spin into account), the  $N$  electrons will fill the  $N/2$  bonding levels,  $s$  electrons going into  $\sigma$  orbitals and  $p$  electrons going into  $\pi$  orbitals, leaving the  $N/2$  anti-bonding levels empty. Can we also reiterate that for a given band, of size  $4\beta$ , the higher the value of  $N$ , the more closely packed will be the resulting levels.

We will see that the 1-D model we have treated in this chapter can be extended to 3-dimensions in which the size and height of permitted bands are related to the co-ordination number, or rather number of bonds, of a given atom.

We can also see that, as shown in Figure I-16, if bonds between atoms in a 1-D chain are alternating, then a central band gap is formed. Elsewhere, when different types of states are involved, a gap in the energy can occur due to the difference in energies of those orbitals, as shown in Figure I-12. Moreover, when different orbitals—for example  $s$  and  $p$  type—mix, bonding and anti-bonding orbitals are formed, and the difference in energy bands corresponds to the energy of the formed band gap. We will look at this problem in 3-D, including the formation of hybrid orbitals—for example  $sp^3$ —in Chapter 2.

## II

---

# Electron and band structure in regular or disordered 3-dimensional environments: localised and delocalised states

## I Introduction

Calculations based on 3-D environments, using weak bonding approximations, follow much the same line as the studies made in 1-D. The dispersion curve  $E = f(k)$  can be traced depending on the different directions under consideration ( $k_x$ ,  $k_y$  and  $k_z$  for a cubic crystal). If these directions are not equivalent, and have a forbidden energy for which the value is direction dependent, then the resulting energy gap in the material is of the form.

$E_G = (E_C)_{\min} - (E_V)_{\max}$  in which  $(E_C)_{\min}$  corresponds to the minimum conduction band (CB) for all directions  $\vec{k}$  considered, and  $(E_V)_{\max}$  corresponds to the maximum valence band (VB) over all directions.

This approximation for the weak bond is, in fact, only applicable to metals. In this Chapter, we shall look at the electronic bands found within 3-D organic solids and see that their intrinsic semiconducting or insulating character can only be realised by considering strong bonding. We shall also consider 3-D regularly networked solids, considering each node an atom which contributes to the electronic properties of the material, *via*:

- (i) a single, s-state electron, and using as example the cubic network to determine the height of the permitted band, otherwise known as the VB.
- (ii) hybridised electrons using the specific example of diamond, in which each carbon atom is at the centre of a tetrahedron and has  $sp^3$  hybridised bonding states (as detailed in Appendix A-1, Section II-2); the generation of the band structure and the forbidden band, which separates bands corresponding to bonding and anti-bonding states, will be described.

Finally, we will look at amorphous materials.

## II Going from 1-D to 3-D: band structure of networked atoms with single, participating s-orbitals (including simple cubic and face centred systems)

### 1 3-D General expression of permitted energy

To simplify eqn (22) in Chapter I, which relates the energy of a strongly bonded electron in 1-D, we can rewrite it as

$$E = E_0 - \alpha - \beta \sum_{t=-1,+1} e^{-ikt a} \quad (1)$$

The sum is for one atom and its two closest neighbours. On considering more than one dimension though, a simple way of writing eqn (1) is

$$E = E_0 - \alpha - \beta \sum_m e^{-i\vec{k}\vec{a}_m}, \quad (2)$$

in which  $\vec{a}_m$  represents the vectors joining the reference atom with its  $m$  closest neighbours. In the case of a cubic lattice, as shown in Figure II-1, the closest neighbouring atoms have vector  $\vec{a}_m$  components:

$$\begin{cases} (\pm a, 0, 0) & \text{in the x axis} \\ (0, \pm a, 0) & \text{in the y axis} \\ (0, 0, \pm a) & \text{in the z axis} \end{cases}$$

The energy thus takes the form  $E = E_0 - \alpha - 2\beta[\cos k_x a + \cos k_y a + \cos k_z a]$ , in which  $k_x, k_y, k_z$  are the components of  $\vec{k}$  in the 3 directions  $Ox, Oy, Oz$ .

In the centre of the zone,  $k = k_0 = 0$  (or  $k_x = k_y = k_z = 0$ ); the energy is minimal and equal to:

$$E = E_0 - \alpha - 6\beta = E(k_0) \quad (3)$$

In the neighbourhood of the central zone,  $k \approx k_0 \approx 0$ , or  $k_x \approx k_y \approx k_z \approx 0$ ,  $\cos k_x a \approx 1 - \frac{(k_x a)^2}{2}$  (ditto for  $k_y$  and  $k_z$ ), and the energy can thus be written as

$$\begin{aligned} E &= E_0 - \alpha - 6\beta + \beta a^2 (k_x^2 + k_y^2 + k_z^2) \\ &= E(k_0) + \beta k^2 a^2. \end{aligned} \quad (4)$$

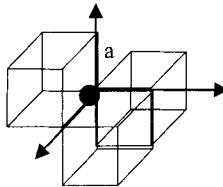


Figure II-1. Geometry of cubic lattice structure.

We can now compare eqn (4) with that obtained by a Mac Laurin development of E using  $k_0$ :

$$E_{(k)} = E_{(k_0)} + (k - k_0) \left( \frac{\partial E}{\partial k} \right)_{k_0} + \frac{(k - k_0)^2}{2} \left( \frac{\partial^2 E}{\partial k^2} \right)_{k_0}. \quad (5)$$

As in the centre of the zone, we now have a tangential horizontal (to be compared with Figure I-10),  $\left( \frac{\partial E}{\partial k} \right)_{k_0} = 0$  and the mass can be effectively defined by

$$m^* = \frac{\hbar^2}{\left( \frac{\partial^2 E}{\partial k^2} \right)_{k_0}}, \quad (6)$$

so that we can obtain from eqn (5), when  $k \approx k_0 = 0$ :

$$E_{(k)} = E_{(k_0)} + \frac{\hbar^2}{2m^*} (k - k_0)^2. \quad (7)$$

Again, in the neighbourhood of the central zone, where  $k_0 \approx 0$ , we now have

$$E_{(k)} = E_{(k_0)} + \frac{\hbar^2}{2m^*} k^2. \quad (7')$$

*Comment:* The mass  $m$  of an electron can be related in the fundamental dynamic equation  $F_T = q(E_{\text{appl}} + E_{\text{int}}) = m\gamma$  with  $E_{\text{appl}}$  which is the empirically applied field and  $\gamma$  is the acceleration undertaken by the electron. The internal field ( $E_{\text{int}}$ ) which is derived from the internal potential generated by the nucleus is not well known and the effective mass  $m^*$  is defined by the relationship  $F_{\text{ext}} = qE_{\text{appl}} = m^*\gamma$ . Eqn (6) is obtained by calculating the work of the external force (see Appendix A-2, Section IV-2).

## 2 Expressions for effective mass, band size and mobility

The identification of coefficients  $k^n$  ( $n = 0$  and  $n = 2$ ) of eqns (4) and (7) yields:

$$\begin{cases} E_{(k_0)} = E_0 - \alpha - 6\beta \\ \beta a^2 = \frac{\hbar^2}{2m^*}, \quad \text{or} \quad m^* = \frac{\hbar}{2\beta a^2}. \end{cases} \quad (8)$$

The size of the band can be deduced from the amplitude of the variation in energy in the first Brillouin zone (described, for 1-D, as the variation in  $k$  zone in Figure I-10):

- when  $k_x = k_y = k_z = 0$ :  $E = E(k_0) = E_0 - \alpha - 6\beta$ ; and
- when  $k_x = k_y = k_z = \frac{\pi}{a}$ :  $E = E\left(\frac{\pi}{a}\right) = E_0 - \alpha + 6\beta$ .

The amplitude in the variation ( $4\beta$  in 1-D) of  $E$ , which is the depth of the permitted band, changes in 3-D to

$$\Delta E = E\left(\frac{\pi}{a}\right) - E(k_0) = B = 12\beta \quad (9)$$

The result given for a simple cubic network can be generalised by introducing a co-ordination number  $Z$ , which denotes the number of closest neighbours, and in

our example it is equal to 6 as made evident in Figure II-1. Eqn (9) can thus be rewritten as

$$B = 2Z\beta. \quad (10)$$

Interestingly enough, when mobility is expressed in the form  $\mu = \frac{q\tau}{m^*}$ , the introduction of  $\beta$  derived from eqn (10) ( $\beta = B/2Z$ ) in eqn (8) gives:  $m^* = \frac{\hbar^2}{Ba^2}Z$ . In terms of  $\mu$ , we have

$$\mu = \frac{q\tau a^2 B}{\hbar^2 Z}. \quad (11)$$

We can thus conclude that semiconductors have narrow permitted bands as  $\Delta E = B$  is small. There is weak coupling between atoms as, following eqn (10),  $\beta$  is also small; in other words, semiconductors display low mobilities.

### III 3-D covalent crystal from a molecular model: $sp^3$ hybrid states at nodal atoms

#### 1 General notes

We will now look at the case of diamond, a material made up of a regular network of  $sp^3$  hybridised carbon atoms. In Appendix A-1, the spatial geometry of bonded carbon is detailed. The bonds are equally spaced when  $sp^3$  hybridisation occurs and the orbitals can be expressed using 4 functions  $|\Psi_1\rangle$ ,  $|\Psi_2\rangle$ ,  $|\Psi_3\rangle$ ,  $|\Psi_4\rangle$  as calculated in Appendix A-1, Section III. To follow the formation of the different electronic states and energy levels in diamond, we will sequentially study each step as shown in Figure II-2, by:

#### a Isolating carbon atoms

Looking at Figure II-2-a and Figure II-2-b, zone (1), we see that the orbitals of isolated carbon atoms, with electronic configuration  $1s^2 2s^2 2p^2$ , are characterised by having two levels,  $E_s$  and  $E_p$ . Note that in Figure II-3, the atoms C, C', C'' and so on, are assumed to be well separated.

As we bring the C', C'', C''', C'''' closer to the reference atom C, s and p bands form following the superposition of wavefunctions. For example, s-orbitals give rise to bonding and antibonding combinations which tend downwards and upwards, respectively. This is detailed further in Appendix A-2, Section I-2.

#### b s And p band hybridisation at the critical point M of Figure II-2(a)

When hybridisation of s and p states is energetically favoured,  $sp^3$  states on atom C, described by functions  $\Psi_1$ ,  $\Psi_2$ ,  $\Psi_3$  and  $\Psi_4$ , are obtained (see Appendix A-1, Section II-2). In the same way, hybrid states of the atom C' are represented by the functions  $\Psi'_1$ ,  $\Psi'_2$ ,  $\Psi'_3$  and  $\Psi'_4$ , and so on, for the other C atoms.



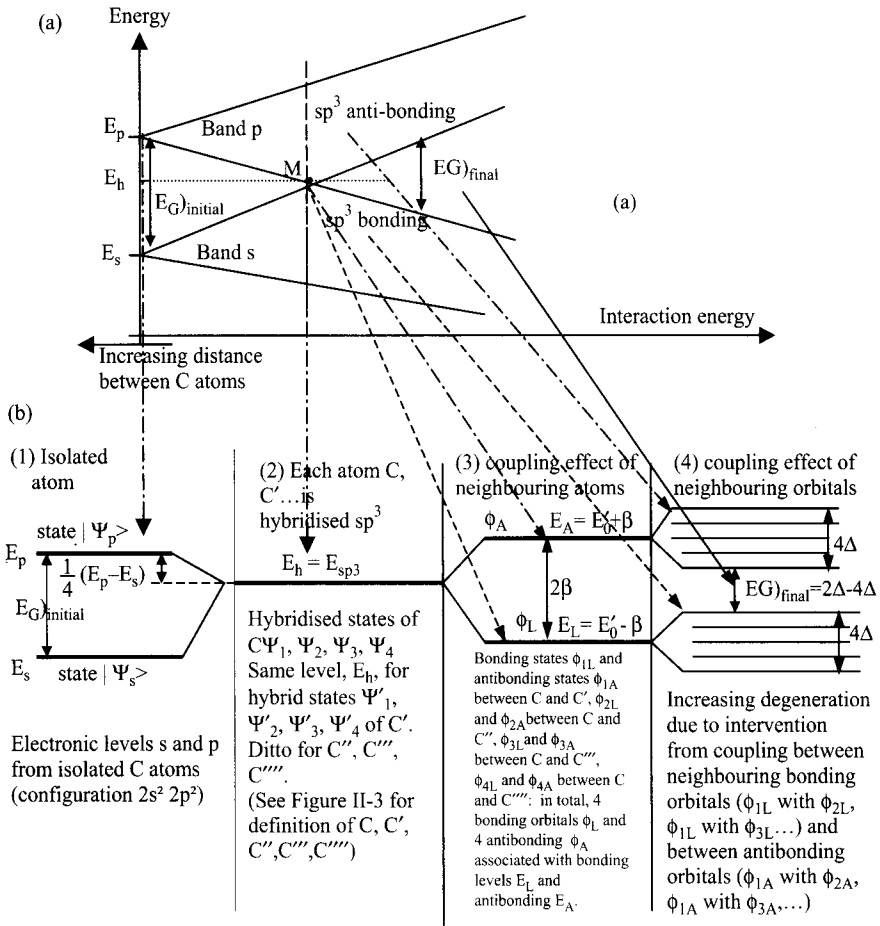


**Figure II-2.** (a) Band formation due to closing C atoms; (b) evolution in electronic energy levels through successive couplings.

Taking all states together, as shown in zone 2 of Figure II-2(b), and represented by the functions  $\Psi_i)_{i=1,2,3,4}$ ,  $\Psi'_i)_{i=1,2,3,4}$  and so on, equivalent to  $4N$  states for a system containing  $N$  atoms, we have energy  $E_{sp^3} = E_h$ .  $E_h$  can be calculated relatively simply using, for example

$$\begin{aligned}
 E_h &= \langle \Psi_1 | H | \Psi_1 \rangle \\
 &= \left\langle \frac{1}{2} (S + \varphi_{2p_x} + \varphi_{2p_y} + \varphi_{2p_z}) \middle| H \middle| \frac{1}{2} (S + \varphi_{2p_x} + \varphi_{2p_y} + \varphi_{2p_z}) \right\rangle \\
 &= \frac{1}{4} \{ \langle S | H | S \rangle + \langle \varphi_x | H | \varphi_x \rangle + \langle \varphi_y | H | \varphi_y \rangle + \langle \varphi_z | H | \varphi_z \rangle \} \\
 &= \frac{1}{4} \{ E_s + 3E_p \},
 \end{aligned}$$

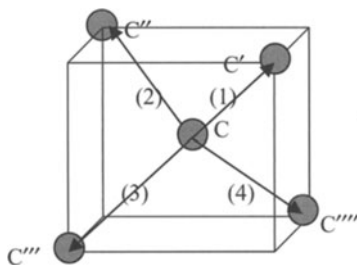


**Figure II-3.** Relative locations of atoms and available  $sp^3$  couplings.

with

$$E_h = \langle \Psi_2 | H | \Psi_2 \rangle = \langle \Psi_3 | H | \Psi_3 \rangle = \langle \Psi_4 | H | \Psi_4 \rangle = \langle \Psi'_1 | H | \Psi'_1 \rangle = \dots = E'_0.$$

$E_p$  and  $E_s$ , respectively, represent the energy levels of 2p and 2s states shown in Figure II-2-b. Thus

$$E_p - E_h = E_p - \frac{1}{4}\{E_s + 3E_p\} = \frac{1}{4}(E_p - E_s). \quad (12)$$

#### c Type A couplings between neighbouring C atoms, as detailed in Figure II-4

Here we consider only couplings (1), (2), (3) and (4), otherwise noted as  $C - C'$ ,  $C - C''$ ,  $C - C'''$ ,  $C - C''''$ , assuming that interactions that could result from other bonds are negligible. The bonding and anti-bonding states appear as shown in zone 3 in Figure II-2-b. This is detailed, qualitatively, in Section 2 just below.

#### d Supplementary effects resulting from type B couplings between molecular orbitals, as shown in Figure II-4

Type B couplings are those between (1) and (2), between (2) and (3) and so on, and result in the appearance of energy bands as shown in zone 4 of Figure II-2-b. A quantitative approach is detailed in Section 3 below.

## 2 Independent bonds: formation of molecular orbitals

Zone (3) in Figure II-2 (b) shows the states which appear following coupling of two  $sp^3$  hybridised orbitals, for example, of C and  $C'$ . For this atomic coupling,  $\Phi$  solutions can be given in the form of a linear combination of each atom's orbitals. As orbital  $|\Psi\rangle$  is for atom C, and orbital  $|\Psi'\rangle$  is for  $C'$ , we now have  $\Phi = c|\Psi\rangle + c'|\Psi'\rangle$ .

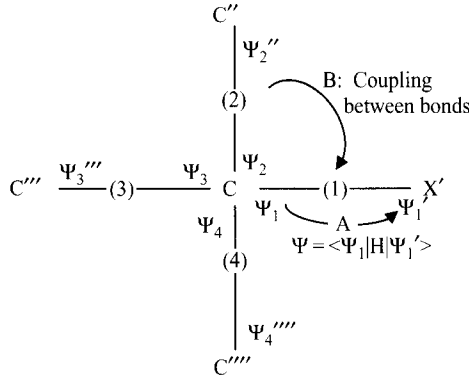


**Figure II-4.** Representation of successive A and B couplings by projecting plan view of Figure III-3.

On using line (1) in Figure II-4 to indicate the bonding between 2 C atoms, the resulting molecular orbital ( $\Phi_1$ ) can be bonding or anti-bonding (see Appendix A-1);

$$\Phi_{1L} = \frac{1}{\sqrt{2}}(|\Psi_1\rangle + |\Psi_1'\rangle) \quad (13)$$

$$\Phi_{1A} = \frac{1}{\sqrt{2}}(|\Psi_1\rangle - |\Psi_1'\rangle)$$

By taking into account pairs belonging to each carbon atom, and assuming them to be independent, the molecular orbitals which appear about our reference atom C are, in addition to  $\Phi_{1L}$  and  $\Phi_{1A}$ :

$$\Phi_{2L} = \frac{1}{\sqrt{2}}(|\Psi_2\rangle + |\Psi_2''\rangle) \quad \text{and} \quad \Phi_{2A} = \frac{1}{\sqrt{2}}(|\Psi_2\rangle - |\Psi_2''\rangle)$$

$$\Phi_{3L} = \frac{1}{\sqrt{2}}(|\Psi_3\rangle + |\Psi_3'''\rangle) \quad \text{and} \quad \Phi_{3A} = \frac{1}{\sqrt{2}}(|\Psi_3\rangle - |\Psi_3'''\rangle)$$

$$\Phi_{4L} = \frac{1}{\sqrt{2}}(|\Psi_4\rangle + |\Psi_4''''\rangle) \quad \text{and} \quad \Phi_{4A} = \frac{1}{\sqrt{2}}(|\Psi_4\rangle - |\Psi_4''''\rangle)$$

The energy levels  $E_L$  and  $E_A$  are, respectively, associated with bonding and anti-bonding states. They have the same form as that determined in Appendix A-1, that is:

$$E_L = E_0' - \beta \quad \text{and} \quad (14)$$

$$E_A = E_0' + \beta.$$

Note that  $E_0' = H_{ii} = \langle \Psi_i | H | \Psi_i \rangle = E_h = E_{sp^3}$  and that the coupling parameter between two atoms under consideration is  $-\beta = H_{ij}' = \langle \Psi_i | H | \Psi_j' \rangle$ .

*Comment* For N atoms in a crystal, the number of bonds of type  $\Phi_L$  is  $2N$  as each carbon atom presents 4 possible bonds each containing 2 electrons, and each shared

between 2 atoms. However, the actual number of valence electrons per atom is 4, resulting from  $2s^2 2p^2 \rightarrow 2t^4$ , in which t represents hybrid states, and therefore the fundamental state carries  $4N$  electrons, which can also be written as  $2 \times 2N$  (the number of electrons per bond multiplied by the number of bonds). All bonding bonds are therefore full when the symmetrically numbered anti-bonding bonds,  $\Phi_A$ , are empty.

### 3 Coupling of molecular orbitals and band formation

For a crystal containing  $N$  atoms, following the reasoning of Section 2, the energy level  $E_L$  (and  $E_A$ ) is degenerate  $2N$  times, corresponding to  $2N$  bonding orbitals. We will now look at the effect of coupling between different molecular bonds on the degeneration of energy levels.

#### a Effect of coupling energy between hybrid orbitals on the same carbon atom

The coupling energy between two hybrid atoms is of the form:  $\langle \Psi_1 | H | \Psi_2 \rangle = -\Delta$ . In terms of either  $\Psi_1$  and  $\Psi_2$  (given in Appendix A-1, Section II-2-c):

$$\begin{aligned} -\Delta &= \left\langle \frac{1}{2}(S + X + Y + Z) | H | \frac{1}{2}(S - X - Y + Z) \right\rangle \\ &= \frac{1}{4}(E_s - E_p - E_p + E_p) = \frac{1}{4}(E_s - E_p). \end{aligned}$$

We can see that the effect is not zero and that we should therefore expect, for a covalently bonded 3-D crystal, a non-zero coupling effect between molecular orbitals bonding two adjacent atoms.

#### b Coupling effects between neighbouring bonding orbitals within a crystal matrix

The coupling within the crystal matrix, shown as B in Figure II-4, corresponds to the form

$$\langle \Phi_{1L} | H | \Phi_{2L} \rangle = \left\langle \frac{1}{\sqrt{2}}(|\Psi_1\rangle + |\Psi'_1\rangle) | H | \frac{1}{\sqrt{2}}(|\Psi_2\rangle + |\Psi'_2\rangle) \right\rangle.$$

Ignoring coupling integrals between non-adjacent electrons, as for example  $\langle \Psi'_1 | H | \Psi_2 \rangle \approx 0$ , results in:

$$\langle \Phi_{1L} | H | \Phi_{2L} \rangle = \frac{1}{2} \langle \Psi_1 | H | \Psi_2 \rangle = \frac{1}{2} \times \frac{1}{4}(E_s - E_p) = -\frac{\Delta}{2}. \quad (15)$$

On modifying energy levels of type  $E_L$ , coupling of molecular bonds results in an increased degeneration to the level of  $E_L = E'_0 - \beta$ .

By analogy to the 1-D system looked at in Chapter 1, wavefunctions of the crystal must be written in the form of a linear combination of either bonding orbitals,  $\Phi_L$ , or

of anti-bonding orbitals,  $\Phi_A$ . These functions, which are characteristic of a regular network, should also satisfy Bloch's theorem and are thus of the form:

$$\left| \Phi_k^L(\vec{r}) \right\rangle = c_0 \sum_s e^{i\vec{k} \cdot \vec{r}_s} |\Phi_L(\vec{r} - \vec{r}_s)\rangle$$

$$\left| \Phi_k^A(\vec{r}) \right\rangle = c'_0 \sum_s e^{i\vec{k} \cdot \vec{r}_s} |\Phi_A(\vec{r} - \vec{r}_s)\rangle$$

These are the Bloch sums for bonding and anti-bonding orbitals, and are for electrons delocalised throughout a whole crystal network in 3-D. They are similar to the wavefunctions used in 1-D to verify Floquet's theory (eqn (10) of Chapter I).

In the same way as that observed for s-orbitals in a 1-D system (Chapter 1) and in a 3-D system (Section II-1 of this Chapter), the functions result in a fragmentation of  $E_L$  and  $E_A$  levels, as shown in going from zone 3 to zone 4 in Figure II-2. We thus obtain  $2N |\Phi_k^L(\vec{r})\rangle$  functions. Having taken into account  $4N$  spin functions we now have a full band of bonding states, justifying the term "Highest Occupied Molecular Orbital" (HOMO), otherwise known as the valence band by physicists. The band of anti-bonding states though is empty and is known as the "Lowest Unoccupied Molecular Orbital", or for physicists, the conducting band. The pair of bands are separated by what is known as the "band gap" of height  $E_G$ .

Quantitatively, we have seen in Section II of this Chapter that for s-orbitals characterised by a coupling parameter  $-\beta = \langle \psi_s | H | \psi_{s\pm 1} \rangle$ , the size of the formed bands is equal to  $2Z\beta$  (eqn (10) of Section II). In the case of Figure II-4 treated here, the co-ordination number ( $Z$ ) equals 4 and the coupling parameter,  $\langle \Phi_{1L} | H | \Phi_{2L} \rangle = -\frac{\Delta}{2}$ . The size of the HOMO and LUMO bands is therefore, following eqn (10),  $B = 2.4 \cdot \frac{\Delta}{2} = 4\Delta$  (zone (4) of Figure II-2-b). In addition, the height of the band gap can be calculated directly from Figure II-2-b using  $E_G = 2\beta - 4\Delta$ . The values of  $\beta$  and  $\Delta$  depend on the network and size of atoms. With diamond having a band gap of around 5.4 eV, it is more of an insulator than a semiconductor. On descending down through column IV of the periodic table, moving from carbon, through silicon to germanium, the size of the atoms increases and the size of the permitted bands also increases to the order of *ca.*  $4\Delta$ . With each successive increase in atom size, the band gap diminishes: C, 5.4 eV; Si, 1.1 eV; and Ge, 0.7 eV.

## IV Band theory limits and the origin of levels and bands from localised states

### 1 Influence of defaults on evolution of band structure and the introduction of 'localised levels'

Figure II-5 continues on from Figure II-2-b by considering the origin of the VB and CB for a perfectly ordered system of tetrahedral carbon atoms. As we have seen, the initial  $s^2p^2$  configuration gives rise to  $4 sp^3$  type molecular orbitals. And each one of

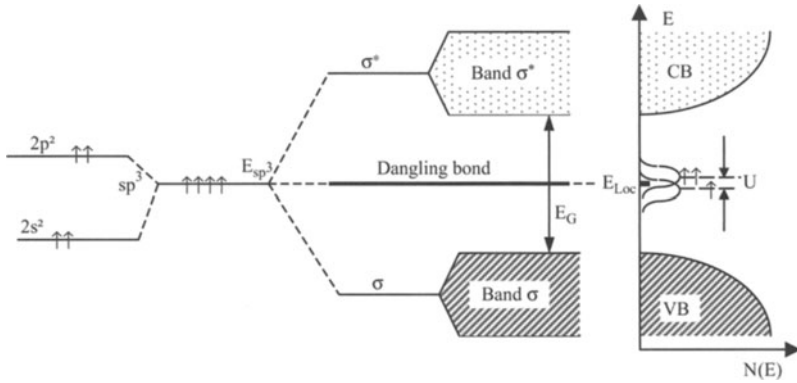


**Figure II-5.** Origin of localised levels associated with dangling bonds of tetrahedral carbon.

these leads to the formation of a bonding  $\sigma$ -orbital and an anti-bonding  $\sigma^*$ -orbital. In going from single molecules to the solid state, the combination of  $sp^3$  orbitals leads to the rupture of  $\sigma$ - and anti-bonding  $\sigma^*$ -orbitals into valence and conduction bands, respectively.

Because of the finite size of a real crystal, however, at the surfaces faults occur as each carbon atom is bonded to 3 rather than 4 carbon atoms. This results in one incomplete  $sp^3$  bond, or “dangling” bond, which contains one electron and, intrinsically, is electrically neutral. The single electron is situated at the level  $E_{sp^3}$ , even if the localised level associated with the electron is  $E_{Loc}$ , and is in the middle of the band gap, given the permitted bands allowed (Figure II-5).

Other faults can give rise to similar levels in a real crystal: vacated sites (generated during the preparation of the crystal); and dangling bonds induced by physical treatment, such as irradiation or ion implantation which, breaks bonds as the crystal is traversed.

The presence of structural faults, caused by dangling bonds, can create disorder, for example fluctuations in bonding angles, and result in an opening of levels and the formation of a default band. The exact positioning of the bands relies on relaxation phenomena which occur in the solid following fault formation, and whether they result from valence or conduction bands.

In Figure II-5, the lower band, near the middle of the band gap, corresponds to a dangling bond containing one electron. It is therefore a donor type band which is neutral and in an occupied state. The upper band, near the middle of the band gap, corresponds to the same fault but has a different charge *i.e.* has received an extra electron, and is an acceptor band which would be neutral if it were empty (see page 344 of [Ell 90]). The energy difference between these two types of faults, of which one is neutral when it is full, the other neutral when it is empty, corresponds to the Hubbard correlation energy ( $U$ ), for which  $U = \langle q^2 / 4\pi\epsilon_0\epsilon_r r_{12} \rangle$ , in which  $r_{12}$  designates the average distance between two electrons on the same site over all possible configurations. We

will now go on to try and detail the effects resulting from these electronic repulsions which up until now have been treated as negligible.

## 2 The effects of electronic repulsions, Hubbard's bands and the insulator-metal transition

In band theory, until now, we have considered that each electron existed in an average potential resulting from a collection of atoms and other electrons. In the case of alkali metals (Li, Na, K. . .), which have one free electron per atom, the transfer of an electron from one atom to its neighbour through a conduction band occurs *via* electronic levels situated just above the Fermi level ( $E_F$ ) and the energy utilised is extremely small, of the order of a fraction of a meV.

### a The model

In utilising Hubbard's model and theories, we can consider that the only important electronic repulsions are those which occur between two electrons which are on the same site (the same atom in a series of alkali metal atoms). The repulsion energy, or Hubbard energy, can be evaluated to ascertain if it is significant for certain materials and can even help indicate the origin of certain metal-insulator transitions. As before, we will use the same chain of alkali metals as shown in Figure II-6-a to evaluate the problem, although we will assume that overlapping between atoms is poor and the transport of electrons from one atom to the next requires a great deal of energy. Movement of an electron thus generates a supplementary repulsive energy which can be estimated by:

- calculating the ionisation energy required ( $I_p$ ) to separate an electron from the atom  $A'_1$  to which it is attached which subsequently becomes  $A_1$  (this change is shown in going from Figure II-6-a to Figure II-6-b); and

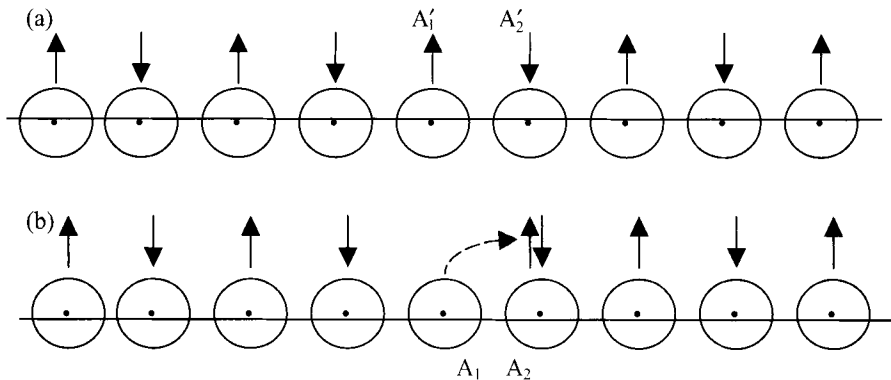


Figure II-6. Highlighting electronic repulsions in a chain of atoms with s-orbitals.

— calculating the energy recovered, or the electron affinity ( $\chi$ ) when the free electron is placed on the independent, adjacent atom  $A'_2$ , which subsequently becomes  $A_2$ .

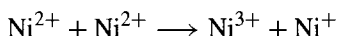
The total energy thus required, equivalent to the repulsive energy, is  $U_H = I_p - \chi$ .

For hydrogen  $I_p = 13.6$  eV and  $\chi = 0.8$  eV, and thus  $U_H = 12.8$  eV, showing how  $U_H$  can attain a relatively high value of several eV.

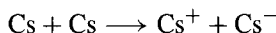
Elsewhere, Mott showed how the repulsive energy can be calculated using  $r_{12}$  [Mot 79], which represents the distance between two electrons on the same site or atom, and  $\psi(r)$  which is the wavefunction corresponding to the value proposed at the end of the preceding Section 1.

$$U_H = \int \int \frac{e^2}{4\pi\epsilon_0 r_{12}} |\psi(r_1)|^2 |\psi(r_2)|^2 dr_1 dr_2.$$

Practically speaking, this energy is particularly important with respect to transition metal oxides, such as NiO, for which electron transport occurs *via* d-orbitals and can be written as:



For a chain of alkali metals, however, the same electron transfer, *via* s-orbitals, is written:



In Figure II-6,  $A'_1 \equiv A'_2 \equiv \text{Cs}$  while  $A_1 \equiv \text{Cs}^+$  and  $A_2 \equiv \text{Cs}^-$ . On removing the arrows in Figure II-6, which represent the division of electrons throughout a chain of atoms, we can consider that for NiO,  $A'_1 \equiv A'_2 \equiv \text{Ni}^{2+}$ ,  $A_1 \equiv \text{Ni}^{3+}$  and  $A_2 \equiv \text{Ni}^+$ . Placing an electron on a  $\text{Ni}^{2+}$ , to form a  $\text{Ni}^+$  ion, would require the energy given by  $U_H = I - \chi$  if the  $\text{Ni}^+$  and  $\text{Ni}^{3+}$  ions, at positions  $A_2$  and  $A_1$  in Figure II-6-b, respectively, are sufficiently far apart. The transported electron can be assumed to pass through a free state, that is its energy  $E_n$  at the level  $n \rightarrow \infty$  tends towards 0, as do the successive energies  $I_p$  and  $-\chi$ , as previously described.

Energy levels of isolated ions can be represented in terms of  $-I_p$  (the energy of an orbital which loses an electron, *i.e.*  $\text{Ni}^{3+}$  or  $A_1$ ) and  $-\chi$  (the energy of a supplementary electron situated on  $\text{Ni}^+$  or  $A_2$ ). When the ions are well separated, as shown in the far left part of Figure II-7, each energy level is separated by  $U_H = I_p - \chi$  which appears as a band gap between the upper and lower levels, the former having received an electron, the latter having lost one.

On bringing the ions closer to one another, as described in going from the left to right side of Figure II-7, transport by charge carriers becomes possible *via* the permitted bands which start to form. These newly formed discrete bands give rise to permitted bands (Hubbard's bands), upper level bands of electrons (in which  $\text{Ni}^+$  can be found) and lower level bands containing holes (in which  $\text{Ni}^{3+}$  resides).

As the size (B) of the bands grows with increasing proximity of atoms, the difference  $U_H - B$  decreases and eventually disappears when B reaches  $U_H$ . Beyond this value—obtained when the atoms are close enough to each other—the upper and lower Hubbard bands overlap and the band gap is removed; this point is also known as the Mott-Hubbard transition from an insulator to metallic state.



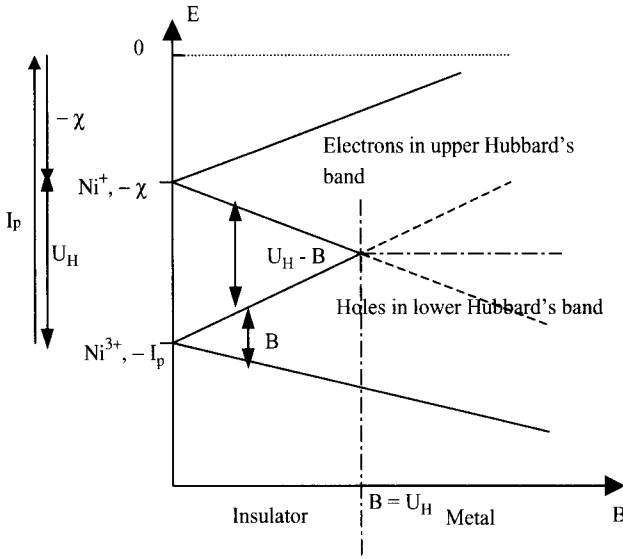


**Figure II-7.** Evolution of Hubbard bands as a function of band size ( $B$ ).  $B = 0$  for atoms far apart but when  $B = U_H$ , the band gap  $U_H - B$  disappears to give a metal-insulator transition.

### b Charge transfer complexes

Charge transfer complexes (CTCs) are materials in which the effective correlation energy is high [And 92]. If the effective energy ( $U_{\text{eff}}$ ) is defined as the difference between the electronic repulsion energy for a site occupied by two electrons ( $U_0$ ) and the electronic repulsion energy between two electrons on adjacent sites ( $U_1$ ) *i.e.*  $U_{\text{eff}} = U_0 - U_1$ , then for a CTC the energy  $U_H$  corresponds to  $U_{\text{eff}}$ .

For a system with  $N$  sites:

- if we can assume that  $U_{\text{eff}}$  is negligible, each site can be occupied by two electrons (spin up,  $\uparrow$ , and spin down,  $\downarrow$ ). In addition, as in Figure II-8-a, if the system is half filled by  $N$  electrons then the material is metallic;
- if the system is one in which  $U_{\text{eff}}$  is high, we can place only one electron per site. Again, if the system carries  $N$  electrons (*i.e.*  $\rho = 1$ , in which  $\rho$  designates the number of electrons per site) then all energy levels are occupied and the band is full as shown in Figure II-8-b. Only  $B$  inter-band transitions are allowed, demanding a high energy of activation ( $E_a$ ), and the system, in other words, is an insulator (Mott insulator) or semiconductor. For example, the complex HMTTF-TCNQF<sub>4</sub>, in regular columns, has  $\rho = 1$ ,  $E_a = 0.21$  eV with a room temperature conductivity  $\sigma_{\text{RT}} = 10^{-4} \Omega^{-1} \text{cm}^{-1}$ ; and
- once again, if the system is one in which  $U_{\text{eff}}$  is high and we can only place one electron per site but  $\rho < 1$  because bonds at the interior of each column are not fully occupied, both  $A$  intra- and  $B$  inter-band transitions are possible with the former requiring, respectively, low and high activation energies. This is shown in Figure II-8-c. As an example, TTF<sup>+0.59</sup>-TCNQ<sup>-0.59</sup> displays a metallic character with  $\rho = 0.59$  and  $\sigma_{\text{RT}} = 10^3 \Omega^{-1} \text{cm}^{-1}$ .

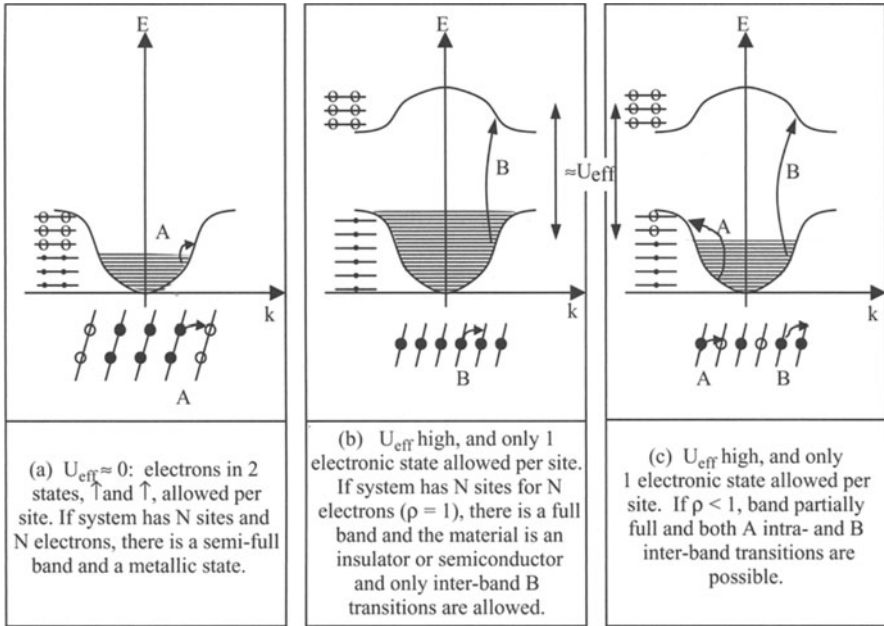


**Figure II-8.** Electron transport with respect to electronic structure. Upper parts of the Figures represent band schemes and lower parts represent electron positions (● = occupied state, ○ = empty state).

**c The Mott transition from insulator to metal: estimation of critical factors**

Different theories have been elaborated to establish, in a quantitative manner, the parameters surrounding transitions from insulator to metallic states. The Thomas-Fermi screened potential can be used [Ell 98], [Sut 93] and the basis of theoretical developments, including the application of magnetism, can be followed up elsewhere [Zup 91]. We will limit ourselves here to saying that this transition can result from competition between localisation effects, themselves resulting from electron Fermi kinetic energies ( $E_F$ ) and the electrostatic energies to which they are subject.

In order to take into account environmental effects and polarisation, two elements must be considered: the permittivity of the medium under study ( $\epsilon_0 \epsilon_r$ ) ( $\epsilon_r$  being the relative permittivity of the material); and the active length ( $a^*$ ) of the electrostatic potential, which takes on the form  $e^2 / 4\pi \epsilon_0 \epsilon_r K_1 a^*$ .  $K_1$  is a constant which accounts for the present-day incomplete knowledge of interaction distances, which can be written simply as  $K_1 a^*$ . It should be noted that  $a^*$  must take on the same form as the first Bohr orbit ( $a_0$ ), that is  $a_0 = [\epsilon_0 \hbar^2] / [\pi m e^2]$ . To obtain  $a^*$  from  $a_0$ ,  $\epsilon_0$  needs once again to be replaced by  $\epsilon_0 \epsilon_r$ , to take into account the effect of the interaction between network and electron thus changing the latter mass from  $m$  to  $m^*$  so that  $a^* = [\epsilon_r \epsilon_0 \hbar^2] / [\pi m^* e^2]$  or  $a^* = \epsilon_r a_0 (m / m^*)$ .

As  $E_F = (\hbar^2/2m^*)(3\pi^2n)^{2/3} = (K_2\hbar^2n^{2/3})/(4\pi^2m^*)$ , in which  $n$  is the electron concentration (page 171 of [Mooser 93]) and  $K_2$  a constant, the condition required to reach the metallic state can be written:  $(\hbar^2n^{2/3})_{n=n_c}/(4\pi^2m^*) \geq Ce^2/(4\pi\epsilon_0\epsilon_r a^*)$ , in which  $C$  is, as yet, an unresolved constant resulting from the introduction of the aforementioned constants  $K_1$  and  $K_2$ . The relationship is thus based on  $n_c$ , at which point the transition occurs. Therefore, we should have  $a^*n_c^{2/3} \geq C(e^2m^*\pi)/(\epsilon_0\epsilon_r\hbar^2)$ , either in terms of the expressions  $a^*$  and  $a_0$ , as in  $(a^*n_c^{1/3})^2 \geq C$ , or expressed as  $a^*n_c^{1/3} \geq D$ , in which  $D = C^{1/2}$ . Experimentally, the constant  $D$  is normally found to be around 8 times the value of  $n_c$  (it has been shown that  $D \approx 0.26$ ) and thus the criteria for the transition is:

$$(a^*n_c^{1/3})^2 \geq 0.26. \quad (16)$$

Physically speaking, this criterion means that all materials can become metallic if they are sufficiently compressed so that the electron density reaches the value  $n_c$ . The corresponding metal-insulator transition (M-I transition, which also occurs at  $n = n_c$ ) is called the Mott transition and originates from localisation of electrons through electrostatic interactions, not from any material disorder. We shall see in the following Section 3 how disorder alone can result in the Anderson transition.

#### d $\pi$ -Conjugated polymers

Polymers conjugated by  $\pi$ -orbitals are, in principle, not subject to Mott transitions as transfers from one site to another in the same chain have  $\beta$  integral values which are too high (typically of the order of  $4\beta \approx 10$  eV for polyacetylene), well above electron-electron interaction energies ( $U$ , below 1 eV for polyacetylene). Figure II-8-a therefore sufficiently describes these materials, although they do display insulating characteristics, which in the case of polyacetylene results from a Peierls distortion due to electron-phonon interactions which open the band gap (Figure II-9).

### 3 Effect of geometrical disorder and Anderson localisation

#### a Introduction

The effect of geometrical disorder has for the most part been studied within theories on amorphous semiconductors developed by Mott and Davies [Mot 71, Mot 79 and Mot 93], and discussed—in French—by Zuppiroli [Zup 91] and Moliton [Mol 91].

The theory is based on two fundamental ideas:

- the first was taken from the work of Ioffe and Regel [Iof 60] who observed that there was no great discontinuity in the electronic properties of semi-metallic or vitreous materials when going from solid to liquid states. It was concluded that electronic properties of a materials cannot be only due to long range order, as was proposed by Bloch for properties of crystals, but are also determined by atomic and short range properties in which the average free path of an electron is inter-atomic. It is worth noting also, that even though a material may be amorphous,

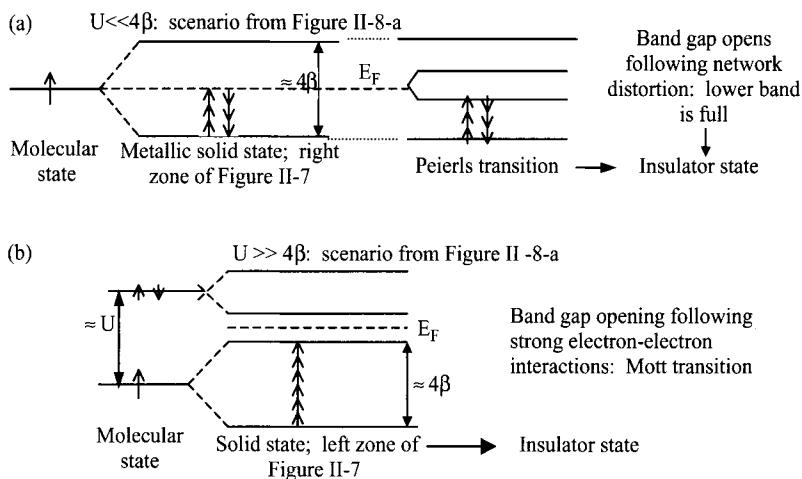


**Figure II-9.** (a) Characteristics of  $\pi$ -conjugated polymers, with the example of polyacetylene under a Peierls transition, verifying that  $U \ll 4\beta$ , in contrast with (b) Mott insulators for which  $U \gg 4\beta$  (and possible for CTCs).

this does not exclude it from having bands. For example, glass, which is a non-crystalline material, is transparent in the visible region of light ( $\approx 1.5 - 3$  eV), that is to say that while absorption of photons with energy below 3 eV does not occur, glass does actually have a band gap of at least greater than 3 eV; and

- the second rests on the evidence given by Anderson [And 58] for a material without long range order that nevertheless have localised states with permitted energy bands for electrons. This theoretical model comes from observations made on certain amorphous semiconductors in which charge carriers cannot move.

## b Limits to the applicability of band theory and Ioffe Regel conditions

Bloch functions, *i.e.*  $\psi_k(\mathbf{r})$ , can be used to describe electron wavefunctions in perfectly crystalline materials. The electronic states are delocalised and spread out over space, as denoted by  $|\psi_k(\mathbf{r})|^2$ . Because of perfect delocalisation, the average free mean path of an electron can be considered infinite. It is only when studying a real crystal that the average free path of an electron takes on significance because of effects due to quasi-imperfections caused by vibrations, called phonons, and imperfections caused for example by doping agents and impurities which perturb the regularity of potential throughout the network. It is only when these electron scattering effects, which limit the free path of electrons are considered, that the statistical average term  $\mathcal{L}$  of the free path length of an electron between two successive collisions can be introduced. In addition, there are two terms to note: "lattice scattering" which indicates collisions due to the material network and for a similar effect caused by ionised impurities, the term "impurity scattering" is used.

On disordering a lattice by introducing vibrations and/or impurities,  $\mathcal{L}$  appears and takes on a decreasing value as disorder increases. If there is a low amount of

impurities, then local levels appear, most notably in the forbidden band (FB), but if the number of impurities increases, the localised levels grow to form impurity bands which can reach a size  $\Delta E_c$ , close to that of the valence band (VB), the conduction band (CB) and the FB introduced in Bloch's theory. Bloch's theory though loses all semblance of reality when values of  $\Delta E_c$  reach the same values of the bands. Put another way, we can go from the crystalline state to the amorphous state with  $\mathcal{L}$  decreasing until Bloch's theory is no longer acceptable. The limit for  $\mathcal{L}$  was fixed to  $k\mathcal{L} \sim 1$  (for a perfect crystal,  $k\mathcal{L} \gg 1$ ) by Ioffe and Regel by following the reasoning of the uncertainty principle, *i.e.*

$$\Delta E \cdot \Delta t \geq \hbar \quad \text{and} \quad \Delta x \cdot \Delta k \geq 1. \quad (17)$$

To arrive at the result shown above, we can consider that the trajectory of an electron after a collision is random, and at the very best can only be defined between two collisions, *i.e.*:

$$(\Delta t)_{\max} = \tau \quad (18)$$

in which  $\tau$  is the relaxation time—the average time between two collisions; and

$$(\Delta x)_{\max} = \mathcal{L} \quad (19)$$

From eqn (17) we can thus directly derive the best precision in  $\Delta E$ ,  $(\Delta E)_{\min}$ , and in  $\Delta k$ ,  $(\Delta k)_{\min}$ , when:

- 1) the equivalence of (17) by  $\Delta E$  is verified.  $\Delta t = \hbar$  and  $\Delta x \cdot \Delta k = 1$ ;
- 2) when  $\Delta t$  and  $\Delta x$  are at their highest value in the equalities just above and equal to  $(\Delta t)_{\max} = \tau$  and at  $(\Delta x)_{\max} = \mathcal{L}$ .

We arrive at:

$$(\Delta E)_{\min} \cdot \tau \approx \hbar, \quad (20)$$

and

$$(\Delta k)_{\min} \cdot \mathcal{L} \approx 1. \quad (21)$$

The question we are therefore brought to ask is with increasing disorder, what are the lowest values that  $\tau$  (and thus the mobility  $\mu = q\tau/m$ ) and  $\mathcal{L}$  can go to while  $(\Delta E)_{\min}$  and  $(\Delta k)_{\min}$  retain acceptable values, values which are compatible with classical theory of bands in a real crystal.

The response can be given by using simple calculations which show that when:

- $\mu \rightarrow 1 \text{ cm}^2 \text{ V}^{-1} \text{ s}^{-1}$  (and  $\tau \approx 6 \times 10^{-16} \text{ s}$ ), from eqn (20)  $(\Delta E)_{\min} \approx 1 \text{ eV}$ . Thus,  $(\Delta E)_{\min} \approx E_G$  (band gap size) or  $(\Delta E)_{\min}$  is the same order of size as the permitted bands. When  $\mu \leq 1 \text{ cm}^2 \text{ V}^{-1} \text{ s}^{-1}$ , uncertainty in the energy of the carriers tends to the same order of size as the permitted and forbidden bands, *i.e.* to such an extent such that the band scheme loses its relevance to real systems. It will be shown though that the Anderson model band scheme has to take into account localised bands with a gap which eventually becomes the mobility gap,  $E_{\mu}$ .

- $\mathcal{L} \rightarrow$  a few Angstroms, that is to say  $\mathcal{L} \approx a$ , in which  $a$  is the lattice constant and is typically of the order of  $3 \times 10^{-8}$  cm, eqn (21) results in  $(\Delta k)_{\min} \approx 1/\mathcal{L} \approx 1/a \approx 3 \times 10^7 \text{ cm}^{-1} \approx k$ . In effect, with  $\lambda = h/mv$  in which  $v = v_{\text{thermal}} \approx 100 \text{ km s}^{-1}$  and  $\lambda \approx 7 \times 10^{-7} \text{ cm}$ , we have  $k = 2\pi/\lambda \approx 10^7 \text{ cm}^{-1}$ , and can directly infer that in a band scheme, conduction electrons will be such that  $k \approx 1/a$ . At these values where  $\mathcal{L} \approx a$ , we therefore have  $(\Delta k)_{\min} \approx k$ , and  $k$  can no longer be considered a good physical parameter to which we can apply quantification. In addition, when  $\Delta k \sim k$  Fermi's sphere is so badly defined that it can, at a limit, be totally deformed and the concept of carrier speed loses significance as  $\hbar k = m^*v$ , just as much as the average free path which is expressed as a function of  $v$  following  $\mathcal{L} = v\tau$ .

Finally, as soon as  $\mathcal{L} \approx a$ , and more strictly speaking as soon as  $\mathcal{L} \leq a$  which occurs when the interaction between an electron and the material network becomes increasingly strong, an electron no longer goes any further than the limits of the atom to which is tied. The electronic wavefunction localises over a small region in space and is generally supposed to diminish exponentially with respect to  $R$  following  $\exp(-\alpha R)$ .

Having followed the work of Mott and Anderson, we are brought to a new concept of localised states. The permitted density of states,  $N(E)$ , always results in an energy band beneath a single  $E_C$  for a conduction band and above a single  $E_V$  for a valence band, and, in other words, an activation energy is necessary for carriers to pass from one state to another with an emission or absorption of a phonon.

**c Anderson localisation**

*α) The model* Systems in which disorder is due to a random variation in the energetic depth of regularly spaced sites (with interstitial distances always equal to  $a$ ) are considered in Anderson's model, and can relate, for example, to a random distribution of impurities. Different authors, including Mott, have tried to take into account lateral, spatial disorder and the results have been close to those of the Anderson model, of which we will limit our discussion to this section.

In Chapter 1, we saw that if we take into account effects resulting from a network of atoms at nodes by constructing a regular distribution of identical potential wells, then a permitted energy band of height  $B$  appears, as shown in Figure II-10.

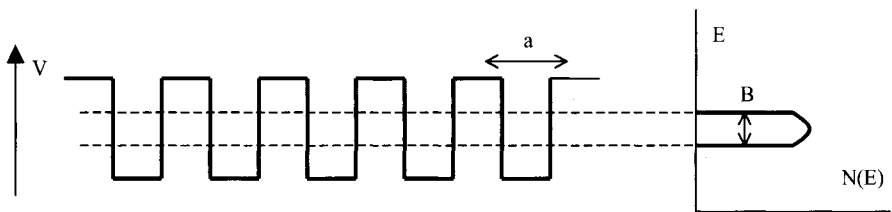


**Figure II-10.** Regular distribution of identical potential wells and permitted band.

In the approximation of strong bonds, we saw in Section II-1 of this Chapter that:

- $B = 2Z\beta$ , with  $Z =$  the number of adjacent neighbours and  $\beta$  the resonance integral between two adjacent sites;
- 

$$m^* = \frac{\hbar^2}{2\beta a^2} = \frac{\hbar^2}{a^2 B} Z \tag{22}$$

so that  $\mu = \frac{q\tau a^2}{\hbar^2} \frac{B}{Z}$ , and semiconductors possessing a narrow B band exhibit low mobilities.

For Anderson’s model we replace the preceding distribution by one of randomly deep potential wells which represent disorder, as shown in Figure II-11.

*β) Variation in wavefunctions with respect to  $V_0/B$  (Anderson) and  $\mathcal{L}$  (Ioffe and Regel)*  
 We will show here how permitted energy bands change into localised states if  $V_0/B$  goes beyond its critical value. In order to do this, we need to look at the following, successive scenarios:

— *Real crystal:  $V_0/B$  is very low and  $\mathcal{L}$  is high*

Here the wavefunction is given by Floquet’s theory (eqn (10) of Chapter 1) which we can write to the order of a normalisation constant:

$$\psi_k(r) = \sum_n e^{ikr_n} \psi_0(r-r_n). \tag{23}$$

The average free path can be estimated from the Born approximation, [page 401 of Smi 61], by realising that the wave vector of an electron ( $k_n$ ) changes to  $k_m$  once the electron has undergone a collision of probability  $P_{nm}$  and that  $P_{nm} = \frac{1}{\tau} = \frac{v}{\mathcal{L}}$ , and in addition [page 16 of Mot 71]  $P_{nm}$  is given by Fermi’s ‘golden rule’:  $P_{nm} = \frac{1}{4} \frac{2\pi}{\hbar} |\Omega|_{moy}^2 N(E_m)$  (eqn (2.20) of [Mol 91] relating to unit volume). For conducting electrons, for which  $E_m \approx E_F$ , spread throughout a volume  $V = a^3$  with a random

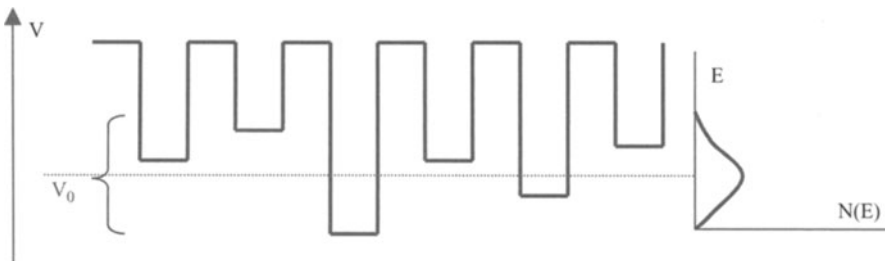


**Figure II-11.** Distribution of randomly deep potential wells.

distribution of wells with depth such that  $|\Omega|_{\text{moy}} = (V_0/2)$ , we obtain:

$$\frac{1}{\mathcal{L}} = \frac{P_{nm}}{v} = \frac{1}{4} \frac{2\pi}{\hbar} \left( \frac{V_0}{2} \right)^2 a^3 \frac{N(E_F)}{v}, \quad (24)$$

in which  $N(E_F)$  is the density of states at the Fermi level and  $v$  the velocity of an electron at the Fermi level.

As  $\mathcal{L}$  is large, the system under consideration is almost a perfect crystal and therefore we can write:

$$N(E) = \frac{4\pi(2m^*)^{3/2}E^{1/2}}{h^3} \text{ and } v = \left( \frac{2E}{m^*} \right)^{1/2}.$$

In using the effective mass given in eqn (22), eqn (24) gives:

$$\frac{a}{\mathcal{L}} = \frac{(V_0/\beta)^2}{32\pi}; \quad \text{and with } B = 2ZI, \quad \frac{a}{\mathcal{L}} = \frac{(2ZV_0/B)^2}{32\pi}. \quad (25)$$

— *System in which  $(V_0/B) \approx 1$  (single disorder value) corresponding to  $\mathcal{L} \approx a$  for weak disorder*

When  $\mathcal{L} \approx a$ , eqn (25) written for a cubic system in which  $Z = 6$  results in  $(V_0/B) = 0.83 \approx 1$ . At this point when  $\mathcal{L} \approx a$  (and  $V_0 \approx B$ ), the disorder is such that  $\Delta k \approx k$  (following Ioffe and Regel), and under such conditions, at each collision,  $k$  randomly varies by  $\Delta k$ , the closest neighbour to  $k$ . In going from one potential well to the next, the wavefunction as detailed in eqn (23) randomly changes and, following Mott, loses its phase memory and should therefore be rewritten using an approximate form:

$$\psi_k(r) = \sum_n A_n \psi_0(r - r_n),$$

with  $A_n = c_n \exp(i\phi_n)$ , in which  $A_n$  is a function with a random phase and a near constant amplitude. Moreover, this amplitude is more constant than the variation between neighbouring potential wells *i.e.*  $V_0$  is low. In a model using two wells with potential depths  $V_1$  and  $V_2$  (as in Miller and Abrahams [Mil 60]) the resulting wavefunction can take on either a symmetrical or antisymmetrical form, respectively,  $\psi_S = A_1\psi_1 + B\psi_2$  or  $\psi_A = A_1\psi_1 - B\psi_2$ . We can therefore show that when  $|V_1 - V_2| \ll |\beta|$  (*i.e.*  $V_0$  is low), so  $A_1 \approx A_2$ , the difference in energy ( $E_1 - E_2$ ) between the two possible states is such that  $|E_1 - E_2| \approx 2|\beta|$  [Mot 79] and [Mol 91]. A representation of the function is shown in Figure II-2-a for a network of several potential wells.

— *System in which  $(V_0/B) > 1$  ( $(V_0/B)$  just above single order value): initial delocalisation and medium disorder*

In a system which corresponds to a great increase in disorder, and for the model of just two wells would correspond to an increase in the depth between the wells as in  $|V_1 - V_2| = V_0$ , the difference in energy,  $|E_1 - E_2|$ , increases to a corresponding level and  $A_1$  differs from  $A_2$ . The amplitudes of the functions are no longer constant and the wavefunction displays increasing disorder both in amplitude and in phase (Figure II-12-b).



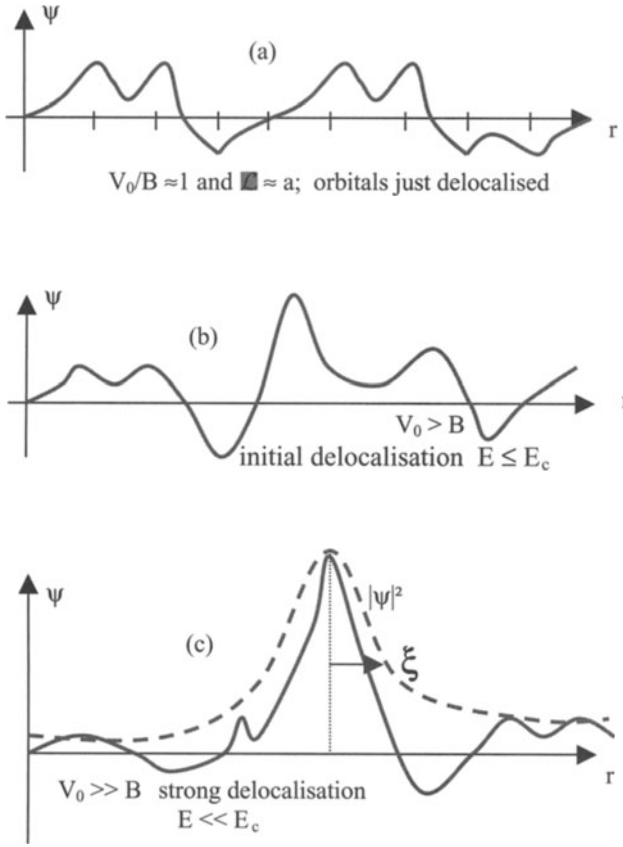


**Figure II-12.** Variations in wavefunction with delocalisation: (a) delocalisation—localisation only; (b) weak delocalisation; and (c) strong delocalisation.

— System in which  $(V_0/B) \gg 1$  ( $(V_0/B)$  well above single order value): strong delocalisation and great disorder

In this system a highly localised state is formed, as shown in Figure II-12-c, and as  $V_0$  increases the localisation is accentuated. In addition, there is no longer propagation along a line of potential wells and states are thus localised. An exponential decrease in the wavefunction starts to appear and is increasingly noticeable with increasing values of  $V_0$ . The wavefunction takes on the form

$$\psi(r) = \left[ \sum_n A_n \psi_0(r - r_n) \right] e^{-\alpha r}$$

and can be rewritten

$$\psi(r) = \left[ \sum_n A_n \psi_0(r - r_n) \right] e^{-r/\xi},$$

in which  $\xi$  is the localisation length.

To conclude, the factor  $V_0/B$  is a crucial term in deciding whether only localised states form ( $V_0/B > 1$ ) or whether both localised and delocalised states can co-exist ( $V_0/B \leq 1$ ).

*$\gamma$ -Band scheme and form of the states density function  $N(E)$*  From a realistic scheme of the distribution of potential wells, we can see that states should be localised within one energy domain and delocalised in another. Accordingly, in Figure II-13 is described a system with non-negligible disorder:

- all states at the tail end of the function  $N(E)$  which correspond to a high enough value of  $V_0$  and from energies  $E(E_c \text{ and } E) E'_c$  appear localised as before in the scheme of potential wells;
- however, the middle of the band corresponds to shallow states with small  $V_0$ , such as  $V_0/B$ , and is a zone of delocalised states which have  $E'_c < E < E_c$ .

**d Localised states, conductivity and Anderson’s metal-insulator transition**

*$\alpha$ -Mott’s definition:* Mott’s definition is based on continuous conductivity relative to electrons with a given energy ( $\sigma_E(0)$ ) and delocalised states are on average, at  $T = 0$  K, those for which  $\sigma_E(0)$  is zero *i.e.*  $\langle \sigma_E(0) \rangle = 0$ . To arrive at an average though, all possible configurations which have the energy  $E$  need to be considered, and while some electrons may have a non-zero energy, the average over all possible states with the corresponding energy  $E$  gives zero as a result. These states and the mobility they represent are in effect thermally activated.

However, at  $T = 0$  K, delocalised states average to give  $\sigma_E(0) \neq 0$ , that is to say metallic behaviour occurs.

*$\beta$ -State properties* In Figure II-13, two types of states—localised and delocalised—are separated by energies  $E_c$  and  $E'_c$  which together are called the ‘mobility

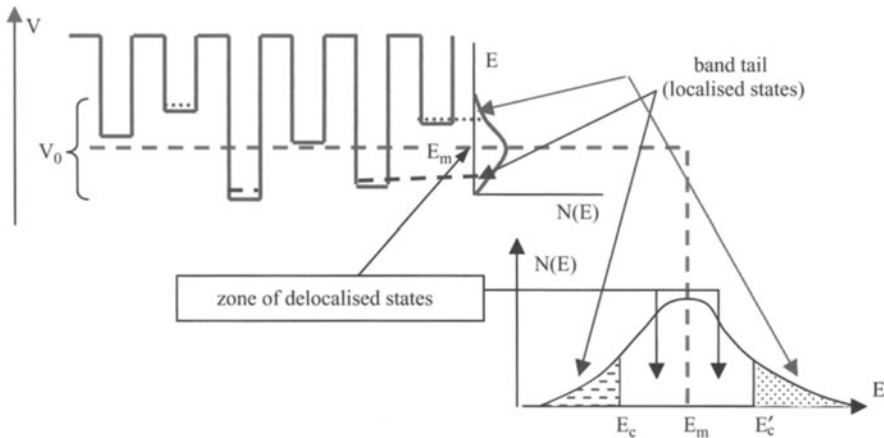


**Figure II-13.** Representation of localised and delocalised states co-existence.

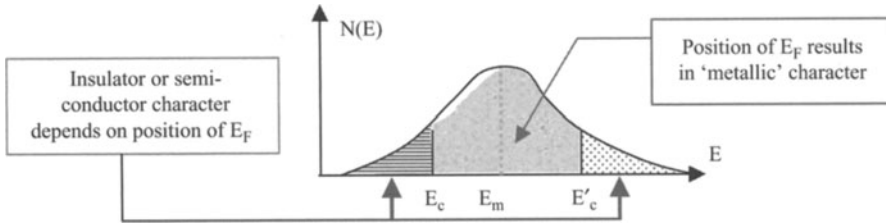


**Figure II-14.** Metallic character resulting from the domain  $E_F$ .

edge'. In the two zones Einstein's relation holds true if  $E_F$  is outside the bands of non-degenerate states. This gives  $\mu = qD/kT$ , but the diffusion coefficients ( $D$ ) have different forms, as in  $D = Pa^2$  in which  $P$  represents the probability of movement to neighbouring sites. This brings us to the origin of the expressions used in Chapter 5:

- when  $E > E'_c$  and  $E < E_c$ ,  $D = (1/6)v_{ph}a^2 \exp(-w_1/kT)$  (with  $v_{ph}$  being the phonon frequency and  $w_1$  the energy of activation) and  $\langle \sigma_E(0) \rangle_{T=0K} = 0$ . Here as  $T \rightarrow 0$ , we can verify that  $D$  and  $\mu$  tend towards zero, much as conductivity; and
- when  $E_c < E < E'_c$ ,  $D = (1/6)v_e a^2$  and  $\sigma_E(0) \neq 0$  where  $v_e$  is the frequency of electronic vibrations.

*$\gamma$ -Slightly disordered media, in which localisation is slight and  $\mathcal{L}$  is small, and the distinction between an insulator or semiconductor and a metal* As in the case of classic, crystalline media, the position of  $E_F$ , as detailed in Figure II-14, is related to the nature of a material. When  $E_F$  is situated in the domain of delocalised states ( $E_c < E_F < E'_c$ ) there is degeneration appropriate for a 'metallic' character. However, when  $E_F$  is situated in the zone of localised states, for which typically  $E < E_c$ , charge carriers can only be thermally excited and conductivity can occur only by jumps or by excitation to  $E_c$ , and indeed at 0 K conductivity tends towards 0 which is typical of an insulator. Materials for which the Fermi level is situated in an energy zone in which states are localised are called Fermi glasses.

*$\delta$ -Metal-insulator or semiconductor transition* For a given material which has a Fermi level fixed by its charge density, displacement of  $E_c$ , for example by increasing the disorder as shown in Figure II-15, moves the Fermi level from an initial state in a domain of delocalised states (metallic) to a zone of localised states. The result is a metal to insulator or semiconductor transition.

*$\epsilon$ -Anderson transition from order to disorder and the change in conductivity* Even though we do not detail transport properties in this Chapter, we should nevertheless introduce an expression for metallic conductivity written in the relatively simple form of  $\sigma = qn\mu = nq^2\tau/m^*$ , in which  $n$  is electron concentration and  $\tau$  is the relaxation time with respect to the Fermi level. With  $\mathcal{L} = v\tau$  we have  $\sigma = nq^2\mathcal{L}/m^*v$ , and on introducing the crystalline momentum,  $\hbar k = m^*v$ , we reach  $\sigma = nq^2\mathcal{L}/\hbar k_F$  in which  $k_F$  is the wave vector at the Fermi surface. We can also note that the number  $n$  of electrons within a unit volume  $V$  ( $V = 1$ ) can be obtained by use of the reciprocal space,

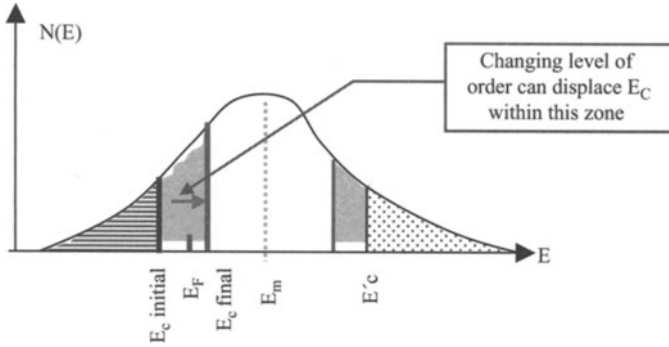


**Figure II-15.** Using disorder to displace  $E_C$  and effect metal-insulator transition.

that is to say the number of cells within the Fermi volume being  $([4/3]\pi k_f^3)/8\pi^3$ , each with volume  $8\pi^3/V = 8\pi^3$  for  $V = 1$ . In taking into account electron spins (*i.e.* doubly occupied cells), we have  $n = 2([4/3]\pi k_f^3)/8\pi^3$  and metallic conductivity can therefore be written as  $\sigma_B = 4\pi k_f^2 q^2 \mathcal{L}/12\pi^3 \hbar$  (*cf.* Section III-1 in Chapter V).

When considering a metallic state, the Fermi level can be considered more or less at the band middle, as in 1-D with  $k_f \propto \pi/a$  (p. 21 of [Mot 93]) and Figure II-14. With increasing disorder,  $E_C$  and  $E'_C$  tend towards each other at the band centre  $E_M (\approx E_F)$  at which point all states are delocalised. This change is called Anderson's transition and is detailed in Figure II-16. Simultaneously,  $V_0/B \geq 1$  with  $\mathcal{L}$  tending towards  $a$ . For its part, with  $\mathcal{L} = a$ , conductivity  $\sigma$  tends towards  $\sigma_{\min} = \sigma_{IR} = (\sigma_B)\mathcal{L}=a = q^2/3a\hbar$ . In mono-dimensional media this abrupt transition is a point of controversy as it is known to occur progressively in 3-dimensions. When  $a$  is of the order of  $3 \text{ \AA}$ ,  $\sigma_{IR} = 700 \text{ S cm}^{-1}$ , often a saturation value for conductivity in rising temperatures.

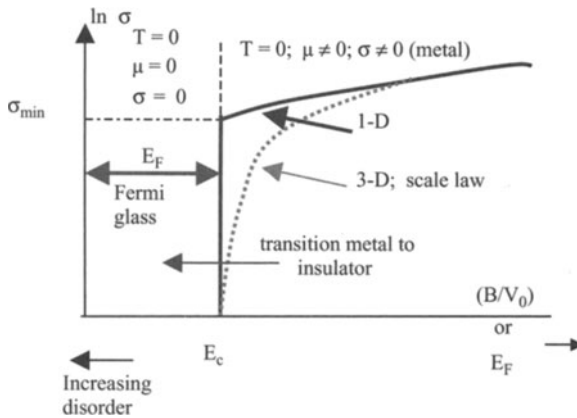


**Figure II-16.** Anderson's transition from metal to insulator at absolute zero following  $1/(V_0/B) = B/V_0$ . The same phenomena occurs as  $E_F$  is displaced from  $E_C$ .

## V Conclusion

The origin of energy bands in a perfect three dimensional crystal, a material which presents a perfect regularity tied to a geometric structure unaltered by any physical reality was presented in this Chapter. In addition, supplementary effects such as dangling bonds, chain ends and holes within the structure were considered. These imperfections introduced into the band gap localised levels which once fluctuated could open to form a band which could split as a function of electron filling, in a manner analogous to the perturbations caused by electron repulsions, which were not taken into account in the band theory.

By introducing modifications of crystal regularity by considering network thermal vibrations (phonons) and defects, both chemical (impurities) and physical (dislocations), the notion of a real crystal was studied. This resulted in determining the free mean pathway of electrons, which could no longer be considered as completely delocalised within the network—as was the case in a perfect crystal. It was shown that an increase in disorder reduced the free mean path length up to the point of localising

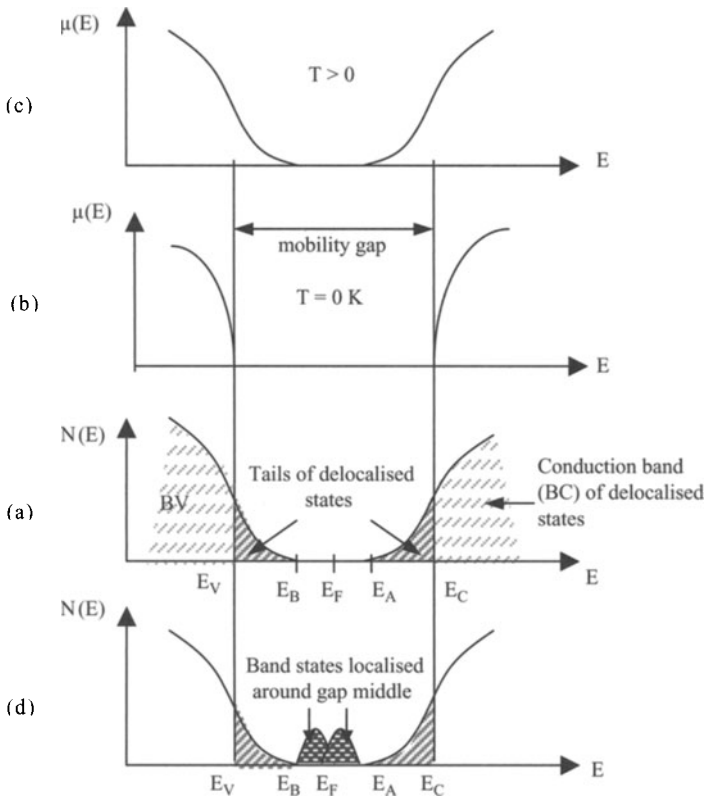


**Figure II-17.** Band models for amorphous semiconductors: (a) following CFO; (b) following  $\mu(E)$  at  $T = 0$  K; (c) following  $\mu(E)$  at  $T > 0$  K; and (d) following that of Mott and Davis.

electrons in neighbourhoods of deep defaults, resulting in energy levels localised at extremities, or “tails”, of permitted bands.

Finally, it can be noted that all models postulate for amorphous media such as crystalline semiconductors that there are conduction and valence bands which are or are not separated by a band gap, depending on the all important band tails. And that:

- bands result in part from short range order (from approximations of strong bonds giving rise to bonding and anti-bonding states, *i.e.* valence and conduction bands separated by a band gap) and from disorder created by phonons or impurities shown by tails of delocalised states. Tail states are neutral when occupied in the case of the valence band and when empty in the conduction band. The Fermi level is thus placed in the middle of the band gap, as shown in Figure II-17 and following the model proposed by Cohen, Fritzsche and Ovshinsky (CFO).
- the form of the bands depends on the type of the implicated orbitals. For p or d orbitals, which are less stretched overall into space than s-orbitals, the form of  $N(E)$  is different and the bands are smaller.
- in a perfect crystal, the band gap is an forbidden energy in which  $N(E) = 0$ , while in an amorphous material it is a mobility gap and  $N(E)$  is not necessarily zero but the mobility  $\mu(E)$  however does become zero at  $T = 0$  K (localised states), as shown in Figure II-17-b and c.

By taking into account the disorder caused by not only phonons and impurities but also by structural defects such as dangling bonds and chain ends, additional offsetting defaults localised in the middle of the band can generate two bands at compensating levels (Hubbard’s bands) following the model of Mott and Davis as shown in Figure II-17-d.

# III

---

## Electron and band structures of ‘perfect’ organic solids

### I Introduction: organic solids

#### 1 Context

Here the construction of a band scheme, including permitted and forbidden bands, will be detailed for ‘perfect’ organic solids. ‘Perfect’ means a neutral solid which has no excess charges and no defaults due to impurities, electronic structural defaults such as topological faults associated with quasi-particles or solitons, and no geometrical faults due to dangling bonds or disorder. The latter, however, will be evoked. All these ‘contributions’ will be detailed in Chapter 4. Coming back to the present Chapter, we will limit ourselves to establishing a band scheme model normally used for physical studies of intrinsically, semiconducting inorganic solids without defaults. Network distortion, due to the stabilisation of the electronic structure of polyacetylene, based on ‘perfectly’ alternating single and double bonds of fixed lengths, will however be considered.

#### 2 Generalities

In preparing optoelectronic components, we need to use materials which go beyond being passive such as the organic solids used as insulators. The latter materials, for example polyethylene based on the repeat unit  $-(\text{CH}_2)_n-$  are dielectric and have very high forbidden bands of at least 5 eV, an energy level situated well outside the optical spectrum, disfavours electronic transport. This results from the considerable energy separation between molecular bonding ( $\sigma$ ) and anti-bonding ( $\sigma^*$ ) orbitals joining  $\text{CH}_2$  groups, which is in turn due to considerable axial overlapping of these orbitals allowed by the polymer geometry [Ngu 94] (see also Appendix A-1). We should realise, however, that energy separation between bonding  $\pi$  and anti-bonding  $\pi^*$ -orbitals is relatively small, as lateral orbitals display limited overlapping. The band gap for molecular or polymeric solids containing such orbitals is typically between 1 and 3 eV, a value which permits the use of their optical and electronic transport properties in the domain of optoelectronics.

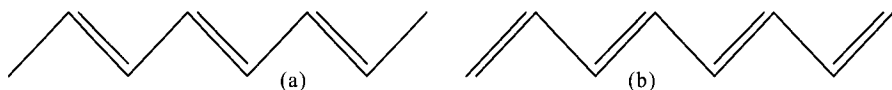


**Figure III-1.** (a) and (b) Energetically equivalent forms of polyacetylene  $-(\text{CH})_x-$ .

Here we will look at organic materials based on polymers displaying  $\pi$ -conjugation and small molecules containing  $\pi$ -bonds. Each material type presents its own advantages and disadvantages.

Polymers often display high thermal stabilities and are generally considered well apt to forming thin films over large surfaces, for example by spin coating. However, this process does require the use of solvents making preparations of films containing more than one coat difficult. In this Chapter we will look at two types of electronic structure of  $\pi$ -conjugated polymers using as examples polyacetylene (Figure III-1) of which the fundamental energy state is degenerate due to two possible configurations, as represented in Figure III-2-a, and poly(*para*-phenylene) (PPP) which is based on the repeat unit structure  $-(\text{C}_6\text{H}_4)_n-$  and, as detailed in Figure III-3-a, has a non-degenerate fundamental energy level. We should also note that the widely used  $\pi$ -conjugated poly(*para*-phenylene vinylene) (PPV), represented in Figure III-3-b, is also non-degenerate.

Materials based on small molecules, however, require evaporation in vacuum chambers and delicate, although now well controlled, handling. New alternative deposition technologies have been developed using ink-jet or roll-to-roll printing. These materials are generally easy to purify, thus reducing reactions and diffusions at electrodes, and can sometimes be better ordered than polymer based materials even to the point of displaying higher charge mobilities, as in the case of crystallised small

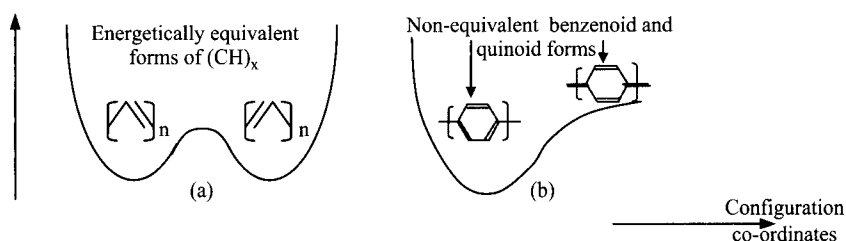


**Figure III-2.** (a) Degenerate  $(\text{CH})_x$ ; and (b) non-degenerate PPP.

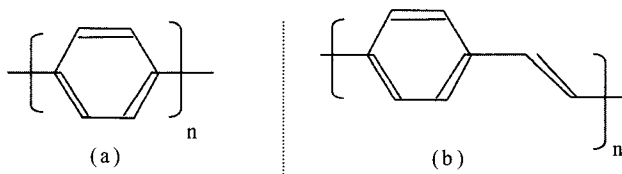


**Figure III-3.** Structure of: (a) PPP; and (b) PPV.



molecules. We will limit ourselves to looking in a more or less qualitative manner at the band structures of two molecules which are widely used:

- 8-Tris-hydroxyquinoline aluminium (Alq<sub>3</sub>) represented in Figure III-4 is an organometallic complex based on a central metal cation co-ordinated with quinolate ligands. To render this material usable in electroluminescence based applications it is prepared as a thin film by evaporation under vacuum, which in itself demands that the complexes have no overall charge and saturated co-ordination numbers [Miy 97]. Alq<sub>3</sub> satisfies this and is the most generally used complex, even if its fluorescent quantum yield is relatively low. It provides films exhibiting good stabilities in electroluminescence and is a good transporter of electrons.
- Fullerene-60 (C<sub>60</sub>) or buckminster fullerene, represented in Figure III-5, is original in that displays a spherical distribution of  $\pi$ -electrons and is constituted of 20 hexagons and 12 pentagons, resulting in each carbon atom being in the same environment and having the same sp<sup>2</sup> hybridisation state (modified by the spherical shape).

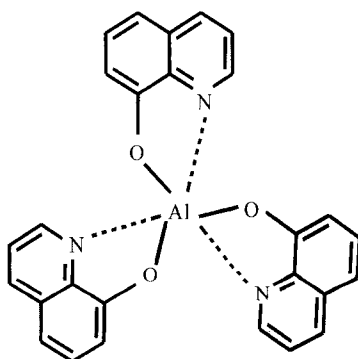


**Figure III-4.** Structure of Alq<sub>3</sub>.



**Figure III-5.** Representation of fullerene-60 showing bond co-ordination.

### 3 Definition of conjugated materials [Ngu 94]; an *aide-mémoire* for physicians and electricians

In the simplest of terms, a conjugated system is one which has alternating single and double bonds. Examples of butadiene and benzene are shown in Figure III-6-a, which has been simplified by excluding bonds to hydrogen atoms. In Figure III-6-a we can see that each conjugated carbon atom has 3 neighbours, with which it forms 3 equivalent  $\sigma$ -bonds resulting from the triangular  $sp^2$  hybridisation of 3 atomic orbitals, which in this example are  $2s$ ,  $2p_x$ , and  $2p_y$ , cf. Appendix A-1, Section II-1-b.

The 4<sup>th</sup> valence orbital of carbon,  $2p_z$ , which is perpendicular to the plane of  $\sigma$ -bonds, undergoes lateral overlapping with other carbon  $2p_z$  orbitals to form  $\pi$ -orbitals. In fact, as shown in Figure III-7-a, the overlap between carbon atoms  $C_1$  and  $C_2$ , and between  $C_3$  and  $C_4$  is dominant, localising double bonds, however, the overlap between  $C_2$  and  $C_3$  is not non-negligible and will lead to a better definition of a conjugated system with laterally overlapping p orbitals.

In Figure-III-7-a there is only 1 orbital at  $C_2$  to assure bonds with neighbouring atoms  $C_1$  and  $C_3$ . There should be 2 orbitals but as there is only 1 we can conclude that there are not enough orbitals or electrons to assure the presence of 2 saturated  $\pi$ -bonds, which require 2 electrons per bond. Similarly, we can see that in the case of graphite shown in Figure III-7-b that at  $C_2$  only a single orbital is present to assure bonds with 3 neighbouring atoms ( $C_1$ ,  $C_3$ ,  $C_4$ ). There are therefore not enough orbitals, as 3 are required, nor electrons, as again 3 are required but only 1 is available, to assure the

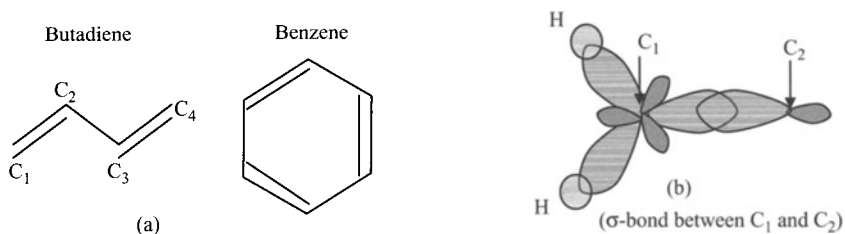


**Figure III-6.** (a) example of conjugated structures; (b) hybrid  $\sigma$ -bond between  $C_1$  and  $C_2$ .

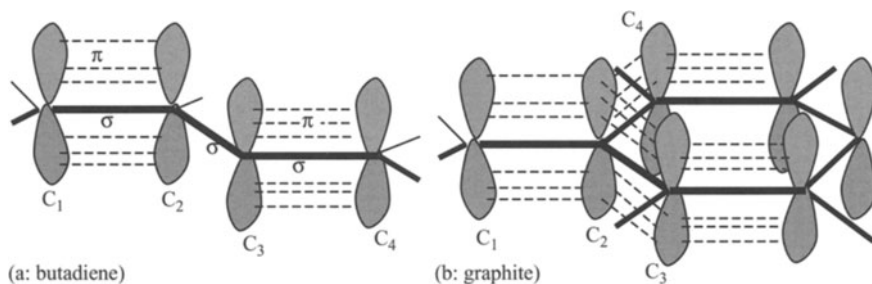


**Figure III-7.**  $\sigma$ - and  $\pi$ -bonds in: (a) butadiene; and (b) graphite (b).

presence of 3 saturated  $\pi$ -bonds. It is this non-saturated character of the delocalised bonds which gives rise to the conductivity of graphite, [Moo 93] associated with an electron cloud between each plane of reticulated atoms.

There are two comments which we can make at this point: (i) a delocalised bond can be defined as one which is common to three or more atoms and displays an equal distribution of electrons; and (ii) qualitatively noting, lateral overlaps, giving rise to  $\pi$ -bonds as shown in Figure III-7 (*cf.* Appendix A-1, Section II), are weaker than axial overlaps which result in the  $\sigma$ -bonds shown in Figure III-6-b. As previously described, the energetic separation between a  $\pi$ -bonding orbital and its corresponding  $\pi^*$ -anti-bonding orbital is less than that between  $\sigma$ - and  $\sigma^*$ -orbitals.

## II Electronic structure of organic intrinsic solids: $\pi$ -conjugated polymers

### 1 Degenerate $\pi$ -conjugated polymers: polyacetylene, the archetypal 'conducting polymer'

Polyacetylene was the starting point for research into conducting polymers developed at the end of the 1970s [Sko 86].

#### a Delocalised $\pi$ -bond structure with unit repetition constant a

Generally speaking, when constructing molecular orbitals, as detailed in Appendix A-1, Section II-1,  $2s^2 2p^2$  carbon states pass *via* an excited state,  $2s 2p_x 2p_y 2p_z$ .  $sp^2$  Hybridisation similarly consists in mixing 1 s-state and 2 p-states, as in our example with the configuration  $2s 2p_x 2p_y$ , resulting in 3 equivalent hybrid orbitals, while having left the 4th orbital ( $2p_z$ ) unchanged. The latter is represented in Figure III-8-a by black spots. We can consider CH units as being linked by  $\sigma$ -bonds formed from a triangular  $sp^2$  hybridisation and represented in Figure III-6-b.  $\sigma$ -Bonds, which assure the structural rigidity of the polymer, give rise to bands of  $\sigma$ -bonding and  $\sigma^*$ -anti-bonding orbitals, which are separated by an appropriately large band gap—given the importance of hybrid orbital interactions. The representation used in Chapter II, Section III for  $sp^3$  orbitals can be used again here in a similar manner for  $sp^2$  orbitals: the  $\sigma$ -bonding orbitals are completely filled by  $3N$   $sp^2$  electrons while  $\sigma^*$ -orbitals are completely empty, so that the electron transport associated with these bands is zero.

As represented in Figure III-8-a, given the geometry of polyacetylene, we can assume that the backbone is one-dimensional relative to  $2p_z$  electrons with unit repetition a. As detailed in Figure III-8-b, with  $N$  carbon atoms in a chain and  $N$   $p_z$  electrons which fill only half of the first band (which can contain  $2N$  electrons as shown in Chapter I, Section VI-2), polyacetylene should behave as a metal (half-filled

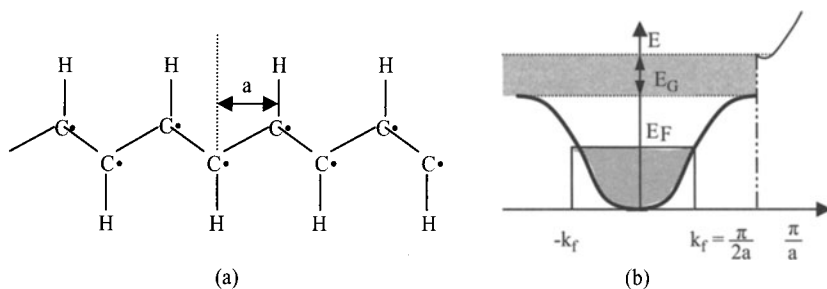


**Figure III-8.** (a) configuration of polyacetylene with unit repetition constant  $a$ ; (b) resulting band scheme, as classically shown, corresponding to a weak bond approximation, however, considering a strong bond approximation yields a similar representation, as shown in Figure I-10 [Mol 88].

last band), however, this is not the case. In order to take into account reality, we need to bring in Peierls distortion, which results in a dimerisation of the chain.

### b Conjugated structure with localised, alternating single and double bonds and repeat unit $2a$

Peierls distortion, in terms of energy, favours dimerised structures, such as shown in Figure III-9-a, in 1-D. As we have seen in Chapter I, Sections V-2 and VI-3, the energy of deformation ( $E_{\text{deform}}$ ) is less than the gain in electron energy following the opening of a band gap ( $E_{\text{relax}}$ ). The unchanged  $\sigma$ -orbitals maintain polymer rigidity, however, the permitted band can only take on  $N$  electrons, as its size has been halved (Figure III-9-b). Therefore,  $N$   $p_z$  electrons from  $N$  carbon atoms remain blocked within this band. We can see that polyacetylene in its natural state is a semiconductor, with a forbidden band gap of the order of 1.5 eV.

Levels associated with defects (solitons) and electronic doping will be detailed in Chapter IV.

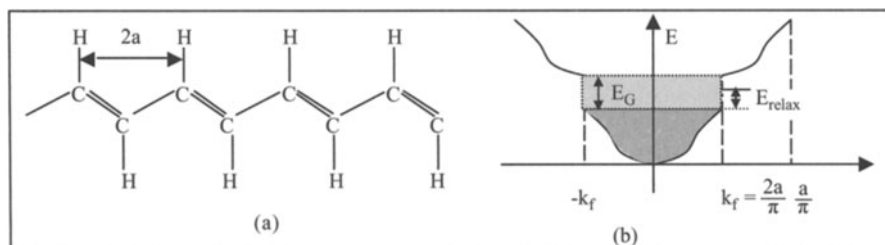


**Figure III-9.** (a) configuration of polyacetylene with period  $2a$ ; (b) band scheme for configuration (a) which can be compared with the representation shown in Figure I-16 of strong bonds.

## 2 Band scheme for a non-degenerate $\pi$ -conjugated polymer: poly(*para*-phenylene)

### a Basics

Here we shall treat PPP, based a chain of benzene rings  $(-\text{C}_6\text{H}_4)_n-$ , in the framework of Hückel theory. We will initially establish the form of the band scheme for an isolated polymer. We will then use techniques previously used for strong bonds, *i.e.* covalent, intramolecular bonds, which are appropriate for organic materials. Intermolecular interactions will not be considered in the initial stages. As mentioned above, overlapping being weaker between  $\pi$ -orbitals than between  $\sigma$ -orbitals, the  $\pi$ - $\pi^*$  separation is weaker than  $\sigma$ - $\sigma^*$  separation. We will thus be limited to studying bands resulting from  $\pi$ - and  $\pi^*$ -molecular orbitals, which correspond to highest molecular orbital (HOMO) and lowest unoccupied molecular orbital (LUMO) bands. These bands, which have an energy interval in which are distributed bonding and anti-bonding states, are thus analogues of valence (VB – the last full band) and conduction (CB – the first empty or partially occupied band) bands, which are traditionally introduced in solid state physics in a band scheme of weak bonds. We shall consider  $\sigma$ -bonds as contributing only a constant bonding force between atoms.

We shall thus obtain a definitive band scheme in three stages:

- in the first stage, we shall determine as simply as possible the energy states of an isolated benzene ring. This can be done by treating the problem in 1-D using results obtained in Chapter I with Floquet's theorem. Appendix A-2, Section II also gives relevant descriptions of  $\pi$ -p and  $\pi^*$ -p orbitals;
- secondly, we shall consider state interactions of a benzene ring within a polymer chain. This will result in a breakdown of  $\pi$  and  $\pi^*$  bands, in a mechanism identical to that detailed in Chapter II, Section III-3 for molecular orbital coupling;
- finally, we shall involve interchain interactions by considering the behaviour of amorphous semiconductors (Chapter II, Section IV), to then propose a definitive band scheme.

### b Energy states and orbitals of an isolated benzene ring

Molecular orbitals of an isolated ring, also considered as a cyclic conjugated polyene, can be obtained by considering linear combinations of atomic orbitals, with Floquet's theorem as detailed by eqn (10) in Chapter I. For a regular system, of repeat unit length  $d$ , molecular orbitals are in the form  $\Psi_k(\vec{r}) = c_0 \sum_s e^{ik \cdot \vec{r}_s} \Psi_s(\vec{r})$  in which functions  $\Psi_s(\vec{r})$  are  $p_z$  type atomic orbitals from 6 benzene carbon atoms each designated by its  $s$  number over which the summation is performed, and  $k$  is determined with the help of Born von Karman cyclic conditions which state that  $\Psi_k(r) = \Psi_k(r + L)$ , in which  $L = Nd$  and being the regular chain length, here containing  $N = 6$  bonds of length  $d$ . Using  $e^{ikL} = 1$  gives  $k$  in terms of  $k_p = 2\pi \frac{p}{Nd} = \pi \frac{p}{3d}$  with  $p$  varying in integers from  $-3$  to  $+3$  corresponding to values in  $k$  from between  $-\frac{\pi}{d}$  and  $+\frac{\pi}{d}$  in the first zone.

Six functions,  $\Psi_k(\vec{r}) = \Psi_{k_p}(\vec{r})$ , associated with 6 energy levels in the form  $E_p = E'_0 + 2\beta_0 \cos(k_p d)$ , correspond to 6 possible values of  $p$  and are represented in Figure III-10, in which are also shown wavefunctions and energy levels for an isolated benzene ring. Here we should note that:

- wavefunctions can be progressive, with one half having propagation in sense  $\psi_{k_p}$ , with the other half in the opposing sense  $\psi_{k_{-p}}$ , or stationary, resulting directly from real and imaginary parts of wavefunctions given by Floquet's theorem (an example is given in Chapter I, Section VII-3). For the energy level  $E_p = \pm 1$ , stationary solutions result in antinodal (real part in cosine) or nodal (imaginary part in sine) solutions in *para* positions;
- $E'_0$  is the Coulombic integral representing energy of a  $2p_z$  electron on a carbon atom, while  $\beta_0$  is the transfer integral, also known as exchange or resonance integral, between two adjacent carbon atoms in the ring; and
- taking spin into account, the energetic separation between HOMO and LUMO is equal to  $2\beta_0$  (empirically determined to be *ca.* 5.5 eV) and the three lowest levels are occupied.

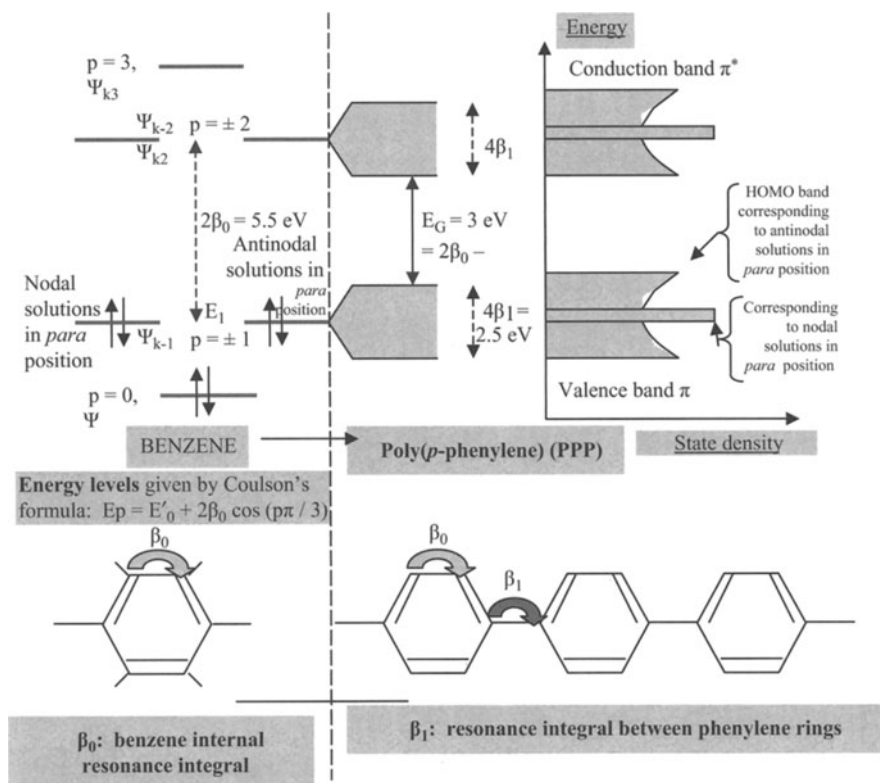


Figure III-10. Energy levels for: left, benzene; and right, PPP.

### c Coupling of orbitals on adjacent polymer rings—generation of $\pi$ - and $\pi^*$ -bands

If we now consider a polymer chain using the inter-ring transfer integral  $\beta_1$  which designates the coupling of adjacent, *para* positioned rings, we have a breakdown of the band of HOMOs and antinodal type LUMOs giving rise to  $\pi$  and  $\pi^*$  bands, each of size  $4\beta_1$ . Evolution of the band scheme can be observed in going from left to right of Figure III-10, and we can also note that energy levels corresponding to nodal solutions for energy levels  $E_1$  and  $E_2$  remain, however, discreet.

Variations in the state density function are shown on the right of Figure III-10, in which we can see an appearance of a clear contribution due to breakdown of  $\pi$ - and  $\pi^*$ -bands (leading eventually to discreet levels corresponding to nodal solutions when stationary solutions are privileged).

While the band gap size of PPP has been experimentally evaluated at 3 eV, the relationship  $E_G = 2\beta_0 - 4\beta_1$  can also be used, given that we can estimate the size of  $\pi$ - and  $\pi^*$ -bands at  $4\beta_1 = 2.5$  eV. These values are well within the order of those determined by electron energy loss spectroscopy.

While this is a rather simplified description of energy levels in PPP, rigorously detailed descriptions can be found elsewhere such as that by J.L. Brédas in [Sko 86] and references therein.

### d Effects due to inter-chain interactions and disorder

We should highlight the fact that the results obtained up to now have only dealt with intra-chain interactions in mono-dimensional models, and that inter-chain interactions, which appear once we reason in 3-D, will modify the results especially at the level of transport processes [Zup 93]. Inter-chain transfer integrals of around 0.1 eV have been obtained for PPV [Gom 93], a polymer with a similar conjugation to that of PPP. We can consider that inter-chain mobilities, which clearly determine to a high degree the total resulting mobility, are thus very much lower. In addition, a sample of PPP normally contains polymers with different lengths of conjugation, and with increasing chain length there is an increase in the distribution size which  $\pi$  and  $\pi^*$  states, situated at band edges, undergo, resulting in bathochromic effects. Of one thing though we can be certain: in using results obtained for amorphous semiconductors, [Sko 86 and Mol 98] these effects will remove the brutal discontinuity observed for an isolated chain at the band edges; instead we will now obtain band tails, resembling those of amorphous semiconductors such as silicon. In addition, as in the case of carbon detailed in Chapter II, Section IV-1, forbidden states in the middle of the band can be added to allow for dangling groups, which can appear especially during thermal (*e.g.* in synthetic procedure) or radiation treatments. We will add these levels to the definitive band scheme after considering electron doping of PPP in Chapter IV.

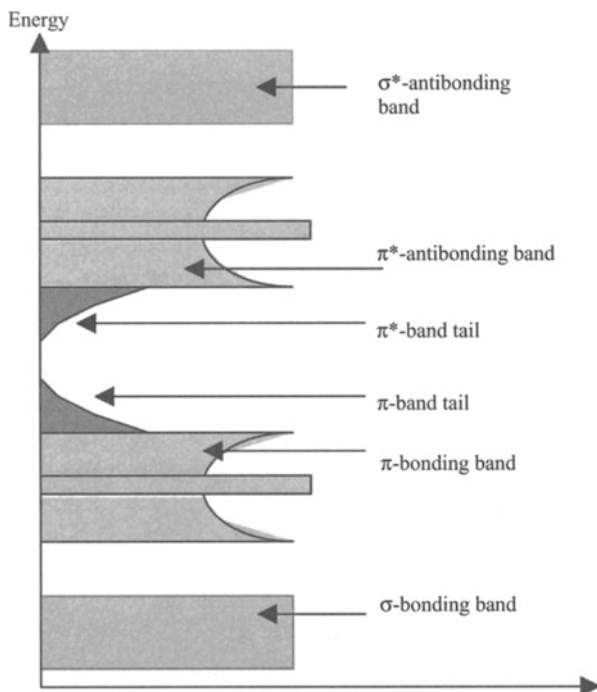


**Figure III-11.** Band scheme for a  $\pi$ -conjugated polymer.

### III Electronic structure of organic intrinsic solids: small molecules

#### 1 Evolution of energy levels in going from an isolated chain to a system of solid state condensed molecules

In polymers, each monomeric unit is joined to its neighbours by strong bonds with transfer integrals  $\beta_1$  which lead to the breakdown of bands (Figure III-10). However, in thin films of small molecules, cohesion is due only to weak Van der Waals forces. The resulting coupling between molecular orbitals is weak due to poor overlapping between orbitals of the molecules in the material. In addition, the greater the distances between molecules, the weaker the interactions between electrons on two neighbouring molecules and the lesser the degeneration observed in going from an isolated to condensed state by valence electrons. The result is that the bands obtained for molecular solids are not very interactive and are narrow.

In a general, qualitative manner, we can nevertheless indicate the way in which a band gap evolves with respect to the size of a total system of molecules. Note that the term 'small molecules' encompasses benzene, anthracene (3 joined phenyl rings) and even tetracene (4 joined phenyl rings) and the discrete occupied levels increase to such



a point that we have a considerable number of energy states for the HOMO [Pop 82]. Finally, the separation, or band gap, between HOMO and LUMO bands decreases with increasing numbers of rings, just as for polymers in which energy levels become more and more 'dense' as we increase chain lengths. It should be noted that the term 'band' here corresponds simply to an energy interval in which HOMO and LUMO levels are situated, without making any strict reference to a Bloch pseudo-continuum of energy levels. It is interesting to remember though that the state, whether neutral or charged, of solid state molecules equally effects the band gap size; polarisation of the solid by ionised molecules actually decreases the band gap [Pop 82].

Without going into some tedious and highly specialised calculations, we shall limit ourselves to simply indicating the electron band structure for two types of molecular solids:

- Alq3 which is pretty much amorphous and is widely used in the field of electroluminescence; and
- C<sub>60</sub> (in the undoped state is called fullerite and in the doped state is called fulleride) crystallises into a cubic face centred (fcc) pattern and shows great potential for use in photovoltaic systems.

## 2 Energy level distribution in Alq3

### a Generalities

Optical spectra of Alq3 evaporated under vacuum into a thin film (solid state) or in solution (diluted in DMF) have been empirically determined to be more or less identical. This has shown that intermolecular interactions are negligible in the solid state and any corresponding breakdown of bands is reduced. If the inverse were true, then we would observe strong intermolecular interactions and a high degree of delocalisation of charge carriers throughout the medium, with for example electrons or holes readily moving from one molecule to the next giving rise to an increased charge mobility and a consequential increase in the size of permitted bands.

As we are looking at Alq3, a large molecule consisting of a central metal cation tied to 3 surrounding ligands, we shall have to consider internal interactions, including those between ligands. A study has been made using semi-empirical determinations of molecular orbitals and associated energy levels giving a method intermediate between the Hückel and *ab initio* methods, which are normally reserved for small systems serving as 'reference models' [Riv 89].

### b Quantitative results from Alq3 proposed by Burrows *et al*

In considering an isolated molecule of Alq3 and assuming it exhibited equal characteristics to a molecule within a thin film, by ignoring external effects due to weak Van der Waals forces as noted above, energy levels were determined by Burrows *et al* [Bur 96]. HOMO and LUMO band energies were estimated using the semi-empirical ZINDO method, which necessitated the use of various molecular configurations. Calculations indicated that there should be 3 small optical transitions corresponding to

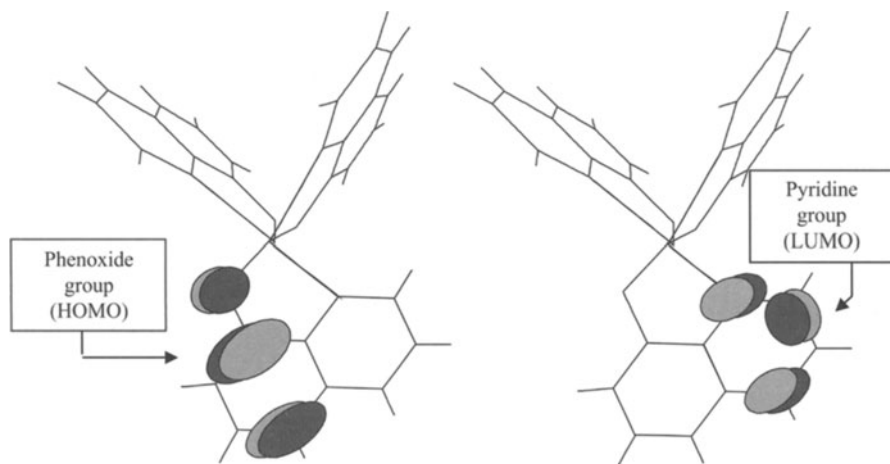


**Figure III-12.** Localisation of full (HOMO) and empty (LUMO) orbitals on Alq3.

wavelengths  $\lambda = 377, 369$  and  $362$  nm equal, respectively, to energies of 3.28, 3.35 and 3.42 eV, and the result was close to that experimentally observed at 385 nm. It was shown in the calculation that two isomers of Alq3 gave very similar results, indicating that solid state thin films of Alq3 are stable, undergoing negligible recrystallisation, and contain both isomers.

Calculations indicated, amongst other things, that  $\pi$ - and  $\pi^*$ -orbitals were localised about quinolate ligands, shown in Figure III-12, and more specifically, full  $\pi$ -orbitals (HOMO) were situated at the ligand phenoxide groups while empty  $\pi^*$ -orbitals (LUMO) were about ligand pyridine groups. The model has been tested and confirmed correct by various studies in which substituents have been placed on the ligands, for example electron accepting groups once placed on the phenoxide group resulted in a bluer emission, in agreement with expected reductions in energy of the highest occupied level.

### 3 Fullerene electronic levels and states

#### a Structure of C<sub>60</sub>

The spherical form of C<sub>60</sub> results from the interstitial placement of 12 pentagons, which never touch, and 20 hexagons, as presented in Figure III-5 [Had 86]. Pentagon sides correspond to simple valence bonds which share from each carbon atom one electron and have length 1.45 Å, while each pentagon is joined *via* double bonds which share from each carbon atom 2 electrons and have length 1.40 Å; each carbon atom is thus shared between one pentagon and two hexagons. Overall, C<sub>60</sub> has strong rotational symmetry consisting of an icosahedral (20 faces) ( $I_h$ ) with six 5<sup>th</sup> order rotational axis, ten 3<sup>rd</sup> order axes, fifteen 2<sup>nd</sup> order axes and one symmetry of inversion.

The full common name of  $C_{60}$  comes from that of American architect Buckminster Fuller who designed similarly structured dome-like buildings.

Double bonds within the structure of  $C_{60}$  result in two particular effects:

- conjugation between pentagons of delocalised  $\pi$ -electrons, resulting in reduced electron-electron repulsions and increased polarisability. The system is highly stable and has an elevated electron affinity, estimated by photoelectron spectroscopy to be around 2.5 to 2.8 eV. Such a value indicates that  $C_{60}$  should be a good electron conductor;
- even considering the non-planar structure, carbon atoms must be considered as undergoing a hybridisation which is part  $sp^2$  and part  $sp^3$  as  $\pi$ -electrons are not purely p type due to the poor pyramidal form of each carbon atom. Accordingly, we shall have to perform a slight 'rehybridisation' of the system by introducing some 2s character (estimated at around 10 %) into the  $\pi$ -orbital.

### b Electronic levels of $C_{60}$ calculated using Hückel approximations

A simple but approximate (given the last remark of the preceding paragraph) method to derive the electronic levels in  $C_{60}$  consists of considering its structure to be based on  $3\sigma$ -bonds and  $1\pi$ -bond per carbon atom. We can see this as an initial step in determining electronic levels of the  $60\pi$ -electrons in the molecule (see also Appendix A-2, Section II).

Hückel's method, briefly considered using a simple example in Appendix A-1, Section II, is based on a method of variations which establishes  $t$  equations determining  $t$  energy levels (each of which may eventually be degenerate) associated with  $t$  electrons in the system. Here,  $t = 1$  to 60. Thus we take following Hückel's approximation (see Section IV-3-b):  $-\alpha = H_{tt}$  and  $-\beta = H_{ts} \delta_{ts}$ , in which  $\delta_{ts} = 1$  if  $s = t \pm 1$  or otherwise  $\delta_{ts} = 0$  which means that only resonance integrals for adjacent neighbours are taken to be non-zero; and that overlap integrals between adjacent orbitals can also be consider negligible. Within the parameter  $-\alpha$ , which has no effect on energy variations, we finally arrive at [Tro 96]:

$$(E_t)_{t=1, \dots, 60} = -\beta \begin{pmatrix} \text{Matrix of} \\ \text{closest} \\ \text{neighbours} \end{pmatrix}$$

The matrix of closest neighbours is that in which the elements are  $(\delta_{ts})_{ts}$  with indices outside the brackets denoting the line and column of element  $\delta_{ts} = 1$ , if  $t$  and  $s$  are first neighbours. A calculation of proper values of this matrix gives the energy scheme, graduated with units in  $\beta$ , shown in Figure III-13. Names given to energy levels originate from corresponding molecular orbitals and their symmetries in group theory.

There are 3 molecular orbitals at  $0.139\beta$  (level  $t_{1u}$ ) and 3 more at  $0.382\beta$  (level  $t_{1g}$ ), so we can expect the molecule to have up to 12 electrons in these levels. The separation of  $h_u$  and  $t_{1u}$  levels can be estimated as  $\Delta E = 0.76\beta$ , while that between  $h_u$  and  $t_{1g}$  is  $\beta$ , and is intermediate to that of anthracene ( $\Delta E = 0.83\beta$ ) and tetracene ( $\Delta E = 0.59\beta$ ).

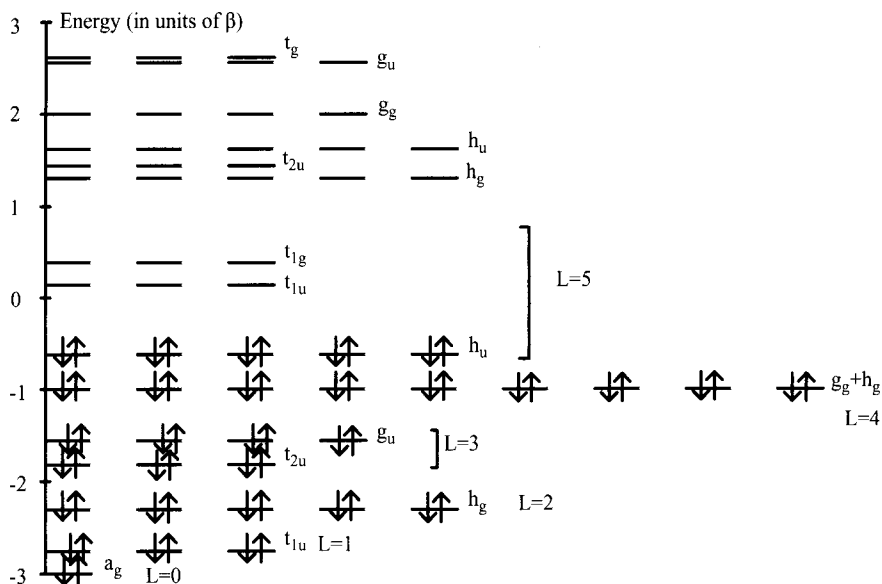


Figure III-13. Energy levels associated with  $C_{60}$  Hückel molecular orbitals

### c Band scheme of solid $C_{60}$

The structure of  $C_{60}$  in the solid state resembles that of a crystal and at ambient temperature centres of gravity of  $C_{60}$ s occupy nodes of a face centred cubic (fcc) structure, however, as a function of time, each molecule turns about its own axis which is randomly and independently orientated with respect to other molecules in the lattice. A molecule can thus be perceived by its neighbours more and more like a uniformly charged sphere.

While strong covalent bonds assure the structure of each individual  $C_{60}$ , only weak Van der Waals forces between each molecule (Figure III-14) assure cohesion. With the overlap of orbitals being poor, the actual energy bands due to accumulated  $C_{60}$  molecules remain narrow. The band derived from the HOMO,  $h_u$ , is a valence band and is completely full, whereas the band derived from the LUMO level,  $t_{1U}$ , is a conduction band and is completely empty. Solid  $C_{60}$  (fullerite) is thus an insulator, or rather, a semiconductor as the band gap is estimated as being somewhere between 1.5 and 1.9 eV (Figure III-15). Formally, a transition between these two bands, of the same u type, is forbidden, however, this selection rule is invalidated by electron-phonon coupling, as has been observed (Chapter VIII).

While the 'band structure' presented in the following Figure III-15 is qualitative, we should remember that in the solid state, molecular orbitals remain narrow and tend towards those of  $C_{60}$  in an isolated state. It has been observed [Kel 92] that absorption spectra of films of  $C_{60}$  are very similar to those of molecular  $C_{60}$ , underlining the weakness of intermolecular interactions in the solid state. In addition, the similarity

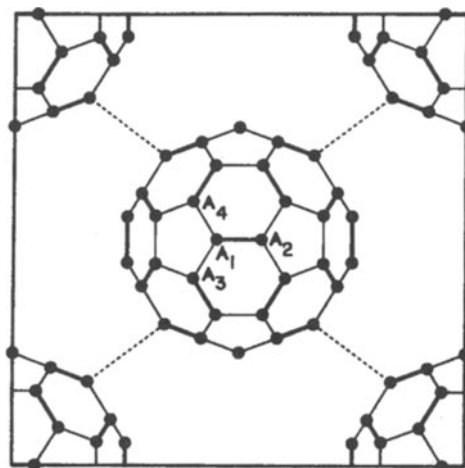


**Figure III-14.** Plan projection (001) of atom position in  $C_{60}$  in solid state structure cfc. Continuous lines, either thick and joining two hexagons as in  $A_1A_2$  or thin and short as in  $A_1A_4$ , represent strong, intramolecular covalent bonds. Dotted lines represent weak, intermolecular Van der Waals.

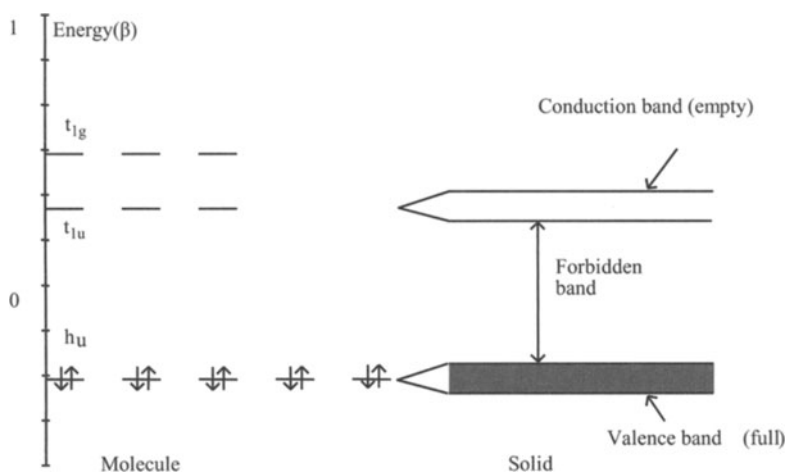


**Figure III-15.** Hückel approximation of the band scheme of solid state  $C_{60}$ .

of spectra obtained for solid state and solvated  $C_{60}$  allowed attribution of solid state bands of energy levels associated with molecular orbitals.

However, ongoing studies are being performed to determine the band structure of  $C_{60}$  in the solid state, their interest being to accurately describe the semiconducting properties of  $C_{60}$ . The calculation methods used are either that of self-consistent field (SCF) or those based on so-called density functions, in particular the approximation

called the Local Density Approximation (LDA). A useful reference for the latter is [Tro 96], and Appendix A-3 details the principle results [Tro 92].

Here we will suffice ourselves with the three main results:

- the band gap can be without an intermediate (at point X in Brillouin's zone, cutting the intersection of the axis  $k_z$  with the upper face of the octahedral and defining Brillouin's zone of the cfc lattice);
- while the band gap has been found to be 1.18 eV [Tro 92], it is more generally estimated to be between 1.5 and 1.9 eV; and
- the greatest valence band size (in X) is between 0.42 eV and 0.58 eV.

## IV Conclusion: energy levels and electron transport

Most of the electronic energy level schemes in this Chapter have been prepared using conclusions from Chapter 1. Within strong bond approximations, for a chain of  $N$  atoms, energies can be written as  $E_p = -\alpha - 2\beta \cos(2\pi p/N)$  in which  $p$  takes on  $N$  integer values such that  $-N/2 \leq p \leq N/2$ , yielding  $N$  values for  $E$ . As shown in Figure I-20, we now know that when  $N$  is low, successive  $p$  energy levels are well separated, and when  $N$  is high, then the spread between different levels is small.

In the limiting case when  $N \rightarrow \infty$ , the cosine argument  $\theta_p = 2\pi p/N$  results in a tendency towards a pseudo-continuity between  $-\pi$  and  $\pi$ ; the electronic spectrum takes on the form  $E_p = -\alpha - 2\beta \cos \theta_p$  and the separation between two successive proper energy values tends towards zero, with a spectrum size which is thus proportional to  $\beta$ . The name 'energy band' is given to proper values of resulting spectra in reference to free or semi-free electrons (weak links  $\Delta E \approx 10^{-7}$  eV  $\rightarrow 0$  for delocalised states). In the more general case in which a chain has a finite length,  $\theta_p$  shows discreet values along with the energy spectrum; a decreasing  $N$  results in an increase in the energy separation between two successive levels to the point at which a pseudo-continuous energy state spectrum can be transformed into a spectrum of discreet energy states. The latter can be observed more easily when it results from small molecules which display a succession of discreet energy states, which may only be slightly enlarged by weak intermolecular interactions (Van der Waals). However, with macromolecules in which  $N$  is large the only the result we can hope for is for an energy band assimilating energy state spectra.

So, in a general and qualitative manner, we can retain from the examples studied that:

- long chains of degenerated polyacetylene with a high value of  $N$  can be considered, using either weak or strong bond approximations, to have to all practical extents a continuous energy band. As we have seen in other cases the energy band is only half-filled with 1  $\pi$ -electron per carbon atom and the material should be *a priori* a conductor, however, a Peierls transition associated with the formation of alternating double and single bands explains its intrinsically insulating character;
- poly(*para*-phenylene), which is non-degenerate, typically displays a conjugation across 10 to 20 phenyl rings. Each ring results in discreet levels which are well

separated (note that for benzene, the band gap between HOMO and LUMO bands is *ca.* 5.5 eV). The coupling between adjacent phenyl rings though results in a breakdown of HOMO and LUMO  $\pi$ - and  $\pi^*$ -bands and results in a band gap of the order of 3 eV between  $\pi$ - and  $\pi^*$ -bands of size *ca.* 2.5 eV;

- Alq3 is an example of a 'small molecule', although relatively speaking it is not actually that small. Semi-empirical calculations (ZINDO) have been used to determine energy levels for an isolated molecule taking into account, at present, 15 configurations in which are included the 15 highest full sites and 15 lowest empty sites. Calculations showed that phenoxide groups were the centre for HOMO levels, whereas pyridine groups had localised LUMO levels. In addition, weak Van der Waals intermolecular interactions do not result in even narrow molecular band breakdowns. This has been indicated by the invariability of spectra of Alq3 in the solid and solvated state, showing no perceptible opening of discrete molecular bands levels. However, when considering electroluminescence, there is a problem in dealing with the continuity (or non-continuity) of energy levels susceptible to receiving injected charge carriers at interfaces. If the energy separation between levels is too great, then there is a risk that any injected charge will not find an accepting energy level. Given the size of the molecule though it is probable that there is a large number of energy levels and consequently energy levels should be sufficiently close to ensure that charge carriers are not blocked. This problem has in fact given rise to some controversies and we will come back to this subject when looking at organic light emitting diodes (OLEDs) in a later Chapter; and
- in fullerene ( $C_{60}$ ) we have a molecule of a not inconsiderable size, thus discrete energy levels can be determined using classical Hückel theory for  $\pi$ -electron based systems.

In Figure III-15, and generalised in Figure III-16, we see that in the solid state small molecules exhibit only a narrow breakdown of levels if intermolecular interactions are weak. As we shall see in Chapter V, charge transport mechanisms and optical

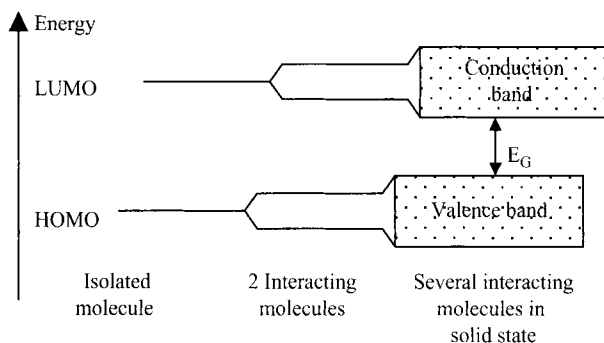


**Figure III-16.** Band structure formation for a molecular system in the solid state in which HOMO and LUMO levels of individual molecules increase in size due to interactions with neighbouring molecules. More these interactions are weak, more narrow the bands become, reducing mobilities.

processes, which control opto-electronic properties, depend directly on the form and nature of energy bands/levels of a medium in the following way:

- if we have a 'pseudo-continuous' band structure, and permitted bands are sufficiently large, then conduction can easily occur between very close levels within bands. This, however, is rarely the case in organic solids;
- if, however, we have a structure in which levels are discreetly spaced, then movement of charge carriers through different energy levels cannot occur without mechanisms allowing barrier crossing, and therefore carrier mobilities and conductivities are reduced. As we have seen before, this similarly applies to narrow permitted bands (see also Chapter II, Section II-2).

We should take note that band structures are actually considerably more complicated than that represented in Figure III-16. Supplementary levels are generated by a wide variety of causes. For example we can construct: discreet levels resulting from dangling bonds; localised levels associated with structural, chemical and other forms of disorder; polaron levels due to lattice localised charges (with a polaron band displaying a specific form of transport); and levels due to traps, or deep wells. Before looking at transport properties in more depth, we shall examine the electronic structure of real organic solids in Chapter IV.



## IV

---

# Electron and band structures of ‘real’ organic solids

## I Introduction: ‘real’ organic solids

In this Chapter we shall complete the band scheme for ‘perfect’ organic solids, obtained in Chapter III, by taking into account electronic contributions in ‘real’ organic solid materials, particularly  $\pi$ -conjugated polymers, due to:

- excess charges either introduced on purpose (doping) or not, including electron-lattice coupling (vibrations) yielding quasi-particles such as polarons or bipolarons;
- topological defaults yielding solitons, including linking of chemical groups;
- structural defaults such as dangling groups due to thermal or radiation treatment, using for example UV or ionic implantation; and
- geometric disorder and its effect on local charges.

From the above, we shall be able to construct a band scheme which, although quite general in nature, will allow us in Chapter V to subscribe to each electronic level appropriate transport processes.

## II Lattice-charge coupling—polarons, bipolarons, polaron-excitons, solitons and their associated energy levels—and $\pi$ -conjugated polymer doping

### 1 Introduction

In this Section we shall look at the effects of introducing excess charges into a distortable organic solid and discover resulting excited states associated with quasi-particles such as polarons, bipolarons, polaron-excitons and solitons which appear depending on the nature of the material under study. We shall define them in

more detail though much later on. Excess charges, either electrons or holes, can be introduced into materials *via* different routes:

- electrical doping by charge transfer from a donor type dopant (n-type) or acceptor (p-type) into an organic solid which is typically a  $\pi$ -conjugated polymer;
- electric field effect doping in which an organic semiconductor or MIS structure (Metal-Insulator-Semiconductor structure) is subject to positive or negative electrical polarisation due to influence from a grill doped with either n- or p-type dopants, respectively;
- unipolar injection of charges into an organic solid using an electrode; and
- bipolar injection of opposed charges (electrons from cathode and holes from anode) which following migration through an organic solid can generate certain quasi-particles.

## 2 Polarons

### a The 'dielectric polaron'

If we take an ionic crystal lattice, as shown in Figure IV-1-a, and then place an electron on an ion, as detailed by the black point in Figure IV-1-b, then we can see that surrounding ions undergo a force due to the additional electron, and this

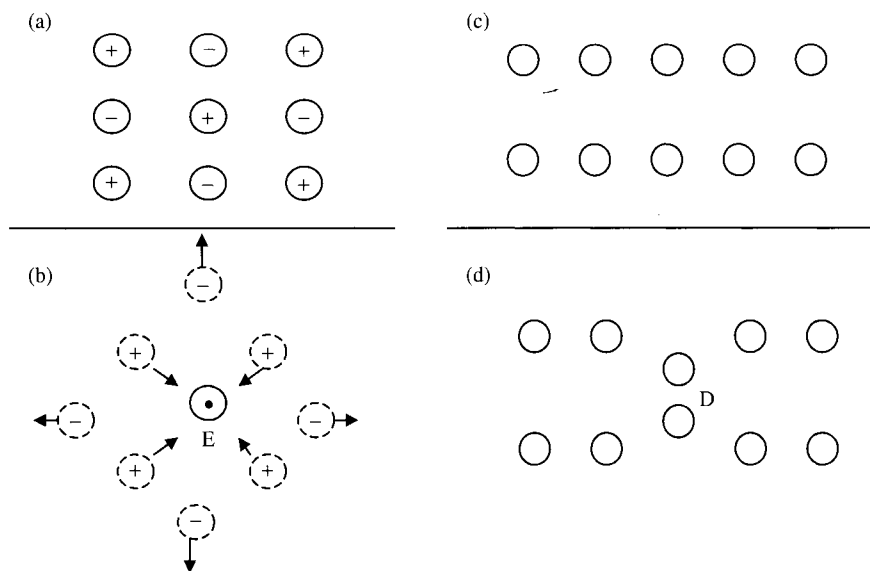


**Figure IV-1.** (a) Lattice of ions in relaxed state; (b) repositioning of ions in directions of arrows following placement of electron at E in the lattice; (c) and (d) polaron formation in covalent materials going from a regular arrangement of rare gas atoms in (c) to a deformed atomic lattice after a hole has been placed at D.

electron-lattice interaction results in a new positions for the ions, as shown in the same Figure by dotted lines. This displacement of ions always results in a reduction of electron energy, and also results in a potential well within which can be found the electron. If the well is deep enough then the electron will find itself in a tied state, incapable of moving to another site unless there is modification in the positions of neighbouring ions. We can label the electron 'self-trapped' and as such, it and its associated lattice deformation is termed a 'polaron'. The term originated from phenomena observed in polar materials, however, such quasi-particles can also occur in covalent materials.

### b Molecular polarons

Molecular polarons form in covalent materials in which the resulting distortion is confined to neighbouring atoms, which can subsequently form a chemical bond while the charge is trapped. A good example is  $V_k$  centres in alkali metal-halogen crystals, in which a hole trapped on a  $Cl^-$  ion results in attracting a neighbouring  $Cl^-$  ion to yield a 'molecular ion' of form  $Cl_2^-$ . Similar phenomena can occur in solid rare gases in which a trapped hole, detailed in Figure IV-1-c and d, and similarly in certain mineral glasses in which dangling bonds at a neutral site ( $D^0$ ) can result in a more favourable local rearrangement such that  $2 D^0 \rightarrow D^+ + D^-$  where  $D^+$  and  $D^-$  are the previously neutral dangling bonds ( $D^0$ ) which have, respectively, lost or gained an electron charge.

We will now go on to detail further the origin of polarons in molecular crystals.

### c Small and large polarons

If the wavefunction associated with a self-trapped electron takes up a space equal to or smaller than the lattice constant, then the polaron is called a 'small polaron' and the deformation is localised only in the neighbourhood of the charge carrier. We shall see this sort of quasi-particle in covalent materials. However, a 'large polaron', sometimes called a 'Fröhlich polaron', is one which forms in polar media in which Coulombic forces are involved and which polarises the crystal along the length of its action. We will not detail the latter polaron (which is covered elsewhere [Cox 87]), and shall essentially consider polarons in molecular or macromolecular media.

## 3 Model of molecular crystals

### a Holstein's model in equation form

Here we shall use molecular crystals to obtain a simple, generalised model for small polarons (following Holstein's model [Hol 59]). We shall consider just one excess electron placed in a regularly aligned but flexible lattice of molecules each of mass  $M$ . With each molecule  $g$  we associate a co-ordinate  $x_g$  which represents the movement of the molecule under harmonic vibration of pulsation  $\omega_0$  with frequency  $\nu_0 = \frac{1}{2\pi} \sqrt{\frac{k}{M}}$ .

We start with a single molecular site, excluding coupling effects with surrounding molecules, on which there is not yet an excess electron. While  $\zeta(r)$  represents the potential energy of an oscillator, the vibration force is  $\vec{F}(r) = -\vec{\text{grad}} \zeta(r)$ . When  $r_0$  is in an equilibrium position, such that  $x_g = r - r_0$  represents the local deformation of a molecule, we have, using a Mac Laurin development,

$$\zeta(r) = \zeta(r_0 + x_g) = \zeta(r_0) + \frac{1}{2} \left( \frac{\partial^2 \zeta}{\partial r^2} \right)_{r_0} x_g^2.$$

The first derivative is in effect zero as  $\zeta(r_0)$  corresponds to a minimum energy position at equilibrium for  $r = r_0$ .

We now have

$$F(r) = -\frac{\partial \zeta}{\partial r} = -\left( \frac{\partial^2 \zeta}{\partial r^2} \right)_{r_0} x_g = -kx_g$$

and with the value of  $k = \left( \frac{\partial^2 \zeta}{\partial r^2} \right)_{r_0}$  given in  $\zeta(r)$  gives  $\zeta(r) = \zeta(r_0) + \frac{1}{2} kx_g^2$ . With  $k$  verifying the harmonic equation

$$F(r) = M \frac{d^2 x_g}{dt^2} = -kx_g,$$

for which the solution  $x_g = X \cos \omega_0 t$  necessitates the introduction of an actual pulsation  $\omega_0 = \sqrt{\frac{k}{M}}$ , we finally obtain  $\zeta(r) = \zeta(r_0) + \frac{1}{2} M \omega_0^2 x_g^2$ .

$\omega_0$  can be estimated for an elongation  $x_g$  of the order of  $a$ , the lattice constant, as vibration energy,  $\frac{1}{2} M \omega_0^2 a^2$ , is of the same order as that of a bond energy  $E_L$  in the molecule and  $E_L \approx 1 \text{ eV}$ . In taking  $a \approx 1 \text{ \AA}$  and  $M = \frac{10^{-3}}{N}$  (hydrogen atom mass  $10^{-3} \text{ kg}$ ), we have

$$\frac{1}{2} \cdot \frac{10^{-3}}{6.02 \times 10^{23}} (10^{-2})^2 \omega_0^2 = 1.6 \times 10^{-19} \text{ J}$$

giving  $\omega_0 \approx 10^{14} \text{ rad s}^{-1}$ . If  $a = 1 \text{ nm}$  though, we now have  $\omega_0 \approx 10^{13} \text{ rad s}^{-1}$  and for heavier atoms, the frequencies are even lower.

On taking into account the coupling between the vibrational movement of a molecule and that of its neighbours, which results in the transfer of vibrational energy throughout the lattice, we have to bring a phenomenon of frequency dispersion  $\omega = f(k)$  into play. The Hamiltonian corresponding to this molecular crystal, into which we have not yet inserted free charges is written [Emi 86] as:

$$H_L = \sum_g \left\{ -\frac{\hbar^2}{2M} \frac{\partial^2}{\partial x_g^2} + \frac{M \omega_0^2 x_g^2}{2} + \sum_h M \omega_0 \omega_b x_g x_{g+h} \right\}$$

in which  $h$  designates the closest neighbour,  $M$  is reduced mass and  $\omega_b$  is the size of the band of optical phonons.

When a supplementary and excess electron is introduced into the lattice we can take account of electron-lattice interactions by considering the excess carrier energy at a site in the lattice. We accept that the energy is a linear function of movements within the lattice, and the greater the induced movement the greater the absolute value of the electron-lattice energy and the more easily that the charge is self-trapped. This trapping is actually be greater than any coupling.

For a carrier localised on a site  $g$ , we can write  $E_g = E_0 - \sum_{g'} f(g' - g)x_{g'}$ , in which  $f(g' - g)$  is a weighting factor which characterises electron-lattice interactions. In assuming that interactions are over short distances in using  $f(g' - g) = A\delta_{g'g}$ , the previous relationship changes to  $E_g = E_0 - Ax_g$ , in which  $E_0$  is the energy of a non-distorted site,  $E_g$  is  $E_0 = 0$  plus a constant and  $A$  represents the electron-site coupling force, as in  $A = -\frac{E_g - E_0}{x_g - 0} = -\text{grad } E$ . In general, we can write  $E_g = E(x_g) = -Ax_g$ .

Thus in the scenario we are considering, molecular deformations induced by the charge carrier are mostly localised around the carrier itself, and it is the presence of vibrational coupling between neighbouring molecules that distribute distortion effects beyond the occupied site. Figure IV-2, otherwise known as an Emin representation, presents a scheme of the distance from equilibrium of diatomic molecules—represented by vertical lines—in a linear molecular crystal about a site with an electron (black dot).

The complete resolution of this problem will require the use of Hamiltonian operators ( $H_e$ ) for strongly bonded electrons in a crystal of covalently bonded molecules, which will add a Hamiltonian for vibrational energies ( $H_L$ ). Results relevant to short range electron-lattice interactions, which we will need to consider here are also discussed in Section 7.1 of [Mol 94].

## b Limiting case of a single molecular site: polaron and bipolaron

$\alpha$  *Polarons and single electrons* In this limiting case we will place 1 excess electron on a single site, the molecule of which undergoes a deformation  $x$ . The potential

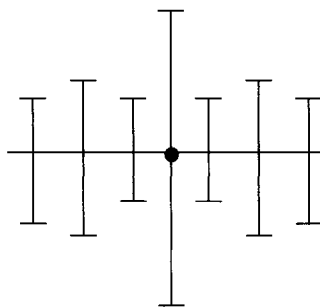


**Figure IV-2.** Scheme of equilibrium separation distances for diatomic molecules in a linear chain, in which an electron (black dot) is placed at the centre of a molecule.

energy of the site can be expressed as:

$$E = \underbrace{M \omega_0^2 \frac{x^2}{2}}_{\text{Vibration energy of molecular site}} + \underbrace{(E_0 - Ax)}_{\text{Energy of electron-lattice interaction (electron-vibration coupling)}} = Bx^2 - Ax \text{ in which } E_0 = 0 \text{ and } B = \frac{1}{2}M\omega_0^2.$$

Vibration energy of molecular site

Energy of electron-lattice interaction (electron-vibration coupling)

Energy when there is no distortion

E is optimised for a value  $x = x_0$  such that

$$\left(\frac{\partial E}{\partial x}\right)_{x=x_0} = 0, \text{ and } M\omega_0^2 x_0 - A = 2x_0 B - A = 0 \iff x_0 = \frac{A}{M\omega_0^2} = \frac{A}{2B}.$$

Following a deformation of the lattice  $x_0$  through vibration and electron-lattice interactions, the energy of electron-lattice interactions is accordingly reduced by  $Ax_0$  ( $-Ax_0$  written algebraically). The system though undergoes a distortion associated with a vibrational energy equal to  $Bx_0^2$  which is such that  $Bx_0^2 = B\left(\frac{A}{2B}\right)x_0 = \frac{1}{2}Ax_0$ .

Overall we can write that energy in the system is reduced by  $E_p$  for which:

$$E_p = Bx_0^2 - Ax_0 = -\frac{1}{2}Ax_0 = -\frac{A}{4B} = -\frac{A^2}{2M\omega_0^2}.$$

Representations of these various energies are shown in Figure IV-3.

Finally we can note that in polar media, the formation of a polaron is highly favoured as the energy 'cost' due to a distortion is less in absolute terms than the energy recovered through a reduction in charge-lattice interactions. The former is actually exactly one half that of the latter.

$\beta$  *Bipolarons and two electrons* Using the model for a single molecular site, we can go on to consider the deformation due to two electrons. System energies can be written:

$$E = \underbrace{M \omega_0^2 \frac{x^2}{2}}_{\text{Vibrational energy}} - \underbrace{2Ax}_{\text{Electron-lattice coupling energy}} + \underbrace{U}_{\text{Coulombic repulsion due to 2 electrons on the same site. We can suppose that } U \text{ varies following } U = U_0 - Cx, \text{ in which } U_0 \text{ is the repulsion at zero deformation.}}$$

On replacing A in the preceding Section by  $2A + C$ , the minimum E is now given by:

$$x = x_1 = \frac{2A + C}{M\omega_0^2} \text{ and } E_{BP} = -\frac{(2A + C)^2}{2M\omega_0^2} + U_0.$$

This system in which there are two electrons localised on a single deformation is called a bipolaron and is stable if the energy required for its formation is less than

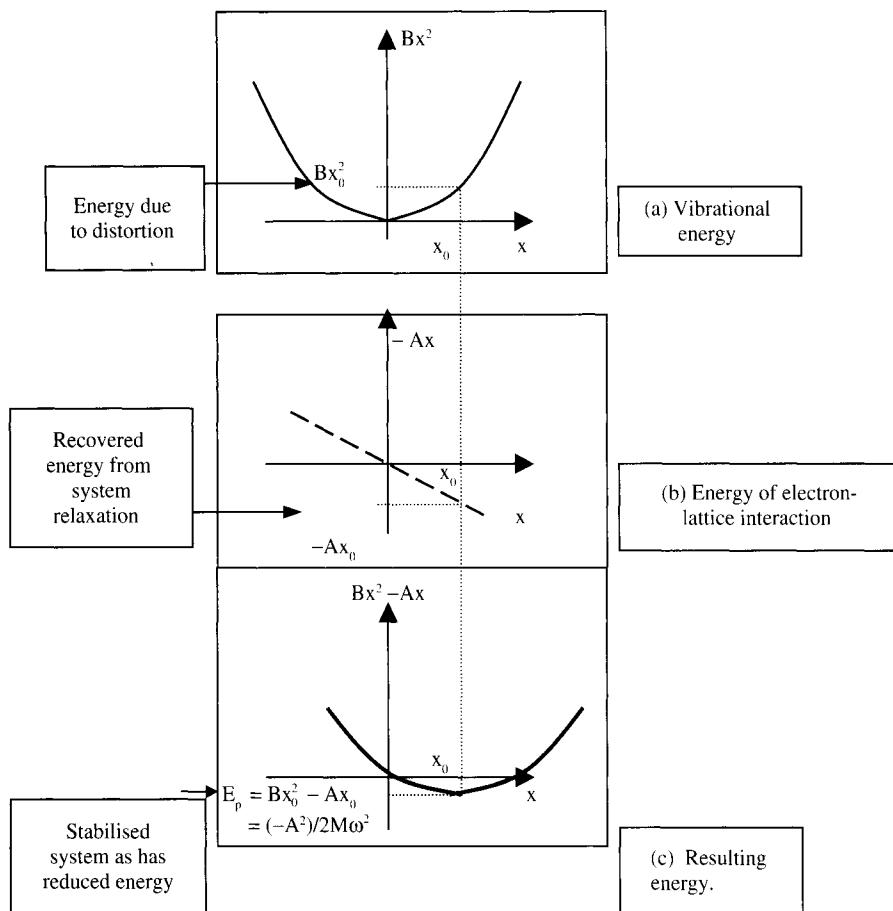


**Figure IV-3.** Different energy terms with respect to lattice deformation by an excess electron.

twice the energy of 2 isolated polarons, *i.e.* when:

$$-\frac{(2A + C)^2}{2M\omega_0^2} + U_0 < -\frac{A^2}{M\omega_0^2}$$

The above relationship can be true when  $A$  and  $C$  are of the same sign and when  $U_0$  is not too high. The deformation  $x_1$  imposed by the two particles (here two electrons, but can also be holes) can be advantageous in overcoming moderate Coulombic repulsions.

#### 4 Energy spectrum of small polaron

As we have just seen, a supplementary electron which distorts a molecule onto which it is placed has an energy reduced by  $-Ax_0 = 2E_p$ , while the vibration energy of deformed molecule increases by  $Bx_0^2 = |E_p|$ , resulting in an overall reduction in

energy for the system equal to  $E_p$  with respect to the energy of an electron in a rigid crystal of molecules, for which  $x_g = 0$ .

Within the limits of the preceding calculation, in which we have ignored vibrational dispersions due to coupling with non-existing neighbouring molecules, we have

$$|E_p| = \frac{A^2}{2M\omega_0^2} \quad (\text{see Figure IV-4}).$$

If we also take into account the possibility that a small polaron (charge carrier and associated lattice deformation) can equally be situated at any other of the geometrical equivalents in a crystal, then we find that the actual states of the system are shared in a polaronic band as shown in Figure IV-4. Using a modified method of that used for strong bond approximations (eqn (2) and following eqns in Chapter II), we can consider that the proper states of a small polaron in a cubic crystal has energy in the form:

$$E_k = -2J \exp(-S)[\cos k_x a + \cos k_y a + \cos k_z a] - E_p,$$

with:

- $k = \sqrt{k_x^2 + k_y^2 + k_z^2}$  as the polaron wavevector, and  $a$  the lattice constant;
- $J$ , the resonance integral between two ‘electronically coupled’ closest neighbours, is in the form  $\exp(-\alpha R)$  to take into account the exponential form of electronic wavefunctions; and
- $\exp(-S)$  is an overlap factor associated with chain vibrations. It represents the superposition integral between two wavefunctions, which detail the vibrational

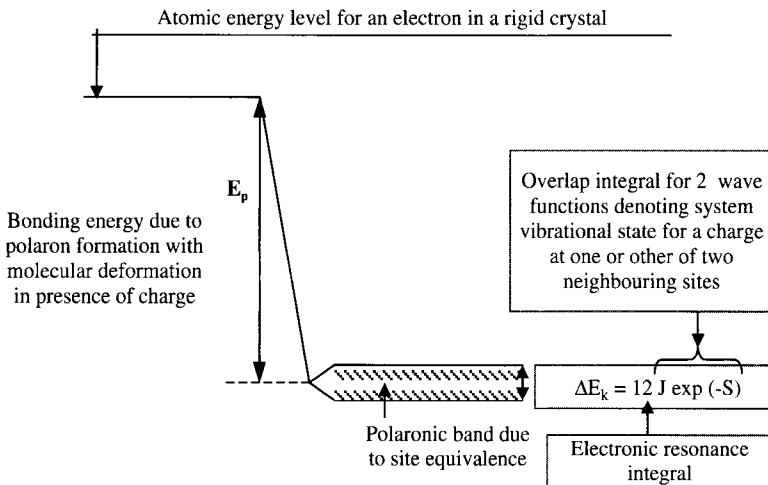


Figure IV-4. Energy scheme for small polaron.



state of the system when the charge carrier is on one or another of two adjacent sites in a crystal. In the limiting case of a rigid lattice, the vibrational wavefunction remains unchanged during charge transfer from one site to its neighbour, and the overlap factor is equal to 1. However, here where we are looking at a distortable lattice, then  $\exp(-S)$  can be considered to relate the necessary overlapping of atomic sites between which the required tunnel effect can occur to allow a complete displacement of atomic site and charge, which is taken into account by  $J$ .

Thinking about it in more depth, we can see that the transfer of a polaron requires in fact two, concomitant tunnelling effects. One is associated with moving a charge between two neighbouring sites (electronic resonance integral), while the other is concerned with displacing the deformation itself and any sites geometrically tied to the deformation.  $\exp(-S)$  is a factor of the same order as the atomic tunnelling effect as we can use it to assimilate atomic site transfers. As it is associated with the high mass of atoms, relative to the charge carriers, its value is extremely low. And thus for a cubic crystal, the polaronic band size is  $\Delta E_k = 12 J \exp(-S)$  and is therefore extremely narrow, of width typically below that of vibrational energies, which are at least  $kT \geq 10^{-4}$  eV at not too low temperatures.

*Comment* We need to remember that displaced deformation is equivalent to an 'exchange' in position for two neighbouring sites. Evidently, it is not two actual atoms which change place but their position relative to the deformation propagated with a charge. However, Figure IV-5 shows how geometrically speaking the exchange is equivalent to an interchange of 2 sites.

## 5 Polarons in $\pi$ -conjugated polymers

Polarons in  $\pi$ -conjugated polymers are of the same type as those we have looked at just above, although local reorganisation can be favoured by there being a stable ionic form of the polymer different to that associated with its neutral state. Here we shall

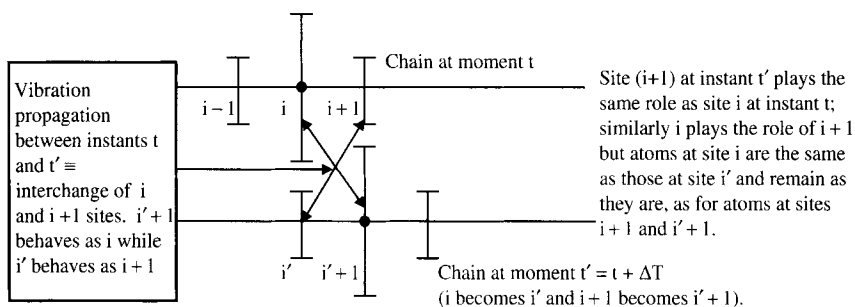


**Figure IV-5.** 'Interchange' of 2 neighbouring sites during vibration (and polaron!) propagation, in which  $i$  and  $i'$  are initial and final states.

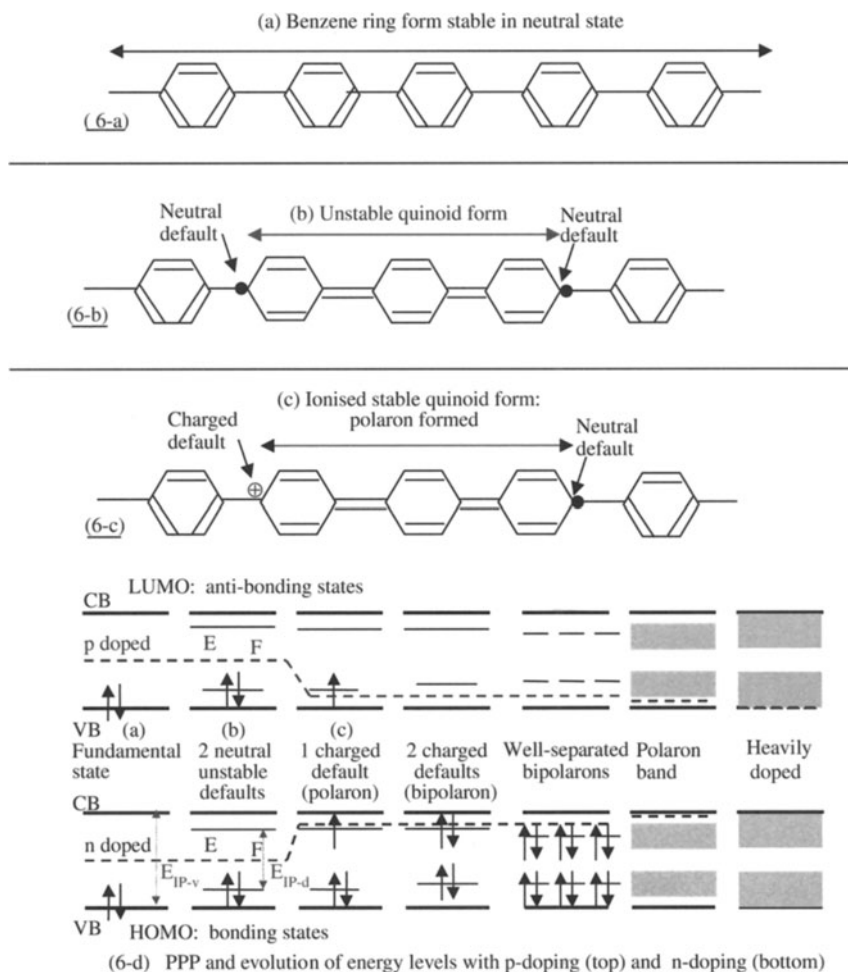


**Figure IV-6.** Representations of: (a) stable benzoic form; (b) unstable quinoid form; and (c) stable once-ionised quinoid form of PPP. Note that to limit Figure size, the distance between defaults has been drawn as 3 benzene rings, instead of 5. Figure (6-d) represents the energy levels corresponding to structures of the: (a) fundamental state; (b) state with two neutral defaults; (c) once-ionised state and then finally to states corresponding to different levels of doping giving rise to simultaneous ionisation of more than one state, with n-doping for negative ionisation (bottom) and p-doping for positive ionisation (top).

use PPP as an example. In the neutral state, the stable structure of PPP is based on benzylic rings, as shown in (a) of Figures IV-6 and IV-7, and as corollary, a structure based on quinoids is unstable, as shown in (b) of Figures IV-6 and IV-7.

As shown in going from Figure IV-6-c to Figure IV-7-c, when a default becomes charged, for example due to charge transfer, a quasi-particle polaron (c) appears.

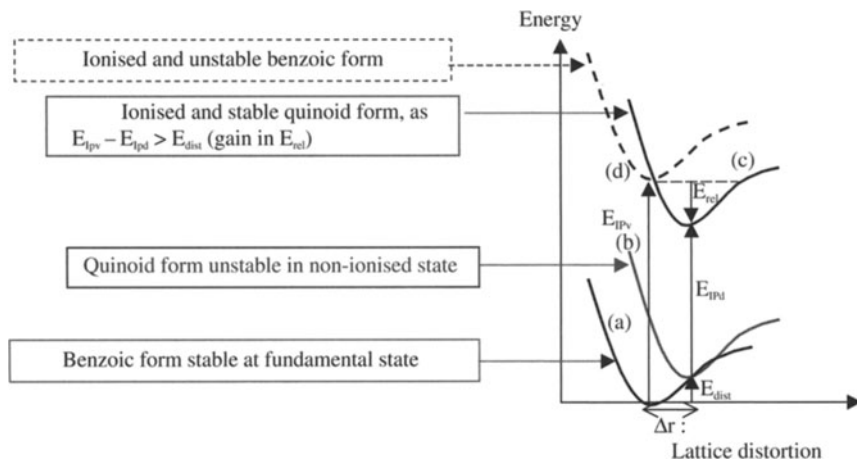


**Figure IV-7.** Configuration curves for PPP chains in neutral and ionised states.

In Figure IV-7 which shows system energy with respect to geometric configuration, we can see that a chain based on quinoids is stable in its ionised state (curve c). In effect, the energy  $E_{dist}$  due to chain distortion in going from benzoic to quinoid forms is more than compensated for by the relaxation energy  $E_{rel}$  which results in going from an unstable ionised benzoic based state (curve d) to the same state based on quinoids (curve c).

Polaron quasi-articles correspond to charge-lattice interactions which self-trap within lattice deformations that they cause. Calculations [Bré 82] have shown that these types of quasi-particles are localised over approximately 5 benzene rings. Figure IV-6 shows a localisation over three rings only, but this is just to limit the actual size of the diagrams—and changes nothing with respect to our understanding of the mechanisms involved.

In Figure IV-6-d we can see the evolution of energy levels with increasing density of introduced charges (doping density) and of the Fermi level, which sits midway between the lowest unoccupied and the highest occupied levels. We can simply note for the moment that levels associated with two neutral defaults (shown in Figure IV-6-b) can be interpreted as coming from a bonding or anti-bonding combination of a non-bonding pair of soliton states situated in the middle of the gap. However, we will look to the actual nature of these sorts of states in Section 7.

## 6 How do we cross from polaron-exciton to polaron?

A simple way of envisaging double electrical charge injection is to think of a positive polaron and a negative polaron which appear opposing electrodes, as shown in Figure IV-8-a and b. With an applied potential field, each polaron migrates across the material towards each other until they eventually meet, at which point they form an excited but neutral species. (The electron and the hole are excited outside of the

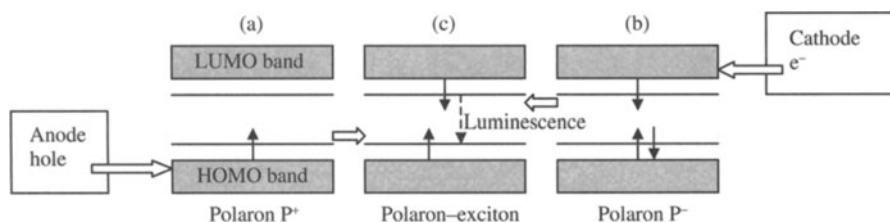


**Figure IV-8.** Electron-hole injecting giving rise to a polaron-exciton.

HOMO and LUMO bands.) It is this species which is called a polaron-exciton and shown as a polaron-exciton singlet in Figure IV-8-c. In later Chapters detailing optical properties, we shall look more fully at the properties of excitons.

Using PPP as the example, Figure IV-9 represents the generation of an intra-chain polaron-exciton (remember also this occurs over 5 rings, but 3 are used here to fit in the representation). We can see that there is a strong coupling between electronic and vibrational excitations as each inserted charge results in a strong geometric distortion of the lattice, which displays a quinoid based structure.

When a radiant combination occurs, sometimes photons with an energy higher than that which separates energy levels of two polarons (or bipolarons) are formed, indicating that lattice coupling and therefore any induced distortions are less than that envisaged by previous models of polarons or bipolarons. The charges which make up the exciton, which is no longer a polaron-exciton (!), are thus tied to each other by an energy of no more than several tenths of an electron volt. This can be due to several factors (which will break any symmetry to the system Hamiltonians) which are subject to numerous controversies [Gre 95, page 46].

## 7 Degenerate $\pi$ -conjugated polymers and solitons [Hee 88]

In defining the soliton, which appears within chains of degenerated polymers such as polyacetylene  $-(CH)_x-$ , we will have defined the complete range of quasi-particles. As shown in Figure IV-10-a, polyacetylene is obtained in the *cis* form directly after its synthesis, however, with increasing temperature it tends towards the *trans* form.

During the isomerisation process, with increasing temperature, faults appear in alternating double and single bonds. These bonds occur during 'dimerisation' as we

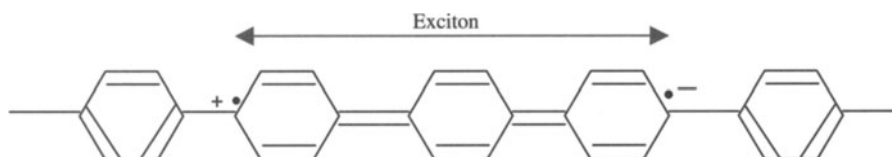


**Figure IV-9.** Representation of intra-chain exciton in PPP.

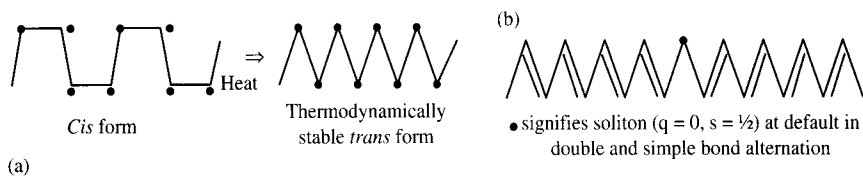


**Figure IV-10.** (a) *Cis – trans* transformation in  $-(CH)_x-$ ; (b) soliton type default in  $-(CH)_x-$  chain.

have seen in Chapter III, Section II-1. Defaults can arise due to the chain being energetically equal on either side, as if two configurations could equally be formed, as is shown in Figure IV-10-b. It has been estimated that such types of defaults can typically form once for every two thousand CH units. The state is, from an energetic point of view, equivalent to a dangling bond, with a  $2p_z$  configuration for the lone electron which makes the soliton shown in Figure IV-11-a. And is therefore midway between  $\pi$ - and  $\pi^*$ -levels, as shown in the left hand side of Figure IV-11-b. As shown on the right hand side of Figure IV-11-b, the Peierls distortion forms a band gap between full and empty bands. Figure IV-11-c shows the state density function where we can see that the soliton (or dangling bond) is situated in the middle of the band gap. The Figure can be compared with that of Figure II-5 for a dangling bond in a tetrahedral carbon system. Overall, the chain remains electrically neutral, as the carbon atom near where the soliton resides is surrounded by 4 electrons. However, the system can give a paramagnetic signal due to the unmatched electron having  $s = \frac{1}{2}$ .

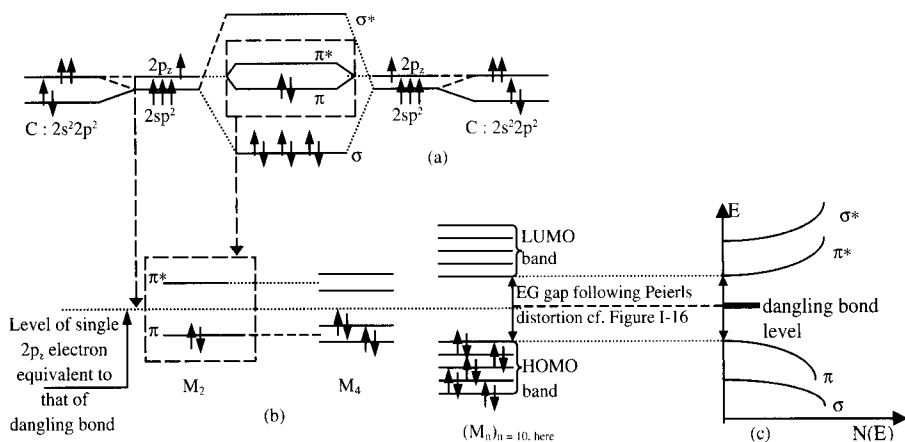


**Figure IV-11.** (a) Representation of bond formation between two groups  $-CH-$ ; (b) energy level evolution with increasing interacting monomers, going from 2 to 4 then to  $n$ ; for a chain of  $n$  monomers Peierls distortion gives rise to gap  $E_G$ ; (c) resulting band scheme generated by Peierls distortion also showing level of dangling bond.

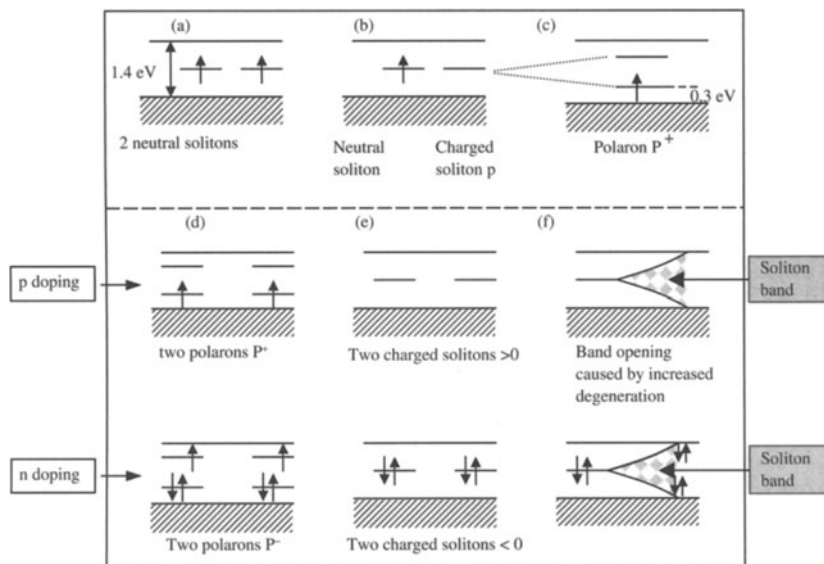


**Figure IV-12.** Energy states favoured during different steps in doping of  $-(\text{CH})_x^-$ , as followed in text.

Now we shall turn our attention to doping effects, with the following dopants: n-type donor (such as alkali metals) which can transfer an electron to  $-(\text{CH})_x^-$ ; and p-type acceptor such as  $\text{I}_2$  or  $\text{AsF}_5$  which are capable of taking an electron from a chain of  $-(\text{CH})_x^-$ . We shall take as example a single chain of  $-(\text{CH})_x^-$  on which there are two solitons corresponding to two excited states, as detailed in Figure IV-12-a. On doping, one of the two solitons is ionised and we thus obtain the associated pair charged soliton-neutral anti-soliton, as shown in Figure IV-12-b. Following their interaction we obtain two levels—one bonding and the other anti-bonding—which correspond to a polaron, and as detailed in Figure IV-12-c is of p-type with an acceptor-type dopant. If we increase the doping, two polarons can be formed as shown in Figure IV-12-d, which give rise to two charged solitons (Figure IV-12-e), and as the doping increases even more, a soliton band will appear and grow until the forbidden band is finally closed by around 30 % w/w of dopant (Figure IV-12-f) [Bré 82].

### III Towards a complete band scheme including structural defaults, disorder and rearrangement effects

#### 1 Which effects can intervene?

As we have just seen, in real organic solids we should account for local interactions due to electronic charges and their associated lattice deformations and vibrations.

In addition, such quasi-particles (polarons, bipolarons and solitons) are characteristic of the sort of doping used, and in contrast to classic covalent semi-conductors based on for example Si or Ge, doping atoms take up interstitial positions rather than substitute atoms in a lattice. The specific electronegativity of dopant atoms, generally alkali metals or halogens, is therefore used to transfer charge to materials such as  $\pi$ -conjugated polymers.

Studies of conduction phenomena have shown that in reality transport properties can be isotropic and therefore charge transport and vibrational energies can only be considered as one-dimensional over short 'local' distances. Hopping mechanisms for inter-chain movement of quasi-particles have been introduced in attempts to account for real effects, such as Kivelson, Brédas or Zuppiroli models for solitons or networks of polarons and bipolarons. Inter-chain transfer integrals have also been introduced. These effects will be discussed when looking at transport mechanisms.

While short range order can be discerned in crystals or certain fibrous polymers, in most materials there is a high degree of long range disorder which generally dominates their properties. We can therefore consider such materials to be amorphous, but recognise that there will be localised states appearing in band tails due to the random distribution of potential wells from electron sites (as shown in the Anderson model). Examples of these can be localised states in between polymer chains or associated with particularly amorphous zones of molecular solids.

## 2 Complete band scheme accumulating different possible effects

### a Construction of density state function

We shall introduce various contributions in order to construct a complete band scheme. Except in one-dimensional media, disorder and electron-lattice interactions do not strictly result in a simple sum of two effects, rather each acts in synergy to produce localised states. Energetically speaking, this can only occur within the energy band gap (polarons) or in the mobility gap (disorder in the case of amorphous semi-conductors) (Emin in [Sko 86]). In order to obtain as general a band scheme as possible (Figure IV-13), we must also associate with the localised states the state density function (Pflüger in [Sko 86] and A Moliton in [Sko 98]) such that:

- the introduced band tails increase with disorder (zones C<sub>5</sub> and C<sub>6</sub> in Figure IV-13); and
- contributions from electron-lattice interactions increase in polaronic or bipolaronic bands with increasing interactions and their electronic effects (zones C<sub>3</sub> and C<sub>4</sub> in Figure IV-13).

On considering the mechanism of charge transport, we can see that charge carriers can be thermally activated towards localised (between which there can be phonon assisted hops) or delocalised (zones C<sub>1</sub> and C<sub>2</sub>) states. The energy involved increases in going from the former to the latter phenomena, and each process appears with an

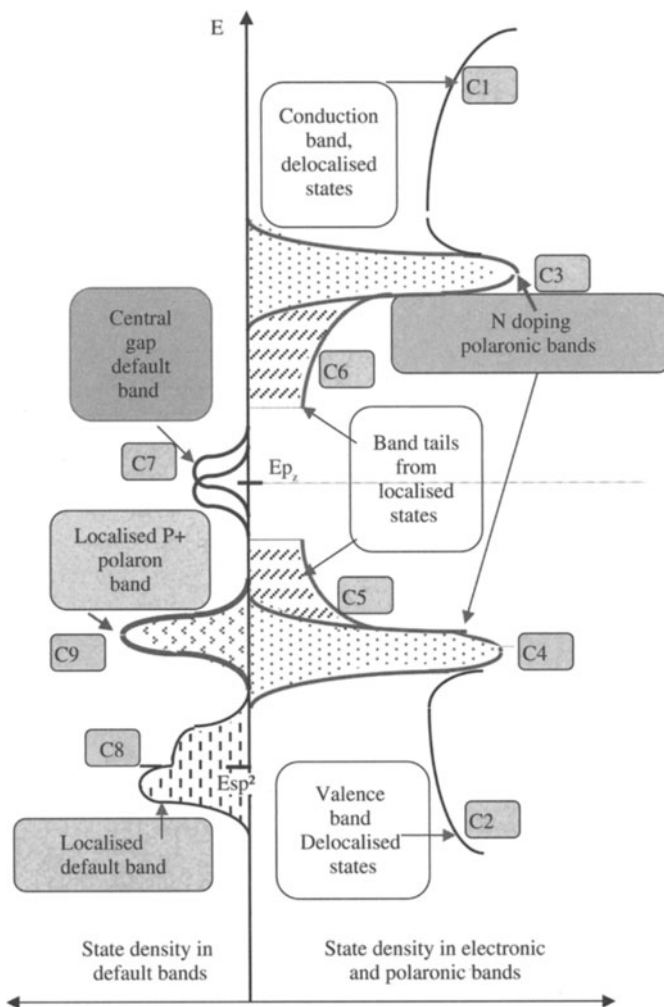


**Figure IV-13.** Band scheme with all envisaged energy levels. To the left are shown state densities resulting from localised defaults i.e. bond ruptures.

increase in temperature. For an intrinsically 'perfect' material the energy is equal, *a priori*, to the half-gap between valence ( $\pi$ ) and conduction ( $\pi^*$ ) bands.

We should note that there can be various perturbations due to thermal effects during synthesis, UV irradiation, ion implantation etc. and structural defaults such as vacancies, dangling bonds or chain ends, which result in conduction mechanisms at the band gap centre. Localised levels are thus introduced (zone C7) of a nature similar to those for carbon in Figure II-5. Geometrical fluctuations, for example changes in bond angles, increase the size of these bands, which in reality split into two bands (Hubbard's bands, zone C7).



### b $\pi$ -Conjugated polymers

As elsewhere detailed for PPP [Mol 98], we can have in reality two types of default bands. Here we shall detail the energy levels formed on combining two carbon atoms which have hybridised states  $2sp^2$   $2p_z$  as shown in Figure IV-11-a. There are  $\sigma$ -bonding and  $\sigma^*$ -antibonding orbitals in addition to  $\pi$ -bonding and  $\pi^*$  antibonding orbitals. If we form an electroactive polymer ( $M_n$ ) from monomer ( $M$ ) containing two carbon atoms, then as the polymer is constructed from alternating single and double bonds the  $\pi$ - and  $\pi^*$  orbitals give rise to HOMO and LUMO bands (Figure IV-11-b) and the resulting state density function represented in Figure IV-11-c. When a default associated with removal of an electron occurs, for example from a dangling bond following chain rupture, localised states which appear depend on the original orbital of the electron, which could be either a  $\pi$ -orbital ( $p_z$ ) or a  $\sigma$ -orbital ( $sp^2$  state) situated (Figures IV-13 and 14), respectively: (i) at the centre of the gap (denoted  $E_p \equiv E_g$ ) separating HOMO and LUMO, and are the only states that we have considered up to now; or (ii) at lower levels than those mentioned in (i) and distributed in the neighbourhood of the primary  $sp^2$  level.

Given that  $(E_p - E_s) \approx 8.8$  eV and that  $E_{sp^2} = \frac{1}{3}(E_s + 2E_p)$ , we have:

$$E_p - E_{sp^2} = \frac{1}{3}(E_p - E_s) \approx 2.9 \text{ eV}.$$

In PPP, the highest point of the valence band is some 1.5 eV below the  $E_p$  level and the state which corresponds to a C–H bond rupture,  $E_{sp^2}$ , is 1.4 eV below the same high point of the valence band, which allows charge transfer to occur from the highest point of the  $\pi$ -band to localised states. This charge transport process results in a decrease in the Fermi level, which otherwise would be at the centre of the gap, placing it nearer the valence band resulting in p-type conduction. Figure IV-14 details evolutions [Mol 94] of energy levels in a band scheme due to generation of dangling bonds (Figure IV-14-b), which can equally induce holes in the valence band (Figure IV-14-c) and can be considered as positive polarons with poor mobility due to their strong lattice attachment resulting from Coulombic interactions with negative charges on the polymer chain, as opposed to chemical doping.

Figure IV-13, which represents the state density function contains not only a default band at the gap centre (zone  $C_7$ ), but due to the inevitability of CH ruptures in polymers, it also has a default band situated at lower energy values (zone  $C_8$  situated around level  $E_{sp^2}$ ).

### 3 Alq3 and molecular crystals

So far in this Chapter we have concentrated on the real behaviour of  $\pi$ -conjugated polymers. Alq3, however, is not much different in its behaviour, as it is now widely thought that polarons do occur in molecular crystals in general (Karl in [Far 01]) as well as specifically in Alq3 (Burrows in [Miy 97]).

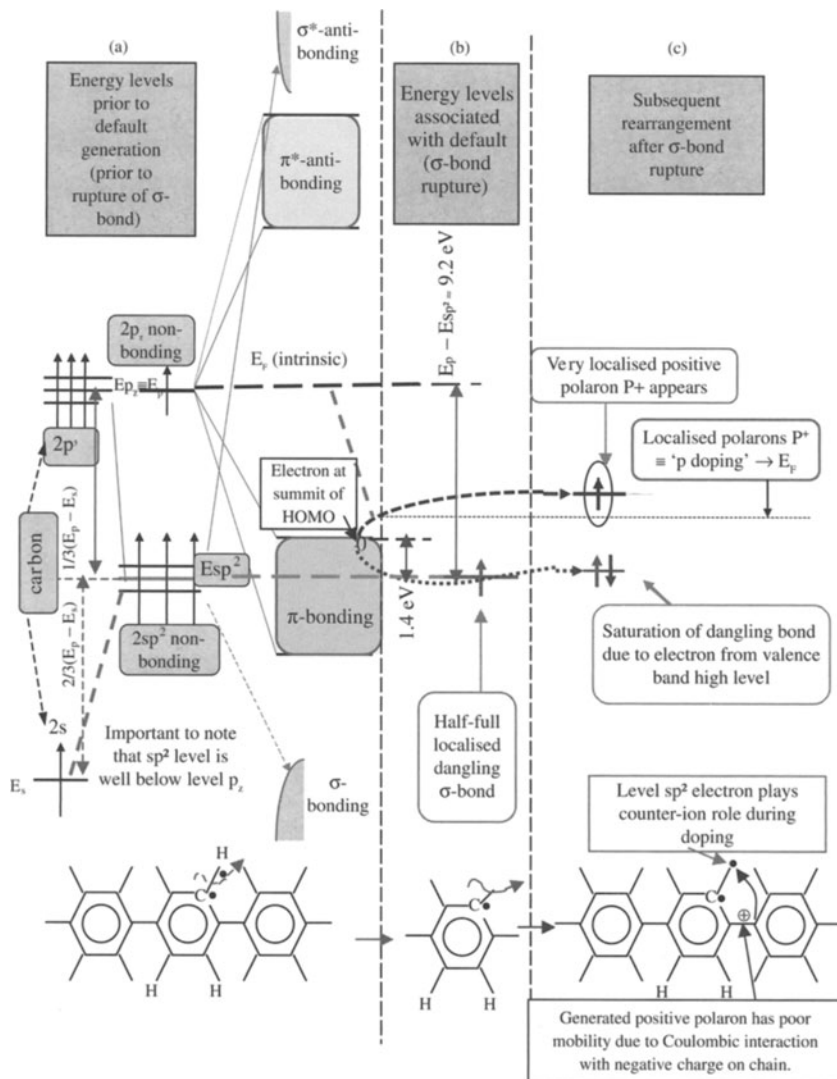


**Figure IV-14.** Energy levels in a  $\pi$ -conjugated polymer which can appear following rupture of C—H or C—C bonds, due for example to thermal effect, irradiation or ion implantation.

### a Structural defects due to a charge presence in Alq3

Structural defects resulting from electron injection into Alq3 which becomes an anion have been studied. According to Chapter III, Section III-2, an injected electron should enter the first empty level localised around pyridine groups. Calculations have shown that Al—O bond lengths should remain unchanged while Al—N bond lengths should change considerably, as the presence of an electron on a quinolate ligand on an

anionic Alq<sub>3</sub> induces an increased interaction with the central cation. The Al—N bond between the host ligand and the central cation should shorten. The host quinolate ligand will though in turn generate repulsions between it and other quinolate ligands due to extra negative charge, and two remaining Al—N ligand bond lengths will accordingly increase.

In order to approximately define the trapping energy associated with an electron injected into Alq<sub>3</sub>, calculations were performed using a neutral Alq<sub>3</sub> of the same geometric structure as its anion. Transition energies 3.07 to 3.20 and 3.34 eV underwent a high red shift of the order of 0.21 eV with respect to the neutral and therefore fundamental state of Alq<sub>3</sub>, representing the electron trap energy depth.

It was also thought by Burrows, in the following manner, that these calculations permitted a further precision of the nature of the traps in Alq<sub>3</sub>. When an electron is localised on a molecule it induces anti-bonding orbital population and the molecule accordingly relaxes into a new structure (Frank-Condon principle). This relaxation towards a lower energy level can be used to automatically trap an electron which could move to a neighbouring molecule through polaronic processes (see Chapter V). Given that there are many possible variants to the Alq<sub>3</sub> structure and accordingly possible calculable energies, due to isomers and thermal vibrations, an exponential breakdown of trap levels leading to distributed levels in the LUMO band is possible. Conduction mechanisms associated with trap levels can therefore appear in otherwise resistive media.

## **b Molecular crystals**

With localisation of a charge carrier, there is a polarisation of its host molecule and its close environment, and due to the influence of a weak (see page 267 of [Pop 82]) polarisation field, the carrier is assimilated with a polaron. When moving, the polaron must overcome a potential barrier associated with potential wells it itself induced in the lattice. Introducing the notion of trap levels, which correspond to distributed localised levels following usual functions (in particular Gaussian), appears necessary once molecular crystals undergo a transition to an amorphous phase, as discussed elsewhere (page 245 in [Pop 82]), and for example observed in vapour deposited thin films of tetracene at  $T < 160$  K.

## **IV Conclusion**

Taking into account all possible electronic levels that appear in an organic solid can at first seem complicated. In order to simplify the complexities presented in Figure III-11, Figure IV-15 sets out practically all envisaged levels for  $\pi$ -conjugated polymers. As for amorphous semi-conductors, we can see that there are foot bands (for  $\pi$ - and  $\pi^*$ -bands) and that states can be just as well associated with any type of disorder, as can charge carriers with the lattice (*i.e.* polarons).

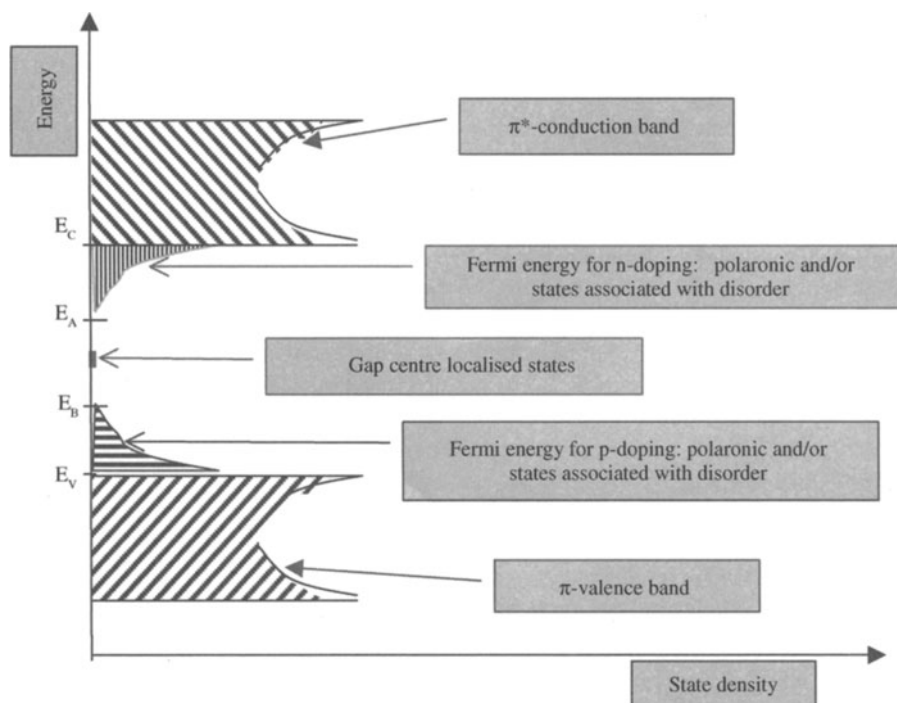


**Figure IV-15.** Simplified band scheme and position of  $E_F$  following doping of  $\pi$ -conjugated polymers.

We shall try and determine the mobility that charge carriers can have in the ‘foot’ or lowest band states. In any case, it must be relatively poor and some of the states tend to behave as though they were like traps in a manner analogous to localised tail band states in amorphous semiconductors. Trap levels and their behaviour will certainly be studied in molecular solids such as  $Alq_3$  and as we have seen here, the existence of the trapping levels is equally associated with a lattice relaxation associated with the charge presence.

Even if it is not possible to consider an universal band scheme for all real organic solids, we can at least now conceive that carrier localisation, on obligatorily distributed energy levels to account for the disorder that each carrier brings, is a common characteristic of these solids. The nature of and treatments to which these materials may be subject (thermal, irradiation) result in a diversity of localised states.

Finally, we can state that transport properties of real organic solids, as in all materials, are conditioned by:

- the position of the Fermi level in the band scheme, as it conditions, along with other effects, the type of transport mechanism which may or may not be thermally active;

- the value of state densities as a function of energy—which determines the number of charge carriers; and
- the nature of these states—on which depends the value and expression of mobility.

We shall now go on to try and define more exactly the laws which characterise the various possible transport mechanisms in Chapter V.

## Electronic transport properties: I Conduction in delocalised, localised and polaronic states

### I Introduction

In this Chapter we shall establish the different laws required for electrical conductivity within a band scheme for organic solids (Appendix A-6 summarises laws for thermoelectrical power). Organic solids can be deemed semiconductors, or in more general terms conductors, especially when considering certain  $\pi$ -conjugated polymers undergoing development at the present time. The laws depend upon the nature of the conduction states involved, which in turn may be due to:

- valence and conduction band delocalised states (HOMO and LUMO bands in strong bonds);
- localised states associated with disorder that governs the depths of wells;
- states localised around the Fermi level in which transport mechanisms by hopping (Hopping to Nearest Neighbour, or HNN) or tunnelling effects (Variable Range Hopping, or VRH) appear; and
- polaronic states due to the localisation of carriers in wells with depths dependent on the ability of the lattice to deform, and with different laws appearing as a function of temperature domain.

The nature of the states implicated in conduction depends on the position of the Fermi level, which is typically situated half-way between the highest occupied level and the lowest unoccupied level. We shall thus describe, with respect to the Fermi level, a scale of energies within a general band scheme in order to characterise the theoretical form of conductivity in each of the states listed above. We shall not go into conduction mechanisms specific to organic solids and insulating states, in which conduction can be limited to space charges and/or intermediate trap levels more normally associated with OLEDs, but rather leave this and conduction limited to electrodes and interfaces to later Chapters.

## II General theories of conduction in delocalised states: Boltzmann's transport equation and the Kubo–Greenwood formula for mobility (see also Appendix A-4)

### 1 General results of conductivity in a real crystal [Qué 88 and Sap 90]: limits of classical theories

The classical theory of conductivity ( $\sigma$ ) was initially elaborated by Drude using a 'billiard ball' model. The relaxation time ( $\tau$ ) (defined as the average interval between two successive collisions undergone by an electron) was assumed to be the same for all electrons, and was used in the following eqn (1):

$$\sigma = \frac{nq^2}{m^*} \tau = \sigma_0 \quad (1)$$

in which  $n$  is the concentration of electrons with effective mass  $m^*$ .

In an alternating field with period ( $\omega$ ), conductivity is given by the relationship

$$\sigma(\omega) = \frac{nq^2\tau}{m^*} \frac{1 - i\omega\tau}{1 + \omega^2\tau^2} \quad (2)$$

The real part is thus written:

$$\sigma_R(\omega) = \frac{nq^2\tau}{m^*} \frac{1}{1 + \omega^2\tau^2} = \sigma_0 \frac{1}{1 + \omega^2\tau^2} \quad (2')$$

and is valid at high frequencies although tends towards  $\sigma_0$  at low frequencies ( $\omega\tau \ll 1$ ).

For a metal, the problem can be resolved in reciprocal space using Fermi–Dirac statistics and globally gives the same result [Qué 88]. If we go on to suppose though that the relaxation time is the same for all electrons, we find that only electrons which have an energy of the order of the Fermi level participate in conduction, remembering of course that the concentration of the  $n$  electrons intervenes in determination of  $\sigma$ . The relaxation time  $\tau$  should indeed be denoted as  $\tau(E_F)$  as it is related to electrons in levels neighbouring  $E_F$  in the case of metals, degenerate semiconductors and semiconductors for which  $E_F$  is in the conduction band.

The hypothesis that  $\tau$  is the same for all electrons, however, is subject to dispute as the relaxation time of any diffused electron depends upon its velocity  $v$ . If  $\sigma_t$  is the section of total efficient diffusion, for isotropic collisions, and  $N$  is the number of particles struck per unit volume, the probability  $P$  of a collision per unit time for an electron at velocity  $V$  is such that [Smi 61]  $P = \frac{1}{\tau} = Nv\sigma_t$ , in which  $\tau$  is the relaxation time such that  $\mathcal{L} = v\tau$ , where  $\mathcal{L}$  is the mean free pathway. Thus, in reality,  $\tau$  depends on  $v$  and thus  $k$ . Equally,  $\tau$  also depends on the direction of electron displacement, and generally can be written in terms of  $\vec{k}$ .

If an electron is diffused by a particle, and the wavevector  $\vec{k}$  varies by a value  $\Delta\vec{k} \ll \vec{k}$ , then the hypothesis that  $\tau = \text{constant}$  is acceptable, however, in the alternate scenario we must take into account the dependence of  $\tau$  on  $\vec{k}$ . In order to perform the required calculations, we can use the state density function ( $N(E)$ ) within energy space.

## 2 Electrical conduction in terms of mobilities and the Kubo–Greenwood relationship: reasoning in reciprocal space and energy space for delocalised states (cf. Appendix A-4)

### a Hypotheses used for calculation

The actual calculations used, detailed in Appendix A-4, were initially developed for inorganic semiconductors. Boltzmann’s transport equation is, however, a semi-classical equation, due to its use of Newton’s law which demands that particles have precisely known positions and moments. In turn we are required to reason in terms of phases in space in which the probability of the presence of a particle is denoted by the function  $f_0(\vec{k}, \vec{r}, t)$ . In addition, quantum mechanics is brought to bear by considering the levels of collisions which are supposed to vary the vector  $\vec{k}$  instantaneously by  $\Delta\vec{k}$  without a variation in the position of charge carriers. From a practical point of view, this results in assuming that the collision duration is negligible with respect to the interval between two collisions for any given particle of energy  $E$ , which corresponds to a value of  $\vec{k}$  given between two collisions.

We should also note that the aforementioned hypotheses of relaxation time is formulated such that following a perturbation the system will revert to its equilibrium, following an exponential law characterised by a relaxation time  $\tau(E)$ . When isotropic collisions occur, it has been shown that the relaxation time is equal to average times between collisions [Lun 00].

### b Formulae for mobility

If the applied field  $E_x$ , with respect to  $O_x$ , is uniform and constant, we obtain for current density ( $J_x$ ), again with respect to  $O_x$ , the following expressions:

- in  $k$  space (from eqn (13) of Appendix A-4):

$$J_x = \frac{q^2 E_x}{4\pi^3 k_B T} \int_k \tau(k) v_x^2 f_0(1 - f_0) d^3k; \text{ and} \quad (3)$$

- in energy space (from eqn (14) of Appendix A-4):

$$J_x = q^2 E_x \int_E \frac{\tau(E) v_x^2}{kT} f_0(1 - f_0) N(E) dE. \quad (3')$$

For isotropic diffusion, in which  $\left(v_x^2 = \frac{v^2}{3}\right)$  and where parabolic energy bands exhibit minimum  $k = 0$ , we can use an approximation of effective mass ( $m^*$ ) which is such that

$$E = \frac{\hbar^2 k^2}{2m^*} = \frac{1}{2} m^* v^2$$



(see Appendix A-4, Section III):

— when  $\tau(E) = \tau$  is constant, we obtain  $J_x = nq\mu E_x$ , in which  $\mu$  is the mobility of charge carrier  $q$  [eqns (16 and 22) in Appendix 4] given by

$$\mu = \frac{q\tau}{m^*}; \quad (4)$$

— when the system is degenerate ( $E_F$  in the conduction band), we obtain to the first order [eqn (23) in Appendix 4]

$$\mu \approx \frac{q\tau(E_F)}{m^*}; \text{ and} \quad (5)$$

— when  $\tau(E)$  corresponds to non-degenerate charge carriers (distributed according to Boltzmann's law)

$$\sigma = \frac{nq^2}{m^*} \langle \tau \rangle, \text{ or } \mu = \frac{q}{m^*} \langle \tau \rangle, \text{ with} \\ \langle \tau \rangle = \frac{\int_0^\infty \tau(E) E^{3/2} \exp\left(-\frac{E}{kT}\right) dE}{\int_0^\infty E^{3/2} \exp\left(-\frac{E}{kT}\right) dE} = \frac{\langle E\tau(E) \rangle}{\langle E \rangle}. \quad (6)$$

This average value for  $\tau(E)$  is sometimes denoted  $\langle\langle\tau(E)\rangle\rangle$  to clearly indicate that it is an average obtained not only from the single component of the distribution function  $N(E) = N(E)f(E) \approx E^{1/2} \exp\left(-\frac{E}{kT}\right)$ , but also from  $EN(E)$ , which can only appear in calculations specific to transport equations.

### c The Kubo–Greenwood relationship

*$\alpha$ -General case*

Eqn (3') permits writing the conductivity in the form:

$$\sigma = q^2 \int_E \frac{\tau(E)v_x^2}{kT} f_0(1 - f_0)N(E)dE, \quad (7)$$

which in turn can be written as the Kubo–Greenwood formula:

$$\sigma = q \int \mu(E)N(E)f(E)[1 - f(E)]dE, \text{ with} \quad (7')$$

$$\mu(E) = \frac{q\tau(E)v_x^2}{kT}. \quad (8)$$

*$\beta$ -Case of isotropic diffusion and the effective mass approximation*

$\left(v_x^2 = \frac{v^2}{3} = \frac{2E}{3m^*}\right)$ : on introducing this expression for  $v_x^2$  and noting that  $\bar{E} = \frac{3}{2}kT$  in eqn (3'), we again obtain the Kubo–Greenwood equation (7') in which

$$\mu(E) = \frac{q\tau}{m^*} \frac{E}{\bar{E}}. \quad (9)$$

Eqn (9), without approximation over  $f_0$ , is more general than eqn (5) which is applicable only to degenerate semiconductors.

### III Conduction in delocalised band states: degenerate and non-degenerate organic solids

#### 1 Degenerate systems

For degenerate systems we must suppose that  $E_F$  enters the conduction band and that we are dealing with ‘metallic’ conductivity. Figure V-1 represents the conduction band in a disordered organic solid with delocalised tail bands. In this degenerate system we can imagine, for example, that the high concentration of charge carriers, which allow the Fermi level to enter the conduction band, is due to a high degree of doping of the  $\pi$ -conjugated polymer which is ‘highly charged’. In addition, in order to imagine a conduction which can occur within a band of delocalised states, we should be using a regime of weak localisation, in other words, the mean free pathway  $\mathcal{L} \geq a$ , and  $V_0/B \leq 1$  (cf. Chapter II, Section IV-3).

#### a Example of a degenerate medium practically without disorder ( $\mathcal{L} \gg a$ )

Conductivity can be expressed using Drude-Boltzmann’s general formula,  $\sigma_B = qn\mu = \frac{nq^2\tau(E_F)}{m^*}$ , in which  $n$  is the concentration of electrons and  $\mu$  is given to the first order by eqn (5).  $\tau(E_F)$  Represents the relaxation time relative to the Fermi level. With  $l = v_F\tau(E_F)$  in which  $v_F$  is the velocity of charge carriers (at the Fermi level) and  $l$  is the mean free pathway we have  $\sigma_B = nq^2l/m^*v_F$ . On introducing the crystalline moment,  $\hbar k_F = m^*v_F$ , we obtain  $\sigma_B = nq^2l/\hbar k_F$ , in which  $k_F$  is the wavevector at the Fermi surface.

If we now consider the system at absolute zero, we can quickly obtain  $n$  as a function of  $k_F$  using reciprocal space. With the number of cells, of volume  $8\pi^3/V = 8\pi^3$  for  $V = 1$ , at the interior of the Fermi sphere being  $([4/3]\pi k_F^3)/8\pi^3$ , and in taking electron spin into account by introducing  $n = 2([4/3]\pi k_F^3)/8\pi^3$  for doubly occupied cells, we obtain metallic conductivity written in the form  $\sigma_B = 4\pi k_F^2 q^2 l / 12\pi^3 \hbar$ . If we set  $S_F = 4\pi k_F^2$  at the Fermi surface, we obtain the following widely used and general formula [Mot 79]:

$$\sigma_B = S_F q^2 l / 12\pi^3 \hbar. \tag{10}$$

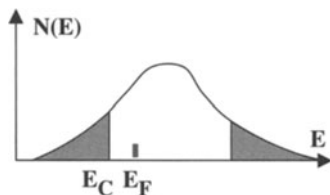


**Figure V-1.** Position of  $E_F$  in degenerate and disordered organic solid for conduction in delocalised states showing conduction band and tails bands of localised states.

**b Low level disorder and the effect of weak localisations ( $\mathcal{L} \geq a$ )**

$\alpha$  *The central principle* Consider first of all the effect of weak localisation of the conductivity detailed just above. If  $\mathcal{L}$  decreases following collisions, multiple diffusions occur. If in addition, the collisions are elastic, generated for example by dopants or impurities spread throughout the material in a random fashion, the wave function ( $\Psi$ ) does not loose its phase memory in a regime of weak delocalisation ( $\mathcal{L} \geq a$ ). Additionally, if  $\mathcal{L}$  is sufficiently large with respect to the wavelength of the wave functions ( $\mathcal{L} \gg \lambda$ ), constructive quantum interference can develop between waves which are following different paths, as shown in Figure V-2. Under these conditions, a backscattering appears along with a diminution in conductivity, which follows the form:

$$\sigma = \sigma_B \left\{ 1 - \frac{C}{(k_F \mathcal{L})^2} \right\}. \tag{10'}$$

To generate the backscattering,  $\mathcal{L}$  must be sufficiently large ( $\mathcal{L} > \lambda$ , or  $\mathcal{L}/\lambda > 1$ , and with  $k = 2\pi/\lambda$ ,  $k\mathcal{L} > 1$ ) to create interferences ( $\delta = m\lambda$  with integer  $m$ ), and yet must also be sufficiently small so that collisions occur to a non-negligible degree, without which  $\mathcal{L} \leq a$  (and  $k\mathcal{L} \leq 1$ ) and we would have a localisation strong enough to provoke a loss in memory of the wavefunction. To sum, this compromise can be reached under a system of weak localisation with  $\mathcal{L} \geq a$ . The quantum interferences are well detailed in [Ger 97], for example.

$\beta$  *Limiting phenomena of quantum interference* Quantum interferences can only occur if the interval between 2 elastic collisions  $\tau$  is much less that that between two inelastic collisions (which modify  $k$  and therefore also the wavefunction phase). The reduction in conductivity decreases when the number of interfering quantum sequences decreases (phonon effect at increased temperatures). The conductivity can then be given by  $\sigma = \sigma_B \{ 1 - C(1 - 1/L)/(k_f l)^2 \}$  [Mot 79].

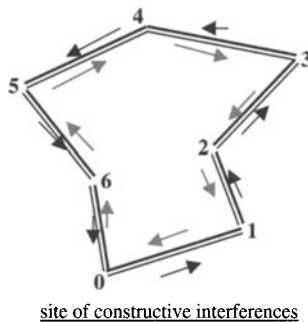


**Figure V-2.** With elastic collisions, two waves corresponding to two directions in a pathway return to 0 in a coherent fashion, resulting in interference, localisation at O and decreasing conductivity.

The term  $(1 - 1/L)$  represents the reduction in diffusion when all collisions are not elastic and  $L$  can represent the length of the sample being studied, the length of inelastic diffusion, or even the cyclotronic radius when a magnetic field ( $H$ ) is applied. In effect, a magnetic field induces a dephasing of trajectories and therefore implicates wavefunctions associated with diffusion transitions; constructive interferences can be made redundant and weak localisation effects diminished; and conductivity increases resulting in positive ‘magneto-conductance’, or rather, negative ‘magneto-resistance’.

We can now consider effects due to variations in potential and reinforcement of disorder. When  $V_0 > B$  or, at the limit,  $V_0 \sim B$ , the state density function exhibits an increase in energy and also a reduction in the state densities denoted by  $g$  for a value corresponding to the band middle (disorder results in state density functions  $N(E)$  being flattened to  $gN(E)$ ). In the principle part of the expression for conductivity—which is proportional to the square of the state density function, as detailed in Eqn 2.18” in [Mol 91]—where a correcting term intervenes,  $q^2$  is replaced by  $(gq)^2$  and thus the conductivity can be written

$$\sigma = \sigma_B g^2 \{1 - C(1 - 1/L)/(gk_f l)^2\}. \quad (16)$$

This last expression for  $\sigma$  corresponds therefore to  $1 \approx a$  and  $V_0 \approx B$ , and relates the expected Anderson transition from metal to insulator. In addition, we can also note that as  $V_0$  increases,  $g$  decreases coherently with conductivity.

### c Law for the variation in conductivity with temperature

It has been shown in 3-D by Altshuler and Aronov, (detailed in Chapter 5 of [Mot 93]) that at low temperatures, where quantum interferences are important, the expression for  $\sigma$  above becomes

$$\sigma = \sigma_B(T_0) + \frac{Ke^2}{4\pi^2\hbar} \left(\frac{kT}{\hbar D}\right)^{1/2} = \sigma_B(T_0) + mT^{1/2},$$

in which  $T_0$  is a reference temperature and  $K$  a constant [Ell 90]. This law is established using  $L = v\tau_i$  and  $\tau_i \propto T^{-p}$ , with  $L$  equivalent to the indice  $i$  corresponding to inelastic collisions which when dominating phonons give rise to  $p = 2, 3$  or  $4$  depending on the temperature. As long distance electron-electron interactions are introduced, a minimum in the state density function results in  $E = E_F$ .

## 2 Non-degenerate systems: limits of applicability of the conduction theory in bands of delocalised states for systems with large or narrow bands (mobility condition)

### a Representation and properties of non-degenerate systems

In non-degenerate systems, the conductivity corresponds to that of a semiconductor, in which  $E_F$  is sufficiently less than  $E_c$  so that an approximation of the Fermi-Dirac function can be made using Boltzmann’s distribution (see Appendix A-4, Section III-2-c).

The Fermi level must therefore be situated midway in the gap between valence and conduction bands (Figure V-3). In analogy to the terminology introduced by Fritzsche [Fri 70] of an ‘ideal amorphous semiconductor’ we are considering an ‘ideal’ system in the sense that we assume that there are no defaults giving rise to numerous, deep states in the band gap. These defaults, localised and degenerated in the gap can arise from impurities and dangling bonds, and the conductivity in these states, often encountered in organic systems, will be detailed in Section 4. Initially we will suppose also that states in the band tails are of low density even if conduction through these delocalised states can occur.

Conductivity can be obtained using the general relationship of Kubo and Greenwood:

$$\sigma = q \int N(E)\mu(E)f(E)[1 - f(E)]dE,$$

which gives eqn (6) for non-degenerate systems.

In a more or less classical fashion, we can equally use the simplifying, following hypotheses:

- $N(E) \approx$  constant in extended states,  $N(E) \approx N(E_C)$
- $\mu$  is zero in the mobility gap  $E_\mu$  and equal to an average value ( $\mu_e$ ) in extended states (with Einstein’s relationship, we can consider that  $\mu_e = \frac{qD_e}{kT}$ ), and thus

$$\sigma = qN(E_C)\mu_e kT \exp[-(E_C - E_F)/kT],$$

following the classical law for semiconductors with

$$\sigma = \sigma_0 \exp\left(-\frac{E_C - E_F}{kT}\right).$$

*Comment 1* In semiconductors, classically speaking, the diffusion constant ( $D_e$ ) is tied to the diffusion length  $L_e$  by  $L_e^2 = D_e \tau_e$ . With  $v_e = 1/\tau_e$  and  $L_e \approx a$ , we have  $D_e = v_e a^2$ . If diffusions are isotropic, *i.e.* equally probable in all 6 directions of a triangular pyramid, we have therefore in one direction  $D_e = (v_e a^2)/6$ . We can also

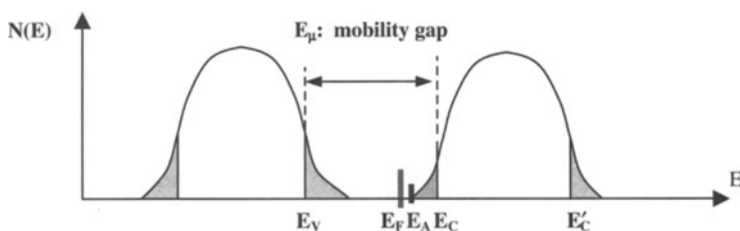


**Figure V-3.** An ‘ideal’ system can induce semiconductivity in delocalised states.

obtain, using the nearest neighbour approximation, as used in obtaining eqn (15) below,  $v_{el} \approx \hbar/ma^2 \approx 10^{15} \text{ s}^{-1}$ .

*Comment 2* In amorphous semiconductors,  $E_C - E_F = \Delta E - \alpha T$  and

$$\sigma = \sigma_0 \exp\left(\frac{\alpha}{k}\right) \exp\left(-\frac{\Delta E}{kT}\right) = C_0 \exp\left(-\frac{\Delta E}{kT}\right)$$

in which

$$\Delta E = E_C(T = 0 \text{ K}) - E_F(T = 0 \text{ K}).$$

We shall now see that, *given the properties of  $\pi$ -conjugated polymers and organic solids*, such as mobility values, band size in terms of the resonance integral  $\beta$ , how *the possibility of conduction through the delocalised band states, developed in II, is barely realisable* [and yields eqn (6) for non-degenerate systems, *i.e.* semiconductors to which approximations for effective masses can be applied].

### b Condition on band size allowing application of effective mass approximation

To define an effective mass, the size of permitted bands ( $B$ ) must be  $B \gg kT$ , otherwise when the band attains a value close to  $kT$  (0.0026 eV at ambient temperature) it is not only the lowest band levels which are occupied but also all levels inside the band due to occupied by thermal effects. The form of the obtained mobility, for a strong bond, is no longer acceptable *i.e.* that of eqn (11) of Chapter II,  $\mu = \frac{q\tau a^2}{\hbar^2} \frac{B}{Z}$ , obtained with the mobility relationship  $\mu = \frac{q\tau}{m^*}$  with a simplified version of  $\tau$  in which was introduced the effective mass  $m^* = \frac{\hbar^2}{Ba^2} Z$  from eqn (8) of Chapter II. So, to obtain an expression for  $m^*$ , we need to use an approximation which involves only the lowest states in the band. Here,  $k \approx 0$  and is centred in the zone for which  $E$  is at a minimum (*i.e.*  $[\frac{\partial E}{\partial k}]_{k \approx 0} = 0$ ), allowing the use of a cosines approximation for energy in a strong bond.

### c Systems for which the permitted band $B$ is large ( $B \gg kT$ ); $\pi$ -conjugated polymers

From the preceding paragraph, we can see that the approximation of effective mass can only be applied to large bands ( $B \gg kT$ ). It is here that the mobility of charge carriers within HOMO and LUMO bands in  $\pi$ -conjugated polymers can be evaluated using

$$\mu = \frac{q\tau a^2}{\hbar^2} \frac{B}{Z}. \quad (11)$$

In addition, we should note that as detailed in Chapter II, Section III-3-B, so that bands conserve a physical significance,  $B > \Delta E$  in which  $\Delta E \approx \frac{\hbar}{\tau}$  [Chapter II,

eqn (20)]. Under these conditions, to obtain conduction in these large delocalised bands, the following should be valid:

$$\mu = \frac{q\tau a^2 B}{\hbar^2 Z} > \frac{qa^2 \Delta E}{\hbar^2 Z} \approx \frac{qa^2}{\hbar} \frac{1}{Z}. \quad (12)$$

The inequality in eqn (12),  $\mu > \frac{qa^2}{\hbar} \frac{1}{Z}$ , is the final condition for conductivity in delocalised bands  $B$ . With  $a$  of the order of several Å, which is about the length of a strong bond in a  $\pi$ -conjugated polymer, and  $Z \approx 2$  we obtain the condition  $\mu > 10^{-1} \text{ cm}^2 \text{ V}^{-1} \text{ s}^{-1}$ . As the typically observed value for conductivity in these polymers is of the order  $\mu > 10^{-4} \text{ cm}^2 \text{ V}^{-1} \text{ s}^{-1}$ , we can conclude that that transport probably does not occur within these delocalised bands.

We have to consider that in  $\pi$ -conjugated polymers any charge mobility due to delocalised states is well reduced by the passage of charge carriers through more localised states, such as intermolecular states. These, for example, include hopping between polymer chains with a pathway possibly tied to interchain polarons, such as 'intrachain or chain-end defaults' which can be due to impurities, faults in conjugation, dangling bonds and traps of all sorts. Mobilities associated with these sorts of transport mechanisms shall be detailed later.

#### d Systems with narrow permitted bands ( $B < kT$ ): small molecules [Wri 95]

Molecular solids, as we have seen in Chapter III, Section III, present narrow permitted bands, as intermolecular interactions operate through weak Van der Waals bonding and a limited overlapping of molecular orbitals. Given the argument presented in the preceding Paragraph b, we find that the effective mass approximation can no longer be applied to an attempt to evaluate charge mobility.

In assuming that any collisions is isotropic and therefore relaxation time is equivalent to the time between two collisions, we can use the general equation for mobility detailed in eqn (8) (see Section II-2). We therefore have  $\mathcal{L} = \tau v_x$ .

We can thus derive (following [Wri 95]) that

$$\mu = \frac{q}{kT} \langle \tau v_x^2 \rangle = \frac{q\mathcal{L}}{kT} \langle v_x \rangle.$$

As  $v_x = \frac{1}{\hbar} \frac{\Delta E}{\Delta k_x}$  [Appendix A-4, eqn (1)], relative to the size of a permitted band we have  $\Delta E \approx B$ , and while  $\Delta k \approx 1/a$  (corresponding to the order of a permitted band of height  $B$  and Brillouin zone in reciprocal space, comparable to the simple representation in Chapter I with  $E = f(k)$ ), we obtain  $v_x \approx \frac{Ba}{\hbar}$ , or in other terms

$$\mu = \frac{q\mathcal{L} Ba}{kT \hbar}. \quad (13)$$

At this level, we can in fact reason in two ways, both of which arrive at reasonable results:

- either that to have a conduction through delocalised states, we need  $\mathcal{L} > a$  (from the second conduction given by Ioffe and Regel, detailed in Chapter III,

Section III-3-b), resulting in the need to verify that:

$$\mu > \frac{qa^2 B}{kT \hbar} \tag{14}$$

And for small molecules with a band size  $B \approx kT$ , we have the same condition as that for the polymers:

$$\mu > \frac{qa^2}{\hbar} \tag{15}$$

On taking  $a \approx 5 \times 10^{-8}$  cm (where  $a$  represents intermolecular distances, which are slightly longer than covalent bonds and we can reasonably assume that  $a^2$  is at least an order of difference greater for small molecules than for polymers), we should have  $\mu \geq 1$  to  $10 \text{ cm}^2 \text{ V}^{-1} \text{ s}^{-1}$ . With  $\mu \approx 1 \text{ cm}^2 \text{ V}^{-1} \text{ s}^{-1}$  and  $a \approx 6 \times 10^{-8}$  cm for anthracene, we do not have the inequality required in eqn (15) *i.e.*  $\mu \geq 5 \text{ cm}^2 \text{ V}^{-1} \text{ s}^{-1}$ ; or

- with the known mobility ( $\mu \approx 1 \text{ cm}^2 \text{ V}^{-1} \text{ s}^{-1}$  for anthracene) and  $B \approx \beta$ , in which the resonance integral for anthracene  $\beta \approx 0.01 \text{ eV}$  with  $a \approx 6 \times 10^{-8}$  cm, we can estimate using eqn (13) that  $\mathcal{L} \approx 3 \times 10^{-8}$  cm. The free mean pathway appears to be considerably less than the intermolecular distance  $a$ , itself incompatible with conduction through delocalised states (Ioffe and Regel).

#### IV Conduction in localised state bands

Here we consider systems with many localised states and corresponding to two particular cases:

- System 1 which classically corresponds to a real (non-ideal), amorphous semiconductor with localised states essentially induced by disorder, thus with a low degree of occupation, such that the Fermi level is below the band tails (Figure V-4) and conduction is in a band of non-degenerated localised states; and
- System 2 which has numerous defaults (such as impurities, dangling bonds and so on) which introduce localised levels deep within the band gap sufficiently occupied by carriers so that the Fermi level is found in this band (Figure V-5) and corresponds to a conduction in a band of degenerated localised states.

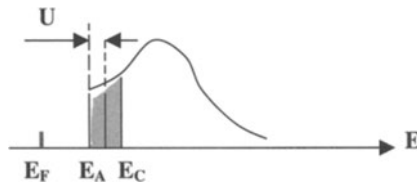
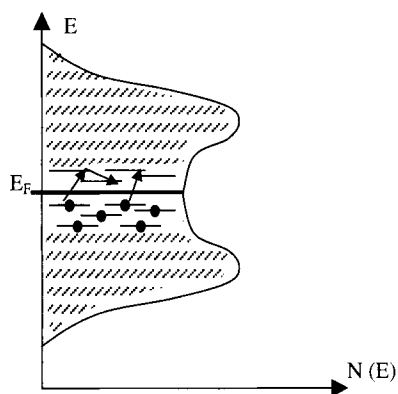


Figure V-4. Position of  $E_F$  in conduction dominated by band tail transport.





**Figure V-5.** Representation of conduction in a band of degenerated, localised states; regions marked with oblique and square lines correspond, respectively, to unoccupied and occupied states.

### 1 System 1: Non-degenerated regime; conductivity in the tail band

In organic solids, and in particular in  $\pi$ -conjugated polymers, disorder effects can result from geometrical fluctuations such as the rotation of a cyclic group or a bond about another bond yielding distortions in a polymer. The resulting fluctuations in potential are, in principal, quite weak (resulting in shallow wells) and operate over relatively long distances. The overall result, throughout the conjugation length of a polymer, is an increase in the distribution of  $\pi$  and  $\pi^*$  states close to band limits. Weak localised states are thus generated at the band edge. The system corresponds to that shown in Figure V-4 which is non-degenerate and  $f_0(1 - f_0) \approx \exp(-[E - E_F]/kT)$ . With wavefunctions being localised, conduction can only occur through thermally activated hops. In each pass from one site to the next, the carrier receives energy from a phonon.

Conductivity is given by Kubo–Greenwood’s functions, as shown in Appendix 5. We still have  $\sigma = q \int \mu(E) f_0(1 - f_0) N(E) dE$ , but this time around,  $\mu = \mu_0 \exp(-\frac{U}{kT})$  and  $\mu_0 = \frac{q\mathcal{L}^2}{\tau_0 kT}$  (see eqn (7), Appendix 5) in which  $U$  represents the energy barrier between localised states and  $\tau_0$  is such that  $\frac{1}{\tau_0} = P_0 = v_{ph}$  in which  $P_0$  represents the probability of a transition from one state to another without an energy barrier (i.e. if  $U$  were equal to zero). Taken into account is the frequency of phonons ( $v_{ph}$ ) which are quasi-particles that stimulate transitions between localised states.  $\mathcal{L}$  corresponds to the mean free pathway between two hops, and in some senses is equivalent to the mean hopping length for localised states conventionally denoted  $R$ .

If we take the typical value for phonon frequency to be  $v_{ph} \approx 10^{13} \text{ s}^{-1}$  and  $U \approx kT$ , we obtain, at ambient temperature, a mobility of the order of  $10^{-2} \text{ cm}^2 \text{ V}^{-1} \text{ s}^{-1}$ , a value lower by two orders than the mobility found in extended states.

Typically, the analytical representation of the band tails is given by a state density function of the form  $N(E) = \frac{N(E_C)}{(E_C - E_A)^s} (E - E_A^s)$  in which  $s = 1$  (linear variation) or  $s = 2$  (quadratic variation). In making  $x = \frac{E - E_A}{kT}$ , and  $\Delta E = E_C - E_A$ , we

obtain [Mol 91]:

$$\begin{aligned} n &= \frac{N(E_C)}{(\Delta E)^s} (kT)^{s+1} \exp\left(-\frac{E_A - E_F}{kT}\right) \int_0^{\frac{\Delta E}{kT}} e^{-x} x^s \exp(-x) dx \\ &= C_s \frac{N(E_C)}{(\Delta E)^s} (kT)^{s+1} \exp\left(-\frac{E_A - E_F}{kT}\right) \end{aligned}$$

in which  $C_s = \int_0^{\frac{\Delta E}{kT}} x^s \exp(-x) dx$  can be calculated by integration of parts with the function  $\Gamma(s + 1) = \int_0^{\infty} e^{-x} x^s dx$ , which is such that  $\Gamma(s + 1) = s\Gamma(s) = s!$ . We finally obtain:

$$\sigma = \sigma_{loc} = \sigma_{01} \left(\frac{kT}{\Delta E}\right)^s C_s \exp\left\{-\frac{E_A - E_F + U}{kT}\right\} \quad (16)$$

with  $\sigma_{01} = qN(E_C)v_{ph} \frac{qL^2}{kT} kT = q^2 N(E_C)v_{ph} R^2$  (here using  $R$  as the classical representation for the mean hopping length), a factor independent *a priori* from  $T$ .

## 2 System 2: degenerate regime; conductivity in deep localised states

System 2 occurs when a material contains a high concentration of defaults and presents a high density of localised states in the band gap. Electronic transport is effected in this band by hopping from an occupied to an empty state with a contribution from a phonon. A high degree of disorder can be introduced by numerous chemical defaults, such as impurities, dopants, (un)saturated dangling bonds and rearrangements following bond rupture (see Chapter IV). The resulting highly localised variations in potential give rise to deep states within the band gap, in which a band of localised states is thus generated about the Fermi level (Figure V-5). Polaron transport will be detailed in the following Section V, and so we will not go into detailing possible lattice relaxations and the formation of highly localised and poorly mobile polarons.

The conduction mechanism in such a band was studied in particular detail for compensated semiconductors, in which a closest neighbour transport mechanism was a dominant feature, and in amorphous semiconductors for which Mott proposed a mechanism based on variable distance hopping. In both cases the transport was effected through two localised levels A and B separated by an energy  $\Delta E$ . Conduction thus corresponded (Figure V-6 (1)) to a thermally assisted ‘hopping’ mechanism *via* a tunnelling effect (2). Except at high temperatures, this transport is favoured, as it only requires energy  $\Delta E$ , with respect to hop ( $H$ ) which, uniquely, is thermally assisted, and necessitates energy  $U \gg \Delta E$ .

In greater detail, the transfer of a carrier from site A to B needs three stages, as shown in Figure V-6:

- Transition 1 in which thermal activation of a carrier between two energetically equivalent levels with the help of phonon energy  $W = \Delta E$  (the two sites A and B appear energetically equivalent to carriers which have this energy);

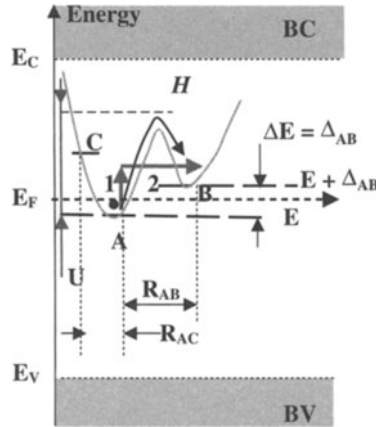


**Figure V-6.** Scheme of transitions during conduction by hopping between localised levels at the order of  $E_F$ .

- Transition 2 for the movement of a carrier through a barrier, and corresponds to a tunnelling effect from one site to another of equivalent energy; and
- an efficient electron-phonon coupling permitting the first step. When  $\Delta E/\hbar$  is larger than the phonon pulsation maximum  $\omega_{\max}$ , the coupling can only occur at the frequency  $\omega_{\max} \approx \nu_{\text{ph}} \approx 10^{12}$  to  $10^{13} \text{ s}^{-1}$ .

**a Conduction due to Hopping to Nearest Neighbours (HNN)**

The probability ( $p$ ) per unit time that a hop will occur between two neighbouring sites A and B is thus a product of the three terms listed just above. The Boltzmann factor,  $\exp(-\Delta E/kT)$ , indicates the probability of transition 1 due to the generation of a phonon with energy  $\Delta E$ . The factor required for transition 2, in which an electron transfers from one site to another, can be expressed as an overlapping factor in the form  $\exp(-2\alpha R)$  with wavefunctions being localised in  $\Psi = \exp(-\alpha R)$ , in which  $R$  represents the spatial distance between adjacent sites and  $\alpha$  the localisation length. The third can be taken into account with  $\nu_{\text{ph}}$ .

Thus, from these three notations, we have:

$$p = \nu_{\text{ph}} \exp\left(-2\alpha R - \frac{\Delta E}{kT}\right). \tag{17}$$

In addition, if  $N(E_F)$  represents the density of states at the Fermi level, and does not vary to a practical degree within the limits  $kT$  about the level  $E_F$ , then  $kT N(E_F)$  represents the electronic concentration in the neighbourhood of  $E_F$  (cf. Appendix A-5, Section III).

In taking eqn (6) from Appendix A-5,  $\mu = \frac{q}{kT} \frac{R^2}{\tau} = pR^2 \frac{q}{kT}$ , Kubo–Greenwood’s relationship gives:

$$\sigma = qkTN(E_F)pR^2 \frac{q}{kT} = q^2R^2\nu_{\text{ph}}N(E_F)\exp\left(-2\alpha R - \frac{\Delta E}{kT}\right). \tag{18}$$

*Comment*

$\mu$  can be evaluated by using Einstein's relationship, *i.e.*  $\mu = \frac{qD}{kT}$ , in which  $D \approx \frac{pR^2}{6}$ . However, this practise is difficult to uphold, as we are dealing with degenerated states, and the latter relationship was strictly established for non-degenerated states.

**b Conductivity according to the Variable Range Hopping (VRH) model**

When  $kT$  attains a 'high enough' value with respect to  $\Delta E$  (typically within a high temperature range), a carrier has enough thermal energy to hop to an empty level of its nearest neighbour. This hop occurs with negligible spatial displacement—following on from the previous HNN model. However, if  $kT$  is of a low value with respect to  $\Delta E$  *i.e.* near low temperatures, the carrier can only hop to energetically close levels, even though they may be spatial speaking far away. *A priori*, the carrier therefore systematically looks for the energetically closest empty level even to the point of disregarding distance. The probability of transitions occurring due to tunnelling effects also diminishes due to an increasingly large barrier. We must therefore look for a compromise which optimises hopping distance giving by the condition

$$\left[ \frac{dp}{dR} \right]_{R' \text{ 'optimised' }} = 0. \quad (19)$$

The value of  $\Delta E$  must therefore be estimated as a function of  $R$ . In order to do this, we can consider that a hop over distance  $R$ , obligatorily, must occur within the volume  $(4/3)\pi R^3$ , and that the number of energy states corresponding to such a hop have an energy of between  $E$  and  $E + dE$  given by  $dN = (4/3)\pi R^3 N(E)dE$ . If we consider only one hop between  $E$  and  $E + \Delta E$  (for  $\Delta E = \Delta_{AB}$ , the length  $R = R_{AB}$ ) and  $dN = 1 = (4/3)\pi R^3 N(E)\Delta E$  (with  $E = E_F$ ), we reach

$$\Delta E = \frac{3}{4\pi R^3 N(E_F)}. \quad (20)$$

In addition, and in agreement with Mott [Mot 79], if we take an average value for  $R$ , the mean hopping distance, then

$$\bar{R} = \langle r \rangle = \frac{\int_0^R \int_0^{\varphi_0} \int_0^{\theta} \Psi^* \mathbf{r} \Psi d\tau}{\int_0^R \int_0^{\varphi_0} \int_0^{\theta} \Psi^* \Psi d\tau} = \frac{\int_0^R \mathbf{r}^3 d\tau}{\int_0^R \mathbf{r}^2 d\tau} = \frac{3}{4} \mathbf{R}, \quad (21)$$

the condition for optimised hops,

$$\left[ \frac{dp}{dR} \right]_{R' \text{ 'optimised' }} \propto \frac{d}{dR} \exp \left[ -\frac{3\alpha R}{2} - \frac{3}{4\pi R^3 kTN(E_F)} \right] = 0,$$

gives:

$$R' \text{ 'optimised' } = R = \left[ \frac{3}{2\pi\alpha N(E_F)kT} \right]^{1/4}. \quad (22)$$

Conductivity, in the form of eqn (18) can thus be written with the optimised value for R:

$$\sigma = \sigma_{VRH} = \sigma_{0v} \exp\left(-\frac{B}{T^{1/4}}\right) = \sigma_{0v} \exp\left(-\frac{T_0}{T}\right)^{1/4}, \quad (23)$$

with

$$\begin{cases} B = B_0 \left[ \frac{\alpha^3}{kN(E_F)} \right]^{1/4}, & \text{in which } B_0 = 2 \left( \frac{3}{2\pi} \right)^{1/4} = 1.66 \\ T_0 = 2^4 \left[ \frac{3\alpha^3}{2\pi kN(E_F)} \right], & \text{and } \sigma_{0v} = q^2 \bar{R}^2 N(E_F) v_{ph} = \frac{9}{16} q^2 R^2 N(E_F) v_{ph}. \end{cases} \quad (24)$$

*Comment*

Eqn (23) comes about through reasoning in 3 dimensions ( $d = 3$ ). The same reasoning with  $d = 2$ , or with  $d = 1$ , can give a general formula eqn (23') in which:

$$\sigma \propto \exp\left[-\left(\frac{T_0}{T}\right)^\gamma\right],$$

with  $\gamma = [1/(d + 1)]$  i.e.  $\gamma = 1/4$  in 3D,  $\gamma = 1/3$  in 2D,  $\gamma = 1/2$  in 1D.

### c Use of Mott's formula (eqn (23))

As  $R^2$  intervenes in  $\sigma_{0v}$ , as in eqn (22), and  $R^2 = f(T^{-1/2})$ , eqn (23) can be rewritten:

$$\sigma = \sigma_{VRH} = \sigma_{0vrh} T^{-1/2} \exp\left(-\frac{T_0}{T}\right)^{1/4}. \quad (25)$$

From which we find that:

$$\begin{cases} \sigma_{0vrh} = A v_{ph} \sqrt{\frac{N(E_F)}{\alpha}}, & \text{with } A = q^2 \frac{9}{16} \left( \frac{3}{2\pi k} \right)^{1/2} \approx 1.54 \frac{q}{k^{1/2}}, \\ T_0 = 2^4 \left( \frac{3}{2\pi} \right) \left[ \frac{\alpha^3}{kN(E_F)} \right] \approx 7.64 \frac{\alpha^3}{kN(E_F)}. \end{cases} \quad (26)$$

These values can be empirically determined from  $\log \sigma \sqrt{T} = f(T^{-1/4})$ , the slope of which is equal, in absolute value, to  $\frac{T_0^{1/4}}{2.3}$ , and the ordinate at the origin ( $T \rightarrow \infty$ ) directly yields  $\sigma_{0vrh}$ . We can thus derive values for  $\alpha$  and  $N(E_F)$ :

- from eqn (27) we have  $N(E_F) = 7.64 \frac{\alpha^3}{kT_0}$ , which used in eqn (26) gives

$$\alpha = \frac{\sigma_{0vrh}}{A v_{ph}} \left( \frac{kT_0}{7.64} \right)^{1/2}; \quad (28)$$

- from eqn (28) in eqn (27) we obtain

$$N(E_F) = \left( \frac{\sigma_{0vrh}}{A v_{ph}} \right)^3 \left( \frac{kT_0}{7.64} \right)^{1/2}. \quad (29)$$

In amorphous silicon (aSi), we thus obtain at ambient temperature  $\alpha = 0.871$  ( $10^{10} \text{ cm}^{-1}$ ), and  $N(E_F) = 3.97 \times 10^{27} \text{ states cm}^{-3} \text{ eV}^{-1}$ .

There are two pertinent comments that can be made at this stage:

- the preexponential coefficient  $\sigma_{0\text{vrh}}$  is often abnormally high, similar to the value of  $N(E_F)$  which we have deduced here. This can result from the value estimated for  $\nu_{\text{ph}}$  in terms of a single phonon transition. B is though pretty much well defined, and reasonably we can fix  $\alpha^{-1} \approx 10 \text{ \AA}$  and thus deduce  $N(E_F)$ . Accordingly we can go on to deduce R optimised (typically *ca.* 80  $\text{\AA}$ ); and
- it is not because the representation  $\ln \sigma\sqrt{T} = f(T^{-1/4})$  is linear that we have Mott's VRH law! We shall see later that percolation 'hopping' can result in the same law.

### d A practical representation of Mott's law for PPP doped by ion implantation

The curve of  $\ln \sigma\sqrt{T} = f(T^{-1/4})$  is shown in Figure V-7 for PPP films, implanted with caesium ions at energies (E) of 30 and 250 keV and flux (D) varying from  $2 \times 10^{15} \text{ ions cm}^{-2}$  to  $10^{16} \text{ ions cm}^{-2}$  [Mor 97]. We can see that the linear law is well adhered to over the temperature range studied, which tends towards low temperatures. Values calculated for  $T_0$  vary between  $3 \times 10^5$  and  $4 \times 10^6 \text{ K}$ , with  $T_0$  tied to  $N(E_F)$  and  $\alpha$  (the inverse localisation length) by eqn (27).

The preexponential factor  $\sigma_{0\text{vrh}}$  generally yields incoherent results [Eil 90]. So, as proposed below, we shall use as a starting point a reasonable value of 1 nm for  $1/\alpha$ , given that interchain distances are around 0.5 nm, in order to determine values

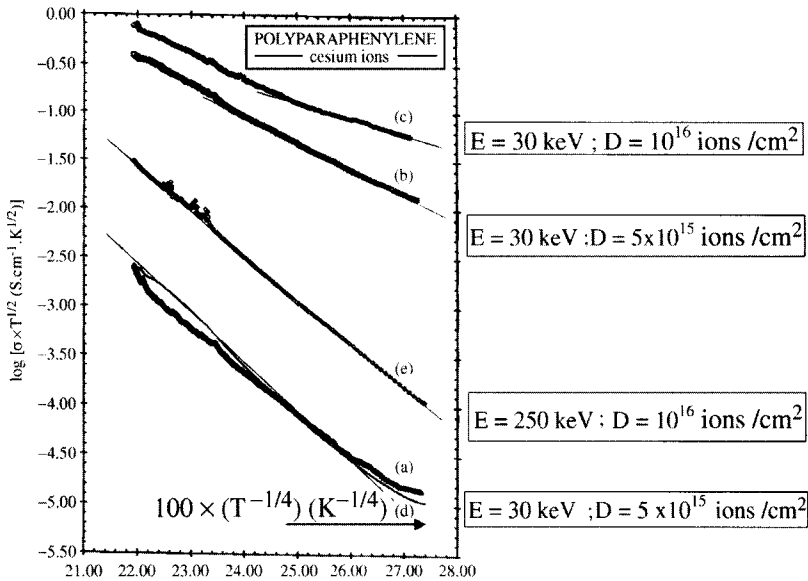


**Figure V-7.** Representation of  $\ln \sigma\sqrt{T} = f(T^{-1/4})$  characteristic of Mott's law for PPP films implanted with caesium ions, with implantation parameters alongside each curve.

for  $N(E_F)$ , which reach from between  $2 \times 10^{19}$  to  $3 \times 10^{20}$  states  $\text{eV}^{-1} \text{cm}^{-3}$ . The result lies is of an acceptable order for localised states associated with a band of deep defaults.

## V Transport mechanisms with polarons

### 1 Displacements in small polaron bands and displacements by hopping

We shall now look at the problem of transport phenomena associated with the displacement of polarons which have an energy spectrum detailed in Chapter IV, Section II-4. Figure V-8 below schematises the corresponding energy levels.

In the scenario in which  $J \neq 0$  ( $J$  is the electronic transfer integral), surplus carriers, *a priori*, are able to move from one site to another within the solid *via* two possible processes:

- The first is called the ‘diagonal’ process and corresponds to a tunnelling effect of a small polaron between adjacent sites with unchanged values for the population of each phonon mode (during transfer of charge between adjacent sites).  $N_q = N'_q$  for all values of  $q$ , in which  $N_q$  and  $N'_q$  are, respectively, numbers of the initial and final occupation states of the phonon and are associated with the  $q$  vibrational mode number. This process corresponds to a simple translation, with a modulus equal or unequal to the footprint of the lattice, the charge carrier and the associated lattice distortion, without changing the vibrational movement of atoms from their equilibrium positions. These processes occur together (tunnelling effect concomitant with the charge and the deformation) with a displacement within the band of the small polaron. The phenomenon is exactly equivalent to that in a non-deformational lattice, in which the occupation of any site by a carrier can be considered using proper states within a Bloch type system. Within the strong bond approximation, the proper values gives rise to a band of size  $12J \exp(-S)$  (for a cubic crystal). The size of the band for a small polaron is particularly narrow, more so if the lattice cannot be deformed ( $\exp(-S) \rightarrow 1$ ), and the mobility of polarons associated with such a process would therefore be very low.
- The second is called the ‘non-diagonal’ process and concerns tunnelling effects assisted by a phonon (hopping) of a single carrier between adjacent sites. The levels occupied by phonons change during the carrier’s transition from site to site, and here  $N_q \neq N'_q$  for certain values of  $q$ .

Finally we should note that the mobility of a small polaron is the sum of two contributions: an associated displacement in the small polaron band and the hopping movement of the polaron itself.

If we consider a small polaron moving within a perfectly ordered material, we should note that the description useful for free carriers (or here, a very mobile polaron) which undergoes random collisions with vibrating atoms is no longer acceptable when the variation in energy of such a diffusion is of the same order as the small polaron band size. In addition, the mobility within the small polaron band can only dominate

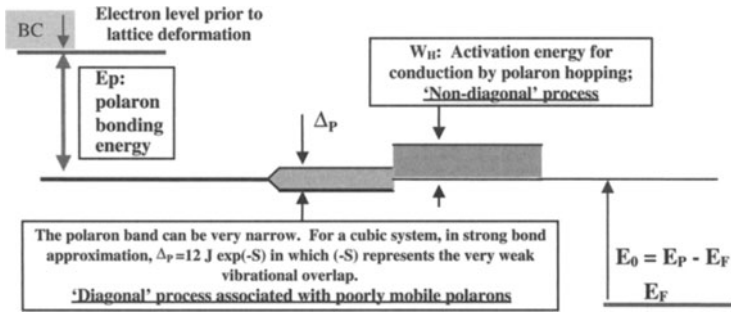


Figure V-8. Energy spectrum associated with polarons.

at low temperatures, even in an ordered crystal. We should also reckon on the band being extremely narrow ( $<10^{-4}$  to  $10^{-5}$  eV) and therefore the hopping regime can be considered only for disordered materials—which is generally the case for the materials we are studying. Energy fluctuations between localised sites are generally estimated to be considerably greater than band sizes. So, only polaron hopping assisted by phonons will be discussed hereon.

## 2 Characteristics of hopping by small polarons [Emi 86]

Charge transport in many polymers is generally supposed to be based on hops assisted by phonons. The charge carrier moves between two spatial localisations accompanied with a change in atomic vibrational states (following the 'non-diagonal' process detailed above).

### a Single and multi-phonon processes

The electron-lattice coupling force depends heavily upon the spatial extent ( $d$ ) of its state: if the state is confined about a single atomic site, the coupling force is extremely high. For highly extended states though, the electron-lattice interaction is much weaker, resulting from electronic states essentially only interacting with atomic vibrations of wavelength  $\lambda$  greater than its characteristic length  $d$ .

An electronic state confined to a single atomic site will give rise to a high electron-lattice interaction force. In addition, if the electronic state extends over a large monomer, its coupling with lattice vibrations will be very weak.

Finally, the transport processes brought into play depend on two factors:

- one is the precise intensity of the electron-lattice coupling. If  $(E_p/\hbar\omega_0) \ll 1$  then the coupling is weak, and if  $(E_p/\hbar\omega_0) \gg 1$  the coupling is strong. (In general terms we can consider that  $\hbar\omega_0$  represents the maximum phonon energy); and
- the other is the energy difference  $\Delta$  between the two sites involved in the transport. (If  $\Delta = 0$ , the two sites are degenerate).

According to the values of these two parameters, transport mechanisms for one or more phonons appear.



$\alpha$  - Mechanism for a single phonon when  $(E_p/\hbar\omega_0) \ll 1$ , and when  $\Delta < \hbar\omega_0$ . Here we have weak coupling with an extended electronic state ( $\approx 10^{-7}$  cm) (if the coupling tends towards zero, we are going towards a rigid lattice). The hopping density is thus dominated by a process which brings into play the minimum number of phonons, which in turn favours only those with the highest energy.

At low temperatures ( $kT < \hbar\omega_0$ ) hopping mechanisms are thermally assisted by phonons (with very low energies  $\approx 10^{-3}$  eV), absorbed by a minimum number in accordance with the principal of the conservation of energy. However, the hops occur over long distances as the states involved are highly extended. At high temperatures ( $kT > \hbar\omega_0$ ) the hopping processes lose their thermally active character and their number increases with temperature following  $T^n$ .

$\beta$  Multi-phonon mechanisms appearing when  $(E_p/\hbar\omega_0) \gg 1$ , both with  $\Delta < \hbar\omega_0$  and  $\Delta > \hbar\omega_0$ . The dominant process brings into play phonons with relatively low energies. A high number of multi-phonon type emissions contribute to the hopping process. Clearly, a strong coupling generate a higher number of phonons than that which necessitates a conservation of energy, however, the actual energy of the phonons remains relatively low. There is a strong possibility though of transitions occurring with this type of process.

Given that  $\Delta$  cannot be excessively high and that the temperature cannot be too low ( $< 10$  K), the calculation for the hopping probability is reduced to a calculation of probability in the degenerated state ( $\Delta = 0$ ) which we can multiply by the term for thermal activation,  $\exp(-\Delta/2kT)$ . We should note though that this is not the only term to rely on temperature; there are two others which can appear:

- one is that tied to hops between degenerated states and corresponds essentially to small polaron hops. At low temperatures ( $T < T_\theta/2$  where  $T_\theta$  is Debye's temperature), the process is dominated by the interaction of charge carriers with acoustic phonons, which give rise to a non-thermally activated mechanism of the variable hopping range (VRH) type. At higher temperatures, the hopping process is independent of the type of phonon with which the carriers interact, and appears as if thermally activated. After detailing its origin in Section b below, Section 3 will show the relevant calculations; and
- the other is related to conduction by percolation which occurs when a rising temperature increases the number of involved sites (which can also have a higher energy) and thus the number of conducting pathways. In appropriate cases, this mechanism can result in a conductivity which varies with  $\exp[-(T_0/T)^{1/4}]$ , in a form which resembles that given by VRH.

### **b Temperature dependence of number of hops (strong coupling)**

Here we shall consider a hop, assisted by phonons, between two strongly localised and separated states. With a charge localised on one of the sites, the deformation of atoms associated with this charge will also result in a potential well around the charge (see Figure IV-5). And this is indeed the polaron effect. In addition, the charge

cannot move without these atoms modifying their positions. Figure V-9, which comes from [Emi 86] illustrates the processes which a carrier follows from moving to an adjacent site with a suitable atomic displacement.

In Figure V-9 (a), both atomic and electronic charge displacements occur through a tunnelling effect (diagonal process). However, in the case of strong electron-lattice coupling, this tunnelling is relatively unlikely as superposition of (atomic) vibrational wavefunctions is poor (*i.e.*  $\exp(-S)$  is small). During their vibrational movement, atoms can find themselves in configurations where the superposition of their (atomic) vibrational wavefunctions is augmented (in process  $b_1$ ). The transport process can thus occur in 3 stages:

- first, atoms go through an appropriate displacement ( $b_1$ );
- second, atomic and charge displacements together give a tunnel effect; and
- thirdly, the displaced atoms relax towards their configuration of lowest energy.

Even though the tunnelling effect in process (b) is easier than process (a), these different movements are more energetic, as energy is required to distort the atomic displacements. In reality, if we give enough energy to the system, a charge can move without needing the intervention of a (atomic) vibrational tunnelling effect as is the case in process (c). In state ( $c_1$ ) atoms are in a configuration which presents, momentarily, two degenerated potential wells (of the same depth). The carrier can use this 'coincidence event' to go to an adjacent site through a tunnelling effect (process  $c_2$ ). Following this, the atomic displacements relax ( $c_3$ ).

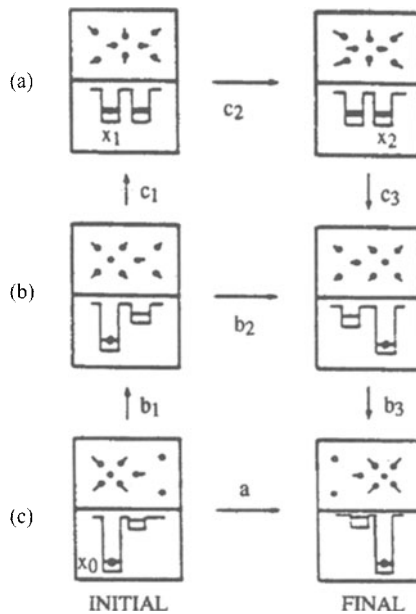


**Figure V-9.** Schematisation of displacement processes at different temperatures: (a) at low temperatures; (b) at intermediate temperatures; and (c) at high temperatures.

During the latter ( $c_1$ ) transition, no (atomic) vibrational tunnelling effects are necessary, only the electronic charge passes uses a tunnelling effect; this type of displacement is called 'semi-classical'.

At the lowest temperatures, process (a) dominates. When the temperature rises, process (b) starts to intervene with an certain inactivated contribution for a number of hops. At high enough temperatures though the semi-classical process (c) predominates; a number of hops are thermally activated and the energy of activation is the minimum energy which we must generate for coincidence configurations (at two atomic sites) to occur.

### 3 Precisions for the 'semi-classical' theory: transition probabilities

#### a Coincidence event

The principle on which for this semi-classical concept is based is the event coincidence which permits the passage of a charge using only its tunnelling effect. In the quantum regime, we still have to consider uncertainty with respect to time and therefore any associated intervals during which the passage occurs. Within classical limits, the event occurs instantaneously (and for us, when two atomic sites are identical that means that the two local electronic levels are identical as in  $-Ax_i(t) = -Ax_{i+1}(t)$ ).

If we suppose a charge carrier occupying a site on a crystal has an associated electronic energy level which is a function of instantaneous positions of atoms of the crystal, we can see that as the atoms continuously change position with their vibrational energy, then the electronic energy of such a carrier will also change. Amongst the variations of distorted configurations resulting from vibrating atoms, there is a probability ( $P_1$ ) that a situation will occur when the electronic energy of one electron at one site is 'momentarily' equal to that on a neighbouring site; such a coincidental event is represented in Figure V-10, following Emin's proposition [Emi 86].

While in classical physics a coincidence event can be considered as an instantaneous event, in quantum mechanics we need to accord a finite time interval. If the time interval during which the coincidence occurs is long with respect to the time required by an electron to pass from one coincidence site to the next (of the order of  $\Delta t \approx (\hbar/\Delta E) \approx (\hbar/J)$ ), then the electron can follow the 'lattice displacement' (or rather, displacement of vibrations) and hop with a probability  $P_2 = 1$  when the coincidence event occurs, in a situation characteristic of an adiabatic approximation. However, if the time required by the electron to hop is long relative to the duration of the coincidence event, then the electron cannot always follow the 'lattice displacement' and the hop probability reduces to  $P_2 < 1$ , in a situation characteristic of the non-adiabatic domain.

#### b Activation energy of small polaron at high temperatures

Here we will establish the expression for the activation energy characteristic of a high temperature regime, before exploiting these results in Section 4 in conjunction

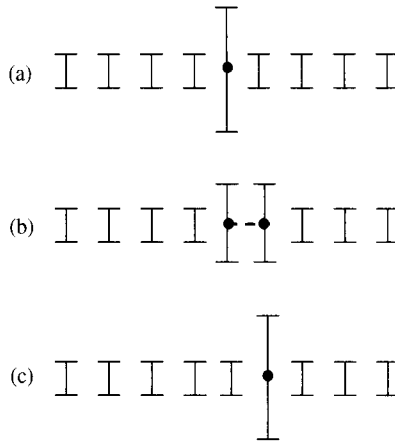


**Figure V-10.** Hopping process for small polaron: (a) the dot represents the position of a carrier on an atomic site; (b) coincidence event is formed; (c) carrier's situation following its transfer and relaxation of surrounding lattice.

with the knowledge that the minimum energy required for a 'coincidence event' is  $W_H \approx -E_p/2$  to derive calculations for conductivity.

Only with the energies of two wells (well for departure and for arrival) being equal can we enter the configuration shown in Figure V-9 c<sub>2</sub> (coincidence event). Using the notations given in Chapter IV, Section II-3, we can write this as  $-Ax_1 = -Ax_2$ , or  $x_1 = x_2$ .

In going from Figure V-9-a to Figure V-9-c<sub>1</sub> the wells from which the charge originates must be deformed with an energy  $B(x_1 - x_0)^2$  in which  $x_0$  and  $x_1$  are, respectively, the deformation of the wells in their initial state (polaronic state associated with a deformation  $x_0$  calculated in Chapter IV, Section II-3-b) and in the state  $c_1$ . The well which 'receives' the charge undergoes a change from non-deformed configuration (non-polaronic wells as in the initial stage shown in Figure V-9-a) to a deformed configuration  $x_2$  (Figure V-9-c<sub>2</sub>), which necessitates an energy  $Bx_2^2$ . The necessary energy overall is therefore  $W = B(x_1 - x_0)^2 + Bx_2^2$ , and with  $x_1 = W = B(x_2 - x_0)^2 + Bx_2^2$ .  $W$ , the minimum energy and denoted  $W_H$  required for a coincidence event can be obtained by minimising  $W$  with respect to  $x_2$ : as  $\frac{\partial W}{\partial x_2} = 4Bx_2 - 2Bx_0 = 0$  and thus  $x_2 = x_0/2 = x_1$ , we obtain  $W_H = \frac{Bx_0^2}{2}$ , and then with  $E_p = -Bx_0^2$  (see Chapter IV, Section II-3 or II-4), we finally have  $W_H = -\frac{E_p}{2}$ .

**c Comments**

*α Comment 1* When the two wells of departure and arrival of the charge are energetically separated by  $\Delta$  at the coincidence event due to disorder (Figure V-9-c), the original equation ( $-Ax_1 = -Ax_2$ ) should now be replaced by  $A(x_1 - x_2) = \Delta$ . This results in [Mot 79]:

$$W_H = -\frac{E_p}{2} \pm \frac{\Delta}{2}.$$

$\beta$  *Comment 2* When the material under study is polar, we are dealing with large polarons and the expression that we have just established,  $W_H = -\frac{E_p}{2}$ , is acceptable only when the localised charge carrier on one site does not modify the distortion of another molecular site, *i.e.* as is found for small polarons. For a polar material, therefore, this expression is no longer applicable, as Coulombic potential wells overlap between the two sites and mutually perturbed.

$\gamma$  *Comment 3* The transfer probability for a small polaron at low temperatures is given by  $C \exp\left(-\frac{W_H}{\frac{1}{4}\hbar\omega}\right) \exp\left(-\frac{\Delta}{kT}\right)$  (page 81 of [Mot 79]), is valid for a temperatures such that  $kT < [(1/4)\hbar\omega]$  and gives rise to non-thermally activated processes when  $\Delta \approx 0$ . For intermediate temperatures, the relationships obtained for high temperatures can be reasonably used, with the condition imposed that we replace  $W_H$  by  $W_H \left(1 - \frac{1}{3} \frac{\hbar\omega}{kT}\right)^2$ . When  $T = \frac{T_0}{2}$ , energy decreases by 8 % and when  $T = \frac{T_0}{4}$ , by 30 %.

#### 4 Relationships for continuous conductivity through polaron transport

We have seen, starting with our study of small polarons in a crystalline system, that the presence of disorder in a non-crystalline system localises charge and slows transfer, thus aiding the formation of small polarons. In order to follow transport phenomena associated with small polarons, we are compelled to consider relationships for continuous conductivity (and if possible thermoelectric power, as detailed in Appendix A-6) with respect to temperature.

Depending on the temperature range envisaged, in Section 2 we saw in Figure V-9 that three transport mechanisms are possible:

##### a Very low temperatures ( $kT < 10^{-4}$ eV)

At very low temperatures, the only process likely to exist is that shown in Figure V-9-a and reproduced in Figure V-11-a below. This process occurs without changing the overall population of phonons and for a charge subject to a double tunnelling effect with a deformation associated with the movement of a polaron within its own, extremely narrow band. For a cubic crystal, the band is of size  $B = 12 J \exp(-S)$  and the effective mass can be written using eqn (22) from Chapter II, *i.e.*  $m^* = \frac{6\hbar^2}{a^2 B} = \frac{\hbar^2}{2a^2 J \exp(-S)}$ . The corresponding mobility is in the form  $\mu = \frac{q\tau}{\hbar^2} 2a^2 J \exp(-S)$ , is proportional to  $\exp(-S)$  and is extremely low, much as the corresponding conductivity. Aside, it is probably worth considering whether or not this process occurs in amorphous semi-conductors [El 90], given that fluctuations in tail energy band sites are perhaps higher at  $10^{-4}$  eV.

##### b At low temperatures

At low temperatures, although not as low as those in (a), we have the process detailed in Figure V-9-b which consists of a charge subject to a double tunnelling effect and a

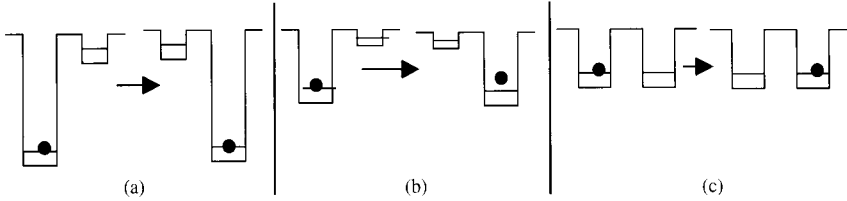


**Figure V-11.** Transport mechanisms at different temperatures. (a) Low T; (b) Intermediate T; (c) ‘Elevated’ T.

vibration assisted by phonon overlapping. The activation energy of this process decreases with temperature (and tends towards zero for conduction in the polaronic band). A variable distance hopping mechanism with these characteristics is probable [Gre 73] following a law of the form  $Ln\sigma \propto -(T_0/T)^{1/4}$ .

### c ‘Elevated’ temperatures

At slightly elevated temperatures, around or just above ambient temperature, the process detailed in Figure V-11-c may occur, requiring a single tunnelling effect coupled with the ‘event coincidence’ due to the same vibrational configuration of two adjacent sites resulting from a thermal energy  $W_H$ .

Here we can write that  $\sigma = qN\mu_p$ , in which  $N$  is the charge carrier density and  $\mu_p$  is the mobility associated with this type of polaron. On using Einstein’s relationship,  $\mu_p = qD/kT$  (with  $D$  in the form  $D = Pa^2$ , in which  $P$  is the probability that a carrier will hop between neighbouring sites and  $a$  is the inter-atomic distance) we end up with:

$$\sigma = \frac{Nq^2a^2}{kT}P.$$

$P$  depends on two probabilities which were defined in Section 3 of this Chapter:

- $P_1$  is the probability for the event coincidence in the form  $P_1 = \nu_0 \exp(-W_H/kT)$  in which  $\nu_0$  is the mean phonon frequency and  $W_H$  is the activation energy required to produce the equivalent of the two sites. As we have seen in Section 3-b,  $W_H = -E_p/2$ , and from Section 3-c, disorder can be represented using the parameter  $\Delta$  for the amplitude of differences between initially occupied and unoccupied sites. We can therefore now say that  $W_H = -E_p/2 \pm \Delta/2$  with  $E_p$  representing, as previously denoted, the polaron bonding energy  $-A^2/2M\omega_0^2$  for an isolated diatomic molecule. This activation energy can, however, be reduced as the lattice slowly relaxes, leading to a correlation between successive hops.
- $P_2$  is the probability of charge transfer during an event coincidence. For the non-adiabatic regime, in which  $P_2 < 1$  as carriers are slower than lattice movements, the relationship

$$P_2 = \frac{1}{\hbar\nu_0} \left( \frac{\pi}{W_HkT} \right)^{1/2} J^2$$

was obtained by Holstein [Zup 91] in which  $J$  is, as before, the electronic transfer integral such that  $J^2 = \exp(-2\alpha R)$ .

Under non-adiabatic conditions, the mobility can be written as:

$$\mu = \frac{qa^2}{kT} P_1 P_2 = \frac{qa^2}{\hbar kT} \left( \frac{\pi}{W_H kT} \right) J^2 \exp \left( -\frac{W_H}{kT} \right) \rightarrow \mu \propto T^{-3/2} \exp \left( -\frac{W_H}{kT} \right).$$

This mobility appears thermally activated over a wide range of temperatures and characterises polaron based conduction. When the temperature is such that  $W_H$  is of the order of  $kT$ , the preexponential term predominates and gives rise to a variation proportional to  $T^{-3/2}$ . We also note that  $N = N_c \exp(-E_0/kT)$ , in which  $E_0$  represents the activation energy necessary for a constant number of carriers, corresponding to an equilibrium value, and  $N_c$  (at approximately  $10^{22} \text{ cm}^{-3}$  is a value higher than that generally seen in non-polaronic theories [Eil 90]) represents the density of equivalent sites initially susceptible to thermally generate carriers on polaronic levels.

We thus arrive finally at an expression for conductivity at 'elevated' temperatures:

$$\sigma = \frac{qa^2}{kT} N_c v_0 P_2 \exp \left( -\frac{E_0 + W_H}{kT} \right) = \sigma_0 \exp \left( -\frac{E_0 + W_H}{kT} \right)$$

In general,  $\sigma_0 \approx 10 - 10^3 \Omega^{-1} \text{ cm}^{-1}$ .

*Comment 1* For a one dimensional model, in which the transfer of vibrational energy giving rise to equivalent sites depends only on one direction we have  $W_H \approx -E_p/2$ . However, with a 3 dimensional model, supposing that energies are propagated equally in all 3 directions, for each direction we have  $W_H = -E_p/6$ .

*Comment 2* It should be noted that for intrinsic carriers,  $E_0$  is less than half of the optical gap. (The optical gap corresponds to an excitation of an electron from the valence band to the conduction band, during which atoms remain unmoved in a rigid lattice). However, when atoms can adjust their position in response to the presence of a carrier, there is a coupling between charge and lattice consisting of small polarons and the energy scheme for this is illustrated in the right hand side of Figure V-12—an extension of Figure V-8. The size of the gap can be deduced from the probability of a level being occupied by either a small negative (localised electron) or positive (localised hole) polaron with the energy difference between them being  $2 E_0$ . With the bands of small polarons being narrow, ( $kT \gg$  polaron band size) the Fermi level can be found midway between the bands of electrons and small polaron holes in an intrinsic semiconductor.

## 5 Conduction in 3-D in $\pi$ -conjugated polymers

It should be said that most calculations concerning  $\pi$ -conjugated polymers have been performed on single chains, without calling into account interchain interactions. And yet, isotropic conductivity is often observed for doped  $\pi$ -conjugated polymers, tending to indicate that interchain charge transport is relatively facile due to the presence of a non-inconsequential overlapping between  $\pi$ -orbitals of adjacent chains. Models of conduction have been elaborated for this scenario, given that electronic transfer between chains is effected either by direct three dimensional coupling or via intermediate doping ions.

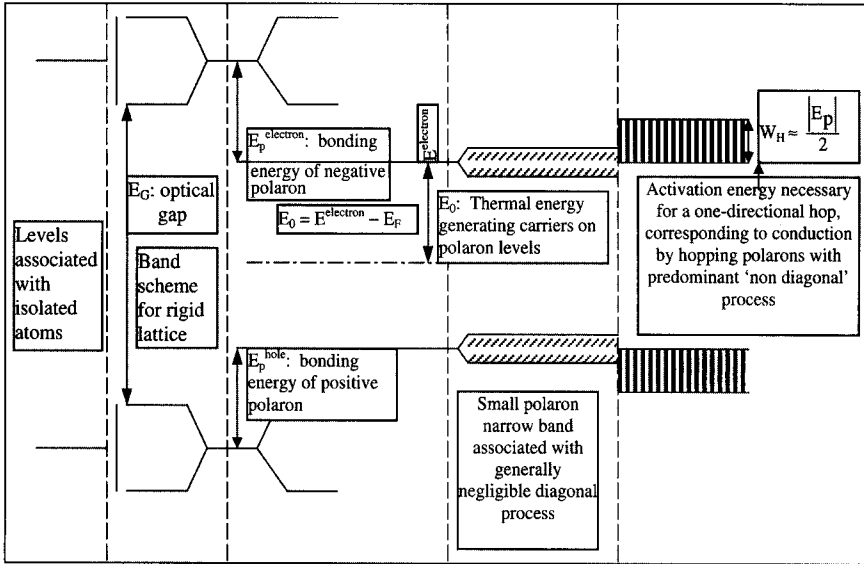


Figure V-12. Energy scheme for charge-lattice coupled system (intrinsic charge generation).

**a Direct 3-D coupling between chains**

Direct, 3-D, interchain coupling is characterised by the transfer integral  $t_{\perp}$  (Figure V-13). In order to perform direct calculations of the band structure in 3-D, we need to know the actual 3-D structure under consideration. While, in general, only relatively incomplete data are available, for polyacetylene (PA) and poly(*para*-phenylene vinylene) (PPV) local determinations of  $t_{\perp}$  integrals have been made yielding values of the order of 0.4 eV [Gom 93]. Such a value assures for polymers like PPV the condition  $(t_{\perp}/t_{//}) \geq 10^{-2}$ , a value generally considered necessary for 3-D transport [Sch 94]. Indeed, it is worth noting here that such transport can be established without resorting to the intervention of polarons.

For PA and PPV apparently reasonable methods have been used to evaluate interchain interaction effects on polaron stabilisation. Using a model identical to that derived for isolated chains, it has been shown that polaron effects are considerably weakened once interchain interactions are taken into account: reasonable values for 3-D coupling were sufficient to destabilise polarons so that they could no longer practically form.

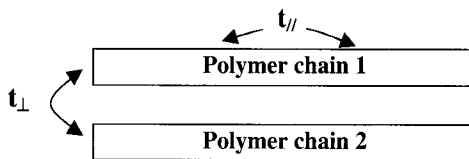
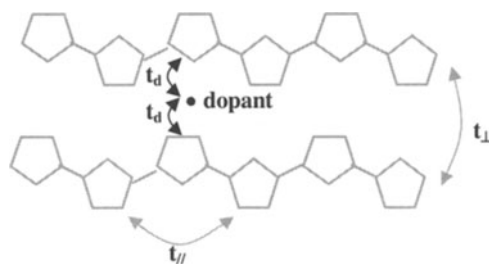


Figure V-13. Intrachain ( $t_{//}$ ) or interchain ( $t_{\perp}$ ) transfer integrals.





**Figure V-14.** Schematisation of dopant bridging showing various transfer integrals.

All the previously mentioned calculations were actually performed using an ideal structure, without geometrical or chemical defaults, and as we have already seen in Chapter III, Section IV, it is disorder, for example due to certain short conjugated sequences, or chemical defaults such as polymer precursors remaining in the material and dopants, which tend to stabilise polarons [Con 97].

### b Chain coupling through intermediate dopant ions [Bus 94]

Interchain coupling has been, in particular, studied for  $(t_{\perp}/t_{//}) \geq 10^{-2}$  not being true, using, for example polypyrrole in which  $t_{//} \approx 2.5$  eV and  $t_{\perp} \approx 0.03$  eV. The presence of a dopant ion inbetween chains which can transfer carriers with equal ease to either one chain or the other—as shown in Figure V-14—can assure coupling; the resulting transfer integral  $t_d \approx 0.5$  to 1 eV is significantly larger than  $t_{\perp}$ .

The electronic charge transferred by dopant or ‘counter-ion’ is distributed on the chains adjacent to the ion. As a result, polaronic species called transverse polarons and bipolarons form across several chains and are centred about the counter-ions (Figure V-15). Calculations have shown that transverse polarons can only exist when the dopants are well dispersed from each other and that at higher doping levels, transverse bipolarons form.

Both the attractive potential induced by the dopant and its tendency to reinforce tunnelling effects stabilise transversal polarons and bipolarons, as shown in Figure V-16.

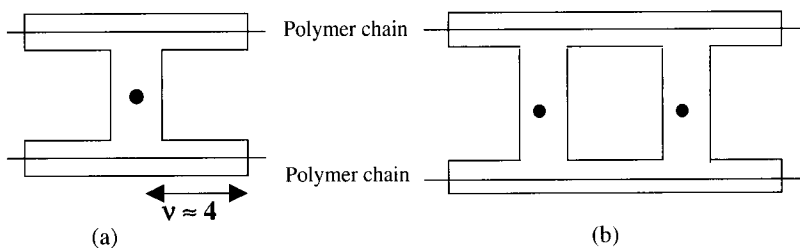
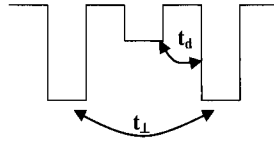


**Figure V-15.** (a) Transverse polaron; and (b) transverse bipolaron.  $v$  is the polaron half size expressed in monomer units.



Dopant centers reinforce transitions between two chains due to tunnelling effects

Figure V-16. Reinforcing interchain transitions with doping centres.

### c Hopping conduction in disordered polymers

On a small scale, when there is a high enough concentration of dopants to connect adjacent chains, then clusters of polarons resembling networks form. We can see though that on a larger scale, there is an inhomogeneous spread of polarons in a disordered polymer network, and the polaronic clusters are separated. A calculation for conductivity by hopping for this configuration has been made using the following, three hypotheses:

- adiabatic hops occur within polaronic clusters;
- non-adiabatic hops occur between polaronic clusters, with the intervention of a phonon;
- electrostatic energy is the principal barrier in the hopping mechanism.

The relationship found for conductivity is [Zup 93]:

$$\sigma = \sigma_0 \exp \left[ - \left( \frac{T_0}{T} \right)^{1/2} \right]$$

Here  $T_0$  depends on both the charge energy of clusters and system granularity such that

$$T_0 = \frac{8U \left( \frac{\bar{\delta}}{\delta} - 1 \right)^2}{k \left( \frac{\bar{\delta}}{\delta} - \frac{1}{2} \right)}$$

where

$$U = \frac{1}{4\pi\epsilon_0\epsilon_r} \frac{e^2}{a}$$

and represents electrostatic repulsion between two electrons separated by distance  $a$ ,  $\delta$  is the lean distance between dopants in a cluster and is independent of cluster size and  $\bar{\delta}$  is the mean distance between dopants assuming a homogeneous distribution and ignoring clusters.

On finally using the representation of a simple inhomogeneous distribution of dopants, supposing that there are no particulates with metallic properties, the obtained law resembles closely that of Sheng (see below), which was established for a granular, metallic system.

## VI Other envisaged transport mechanisms

This Section contains a relatively short summary of the different models, and their laws, used to interpret the behaviour of conductivity in organic solids.

### 1 Sheng's granular metal model

Sheng's model was formed in order to comprehend the observed conductivity of heterogeneous systems composed of nano-particles within an insulating ceramic matrix and supposes that the metallic clusters have free charges which can pass through the matrix following a tunnelling effect. The charge transfer is limited by the energy  $E_{Ch}$  necessary for an electron to hop from one particle to the next, which will form a positive charge on the particle it has left and a negative charge on the particle to which it has arrived. Using the idea of a charged capacitor as a reference, we can suppose that the system will have a charging energy. The law obtained is in the form

$$\sigma = \sigma_0 \exp \left[ - \left( \frac{T_0}{T} \right)^{1/2} \right],$$

with  $T_0$  dependent on  $E_{Ch}$ , the distance between grains and the transparency of the barrier between grains.

### 2 Efros—Shklovskii's model from Coulombic effects

In Mott's model of variable distance hopping, it is supposed that charges have negligible interactions between each other. When Coulombic interactions between a charge and a remnant positive hole become dominant (with opening of a Coulombic band gap as detailed in Chapter II, Section IV-2), the mean hopping distance can be evaluated to give, in all dimensions, a law of the type:

$$\ln \rho \propto (T_0/T)^{1/2}, \quad \text{in which } \sigma = \sigma_0 \exp(-T_0/T)^{1/2}.$$

Sheng also showed that this law resembled his own, with the Coulombic repulsions simply playing the role of charge energy.

### 3 Conduction by hopping from site to site in a percolation pathway

Conduction along a percolation pathway within a lattice is modelled. It is supposed that the conductivity  $\sigma = G_m/R_m$ , where  $G_m$  is the characteristic conductivity and  $R_m$  is the characteristic dimension of the lattice. The percolation limit is assumed to be reached once the limiting value of  $G_m$  is equal to  $G_C$  which is in turn defined as the greatest conductance permitting a continuous passage throughout the lattice for all charge movements ( $G_{ij}$ ) between sites  $i$  and  $j$  which are such that  $G_{ij} > G_C$ . The obtained law, which resembles that of VRH, is  $\sigma = \sigma_0 \exp(-AT^{-1/4})$ .

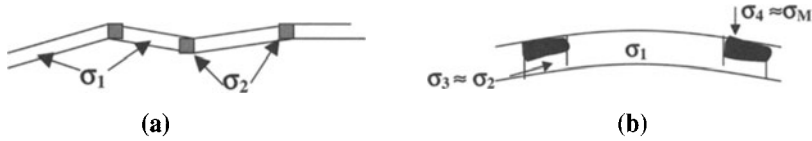


**Figure V-17.** Heterogeneous systems with: (a) moderate dopant concentration; and (b) high concentration.

#### 4 Kaiser’s model for conduction in a heterogeneous structure

Conductivity in a heterogeneous structure was modelled by Kaiser [Kai 89] in order to account for the behaviour of  $\pi$ -conjugated polymers doped to varying degrees. Here we shall detail only expressions for continuous conductivity, although those for thermoelectric power can be followed in Appendix A-6.

In order to understand a variety of behaviours, models of heterogeneous polymers with 2 or 3 domains were proposed [Mol 98]. As shown in Figure V-17-a, the former system was considered to consist of fibrils (Region 1) within a matrix (Region 2) with the conductivity such that  $\sigma^{-1} = f_1\sigma_1^{-1} + f_2\sigma_2^{-1}$  where  $f_i$  being a factor in the form  $f_i = L_iA/pLA_i$  with  $p$  representing the number of conducting pathways given here by the same ratio  $\frac{L_i}{A_i}$  of length over sectional area ( $L$  and  $A$  are the sample length and cross sectional area respectively).

When  $\sigma_1 \gg \sigma_2$  due to the presence of sufficient dopants, we have  $\sigma \approx f_2^{-1}\sigma_2$  and the evolution of  $\sigma$  is pretty much guided by the term  $\sigma_2$ . This means that transport mechanisms assisted by tunnelling effects are dominant, while at low temperatures the hopping mechanism (VRH) proposed by Mott are of relevancy. It should be noted that  $\sigma$  can be high due to the term  $f_2^{-1}$  which is proportional to  $L/L_2$  with  $L$  being high relative to  $L_2$ , the thin inter-fibril barrier).

At high levels of dopant, in order to account for a finite value for  $\sigma$  at temperatures tending to 0 K and the increase in thermoelectric power with  $T$  at low temperatures, the preceding representation using fibrils needs to be modified as shown in Figure V-17-b. Two parallel domains are substituted, the first of which (conductivity  $\sigma_3$ ) continues to represent inter-fibril hopping, while the second introduces, like an amorphous metal, a supplementary component ( $\sigma_4$ ) in the form  $\sigma_4(T) = \sigma_{40} + \alpha T^{1/2}$ , in which  $\sigma_{40}$  and  $\alpha$  are constants. Overall, this gives  $\sigma^{-1} = (f_1\sigma_1)^{-1} + (g_3\sigma_3 + g_4\sigma_4)^{-1}$ .

### VII Conclusion: real behaviour of conducting polymers and the parameter $w = -d(\log \rho)/d(\log T)$

#### 1 A practical guide to conducting polymers

At the level of the actual, practical behaviour of polymers, an article by J P Travers [Tra 00] is of considerable use as it details magnetic characterisations of different molecular structures which may be used to determine charge origins. Here though we cannot focus only on electrical transport, and can at best give a summary of the

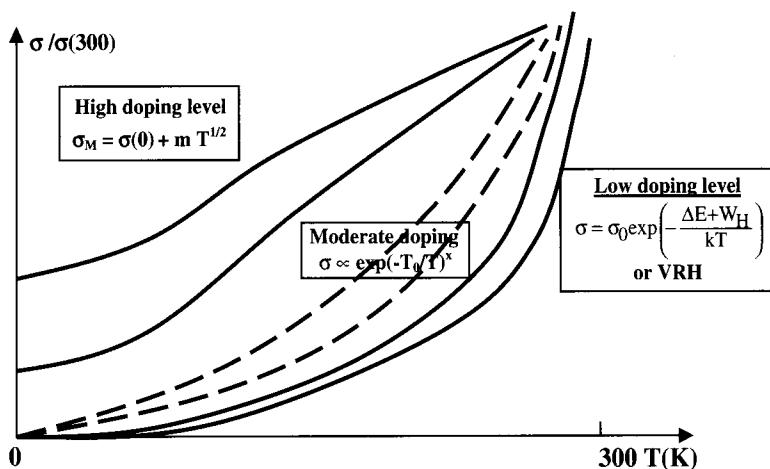


Figure V-18. Conductivity of doped CPs at different temperatures.

three principal classes of conducting polymers (CP) with respect to the conductivities shown in Figure V-18:

### a Highly doped CPs

These polymers exhibit a 'metallic' character (degenerate medium with  $E_F$  in delocalised states due to a disordered system). Conductivity parallel to the chain axis can be expressed using Drude-Boltzmann's relationship (Section III-I-a):

$$\sigma = \sigma_{//} = \frac{nq^2 \mathcal{L}}{\hbar k_F}$$

Given that  $k_F = \frac{\pi}{a}$ , we obtain

$$\sigma_{//} = \left( \frac{nq^2 a^2}{\pi \hbar} \right) \left( \frac{\mathcal{L}}{a} \right)$$

(equation retained by Kivelson and Heeger [Kiv 88].

With respect to temperature:

- at low temperatures with poor localisations, we have seen from Altshuler and Aronov's law that

$$\sigma = \sigma(0) + mT^{1/2};$$

- at slightly higher temperatures, inelastic collisions are controlled by electron-electron interactions, with  $l \propto T^{-1}$ , resulting in  $\sigma \propto T$  (Mott's linear law); and
- at higher temperatures, collisions with phonons dominate with  $l \propto T^{-1/2}$ , again giving  $\sigma \propto T^{1/2}$  in a law identical to that proposed by Kaiser for highly doped heterogeneous systems.

**b Moderately doped CPs**

For polymers with a moderate level of doping, we can suppose that:

- $E_F$  tends to be outside extended states, with states more or less localised within the gap. There are different theories, however, they result in laws essentially following  $\sigma \propto \exp(-T_0/T)^x$ .
- there is a heterogeneous structure [Kai 89], with conducting fibrils separated by an electric barrier:  $\sigma^{-1} = f_1 \sigma_1^{-1} + f_2 \sigma_2^{-1} \Rightarrow$  (and with  $\sigma_1 \gg \sigma_2$ ,  $\sigma \approx f_2^{-1} \sigma_2 \rightarrow$  VRH (tunnelling effect) again in the form  $\sigma \propto \exp(-T_0/T)^x$ ).

**c CPs with low levels of doping**

Here,  $E_F$  is within a quite large gap of few states.

Whatever our point of view concerning polaronic states or states tied to localised defaults, we keep coming back to a VRH based law at low temperatures, while at higher temperatures a thermally activated law is more appropriate.

**2 Temperature dependence analysed using the parameter**

$w = -[(\partial \ln \rho) / \partial \ln T]$

We can suppose that in the majority of cases, resistivity can be expressed using the general formula [Zab 84]  $\rho = BT^{-m} \exp(T_0/T)^x$ . We can go on to derive  $\ln \rho = \ln B - m \ln T + \left(\frac{T_0}{T}\right)^x$ , giving also  $\frac{d \ln \rho}{dT} = -\frac{m}{T} - x \frac{T_0^x}{T^{x+1}}$ . Finally this yields  $-T \frac{d \ln \rho}{dT} = m + x \left(\frac{T_0}{T}\right)^x$ , and  $w = -\frac{d \ln \rho}{d \ln T} = m + x \left(\frac{T_0}{T}\right)^x$ .

**a In the VRH regime**

In this domain, we have  $m = 0$  and  $x = 1/4$  in 3-D, with  $w = \frac{1}{4} \left(\frac{T_0}{T}\right)^{1/4}$ . Following the preceding law, we have  $\ln w = \ln(xT_0^x) - x \ln T = A - x \ln T$ . In Figure V-19, the curve representing  $\ln w = f(\ln T)$  in an insulator-semiconducting domain shows it to be a straight line with a negative slope  $-x = -0.2$ .

We can also note that  $(T_0/T)^x = (T_0 T^{1-x})/T = \epsilon(T)/T$  so that:

- when  $x = 1$ ,  $\epsilon(T) = T_0 = \text{constant}$ , and we are in a thermally activated regime with  $\rho = \rho_0 \exp(\Delta E/kT)$  in which  $\Delta E = kT_0$ ; and
- when  $x = 1/4$ ,  $\epsilon(T) = (T_0 T^{3/4})$  which is such that  $\epsilon(T)$  decreases with T in a behaviour characteristic of VRH *i.e.* activation energy  $k\epsilon(T)$  decreasing with T.

**b Close to metal-insulator transition**

Resistivity is not thermally activated and  $\rho(T) \approx T^{-m}$ . Thus we have  $T_0 = 0$ , with  $\ln w = \ln m = \text{constant}$ . The representation  $\ln w = f(\ln T)$  is a straight horizontal

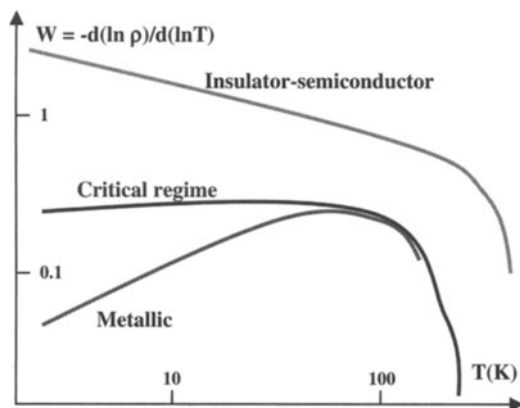


**Figure V-19.** Ln curves for  $w(T)$  as a function of temperature for PANI doped with camphorsulfonic acid under three regimes: metallic, critical (M-I) and insulator.

line, as shown in Figure V-19. This law corresponds to the TCR (temperature coefficient ratio)  $\alpha_p = (1/\rho)(\delta\rho/\delta T) < 0$ , while a real metallic character follows  $\alpha_p > 0$ .

### c True metallic behaviour

True metallic behaviour could be observed with polyaniline (Pani) [Men 93] with  $\rho(T)$  increasing very slightly with  $T$  at low temperatures with a system changing from a characteristic power law under critical regime (close to the M-I transition) to purely metallic behaviour.

# VI

---

## Electron transport properties: II. Transport and injection mechanisms in resistive media

### I Introduction

In the preceding Chapters, we have attempted to define the structure and nature of electronic levels following charge insertion into organic materials, in no particular order, by doping, electron injection or photoexcitation.

In organic electroluminescent diodes, doping agents need to be removed as they can quench luminescence. Given that the materials in these types of components are more like insulators than conductors, it is useful to understand:

- electron and hole injection at the cathode and the anode, respectively; and
- transport of electrons and holes at the electrode interface or within the organic layer.

As we shall see, different mechanisms can be envisaged. The I(V) characteristics (current – voltage characteristics) of an electronic structure are often studied and explained in terms of charge injection either under field (Schottky) or tunnelling effects. Alternatively, results can be interpreted using models based on current flow limited by space charges (SCL). The aim is to reduce the threshold potential of a diode, and depending on the dominant process, it should be possible to improve the electronic properties of the metal used for the electrode or the mobility of carriers within the organic layer.

In this Chapter, we shall present the various possible charge mechanisms for charge injection at interfaces and study how, classically, electron transport is envisaged in near-insulating materials such as undoped organic solids, which display conductivities of the order of  $10^{-10}\Omega^{-1}\text{cm}^{-1}$ . An example of which is well purified poly(*para*-phenylene) (PPP), which exhibits conductivity around  $10^{-15}\Omega^{-1}\text{cm}^{-1}$ .

### II Basic mechanisms

#### 1 Injection levels

In order to attain significant electric currents within components, such as electroluminescent diodes, charge carriers are required to be injected in a high enough



concentration to energetically high levels using a sufficiently intense electric field ( $E_a$ ). The initial thermal equilibrium shown in Figure VI-1-a is broken, giving rise to thermally excited carriers at the outer edges of conduction bands (CB) (in the case of electrons) and a pseudo-equilibrated regime (Figure VI-1-b). The Fermi level ( $E_F$ ) yields Fermi pseudo-levels for electrons ( $E_{Fn}$ ) and holes ( $E_{Fp}$ ) with a considerable increase in charge concentration [Mat 96].

### 2 Three basic mechanisms

Classically, outside of equilibrium, three types of current can be considered:

- (A) At electrodes, the current of carriers is produced by:
- thermoelectronic emission;
  - emission due to field effects (Schottky); and
  - emission due to tunnelling effects;

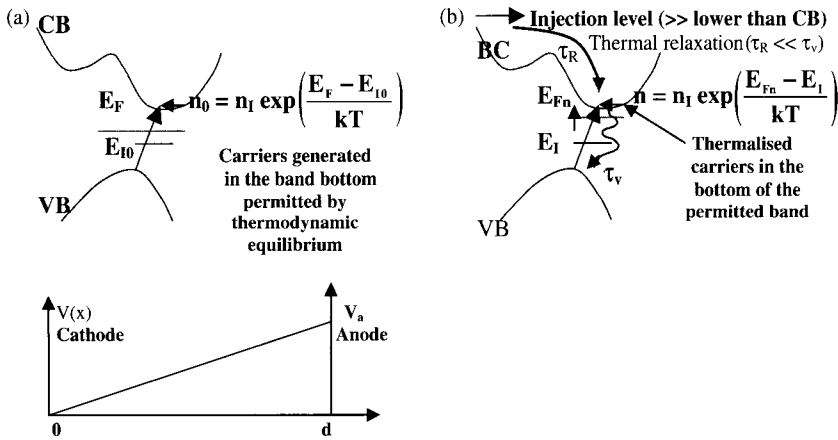


**Figure VI-1.** (a) Thermodynamic equilibrium ( $E_F, n_0$ )

If the applied field ( $E_a$ ) is weak, carrier concentration in permitted bands is unmodified and there is no injected space charge ( $\rho = 0$ ). Conduction is assured only by internal charges, of concentrations  $n_0$  and  $p_0$ , at thermodynamic equilibrium. For electrons,  $J_n = q n_0 \mu_n E_a$ . Integration of Poisson's equation,  $\Delta V = 0$ , with limiting conditions,  $V(0) = 0, V(d) = V_a$ , gives  $-\frac{dV}{dx} = E(x) = \text{Constant} = E_a = -V_a/d$ , that is:  $V(x) = (x/d)V_a$  (ohmic regime).

(b) Outside thermodynamic equilibrium ( $E_{Fn}, n$ )

Charge carrier concentration in bands is modified by  $E_a$  (the mean applied electric field, as defined by  $E_a = -V_a/d$ , in which  $V_a$  is the applied field at the insulator/semiconductor). Tied to carrier injection and the high resistivity of the material is space charge with  $\rho \neq 0$ .  $E_a$  is sufficiently high to introduce by emission or injection from electrodes concentration of carriers breaking down the initial thermodynamic equilibrium. The current,  $J$ , being governed by intrinsic properties of material, is no longer ohmic and is either:

- limited by trickling properties of charges introduced in the material volume ( $J_{Ev}$ ); or
- limited by current produced at electrodes ( $J_C$ ).  $J = J_{Ev}$  if  $J_{Ev} < J_C$ ;  $J = J_C$  if  $J_C < J_{Ev}$ .

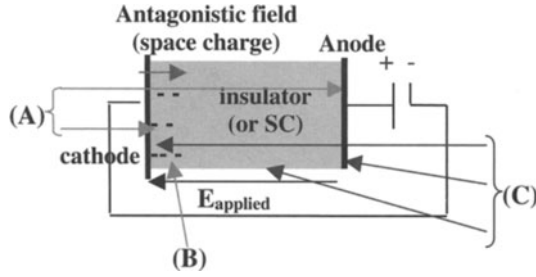


**Figure VI-2.** Three basic mechanisms A, B and C.

- (B) Current of a single carrier type at one electrode limited by the space charge in the electrode locality ( $J_{\text{SCL}}$ ). In the presence of trapping levels in the insulating volume, the space charge limiting law must be modified to account for reduced mobility of carriers; and
- (C) Current due to double charge injection at each electrode controlled by the insulating volume. Current is limited by space charges (or electrode currents as they limit injection) and a concentration of recombination phenomena.

In the following Section we shall look at each of these currents in more detail.

### III Process A: various (emission) currents produced by electrodes

Typically these currents occur when the metallic electrode and insulator contact is rectifying (if  $W_{\text{M}}$  and  $W_{\text{SI}}$  are, respectively, work functions for the electrodes and the insulator or semiconductor, when  $W_{\text{M}} > W_{\text{SI}}$ ). Depending on the strength of the applied electric field ( $E_{\text{a}}$ ), three types of electric current can be identified and are detailed below.

#### 1 Rectifying contact (blocking metal $\rightarrow$ insulator)

Figures VI-3-a and b show the rectifying contact with  $W_{\text{M}} > W_{\text{SI}}$ . Under these conditions, on contact electrons are emptied into the metal (M) from the insulator (I). In I there appears a positive space charge over a relative large distance ( $L$ ) due to the low electron density in I. This is called the depletion zone.

$V_{\text{a}}$	M side barrier	I or SC side barrier	Result <i>vis à vis</i> electron passage
0	$W_{\text{B}}$	$qV_{\text{d}}$	
$<0$ SC side (direct polarity)	$W_{\text{B}}$	$qV_{\text{d}} - qV_{\text{a}}$	I or SC $\rightarrow$ M eased M $\rightarrow$ I or SC remains difficult
$>0$ SC side (inverse polarity)	$W_{\text{B}}$	$qV_{\text{d}} + qV_{\text{a}}$	I or SC $\rightarrow$ M difficult M $\rightarrow$ I or SC always difficult

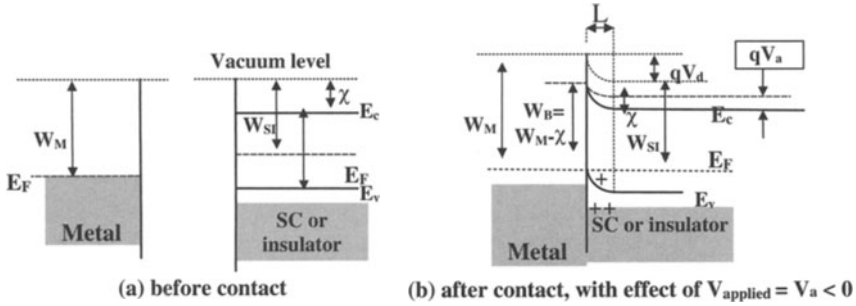


Figure VI-3. Metal-insulator contact with  $W_M > W_{SI}$ .

The Table above summarises characteristics for a contact with  $W_M > W_{SI}$  which is effectively blocking with respect to electron injection ( $M \rightarrow I$ ). Only a thermo-electronic emission can occur from  $M$  (which tends to saturate in the form  $J_{0SCH} = A^*T^2 \exp(-[W_B - \Delta W]/kT)$  due to emission by field effects). With a high value of  $E$ , a tunnelling effect (generated with a narrow barrier) can allow thermoelectric emission through this blocking contact (Fowler–Nordheim equation).

**2 Thermoelectronic emission ( $T \neq 0$ ;  $E_a = 0$ )**

The Dushman-Richardson law (deduced from distribution of electron velocities in metals given by Maxwell-Boltzmann’s equation in Appendix A-7) covers the emission process detailed in Figure VI-4. The emitting current density at saturation is given by  $J_{0sT} = A^*T^2 \exp(-W_B/kT)$ , with  $W_B = W_M - \chi$  in which  $W_M$  is the metal work function,  $\chi$  is electron affinity of insulator or semiconductor and  $A^*$  is the modified Richardson constant from  $A^* = (4\pi qm^*k^2)/h^3$ .

**3 Field effect emission (Shottky):  $E_a$  is ‘medium intense’**

In this process, the electric field ( $E_a$ ) reduces the potential barrier by  $\Delta W = q(qE_a/4\pi\epsilon)^{1/2}$ . The law used in Process 1 to give the saturation current here becomes

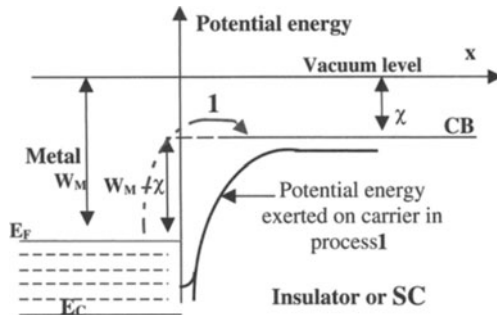
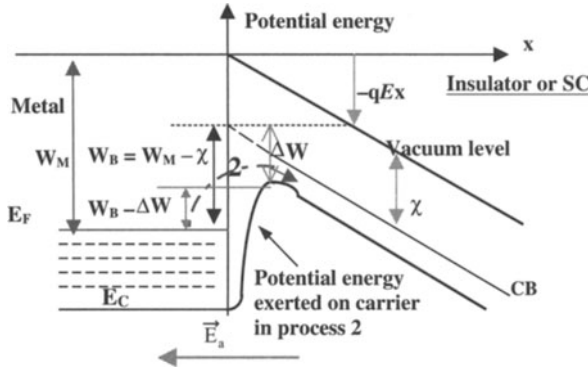


Figure VI-4. Emission process by thermoelectric effect.



**Figure VI-5.** Emission process due to Schottky field effect.

$J_{0SCH} = A * T^2 \exp(-[W_B - \Delta W]/kT)$  (as in Figure VI-5 and Appendix A-7). With  $T$  constant, theoretically  $\log J_{0SCH} = f(\sqrt{E_a})$  remains linear, however, at low  $E_a$ ,  $J$  is often observed to depart from a straight Schottky line due to the appearance of space charge near the emitting surface (see Figure VI-21).

#### 4 Tunnelling effect emissions and Fowler–Nordheim’s equation

At high values of  $E_a$ , the potential energy curves steepens and the potential barrier observed by electrons narrows considerably, only to be crossed through Process 3, which corresponds to a tunnelling effect (Figure VI-6 and Appendix A-7). The current density is given by Fowler–Nordheim’s equation:

$$J_{0FN} = \frac{q^3 E_a^2}{8\pi h W_B} \exp\left[-\frac{4}{3} \left(\frac{2m}{\hbar^2}\right)^{1/2} \frac{W_B^{3/2}}{qE_a}\right].$$

$\log(J_{0FN}/E_a^2) = f(1/E_a)$  is a straight line with slope  $W_B$ .

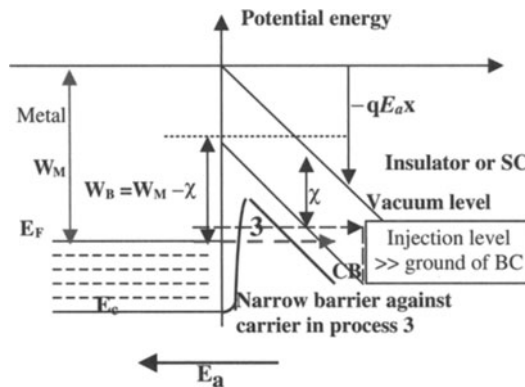


**Figure VI-6.** Tunnelling effect emission process.

## IV Process B (simple injection): ohmic contact and current limited by space charge

Current limited by space charge occurs when the contact is ohmic, that is to say that the electrode behaves as though it is an infinite reserve of charge and the current flow is not determined by the volume of the emitting material. Given that the latter is close to being an insulator, the formed space charge opposes the trickle of current through the material within the neighbourhood of the electrode-material interface. At a sufficiently high applied field ( $E_a$ ), space charges are pressed right back to the interface and can effectively enforce a saturation current. Here, we shall look at the different stages involved.

### 1 Ohmic contact (electron injection)

#### a Definition

A metal-insulator (M – I) contact is ohmic when its resistance (impedance) is negligible compared to that of the insulator or semiconductor volume. As a consequence, free carrier density near the contact is considerably greater than that in the material volume, which is generated thermally, and ohmic contact can act as a charge reservoir. The conduction is controlled and limited by the insulator volume impedance and any possible recombination phenomena.

#### b Comment

The use of the term ‘ohmic’ is not particularly exact. Under high fields the concentration of charge carriers rapidly overshoots the concentration  $n_0$ , which gives rise to the ohmic law generated intrinsically in the material volume. However, with increasing field strength, we can find that  $n$  rapidly exceeds  $n_0$  due to inequilibrium charge injection, resulting in the  $I(V)$  law becoming non-linear and thus non-ohmic.

#### c Realisation and schematisation

Ohmic contact is obtained when  $W_M < W_{SI}$ .

As shown in Figure VI-7, once contact is attained, equilibration of Fermi levels ( $E_F$ ) generates a negative space charge ( $\rho$ ) on the side of the insulator which extends over a narrow accumulation zone—due to carrier accepting state densities being large,  $N_c \approx 10^{19} \text{ cm}^{-3}$ —and thus of low resistance. The result is a curve in bands with a reduction in the  $M \rightarrow I$  barrier, such that it equals  $W_M - \chi$ . If  $(W_M - \chi) \approx 0$  or is negative, then the contact is ohmic.

With the application of  $E_a$  in the sense shown in Figure VI-8, *i.e.* directed from the I to M and thus with  $V_a > 0$  at I, it is the whole volume of the very resistive I which suffers the drop in potential, in a drop which decreases with  $V_a$ . On taking into account the antagonistic effect of  $E_{\text{internal}}$  (due to  $\rho$  and directed  $M \rightarrow I$ ) and  $E_a$ , the conduction

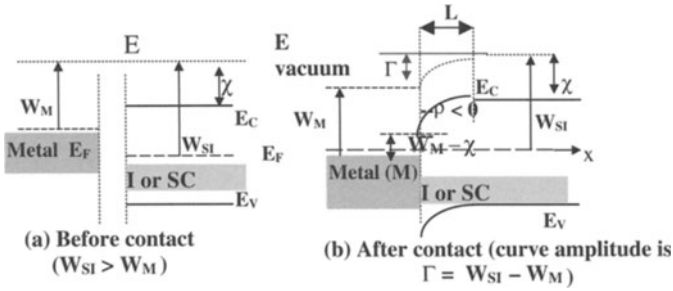


**Figure VI-7.** Metal-insulator contact with  $W_M < W_{SI}$ .

band in I (denoted by  $E_C$  in Figure VI-8) goes through a maximum at  $x = L_c$ , at which point  $dV/dx$  is zero, as is  $E_{resulting}$  ( $V$  being the resulting potential). Therefore, the two effects of internal and external fields compensate one another exactly at  $x = L_c$ , a point which is called the ‘virtual cathode’. As  $E_a$  reaches ( $V_1 \rightarrow V_2$  with  $V_2 \gg V_1$ ),  $L_c \rightarrow L'_c$  with  $L'_c < L_c$ ; the virtual cathode tends towards zero and space charge at this point is repressed. The result is that current can more easily pass through I to a value which is the saturation current limited by space charge  $J_{SCL}$ .

**2 The space charge limited current law and saturation current ( $J_s$ ) for simple injection in insulator without traps**

**a Hypotheses for simple cathodic injection of electrons**

- 1) A band model is applicable to the treatment of the injection of carriers with a current non-limited by an electrode (for example with perfect ohmic contact).

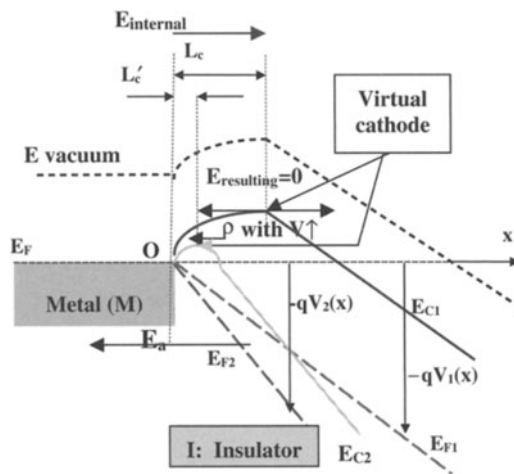


**Figure VI-8.** Effect of applied field ( $E_a$ ) in which polarisation  $V_a > 0$  on insulator, with  $V_a = V_1$  or  $V_2$  such that  $V_2 > V_1$ .

Considerable controversy surrounded whether or not band models, necessary for the description of an ohmic contact, could be applied to organic solids. A model does indeed exist for organic solids [Pfu 86], [Mol 96 and 98] (for polymers, see Figure VI-8) and is close to that of amorphous semiconductors. It should be said that even in inorganic semiconductors, a representation of continuous bands is an approximation. The most important point remains the existence of energy levels within an insulator that can accept, at the interface, injected charges, whether those levels are localised or not. Either way, effects on the resulting mobilities are taken into account because this parameter is included in the final expression for current density.

- 2) Carrier mobilities are independent of  $E_a$  and dielectric permittivity ( $\epsilon$ ) is NOT modified by charge injection. Poole-Frenkel or impact ionisation effects are not considered.
- 3) Electric field is assumed high enough to consider the following current components negligible:
  - current due to thermally generated carriers with density  $n_0$ : ohmic current due to these carriers is negligible under a high injection regime as  $n \gg n_0$ ;
  - current due to diffusion. Here we can note that the applied potential is considerably higher than the thermal potential  $kT/q$ . The derived term for current (conduction) is dominant with respect to that of diffusion:

$$\begin{aligned} J &= \sigma E + qD_n \text{grad } n = qn(x)\mu_n E(x) + q(kT/q)\mu_n (dn/dx) \\ &= \mu_n \rho_l(x) E(x) + \mu_n (kT/q) (d\rho_l(x)/dx) \approx \mu_n \rho_l(x) E(x). \end{aligned}$$

*Comment:* with the form found *a posteriori* for  $\rho_l(x) \approx x^{-m}$  (and  $m \approx 1$ : see following Section c) we have:

$$\frac{J_{\text{diff}}}{J_{\text{derived}}} \approx \frac{kT}{exE(x)} = \frac{kT}{eV(x)}$$

at  $T_{\text{ambient}}$  we have  $kT = 0.025 \text{ eV}$ ; with  $V(x) \gg 0.025 \text{ V}$  the approximation is justified.

- 4) We consider that the system is one dimensional with two planes, the first at  $x = 0$  for the cathode, injecting electrons, and the second at  $x = d$  for the collecting anode.  $E_a$  is sufficiently intense for the resulting field at the cathode to be zero (the same for both real and virtual cathodes);  $E(x = 0) = -(dV/dx)_{x=0} = 0$ . The current in this situation is the saturation current ( $J_s$ ) following Mott's approximation and is the maximum current which can transverse the insulator.

### b Mott-Gurney's expression (1940)

Preamble: in a stationary regime, derivative of  $\vec{J} = 0$ , or rather  $J = \text{constant}$  with respect to  $x$ , such that  $J = qn(x)\mu E(x)$ . Thus, to realise  $J_s$ , we just need to calculate it with respect to  $x = d$ .

Form of  $E(x)$ : Poisson's equation gives

$$\frac{dE(x)}{dx} = \frac{\rho(x)}{\epsilon} = \frac{qn(x)}{\epsilon} = \frac{J}{\epsilon\mu E(x)}.$$

By integrating  $2E(x) \frac{dE(x)}{dx} = \frac{d[E(x)]^2}{dx} = \frac{2J}{\epsilon\mu}$ , and using limiting conditions ( $E(0) = 0$  for  $J = J_s$ ) we have:

$$E(x) = - \left[ \frac{2}{\epsilon\mu} J_s x \right]^{1/2}. \quad (1)$$

(Notice the negative sign which has been used as  $V_a > 0$  and the mean field ( $E_a$ ) is defined by:  $\int_0^d -dV = -V_a = \int_0^d E(x)dx = E_a d$ , or  $E_a = -\frac{V_a}{d}$ ).

- Expression for  $J_s$ : here

$$\int_0^d -dV = -V_a = \int_0^d E(x)dx = - \left( \frac{2J_s}{\epsilon\mu} \right)^{1/2} \int_0^d x^{1/2} dx = - \left( \frac{2J_s}{\epsilon\mu} \right)^{1/2} \frac{2}{3} d^{3/2},$$

and leads to

$$J_s = \frac{9}{8} \epsilon\mu \frac{V_a^2}{d^3} = \frac{9}{8} \epsilon\mu \frac{E_a^2}{d}. \quad (2)$$

### c Graphical representation as in Figure VI-9

Placing eqn (2) into eqn (1) gives

$$E(x) = - \frac{3}{2} \frac{V_a}{d} \left( \frac{x}{d} \right) = \frac{3}{2} E_a \left( \frac{x}{d} \right)^{1/2},$$

and  $E(d) = \frac{3}{2} E_a$ .

Additionally,

$$V(x) = - \int_0^x E(x) dx = - E_a d \left( \frac{x}{d} \right)^{3/2},$$

and thus  $V(x) = V_a \left( \frac{x}{d} \right)^{3/2}$ . The potential energy  $W(x)$  of an electron can be directly deduced from  $V(x)$  as  $W(x) = -qV(x)$  (Figure VI-9-b insert).

The charge density ( $\rho$ ) has the form

$$\rho(x) = \epsilon \frac{dE}{dx} = \frac{3\epsilon E_a}{4d} \left( \frac{x}{d} \right)^{-1/2}.$$

*Comment 1* We can see that the empirically derived curve of the law for  $J_{SCL}$  can yield determination of electron mobility  $\mu$ .



*Comment 2* Here we consider up to what frequency the static characteristic  $J_s = f(V_a)$  can be applied.

So that eqn (2), for a stationary regime (derivative  $\bar{J} = 0$ ), can be applied to a dynamic regime, the transit time of an electron ( $t_s$ ) through thickness  $d$  must be less than the period ( $T$ ) of the applied electric signal *i.e.*  $t_s < T = 1/\nu$ . In other terms, the critical frequency ( $\nu_c$ ) of the applied field cannot go higher than the point at which  $t_s = 1/\nu_c$ .

With  $dt = \frac{dx}{v_n}$  in which  $v_n = -\mu_n E$ , we have

$$t_s = \int dt = \int_0^d -\frac{dx}{\mu_n E(x)};$$

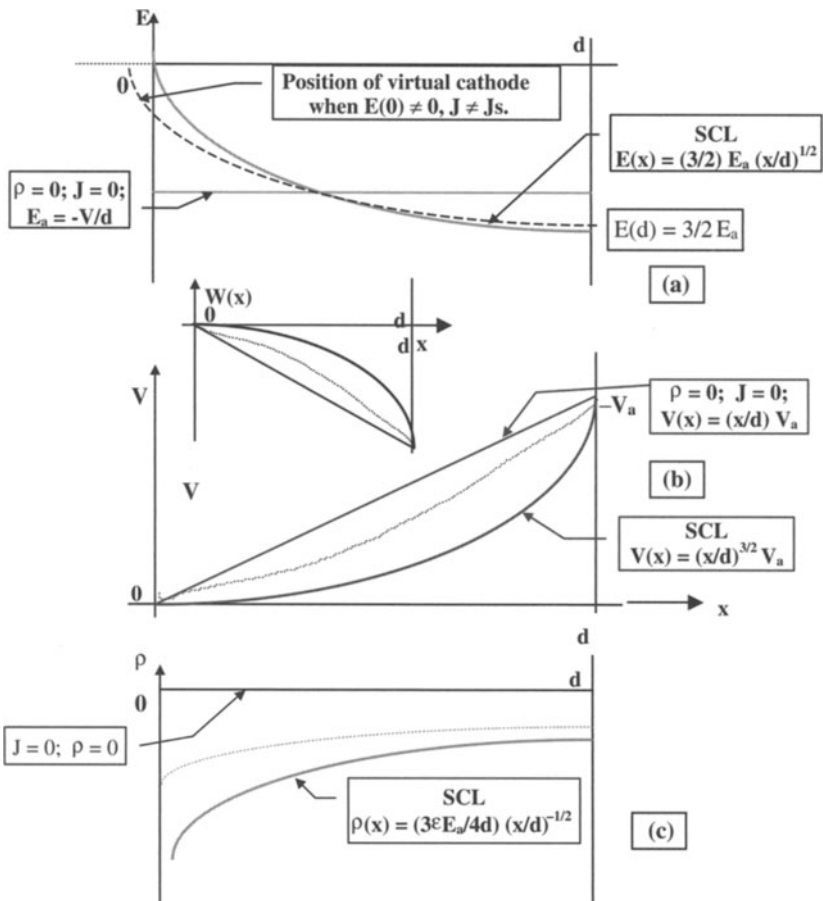


**Figure VI-9.** Representations (a)  $E(x)$ ; (b)  $V(x)$ ,  $W(x)$  and (c) of  $\rho(x)$ ;  $J = \sigma E = \mu \rho(x) E(x) = \text{constant}$  is observed as if  $\rho(x)$  is small,  $E(x)$  is large and *vice versa*.

following eqn (1)

$$E(x) = - \left[ \frac{2}{\epsilon\mu} J_s x \right]^{1/2},$$

and therefore,

$$t_s = \left[ \frac{\epsilon}{2\mu J_s} \right]^{1/2} \int_0^d x^{-1/2} dx = \left[ \frac{2\epsilon}{\mu J_s} \right]^{1/2} d^{1/2}.$$

Taking into account eqn (2), we obtain  $t_s = \frac{4}{3} \frac{d}{\mu V_a}$  and the relationship  $t_s < 1/v$  gives

$$v < v_c = \frac{1}{t_s} = \frac{3}{4} \frac{\mu V_a}{d}. \quad (3)$$

In terms of actual numbers, when  $V_a = 5 \text{ V}$  and  $d = 1 \mu\text{m}$ , we obtain  $v_c \approx 60 \text{ GHz}$ .

### 3 Transitions between regimes

#### a Transition at very low potential

Generally speaking, at very low potentials,  $J(V)$  exhibits a transition at the threshold voltage ( $V_\Omega$ ) going from intrinsic conduction to SCL regimes (see Figure VI-10). In effect, at sufficiently low potentials, the concentration of injected carriers ( $n$ ) remains considerably lower than intrinsic carriers ( $n_0$ ), which are generated by thermodynamic equilibria, and conductivity follows classical the ohmic law:  $J_\Omega = qn_0\mu V_a/d = qn_0\mu E_a$ .

$V_\Omega$ , the voltage at which the current density ( $J$ ) starts to deviate from the ohmic law towards a quadratic SCL law, is such that  $(J_\Omega)_{V=V_\Omega} = (J_s)_{V=V_\Omega}$ , which yields  $V_\Omega = \frac{8}{9} \frac{qn_0 d^2}{\epsilon}$ . In effect, only  $V_\Omega$  may be used to estimate  $n_0$ .

#### b Towards high tensions: transitions between regimes

$\alpha$  *With a blocking contact* The current density  $J_{0sT}$  at an electrode follows, primarily, the law of thermodynamic emission, while in the mass of the material, the

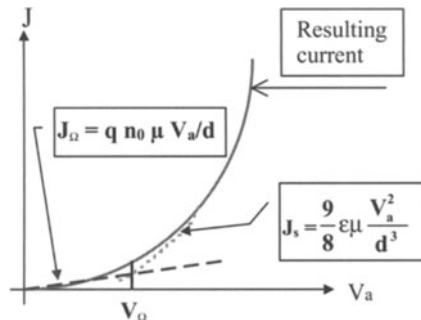


**Figure VI-10.** Transition tension from equilibrated thermodynamics to the SCL law.

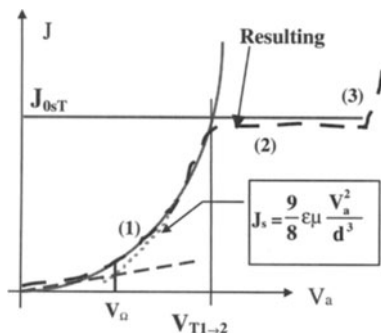


**Figure VI-11.** Possible transitions between different regimes with increasing potential.

current is limited by space charge and tends towards  $J_{SCL} = J_S$ . The following are possible:

- 1 if  $J_{SCL} < J_{0sT}$ , the SCL law is limiting and therefore represents the current through the structure;
- 2 if  $J_{SCL} > J_{0sT}$  (in  $V_a = V_{T1-2}$ ) the thermoelectric emission law (Richardson) conditions the current going through the structure; and
- 3 When  $E_a$  is very high,  $J_{0sT}$  gives way to field effect emissions and then to tunnelling emissions. If  $J_{0T}$  represents the current densities emitted at the electrodes, depending on whether  $J_{SCL} < J_{0T}$  or  $J_{SCL} > J_{0T}$  the current through the structure will follow, respectively, the SCL law or the laws governing the electrodes ( $J_{0T}$ ).

$\beta$  *If the contact is ohmic* By principal  $J = J_{SCL}$  (few traps) (or, as we shall see in the following Section,  $J = J_{TFL}$  if there are many traps). *At highly elevated field strengths*, power laws for  $E$  ( $E^2$  for SCL,  $E^m$  for TFL) can result in extremely high volume currents with  $J_{SCL}$  higher than the injection currents ( $J_{Electrodes}$ ) generated at the levels of contacts, which in themselves never perfectly ohmic as they are never actually infinite reserves of current. At extremely elevated field strengths,  $J_{SCL} > J_{Electrodes}$  is possible and throughout the structure, a transition from SCL (or TFL) to an emission law by tunnelling effects (controlled by the electrode) can appear.

## 4 Insulators with traps and characteristics of trap levels

### a Origin and distribution of traps in organic solids

Organic solids are often far from 'ideal' and contain traps due to imperfections which interact with injected charge carriers. The traps control the current volume of carriers and the characteristics of  $J(V)$ .

There are two types of energetic distributions of traps which are generally cited:

- due to discreet trap levels generally due to chemical impurities;
- a continuous distribution of traps, generally due to structural defaults, of exponential Gaussian form with maximum density at the band edge.

These traps—neutral when empty and charged when full—exert a weak radius of action and can be spatially modelled by an exponential law. The electric field  $E_a$  only slightly modifies (to the order of  $\Delta E_T \approx \text{meV}$ ) the potential barrier ( $U$ ) as shown in Figure VI-12-a, and trapping-detrapping follows Randall and Wilkins's law, that is  $p = \nu_0 \exp(-U/kT)$ .

We should note that two depths of trap can be considered from a thermodynamic point of view, as presented in Figure VI-12-b, with respect to electron traps. That is to say that the electron (and hole) Fermi pseudo-level ( $E_{Fn}$  and  $E_{Fp}$ ) has a factor of degeneracy ( $g_n$  or  $g_p$ ) due to occupation by an electron or hole. The probability of an electron being captured by a trap at energy level  $E_t$  is given by:

$$f_n(E_t) = 1/[1 + g_n^{-1} \exp\{(E_t - E_{Fn})/kT\}].$$

From the probability of trap occupation, we can distinguish between two types of trap:

- shallow traps corresponding to levels  $E_t (\equiv U)$  and situated, for electrons, well above the Fermi pseudo-level of a weak applied field ( $E_{Fn0}$ ) (giving a state approaching that of a thermodynamic equilibrium such that  $E_{Fn0} \approx E_F$ ). In a regime close to equilibrium, most shallow traps are empty, while outside equilibrium (strong injection with  $E_{Fn} \rightarrow E_t$ ), some shallow traps are filled;
- traps with levels  $E_t$  below  $E_{Fn0}$  for electrons, in other words deep traps, are mostly filled with carriers at thermodynamic equilibrium, and in a regime of strong injection ( $E_t < E_{Fn0} < E_{Fn}$ ), practically all traps are filled.

### b Order of size of trap densities

- Trap density in a solid is typically of the order  $N_t \approx 10^{18} \text{ cm}^{-3}$ .
- If we take for example a cfc lattice, which contains an average of 4 atoms per unit and has a unit parameter of *ca.* 0.4 nm, atomic density is *ca.*  $4/(4 \times 10^{-8})^3 \approx 6 \times 10^{22} \text{ cm}^{-3}$ . The ratio  $\frac{\text{default density}}{\text{atom density}} \approx 0.2 \times 10^{-4}$  *i.e.* less than 1 default every 10000 atoms.

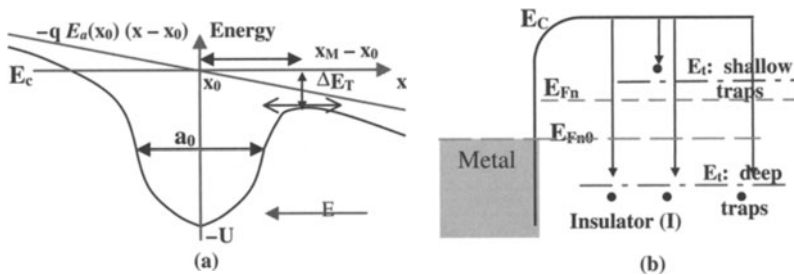


**Figure VI-12.** (a) spatial modelling of a neutral trap; and (b) electron injection levels in an insulator with deep and shallow electron traps.

### c Trapping-detrapping statistics for traps in the discreet level $E_t$

The volume density of trapped electrons ( $n_t$ ) can be given using  $n_t = N_t f_n(E_t)$  in which  $f_n(E_t)$  is the probability of electron capture by a trap of energy level  $E_t$ . Note here that  $E_t \equiv U$ , the trap depth; see Figures VI-12-a and b.

Additionally, if  $c$  is the capture coefficient of a trap and  $n$  is the density of mobile carriers (with  $n = N_C \exp[-(E_C - E_{Fn})/kT]$ ), the number of carriers trapped by necessarily empty per unit time is equal to  $cn$ . As  $(N_t - n_t)$  is equal to the volume density of empty traps, the number of trapped carriers per unit volume and unit time is therefore  $cn(N_t - n_t)$ , which represents the level of total trapping. The alternate process though is that of detrapping in which traps liberate  $p$  electrons per unit time ( $p$  is given by  $p = \nu_0 \exp(-U/kT)$ ). As  $n_t$  is the number of occupied per unit volume, the number of electrons detrapped per unit volume and unit time is  $pn_t$ , which represents the overall detrapping.

At equilibrium, the degree of trapping and detrapping is equal and therefore we have

$$pn_t = cn(N_t - n_t), \quad \text{or} \quad n_t = \frac{N_t}{1 + p/cn} \quad (4)$$

where  $p/cn$  the ratio of probabilities of detrapping from a full trap to trapping by an empty trap.

We can now envisage different scenarios:

- $n_t \ll N_t$  (low degree of trapping): we have  $\frac{n_t}{N_t} = \frac{1}{1+p/cn} \ll 1$  *i.e.*  $p/cn \gg 1$ , which leads to:  $\frac{n_t}{N_t} \approx \frac{1}{p/cn}$ , that is

$$\frac{n}{n_t} = \frac{p}{cN_t} = \frac{\nu_0}{cN_t} \exp(-E_t/kT).$$

Numerically, with  $E_t = 0.25$  eV,  $N_t \approx 10^{18} \text{ cm}^{-3}$ ,  $c = 10^{-10} \text{ cm}^3 \text{ s}^{-1}$ ,  $\nu_0 = 10^{10} \text{ s}^{-1}$ , and at  $T = 80$  K we have  $\frac{n}{n_t} \approx 10^{-14}$ , while at  $T = 300$  K we obtain  $\frac{n}{n_t} \approx 10^{-4}$ . In both cases there is a very high proportion of trapped electrons with respect to free, mobile electrons, even though there is a low concentration of traps.

- $n_t \approx N_t$  (high degree of trapping): this occurs when  $p \rightarrow 0$  (very low detrapping probability) *i.e.* when  $E_t \equiv U \gg kT$  and is due to very deep traps, or at a limit, very low temperatures.

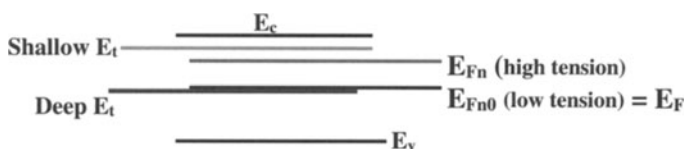


Figure VI-13. Location of energy levels for shallow and deep traps.

## 5 Expression for current density due to one carrier type ( $J_{sp}$ ) with traps at one discreet level ( $E_t$ ); effective mobility

### a At low tensions

$n_0 \gg n$  and the density of thermally generated carriers ( $n_0$ ) is well above the density of injected charges ( $n$ ) and the current undergoes runaway (current emitted or injected). In the presence of traps of density  $N_t$ , we have  $n_0 = n_{of} + n_{ot}$  in which:

- $n_{of} = N_c \exp(-[E_c - E_{Fn0}]/kT)$  and is the density of free charges (not trapped) of mobility  $\mu_{of}$  (with a Fermi pseudo-level in this low tension regime  $E_{Fn0} \approx E_F$ : Fermi level at thermodynamic equilibrium).
- $n_{ot} = N_t f_{n0}(E_t) = \frac{N_t}{1 + g_n^{-1} \exp[(E_t - E_{Fn0})/kT]}$  density of charged traps.

Ohm's law, with respect to free carriers, is (with  $\mu_{of} = \mu_n$ )

$$J_\Omega = q n_{of} \mu_{of} E_a \quad (5)$$

#### $\alpha$ Two limiting cases

- Shallow traps:  $E_t > E_{Fn} > E_{Fn0}$ , so  $\exp[(E_t - E_{Fn0})/kT] \gg 1$  and  $n_{ot} \approx 0$ :  $n_0 = n_{of} + n_{ot} \approx n_{of}$ . Ohms law remains unchanged when there are no traps:  $J_\Omega = q n_0 \mu_{of} E$ .
- Deep traps:  $E_t \leq E_{Fn0}$ , and  $n_{ot} \neq 0$ . For Ohm's law, beyond the general eqn (5), we can also write

$$J_\Omega = q n_0 \mu_{eff} E = q (n_{of} + n_{ot}) \mu_{eff} E \quad (6)$$

which defines the effective mobility, the value of which can be obtained on equalising eqns (5 and 6) to give  $\mu_{eff} = \frac{n_{of}}{n_{of} + n_{ot}} \mu_{of}$ .

#### $\beta$ Important comments

- General expression for mobility:  
In a general manner  $\theta = n_{of}/n_{of} + n_{ot}$  with  $\mu_{eff} = \theta \mu_{of}$ . With shallow traps ( $n_{ot} \approx 0$  and  $n_0 \approx n_{of}$ ):  $\theta \approx 1$  and  $\mu_{eff} \approx \mu_{of}$ .
- Under a continuous regime  $V < V_\Omega$ , and ohmic conduction is predominant but does not prevent carrier injection, which is in the minority at low tensions. Accordingly, a transitory regime is generated corresponding to trapping of injected carriers which is associated with the appearance of current peaks; it is only once carriers are trapped that linear, ohmic conduction can be observed. If we take the curve of a second characteristic  $J(V)$ , we can then see a much smoother transition, practically without peaks (as traps responsible for current peaks are filled).

### b Form of J at higher tensions (injection)

At higher tensions, the Fermi pseudo-level is  $E_{Fn}$  and we have:

- $n = N_c \exp(-[E_c - E_{Fn}]/kT)$  for density of free, untrapped charges with mobility  $\mu_f = \mu_n$ ,
- $n_t = N_t f_n(E_t) = \frac{N_t}{1 + g_n^{-1} \exp[(E_t - E_{Fn})/kT]}$  for density of trapped charges.

Thus  $\theta \rightarrow \theta_n = n/(n + n_t)$  and  $\mu_{\text{eff}} = \theta_n \mu_n$ .

Under a regime of charge injection, whether traps are deep or shallow, injected carriers are distributed between free and trapped carriers. The result is the mean effective mobility, which can equally be obtained through using a Poisson distribution.

$\alpha$  *Effective mobility* with  $\rho_{\text{mobile}} = nq$  and  $\rho_{\text{trap}} = n_t q$ , Poisson's equation gives:

$$\frac{dE}{dx} = \frac{\rho_{\text{mobile}} + \rho_{\text{trap}}}{\epsilon} = \frac{(n + n_t)q}{\epsilon}.$$

With  $J = n q v = n q \mu_n E$ :

$$E \frac{dE}{dx} = \frac{J}{n\mu_n} \frac{n + n_t}{\epsilon} = \frac{J}{\mu_{\text{eff}} \epsilon} \quad (7)$$

with

$$\mu_{\text{eff}} = \mu_n \frac{n}{n + n_t}. \quad (8)$$

As  $n + n_t > n$ , in all cases,  $\mu_{\text{eff}} < \mu_n$ . (When there is a low degree of trapping, it is possible to write

$$\mu_{\text{eff}} = \mu_n \frac{1}{1 + n_t/n} = \frac{1}{1 + cN_t/p} = \frac{p}{p + cN_t};$$

and as  $n_t/n \gg 1$ ,  $\mu_{\text{eff}} \ll \mu_n$ ).

$\beta$  *Expression for J* Integration of eqn (7) gives, for E, a solution which resembles that of eqn (1), with the precision that the effective mobility ( $\mu_{\text{eff}}$ ) replaces the mobility  $\mu_n$  ( $\equiv \mu$  by notation).  $J_s$  (denoted in the presence of traps as  $J_{sP}$ ) is thus given by eqn (2), in which  $\mu$  is replaced by  $\mu_{\text{eff}}$ :

$$J_{sP} = \frac{9}{8} \epsilon \mu_{\text{eff}} \frac{V_a^2}{d^3} = \frac{9}{8} \epsilon \mu_{\text{eff}} \frac{E_a^2}{d}. \quad (9)$$

*Comment* Current density can also be written either as  $J = q n \mu_n E_a$ , or as  $J = q(n + n_t)\mu_{\text{eff}} E_a$ . The equality of these two relationships gives  $\mu_{\text{eff}} = \theta_n \mu_n$  again with  $\theta_n = n/(n + n_t)$ . By comparing eqn (9) with

$$J = q(n + n_t)\mu_{\text{eff}} E_a \quad (9')$$

shows that  $(n + n_t) \propto E_a$  and that in (9'), J is not ohmic. Physically speaking, this is quite normal, as the concentration (n) depends upon the value of  $E_a$  under a high tension regime.

#### $\gamma$ Trap effects on conduction

- If the concentration of traps  $N_t$  increases, in accordance with eqn (4)  $n_t$  also increases, such that  $\mu_{\text{eff}}$  (given by eqn (8)) decreases along with  $J_{sP}$ ; the material no longer appears insulating;
- If  $E_t$  increases, or if T decreases, p drops and  $n_t$  increases; once again  $\mu_{\text{eff}}$  decreases along with  $J_{sP}$ .

$\delta$  *Frequency limit for  $J_{SP}$  as expressed for a static system* Given eqn (3), which concerns a system without traps  $v < v_c = \frac{1}{t_s} = \frac{3}{4} \frac{\mu V_a}{d}$ ,  $\mu$  must be replaced by  $\mu_{eff}$ , and the limiting condition for eqn (9) corresponds to frequencies such that:

$$v < v_{ceff} = \frac{1}{t_{seff}} = \frac{3}{4} \frac{\mu_{eff} V_a}{d^2}. \quad (10)$$

As  $\mu_{eff} < \mu$ ,  $v_{ceff} < v_c$  and can be explained by the fact that the transit time increases as carriers spend more time in traps such that transit time in the presence of traps ( $t_{seff}$ ) is  $t_{seff} > t_s$ , and thus  $v_{ceff} = \frac{1}{t_{seff}} < v_c = \frac{1}{t_s}$ . On performing the quotient  $\frac{(10)}{(3)}$  we obtain

$$\frac{v_{ceff}}{v_c} = \frac{\mu_{eff}}{\mu} = \frac{n}{n + n_t} = \frac{J_{SP}}{J_s}.$$

Using the calculation in Section 4-c above, in a system with low level doping it is evident that  $J_{SP} \approx 3V_a^2$  at 300 K and  $J_{SP} \approx 10^{-14}V_a^2$  at 80 K, which yield limiting frequencies of, respectively,  $v_{ceff} \approx 4$  MHz and  $v_{ceff} \approx 7$   $\mu$ Hz. At low temperatures, we are limited to  $\mu$ Hz, which correspond to excessively long signal periods (greater than  $10^6$  s).

### c Characteristics of $J_{SP} = f(V)$ for levels of discreet, shallow and deep traps (Figure VI-14)

$\alpha$  *System with discreet shallow traps* When there is a low enough level of traps and the system is placed under a tension sufficiently high, so that  $n_0$  is negligible with respect to injected charge density and the Fermi pseudo-level is below the trap energy

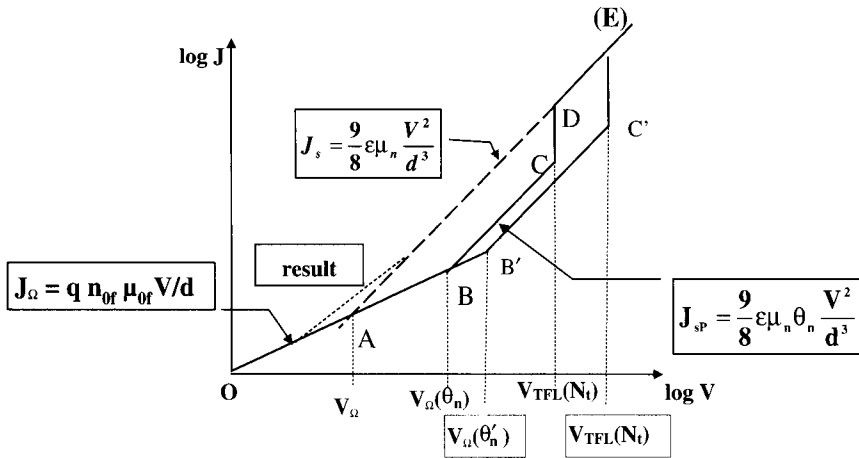


**Figure VI-14.** SCL law in presence of discreet, shallow traps. At low tensions, the law is ohmic ( $J_\Omega$ ); at higher tensions ( $V > V_\Omega$ ) current follows  $J_{SP}$  law, which is the SCL law modified by carrier mobility which, on average, reduces *i.e.*  $\mu_{eff} = \mu_n \theta_n$  with  $\theta_n < 1$ . When all traps are filled ( $V = V_{TFL}$ ) the system returns to following the SCL law (current  $J_s$ ).



level, the above cited SCL law ( $J_{SCL}$ ) tends towards a new law ( $J_{SP}$ ) which can be written

$$\theta_n = \frac{n}{n + n_t} : J_{SP} = \frac{9}{8} \epsilon \mu_n \theta_n \frac{V^2}{d^3}$$

and varies as  $V^2/d^3$  but with a reduced charge carrier mobility (Figure VI-14). At even higher tensions ( $V \geq V_{TFL}$ ) all traps fill and the system returns to the normal SCL law. Transitional tensions,  $V_\Omega$  and  $V_{TFL}$ , are shifted towards higher tensions when trap density rises ( $N'_t > N_t$  and  $\theta'_n < \theta_n$ ).

For very shallow traps, where  $E_t \gg E_{Fn0}$ , and at thermodynamic equilibrium the concentration of carriers in traps levels is given by:

$$n_{t0} = \frac{N_t}{1 + g_n^{-1} \exp[(E_t - E_{Fn0})/kT]} \approx 0.$$

And the density of non-occupied traps at thermodynamic equilibrium is thus  $N_t - n_{t0} \approx N_t$ ; application of a tension up to  $V = V_{TFL}$  results in the filling of initially empty  $N_t$  traps. We can use Poisson's equation to detail the tension  $V_{TFL}$  in a corresponding field  $E_{TFL}$ :  $\frac{dE_{TFL}}{dx} = \frac{qN_t}{\epsilon}$ . By twice integrating this equation from 0 to  $d$ , we arrive at  $V_{TFL} = \int_0^d E_{TFL} dx = \frac{qN_t d^2}{2\epsilon}$ . (From  $V_{TFL}$ , it is possible to derive  $N_t$ ).

*$\beta$  System with discreet, deep traps* The mechanism for a system with deep traps shown in Figure VI-15 exhibits, at not too elevated tensions, very low effective mobility and thus a low current limited by space charge effects (essentially associated with trapped charges). The ohmic regime continues up to the point at which all traps are filled, which occurs at a sufficiently high tension ( $V_{TFL}$ ), and then current follows the SCL law, characterised by the current density  $J_S$ .

For deep traps, we have  $E_t < E_{Fn0}$ , and at thermodynamic equilibrium the concentration in trap levels of carriers is

$$n_{t0} = \frac{N_t}{1 + g_n^{-1} \exp[(E_t - E_{Fn0})/kT]} \neq 0.$$

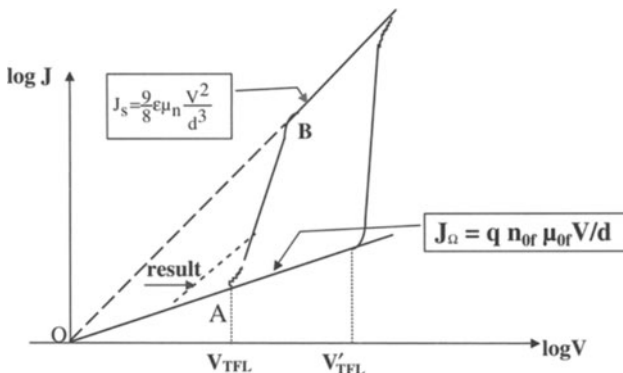


Figure VI-15. Current tension characteristics for system with discreet, deep traps.

At thermodynamic equilibrium, the density of unoccupied traps is thus  $N_t - n_{0t}$ . With applied tension  $V_{\text{TFL}}$  results in the filling of the  $(N_t - n_{0t})$  traps and an associated charge density of  $q(N_t - n_{0t})$ . Poisson's equation allows determination of

$$V_{\text{TFL}} = \int_0^d E_{\text{TFL}} dx = \frac{q(N_t - n_{0t})d^2}{2\epsilon}.$$

*Comment* We should note that while these characteristics have been observed, especially for systems with shallow traps, only the first two parts of the curve generally appear (region in OABC of Figure VI-14); at higher tensions, diodes have a tendency to undergo premature degradation!

## 6 Deep level traps distributed according to Gaussian or exponential laws

### a Distribution form

We can consider different forms of distribution for traps, that of exponential or Gaussian. Here we shall develop the former, and in the next Section, the latter.

We can suppose that the density of traps per unit energy, centred about energy  $E$ , is of the form:  $g(E) = (N_t/kT_t) \exp(-[E_c - E]/kT_t)$  in which  $N_t$  is the total density of trap levels and  $T_t$  is a constant characteristic of the decrease in trapping energy with depth  $E$ . Taking  $T_t = E_t/k = mT$  in which  $E_t$  represents the characteristic energy of traps with respect to  $E_c$  and  $m$ , also, is characteristic of trap distribution, given that for a high value of  $m$ , the decrease in distribution is less than that of Boltzmann, in which  $m = 1$ .

When  $T_t \gg T (E_t \gg kT)$  and traps levels are mostly under  $E_c$  giving rise to a non-degenerate distribution of traps represented by Fermi-Dirac's distribution), we can suppose that for  $-\infty < E < E_{\text{Fn}}$  we have  $f_n(E) \approx 1$  and for  $E > E_{\text{Fn}}$  we have  $f_n(E) \approx 0$  (as if  $T = 0$ ). Given these hypotheses, the concentration of filled trap levels is

$$n_t = \int_{E_{\text{min}}}^{E_{\text{max}}} g(E)f_n(E)dE = \int_{-\infty}^{E_{\text{Fn}}} \frac{N_t}{kT_t} \exp\left(-\frac{E_c - E}{kT_t}\right) dE = N_t \exp\left(-\frac{E_c - E_{\text{Fn}}}{kT_t}\right).$$

With  $n = N_c \exp(-[E_c - E_{\text{Fn}}]/kT)$  we obtain

$$n_t = N_t \left(\frac{n}{N_c}\right)^{T/T_t} = N_t \left(\frac{n}{N_c}\right)^{1/m}.$$

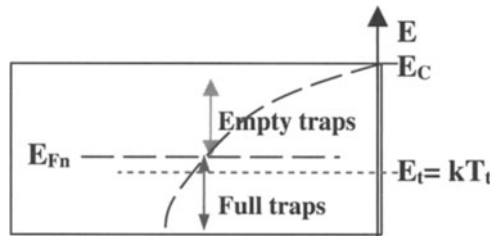


Figure VI-16. Representation of an exponential distribution of traps.

**b Form of saturation current for an exponential distribution ( $J_{exp}$ )**

On multiplying the two parts of the Poisson equation by  $[(m + 1)/m][E(x)]^{1/m}$  we obtain:

$$\left(\frac{m + 1}{m}\right) [E(x)]^{1/m} \frac{dE(x)}{dx} = \frac{d[E(x)]^{(m+1)/m}}{dx} = \frac{m + 1}{m} [E(x)]^{1/m} \frac{q}{\epsilon} (n + n_t).$$

If  $n_t \gg n$  (that is  $N_t \gg N_c$ ) and  $E(0) = 0$  and  $n = J_{exp}/q\mu_n E(x)$  (denoting the current density in this exponential distribution of traps by  $J_{exp}$ ), integration over the interval  $[0, h]$  gives us:

$$E(h) = \left[ \left(\frac{m + 1}{m}\right) \frac{qN_t}{\epsilon} \left(\frac{J_{exp}}{q\mu_n N_c}\right)^{1/m} \right]^{\frac{m}{m+1}}.$$

On using the confined integral (which gives limiting conditions)  $V = \int_0^d E(h)dh$  we arrive at:

$$J_{exp} = q^{(1-m)} \mu_n N_c \left(\frac{2m + 1}{m + 1}\right)^{m+1} \left(\frac{m}{m + 1} \frac{\epsilon}{N_t}\right)^m \frac{V^{m+1}}{d^{2m+1}}.$$

The resulting equation below is generally known as the Tapped Charge Limited Current (TCL) law and its shape is shown in Figure VI-17.

$$J_{TCL} = J_{exp} \propto V^{m+1}/d^{2m+1}.$$

Qualitatively speaking, with increasing current the Fermi pseudo-level increases towards  $E_C$  (bottom of conduction band) and traps below  $E_{Fn}$  fill up. There is a progressive reduction in the number of empty traps, and fresh injected charges are increasing distributed towards free states (in which charges have density  $n$ ). The effective mobility, as great as  $n$  is high, increases with  $V$  following a high power law

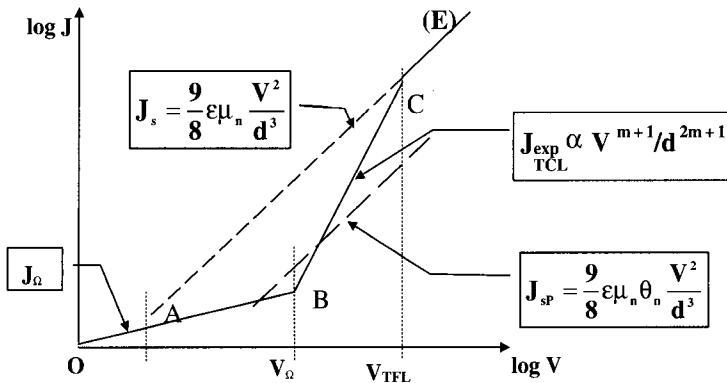


**Figure VI-17.** Current tension characteristics for exponentially distributed traps.

$V^{m+1}$  in which  $m$ , as we already have seen, is characteristic of the mean depth ( $E_t$ ) of trap levels  $E_t = kT_t = kmT$ .

When all traps are filled, a transition from a TCL current (with carriers exponentially trapped) to a SCL current (with non-trapped carriers) takes place. The tension of this transition ( $V_{TFL}$ ) can be obtained at  $J_s = J_{TCL}$ , that is

$$V_{TFL} = \frac{qd^2}{\epsilon} \left[ \frac{9 N_t^m}{8 N_c} \left( \frac{m+1}{m} \right)^m \left( \frac{m+1}{2m+1} \right)^{1+1} \right]^{\frac{1}{m-1}}$$

We should note therefore that the two slopes of  $\ln J = f(\ln V)$  for  $J_s$  and  $J_{TCL}$  are different in contrast to those of  $J_s$  and  $J_{SP}$  which give parallel lines of slope 2.

As we have done for traps associated with discrete levels, we can now determine  $V_\Omega$ , the tension characteristic of a transition from the ohmic regime at low tensions (following  $J_\Omega = qn_0f\mu_n \frac{V}{d}$ ) to a TCL regime. Thus  $V_\Omega$  can be obtained when  $J_\Omega = J_{exp}$ , that is:

$$V_\Omega = \frac{qd^2 N_t}{\epsilon} \left( \frac{n_{of}}{N_c} \right)^{\frac{1}{m}} \left( \frac{m+1}{m} \right) \left( \frac{m+1}{2m+1} \right)^{\frac{m+1}{m}}$$

### c Example of exponential distribution

The example of copper  $\alpha$ -phtalocyanine is used [Kao 81].

Empirically obtained results, detailed in Figure VI-18, showed that:

- in the non-ohmic zone, the slope ( $m$ ) decreased with increasing temperatures (as  $mT = T_t = E_t/k = \text{constant}$  for a given material and as  $T$  increases,  $m$  decreases);

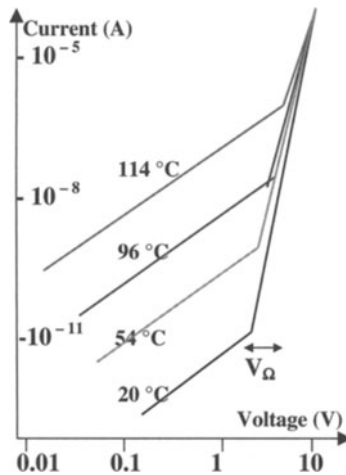


Figure VI-18. Idealised representation of  $J_{exp} = f(V)$  for  $\alpha$ -CuPc.

- $V_{\Omega}$  increases with increasing  $T$ ;
- $N_t \approx 10^{15} \text{ cm}^{-3}$ .

#### d Gaussian trap distribution

A Gaussian trap distribution can be denoted by

$$g(E) = \frac{N_t}{(2\pi)^{1/2}\sigma_t} \exp\left[-\frac{(E - E_{tm})^2}{2\sigma_t^2}\right]$$

in which  $E_{tm}$  is the level at which there is the highest trap density and  $\sigma_t$  standard deviation.

Two types of trap distributions can also be considered:

- *Shallow traps* which are supposed to be such that  $E_{tm} > E_{Fn}$  and any current resembles  $J_{SP}$  (due to discrete trap level) *i.e.*  $J_G \propto V^2/d^3$ .
- *Deep traps* correspond to  $E_{tm} < E_{Fn}$  and the current resembles that of  $J_{exp}$ , and the parameter  $m$  should be replaced by a parameter of the form:  
 $m \rightarrow (1 + 2\pi^2/16k^2T^2)^{1/2}$  [Kao 81] which the expression for current remains of the form  $J_{Gaus.} \propto V^{m+1}/d^{2m+1}$ .

## V Double injection and volume controlled current: mechanism C in Figure VI-2

### 1 Introduction: differences in properties of organic and inorganic solids

Here we shall review only media in which there are only direct band to band recombinations, termed ‘bimolecular’ [Kao 81] but no traps or recombination centres. The level of band to band recombination ( $R$ ) is defined by the equation  $\frac{dn}{dt} = \frac{dp}{dt} = -R = -C_R np$  where  $C_R = \langle v\sigma_R \rangle$  and is the recombination constant,  $\sigma_R$  is the effective recombination surface (the sectional area through which a carrier must pass to recombine) and  $v$  is electron and hole velocities. If carriers hop over barriers more by electric field effects than thermal agitation then we should denote their velocity, which depends on the applied field and carrier mobility, using  $v = (\mu_n + \mu_p)E_a$ .

#### a Inorganic solids

The carrier mobilities are large and constants  $C_R$  are low. In fact, the latter is generally so low that bimolecular recombinations can be considered negligible, and in order to favour recombinations—which are no longer ‘bimolecular’—centres must be introduced into the material. The velocity ( $v$ ) is of the order of thermal electron and hole velocities and is independent of the applied field. In addition, for a volume controlled current (VCC), the negative and positive space charges at the electrodes are of the same order of size as those under SCL for simple charge injection with overlapping

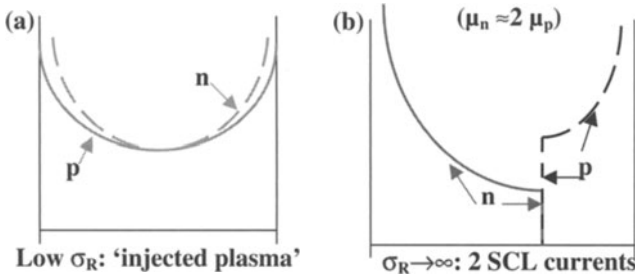


**Figure VI-19.** Double injection and spatial distribution of charge densities in: (a) inorganic and; (b) organic materials.

in the crystal volume (without recombining), and therefore mostly cancel each other out ('injected plasma' in Figure VI-19-a). The result is a current which is no longer limited by space charges and can thus reach high values.

## b Organic solids

In contrast to inorganics, carriers in organic solids exhibit low mobilities and high values of the constant  $C_R$ , so 'high density injected plasmas' become highly improbable. Due to the high value of  $\sigma_R$  generally encountered, there is no zone in which electrons and holes can overlap (if there were, there would be an infinite recombination current). The result is that electron current exists only at the cathode and hole current only at the anode: the two meet and annihilate each other at a plane separating the two regions, as shown in Figure VI-19-b.

## 2 Fundamental equations for planar double injection (two carrier types) when both currents are limited by space charge: form of resulting current $J_{VCC}$ (no trap nor recombination centres)

**a As for SCL, the following hypotheses are used (as both carrier currents are limited by space charges):**

- the band model is applicable;
- $E_a$  is sufficiently high to consider  $J_{intrinsic}$  and  $J_{Diffusion}$  negligible;
- mobilities  $\mu$  and  $\epsilon$  are not modified by  $E_a$ ; and
- there is perfect ohmic contact (infinite charge reserve) at the metallic cathode (at  $x = 0$ ) and anode (where  $x = d$ ). We therefore have:  $n(0) = \infty$ ;  $p(d) = \infty$ ;  
 $E(x = 0) = E(x = d) = 0$ ;  $\int_0^d E(x) dx = -V$ .

## b Parmenter and Ruppel's equation: general example

In general, double injection is assumed to be governed by:

- equations for current:  $J_n = n q \mu_n E$ ,  $J_p = p q \mu_p E$  and  $J = J_n + J_p$ ;

- equations of continuity:  $\frac{1}{q} \frac{dJ_n}{dx} = R$  and  $-\frac{1}{q} \frac{dJ_p}{dx} = R$ ; and
- Poisson's equation:  $\frac{dE}{dx} = \frac{\rho}{\epsilon} = \frac{q}{\epsilon} [p(x) - n(x)]$ .

Given the preceding limits and some rather long equations detailed elsewhere [Kao 81, p 259], the resulting current ( $J_{VCC}$ ) is given by  $J_{VCC} = \frac{9}{8} \epsilon \mu_{\text{eff}} \frac{V^2}{d^3}$  in which  $\mu_{\text{eff}}$  is the effective mobility which is of the complicated form  $\mu_{\text{eff}} = (8q \mu_n \mu_p / 9\epsilon \langle v\sigma_R \rangle) f(\alpha, \beta, \mu_n, \mu_p)$ , with  $\alpha = 2q/\epsilon$ ,  $\beta = \langle v\sigma_R \rangle$ .

### c Limiting case 1: $\langle v\sigma_R \rangle$ is low (as for inorganics)

When  $\sigma_R$  is low,  $\mu_{\text{eff}}$  takes on a high value:

- poor recombination is not an obstacle to the penetration of electrons and holes within the sample, and the condition of overall neutrality is retained within the volume given for  $n \approx p$  ('injected plasma' shown in Figure VI-19-a); and
- there is no space charge to limit current so  $\mu_{\text{eff}}$  and  $J_{VCC}$  are high.

### d Limiting case 2: $C_R$ and $\langle v\sigma_R \rangle$ are high ( $\sigma_R$ high, as for organic solids)

Here we have two SCL currents with a weak overlap of space charges.  $J_{VCC}$  can be calculated directly when  $C_R$  is large [Hel 67] and recombinations are highly efficient and, consequently, there is a very thin space charge overlapping layer. We can thus consider that for the 2 SLC currents produced at each electrode, the two converging currents annihilate each other.

Sequentially, it is assumed that:

- tensions and the thickness of layers for each—well separated—charge type can be summed:

$$L = L_n + L_p \text{ et } V = V_n + V_p; \quad (1)$$

- the electric field does not undergo any great discontinuity in going from one part to another in the recombination zone and therefore

$$V_n/L_n = V_p/L_p; \text{ and} \quad (2)$$

- current associated with electrons (over  $L_n$ ), or with holes (over  $L_p$ ), is such that  $J_n = J_p = J_{VCC} = \text{constant}$ . With each  $J_i$  being of the form  $J_i = (9/8)\epsilon\mu_i V_i^2/L_i^3$ :

$$1 = \frac{J_n}{J_p} = \frac{\mu_n (V_n/L_n)^2 (1/L_n)}{\mu_p (V_p/L_p)^2 (1/L_p)} = \frac{\mu_n L_p}{\mu_p L_n}, \text{ so } \mu_n/\mu_p = L_n/L_p = V_n/V_p. \quad (3)$$

It should be noted that when  $\mu_n > \mu_p$  then  $L_n > L_p$  and the more mobile carriers travel the furthest.

From eqn (3),

$$V_n = V_p \mu_n / \mu_p, \quad (4)$$

which inserted in eqn (1) gives  $V_p = V/(1 + \mu_n/\mu_p)$ .

Placing  $V_p$  in  $J_p = J_{VCC}$  finally gives  $J_{VCC} = \frac{9}{8}\epsilon(\mu_n + \mu_p)\frac{V^2}{L^3}$ .

The resulting current is the sum of two individual currents limited by space charge, and therefore the effective mobility is actually the sum  $\mu_{eff} = \mu_n + \mu_p$ . As shown in Figure VI-19-b, the electron current exists only at the cathode and the hole current only at the anode; on meeting they annihilate one another at a plane which divides the space and has a position determined by the values of  $\mu_n$  and  $\mu_p$ .

We can finally note that, like  $\mu_{eff}$ ,  $J_{VCC}$  is relatively weak.

*Comment* if  $\mu_n \gg \mu_p$  or  $\mu_n \ll \mu_p$  we have, respectively, either  $\mu_{eff} \approx \mu_n$  or  $\mu_{eff} \approx \mu_p$  and again find that current is limited by space charge (SCL) associated with a single carrier type, as is often the case in organic solids. However, we should note that often in these media,  $J_n \neq J_p$  and the preceding calculation is therefore not necessarily appropriate (even though—as we shall see in later Sections—optimisation of the efficiency of OLEDs can result in  $J_n \approx J_p$ ).

### e Limiting case 3: real example of continuously high but constrained $C_R$

$C_R$  does not tend towards infinity, imposing a degree of overlap between the two space charges [Hel 67].  $n(x)$  can therefore be expressed as a function of  $W$ , the size of the recombination zone, for which:

- $J = J_n + J_p = q[n(x)\mu_n + p(x)\mu_p]E(x) = \text{constant}$ ; and (5)
- taking into account that the recombination zone is actually rather thin with respect to the overall film thickness, the electric field can be assumed constant, so the continuity equation gives, for electrons: charge  $-q$  and velocity  $v_n = -\mu_n E$ , with  $J_n = -qn v_n = qn\mu_n E$ . Bringing in  $\frac{dn}{dx} = \frac{dp}{dx} = -R = -C_R np$  yields:

$$(dJ_n/dx) = q\mu_n E(dn/dx) = qC_R n p. \quad (6)$$

(Similarly for holes,  $(dJ_p/dx) = q\mu_p E(dp/dx) = -qC_R n p$ ).

Using eqn (5) to eliminate  $p$  in eqn (6) derives  $n(x)$ :

$$n(x) = \frac{n_\infty}{1 + \exp[2(L_h - x)/W]} \text{ with } W = \frac{2qE^2\mu_n\mu_p}{JC_R}, \text{ or as}$$

$$E = (3/2)V/L, \quad W = \frac{4q\mu_n\mu_p L}{C_R\epsilon(\mu_n + \mu_p)} :$$

in which, by definition,  $W$  is the size of the recombination zone.

The size of  $W$  is inversely proportional to  $C_R$ , (as in the limiting case 2 shown detailed in Section d).

## 3 Applications

### a Practical application of double injection in organic solids

From the relationship for current density in organic solids for double injections with a high value of  $C_R$ ,  $J_{VCC} = \frac{9}{8}\epsilon(\mu_n + \mu_p)\frac{V^2}{L^3}$ , we can see that if  $\mu_n \gg \mu_p$  or  $\mu_n \ll \mu_p$ ,



we obtain  $\mu_{\text{eff}} \approx \mu_n$  or  $\mu_{\text{eff}} \approx \mu_p$  and current is limited by space charges (SCL) associated with single carriers. This is what happens in organic solids, where with two SCL currents we have either:

- at  $\mu_n \gg \mu_p$  (as in molecular solids such as Alq3),  $\mu_{\text{eff}} \approx \mu_n$  and the recombination zone is situated close to the hole ‘injecting’ anode while the current is essentially an ‘SCL’ current of electrons; or
- at  $\mu_n$  being around two orders lower than  $\mu_p$  (as in conjugated polymers in which poor electron mobility is generally associated with traps due to oxygen impurities [Gre 95, p74]),  $\mu_{\text{eff}} \approx \mu_p$  and the recombination zone is situated close to the electron ‘injecting’ cathode while the current is essentially an ‘SCL’ current of holes.

### **b Both electron and hole currents are limited by electrodes (rather than SCL effects as above)**

The problem can be treated as a superposition of two individual currents, although modification of the level of injection can occur at the contacts if electrons-hole recombinations are incomplete.

### **c Application to electroluminescence**

To obtain electroluminescence it is essential to control the level of injection and transport of the two currents, each associated with a different carrier, so that:

- the currents are at equilibrium so that there is no single dominating current which could otherwise traverse the diode without meeting current of the opposite sign; and
- the currents meet each other in the volume of the material and, if possible, not near the electrodes where recombinations do not yield radiation.

As we shall see, various strategies have been devised:

- if current is electrode governed, barriers at the electrodes can be adjusted for electrons (Ca) and holes (ITO) so that currents are of the same order of size. Barriers can be brought to the same low level by adjusting either the work function of the chosen metal electrode, the electron affinity or the ionisation energy of the organic volume; and
- if current is controlled by the volume of the diode, then we can choose layers of materials which go in between each electrode and the volume of the material which exhibit mobilities equilibrating the two SCL currents. Recombinations can then occur within a layer specifically optimised for high quantum emission yields.

Another strategy consists in generating a confinement layer which can be formed from ‘heterojunctions’ which exhibit at least bilayer structures allowing recombination of opposing carriers to be confined at a plane normal to their trajectories.

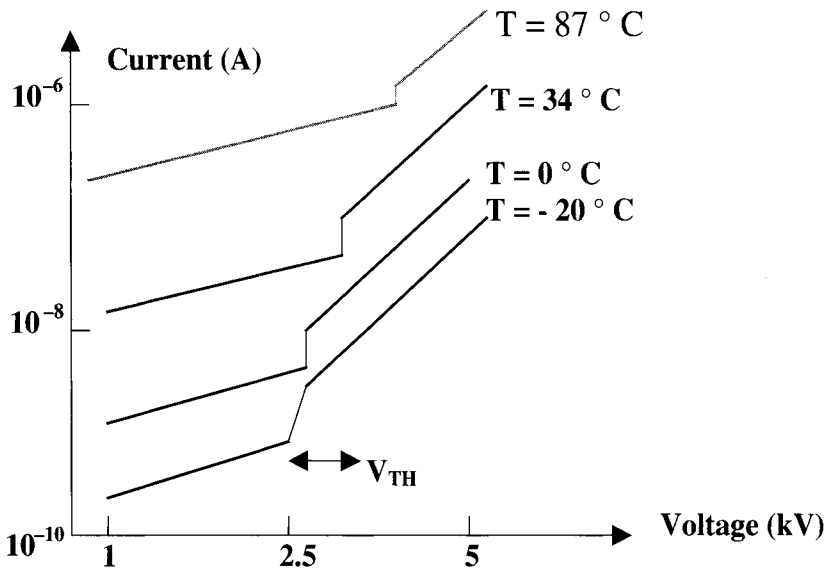


**Figure VI-20.** Single to double injection transition using example of anthracene with gold electrodes (after Hwang and Kao (1973) [Kao 81]).

#### d Transition from single to double injection

At low field strengths, one electrode can already inject for example electrons, while the other cannot yet inject holes. At a higher value of  $E_a$  (and thus from a single field) the second electrode can in turn inject (as shown in the example in Figure VI-20 below for anthracene with gold electrodes):

- at tensions  $V < V_{TH}$  only for electroluminescence,  $J \propto V^2$ , a characteristic of a solid with single (hole) injection (and discrete hole traps);
- at tensions  $V > V_{TH}$ ,  $J \propto V^n$  where  $n > 6$ , a characteristic of a high current which can be associated with electron injection by field effects, which in turn can result from a sufficient accumulation of space charge at the cathode to favour electron emission by tunnelling effects.

When there is double injection, the currents are summed, but if one is considerably greater than the other, the largest will determine the resulting law.

## VI The particular case of conduction by the Poole–Frenkel effect

Solids which contain ionisable centres, which act as though they are Coulombic traps, can exhibit conduction through the Poole–Frenkel effect.

### 1 Coulombic traps

When these Coulombic traps are empty they are positively charged (having charge +q prior to capturing an electron) and neutral when full. Typically, the potential energy of an electron (located by x) in a Coulombic trap (centred at x<sub>0</sub>) can be expressed as:  $U(x) \approx -q^2/4\pi\epsilon|x - x_0|$ .

If E<sub>t</sub> represents the bonding level, the ionisation energy (of modulus equal to E<sub>t</sub>) is modified (by a drop of ΔE<sub>PF</sub>) by an applied field E.

Given that  $U = -qE(x_0)(x - x_0) - q^2/4\pi\epsilon|x - x_0|$ , applying the condition  $0 = (dU/dx)_{x=x_M}$  allows determination of  $(x - x_0)_M = [q/4\pi\epsilon E(x_0)]^{1/2}$  and

$$\Delta E_{PF} = (q^3 E / \pi \epsilon)^{1/2} = \beta_{PF} E^{1/2}, \text{ with } \beta_{PF} = (q^3 / \pi \epsilon)^{1/2}.$$

The initial barrier (E<sub>t</sub>) is now in the applied field (E) E<sub>t</sub> - ΔE<sub>PF</sub>.

For organic materials (insulators), ε is low (≈ 3) and (x - x<sub>0</sub>)<sub>M</sub> is ‘high’: (x - x<sub>0</sub>)<sub>M</sub> (in μm) ≈ 40/√E (E in V m<sup>-1</sup>) that is (x - x<sub>0</sub>)<sub>M</sub> ≈ 100 nm. In addition, ΔE<sub>PF</sub> is also high, and ΔE<sub>PF</sub> (in eV) ≈ 8 × 10<sup>-5</sup>√E. With E in V m<sup>-1</sup>, ΔE<sub>PF</sub> ≈ 0.1 eV for E ≈ 10<sup>5</sup> V m<sup>-1</sup>.

If E increases, (x - x<sub>0</sub>)<sub>M</sub> decreases and the electronic emission process tends towards tunnelling effects.

### 2 Conduction due to Poole–Frenkel effect (as opposed to Schottky effect)

The Poole–Frenkel effect, sometimes called the Schottky internal effect, occurs within solids where electrons move from ionisable centres. The ions, being near immobile, do not contribute directly to the conduction.

If n(0) is the concentration of electrons trapped within a solid in the absence of an electric field, once a field is applied the barrier observed by electrons is reduced by an amount ΔE<sub>PF</sub> = β<sub>PF</sub>E<sup>1/2</sup>, with β<sub>PF</sub> = (q<sup>3</sup>/πε)<sup>1/2</sup>. The concentration of electrons thus

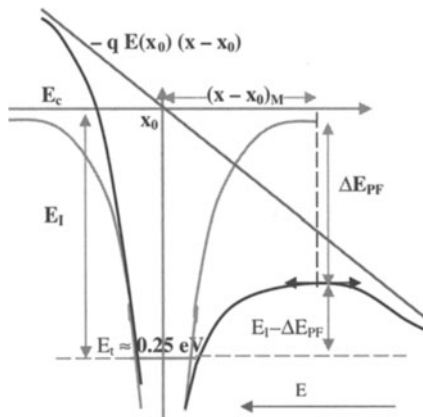
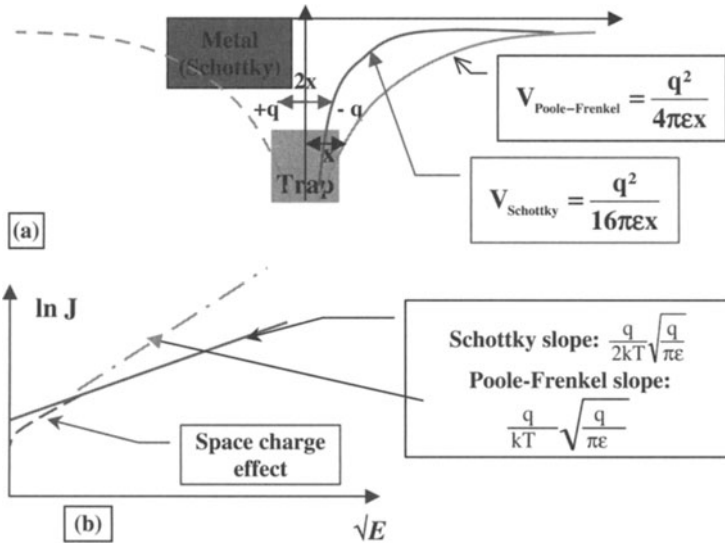


Figure VI-20. Electric field effect on a Coulombic trap.



**Figure VI-21.** (a) Poole-Frenkel and Schottky potentials; and (b) representation comparing Poole-Frenkel and Schottky laws.

changes to  $n(E) = n(0) \exp(\Delta E_{\text{PF}}/kT) = n(0) \exp(\beta_{\text{PF}} E^{1/2}/kT)$ , and conductivity then follows an exponential law,  $\exp(\beta_{\text{PF}} E^{1/2}/kT)$ .

The Poole-Frenkel law is of the same form as that found for a Schottky emission. However, the latter law follows more exactly  $\exp[\beta_{\text{PF}} E^{1/2}/2kT]$ , as in place of a Coulombic force ( $1/4\pi\epsilon x^2$ ), the image force ( $1/4\pi\epsilon[2x]^2 = 1/16\pi\epsilon x^2$ ) intervenes in Schottky emissions (Figure VI-21-a). In both cases a linear law is retained, that is  $\ln J = f(\sqrt{E})$  (in Figure VI-21-b), and in reality it is difficult to distinguish between the two mechanisms even though the slopes differ by a factor of 2 and the physical origins of the two laws are different (the Schottky effect is a limitation of current by electrode emission, while the other is a current limitation due to the material volume). This inexactitude (in terms of the one-dimensional representation of transport) is due to uncertainty in the value of  $\epsilon$  (for the field under study), arising from the possible stepped placement of wells giving a detrapping on a neighbouring site rather than in the conduction band.

As we shall see in Chapter X, the Poole-Frenkel law is in fact particularly useful in justifying transport laws proposed for organic LEDs, where mobility under an applied electric field is thought to follow a law of this type.

## VII

---

# Optical processes in molecular and macromolecular solids

## I Introduction

In this Chapter, we shall look at the origins of optical properties of:

- a solid matrix into which has been inserted transition metal or rare earth atoms. While this may not directly concern organic solids, it is a field of considerable importance in optoelectronics in general, and has given rise to applications for example, in telecommunication systems and electroluminescence; and
- molecular or macromolecular solids.

As an *aide-mémoire*, Appendix A-8 details the successive appearance of energy levels within an isolated atom following perturbations of decreasing intensity.

Optical properties, in general, are governed by:

- the separation of energy into quantum levels in atomic or molecular based structures which condition the wavelengths of emitted or absorbed light; and
- the transition rules, otherwise termed 'selection rules', which determine permitted transitions between quantum levels.

The above rules are based on the conservation of total kinetic momentum within a system associated with the emission or absorption of a photon when an electron transfers from one energy state to another. However, in a more rigorous manner, we can also say that any variation in the kinetic momentum of an electron implicated in a radiating transition should equal 1. By definition, any radiating transition is one which employs the emission or absorption of a photon, which is a boson type particle. Indiscernible particles do not follow the Pauli principle [Bla 67, p8] and any number of bosons can occupy the same quantum state, however, the state function must remain symmetric—with respect to permutation of co-ordinates between two particles—and associated with a whole spin number (from the symmetry postulate [Coh 73, p1374] and thus also Pauli's principle [Lev 68, p99]). So, for a photon,  $S = 1$ .

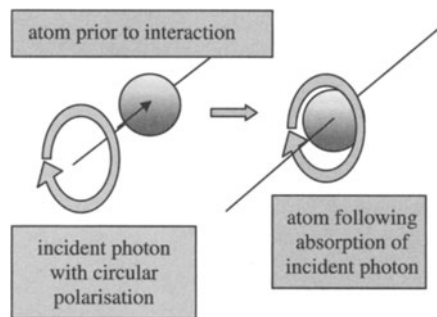


**Figure VII-1.** Schematised atom-photon interaction in which circularly polarised photon transfers its kinetic momentum to an electron at the periphery of the atom (process of absorption). Variation in kinetic momentum of the electron accords with  $\Delta l = \pm 1$ .

Selection rules governing radiating transitions take into account gains or losses in kinetic momentum due to photon absorption or emission, respectively. The process is schematised in Figure VII-1.

## II Matrix effects due to insertion of atoms with incomplete internal electronic levels (transition metals and rare earths)

### 1 Electronic configuration of transition elements and rare earths

Mendeleev's periodic table generally follows the sequential filling of atomic levels by electrons as given by Klechkowski's rule and detailed in Appendix A-8 [Arn 91, Chapter 9]. Columns IA and IIA correspond to the s block, while columns IIIA to VIIA, along with column VIII for rare gases, correspond to the p block. Horizontal levels in the table are filled with respect to the number of electrons added, respectively, to s and p layers.

The d block, however, corresponds to transition metals which follow the series  $nd$  ( $n = 3, 4, 5$  and  $l = 2$ ) filled as  $(n + 1)s$ . If we take the example of scandium, for which  $Z = 21$ , and using (Ar) to denote the base electronic configuration of argon, we can write its configuration as  $[\text{Ar}] 3d^1 4s^2$ . The result is that for these 'transitional' elements, the electronic layer  $nd$  below the outermost layer is incomplete. Rare earths, which belong to block f, exhibit a similar electronic disposition. Their internal  $4f$  layer, which is at  $[n + 1] = 7$ , is incomplete and is filled only when the series  $5s$ ,  $5p$  and  $6s$  reach the full configuration of  $5s^2$ ,  $5p^6$  and  $6s^2$ . An example is that of erbium ( $Z = 68$ ) which has the configuration  $[\text{Xe}]4f^{12}6s^2$ .

*Comment:* The use of Klechkowski's rule does involve some exceptions, which incidentally do not detach notably from its use [Arn 91, p75]. For example, chromium (Cr) and copper (Cu) have configurations that stray slightly from the rule each having only 1  $4s$  electron instead of 2 and an additional  $3d$  electron.

## 2 Incorporation of transition metals and rare earths into dielectric or a semiconductor matrix: effects on energy levels

The optical properties of a matrix are controlled by the conventional band scheme, drawn in reciprocal space and shown in Figure VII-2 where  $E = E(k)$ . The size of the forbidden band generally controls emission and absorption spectra. Vertical (direct) transitions are the most probable, when possible, as given the same  $k$  position at the extreme edges of valence and conduction bands a two particle electron-photon transition which conserves energy and quantity of movement is allowed.

Low concentrations of transition metal and rare earth ions incorporated into solid matrices (for example, by ion implantation) can give rise to particular optical properties. For examples, lasing effects are observed on incorporating  $\text{Cr}^{3+}$  in  $\text{Al}_2\text{O}_3$  and doping of silicon fibres with erbium can permit integration of  $1.54\ \mu\text{m}$  lasers into optical fibres for telecommunications. These changes in optical properties are due to the increase in degeneration of energy levels associated with the electronic configurations of transition metal and rare earth ions. In order to understand these systems, the strengths of the different effects which are brought to bear, such as exact electronic repulsions given by the Hamiltonian  $H_{ee}$ , spin-orbit coupling given by  $H_{O,S}$ , and the crystal field effect resulting from the environment and characterised by  $H_{CC}$ , will all depend of the type of ions used.

### a Rare earth ions

Electrons in the  $4f$  layer are well buried within the atom. The full, external layers,  $5s^2$ ,  $5p^6$  and  $6s^2$ , which have wavefunctions with greater external radii than  $4f$  remarkably well protect the exterior layer (crystalline) of the  $4f$  electrons, so in general for rare earths  $H_{ee} > H_{O,S} > H_{CC}$ . Up to and including  $H_{S,O}$ , we have more or less the same

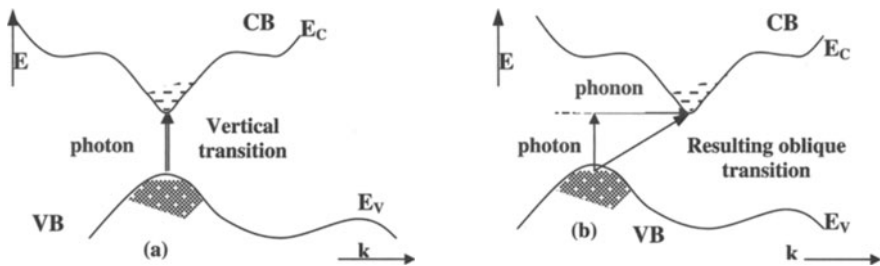


**Figure VII-2.** Transitions in a solid with conduction band (CB) and valence band (VB):

- vertical (direct) transition, most probable as is associated with only two particles, electron and photon (with  $k_{\text{photon}} = 2\pi/\lambda \approx 10^{-3}\text{\AA}^{-1} \approx 0$ ). The photon assures energy conservation during transition between VB and CB with  $\Delta E = E_{C\text{min}} - E_{V\text{max}} = h\nu$ ;
- oblique (indirect) transition, of little probability as associated with three particles, electron, photon and phonon (with  $\Delta k_{\text{phonon}}$  sufficiently high to allow conservation of quantity of movement).

behaviour for atoms in the isolated state as in a matrix, so the crystalline field effect can be considered negligible. Spectroscopic and luminescence properties associated with 4f internal transitions are thus little influenced by exterior perturbations, to the point where they are practically independent to the host material and even temperature.

Insertion of these atoms in a matrix can be accomplished by ion implantation, although this method does necessitate annealing the material to activate the optical properties of the implanted ions. Annealing induces the formation of ‘packets’ of emitters which have dimensions of the order of several microns. The observed luminescence does not seem to be due only to implanted erbium ions, for example, but also their association with other elements, in particular oxygen [Fav 93]. An interpretation is given in Section 3-b.

## b Transition metal ions

d Layer electrons of transition metal ions are only poorly shielded from the exterior, such that perturbation due to crystalline field effects is greater than that of spin-orbit coupling. Typically,  $H_{ee} > H_{CC} > H_{O,S}$ , and the crystal field effect can be sufficiently strong to directly interact on LS terms (degenerated  $[2L + 1][2S + 1]$  times) due to the correlation (exact interaction) between electrons in the same atom. The crystal field effect (often denoted by a quadratic potential  $V : V = Ax^2 + By^2 + Cz^2$ ) starts (before spin-orbit coupling effects) to partially raise degeneration of LS terms. In a typical case, it raises orbital degeneration leaving only spin degeneration or order  $[2S + 1]$  [Mol 81]. The obtained Hamiltonian can therefore only be expressed as a function of spin order and is denoted the spin Hamiltonian.

At this level, two different cases can be envisaged:

- either perturbation introduced by an exterior magnetic field is smaller than that resulting from spin-orbit coupling, as in Figure VII-3, in which case spin-orbit coupling—which interacts after the crystal field effect—does not raise remaining spin degeneration. The resulting perturbation does not even displace levels associated with correlations, but only modifies the states (wavefunctions) corresponding to the latter. Only the intervention of perturbation by an exterior magnetic field

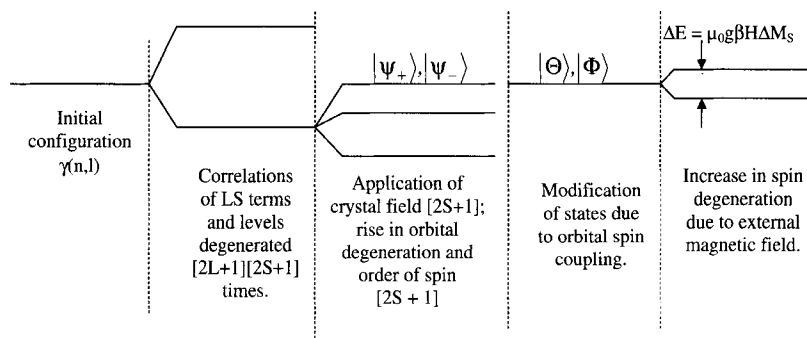


Figure VII-3. Increase in degeneration when magnetic field effect is relatively weak.



$\vec{H}$  (which introduces a perturbation Hamiltonian of the form  $\mu_0 g \beta \vec{S} \cdot \vec{H}$  where  $g$ , while written as a scalar corresponds to a tensor and  $\beta$  is Bohr's magneton) raises the degeneration of energy levels; or

- perturbation introduced by an external magnetic field  $\vec{H}$  is greater than that produced by spin-orbit coupling; the latter simply displaces levels appearing due to the magnetic field. An example, with iron atoms, is shown in Figure VII-4.

The structure which appears on application of  $H$  (Zeeman effect applied to solids) can be evidenced by electronic paramagnetic resonance (EPR). A study of transition probabilities between Zeeman levels yields the selection rule  $\Delta M_S = \pm 1$  [Mol 81].

### 3 Transitions studied for atoms with incomplete layers inserted in a matrix

#### a Transition metal ions

When isolated, iron has the configuration  $[Ar] 3d^6 4s^2$ . Excited states have configurations  $3d^7 4s^1$  then  $3d^6 4s^1 4p^1$  and then  $3d^8$ . The lowest energy levels of these configurations are, respectively, 0.85 eV, 2.4 eV and 4.07 eV above the lowest, fundamental level, which has configuration  $3d^6 4s^2$ .

Once introduced into a matrix as impurities, that is to say at very low concentrations, these elements loose one or more electrons. Generally, iron becomes the cation  $Fe^{3+}$  which has the unexcited configuration  $[Ar] 3d^5$  and, 23 eV higher, has the excited configuration  $[Ar] 3d^4 4s^1$ . Optical properties, which arise from differences in energy generally less than 3 or 4 eV, can only arise from internal transitions to the non-excited configuration  $[Ar] 3d^5$ , shown in Figures VII-3 and VII-4. Under the influence of crystal field effects, which modify energy separations, transitions

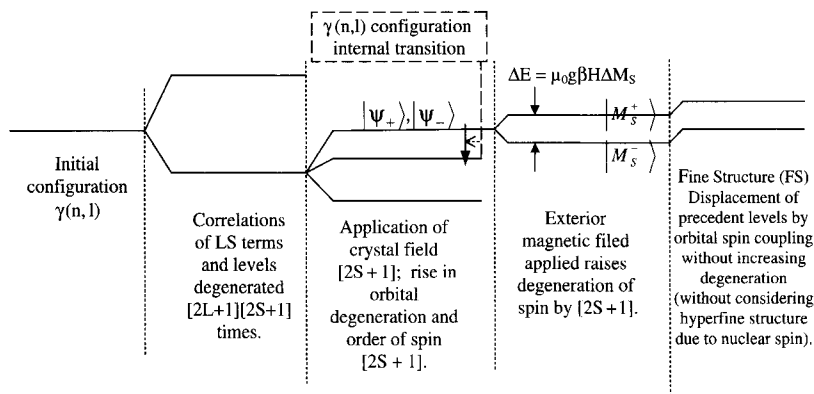


**Figure VII-4.** Increase in degeneration for example of iron with perturbation due to magnetic field greater than orbital spin coupling.

internal to the  $nd$  configuration, as shown in Figure VII-4, can give rise to quite large separations and spectral lines.

In diatomic molecules, which are the classic examples, internal electronic transitions modify interaction forces and therefore the distance between the two atomic nuclei. In other words, the passage of an electron to an excited state reduces the bonding state, allows increased nuclear repulsions and an increased distance between the nuclei.

Similarly, transition metals implanted into a matrix have electronic states, characterised by their configuration, and subsequent effects such as those of crystal field, based on the position and movement of their respective nuclei at co-ordinate ( $r$ ), the latter being located with respect to the mean position of a stable state at the minimum of the configuration curve  $E = E(r)$ , which has a form corresponding to that of an harmonic oscillator. Energy levels within the oscillator are tied to the vibrational states of the system, characterised by quasi-particles called phonons, and coupling between the electronic states and the positions of the nuclei (*i.e.* the relation between the states of electrons and their ions) is called electron-phonon coupling. With increasing separation in excited and fundamental configuration curves  $\Delta r (= r_{exc} - r_f)$ , there is a proportional increase in the electron-phonon coupling. The vertical transition, associated with the Franck-Condon principal which states that the electronic transition is sufficiently rapid to leave the co-ordination ( $r$ ) for the transition metal ion nuclei unchanged, occurs between two states with the same difference in vibrational levels (large variation in vibrational quantum number ( $v$ ) with quantification of phonons) as excited and fundamental electronic configuration curves are shifted (see Figure VII-5).

As shown in Figure VII-6 (transitions F-E), once an electron has been excited, it can loose its energy [Pan 71, p167]:

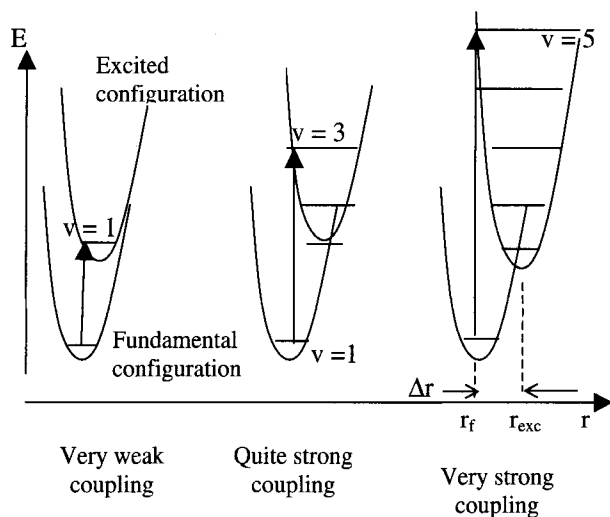


**Figure VII-5.** Configuration curves of different bonds for fundamental and excited states.

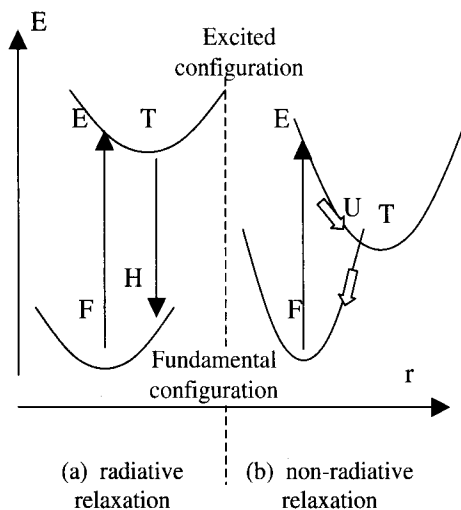


**Figure VII-6.** (a) Radiative and (b) non-radiative relaxations.

- by radiation (Figure VII-6-a). The excited system at point E has vibrational level  $> 1$  and on going from E to T loses quanta of vibrational energy to the lattice in the form of phonons. Thus, thermally energetic electrons are in the lowest part of the potential curve at the fundamental vibrational level ( $v = 1$ ) of the excited configuration. Electrons then relax through the radiative vertical transition TH, which involves the emission of a photon with an energy smaller (and therefore greater wavelength) than that associated with the vertical transition FE. This increase in wavelength is called 'Stoke's shift'. Finally, by phonon emissions, the system relaxes from H to F where the electron returns to its lowest electronic and vibrational level; or
- by a non-radiative pathway (Figure VII-6-b). Here the potential curve associated with the fundamental state intercepts between points E and T the curve associated with the excited electronic state at point U. T is the fundamental vibrational level of the excited system. The system excited to E now relaxes by emitting phonons, first going from E to U through the lattice associated with the excited electronic configuration, and second from U to F into the fundamental configuration system.

### b Rare earth ions

As we have seen already, the interior, incomplete 4f electron layers, which according to Kleschkowski's rule are filled last, of rare earths are protected by external, full layers, notably  $5s^2$  and  $5p^6$ . The upshot of this configuration is that properties of luminescence associated with internal 4f transitions, are relatively insensitive to external effects such as crystal potential and temperature from a surrounding matrix. Indeed, the configuration curves  $E = f(r)$  do not to any practical extent shift between fundamental and excited states for transitions occurring between electrons of the same

4f configuration. Differences between energy levels can thus be reduced to simple differences between flat levels associated with the minima of configuration curves, as detailed in Figure VII-7.

Erbium is of particular interest as the wavelength of its emitted light ( $1.536\ \mu\text{m}$ ) is very close to the maximum transmission wavelength in silicon optical fibres ( $1.55\ \mu\text{m}$ ). The emission is in fact generated by the cation  $\text{Er}^{3+}$  which has configuration  $4f^{11}$  [Mom 95, p35]. The fundamental spectral term is  $S_{\text{max}} = 3 \times \frac{1}{2} = 3/2$ ,  $(\Sigma m_l)_{\text{max}} = (M_L)_{\text{max}} = 3 + 2 + 1 = 6$  and so  $L_{\text{max}} = 6$ . From  $J = L + S$  (as in the second half layer) we have  $J = 15/2$ . The fundamental term is thus  ${}^4I_{15/2}$  while the first excited LS term following spin-orbit coupling (see Appendix A-8, Figure 2) corresponds to  $J = L + S - 1 = 13/2$  and is denoted  ${}^4I_{13/2}$ .

For the transition  ${}^4I_{13/2} \rightarrow {}^4I_{15/2}$  (which should give a fine spectral line as it is associated with spin-orbit coupling terms), the selection rules ( $\Delta S = 0$ ,  $\Delta L = \pm 1$  or  $0$ ,  $\Delta J = \pm 1$  or  $0$ ) are well respected but the supplementary condition,  $\Delta l = \pm 1$  in which  $l$  is the kinetic momentum of a 4f electron undergoing the transition, is not verified (as this electron does not change configuration and remains 4f). This forbidden transition corresponds to Laporte's rules which, as we shall see in more detail for molecules, indicates that electron dipolar transitions (through oscillating dipole radiation) are forbidden within the same configuration, as during an interior transition there is no inversion of orbital sign and the dipole moment of the transition is cancelled out because initial and final states have the same, retained parities. However, the rule is often partially violated, as mixtures of excited orbitals (associated with alternate configurations) with inverse parities are formed. It should be noted also that the probabilities of transitions between states  ${}^4I_{15/2}$  (generally denoted state  $T_1$ ) and  ${}^4I_{13/2}$  (state  $T_2$ ) are in fact low and the resulting spectral lines are weak. In addition, the lifetimes of excited states ( $T_2$ ) are long, as return to the fundamental state ( $T_1$ ) has a low probability, which leaves open the possibility of a secondary excitation from the  $T_2$  state to an even higher energy state  $T_3$ . The wavelength  $\lambda_2$  associated with a return to the fundamental state (transition from  $T_3$  to  $T_1$ ) is consequently shorter

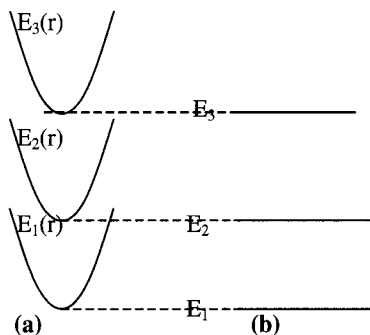


**Figure VII-7.** For rare earth ions inserted into a matrix, we see a reduction to plateau of configuration curves (b) associated with different excited levels (a).

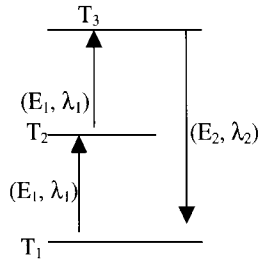


**Figure VII-8.** 'Up conversion' using long lived  $T_2$  level.

(as of higher energy  $E_2$ ) than  $\lambda_1$  associated with the excitation. Figure VII-8 details further this so-called 'up conversion'.

### III Classic optical applications using transition and rare earth elements

Applications for transition and rare earth elements include optical emitters and, in particular, electroluminescent components. Erbium, as noted above, is used in generating lasing effects. All these components are produced by inserting optically active ions into insulating or semi-conducting matrices. These ions are the origin of fluorescing phenomena and bring into play either transitions between flat 4f layers (rare earths) or, principally, alterations in vibrational states (transition elements). Matrices can be doped either during the growth of layers by epitaxy or by ion implantation. The rest of this Section will deal with certain properties utilised in components, which in turn are detailed in Chapter IX on optoelectronic emitters.

#### 1 Electroluminescence in passive matrices (see also Chapter IX, Section VII)

Shock ionisation, brought about by collisions of carriers on a lattice, can generate carriers at excited levels on luminescent centres. Until recently, these centres were typically based on phosphorescing inorganics (for example, ZnS activated by  $Mn^{2+}$ ) and were introduced either using a dielectric bonding material (Destriau's effect) or in a structure permitting reinforcement of charge injection (such as MIS structure, Schottky junction and thin multi-layer films corresponding to ACTFEL structures).

An example of the direct relationship between the crystal effect and transition metal ions is that of manganese inserted into  $ZnF_2$ : the former produces an orange emission centred at 580 nm and the latter has emissions shifted towards longer wavelengths (towards yellow) with the principle emission at 585 nm (2.12 eV) along with others detailed in Figure VII-9 [Bren 99, p706].

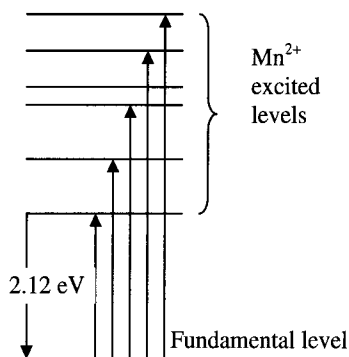


Figure VII-9. Emission lines of  $\text{Mn}^{2+}$  inserted in ZnS.

## 2 Insertion into semiconductor matrix

It has been shown that for erbium to undergo photoluminescence, the band gap of the host semiconductor must be larger than the energy (0.805 eV) associated with the wavelength ( $1.536 \mu\text{m}$ ) of the transition  $^4\text{I}_{13/2} \rightarrow ^4\text{I}_{15/2}$ . In addition, the intensity of luminescence decreases with the excitation temperature, just as much as the decrease in the semiconductor gap; at ambient temperature, the emission is only detectable for semiconductors with a gap superior or equal to that of InP at 1.25 eV.

It should be noted that the concentration of doping ions can modify photoluminescence intensity, which reaches a maximum at a certain concentration. In the example of erbium this maximum is found at approximately  $10^{18}$  ions erbium  $\text{cm}^{-3}$  when implanted in a layer of InP, although the value is independent of the host matrix, be it InP or GaAs. At low ion concentrations when ions are independent of each other in a matrix, in general, luminescence increases steadily with an increase in ion concentration, however, at higher concentrations when ions are in closer proximity, then excitation energies which would otherwise be used for radiative emissions can be lost to transfers between ions. The result is that above a certain concentration (often of the order of 0.1 to 10 %) the luminescence decreases. The above process corresponds to a crossed relaxation.

Co-doping can result in an increase in intensity of luminescence. For example, silicon doped with erbium shows a two fold increase when doped with erbium and oxygen. This process is recognised to be due to the presence of acceptor levels on oxygen 0.35 eV higher than the highest point of the silicon valence band. Recombinations in the forbidden silicon band with these localised levels is equivalent to an energy of  $1.12 - 0.35 = 0.77$  eV, a value of the order of that required to excite  $\text{Er}^{3+}$  ions (transition  $^4\text{I}_{15/2} \rightarrow ^4\text{I}_{13/2}$  of 0.805 eV).

Luminescence dependent on the direction of an applied polarisation (tension) can be obtained by inserting ions in zones of pn junctions. Possible variations are:

- using direct polarisation where ions introduced into a p zone allow radiative recombinations from electron-hole pairs and the resulting radiation, as virtual phonons, excites the inserted luminescent ions. If recombinations are

non-radiative, then the de-excitation energy can nevertheless be transferred to a luminescent ion which in turn can re-emit photons with energy less than or equal to the received energy; and

- using inverse polarisation, the excitation of rare earth or transition element ions results from shocks due to hot carriers (in the Zener characteristic zone) such as electrons injected from zone p into zone n, in which they undergo collisions. The n zone is thus preferentially doped.

### 3 Light amplification: erbium lasers

In systems using fibre optic transmissions, losses during propagation necessitate the periodic use of signal amplification along the length of the fibre. Initial designs, which were relatively expensive, used transducers to transform the optical signal to an electronic signal, which was amplified, and then back again to an impulse optical signal. A more modern technique though is to use silicon optical fibres doped (over distances of around 30 m) with a low concentration of  $\text{Er}^{3+}$  cations, as schematised in Figure VII-10-a. Along the distance,  $\text{Er}^{3+}$  cations are excited using a semiconductor emitted laser beam of wavelength typically between 1.48 and 0.98  $\mu\text{m}$  and a 'pumping' intensity that decreases on going through the doped zone, described in Figure VII-10-b. When luminescent impulse signals traverse the doped and 'pumped' region of the cable, they receive an energy due to the  $\text{Er}^{3+}$  ions, as illustrated in Figure VII-10-c.

Radiation of wavelength  $\lambda = 0.98 \mu\text{m}$  excites  $\text{Er}^{3+}$  cations from their fundamental state  $^4\text{I}_{15/2}$  to their excited higher state  $^4\text{I}_{11/2}$ , which in turn rapidly relax without radiation to the  $^4\text{I}_{13/2}$  level. This process is one of 'pumping' and the laser used acts as a 'pump'. Radiation with  $\lambda = 1.48 \mu\text{m}$  excites  $\text{Er}^{3+}$  ions directly to  $^4\text{I}_{13/2}$  which has a long lifetime. An impulse at  $\lambda \approx 1.48 \mu\text{m}$  traversing the system empties all these excited levels so that the pumping energy is added to the luminescent impulse signal in such a way that it conserves its coherence.

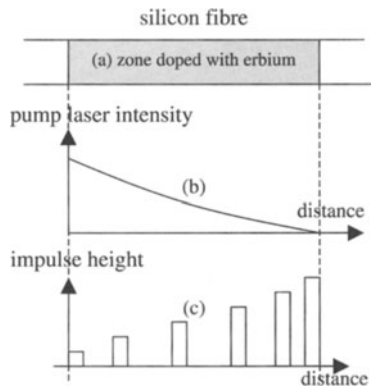


**Figure VII-10.** Zone (a) shows silicon fibre doped with erbium and subject to a 'pump' laser to amplify luminescent impulses (c).

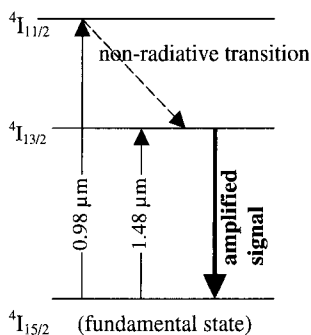


Figure VII-11. Laser pumping over three levels.

## IV Molecular edifices and their general properties [Atk 00]

### 1 *Aide-mémoire*: basic properties

As we have seen in Chapter 1, macrostructures consist of molecules of atoms bonded by intramolecular forces. The solidity of the edifice relies on intermolecular forces. Molecular spectra are richer than those of atoms due to the possible rotations and vibrations. However, the energy of these rotations and vibrations, which is of the order of  $\Delta E_r \approx 0.005$  eV and  $\Delta E_v \approx 0.1$  eV, means that associated spectra are not in the visible region, a region essentially explored for electroluminescent and photovoltaic components. However, it is worth noting that while only electronic spectra have energies  $\Delta E_e \approx 2$  to 6 eV, tied to electronic transitions at the interior of molecular orbitals, these relatively large energies can also excite rotational and vibrational levels to the point where electronic spectra are close to these absorption bands and can become very complex. We shall define electronic terms for molecules after a brief introduction using simple systems of diatomic molecules.

#### a Heteronuclear diatomic molecules

In the example of a diatomic molecule, the axis which joins both atoms is denoted Oz. This axis of symmetry is such that the Hamiltonian remains invariant during rotation about the axis. The result is that  $L_z$  and H are commutative such that they can have the same system of proper functions. We normally introduce an absolute value  $\Lambda \hbar = |M| \hbar$  projecting kinetic momentum over the axis of symmetry Oz. With  $M = 0, \pm 1, \pm 2, \dots$  we have  $\Lambda = 0, 1, 2, \dots$  which, respectively, correspond to states  $\Sigma, \Pi, \Delta, \dots$

In fact, when  $\Lambda \neq 0$ , for the same energy there are two possible states. They are distinguished from one another by the direction of the projection of kinetic momentum at Oz, and an inversion of sign following a symmetry operation on a plane containing the Oz axis ( $L_z$  is not invariant with this symmetry operation O) which has invariant energy during the operation. The latter invariance is due to symmetry of the molecule on this plane, and assures the conservation of the Hamiltonian. This degeneration



explains the choice of  $\Lambda = |M|$  to characterise the energy states of the molecule, rather than  $M$  for which the two values would give the same value of energy when  $M \neq 0$ . It should be noted that at the particular case of  $\Lambda = 0$  ( $\Sigma$  state), corresponding to when the kinetic momentum projection is zero,  $L_z$  and  $O$  are commutative and are can have the same system of proper functions with  $H$ . As two successive applications of the operator  $O$  brings the system back to its starting point, the proper values of  $t$  are such that  $t^2 = 1$  with  $t = \pm 1$  (see comment below).  $\Sigma$  states can give rise, in fact, to two states  $\Sigma^-$  or  $\Sigma^+$ , depending on whether or not the wavefunction changes sign on application of the operator  $O$ .

Just as in an atom, for its part the composition of all electron spins in a system yield a total resulting spin of value  $S$ , and the molecular term or 'multiplicity' is thus denoted carrying the value  $(2S + 1)$  at the upper left hand corner of the letter defining the value of  $\Lambda$ .

*Comment:* brief look at the form of proper values associated with operator  $I$  which transforms variable  $x$  to  $-x$

Looking for proper functions of  $I$  such that  $I\psi(x) = t\psi(x)$  in which  $t$  is the proper value, also with (defining property of  $I$ )  $I\psi(x) = \psi(-x)$ , so that  $I\psi(x) = t\psi(x)$  and  $I\psi(x) = \psi(-x)$  leads to multiplying the left hand side of the two equal parts by  $I$  so that:

$$I(I\psi(x)) = tI\psi(x) = t^2\psi(x) = I, \psi(-x) = \psi(x).$$

This gives  $t^2 = 1$ , that is  $t = \pm 1$ , which results in  $\psi(-x) = \pm\psi(x)$ . This demonstrates that proper functions associated with  $I$  are either symmetric, as in  $\psi^+$ , or antisymmetric as in  $\psi^-$ . In addition, if  $H(x)$  is a Hamiltonian such that  $H(x) = -\frac{\hbar^2}{2m} \frac{d^2}{dx^2} + V(x)$  with  $V(x) = V(-x)$ , then  $H(x) = H(-x)$ . Thus  $I H(x) = H(-x) = H(x)$  and the Hamiltonian is invariant with respect to  $I$ ; it can commute with  $I$  and have the same proper functions as  $I$  and the proper functions of this Hamiltonian are symmetric or antisymmetric (most basic courses in quantum mechanics can give comparable notes).

## b Homonuclear diatomic molecules

Here molecules of the type  $A_2$  are considered, where  $A$  is an atom on the second line of Mendeleev's periodic table. In these discussions, the carbon-bond-carbon system is deemed the most important, due to its centrality to the nature of small molecules and polymers, whatever the type of bond.

As in Chapter I (and in Appendix 1-1), we can consider two types of molecular orbitals:

- $\sigma$ -orbitals which have the straight line joining the two covalently bonded atoms as an axis of symmetry (for example, axis  $Oz$ ); and
- $\pi$ -orbitals which have a plane of symmetry which includes the axis  $Oz$  joining the two atoms and is perpendicular to an axis normal to  $Oz$  such as  $Ox$  or  $Oy$ .

If after a symmetry operation with respect to the centre of symmetry of the molecule, the orbital sign does not change the molecules are termed as having even-parity and are denoted *g* for *gerade* (from the German word for even). If the same operation results in an inversion in the same sign, then the molecule is denoted *u* for *ungerade*.

In Figures 9 and 10 in Appendix A-1 (in which it is the axis *Ox* which joins atom centres, although this changes none of the reasoning) we can see that:

- bonding  $\sigma$ -orbitals have even-parity and are denoted  $\sigma_g$ , while antibonding  $\sigma$ -orbitals have odd-parity and are denoted  $\sigma_u^*$ ; and
- bonding  $\pi$ -orbitals have odd-parity and are denoted  $\pi_u$ , while antibonding  $\pi$ -orbitals have even-parity and are denoted  $\pi_g^*$ .

We can also note that symmetry operations with respect to the central symmetry change  $\vec{r}$  to  $-\vec{r}$ . This operation is called an operation of parity (*I*), which is such that the homonuclear molecule rests invariant under its effect.

## 2 Selection rule with respect to orbital parities for systems with centre of symmetry

In classic terms, the emission of a photon following an electronic transition is considered due to a type of electric dipole oscillating the atom or molecule (see also J.P. Perez, Masson 1996, Chapter 20 or a comparable textbook on electromagnetism or dipole ray theory). The operator associated with the dipole momentum of a structure of atoms or molecules can be given in the form:

$$\hat{M}(\vec{r}_1 \dots \vec{r}_n) = (-e) \sum_{i=1}^n \hat{r}_i,$$

in which  $\vec{r}_i$  locates the position of electrons. This operator is of odd-parity as it changes sign when all  $\vec{r}_i$  are transformed to  $-\vec{r}_i$ . Its matrix element (transition dipole moment) between states 1 and 2, characterised by wavefunctions  $\psi_1(\vec{r}_1, \dots, \vec{r}_n)$  and  $\psi_2(\vec{r}_1, \dots, \vec{r}_n)$ , is of the form:

$$d = \iint \psi_1^*(\vec{r}_1, \dots, \vec{r}_n) \hat{M}(\vec{r}_1, \dots, \vec{r}_n) \psi_2(\vec{r}_1, \dots, \vec{r}_n) d\tau_1, \dots, d\tau_n.$$

We can therefore remark that:

- under the effect of a transformation associated with an inversion operator *I* which transforms  $\vec{r}_i$  to  $-\vec{r}_i$  (and also therefore  $\vec{M}$  to  $-\vec{M}$ ),  $\psi_1$  and  $\psi_2$  are transformed to  $\varepsilon_1 \psi_1$  and  $\varepsilon_2 \psi_2$  with  $\varepsilon_1 = \pm 1$  and  $\varepsilon_2 = \pm 1$ : under the effect of *I*, *d* also becomes  $-\varepsilon_1 \varepsilon_2 d$ ; and
- in systems which have centres of inversion (symmetry), *d* is invariant under the effect of a transformation associated with the inversion operator *I*.

The upshot is that for systems with centres of inversion then  $d = -\varepsilon_1\varepsilon_2 d$  and  $-\varepsilon_1\varepsilon_2 = 1$  if  $d \neq 0$ , and for systems such that  $\varepsilon_1\varepsilon_2 = 1$  (*i.e.* systems which conserve the same orbital parities during transition from state 1 to state 2), obligatorily  $d = 0$ , *i.e.* it is a forbidden transition.

For complexes which have a centre of symmetry, the selection rule (called Laporte's rule) indicates that the only electronic transitions allowed are those which implicate a variation in parity, that is those of the type  $g \rightarrow u$  and  $u \rightarrow g$  are allowed, while transitions  $g \rightarrow g$  and  $u \rightarrow u$  are not.

We can see here that  $\pi_u \rightarrow \pi_g^*$  transitions are allowed. We can also note that if the centre of symmetry is broken (for example, by vibrational effects) then this rule is no longer respected and transitions  $g \rightarrow u$  and  $u \rightarrow g$  become possible. These transitions are called vibronic transitions.

### 3 More complicated molecules: classical examples of existing chromophores

In this Section we shall present some examples of various types of chromophores, which have groups of atoms on which transitions are localised.

#### a Transition metal complexes

*$\alpha$  Introduction: some notions on ligand field theory* Transition metals have an incomplete d orbital and in order to interpret the origin of the optical properties of the complexes of these metals, which consist of the metal tied to surrounding ligands, molecular orbital theory has been adapted under the term 'ligand field theory'. This theory takes into account the highly symmetric structures about the central metal ion that these complexes often present.

The ligands, when for example carrying a pair of free electrons localised towards a central atom, act as centres of electrostatic repulsion which force back the approaching d electrons of the metal atom. Two types of orbitals associated with d electrons can appear:

- those which are directed at the ligands and are denoted  $e_g$ ;
- those which are directed into spaces in between ligands, and for example are denoted  $t_{2g}$ .

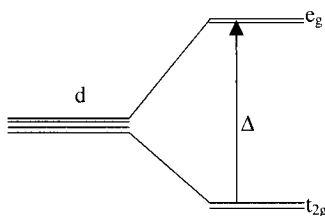


**Figure VII-12.** Energy level separation according to ligand field theory.

Given the presence of these electron repulsions, an electron in the first type of orbital has a disfavoured potential energy with respect to an electron in the latter orbital.

The stabilities of these sorts of complexes can be explained by the approach of ligands to the central metal cation resulting in a decreasing energy of the system, due to favourable interaction energies between the cation and those pairs of free electrons mentioned above. In addition, we have also seen that the energies of  $t_{2g}$  orbitals are favourable with respect to  $e_g$  orbitals.

The orbitals between the central cation and the ligands are filled, first of all, at the  $t_{2g}$  orbital, into which we introduce unpaired electrons. The filling up of orbitals continues with respect to the value of  $\Delta$ . At low values of  $\Delta$ , Hund's rule results in non-paired spins ( $S$  being the maximum) and generates the filling up of the  $e_g$  level, as the reduction in energy due to  $S_{\max}$ , which minimises electronic repulsions, is energetically more advantageous than the increase in energy associated with  $\Delta$ . However, at high  $\Delta$  values, Hund's rule is no longer sufficiently relevant with respect to decreasing energy before the energy jump  $\Delta$  and we obtain a pairing of spins in  $t_{2g}$  levels.

*$\beta$  Transitions in transition metal complexes* Transition metal complexes are often highly coloured. As we have just seen, ligands separate d levels into two subgroups, for example  $e_g$  and  $t_{2g}$  in the case of octahedral complexes, which have a transition corresponding to around 500 nm that is *a priori* forbidden (as is d – d and  $\Delta l = 0$  for isolated atoms following Laporte's rule for centre-symmetrical systems). However, it becomes possible due to vibronic transitions in the octahedral complex.

Charge transfer transitions can also occur. They correspond to the transfer of an electron from the central atom to the ligands or *vice versa*. An example is that of the purple colour of the permanganate ion  $\text{MnO}_4^-$  which is interpreted as being due to a transfer from the ligand to the metal.

## **b Molecules with double bonds**

*$\alpha$  Conjugated molecules* For radiative transitions due to the transition of an electron from a  $\pi$ -orbital to a  $\pi^*$ -orbital (absorption) or from a  $\pi^*$ -orbital to a  $\pi$ -orbital (emission) in:

- an isolated non-conjugated double bond the gap is of the order of 7 eV; and
- a conjugated double bond, that is one which makes up part of a conjugated system, packing energy levels to an increasing degree with conjugation, is such that the gap is bathochromically shifted (increase in wavelength) towards the visible region.

The transition is called a  $\pi - \pi^*$  transition. (It is worth noting that the symmetries of  $\pi$ -orbital (u) and  $\pi^*$ -orbital (g) permit proper accordance with Laporte's rule for centre-symmetric systems).

$\beta$  *Free electron pairs* In compounds containing carbonyl groups ( $>C=O$ ) which are active at 290 nm, the transition is due to non-bonding electrons situated in a free pair on the oxygen. In a transition called a  $n-\pi^*$  transition, one of the electrons is excited to a vacant  $\pi^*$ -orbital.

## V Detailed description of the absorption and emission processes in molecular solids: role of electron-lattice coupling (electrons-phonons)

### 1 Electron-lattice coupling effects during electron transitions

The titled coupling effects, described in Chapter IV, give rise to the fine structure of electron transitions due to lattice conformations, characterised by positions of atoms determining the system configuration for each electronic level. As detailed in Section IV-1, with respect to energies of optical transitions (typically in the optical domain, that is from 1.5 to 3 eV, equivalent to the order of size of organic solid bands), vibrational energies associated with various lattice configurations are negligible. These latter energies give rise to absorption and emission spectra in the near infra-red. Notably, electron-lattice coupling can yield molecular electronic spectra constituted by a collection of lines called emission or absorption bands.

Detailed here are transitions in conjugated materials, as schematised in Figure VII-13. The overlapping of  $p_z$  orbitals from adjacent sites give rise to molecular  $\pi$ -orbitals, and with an electron coming from each site, the lower half of these molecular orbitals are filled, forming bonding  $\pi$ -orbitals, and the upper half which would otherwise yield antibonding  $\pi$ -orbitals, remain empty. Following excitation, the electron transition  $\pi \rightarrow \pi^*$  is accompanied by a change in electron distribution and therefore a change of forces and equilibrium distances between neighbouring atoms. The transitions between fundamental and excited electronic states are vertical and follow the Franck-Condon principal. This is justified by the fact that the mass

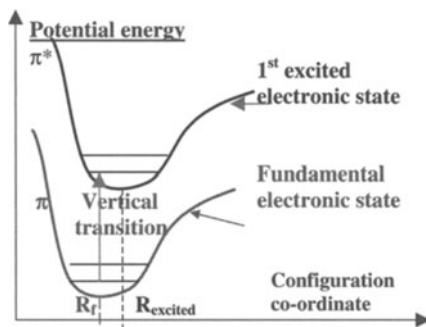


**Figure VII-13.** Configuration of excited and fundamental electron states.

of an electron is considerably less than that of a nucleus and any movement of electrons (transitions, change in energies) occurs during extremely short time intervals (of the order of  $10^{-15}$  s) with respect to the times required for a nucleus to move (approximately  $10^{-13}$  s). We can see, qualitatively, that the height and thus the energy of electron transitions depends on the values of the configuration co-ordinates and vibration levels. From a quantitative perspective, selection rules will can be used to determine absorption and emission spectra.

## 2 Selection rules and allowed transitions

In the adiabatic Born-Oppenheimer approximation, in which movement is slow and the movement of nuclei is negligible with respect to that of electrons, and assuming rotational energies to be negligible, the energy of a molecule can be written as  $E_t = E_e + E_v$  with wavefunction  $\psi_t = \psi'_e \psi_v$  in which the indices e and v indicate electron and vibrational components. The electron wavefunction can be written  $\psi'_e = \psi_e \psi_s$  by separating the spatial co-ordinates of electrons and their spins. This is Russell-Saunders coupling, corresponding to a weak spin-orbit interaction energy, and the separation of spin and orbital movement can give the wavefunction as a product of two wavefunctions, each specific to each type of movement. Using an electron dipole approximation, the probability of a transition between initial (i) and final (f) states is thus given in the following form:

$$P_{if} \propto |\langle \psi_{ei} | \hat{M} | \psi_{ef} \rangle|^2 |\langle \psi_{vi} | \psi_{vf} \rangle|^2 |\langle \psi_{si} | \psi_{sf} \rangle|^2$$

in which  $\hat{M}$  is the dipole momentum operator. Thus, allowed dipolar transitions are such that:

- $\hat{T}_{if} = \langle \psi_{ei} | \hat{M} | \psi_{ef} \rangle \neq 0$ . If the dipole momentum operator is of odd-parity ( $M \equiv e r$ ), then  $\hat{T}_{if}$  will be non-zero only if the states i and f are of opposed parity. This is found for example with bonding and antibonding orbitals as detailed in Section IV-2 (HOMO and LUMO orbitals – see also Figure VII-13); and
- allowed electron transitions between different vibrational levels have intensity increasing with the factor  $\langle \psi_{vi} | \psi_{vf} \rangle$ , which can be noted more simply as  $\langle \psi_{vi} | \psi_{vf} \rangle = \langle \psi_v | \psi_{v'} \rangle = S_{vv'}$  and represents the importance of the superposing vibrational wavefunctions of initial and final states.  $|S_{vv'}|^2 = |\langle \psi_v | \psi_{v'} \rangle|^2$  is called the Franck-Condon factor.

The vibronic levels (due to electron-phonon coupling) appear just as well in absorption as in emission spectra (Figure VII-14). Because of the role played by the Franck-Condon factor, the most intense transitions are those which arise from the maximum zone of the vibrational wavefunction and arrive at points of the wavefunction which are the highest possible given the vertical condition applied to the transition. In absorption this means a departure from the 'bell-shape' of the Gaussian curve of the fundamental state towards the region of the curve representing the oscillating excited state. In Figure VII-14 (a for absorption, b for emission), increasing probabilities of vertical transitions are represented by increasingly thick lines. These probabilities are indicated in the amplitudes of absorption and emission spectra (Figure VII-14-c).

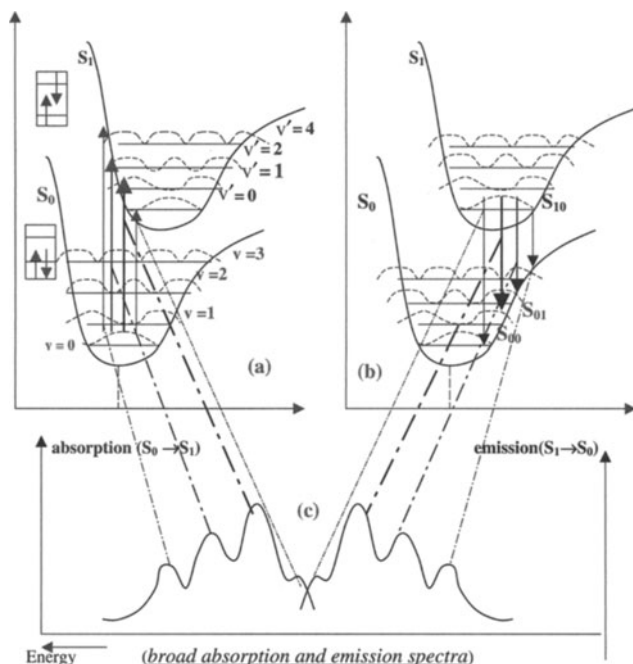


**Figure VII-14.** Vertical transition intensities in: (a) absorption; and (b) emission; (c) resulting absorption and emission spectra.

In addition to the transition rules concerning the orbital movement of electrons, the selection rule for spin needs also to be taken into account in that  $\langle \psi_{si} | \psi_{sf} \rangle \neq 0$ . This condition comes from the form of the electron wavefunction, which was initially written  $\psi'_e = \psi_e \psi_s$  on assuming that spin-orbit interactions are of a low energy (Russell-Saunders's coupling). Thus, we should have  $\langle \psi_{si} | \psi_{sf} \rangle \neq 0$  which means that spin states should be identical and  $S$  should be conserved during transitions. The initial and final states must be of the same multiplicity *i.e.* being equal to  $2S + 1$  with the quantum number  $M_s$  such that  $M_s = -S, -S + 1 \dots 0 \dots S - 1, S$ . Thus in the absence of spin-orbit coupling, transitions between singlet ( $S = 0$ , denoted  $S$ ) and triplet ( $S = 1$ , denoted  $T$ ) states are forbidden. It is for this reason that in Figure VII-14 transitions are between singlet states.

### 3 Modified Jablonsky diagram and modification of selection rules: fluorescence and phosphorescence

#### a Yields from radiating states

For a singlet state  $S = 0$  and  $M_s = 0$ , there is only one state represented by the spin wavefunction  $\psi_{S=0, M_s=0} = \psi_0 0$ . However, for the triplet state where  $S = 1$

and  $M_s = -1, 0, 1$ , there are three possible states corresponding to three spin wavefunctions  $\psi_{1-1}$ ,  $\psi_{10}$  and  $\psi_{11}$ . The statistics of spin therefore indicate that there are three triplet states for each singlet state. For electroluminescence, following the random injection of charge carriers, we should obtain the same distribution of states at excited levels and the return to the fundamental state (which is a simple singlet state as electrons at this level cannot be distinguished by their spin state, which must be different) does not occur radiatively except for electrons leaving excited singlet states. The three triplet excited states do not, *a priori*, recombine radiatively with the only singlet fundamental state, leaving at best only 25 % efficiency with respect to radiative efficiency.

### b Possible deviation from selection rule

In reality, it has been empirically observed [Pop 82] that transitions between states with different multiplicities are  $10^3$  to  $10^5$  times slower than those between states of the same multiplicity. The correspondingly weak transitions are due to residual, weak spin-orbit coupling which exist in all molecules (denoted by the coupling term  $j_j$  and detailed further in Appendix A-8, Section II). With increasing atomic weights though these transitions can become more intense with mixing of orbital movements and spin. In organic molecules, replacing hydrogen atoms with those of bromine or iodine can reinforce forbidden 'inter-system' transitions. The different transitions can therefore be represented with the help of the modified Jablonsky diagram shown in Figure VII-15.

Finally, the excitation of an electron from a  $\pi$ -orbital to a  $\pi^*$ -orbital results in—beyond changing the equilibrium geometry of the molecule—a first excited state

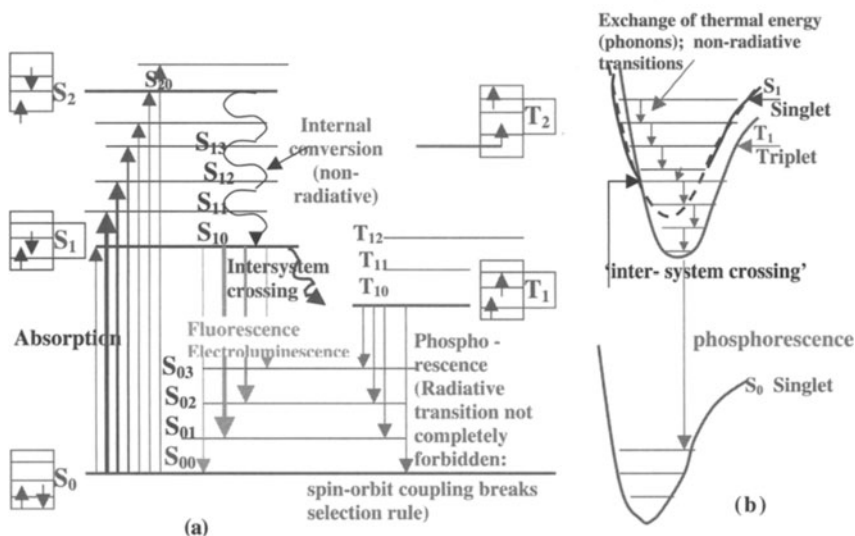


**Figure VII-15.** (a) Jablonsky diagram indicating characteristic fluorescence and phosphorescence transitions; and (b) inter-system crossing from singlet to triplet states.



which can be (Figure VII-15-a) either a singlet state  $S_1$  (which with vibronic levels yields levels  $S_{10}, S_{11}, S_{12}, S_{13} \dots$ ) or a triplet state  $T_1$  (which with vibronic levels yields levels  $T_{10}, T_{11}, T_{12}, T_{13} \dots$ ) and that in emission there are two possible mechanisms:

- fluorescence is practically instantaneous after the molecule has been excited by light. The process starts with the excited molecule descending through its vibrational levels in an internal conversion process detailed in Figure VII-15-a in which energy is given to neighbours by collisions. On reaching the lowest vibrational state, of the same multiplicity ( $S_{10}$ ) as the fundamental level ( $S_{00}$ ), the molecule spontaneously emits a fluorescing ray during subsequent transitions, which respect classic selection rules (see Figure VII-14-b). The intensity of the emitted rays depends on the Franck–Condon factor and the energy of those same rays are less than that of absorbed rays, as detailed in Figure VII-14-c in which we can see that emitted rays are red-shifted, have the longer wavelengths and have undergone a ‘Stokes shift’ or Franck–Condon displacement; or
- phosphorescence which occurs a considerable time after the absorption event. This emission results from the presence of excited triplet states. At the intersection of the two configuration curves, shown in Figure VII-15-b, the two states have the same geometry and for molecules which have strong spin-orbit interactions (for example those which contain atoms, typically, heavier than mercury) the molecule can undergo a reverse in orientation with respect to the spins and pass into a triplet state. After a descent through the vibrational levels to the lowest vibrational fundamental level of the triplet state, the energy remains trapped due to Russell–Saunders coupling which forbids triplet-singlet transitions. As we have already seen, intervention by non-negligible spin-orbit coupling can modify the selection rules (as we can no longer separate spatial co-ordinates of electrons and their spin and thus write the electron wavefunction simply as  $\psi'_e = \psi_e \psi_s$ ) so that the molecules can slowly emit.

Electroluminescence brings into play the same transitions as those detailed above. We shall now go on to see how quantum yields can be improved in these systems.

## 4 Experimental results: discussion

### a Empirical results

Figures VII-16 and VII-17 show spectra obtained for absorption and electroluminescence of Alq3 and poly(*para*-phenylene vinylene) (PPV), respectively.

In both cases we can see a displacement of the emission to the red. Alq3 shows both spectra to be of approximately the same size. PPV, however, shows an absorption spectra larger than that of emission, and Figure VII-17 is less symmetrical than portrayed by the theory shown in Figure VII-14-c. This could be due to the distribution of the conjugated lengths of the polymer, with shorter conjugated segments contributing to a shift towards higher energies. All conjugated segments, whatever their length,

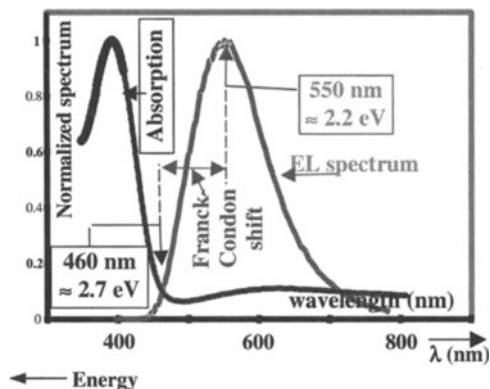


**Figure VII-16.** Absorption and electroluminescence spectra of Alq<sub>3</sub>.

participate in absorption, resulting in a wider spectrum, and the preferential diffusion of excitations to lower energy segments gives rise to these emissions [Gre 95].

## b Discussion

*α Configuration diagram extended to polymers* Considerable discussion has been made concerning the application of a model representing electronic spectra, shown in Figure VII-14, to conjugated polymers which *a priori* present very delocalised orbital bands. This is an issue of extending a description of states with the help of localised molecular orbitals (small molecules which display essentially discrete energy levels) to polymers. It is possible because of the effect of electron-lattice interactions (see Figures IV-6 and IV-7 for the same systems in Figures VII-13 and VII-14) found in conjugated polymers which give rise to sufficient localisations of states during radiative emissions (excitonic states). See also discussion in Section VI-2 concerning the nature of excitons in polymers where empirical results indicate, overall, that the

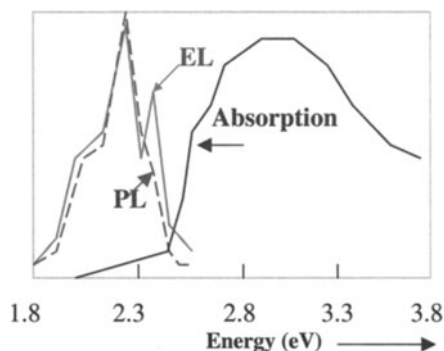


**Figure VII-17.** Absorption, photoluminescence (PL) and electroluminescence (EL) spectra of PPV.

argument is correct. However, in certain cases, difficulties with this approach should not be ignored.

$\beta$  *Extending excitations: notion of excitons* In the discussion just above, an excited electron was seen as being localised on a single molecule, however, this is not strictly true when considering recombinations, a reasoning also generally applicable to polymers.

In reality, in polymers as in small molecules, the generation of an electron-hole pair, by photoexcitation or double electronic injection, results in an excited but neutral state with a limited, finite life time. This state is termed an exciton and is constituted of an electron and a hole paired by excited energy states within the limits of permitted bands (LUMO and HOMO bands, respectively). The occupation of these excited state, the LUMO by the electron, the HOMO by the hole, is termed a non-recombined exciton and has unpaired electron spins, while recombination results in a double population at the HOMO level (obligatorily a singlet state tied to paired carriers).

In an organic crystal, recombination of electron and hole is generally Coulombic in origin, while capture is termed Langevine. In effect, the Coulombic bonding energy between an electron and hole is greater than thermal energy ( $[q^2/4\pi\epsilon r] > kT$ ) when  $r < r_c = (q^2/4\pi\epsilon kT)$ . As for organic solids,  $\epsilon$  is small ( $\approx 3$ ) and  $r_c$  is large ( $\approx 20$  nm), so with surface area of efficient capture defined by  $\sigma_r = \pi r_c^2$  (of the order of  $10^{-11}$  cm<sup>2</sup>), capture is relatively easy. A simple calculation of charge distribution within an organic solid shows that all charges are found within the same Coulombic sphere as opposed charges. A bonded electron-hole state corresponding to a neutral quasi-particle (exciton) forms in such a way. In addition, given the poor mobility of carriers in organic solids, the carriers can only combine through processes detailed in the above Sections 1 to 3. However, as we have seen, depending on the solid, the excited electron-hole pair can be localised on the same molecule or over different molecules. In addition, important effects can result when the excited molecules are close together (as in aggregates).

## VI Excitons

### 1 Introduction

In general terms an exciton can be defined as an elementary excitation of a polyelectron insulator [Uet 86]. Thus the excitation of an electron from a valence band generates an excited electron-hole pair, which as a quasi-particle is subject to a number of interactions. These include Coulombic interactions (described in previous Section) between the electron-hole pair and other interactions caused by interatomic, intermolecular and excited system dipole-dipole forces. These interactions effect energy levels and the optical transitions in the solid. Simply put, we can suppose that an electron and a hole generated by excitation mutually attract to form an associated, bonded state called an exciton much in the same way as an electron and a positively charged defect are tied within a solid by an electrostatic force.

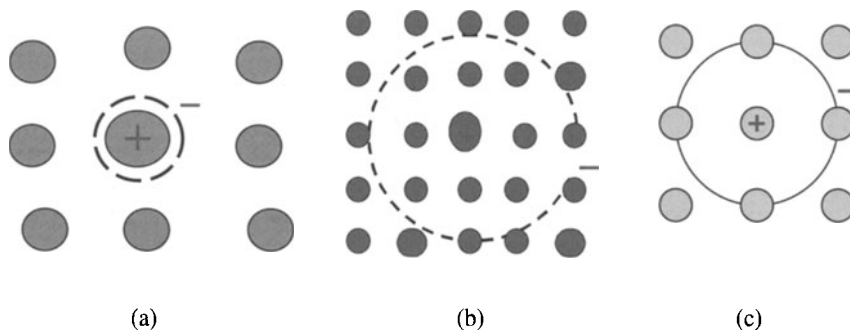


**Figure VII-18.** Various excitons represented: (a) Frenkel exciton; (b) Wannier exciton; (c) charge transfer exciton.

Depending on the nature of the solid, the excited state of electron and hole pair can be localised on one or more molecules. The former is called a Frenkel exciton, and is detailed in Figure VII-18-a. For an electron and hole separated over several molecules, the result is called a Wannier exciton (Figure VII-18-b). The intermediate between these two is the charge transfer exciton, where electron and hole are on adjacent molecules, as shown in Figure VII-18-c.

## 2 Wannier and charge transfer excitons

In solids with large permitted bands (size  $B$ ) such as semiconductors, electrons or holes exhibit high mobilities ( $\mu$ ) with  $\mu$  proportional to  $B$ , as detailed in band theory for covalent solids. Holes and electrons can therefore easily separate giving rise to low interaction energies.

Given that an electron and hole pair, with energy levels schematised in Figure VII-19-a, are:

- buried within a continuous medium with permittivity given as  $\epsilon = \epsilon_0 \epsilon_r$  where  $\epsilon_r$  is relatively high for a reasonably well conducting medium (quite high mobility); and
- trace an orbit around one another in the material; thus their bonding energy ( $E_n$ ) can be evaluated by using the analogy of semiconductors where we introduce charged states due to acceptor or donor type impurities.

The energy  $E_n$  is thus given by the expression:

- derived from a hydrogen based model for which quantified energy levels are of the form  $-m^*e^4/32\pi^2\epsilon^2\hbar^2n^2$  where  $m^*$  is the effective mass of the system; and
- is such that for a limited state, non-bonded ( $n \rightarrow \infty$ ) with the electron-hole system, the energy is equal to  $E_G$  (material gap) which effectively corresponds to the liberation of these two particles from conduction and valence bands.

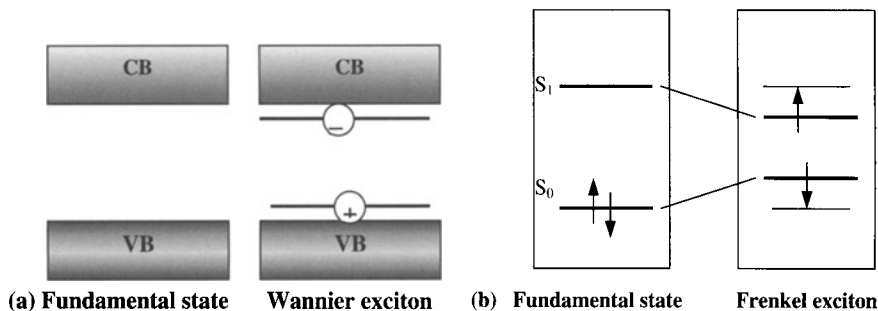


**Figure VII-19.** Representations of excited states in: (a) classic semiconductor band scheme (Wannier exciton); and (b) molecular state with discrete levels (Frenkel exciton).

On using the highest point of the energy band to define the positions of bands due to bonded excited exciton states ( $E_n$ ), which are below the minimum of the conduction band, (situated at  $E_G$  with respect to the highest point of the valence band) where the electron and hole attract one another with the Coulombic potential

$$U(r) = -e^2/4\pi\epsilon r, E_n = E_G \frac{m^* e^4}{32\pi^2 \epsilon_0^2 \epsilon_r^2 \hbar^2 n^2}, \text{ with } m^* = \frac{m_e m_h}{m_e + m_h}.$$

The radius of the exciton ( $r_n$ ) can be evaluated using the electron-hole distance again for a system based on hydrogen and is therefore of the form  $r_n = n^2(4\pi\epsilon_0\epsilon_r\hbar^2/m^*e^2)$ . The distance  $r_1$  at  $n = 1$ , the lowest energy level for a Wannier exciton and thus the most bonded exciton state (like a 1s orbital), is the shortest. From these expressions for  $E_n$  and  $r_n$ , we can see that bonding strength is dependent, essentially, on two parameters:

- the dielectric permittivity of the medium: the larger it is, the weaker the electron-hole attraction; and
- the effective mass of electron-hole pairs: the smaller it is, the greater the electron-hole distance (and by consequence the harder it is to retain the exciton).

Thus for semiconductors which exhibit a large permitted band, high permittivities and charge mobilities  $\mu$  (with a low effective mass  $m^*$  as, classically,  $\mu = q\tau/m^*$ ), only low bond energies can appear (Wannier excitons). For semiconductors with an indirect gap, excitations of the lowest energy are forbidden as they require phonon intervention. For example, Wannier excitons have only been observed in semiconductors such as GaAs with a direct gap.

For polymers, Wannier excitons have been theoretically envisaged in PPV [Gre 95]. The bonding energy of the exciton was found to be around 0.4 eV within an ellipsoid geometry with main axis 2 nm and secondary axis 0.4 nm. These values are representative of molecular excitons with a high degree of localisation on a chain under strong electron-lattice interactions (and electronic and vibrational state coupling). Polymers with a wide gap (insulators) must, nevertheless, present a weaker intra-chain delocalisation and inter-chain interactions can be comparatively greater. Charge

transfer excitons (intermediate to Wannier and Frenkel excitons) are possible. The optimisation of interchain contacts can result in excitons termed excimers (excitons shared over several identical molecular units) or exciplexes (excitons shared over 2 or more different molecular units).

The bonding energy of a charge transfer exciton is given by:  $E_{CT} = I_p - E_A - P - C$  in which:

- $I_p$  is the donor ionisation potential (hole site);
- $E_A$  is the acceptor electron affinity (electron site);
- $P$  is the polarisation energy of the lattice by the electron-hole pair; and
- $C$  is the Coulombic attraction energy of the electron-hole pair.

Using this method, the correct bonding energies for tetracene were calculated with a Coulombic energy for a hole placed at the origin with an electron centred on neighbouring molecules [Wri 95, p109].

### 3 Frenkel excitons

In an inverse scenario to that detailed above, in molecular crystals, the formation of Wannier excitons necessitates a radius of excitation ( $r_n$ ) considerably greater than the intermolecular space available. For materials which are good insulators,  $\epsilon_r$  is low—along with mobility—due to poor contacts between molecules, and electron-hole interaction energy is great and  $r_n$  is low. The result is that the exciton remains localised on a single molecule, corresponding to a Frenkel exciton [Kao 81].

In molecular crystals, the covalent bonds between atoms that make up the molecule are much stronger than intermolecular Van der Waals bonds. As we have already seen in Chapter III, Section III-2, transitions between electronic levels of a practically isolated molecule in a diluted state and one in a condensed, solid state are only weakly displaced in frequency. On the basis of an excited state on a strongly bonded host molecule, Frenkel excitons were generally used to explain luminescence phenomena in molecular crystals. The corresponding energy scheme is detailed in Figure VII-19-b. Frenkel excitons thus correspond to a strong bond approximation with the excitation localised on the same molecule (see Section V) or on an adjacent neighbour. Frenkel excitons have been observed during  $\pi$ - $\pi^*$  transitions in aromatic molecules such as anthracene. Another example is that of excitations in ligands fields of d electrons, observed for example in nickel oxide [Cox 87, p225].

While the particles that make up the electron-hole pair are bonded to one another on the same lattice site, together they constitute a quasi-particle which can move through the crystal by transferring energy to neighbouring sites. This representation of energy migration is confirmed by the fact that in crystals which contain impurities, the latter can trap excitations. It is in this manner that anthracene (which fluoresces on optical excitation), once doped with several parts per million of tetracene, sees its own fluorescence decrease and that of tetracene appear. This effect demonstrates that tetracene efficiently traps excitons, which can move across relatively large distances without relaxing. Given the relatively low concentrations of impurities, the distance covered can be of the order of a hundred molecules or more.

The movement of excitons can be due to overlapping of orbitals between adjacent sites. However, it should be noted that during the permitted  $\pi$ - $\pi^*$  transitions, it is the electrostatic interaction tied to the dipolar momentum which gives rise to the greatest coupling energy between fundamental and excited states. This term is expressed in the form  $\mu_{ij}^2/R^3$  in which  $\mu_{ij}$  is the dipolar momentum for the transition between fundamental (i) and excited (j) states.

For adjacent molecules of different types, the excitation energy transfer mechanisms with long (dipolar interactions) and short (orbital overlapping) action radii will be detailed, along with Förster and Dexter transfers, in the following Section 7. These transfers help explain the interest in the use of optical doping of fluorescent molecules especially for organic LEDs and can also help get round selection rules to increase LED yields (Chapter X). Beforehand though we shall look at the interaction effects due to neighbouring excited molecules which can result in particular properties, especially for example in aggregates. These effects include:

- interactions between two identical molecules without bond formation (termed a physical dimer) in which discrete levels appear and the result, in terms of transitions, depends on the orientation of each of the molecular dipoles;
- interactions between identical molecules in the same chain for which there is a breakdown of the preceding levels, associated with excited electronic states representing Frenkel exciton wavefunctions. The resulting band is called an exciton band and while it does not appear optically (due to the rule  $\Delta k = 0$ ) there is, however, an observable change called Davydov's displacement; and
- interactions between molecules, which in crystallographic terms are unequal (or have two different axes) and the preceding band breaks down into as many bands as there non-equivalent crystallographic axes in a process termed Davydov's breakdown.

In the following Section each effect will be described, although the first will be detailed most thoroughly.

## 4 States, energy levels and transitions in physical dimers

### a States and energy levels

A physical dimer is made of two identical molecules which are close to one another but do not have a chemical bond. With respect to individual single molecules, there are spectroscopic modifications due to intermolecular interactions. In order to understand them more fully, we can write their Hamiltonian in the form  $H = H_1 + H_2 + V_{12}$ , in which  $H_1$  and  $H_2$  are Hamiltonians of the isolated molecules and  $V_{12}$  the intermolecular potential energy. Having  $\psi_1$  and  $\psi_2$  as wavefunctions of the fundamental states of molecules 1 and 2 (neglecting spin and vibration states), of the dimer can be approximated by the wavefunction  $\psi_f = \psi_1\psi_2$  denoted eqn (4-1), and is no more than an approximate solution to the problem as in the physical dimer there is also the intervention of the interaction term  $V_{12}$ . Given this approximation of the wavefunction, the energy of the fundamental state is in the form  $E_f = E_1 + E_2 + \langle \psi_1\psi_2 | V_{12} | \psi_1\psi_2 \rangle$

where  $E_1$  and  $E_2$  represent state bonding energies of single molecules and the latter term,  $W = \langle \psi_1 \psi_2 | V_{12} | \psi_1 \psi_2 \rangle$ , corresponds to the Coulombic bonding energy of the pair of molecules in their fundamental state. In reality, the calculation in this approximation is in disagreement with observed results and it necessitates a slight readjustment. To do this, it is necessary to consider the interaction effects of the two molecules 1 and 2 excited to equivalent  $\psi_1^*$  and  $\psi_2^*$  states, respectively, if the molecules are the same. In the limiting case, if only one of the molecules is excited which rests on the same molecule, then  $V_{12} = 0$ , and the state of the system is denoted by wavefunctions  $\psi_1^* \psi_2$  or  $\psi_2^* \psi_1$  to which there are the same, corresponding energy states  $E_1^* + E_2$  or  $E_1 + E_2^*$ . However, if  $V_{12} \neq 0$ , as is the case in physical dimers, then the electronic energy is no longer localised at one molecule but oscillates between the two molecules of the system. The dimer is therefore not degenerate. The variations in energy depend on the interaction energy and, therefore, the orientation of the two molecules. If the two molecules are identical then, *a priori*, each of these molecules has the same probability of being excited. The physical dimer once excited can therefore be developed following a linear combination using the possible wavefunctions  $\psi_1^* \psi_2$  and  $\psi_2^* \psi_1$  of the initial system (single excitation on one molecule with  $V_{12} = 0$ ). We can therefore write:

$$\psi_{E_{\pm}} = \frac{1}{\sqrt{2}} (\psi_1^* \psi_2 \pm \psi_2^* \psi_1) \quad (1)$$

Denoting the energies of excited 'monomers' as  $E_1^*$  and  $E_2^*$ , the corresponding energies (to  $\psi_{E_{\pm}}$  states) of the excited dimer system are in the form  $E_{\pm} = E_1^* + E_2 + W' \pm \beta$  with:

- $W' = \langle \psi_1^* \psi_2 | V_{12} | \psi_1^* \psi_2 \rangle = \langle \psi_1 \psi_2^* | V_{12} | \psi_1 \psi_2^* \rangle$  being the Coulombic energy for interactions due to the charge distribution on excited molecule 1 and unexcited molecule 2 (or *vice versa*) in a term which depends on polarisation or the polarisability of the media in excited and fundamental states; and
- $\beta = \langle \psi_1^* \psi_2 | V_{12} | \psi_1 \psi_2^* \rangle$  being the resonance interaction energy depending on the overlap of the two molecular orbitals.

Figure VII-20 shows the energy levels for a physical dimer. We can see that  $W$  and  $W'$  are negative and that with  $\beta < 0$ , the level  $E_+$  is lower than level  $E_-$ . The two possible transitions  $+$  and  $-$  are also shown.

## b Possible transitions

In fact, depending on the orientation of the two molecules [För 65], one of the possible transitions  $+$  or  $-$  is forbidden, and in effect, for a dimeric system, the transition momenta between the fundamental  $\psi_1 \psi_2$  state and the two, possible excited  $\psi_{E_{\pm}}$  states are in the form (see also Section IV-2)

$$\vec{M}_{\pm} = \left\langle \psi_1 \psi_2 \left| -e \left( \sum_{i1} \vec{r}_{i1} + \sum_{i2} \vec{r}_{i2} \right) \right| \psi_{E_{\pm}} \right\rangle,$$





of the dimer take on two, non-zero values to give two possible transitions of energy separation  $\Delta E = 2\beta$ , permitting evaluation of  $\beta$ .

## 5 System containing an infinite number of interacting molecules and exciton band: Davidov displacement and breakdown

### a Qualitative description of interaction effects due to n interacting molecules and the exciton band

Instead of a physical dimer of just two molecules, detailed here is a chain of n identical molecules. This jump is analogous to going from studying the electronic structure of a covalent bond between two atoms to looking at a one dimensional covalent semiconductor, as in Chapter I. Instead of there being discrete levels for two bodies, there is an energy band in a 1-D crystal of infinite length and band size dependent on the degree of orbital overlap.

The discrete levels  $E_+$  and  $E_-$  shown in Figure VII-20 each give rise to a band of narrow levels which are termed crystal exciton bands.

### b Linear chain of N identical molecules spaced d apart

If there is only one molecule (i) excited to wavefunction  $\psi_i^*$  while all other molecules denoted by  $n \neq i$  remain in their unexcited state  $\psi_n$ , the wavefunction for the system can be written:

$$\Psi_i = \psi_i^* \prod_n \psi_n.$$

In reality, the wavefunction to which a particular molecule is excited is not actually a good physical solution (as we have seen for the dimer). And as in band theory where we use a linear combination of atomic orbitals, here we must also use a linear combination of all excited states of the form  $\Psi_i$  which can appear. The eventual wavefunction should therefore be looked for in the form  $\Psi = \sum_{i=1}^n c_i \Psi_i$  and the resulting solutions to the wavefunctions are subject to the same considerations as those used for band theory (limiting conditions especially) which are of the form

$$\Psi_k = \frac{1}{\sqrt{N}} \sum_{p=1}^N e^{ikpd} \Psi_p$$

where d represents the distance between molecules.

The function  $\Psi_k$  is such that an excitation is not confined to one molecule but rather delocalised over a whole chain, and is the wavefunction of an excited, neutral but mobile state of the crystal: it denotes the exciton with wavevector k.

Just as in the LCAO method, we can calculate the energy  $E(k)$  associated with the  $\Psi_k$  state. Denoting the interaction energy between two adjacent molecules by  $\beta$  and the transition energy relative to a system of isolated molecules (gaseous phase)

by  $E_0$ , we obtain

$$E(k) = E_0 + (W - W') + 2\beta \cos(kd).$$

Interaction therefore results in the appearance of a band of size  $4\beta$  (Figure VII-22-a). In reality, and from a spectroscopic viewpoint, this band should not appear as the selection rule  $\Delta k = 0$  states that only a single electron associated with  $k = 0$  can result. So, the excitation energy  $E$  is simply displaced (by  $(W - W') + 2\beta$ ) with respect to that of isolated molecules. This is called Davidov's displacement and can be clearly observed, for example in charge transfer components formed from  $[\text{Pt}(\text{CN})_4]^{2-}$ .

### c Linear chain consisting of two types of different molecules

This more complex case can be treated using the analogy of an 1-D, AB type crystal with a strong bond approximation (see Chapter I, Section V). Each  $\Psi_k$  function can be seen as a linear combination of all possible linear combinations such that

$$\Psi_k = \frac{1}{\sqrt{N}} \sum_{p=1}^N e^{ikpd} (a_p \Psi_p^A + b_p \Psi_p^B)$$

where  $\Psi_p^A$  and  $\Psi_p^B$  represent wavefunctions for the A and B molecules excited at site  $p$ . For each value of  $k$ , and in particular  $k = 0$ , which corresponds to the optical region, there are the two possible transitions a and b (Figure VII-22-b) associated with different values of  $a_p$  and  $b_p$ . The interaction between two different molecules A and B results in a Davidov breakdown of the transition. This effect has been observed for anthracene, which gives rise to two forms through a translation of its unit cell.

The intensity of the breakdown ( $W_D$ ) depends on the interactions between the non-equivalent molecules (through a plane for anthracene) and the  $4\beta$  size of each band depends on both sorts of intermolecular interactions. From a practical point of view (for example phtalocyanines [Wri 95]), the spectral peaks from a solid are displaced and spread out with respect to those from a solution.

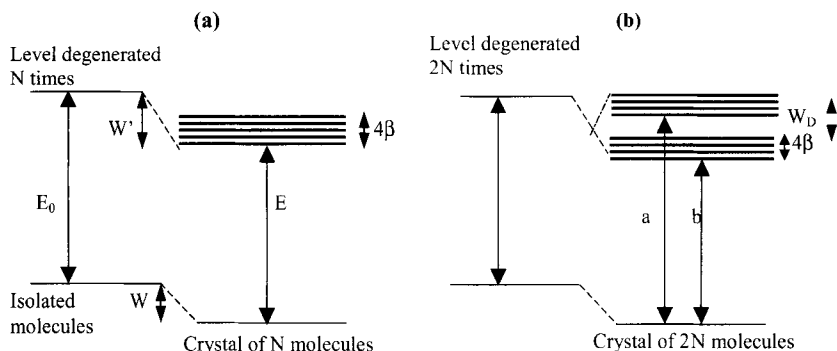


**Figure VII-22.** Energy levels of excited states for a chain of: (a)  $N$  identical molecules; or (b)  $2N$  AB type molecules.

## 6 Aggregates [Fav 01]

### a Aggregate forming systems

In general, colouring agents in solution display wide and unstructured absorption spectra. However, certain ionic colouring agents, which carry charges paired with counter ions, in sufficiently concentrated aqueous solutions show a particularly discreet and intense absorption band red-shifted with respect to the same agents alone. This band is indicative of the formation of molecular aggregates (uni-dimensional) which are generally called 'J aggregates', and have as example pseudoisocyanine. More precisely, for an isolated molecule, or one which is in a very dilute solution, the same absorption band has a frequency  $\nu_1 \approx 19000 \text{ cm}^{-1}$ , while at higher concentrations, this band decreases at the expense of a second band which has higher energy and is situated at  $\nu_2 \approx 21000 \text{ cm}^{-1}$ . At even higher concentrations of the same molecule, a narrow band (width  $\Delta\nu \approx 180 \text{ cm}^{-1}$ ) with a lower energy appears which is the J band and has  $\nu_J \approx 17500 \text{ cm}^{-1}$ .

### b Origin of observed effects

The above observations detail a process in which the system is not at too great a concentration, and any formation of dimers occurs at the expense, twice over, in the concentration of monomers.

If the transitional momenta of the two molecules in a dimer are parallel to each other and perpendicular to the axis of the dimer—as shown in Figure VII-21-b—it is the upper level which corresponds to the permitted transition and thus also absorption. Accordingly, there is a blue-shift. Transitions to the lower level are forbidden, so that following relaxation from the higher to the lower level, any fluorescence of the system will be very weak and will penalise any electroluminescence (Figure VII-23-a); the pair of molecules take on the co-ordination of an 'H aggregate' (the H resembles the geometric form). However, once the system is relaxed, the return from excited to fundamental states is improbable and the excitation (exciton) can diffuse over relatively long distances ( $\approx 100 \text{ nm}$ ) displaying a property which can benefit photovoltaic

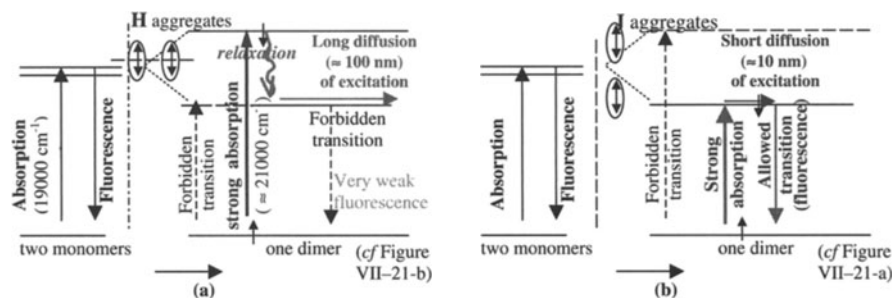


**Figure VII-23.** Transitions and excitation diffusion for: (a) H aggregate; and (b) J aggregate.

effects, where the necessary separation of hole and electron is favoured by the presence of a capable electric field (see volume heterojunctions detailed in Chapter XI).

In addition, the J band which appears at the highest concentrations shifts towards low energies (red-shift as detailed in Figure VII-21-a). As the corresponding fluorescence is rather intense we must suppose that molecules at the centre of J aggregates (the letter J symbolises the bottom to head alignment of the molecules) are orientated so that which ever level absorbs or emits, the bottom to head alignment is retained. This positioning of the molecules is beneficial to electroluminescence (Figure VII-23-b) but penalises any photovoltaic properties. Excitons can recombine easily and therefore diffuse only over short distances, leaving little chance that they will meet a centre, such as a volume heterojunction which could give rise to a potential difference permitting their separation.

To conclude, in order to obtain fluorescence the parallel arrangement of molecular transition momenta are proscribed for condensed materials. However, if aggregates do form, then at least type H aggregates should be avoided, while type J (which have linearly trained dipole momenta) are preferred. In photovoltaic systems, the inverse is true: J aggregates should be avoided as they display low exciton diffusion lengths, while H aggregates are favourable to the separation of holes and electrons.

We can note that the coupling effect detailed here has been observed in the  $\pi$ -conjugated polymer poly(*para*-phenylene) (PPP) in its ladder form (LPPP). In addition, a line shifted towards the yellow appears for PPP films, while a blue line is associated with isolated polymer chains. In addition, the fluorescence quantum yield for PPP goes from 0.4 in solution to 0.1 in the solid state [Lem 95], an effect attributed to non-radiative traps in the solid, condensed state films.

In the solid state, needle shaped molecules tend to orientate themselves parallel with respect to their principal axis, so that the dipolar transition moment for the lowest excited state is also directed in the same direction. Oligophenylenes, which have this structure, exhibit quantum yields in solution of the order of 10 % but extremely low yields in the solid state (less than  $10^{-3}$ ) [Sch 00].

Low quantum yields in electroluminescent diodes are generally blamed on local order. In order to increase yields, films with amorphous structures which avoid crystallisation are sought.

## 7 Förster and Dexter mechanisms for transfer of electron excitation energy

### a Possible mechanisms for excitation transfer between donor and acceptor molecules

The principal mechanism for energy transfer is from an excited donor molecule ( $D^*$ ) to a molecule which acts as an acceptor (A). The transfer can be written in the form  $D^* + A \rightarrow D + A^*$ . It is in this way that optically doped organic films transfer an excitation (exciton) from a host molecule to an 'invited' (doping agent) molecule, in an effect which can reinforce luminescence of invited molecules to the detriment of host molecules. A system can therefore evolve by going from the initial state  $\Psi_i = \Psi_{D^*+A}$  to the final state  $\Psi_f = \Psi_{D+A^*}$ . The probability of such a transition can be written,

using Fermi's golden rule, in the form  $P_{if} \propto |\langle \Psi_i | H^{(1)} | \Psi_f \rangle|^2 N(E)$  where  $N(E)$  is the density of states in the donor-acceptor system at the energy state under study. In organic materials, the probability of transfer of  $k_{ET}$  excitons per unit time is high when going in the direction donor to acceptor. Once the acceptor is in an excited state, it relaxes to the lowest vibrational state with a probability much greater than that associated with a return of excitation from  $A^*$  towards a donor molecule  $D$ . The term  $H^{(1)}$  embraces the interaction terms between donor and acceptor which assure the passage of the excitation. These terms can be divided into two groups:

- electrostatic interactions (Coulombic interactions due to preponderant dipole-dipole interactions) which gives rise to Förster type transfers; and
- direct exchange interactions between molecules adjacent to donors and acceptors (for example, hopping or excitation diffusion between overlapping electron clouds of adjacent  $D^*$  and  $A$  molecules) which give rise to Dexter transfers.

### b Properties of long distance Förster transfers (3 to 10 nm)

If  $\tau$  represents the lifetime of an excitation  $D$  in the absence of a transfer towards  $A$  (the lifetime of an exciton localised on  $D$  has probability of de-excitation per unit of  $k_D = 1/\tau$ ), the probability of excitation transfer per unit time *via* the Förster mechanism is given by:

$$k_{ET}(R) = \frac{1}{\tau} \left( \frac{R_0}{R} \right)^6$$

where  $R$  is the donor-acceptor distance and  $R_0$  is the Förster radius which is such that  $R = R_0$  when  $k_{ET} = k_D$ . Dipole-dipole interactions are non-negligible up to distances as long as 10 nm in organic media, due to strong electron-lattice interactions which result in an increase in emission or absorption spectra.

Spins of both  $A$  and  $D$  molecules are conserved during Förster transitions under a condition imposed by allowed dipolar transitions in the donor and acceptor molecules,

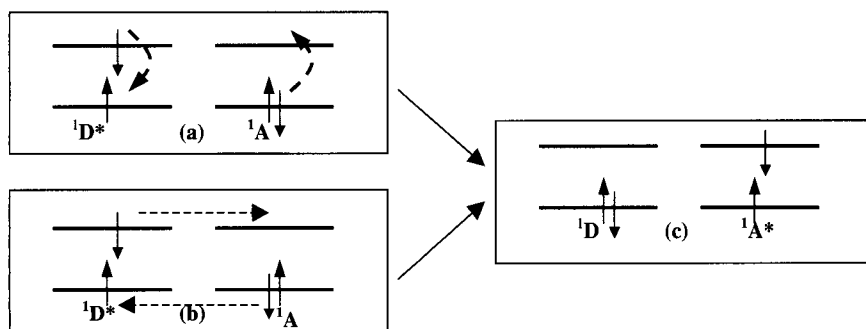
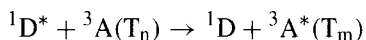
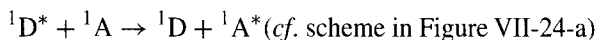


**Figure VII-24.** Excitation transfer, between singlet states, from  $D^*$  to  $A$  following the: (a) Förster mechanism; and (b) Dexter mechanism. (c) Shows state following excitation transfer according to  ${}^1D^* + {}^1A \rightarrow {}^1D + {}^1A^*$ .



**Figure VII-25.** Dexter transfer with conservation of exciton state (example here is triplet):  ${}^3\text{D}^* + {}^1\text{A} \rightarrow {}^1\text{D} + {}^3\text{A}^*$ .

so we find that the following transitions are allowed:



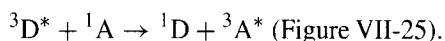
in which  $\text{T}_n$  and  $\text{T}_m$  are, respectively, spectral terms for the molecule A in vibrational state  $n$  and the excited molecule  $\text{A}^*$  in the vibrational state  $m$ . In the latter transfer, the spin configuration of the exciton is changed. In the Förster mechanism, transferred excitons can undergo a change in spin, as in the example here where the spin goes from singlet to triplet.

In contrast, the triplet-singlet transition ( ${}^3\text{D}^* + {}^1\text{A} \rightarrow {}^1\text{D} + {}^1\text{A}^*$ ) is *a priori* forbidden. Nevertheless, it can occur because the lifetime of the  ${}^3\text{D}^*$  can be long, and although the probability of exciton transfer per unit time ( $k_{\text{ET}}$ ) from  ${}^3\text{D}^*$  to  ${}^1\text{A}$  remains small, it can be higher than the probability per unit time for the transition  ${}^3\text{D}^* \rightarrow {}^1\text{D}$ .

### c Properties of short distance Dexter transfers (0.6 to 2 nm)

In contrast to the Förster mechanism, the Dexter mechanism does not rely upon allowed transition probabilities in donor and acceptor molecules. The Dexter transfer displays a probability in physical coherence with the proportional overlap surface of donor and acceptor molecular orbitals. It is a transfer over short distances and subsides exponentially with distance.

Only the total spin of the system is conserved ( $\text{D}^*\text{A}$  then  $\text{DA}^*$ ) during the transfer of excitation *via* overlapping electron clouds, and an exciton transferred this way retains its spin configuration: a singlet exciton retains its singlet state in the same way as a triplet exciton remains a triplet. In addition, the Dexter transfer is the only one which allows energy transfer from the donor triplet state to the acceptor (in the Förster transfer, the transfer of energy from donor triplet state to acceptor triplet state is forbidden due to the condition requiring spin conservation of each type of molecule involved in dipole-dipole interactions). The Dexter transfer of energy between donor and acceptor triplet states can be represented by:



The Dexter transfer is further illustrated in Figure VII-24-b in which there is a transfer of excitation energy between singlet states, as was the case for the Förster transfer.

**Components: organic light emitting diodes,  
photovoltaic cells and electro-optical modulators**



## VIII

---

# Fabrication and characterisation of molecular and macromolecular optoelectronic components

This Chapter describes general methods used in the fabrication of organic optoelectronic components with two specific examples which have undergone considerable development during the last decade. One is that of the electroluminescent diode (from 'small' molecules to give OLEDs, or from polymers to give PLEDs) and the other is the optical guide which is inserted into the arms of an electro-optical modulator in a Mach-Zehnder configuration. Given that the latter will be presented in detail in a later publication [Luc 03], the description here is restricted to the essential points. This Chapter uses many of the methods detailed in three PhD theses (in French) [Ant 98, Mou 99 and Tro 01].

## I Deposition methods

Deposition techniques depend essentially on the nature of the organic materials being handled. The use of vapour deposition methods for polymers is difficult, due to the necessarily high temperatures required which entail possible chain degradation, so polymers are normally processed using spin coating from the liquid state. Small molecules are easier to vaporise and are often deposited, through sublimation, under vacuum. Appendix A-11, Section II gives specific details of some optically and electronically active polymers whereas Appendix A-11, Section III presents similar, widely used small molecules.

### 1 Spin coating

As shown in Figure VIII-1, a small quantity (several drops) of a liquid material is spread over a flat surface. The substrate spins with a predetermined acceleration, rate and period in order to control the thickness of the film, which is spread uniformly due to centrifugal forces. Occasionally, effects caused by the substrate edge can arise. Typical examples of films are those prepared from poly(3-octathiophene) (P3OT), poly(phenylene vinylene) (PPV) and polyimides. Each material requires its own specific techniques in order to yield homogeneous films. Mostly, these materials

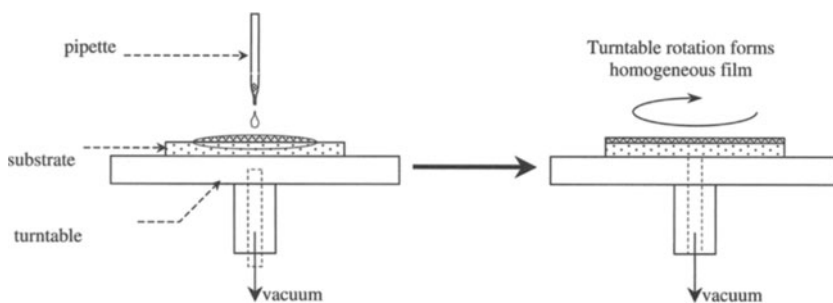


**Figure VIII-1.** Spin coating.

are turned into films using their solutions and once spread often require evaporation of the solvent and annealing of the polymer to obtain the appropriate optical properties. In the case of LEDs, this often means trying to avoid the formation of a polycrystalline material, which would otherwise reduce recombinations (see H type aggregates in Chapter VII, Section VI-6) and would lead to crystal joints limiting electron transport, and diffusion losses in guides.

## 2 Vapour phase deposition

Vapour phase deposition consists of placing a material in a metallic pan, as shown in Figure VIII-2, which is then placed under a high tension and, with a high current, the material is heated and vaporised within the evacuated chamber. A substrate is

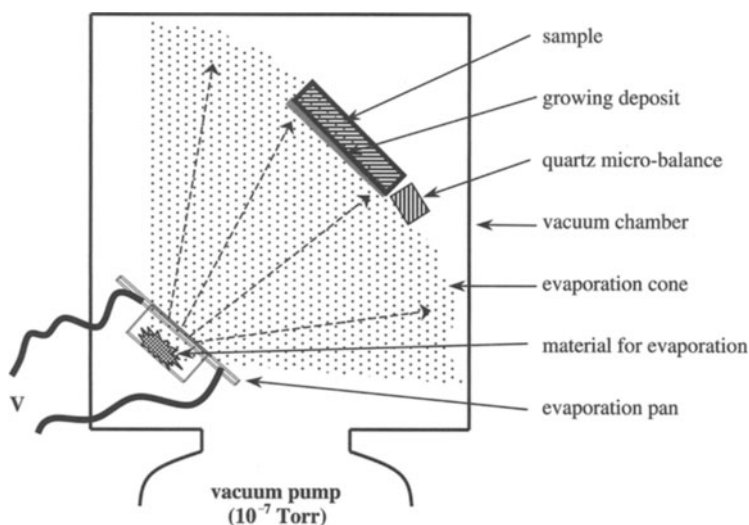


**Figure VIII-2.** Equipment used for deposition by evaporation.

positioned within the cone shaped pathway of vapour so as to trap condensing material. The substrate, through its support, can have its temperature adjusted with respect to the required properties of the condensed layer. Small molecules, such as Alq<sub>3</sub> can be deposited using this method.

The pans are typically made from molybdenum in two parts: a curved base to accept the material and a cover pierced with several small holes so as to multiple the number of vapour cones and limit rapid clogging of the chamber.

The vacuum is generated by a secondary turbomolecular or diffusion pump, in addition to a primary pump, and is of the order of  $10^{-6}$  to  $2 \times 10^{-6}$  mbar. The working temperature is controlled with a thermocouple placed in the pan. The thickness of the deposited sample can be calculated using a quartz balance. This works by altering its vibrational frequency with respect to the mass of deposited material; normally a straight calibration curve can be prepared showing variations in frequency ( $\Delta f$ ) with respect to film thickness (measured using for example a Dektak micrometer) for a particular material.

It is worth noting that metal electrodes (calcium and aluminium for OLED cathodes and gold for electro-optical modulators) are deposited using this method, often using masks to predetermine the design of the electrodes.

Generally speaking, the system often includes a series of pans so that successive depositions of organic solids can be made without exposing the formed multi-layer films to air (Figure VIII-3).

### 3 Polymerisation in the vapour phase (VDP method)

Vapour Deposition Polymerisation (VDP) involves either:

- the thermodynamic relaxation of a monomer, condensed on a cold substrate, invoking its own polymerisation (Figure VIII-4). Examples are those of poly(*para*-phenylene xylilene) (PPX) and its halogenated derivatives [Jeo 91]; or
- the co-evaporation of different monomers, from different pans as shown in Figure VIII-3, which, with precise temperature control of pans and carrying substrates, allow co-polymerisation to yield, for example, polyimides of the type PMDA-ODA [Brou 01].

Materials obtained using this technique often exhibit very good optical properties. In the case of PPX, a remarkable transmission has been observed in the visible spectrum [Jeo 91], which can be explained by its large gap (around 4 eV) making it an excellent candidate to encapsulate optoelectronic components functioning in the visible spectrum (electroluminescent diodes or photovoltaic cells).

The procedures described here can also be used to prepare photoguides based on polymers, for example, either by adjusting the function indices of the monomers (brominated or chlorinated PPX) or, in the case of polyimides, by doping with a colouring agent such as DR1.

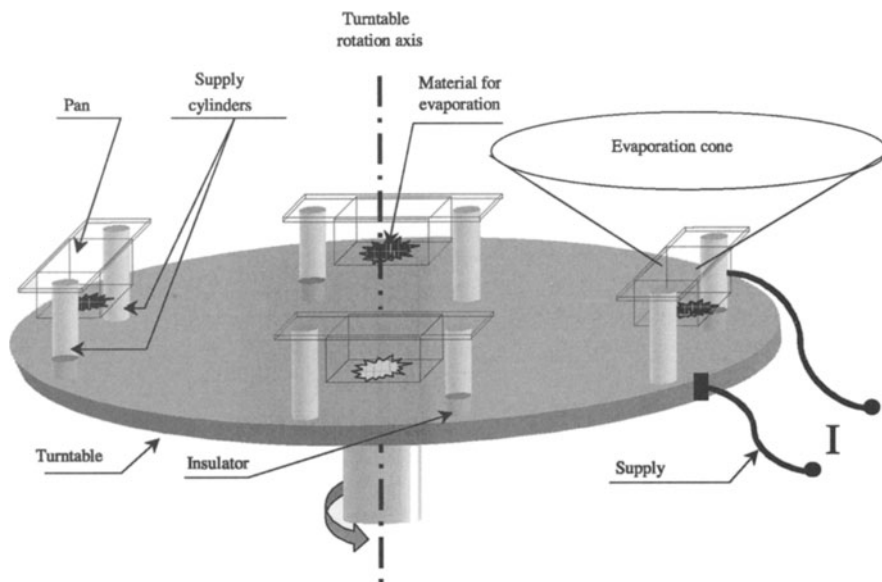


Figure VIII-3. Representation of a multi-pan turntable [Tro 01].

#### 4 Film growth during vapour deposition: benefits due to deposition assisted by ion beams [Mül 89 and Smi 90]

##### a Configuration used for deposition

The titled technique combines classical Joule evaporation effects with those due to an ion beam. The result is the modification of, for example, structural, interfacial and physical properties of the deposited film. Here we shall try and show how the ion beam works during film growth.

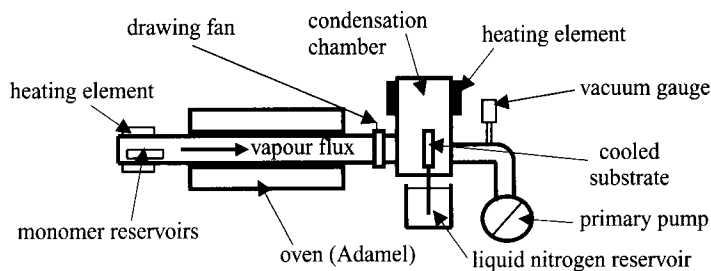
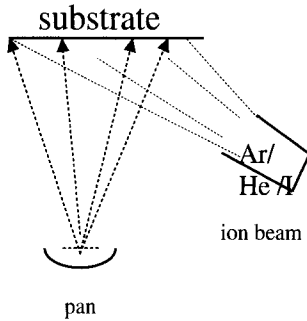


Figure VIII-4. Polymerisation from the vapour phase (VDP).



**Figure VIII-5.** Simplified configuration of ion beam assisted deposition (IBAD).

### b General points: nucleation and film growth

$\alpha$  *nucleation* Individual atoms which hit the film surface continue to diffuse until (Figure VIII-6) they are:

- evaporated;
- used up in the growth of a sufficiently large site; or
- captured by an existing cluster or trapped by a particular site.

The accumulation of atoms continues at a certain speed (of the order of  $R_v = p(2\pi MkT)^{-1/2}$  where  $p$  is pressure and  $M$  is molecular mass) and proceeds at a rate dependent on activation energies.

$\beta$  *Ways in which thin films grow* Initial film growth is conditioned by interactions between the film and the substrate, and can result in various types of growth:

- when interactions between condensing films are stronger than those with the substrate, we obtain the growth of thick islands prior to the whole of the substrate being covered (Figure VIII-7-a), as described by the Volmer-Weber model;
- when interactions are stronger with the substrate and singularly decrease with each added layer, we obtain the formation of successive layers (Figure VIII-7-b), as described by the Franck-van der Merwe model; and
- when a Stranski-Krastanov type growth occurs (Figure VIII-7-c) it is due to the loss of monotonic differences between films, and results in a mixed growth.

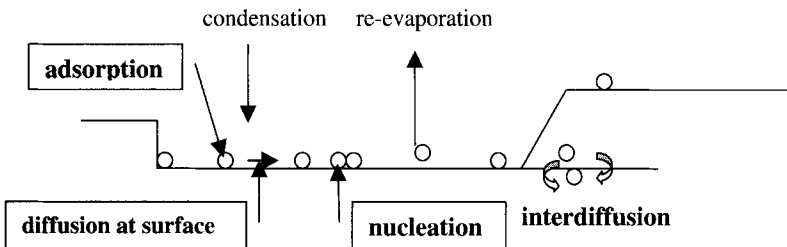


**Figure VIII-6.** Various possible mechanisms accompanying film growth.

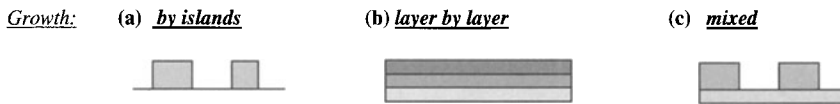


**Figure VIII-7.** Various routes to film growth.

During growth *via* the formation of islands, there is a second step corresponding to stable nucleation and coalescence of clusters (fusion of islands). Once beyond this step, canals can exist leaving a passageway through layers to the substrate below. Once growth is finished, diffusion can occur across the surface, filling the canals.

$\gamma$  *Development of microstructure in thick films* Movchan–Demchishin’s diagram is usually used to represent the development of film structure with respect to the ratio  $T_s/T_m$ , in which  $T_s$  is the temperature of the substrate and  $T_m$  is the melting point of the material. Different zones can appear:

- Zone 1, where  $T_s/T_m = 0.2$  to  $0.4$ , is a zone in which shadow effects dominate and the diffusion of adatoms (atoms added to the surface) is too weak to overcome shadows formed by lower layers. The result is a formation of a mesh (tubes) of column-like aggregates which exhibit poor adherence;
- Zone 2,  $T_s/T_m = 0.6$  to  $0.7$ , where we obtain columnar crystals with curved surfaces in a process dominated by diffusion effects of adatoms at the surface, and the deposited film exhibits a good adherence; and
- Zone 3,  $T_s/T_m = 0.9$ , where the columns recrystallise to give equiaxial crystals in a mechanism dominated by diffusion through volume which aims to minimise mechanical constraints.

In fact, the dense microstructure of Zone 3 obtained from adatoms with a substrate at high temperatures can also be obtained using highly energetic adatoms obtained with an assisting beam, as in the ion beam assisted deposition (IBAD) process.

### c Ion effects on obtained films

$\alpha$  *Ion – solid interactions (particular points in systems at low temperatures)*

Thermal spikes

- Origin of thermal spikes: when ions weakly penetrate the film surface, thermal spikes can result when the local temperature (energy from ion depositions) goes above the melting point of the solid. This mechanism is facilitated when the cooling time (time required to dissipate energy) is longer than the time required to stop ions.
- Effects due to thermal spikes: energy dissipation though thermal conductivity following thermal spikes activates hops of atoms in porous zones between adjacent sites.
- Modelling: for the present time, effects of thermal spikes have been modelled using classical equations of thermal conductivity. When the ratio of bombarding

to incident ions (factor  $R$ ) is close to 1, then the growth of porous micro-columns is arrested, spikes occur and initially empty zones are closed up. This model does not plan for an increased density in zone 1, as it supposes that there is a single isotropic arrangement of atoms due to the thermal spike.

*The limit for the approximation of binary collisions*

When the velocity of particles is low (*i.e.* energy  $E < ca. 100 \text{ eV}$ ) multiple interactions are involved and the classical model, based on binary collisions and performed using the TRIM program, is no longer valid. Indeed, the assumptions that are used, that collisions are violent and only very close incident particles are involved, requires modification using a dynamic method in which co-operative displacements at the interior of the excited solid are developed.

$\beta$  *Ion bombardment effects during initial nucleation and growth of thin films* In general, ion beam bombardment can induce:

- an increase in the size of island-like particles; and
- a decrease in their number density.

These two effects have been attributed, but not directly associated, to an increase in adatom mobilities.

While the final result does not correspond to a set of general rules, it has been shown that the application of IBAD:

- to a crystalline substrate increases nucleation sites; or
- to an amorphous substrate increases the size of islands (increasing diffusion and mobility of adatoms).

**d Effect of IBAD on thin films**

On applying IBAD to thin films, normally, there is a modification of the film density and a collapse in zone 1 of Movcham's diagram. The size of the grains generally decreases as the columnar structure disappears (if the crystal size increases then there are other effects operating such as a rise in temperature). As we have seen though, the thermal spike is not representative of this mechanism of densification. Other, different models have been proposed and are detailed below.

$\alpha$  *Cascading collision model (Figure VIII-8)* The titled model works by accounting for the transfer of momentum from incident ions to remote or pulverised atoms by:

- incident ions being either retro-diffused or incorporated into the film structure; and
- incident ions producing phonons, vacancies, electronic excitations and atoms propelled away from the surface. The latter can either leave the surface as pulverised atoms, or penetrate deeper into the film where they are trapped at interstitial sites, and in preference those sites are favourable to open zone closure.

Vacancies close to the surface produced by ion bombardment, are partially filled by atoms from the vapour phase. At a high enough  $R$  value (ration ion/vapour) the

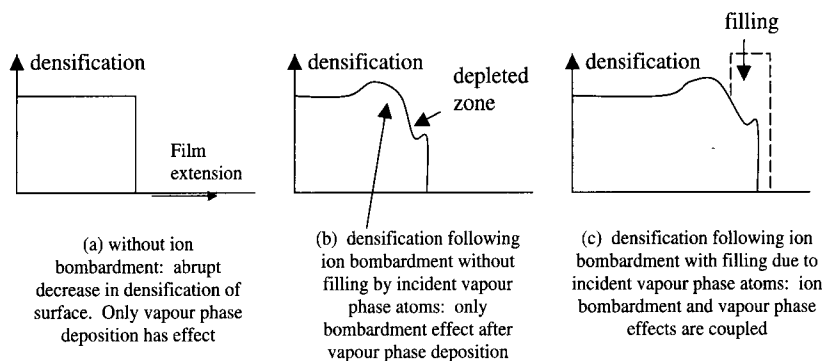


**Figure VIII-8.** Film densification with and without ion bombardment.

latter mechanism results in a densification from the surface to the bottom of the film, so that the film no longer grows as porous columns but as a dense material.

$\beta$  *Estimations with respect to vapour phase atom and ion beam fluxes* Estimates using the ratio of ion to atom fluxes ( $R = J_I/J_A$ ) have been performed.

With  $E = 100$  eV, typically, a value of  $R = 10^{-2}$  has been obtained [Cuo 89].

It has also been shown that the ratio can be optimised when  $J_A/J_I \gg Y$ , that is the degree of pulverisation and is fulfilled when  $E < 1$  keV (where  $E > 1000$  keV), assuring a low degree of pulverisation.

$\gamma$  *2-D simulation of molecular dynamics* This method uses Lennard-Jones potentials to describe interactions between atoms on a zero temperature substrate. Figure VIII-9 shows the filling up of empty zones and the surface movement of atoms caused by a series of incident ions. Simulations have shown that the empty spaces are filled by atoms already well within the film or by atoms from the vapour phase.

$\delta$  *Example of expected modification of OLED interfaces* Finally we can consider the action of IBAD on OLEDs and their behaviour [Mol 00]:

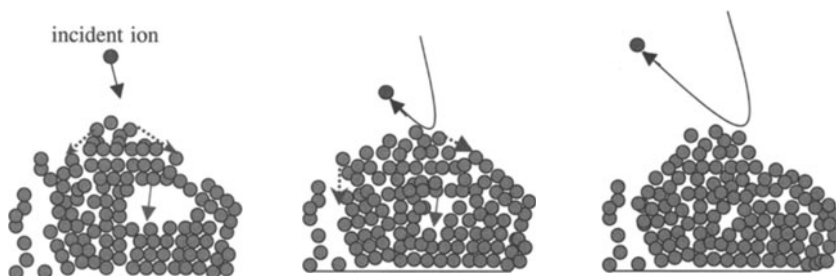


**Figure VIII-9.** Dynamic molecular simulation of atomic rearrangement, in which atoms are pushed into the bulk, and the material collapses and becomes more dense. Dashed arrows show surface diffusion.



- when used with respect to the injection of carriers (especially with respect to the anodic side as can be experimentally shown); and
- when used with respect to the limitation of interface defaults (for example oxygen or non-radiative centres) allowing an increase in fluorescence yields ( $\Phi_f$ ).

The results obtained using this system can be interpreted using the general effects due to a low energy ion beam during layer deposition, which are notably:

- an interface (ITO/Alq<sub>3</sub>) effect. Here, ion bombardment directly effects nucleation during the first steps of film formation. The result, as detailed in Figures VIII-10-a and VIII-10-b, is a decrease in porosity at the interface, an increase in the specific surface contact area and a reinforcement of hole injection at the ITO anode; and
- a volume effect due to layer densification following collisions between incident ions and deposited atoms or molecules. The result is a limitation in the number of traps contributing to luminescence extinction and an increase in the layer resistivity (densification of zone 1 according to Thornton's model).

### 5 Comment: substrate temperature effects

While there are many parameters available when using ion beam assisted deposition, such as the nature of the ions used, their energies, their flux and the density of ionic current, a more classical variation can be introduced through varying the substrate temperature (see also preceding Section 4-b-γ).

Using this technique, a complete study was made of *para*-sexiphenyl film depositions [Ath 96] in which an order-disorder transition was demonstrated at 290 K. In addition, it was shown that depositions performed at a low speed but with a hot substrate resulted in the formation of crystallites (of size *ca.* 2 μm). Optimisation to obtain a good crystalline film, led to the use of a very slow deposition rate (0.01 nm sec<sup>-1</sup>) and a very high substrate temperature (200 °C). Indeed, the nature of the substrate can also have an effect: crystalline substrates (silicon) tend to decrease crystallinity with respect to amorphous substrates such as glass.

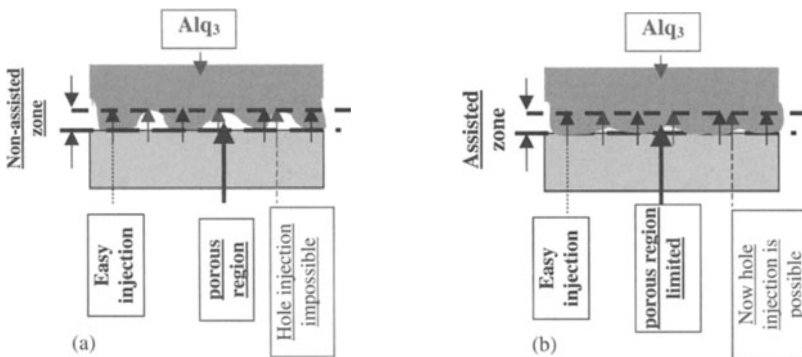


**Figure VIII-10.** (a) Injection without IBAD; (b) Injection using IBAD.

## II Fabrication methods: OLEDs and optical guides for modulator arms

### 1 OLED fabrication

#### a Component structures (see Figure VIII-11)

Classically, the structure of an OLED is based on the layering of organic materials onto indium tin oxide (ITO) covered glass. The ITO serves as an anode; it is generally chosen as its workfunction is particularly well adjusted to favour the injection of holes into organic solids and is used to give a transparent layer. In its most simple and typical form, the OLED is composed of layers which serve for hole injection and transport, and electron injection and transport. The latter is in contact with the cathode and has a low workfunction; calcium is widely used along with a protecting layer of aluminium against air.

Figure VIII-12 shows the necessary stages in the preparation of organic LEDs.

#### b Substrate preparation [Tro 01]

The normal starting point is a plate of glass covered on one side with ITO, bought from a manufacturer such as Balzers or Merk display technologies who use similar fabrication techniques. The square resistance of ITO (of the order of  $R = 4$  to  $20 \Omega/\text{square}$  if possible) can be controlled by the procedure used and any treatments [Tah 98 and Wu 97]; its transmittance is of the order of 90 %. The plates are then cut into squares using a diamond cutter, the size of which for laboratory tests is several  $\text{cm}^2$ .

So that the same glass support can be used to ensure a firm contact with the cathode without touching the anode (see Figure VIII-13), a strip of ITO is removed using a four step chemical etching process. The four steps are: protection of the templated surface using a varnish or strips of rubber; immersion of the samples into a hydrochloric acid bath at  $50^\circ\text{C}$  for several minutes; sample rinsing with water; and removal of the varnish with acetone.

Cut and etched samples are then cleaned using chemicals in an especially important stage with respect to the preparation of electroluminescent diodes. ITO, in fact,

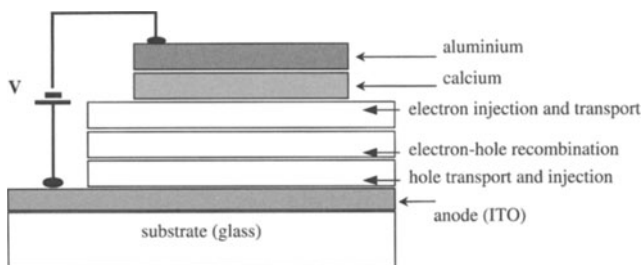
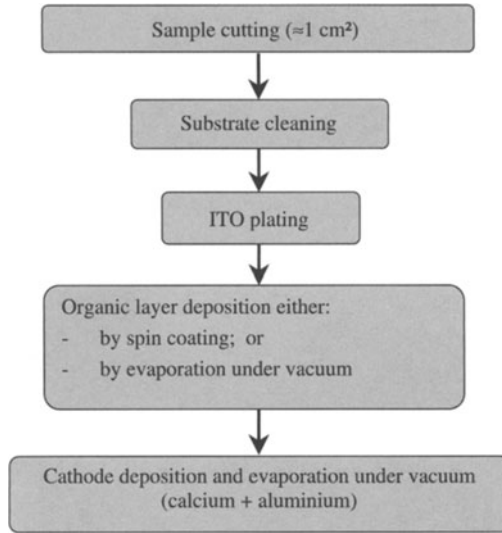


Figure VIII-11. Multi-layer diode structure.



**Figure VIII-12.** Successive stages in the preparation of organic LEDs.

plays a central role in the ageing process and it is essential to have as clean surfaces as possible, given that this can limit the diffusion of impurities into the organic material.

The washing process consists of several stages in which the samples are exposed to:

- deionised water at 60 °C and ultrasound for 5 minutes;
- acetone at 55 °C and ultrasound for 5 minutes;
- ethanol at 60 °C and ultrasound for 5 minutes;
- deionised water at 60 °C and ultrasound for 5 minutes;
- deionised rinsing;
- oven drying at 60 °C for 1 h.

*Comment:* it has been shown that supplementary treatments such as plasma or ultrasound can further improve the properties of ITO.

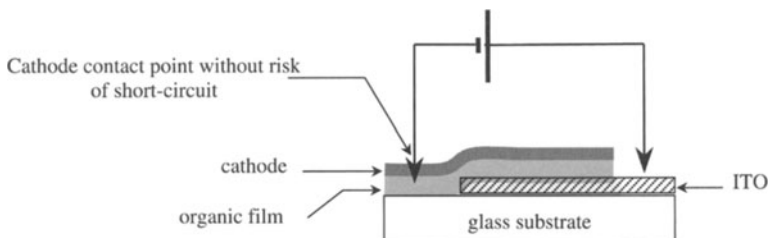


**Figure VIII-13.** Etching ITO to remove possible anode-cathode short circuit.

### c LEDs fabricated for testing: support configuration

Figure VIII-14 details the layout used to place 6 electroluminescent diodes on the same ITO substrate. Emitted light traverses the ITO and the glass substrate.

So called 'on top' configurations, with the ITO deposited last onto the hole injection layer are no less interesting than the configuration already discussed. This type of structure allows the cathode metal to be isolated from air thus limiting secondary reactions, however, the technology required to deposit ITO is demanding and generally involves the use of double pulverisation and deposition using 'Dual Ion Beam Sputtering' (DIBS), or the use of a liquid dispersing agent.

## 2 Fabrication of modulator guides/arms from polymers

### a The importance of polymer based couplers/guides

The wide range of fabrication techniques available to make polymer waveguides allows a degree of flexibility when preparing these optical connectors. The combination of different techniques can permit greater versatility in the final product, which can be manufactured reliably and cheaply.

These optical connectors can be used to link optoelectronic components, to work inside specific modules or even between various modules. Optical interconnections are used in integrated optical circuits, waveguides and space transmissions. Optical systems integrating polymer based materials are now generally considered the solution for use in connecting, coupling and interfacing with electronic components.

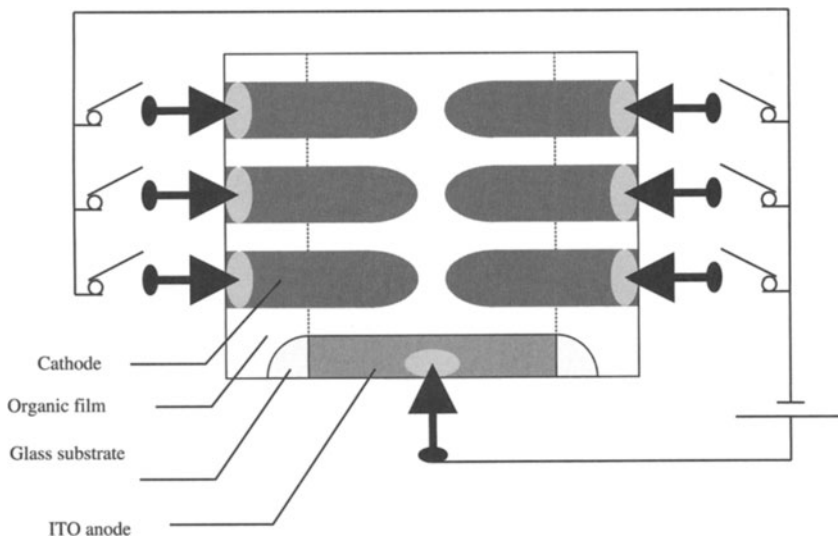


**Figure VIII-14.** Classic set up for testing 6 LEDs.

While optical fibres are used for point-to-point links between emitters and receptors, the actual topologies used require the use of passive components to distribute beams of light to the various 'clients', a job which is fulfilled by optical couplers.

### **b Fabrication technology used for polymer guides**

Mostly, geometric guide forms are determined using lithographic techniques. A few techniques involve direct writing with a laser or a beam of electrons. There are in fact four principal techniques used in the preparation of polymer guides:

$\alpha$  *Etching* Etching corresponds to the control and selective removal of material to realise the required structure. The possibility of being able to etch polymers with a high degree of precision permits the use of direct techniques to obtain waveguides. For example, a polyimide spread over a rigid substrate by spin coating can be eliminated at localised points using either an adequate reactive ionic solvent or by etching to yield a grooved channel.

$\beta$  *External diffusion* A large number of polymers are well suited to receiving doping agents (even selectively). However, certain materials trapped within the polymer, particularly those with low molecule weights, can be thermally diffused to the exterior of the material (polycarbonates are a good example). Zones treated using these properties can give rise to optical guides.

$\gamma$  *Polarisation and localised reactions* We can selectively create zones corresponding to optical guides by using molecular doping agents polarised in the same direction. Localised oxidation reactions can lead to bridging reactions within a guide zone.

$\delta$  *Induced diffusion and polymerisation* Guides can also be obtained by using the controlled diffusion of monomers within a polymer matrix.

The above techniques exploit properties particular to polymers using specially designed apparatus. We shall limit ourselves to detailing the etching process, which is the most widely used of techniques.

### **c Guide fabrication by etching**

Figure VIII-15 shows the two principal steps required in etching. Firstly, to define the geometrical form of the optical component, masks are prepared through the use of a photoresist which is itself made of photosensitive resins *i.e.* organic materials, and then secondly the organic film is etched (or in some cases photo-polymerised) using the mask.

$\alpha$  *Photosensitive resins for mask fabrication* Generally, resin based polymers are used in the preparation of etching masks, which are subsequently used to etch thin films formed from insulating, metallic or semi-conducting materials. Two types of resin are available: positive resins in which the treated part becomes soluble (developable) in a selective solvent; and negative resins which once treated become insoluble.

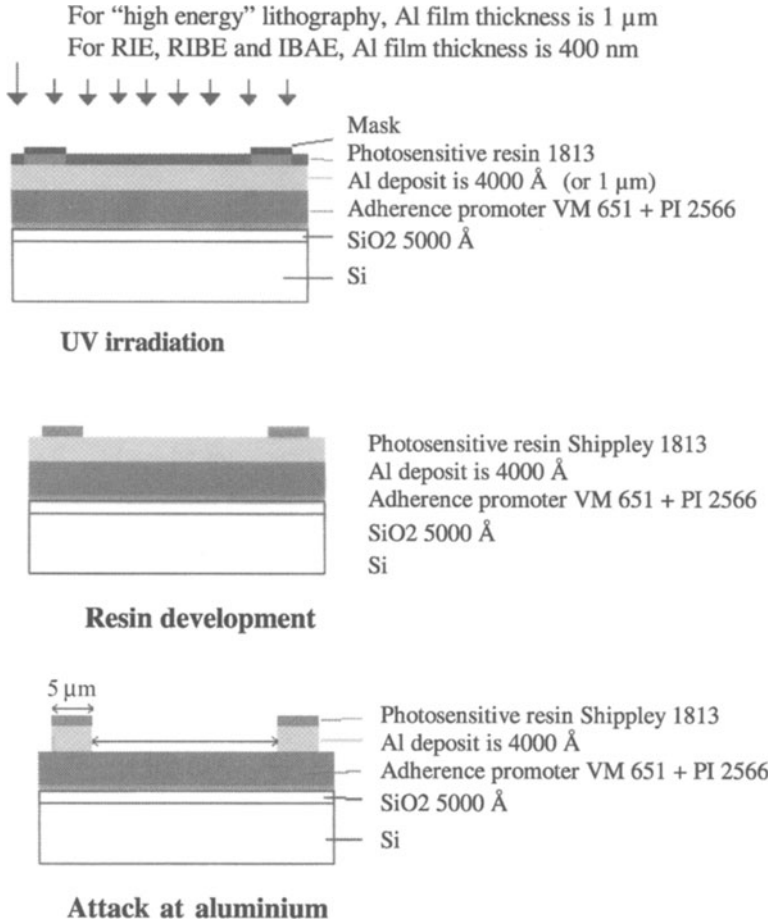


**Figure VIII-15.** Principle used for polymer based lithography (example is polyimide PI 2566, Du Pont).

The form of the mask is defined by a tracing UV light over its surface. Subsequent development using a wet process results in perpendicular walls (negligible ‘under-etching’), if the UV is used in perfect parallel beams. Different developing liquids can be used, such as acids (HF, HCl, H<sub>2</sub>SO<sub>4</sub>, HNO<sub>3</sub>, H<sub>3</sub>PO<sub>4</sub>), bases (KOH, NaOH, NH<sub>4</sub>OH) and oxidising agents (H<sub>2</sub>O<sub>2</sub>, N<sub>2</sub>H<sub>4</sub>).

These resins must, in addition, be able to resist the wet or dry processes used in the following second step. If this is not the case, then a supplementary step using aluminium is required (see Figure VIII-15).

*β Etching of optical structures (polymer guides)* Wet etching can be used in the preparation of polymer guides, however, there is the non-negligible problem of

'under-etching'. Wet development proceeds in an isotropic manner and can attack supporting zones around the mask, resulting in non-rectilinear profiles altering the geometrical definition of the guide.

At present, the tendency is towards dry procedures which use gases in the form of plasmas. As the size of the details required decreases towards  $1\ \mu\text{m}$ , design duplication at such high resolutions is no longer possible without anisotropic etching. This can be achieved using a masked ion beam which, perpendicular to the target, results in film pulverisation. In addition, in terms of economics, safety and environmental hazard, wet chemical processes are onerous and necessitate strict security controls.

The final thickness of the guide is equal to the initial thickness of the film.

Typically the guide section is rectangular or cubic in shape. The strips present an interface with air and exhibit high refractive indexes and typically function as multi-modal guides. Such channels can eventually be filled by a second polymer with a different indice. We can thus obtain embedded guides which can function in mono- or multi-mode. Simultaneously, the second polymer can act as a protective layer against external shocks. Guides fabricated in such a way exhibit uniform profiles and indices, resulting in well-defined properties.

In order to limit losses during use, a great deal of care is required to arrive at smooth etched walls with definition greater than  $0.1\ \mu\text{m}$ .

Dry etching can be, in practical terms:

- completely 'physical' where ionic etching with inert gases, such as argon ions, are used to physically pulverise the material surface;
- a combination of 'physical' and chemical etching, for example the use of reactive  $\text{CF}_4$  ions to etch Si surfaces; or
- purely chemical, for example the use of oxygen plasma to remove, by oxidation, a photosensitive resin resulting in the production of volatile gases which can be readily evacuated.

Appendix A-9 gives further details.

The etching mechanisms depend both upon the nature of the gas used in the plasma (which gives rise to reactive ions or species) and the technology employed, which uses one of three principal configurations.

- plasma etching or reactive ion etching (RIE) where substrates are placed on the lower electrode placed with respect to a radio frequency plasma;
- reactive ion beam etching (RIBE) where a beam of reactive ions, for example  $\text{O}^+$ , are accelerated towards the substrate from a source; and
- ion beam assisted etching (IBAE) which couples the effects of an incident ion beam (which for example can be inert gas ions such as  $\text{Ar}^+$  or reagents such as  $\text{O}^+$ ) with the effects of a flow of reactive gas such as molecular oxygen.

Figure VIII-16 schematically summarises the different techniques which can be brought into play in various etching processes.

In all these processes, the etching reactions are initiated by ions which are accelerated perpendicular to the film surface. Consequently, these processes can result in high contrasts with practically vertical walls and examples include that of polyimide films

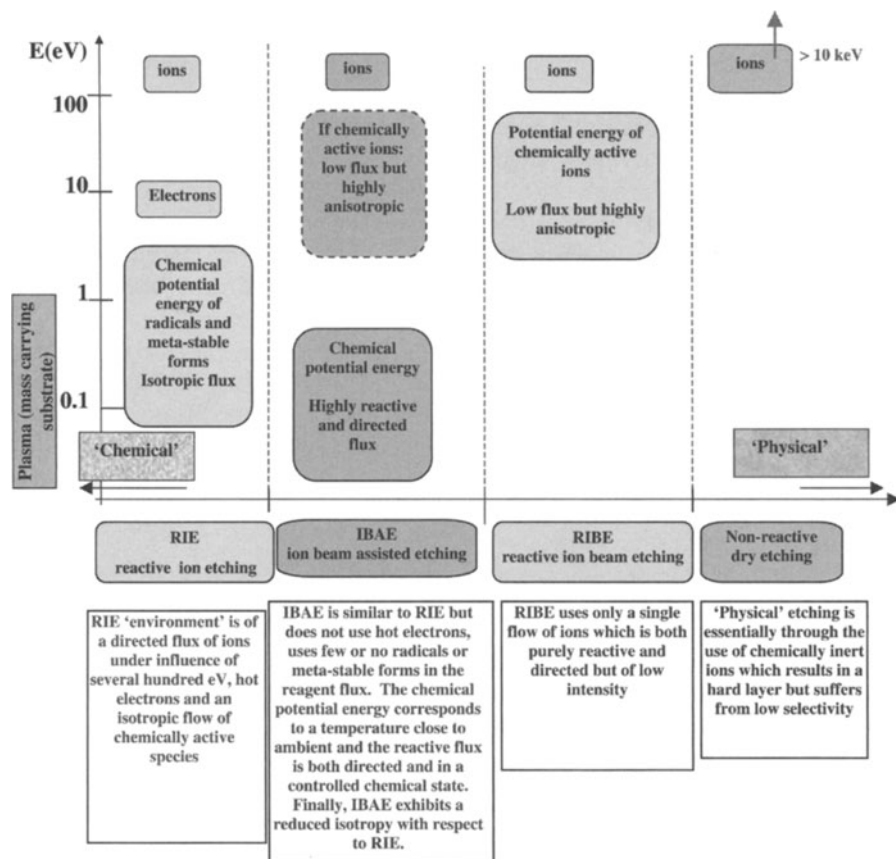


**Figure VIII-16.** Comparison of techniques in the etching process (RIE, IBAE, RIBE, and non-reactive dry etching).

which have been totally converted. In addition, these dry processes are considerably more reproducible than wet processes, and because of the wide variety of available parameters (reactor pressure, gas composition and flow speed, radio frequency power, energy and current density of ion beam), control can be exerted over characteristics such as etching speed, etching selectivity with respect to materials used, and the lateral wall angles of etched features.

While these technologies were initially developed for inorganic electronic/optoelectronic applications (etching Si with  $\text{CF}_4$ ) they are also well applicable to polymers. Indeed, the latter can be actually quite resistant to such processes, due to the strong backbone links which make up the polymer chains (particularly so for polymers containing aromatic or polar groups), but the use of these materials with aluminium masks and reactive beams containing oxygen, which reacts with carbon based chains, can yield remarkable results. Figure VIII-17 shows an example [Cor 01]. Transmission losses, estimated using the 'cut-back' method, are around 0.5 to



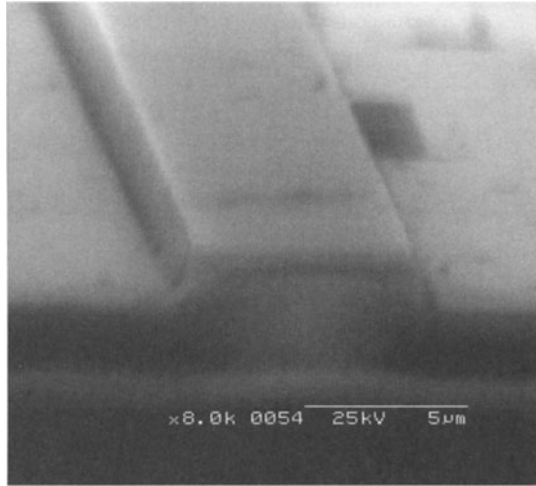


**Figure VIII-17.** Polyimide guide obtained using RIBE and cleaving ( $O^+$  ion beam with energy 2.5 keV).

4 dB  $cm^{-1}$  in TE mode where TM has  $\lambda = 1.3 \mu m$  and  $\lambda = 1.55 \mu m$ . (This destructive method measures the transmission of a guide through successive and progressive reduction in wavelength used; Section IV-2 has further details).

### III Photometric characterisation of organic LEDs (OLEDs or PLEDs)

Photometry is the term used to describe the characterisation of rays from system containing luminescent units [Des 91]. From a study of the energy of the rays, photometry can yield an evaluation of luminosity, which can also be described in visual terms when the detector is the human eye. The terminology used takes account of this binary aspect by using in the notation the indice 'e' for energetic terms and 'v' for visual terms.

#### 1 General definitions

##### a Energy and luminescence fluxes

In general, flux characterises the rate of flow of rays:

- Energetic flux (radiant)  $\Phi_e$  emitted by a light source is quotient of the quantity of energy  $dW_e$  transmitted during time  $dt$  at an interval  $dt$ . We can therefore write this as:

$$\Phi_e = \frac{dW_e}{dt} \quad (1)$$

If the flux is uniform over time  $t$  then  $\Phi_e = W_e/t$  and is expressed in watts (W).

— The luminous flux  $\phi_v$  is defined with respect to the sensitivity of the human eye to different wavelengths of light. The value is expressed in lumen (lm).

To convert from energetic to luminous scales the constant  $K_m = 683 \text{ lm W}^{-1}$  is multiplied by the diurnal photo-response  $V(\lambda)$  of the human eye. The function  $V(\lambda)$  is zero outside of the visible spectrum, which is between  $\lambda_1 = 380 \text{ nm}$  and  $\lambda_2 = 780 \text{ nm}$ . The diurnal photo-response reaches its maximum at around  $555 \text{ nm}$ , as shown in Figure VIII-18, in which  $[V(\lambda)]_{\text{Max}} = 1$  at  $\lambda \approx 555 \text{ nm}$ . Night vision, however, results in the same maximum moving to  $\lambda \approx 510 \text{ nm}$ .

*α Relationship between energetic and luminous flux for a monochromatic or pseudo monochromatic source* Given the above indicated variation required when going from energetic to luminous (visual) scales, for a monochromatic source with a given emission wavelength  $\lambda_d$ , the luminous flux ( $\Phi_v$ ) can be written as a function of the energetic flux ( $\Phi_e$ ):

$$\Phi_v = K_m V(\lambda_d) \Phi_e. \tag{2}$$

Classically, eqn (2) is also used for a polychromatic source with a maximum emission centred around the given wavelength  $\lambda_d$ ; eqn (2) can therefore also be applied to a pseudo monochromatic source.

*β Relationship between energetic and luminous flux for a polychromatic source* More rigorously speaking, the flux contributed over all energies  $E (= h\nu = hc/\lambda)$  should be taken into account when considering a polychromatic source. The spectral distribution on a photometric scale, here the flux ( $\Phi$ ), is characterised by the function  $\Phi'(\lambda)$  in which  $\Phi'$  is the spectral scale defined by:

$$\Phi'(\lambda) = \lim_{\delta\lambda \rightarrow 0} \left( \frac{\delta\Phi}{\delta\lambda} \right)$$

where  $\delta\Phi$  is the fraction of flux  $\Phi$  contained in a spectral band of size  $\delta\lambda$  about the wavelength  $\lambda$ . Knowing  $\Phi'(\lambda)$ , we can now calculate the total flux  $\Phi(\lambda_a, \lambda_b)$  within

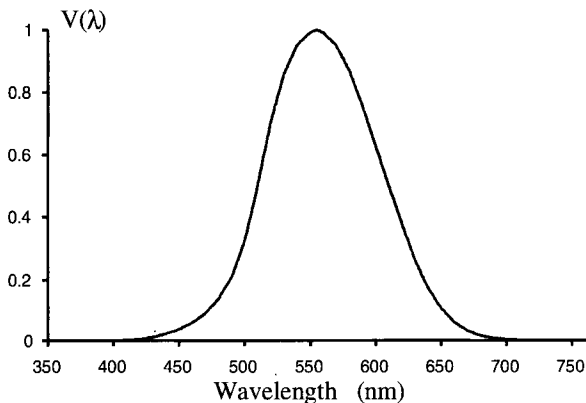


**Figure VIII-18.** Photo-optical response normalised with respect to the human eye:  $V(\lambda)$

a spectral band  $[\lambda_a, \lambda_b]$ :

$$\Phi(\lambda_a, \lambda_b) = \int_{\lambda_a}^{\lambda_b} \Phi'(\lambda) \cdot d\lambda \quad (3)$$

Once we know the total energetic flux ( $\Phi_e$ ), which as detailed later on is measured by a photodiode, then when studying for example diode electroluminescence, the normalised electroluminescent spectra ( $\Sigma$ ) needs to be measured to find the spectral energetic flux ( $\Phi'_e(\lambda)$ ). It should be noted that:

- $\Sigma = \int_0^\infty S(\lambda) \cdot d\lambda$ , corresponding to the sum over the area of an empirical normalised spectra; and
- $\Phi_e = a\Sigma$ , in which 'a' is a constant.

We can go on to deduce that  $\Phi'_e(\lambda) = a S(\lambda)$ , that is:  $a = \frac{\Phi_e}{\Sigma} = \frac{\Phi'_e(\lambda)}{S(\lambda)}$ .

On knowing the electroluminescence spectra, we can thus go from the energetic flux  $\Phi_e$  to the spectral energetic flux  $\Phi'_e(\lambda)$  as in:

$$\Phi'_e(\lambda) = \frac{\Phi_e \cdot S(\lambda)}{\Sigma} = \frac{\Phi_e \cdot S(\lambda)}{\int_0^\infty S(\lambda) \cdot d\lambda} \quad (4)$$

For a given wavelength  $\lambda$ , the general method used to convert from an energetic scale to a luminous (visual) scale once applied to a spectral scale permits, for the latter, the eqn (5) to be written, in a form which resembles that of eqn (2):

$$\Phi'_v(\lambda) = K_m V(\lambda) \Phi'_e(\lambda). \quad (5)$$

On applying eqn (3), the luminous flux is given in the form:

$$\Phi_v = \int \Phi'_v(\lambda) d\lambda = K_m \int V(\lambda) \Phi'_e(\lambda) d\lambda, \quad (6)$$

in which  $\Phi'_e(\lambda)$  is given by eqn (4).

### b Energetic and luminous intensities: definition of the candela

$\alpha$  *Energetic intensity (radiant)* The energetic intensity ( $I_e$ ) is defined as the ratio between the emitted energetic flux ( $d\Phi_e$ ) and the solid angle ( $d\Omega$ ) in which it is emitted:

$$I_e = \frac{d\Phi_e}{d\Omega}. \quad (7)$$

If the emitted flux within a given solid angle ( $\Omega$ ) is constant, then  $I_e = \frac{\Phi_e}{\Omega}$ ; the radiant intensity is thus expressed as watt per steradian ( $W \text{ sr}^{-1}$ ).

$\beta$  *Luminous intensity* The luminous intensity ( $I_v$ ) is defined by the equation  $I_v = \frac{d\Phi_v}{d\Omega}$ ; when  $\Phi_v$  is a constant within  $\Omega$ ,  $I_v = \frac{\Phi_v}{\Omega}$ .  $I_v$  is expressed in lumen per steradian ( $\text{lm sr}^{-1}$ ), otherwise denoted the candela (cd).

The International Commission on Illumination (CIE for Commission Internationale de l'Eclairage) defined the candela as a luminous intensity, in a given direction, for a source which emits a monochromatic beam with frequency  $5.40 \times 10^{14}$  Hz (corresponding to wavelength 555 nm) and energetic intensity in that direction of  $\frac{1}{683}$  W  $\text{sr}^{-1}$ . This definition takes into account the constant  $K_m$  ( $683 \text{ lm W}^{-1}$ ) which was introduced above.

For a monochromatic ( $\lambda = \lambda_d$ , or pseudo-chromatic ray

$$I_v = K_m V(\lambda_d) I_e. \quad (8)$$

For a polychromatic source, however, the reasoning we applied to tie  $\Phi_v$  to  $\Phi'_e$  can be used again to relate  $I_v$  and  $I'_e$ . This gives a relationship between the latter two quantities an equation which resembles eqn (6) for  $\Phi_v$  and  $\Phi'_e$ :

$$I_v = K_m \int V(\lambda) I'_e(\lambda) d\lambda, \quad (9)$$

where  $I'_e$  is given by an analogous relationship to eqn (4), *i.e.*

$$I'_e(\lambda) = \frac{I_e \cdot S(\lambda)}{\Sigma} = \frac{I_e \cdot S(\lambda)}{\int_0^\infty S(\lambda) \cdot d\lambda}. \quad (10)$$

### c Energetic and luminous luminance

$\alpha$  *Energetic luminance* The energetic luminance ( $L_e$ ) of a source is defined as the ratio of the emitted energetic intensity to the area of apparent emitting surface ( $S_a$ ):

$$L_e = \frac{I_e}{S_a} = \frac{1}{S_a} \frac{d\Phi_e}{d\Omega}; \quad (11)$$

for a constant flux,

$$L_e = \frac{I_e}{S_a} = \frac{\Phi_e}{\Omega S_a}. \quad (12)$$

Energetic luminance is expressed in  $\text{W sr}^{-1} \text{ m}^{-2}$  and is the flux emitted in a unit solid angle per unit of apparent source surface.

#### *Comment: the physical significance of luminance*

If  $A_s$  is the surface area of a source, the apparent surface is  $S_a = A_s \cos \alpha$ , as detailed in Figure VIII-19. The luminance in the direction  $OO'$  is the intensity per unit apparent surface and characterises the aspect observed by an observer at  $OO'$ .

By defining the light incident on a screen from a luminous point on a surface  $A'_s$ , with the help of the relationship  $E = \frac{\Phi_e}{A'_s} = \frac{\Phi_e}{\Omega} \frac{\Omega}{A'_s} = I_e \frac{\Omega}{A'_s}$ , we can conclude that 2 sources of the same intensity result at the same screen in the same effective lighting. These two sources can come from different surfaces, for example, the large surface such as that provided by a fluorescent tube or a small surface due to say a lamp filament. And the fluorescent tube will appear to be less bright than the filament and it is this characteristic which is placed in terms of source luminance.

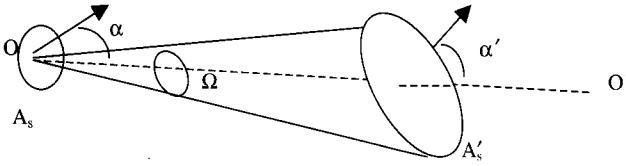


Figure VIII-19. Surface apparent to a screen.

$\beta$  *Expression for visual luminance* The visual equivalence ( $L_v$ ) of luminance is defined by

$$L_v = \frac{I_v}{S_a} = \frac{1}{S_a} \frac{d\Phi_v}{d\Omega}; \quad (13)$$

when the flux is constant

$$L_v = \frac{I_v}{S_a} = \frac{\Phi_v}{\Omega S_a} \quad (14)$$

which is expressed in  $\text{cd m}^{-2}$ .

For a monochromatic or pseudo-monochromatic source, the visual luminance can be determined, if we know the (constant) energetic flux of a source, using eqns (14) and (2) to give:

$$L_v = \frac{\Phi_v}{\Omega S_a} = \frac{K_m V(\lambda_d) \Phi_e}{\Omega S_a} \quad (15)$$

For a polychromatic source, there is the relationship between  $L_v$  and  $L'_e$  which again resembles eqn (6) for  $\Phi_v$  and  $\Phi'_e$  and which is:

$$L_v = K_m \int V(\lambda) L'_e(\lambda) d\lambda \quad (16)$$

where  $L'_e$  is given again by a relationship analogous to eqn (4) *i.e.*

$$L'_e(\lambda) = \frac{L_e \cdot S(\lambda)}{\Sigma} = \frac{L_e \cdot S(\lambda)}{\int_0^\infty S(\lambda) \cdot d\lambda}. \quad (17)$$

## 2 Internal and external fluxes and quantum yields: emissions inside and outside of components

### a Restrictions limiting the passage of the internal ray to exterior of an OLED

Figure VIII-20 details an emission from an OLED towards the exterior. The ray emitted by the emitting layer reaches the organic phase-air interface at an angle of incidence  $\theta$  which can be greater or less than the critical angle  $\theta_1$  defined by the relationship  $n \sin \theta_1 = n_{\text{air}} = 1$ , in which  $n$  is the refractive indice of the organic material. When  $\theta > \theta_1$ , the flux is transmitted to the exterior, however, when  $\theta < \theta_1$ , the flux undergoes a total internal reflection and is, *a priori*, returned back into the OLED structure without reaching the exterior.

*Preliminary comments*

$\alpha$  neglected effects When  $n = 2$ ,  $\theta_1 \approx 30^\circ$ , which being quite a small incident angle and not far from the normal incidence means that we can use the reflection coefficient in the form  $R \approx \left(\frac{n-1}{n+1}\right)^2$ , which yields a coefficient of transmission of  $T = 1 - R \approx 75\%$ . However, if  $n = 1.5$ , we have  $T \approx 96\%$ , although  $\theta_1 \approx 40^\circ$  which renders debatable the use of the equation  $R \approx \left(\frac{n-1}{n+1}\right)^2$ . Given the relatively low indices that organic materials exhibit, T is generally accepted without correction and is approximated to  $T \approx 100\% = 1$  when  $\theta < \theta_1$ .

In addition, the organic, ITO and glass layers are assumed to be uniform and the indice under consideration remains that of the organic material and air only.

$\beta$  Effects due to limiting angle As shown in Figure VIII-20, the limiting angle imposes the restriction upon the emitting rays so that only that with angle  $\theta < \theta_1$  can leave the structure, so:

- at the OLED interior, in the recombination zone, emissions going towards the frontal surface occur in a half space, that is

$$\Omega_1 = \int d\Omega_1 = 2\pi \int_{\theta=0}^{\theta=\pi/2} \sin \theta d\theta = 2\pi;$$

- the portion of flux which can leave the OLED is emitted from the emission zone within a solid angle limited to

$$\Omega_2 = 2\pi \int_{\theta=0}^{\theta=\theta_1} \sin \theta d\theta = 2\pi(1 - \cos \theta_1).$$

Given that  $\sin \theta_1 = 1/n$ , the term C can be calculated by through  $C = [1 - \cos \theta_1]$  so that we have

$$C = [1 - (1 - \sin^2 \theta_1)^{1/2}] = \left[1 - \left(1 - \frac{1}{n^2}\right)^{1/2}\right] \approx \left[1 - \left(1 - \frac{1}{2n^2}\right)\right] = \frac{1}{2n^2};$$

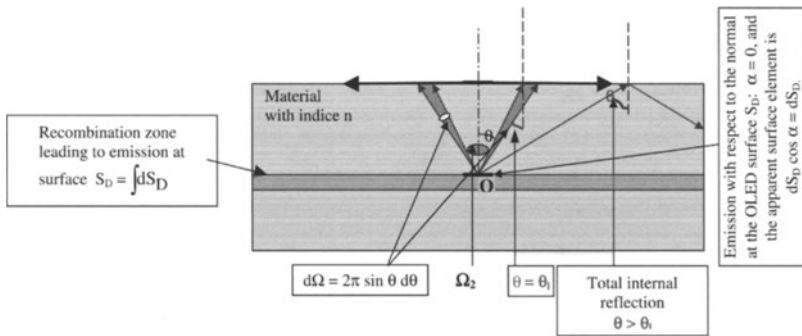


**Figure VIII-20.** Schematisation showing how only certain emitted rays are allowed to escape to exterior due to critical solid angle  $\Omega_2$  of the surface angle  $\theta_1$  ( $\Omega_2 = 2\pi[1 - \cos \theta_1]$ ).

finally we obtain  $\Omega_2 = \frac{\pi}{n^2}$  from which can be deduced that:

$$\Omega_2 = \frac{\Omega_1}{2n^2}. \tag{18}$$

From eqn (18), it is evident that the solid angle ( $\Omega_2$ ) which is used is only a fraction of the total emission angle ( $\Omega_1$ ) and that external yields are considerably effected. In effect, the external flux is only a fraction of that emitted.

Additional comment: If we also bring into play emissions towards the back of the device, that is towards the cathode, then  $\Omega_1$  can be obtained by taking an integral  $\theta$  equal to  $[-\pi/2 \text{ to } \pi/2]$ . On assuming that the cathode is a perfect reflector, then  $\Omega_2$  is obtained by integrating over  $\theta$  from  $[-\theta_1 \text{ to } \theta_1]$ . In both cases the the result is simply multiplied by 2, however, the relationship between  $\Omega_1$  and  $\Omega_2$  in eqn (18) remains unchanged.

**b Isotropic internal and external emissions according to Lambert’s law [Gre 94]**

Here we return to looking at the emitting material/air interface but with a ray incident to this interface with  $\theta < \theta_1$ . Refraction laws modify the geometry of the solid angle cones of the emission, as shown in Figure VIII-21. We now have  $n \sin \theta = \sin \varphi$ , which upon differentiation becomes  $\frac{d\theta}{d\varphi} = \frac{\cos \varphi}{n \cos \theta}$ . As  $n \cos \theta = \sqrt{n^2(1 - \sin^2 \theta)}$ , or using Snell-Descarte’s law  $n \cos \theta = \sin \varphi$ , we finally obtain  $\frac{d\theta}{d\varphi} = \frac{d\theta}{d\varphi} = \frac{\cos \varphi}{\sqrt{(n^2 - \sin^2 \varphi)}}$ . The elementary solid angles  $d\Omega_2$  and Figure VIII-21 are such that

$$\frac{d\Omega_2}{d\Omega_r} = \frac{\sin \theta \, d\theta}{\sin \varphi \, d\varphi} = \frac{1}{n} \frac{\cos \varphi}{\sqrt{(n^2 - \sin^2 \varphi)}}.$$

When  $n \approx 2$  and  $\sin^2 \varphi$  is well below 1, then  $\sin^2 \varphi \ll n^2$  and  $\frac{d\Omega_2}{d\Omega_r} \approx \frac{\cos \varphi}{n^2}$ . This equation indicates that a ray emitted directly towards the exterior at a solid angle  $\Omega_2$  approximately follows Lambert’s law[Gre 94].

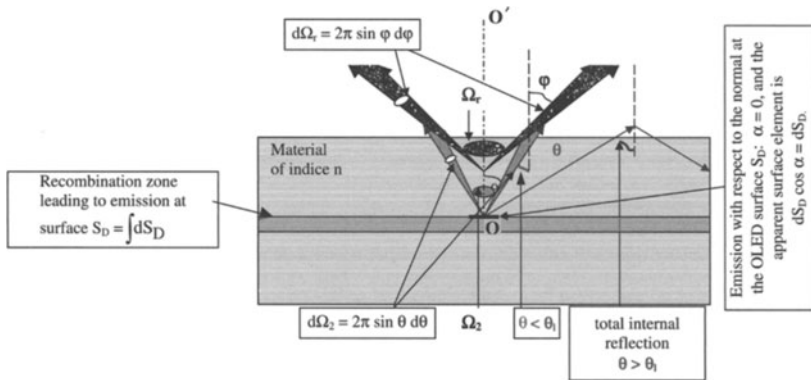


**Figure VIII-21.** Internal and external emissions of an OLED

### c Determination of internal and external emitted fluxes

We shall limit ourselves in this subsection to calculating only fluxes emitted towards the front of the device structure. As indicated in the end-comment of the preceding subsection, to take into account emissions towards the rear of the device, the results need only to be multiplied by 2, assuming that the metallic cathode presents a perfect reflecting surface. All ratios of emitted fluxes and thus yields remain otherwise unchanged.

*α Total internal flux emitted inside the structure* The luminous intensity directly emitted by the source is denoted as  $I_{0\text{int}}$ . Assuming the material to be homogeneous and having no internal interface, the internal emission from the recombination zone is isotropic and the total emitted flux inside the forward half space can be written in the form:

$$\Phi_{\text{Tint}} = \int_{1/2\text{space}} I_{0\text{int}} d\Omega = 2\pi I_{0\text{int}} \int_0^{\pi/2} \sin \theta d\theta = 2\pi I_{0\text{int}}. \quad (19)$$

*β Fraction of total internal flux emitted towards the exterior* The emission with luminous intensity  $I_{0\text{int}}$  remains isotropic in nature, however, the emission angle is limited to  $\theta_1$ , as we saw in Section a. By denoting  $\Phi_{\text{ie}}$  as the flux from the interior towards the exterior, we now have:

$$\Phi_{\text{ie}} = 2\pi I_{0\text{int}} \int_0^{\theta_1} \sin \theta d\theta = 2\pi I_{0\text{in}} (1 - \cos \theta_1) = 2\pi I_{0\text{in}} \frac{1}{2n^2} = \pi I_{0\text{in}} \frac{1}{n^2} \quad (20)$$

*γ Emitted exterior flux* If luminous intensity emitted with respect to the normal to the surface of the LED is denoted by  $I_{0\text{ext}}$ , then as detailed above, the emission follows Lambert's law ( $I_{\text{ext}} = I_{0\text{ext}} \cos \varphi$ ) and the total external flux ( $\Phi_{\text{ext}}$ ) emitted over the forward half space is thus in the form:

$$\begin{aligned} \Phi_{\text{ext}} &= \int_{1/2\text{space}} I_{0\text{ext}} \cos \phi d\Omega; \Phi_{\text{ext}} = 2\pi I_{0\text{ext}} \int_0^{\pi/2} \cos \varphi \sin \varphi d\varphi \\ &= 2\pi I_{0\text{ext}} \int_0^{\pi/2} \sin \varphi d(\sin \varphi) = \pi I_{0\text{ext}}. \end{aligned} \quad (21)$$

*δ Relationships between fluxes* Given that the emitted external flux is a fraction of the total internal emitted flux, and conserving the overall beam power,  $\Phi_{\text{ie}} = \Phi_{\text{ext}}$ , and thus  $\pi I_{0\text{in}} \frac{1}{n^2} = \pi I_{0\text{ext}}$ , from which can be deduced that  $I_{0\text{in}} = I_{0\text{ext}} n^2$ . Placing this expression into eqn (19) gives:

$$\Phi_{\text{Tint}} = 2\pi n^2 I_{0\text{ext}} \text{ or } \Phi_{\text{ext}} = \frac{1}{2n^2} \Phi_{\text{Tint}}. \quad (22)$$



We can obtain the same result directly by the division of eqns (20)/(19) as  $\Phi_{ie} = \Phi_{ext}$ . The factor  $1/2n^2$  represents the actual yield or 'optical yield' of rays emitted from the LED.

#### d External and internal quantum yields

$\alpha$  *External quantum yield* The external quantum yield ( $\eta_{ext}$ ) is defined as the ratio of the number of photons emitted by a diode ( $N_{phext}$ ) in to the external half space over a time  $t$  divided by the number of electrons injected ( $N_{el}$ ) over the same period of time.

$\eta_{ext}$  can be expressed therefore in the relationship:

$$\eta_{ext} = \frac{N_{phext}}{t} \frac{t}{N_{el}} = \frac{N_{phext}}{N_{el}}. \quad (23)$$

If  $I_c$  represents the current injected into an electroluminescent structure, we have:  $I_c = Q/t = N_{el}q/t$ , where  $q$  is the value of elementary charge ( $q = 1.6 \times 10^{-19}$  C). Thus:

$$\frac{N_{el}}{t} = \frac{I_c}{q}. \quad (24)$$

For a given wavelength  $\lambda_d$ , the energy of the photons is determined by  $E_{ph} = hc/\lambda_d$ . With the emitted external flux being  $\Phi_{ext} = W_e/t$  (eqn (1) for constant flux over time  $t$ ), now

$$N_{phext} = \frac{W_e}{E_{ph}}, \text{ that is } \frac{N_{phext}}{t} = \frac{\lambda_d}{hc} \Phi_{ext}. \quad (25)$$

From eqns (24) and (25), eqn (23) for  $\eta_{ext}$  can be written, for a pseudo-monochromatic ray, as

$$\eta_{ext} = \frac{q\lambda_d}{hc} \frac{\Phi_{ext}}{I_c}. \quad (26)$$

$\beta$  *Internal quantum yield* The internal quantum yield is defined in the same way as the external quantum yield, with the exception that the number of photons emitted internally in the half space ( $N_{phint}$ ) is used:

$$\eta_{int} = \frac{N_{phint}}{t} \frac{t}{N_{el}} = \frac{N_{phint}}{N_{el}}.$$

With  $\frac{N_{phint}}{t} = \frac{\lambda_d}{hc} \Phi_{int}$  (in an expression similar to eqn (25), but for internally emitted photons), we have

$$\eta_{int} = \frac{q\lambda_d}{hc} \frac{\Phi_{int}}{I_c}. \quad (27)$$

Given eqn (22), on making the division eqns (26)/(27), we directly obtain:

$$\eta_{ext} = \frac{1}{2n^2} \eta_{int}. \quad (28)$$

### 3 Measuring luminance and yields with a photodiode

#### a General notes on photodetectors: sensitivity and spectral sensitivity

Typically, a photodetector, or photodiode, gives to a responsive current ( $I_{\text{pho}}$ ) in a form arising from two origins:

- dark current ( $I_0$ ) which appears once the photodiode is placed under darkness while polarised in the same way as when exposed to light. This current  $I_0$  can arise from two causes. The first is of thermal origin and is associated with the liberation of conducting electrons by thermal excitation, and the second is associated with the generation of charge carriers by ambient beam effects (natural rays); and
- photoelectric current ( $I_p$ ) associated with the formation of photo-carriers, such as particularly mobile photo-electrons.

$\alpha$  *Sensitivity* For a given photodetector subject to a luminous flux, consisting not necessarily of mono-chromatic light, there is a resulting current:

$$I_{\text{pho}} = I_0 + I_p.$$

Normally, if conditions remain unchanged during the analysis then the current  $I_0$  remains constant, however,  $I_p$  will change proportionally with the received flux ( $\Phi_e$ ), as long as the photodetectors acts linearly. So:

$$I_{\text{pho}} = I_0 + \sigma\Phi_e$$

And this expression is only valid for fluxes which are such that  $\Phi_e < \Phi_S$ ,  $\Phi_S$  being the level above which the photodetector is saturated, as detailed in Figure VIII-22.

In general terms, the sensitivity of a photodetector is defined by its characteristic slope shown in the above Figure, *i.e.*  $\sigma = \frac{dI_{\text{pho}}}{d\Phi_e}$ . For a non-linear photodetector, the value is dependent on the incident flux. However, for a linear photodetector,  $\sigma$  is a constant, up to  $\Phi_e = \Phi_S$ , and takes on the form:

$$\sigma = \frac{I_p}{\Phi_e} \tag{29}$$

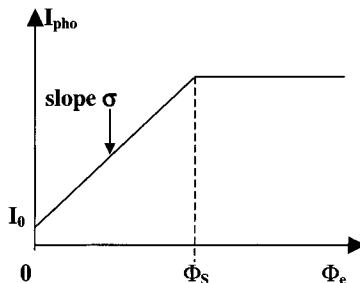


Figure VIII-22. Linear photodiode characteristics.

$\beta$  *Spectral sensitivity* The spectral sensitivity, for a particular ray of light of wavelength  $\lambda$ , is defined by the relationship

$$\sigma(\lambda) = \frac{dI_{\text{pho}}(\lambda)}{d\Phi_e(\lambda)} = \frac{dI_p(\lambda)}{d\Phi_e(\lambda)} = \frac{I'_p(\lambda)}{\Phi'_e(\lambda)}. \quad (30)$$

For a photodetector exposed to a monochromatic beam of a given wavelength  $\lambda_d$  and flux  $\Phi_e(\lambda_d)$ , the total number of photons received by the detector per second ( $n_p$ ) is  $n_p = \frac{\lambda_d \Phi_e(\lambda_d)}{hc}$ . If  $T$  is the transmission coefficient of the photodetector window and  $\eta$  the quantum efficiency of the detector (*i.e.* the number of electron-hole pairs produced by incident photons), the actual number of electron-hole pairs generated per second is of the form

$$G = \eta T n_p = \eta T \frac{\lambda_d \Phi_e(\lambda_d)}{hc} = G(\lambda_d).$$

This coefficient, just like the intensity  $I_{\text{pho}}$  of the resulting current, is dependent on the wavelength of the incident light. For a linear detector, the component  $I_p$  of  $I_{\text{pho}}$  is in the form  $I_p = FqG$  where  $F$  is a factor of amplification. On taking into account

$$I_p(\lambda_d) = FqG(\lambda_d) = Fq\eta T \frac{\lambda_d \Phi_e(\lambda_d)}{hc},$$

we arrive at

$$\sigma(\lambda_d) = \frac{dI_p(\lambda_d)}{d\Phi_e(\lambda_d)} = Fq\eta T \frac{\lambda_d}{hc},$$

which can also be written

$$\sigma(\lambda_d) = \frac{I_p(\lambda_d)}{\Phi_e(\lambda_d)}. \quad (30')$$

If the light is polychromatic, the current  $I_p$  is therefore such that:

$$I_p = \int dI_{\text{ph}} \stackrel{(30)}{=} \int \sigma(\lambda) d\Phi_e(\lambda) = \int \sigma(\lambda) \Phi'_e(\lambda) d\lambda = \int I'_p(\lambda) d\lambda. \quad (31)$$

We thus have:

$$\frac{I_p}{\Phi_e} = \frac{\int \sigma(\lambda) \Phi'_e(\lambda) d\lambda}{\Phi_e} \stackrel{(4)}{=} \frac{\int \sigma(\lambda) S(\lambda) d\lambda}{\int S(\lambda) d\lambda} = \sigma_{\text{av}}; \quad (31')$$

and the value  $\sigma_{\text{av}}$  then obtained for the ratio  $I_p/\Phi_e$  appears as an effective (average) sensitivity. Furthermore, eqn (31') also gives:

$$\Phi_e = I_p \frac{\int S(\lambda) d\lambda}{\int \sigma(\lambda) S(\lambda) d\lambda}.$$

With eqn (4) we reach:

$$\Phi'_e(\lambda) = I_p \frac{S(\lambda)}{\int \sigma(\lambda) S(\lambda) d\lambda}. \quad (32)$$

In addition, eqn (30) gives  $\Phi'_e(\lambda) = I'_p(\lambda)/\sigma(\lambda)$ , which leads, by comparison with the previous eqn, to

$$I'_p(\lambda) = I_p \frac{\sigma(\lambda)S(\lambda)}{\int \sigma(\lambda)S(\lambda) d\lambda}. \quad (32')$$

## b Example photodiode set-up [Ant 98]

Photometric measurements are typically performed with a photodiode that has as large a surface area as possible, for example of the order of 100 mm<sup>2</sup>.

$\alpha$  *Example values for  $\sigma(\lambda)$*  As an example, Table VIII.1 shows values given by Radiospares for a standard diode, with spectral response between 350 and 1150 nm, for  $\sigma(\lambda)$  at different given wavelengths  $\lambda = \lambda_d$ .

$\beta$  *Device set-up* In order to measure the luminance of OLED components, the photodiode is placed up against a window open to the OLED and is connected to an amplifier. Thus by the action of a resistor ( $R_C$ ) placed in the circuit detailed in Figure VIII-23, the assembly permits determination of the value of  $I_p$  from the voltage ( $V_p = R_C I_p$ ) indicated by a multimeter.

(Technical note: the amplifier typically used for this sort of assembly is powered by a tension ( $V_a$ ) equal to 18 V, while the tension applied at the photodiode ( $V_{pho}$ ) is of the order of 10 V. The potentiometer, tied to an operational amplifier, allows this offset tension to be disregarded. The charge resistance is fixed at 995 ohms).

$\gamma$  *A classic set-up for measuring luminance: representation of  $\Omega$  and apparent OLED surface ( $S_a$ )* In general terms,  $S_a$  is the apparent emitting diode surface, and is such that  $S_a = A_s \cos \alpha$  (see Figure VIII-19). Practically speaking, the measurement of a beam emitted by an OLED is effected by placing a photodiode at the window of the measuring cell, as shown above in Figure VIII-24. The surface of the photodiode is perpendicular to the beam direction, so if we designate the surface of the OLED by  $S_D$ , the apparent surface  $S_a$  is such that  $S_a = S_D$ .

Typically, the surface of the photodiode ( $S_{ph}$ ) is around 1 cm<sup>2</sup> while the surface of the OLED is more like several mm<sup>2</sup>. In effect, the source acts as a point with respect to the receptor.

**Table VIII.1.** Principal sensitivity values for a standard photodiode

$\lambda(\text{nm})$	$\sigma(\lambda)(\text{A W}^{-1})$	$\lambda(\text{nm})$	$\sigma(\lambda)(\text{A W}^{-1})$
400	0.12	600	0.32
450	0.2	650	0.35
500	0.25	700	0.38
550	0.28	750	0.42

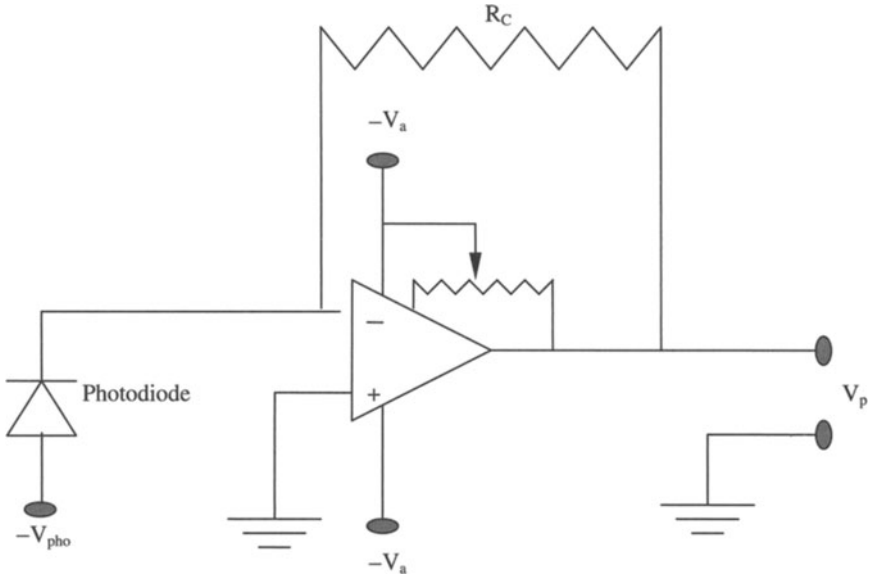


**Figure VIII-23.** Amplified photodiode set-up.

The half angle at the apex ( $\phi$ ) is such that  $\tan \phi = r/D$ . Given typical values, that is with  $r \approx 5$  mm and  $D \approx 40$  mm,  $\phi \approx 7^\circ$ . The solid angle is therefore  $\Omega = \Omega_{ph} \approx 0.05$  sr.

The coefficient  $1/\Omega S_a$  which appears with equal use in eqns (12, 15 and 16) for luminance in monochromatic and polychromatic 'configurations' is effectively such that  $S_a = S_D$  and  $\Omega = \Omega_{ph}$ .

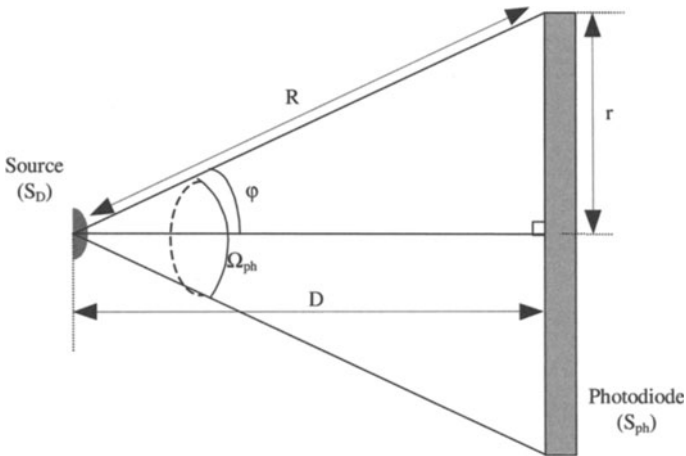


**Figure VIII-24.** Simplified scheme of diode/photodiode arrangement.

### c LED luminance determination using the present example of an OLED

$\alpha$  *A mono- or pseudo-monochromatic LED* ( $\lambda = \lambda_d$ ) In practical terms, if  $I_p = I_p(\lambda_d)$  is the current generated by a photodiode under a beam of light emitted by an LED at a solid angle  $\Omega_{ph}$ , then given eqn (30'),  $\Phi_e(\lambda_d)$  is the flux  $\Phi_{ph}$ , and we can write:  $\sigma(\lambda_d) = I_p/\Phi_{ph}$ .  $I_p$  is such that  $V_p = R_c I_p$  (see preceding Section  $\beta$ ).

From eqn (12),

$$L_e = \frac{\Phi_e}{\Omega S_a} = \frac{\Phi_{ph}}{\Omega_{ph} S_D} = \frac{I_p}{\Omega_{ph} S_D \sigma(\lambda_d)} = \frac{V_p}{R_c \Omega_{ph} S_D \sigma(\lambda_d)}. \quad (33)$$

Introducing eqn (33) directly into eqn (15) directly gives:

$$L_v = \frac{K_m V(\lambda_d) V_p}{R_c \Omega_{ph} S_D \sigma(\lambda_d)}. \quad (33')$$

We can also write

$$L_v = \frac{K_m V_p}{R_c \Omega_{ph} S_D} \frac{V(\lambda_d)}{\sigma(\lambda_d)} = \frac{K_m V_p}{R_c \Omega_{ph} S_D} D \text{ where } D = \frac{V(\lambda_d)}{\sigma(\lambda_d)}. \quad (34)$$

It is eqn (34) which is widely applied, even to polychromatic sources, however, as we shall see in such cases, the factor D should be replaced by a factor called 'A' which will be defined below. Clearly, the ratio A/D will indicate the extent to which the approximation of a polychromatic to a monochromatic source remains correct.

$\beta$  *Polychromatic source* Following eqn (30), we have  $\sigma(\lambda) = I'_p(\lambda)/\Phi'_e(\lambda)$ ; from eqn (12) we can write,  $L'_e = \Phi'_e/\Omega_{ph} S_D$  and  $\sigma(\lambda) = I'_p(\lambda)/\Omega_{ph} S_D L'_e(\lambda)$ . On deducing that  $L'_e = \frac{1}{\Omega_{ph} S_D} \frac{I'_p(\lambda)}{\sigma(\lambda)}$ , we can go on to substitute the value of  $I'_p(\lambda)$  given by eqn (32'), to give:

$$L'_e = \frac{I_p}{\Omega_{ph} S_D} \frac{S(\lambda)}{\int_0^\infty \sigma(\lambda) S(\lambda) d\lambda}. \quad (35)$$

On transferring the value of  $I_p = V_p/R_c$  in to eqn (35), we obtain

$$L'_e(\lambda) = \frac{V_p}{R_c \Omega_{ph} S_D} \frac{S(\lambda)}{\int_0^\infty \sigma(\lambda) S(\lambda) \cdot d\lambda}. \quad (36)$$

The desired expression is finally obtained by introducing eqn (36) into eqn (16):

$$L_v = \frac{V_p K_m}{R_c \Omega_{ph} S_D} \frac{\int V(\lambda) S(\lambda) d\lambda}{\int \sigma(\lambda) S(\lambda) d\lambda}, \quad (37)$$

which can also be written as

$$L_v = A \frac{V_p K_m}{R_c \Omega_{ph} S_D}, \text{ with } A = \frac{\int V(\lambda) S(\lambda) d\lambda}{\int \sigma(\lambda) S(\lambda) d\lambda} = \frac{V_{av}}{\sigma_{av}}. \quad (38)$$

( $\sigma_{av}$  is defined by  $\sigma_{av} = \int \sigma(\lambda) S(\lambda) d\lambda / \int S(\lambda) d\lambda$  and  $V_{av}$  in a same way by  $V_{av} = \int V(\lambda) S(\lambda) d\lambda / \int S(\lambda) d\lambda$ ).

**Table VIII.2.** Comparison of A and D terms for green and blue diodes.

Diode	A ( $\text{lm A}^{-1}$ )	D ( $\text{lm A}^{-1}$ )	A/D
Green (532 nm)	1485	2224	0.67
Blue (467 nm)	698	256	2.92

$\gamma$  *Numerical application [Tro 01]* By way of example, and for two different OLEDs, Table VIII.2 lists values for D (pseudo-monochromatic) and A (polychromatic) terms. The latter is calculated by numerical integration of empirical values obtained over the electroluminescent spectrum. One of the OLEDs emits light centred on the green light ( $\lambda_d = 532$  nm), while the other is centred on blue light (around  $\lambda_d = 467$  nm). We can see that the coefficients A and D are neither equal nor proportional.

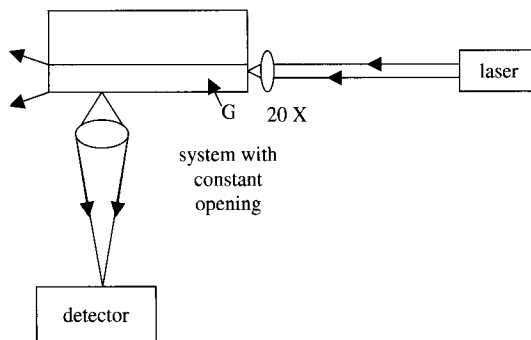
The use of the pseudo-monochromatic approximation results in:

- overestimation of polychromatic luminance for an OLED which emits in the green region as  $D_{\text{OLEDgreen}} > A_{\text{OLEDgreen}}$ ; and
- underestimation of polychromatic luminance for an OLED which emits in the blue region as  $D_{\text{OLEDblue}} < A_{\text{OLEDblue}}$ .

We can thus see the interest in determining luminance through a polychromatic ‘configuration’ which does not penalise blue OLEDs, that in principle exhibits lower luminances than green OLEDs. It is worth noting though that the precision available for polychromatic observations is tied to that of the experiment used to determine the electroluminescent spectrum.

#### d Characterising yields

$\alpha$  *External yield* The external yield is given by eqn (26), that is  $\eta_{\text{ext}} = \frac{q\lambda_d}{hc} \frac{\Phi_{\text{ext}}}{I_c} \cdot \Phi_{\text{ext}}$  has already been calculated using eqn (21), and  $\Phi_{\text{ext}} = \pi I_{0\text{ext}}$ . With the luminous

**Figure VIII-25.** Schematisation of the equipment used to measure losses due to propagation.

intensity given by eqn (7), which represents the flux within a solid angle unit, here  $I_{\text{ext}} = \frac{\Phi_{\text{ph}}}{\Omega_{\text{ph}}}$ . With eqn (29), which is such that  $\Phi_{\text{ph}} = \frac{I_p}{\sigma(\lambda)}$ , we obtain  $I_{\text{ext}} = \frac{1}{\Omega_{\text{ph}}} \frac{I_p}{\sigma(\lambda)}$ . In addition,  $I_{\text{ext}} = I_{0\text{ext}} \cos \varphi$ , and with  $\varphi \approx 7^\circ$  and  $\cos \varphi = 0.992 \approx 1$ ,  $I_{\text{ext}} = I_{0\text{ext}} = \frac{1}{\Omega_{\text{ph}}} \frac{I_p}{\sigma(\lambda)}$ . Finally,  $\Phi_{\text{ext}} = \pi I_{0\text{ext}} = \frac{\pi}{\Omega_{\text{ph}}} \frac{I_p}{\sigma(\lambda)}$ , and  $\Phi_{\text{ext}} = \frac{\pi}{\Omega_{\text{ph}}} \frac{V_p}{R_c \sigma(\lambda)}$ . Placing this into eqn (26) yields:

$$\eta_{\text{ext}} = \frac{q}{hc} \frac{\pi}{\Omega_{\text{ph}} R_c} \frac{\lambda}{\sigma(\lambda)} \frac{V_p}{I_c} \tag{39}$$

$\beta$  *Internal yield* According to eqn (28), we have  $\eta_{\text{int}} = 2n^2 \eta_{\text{ext}}$ , which allows us to write

$$\eta_{\text{int}} = \frac{q}{hc} \frac{2\pi n^2}{\Omega_{\text{ph}} R_c} \frac{\lambda}{\sigma(\lambda)} \frac{V_p}{I_c} \tag{40}$$

### IV Characterisation of polymer based linear wave guides [Col 98 and Ebe 93]

The titled characterisation is generally performed using wavelengths used in telecommunications, that is 1.3 and 1.55  $\mu\text{m}$  and allows analyses of:

- light transversally diffused by the guide;
- losses due to propagation, injection and diffusion at the extreme surfaces; and
- the transversal profile of the beam issued from the guide.

#### 1 Measuring transversally diffused light

Figure VIII-23 schematises the equipment used to specifically measure losses due to propagation within the guide, a loss especially important when using polymer based materials.

The source used in the system is a fibre based laser diode, which emits a transversally sinusoidal beam. A collimator, placed at the exit of the fibre, gives rise to a plan limited wave with a divergence minimised by diffraction. A 20 $\times$  multiplying lens ‘injects’ the wave into the guide (G) and the position of the lens and the guide are optimised with the aid of micro-positioning elements. Light diffused by the guide

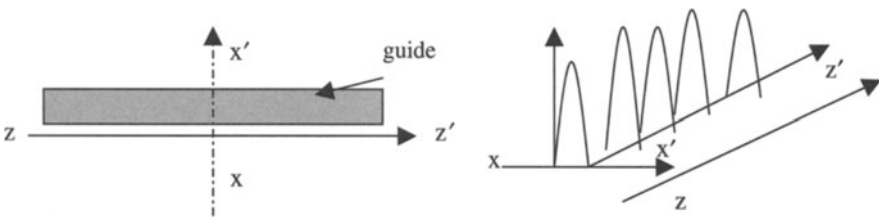
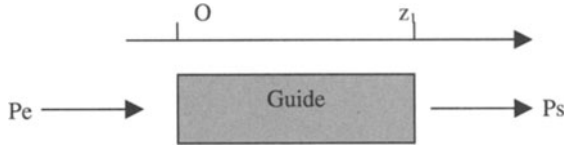


Figure VIII-26. Configuration for analysis of transversal.





**Figure VIII-27.** Configuration used to measure losses by 'cut-back'.

and perpendicular to propagation direction  $zz'$  is analysed using a camera equipped with a vidicon tube (sensitive in the range 400 to 1800 nm). The video signal, resulting from a sweep parallel to  $xx'$  is digitised and treated with a computer program (Figure VIII-26).

## 2 Loss analyses using 'Cut - Back' and 'Endface Coupling' methods

### a 'Cut - Back'

Initially, a collimated laser wave is injected into the guide using a  $20\times$  lens and global losses are determined by observing the difference in power between the injected ( $P_e$ ) and exit ( $P_s$ ) light, as detailed in Figure VIII-27.

Following the simple principle method of 'cut-back', measurements are repeated using different lengths of guide ( $z_i$ ), yielding a curve shown in the upper part of Figure VIII-29 with a slope due to propagation losses.

### b 'Endface Coupling' [Ebe 93]

The method of 'endface coupling' uses the set-up shown in Figure VIII-28 and allows differentiation of losses due to injection from other losses. A light beam traverses the guide from edge 1 to edge 2 initially in order to select the modal profile exactly adapted to the guide. An autocollimator made from a  $10\times$  lens and a mirror M injects across

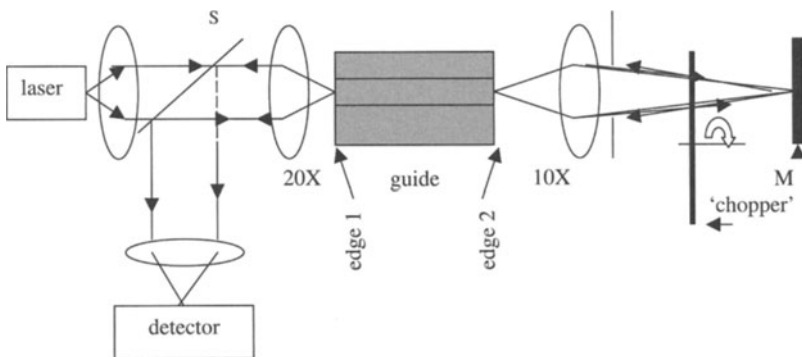


**Figure VIII-28.** Layout for 'endface coupling' equipment.

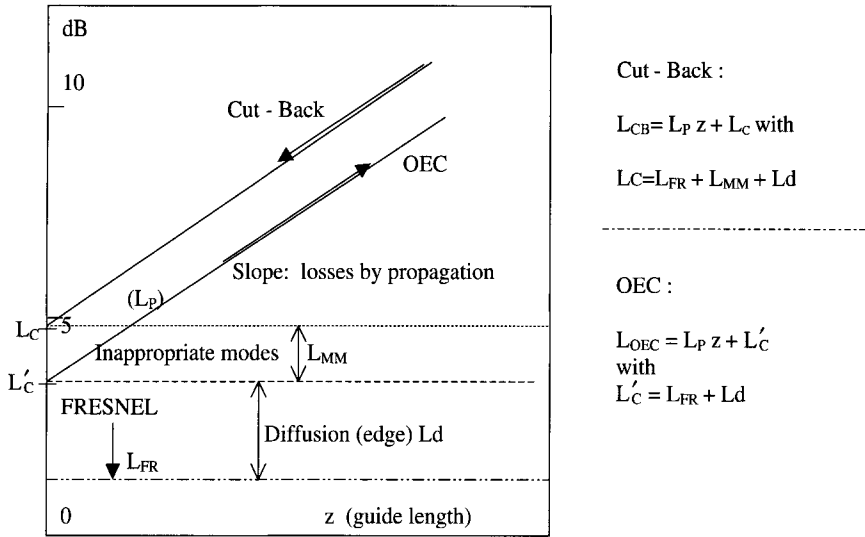


**Figure VIII-29.** Curves permitting analysis of different optical losses (see text for definition of parameters).

side 2 the initially filtered mode without any losses due to interference. With several guide lengths, we can obtain the curve denoted by letters OEC in Figure VIII-29.

**c Curves representing optical losses**

Figure VIII-29 shows various curves which allow analysis of the relative weight of different losses:

- $L_{CB}$  losses measured by 'Cut - Back';
- $L_{OEC}$  losses measured by 'Optimum Endface Coupling';
- $L_P$  losses due to propagation;
- $L_{FR}$  losses due to FRESNEL (reflection);
- $L_d$  losses due to diffusion at terminal edges; and
- $L_{MM}$  losses by injection due to imperfect covering of injected and modal profiles.

# IX

---

## Organic structures and materials in optoelectronic emitters: applications and display technologies

### I Introduction

During the last half of the 20th century there has been an extraordinary development in communication and information technologies. The dominant tool used for visualisation in televisions, computers, radar screens, medical imaging, to give just a few examples, has been the cathode ray tube (CRT). Recent requirements, for portable computers, phones, watches and so on, which require lightweight, unwieldy screens operating at low voltages, have also vitalised the development of new electrical components such as light emitting diodes (LEDs) and, less recently, screens based on liquid crystals. Given the rapid pace of development in display technologies and its results (micro-point plasma screens, electroluminescent screens based on inorganic and subsequently organic materials) it is now possible to imagine performances which were previously inconceivable in devices such as wide-screen (greater than 35") high definition televisions, light ultra-thin screens which could be easy to move or store, and flexible screens permitting ergonomic designs in cars and civil and military aircraft (dashboards, screens in helmets for weapons sighting and so on).

In this Chapter, we have chosen to present the main types of display systems, and then to compare organic component technology against that of classic components. We shall also rapidly detail the process of converting an incoming electrical signal into visual information in optoelectronic components. This process is typically due to luminescence (luminous emissions not entirely thermal) which can be provoked *via* various routes, such as photonic excitation (generally in the ultraviolet), excitation caused by excited particles (cathodic luminescence due to electrons), and application of an electrical field (electroluminescence) to give the principal examples [cur 56].

### II How CRTs work

CRTs operate on the principle of cathodoluminescence. This is due to the impact of a beam of accelerated electrons on a surface dotted with 'phosphors' points, or contacts, which on relaxation to an equilibrium state following excitation, emit light in the

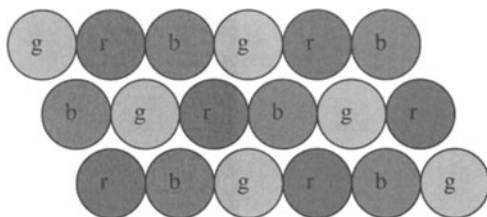


**Figure IX-1.** Arrangement of ‘phosphorus’ blue (b), green (g) and red (r) contacts on a cathode screen.

visible region. Sections VII-1 and VII-2 detail the process of electroluminescence in inorganic materials and, in particular, these ‘phosphor’ contacts.

Luminous emissions from colour televisions are seen by the human eye in an additive process, in a manner similar to that observed through impressionist paintings which are based on the juxtaposition of coloured points (pointillism) [Til 00]. Each luminous element, called a pixel (from the contraction of ‘picture element’), is in fact the product of three ‘sub-pixels’ (contacts placed as shown in Figure IX-1) each generating one of the three primary colours (blue, green and red). Each contact is composed differently to give the different colours: activated silver with zinc sulfide (Ag: ZnS) for blue, activated copper and zinc and cadmium sulfide (Cu:(Zn,Cd)S) for green, and activated europium and yttrium oxysulfide ( $\text{Eu}^{3+}$ :  $\text{Y}_2\text{O}_2\text{S}$ ) for red.

### III Electroluminescent inorganic diodes

Electroluminescent inorganic diodes underwent expansion in use towards the end of the 1960s due to their low cost (per industrially produced unit), their long lifetimes, their ability to emit light over a wide spectral range and their ease of control by a simple electronic circuit. They are widely used in domains requiring small emitters (digital displays for measuring devices and some calculators) and as calibration standards. While their individual price is low, the large number required to make a high definition screen from them makes such an overall cost prohibitive, adding incentive to finding alternative display technologies.

#### 1 How they work

In relatively simple terms, an LED is made from a directly polarised pn junction. Under the effect of this polarisation ( $V$ ), charge carriers are injected from one region, where they are in the majority, to the other, where they are a minority. So electrons from the n side are injected into the p side, while holes are injected from the p side into the n side. Figure IX-2 shows this crossover.

During the diffusion of the charge carriers, which for electrons is of length  $L_n$  and for holes is of length  $L_p$ , the minority carriers can recombine with majority carriers (minority electrons with majority holes in zone p and minority holes with majority

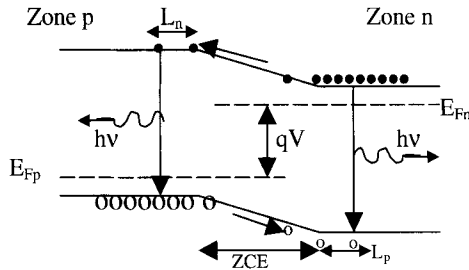


**Figure IX-2.** Radiative recombination zones in a light emitting pn junction working under direct polarisation.

electrons in zone n). Usually we neglect the number of recombinations in the zone ZCE (Figure IX-2) which tends to be particularly narrow under typical tensions ( $V$ ) [mat 96].

If the semi-conductor used is at direct gap (that is with the minimum conduction band and maximum valence band, in reciprocal space, at the same wavevector value), then electron-hole recombinations are facile as a third assisting particle is not required (such as a phonon for which the wavevector assures the conservation of the quantity of movement for indirect transitions—which are oblique and characteristic of semiconductors with an indirect gap such as silicon). The emission of photons corresponding to this recombination occurs with energy of the order of the size of the band gap. For GaAs (direct gap) this is equal to 1.43 eV, an emission with a wavelength ( $\lambda$ ) of 0.86  $\mu\text{m}$  and in the near infrared.

## 2 Display applications

To use semiconductors in displays requires the use of GaP which exhibits an indirect band gap of around 2.3 eV. Due to this indirect gap (and to reinforce radiative recombinations) impurities such as nitrogen are introduced into the semiconductor to form donor type states close to the conduction band [bre 99]. Excitonic radiative emissions can thus be generated in the green region of the visible spectrum with GaP(N). Other colours can also be obtained, for example by doping GaP with zinc or oxygen, or by using mixtures of semiconductors such as  $\text{GaAs}_{1-x}\text{P}_x$ . In the latter case, the direct gap in GaAs increases with the concentration of phosphorus. With a direct transition, a red emission can be obtained using 40% phosphorus, while orange and yellow emissions occur on adding nitrogen to varying compositions of  $\text{GaAs}_{1-x}\text{P}_x$ . Finally, blue emissions can be obtained using GaN or with the alloy InGaN.

## 3 Characteristic parameters (see also Chapters VIII and X for further definitions)

The internal quantum yield, which is defined as the ratio of photons produced to the number of injected electrons, can reach 50% in direct gap semiconductors. However, the external energetic yield ( $\eta$ ) which represents the ratio of luminous energy to the

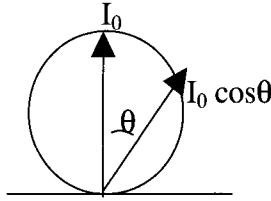


Figure IX-3. Lambert's emission represented.

electrical energy supplied is typically of the order of 1 to 10 %. The mechanisms which result in this difference can be classed into three types:

- the absorption of photons by the material which they traverse (for which multi-layer structures of materials with gaps above the emissions energy have been designed, so as to limit such absorptions);
- Fresnel losses which result from a difference in the refraction indices of the diode and air giving rise to the reflection of a part of the wave and its associated power; and
- losses due to total internal reflection when photons emitted strike the diode/air interface at an angle greater than the limiting angle  $\theta_1$  (indice of diode is greater than indice of air) and remain trapped within the diode.

As detailed in Chapter VIII, the luminous intensity varies according to Lambert's angular law (Figure IX-3), that is  $I(\theta) = I_0 \cos \theta$  in which  $I_0$  is the intensity in the direction normal to the surface and  $\theta$  is the emission angle (against the normal). Therefore, if  $\theta$  increases,  $\cos \theta$  decreases along with the luminous intensity emitted in the same direction.

#### 4 In practical terms

Electrons exhibit a higher mobility than holes, and the level of electrons injected into zone p is greater than the number of holes in zone n. The result is that zone p is the principal centre for radiative emissions and is thus used as the emitting face of the diode (Figure IX-4).

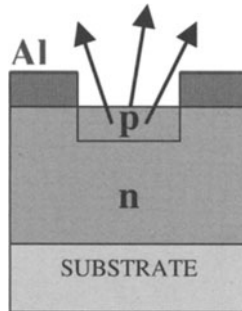
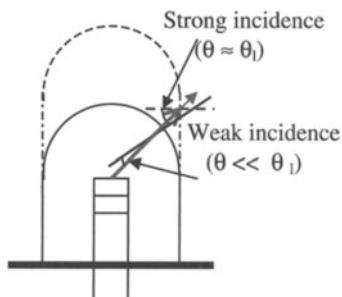


Figure IX-4. Structure of a typical LED.



**Figure IX-5.** The role of the position of the dome.

Finally, practically speaking, LEDs are encapsulated with a transparent resin dome which serves three functions:

- protection of the diode and its connectors from the exterior;
- reduction in the difference in indices of the diode and air, thus increasing the overall yield of the diode (reduction in Fresnel losses); and
- reduction of total internal reflection effects by generating an incidence angle at the dome lower than the limiting angle  $\theta_1$  (see Figure IX-5).

It is notable that for LEDs placed at the summit of the encapsulation dome (the continuous line in Figure IX-5), the largest part of emitted light hits the surface at an angle below the limiting angle. A diode of this type generates a greater angle of view (when looking at the diode) than a diode which has the emitting centre towards the rear of the dome, which emits light that falls on the sides of the dome with an angle close to or greater than the limiting angle.

## IV Screens based on liquid crystals

### 1 General points

Liquid crystals (LC)s were developed near the beginning of the 1960s for flat screens and, given the investment made at that time by industry (for example by Thomson LCD), this system remains the most widely used in technologies such as watches, calculators, computer screens and portable telephones. World wide, the market for LC based screens is valued at around 30 billion dollars, just below that of cathode ray tubes.

The liquid crystal state is a mesophase, a state in between those of a crystalline solid and an amorphous liquid [Til 00]. There are three main types of mesophase:

- Timmerman's globular molecules which give rise to plastic crystals;
- discotic, resulting from flat molecules; and
- calamatic, resulting from long molecules which can be in piled layers (smectic LCs) or grouped in clusters (nematic LCs) in which the molecules are aligned parallel to one another (depending on thermal effects).

## 2 How liquid crystal displays work

Liquid crystal displays (LCD)s operate by using two basic properties of LCs:

- the molecules can modify the direction of polarisation of an incident wave of light; and
- the molecules can be easily moved by the application of an external electrical field, which interacts with an orientated assembly of molecules and their orientated dipole moments (unlike thermal agitation which randomly moves individual dipoles). Even weak fields can vary by a considerable degree the orientation of the molecules.

In practical terms, there are two main types of system: [Car 84]

### a 'Guest-host' type displays

These displays use dichroic dyes (denoted 'guests') orientated by the crystal liquid molecules (the 'hosts'). The elongated dye molecules absorb the component light vector parallel to the molecules' axes (see Figure IX-6) but not the perpendicular components (due to dichroism). Depending on the direction of the molecules, determined by an applied electric field, an incident wave polarised parallel to the molecules (which have an initially homogeneous arrangement) would be reduced or become non-existent.

It is in this manner that displays can be prepared using nematic LCs with dichroic dyes introduced into sandwiched cells, constituted of glass plates, 5 to 200  $\mu\text{m}$  apart, covered with the transparent conductor ITO (a mixture of indium and tin oxides). In reality, two optoelectronic effects may be observed: the first corresponds to an inversion of contrast (from an initial homogeneous orientation as in Figure IX-7-a) and the second a normal contrast (from an initial homotropic orientation as shown in Figure IX-7-b).

### b Displays made with helical nematic liquid crystals

These are the most widely used and are based on the rotation of the plane of polarisation of light by  $90^\circ$  by 'twisted' nematic liquid crystals, in a configuration shown in Figure IX-8.

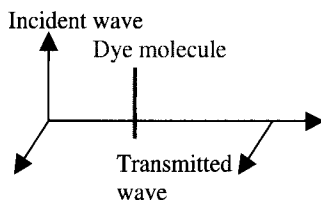
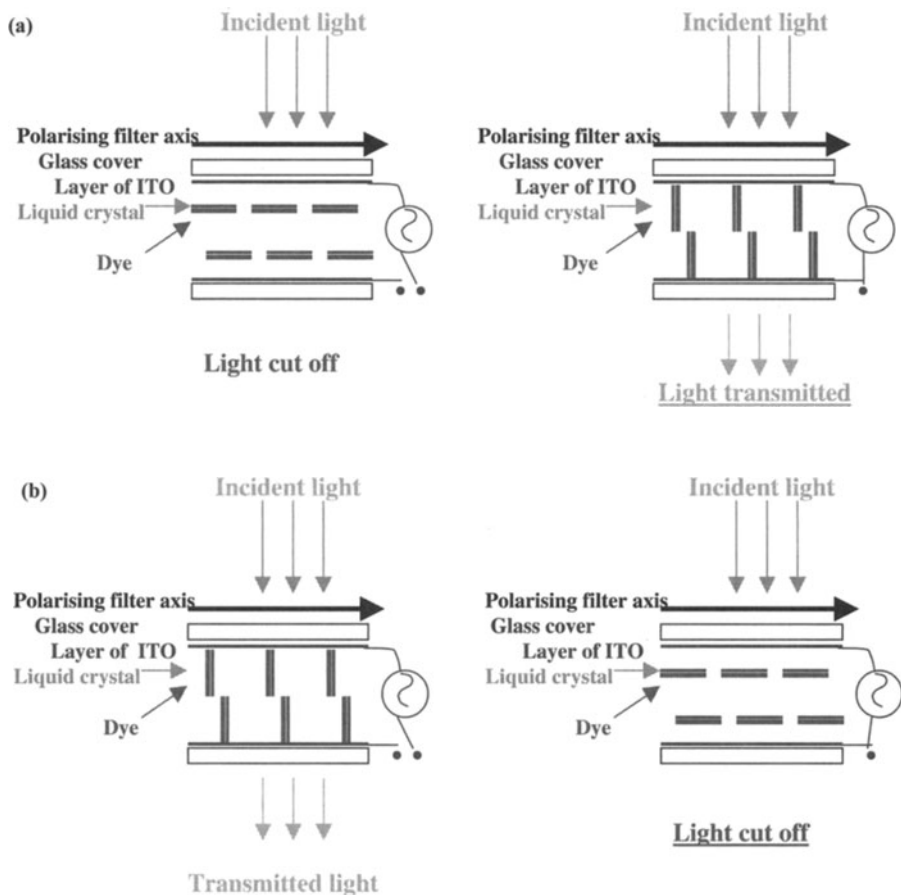


Figure IX-6. Using a dye to modify wave polarisation.





**Figure IX-7.** (a) Initially homogeneous orientation: inverted contrast; and (b) Initially homotropic orientation: normal contrast.

The liquid crystal is encapsulated between two glass sheets around  $10\ \mu\text{m}$  apart each covered by a transparent ITO electrode. The glass sheets are surface treated so that on contact with the liquid crystal, the molecules of the latter align themselves along a given direction. In addition, the directions of molecules at the two electrodes are such that there is  $90^\circ$  between them. As shown in Figure IX-8-a, a polarising filter, on the upper side, allows only incident light orientated parallel to the LC molecules through. Throughout the thickness of the LC layer, the molecules turn this single light component so that on reaching the lower face, the light is polarised parallel to the second polarising filter. Thus, in this relaxed state, the system appears transparent. Once a tension is applied, using the electrodes detailed in Figure IX-8-b, the electric field orientates the LC molecules so that they are parallel to the propagation component of the incident light. The LC molecules no longer turn the direction of the polarised traversing light and therefore, when the light reaches the lower face, it arrives with a component perpendicular to the second filter and the system now appears opaque.

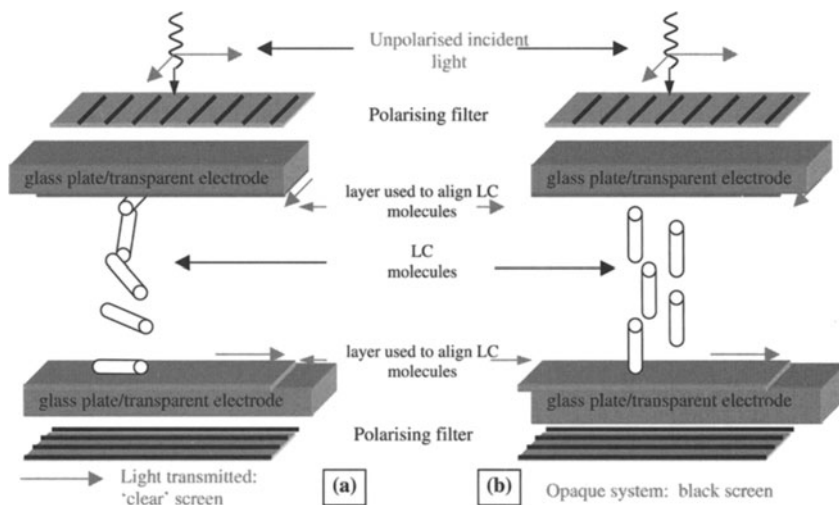


**Figure IX-8.** (a) Without polarisation of light in between electrodes, LC are in helical form and system allows light to pass: observer sees transparent system; (b) With electric field applied ( $\approx 1$  V), the initial orientation of molecules is disturbed and light is no longer turned to pass through the second polarising filter: the observer sees an opaque system.

The response time of such a system can be of the order of several tens of milliseconds, a value which permits the use of these materials for display technologies (which rely upon the persistence of perception of light of the human eye).

### 3 LCD screen structure and the role of polymers

Screens are made up of a matrix of rows and columns of pixels (to give a matrix screen). Colours are obtained by dividing each pixel into three sub-pixels (red, green and blue), each of which can be individually addressed. A side view is given in Figure IX-9.

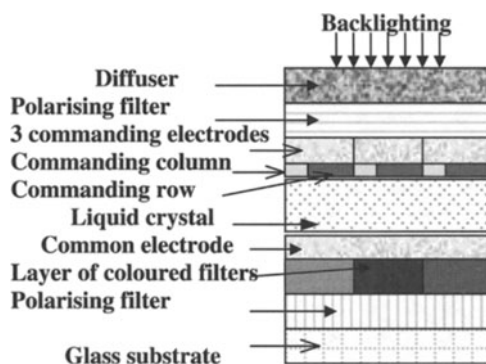


**Figure IX-9.** Cross section of a LCD pixel.

Polymers are involved at several levels in the manufacture of LCD screens and help in reducing their energy consumption and facilitating their use, by introducing qualities such as low weights, flexibility and so on [bro 01]. They are used in particular in the following ways:

- photosensitive polymeric resins used in the photolithographic processes;
- in constructing the screen and the walls of each cellular pixel which contains active materials;
- in aligning and orientating layers of liquid crystals, with the recent use of polymers that have improved the viewing angle and have allowed, using a stamped film layer of polyimide, control over the alignment of molecules in each sub-pixel; and
- optical functionalisation of screens, whereby stretched polyvinyl based polarising filters are protected by cellulose triacetate, which are filters coloured by photosensitive acrylates. Diffusion of light can be obtained using a stretched polyester film. Indeed, mixtures of birefringent polymers can be used to generate reflections by diffusion of otherwise untransmitted, polarised light permitting a recovery of this unused light. Using these techniques has allowed an increase in the luminance of screens, from around  $200 \text{ cd m}^{-2}$  for the more classical systems based on back-lighting to around  $500 \text{ cd m}^{-2}$ , a value similar to that obtained with cathode ray tubes.

#### 4 Addressing in LCD displays [Dep 93]

Multiplex addressing (reaching any single pixel at a given moment) necessitates a system for addressing each pixel in a display[bar 00]. In passive matrixes, as shown in Figure IX-10-a, each pixel is addressed *via* the use of a system of electrodes placed in rows, placed for example on the upper glass plate, and in columns, placed for

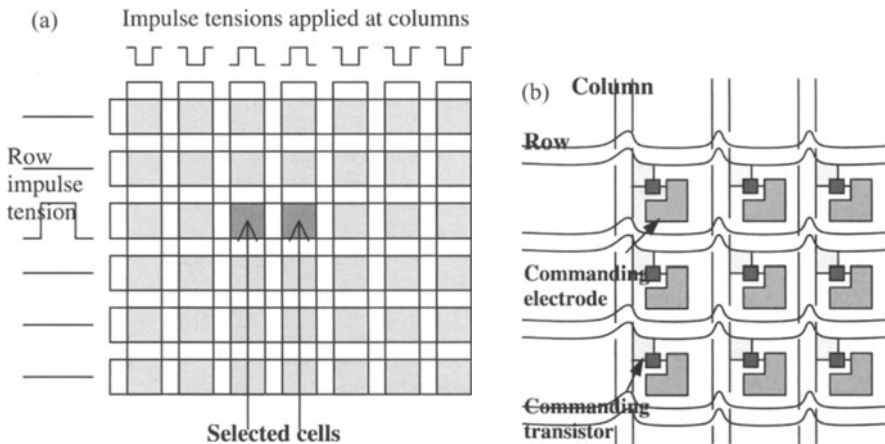


**Figure IX-10.** (a) Passive matrix addressing; and (b) Active matrix addressing.

example on the lower glass plate. At each intersection is a pixel. The surface of the screen is swept in a 60th of second by the electrical excitation of each row while each column is subject to a tension sufficient to produce the required excitation of each pixel. Pixels which are not selected for illumination are subject only to a low or residual tension, the latter of which increases as the resolution of the screen is increased. Indeed, to increase the resolution, along with the number of rows, the tension needs to be increased to maintain an overall average luminance of the order of 200 or 300  $\text{cd m}^{-2}$ ; any increase in resolution also necessitates a decrease in contrast as otherwise some pixels would be illuminated simply by going over the threshold tension.

In order to resolve the problem of decreasing contrast with increasing resolution, active matrixes are used which have individual command transistors associated with each pixel. These transistors are called thin film transistors (TFT) and consist of two electrodes for the entrance and exit of current which flows under the control of a third gate electrode. Hydrogenated amorphous or polycrystalline silicon has been widely used although electroactive polymers have been used as organic electronic/optoelectronic materials. Examples of polymers developed for such use are poly(*para*-phenylene vinylene) (PPV) [gre 95] and polythiophene, and such materials being more and more widely used. A more detailed description of the function of organic transistors can be found elsewhere [hor 00].

## 5 Conclusion

In conclusion, the technology used for LCDs is now very wide spread and has given rise to screens which operate at low power rates. One of the major limits of the technology, however, is the viewable angle of LCD displays, at around  $30^\circ$  to  $40^\circ$ , which results from the technology itself (molecular alignment forming a directional guide), although some progress has been made in improving this [jon 99]. Hitachi and NEC have realised displays with excellent viewing angles by using coplanar electrodes which control, in the same plane, the optical commutation of the liquid crystals. In addition, very wide screen displays, for example for use as wall televisions, have been prepared (from 1990 on by Tektronix) by replacing the TFTs by plasma canals which successively trigger each row of pixels.

## V Plasma screens

Plasma screens were developed around the beginning of the 1970s following the demand in flat screens. Monochromic plasma screens operate by emitting orange-red light from ionised gas, much in the same way as neon tubes [dep 93]. The gas, confined within a series of small cavities each positioned at the intersection of upper and lower electrodes (which determined the size of the pixels, as shown in Figure IX-11), is excited to the plasma state by applying a certain, selective tension. Displays made using this technology exhibit high brilliance and good lifetimes and stabilities. However, they require a considerable amount of energy to operate (and run

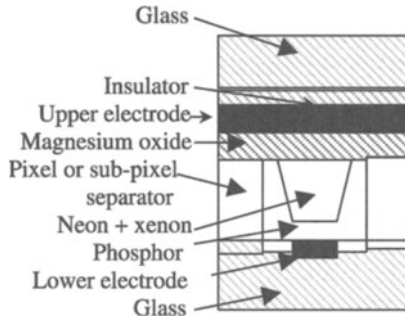


**Figure IX-11.** Cross section of a plasma screen.

at around 200 V). Other colours can be made by indirect excitation of luminescent substances (again using primary colours) with a plasma that emits in the ultra-violet, an example of which is a gaseous mixture of neon and xenon.

The geometry of each sub-pixel, which emits either red, green or blue, is shown in Figure IX-11. The cavity, containing the excitable gas is covered with one of three phosphors. The layer of magnesium oxide is there as a dielectric to reinforce the electric field within the cavity [Til 00].

## VI Micro-point screens (field emission displays (FED))

FEDs are microelectronic components which approximate to miniature cathode ray tubes [Bre 99]. In a FED, electrons are emitted from a cathode and collide with a phosphor to give an excitation and thus a luminous emission. Cathodes are assembled above an insulating layer, as shown in Figure IX-12. Each pixel contains three phosphors and three metallic electrodes which play the role of gates for each colour.

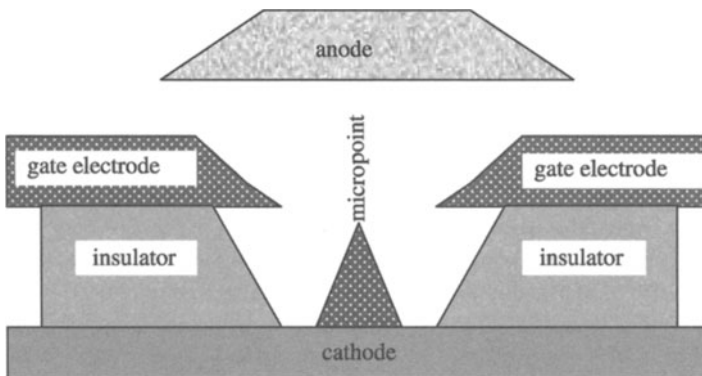


**Figure IX-12.** Cross sectional structure of a micro-point screen (FED).

A pixel is activated firstly by the application of a threshold tension (cathodic tension). Any current that flows is controlled with the help of a variable tension applied *via* the gate electrode. This controlled current of electrons is then accelerated towards the anode. The primary electronic current, which has a more or less radial propagation, is then focussed by use of gate electrodes placed about the micro-point cathode so that the electrons reach the anode in a nearly parallel beam.

FED based screens exhibit several advantages over cathode ray tubes and vacuum tubes:

- they can produce a higher current density during thermo-ionic emission than that encountered in vacuum tubes; and
- they do not require filament heating as electrons are generated by a field effect obtained at the extremity of a micro-point cathode, where the field is sufficiently intense to develop electrons through tunnelling effects across a reduced, narrow potential barrier between micro-point tip and the vacuum (see also Annex A-7, Section III).

With respect to LEDs based on semi-conductors, FEDs also present some advantages:

- no losses due to dissipation (*i.e.* no collisions between electrons in the vacuum while electrons may collide with a semi-conductor lattice);
- operation practically independent of temperature; and
- no perturbations due to ionising rays.

However, FED based screens do pose some disadvantages, for example the minimum distance required between anode and cathode to reduced sparking, and the non-directed emission of electrons tending to limit the obtainable degree of resolution.

## VII Electroluminescent screens

### 1 General mechanism

Electroluminescent screens function using Destriau's effect [mat 96], in which radiative recombinations are generated by the application of an electric field to a powdered semiconductor dispersed within a dielectric matrix, as shown in Figure IX-13-a. The semiconductor is normally the mixture of an inorganic material from groups II–VI, with a relatively large forbidden band of around 2 to 3 eV, and an activator made of a transition metal (typically copper or manganese) or a rare earth. In addition, fillers such as NaCl or KCl may be used as they are easily melted and on cooling they favour the formation of crystals and the insertion of the activators.

The electric field plays the role of carrying the concentration of free charge carriers above its equilibrium value; a return to equilibrium results in recombinations and, in the case of radiative recombinations, the emission of photons. The concentrations, outside of equilibrium, can be generated (and can accumulate) by applying a strong enough field. In general:

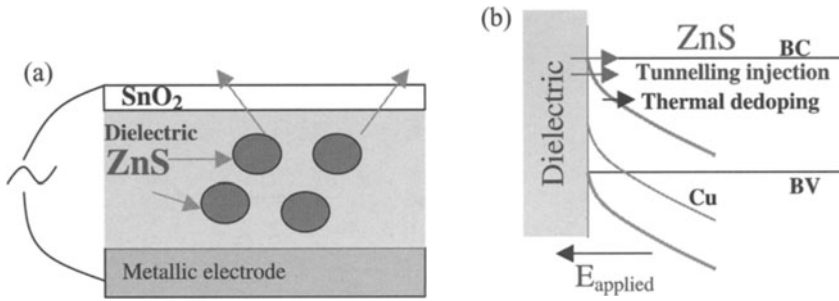


**Figure IX-13.** (a) Structure assisting the Destriau effect; (b) Mechanism of charge injection into electroluminescent ( $\text{ZnS}[\text{Cu}]$ ).

- when  $E_a < 10^8 \text{ V m}^{-1}$ , shock ionisation processes (with  $W_{\text{ionisation}} = q E_a l$ , where  $l$  is the distance covered by an accelerated carrier between two impacts) shift electrons into the conduction band of the semiconductor from valence or impurity bands; or
- when  $E_a > 10^8 \text{ V m}^{-1}$ , carriers can be injected through tunnelling effects at the interfaces (see Figure IX-13-b) to increase the density of carriers available through shock ionisation.

The component structure of electroluminescence will vary depending on the type of applied tension (alternating or direct).

## 2 Available transitions in an inorganic phosphor

In the band scheme of an inorganic phosphor there are permitted bands associated with activators (otherwise called luminescent centres when they induce radiative transitions). There are two possible types of centre within a phosphor:

- those which introduce into the forbidden band localised levels close to the valence band; this is the 'classic' model of Cu centres in ZnS which give rise to a level at several tens of eV above the valence band that has a high probability of capturing holes; and
- those which reinforce both the fundamental level I close to the valence band and the excited level II just below the conduction band. Levels I and level II exhibit high probabilities of capturing holes and electrons, respectively. An example of such an activator is  $\text{CuCl}$ , [dep 93] although  $\text{Mn}^{3+}$  is more widely used along with rare earth ions [mom 95].

There are other bands, very close to the conduction band, which also exist. They are associated with structural defaults (and thus the preparation of the phosphor) and act as trap levels. Electrons caught within these bands may be thermally released with a probability given by the Randall–Wilkins law, which supposes that electrons within the traps have a Maxwell type distribution of thermal energies (see also Chapter VI,

Section IV-4). It can be written in the form

$$p = \nu_0 \exp(-U_s/kT),$$

where  $U_s$  is the energetic depth of the trap with respect to the edge of the conduction band and  $\nu_0$ , *a priori*, is a constant which takes on a value of the order of the frequency of phonons ( $\approx 10^{12} \text{ sec}^{-1}$  according to Mott and Gurney) although it does tend to vary with temperature and typically has been found to have a value around  $10^8 \text{ sec}^{-1}$  in phosphors [ran 45].

Figure IX-14 shows a representative energy diagram for activated phosphors [fri 85].

There are various transitions which can be envisaged:

- A: an activator is excited, recombination occurs and an electron returns to the fundamental level;
- B: excitation, in the conduction band, of an electron at an activator and a recombination with another activator centre;
- C: same as B but with a delayed recombination due to the passage of electrons *via* trap levels, which they escape through thermal energy;
- D: band to band generation due to energetic beams ( $>2$  to  $3 \text{ eV}$ ) whereby a free hole generated from the valence band is displaced until it recombines with an electron in the neighbourhood of an activator. The latter acts as a radiative centre, and an activator electron falling from the valence band to recombine with a hole results in a positive ion at the activator itself, which may in turn may capture, radiatively, an electron from the conduction band; and
- E: the same process as D but a similar delay to that in process C in which electrons are delayed by traps.

Generally speaking, the term ‘fluorescence’ is used for immediate relaxations (for example, cutting out trap levels and within a time  $\tau \approx 10^{-8} \text{ s}$ ) while the term ‘phosphorescence’ is used for recombinations which occur after a delay  $\tau > 10^{-7} \text{ s}$ .

*Comment* It is worth noting that while an increase in temperature may help detraping of electrons, it can also lead to an extinction of luminescence. This is due to electrons excited from the valence band to empty levels of the activation centres,

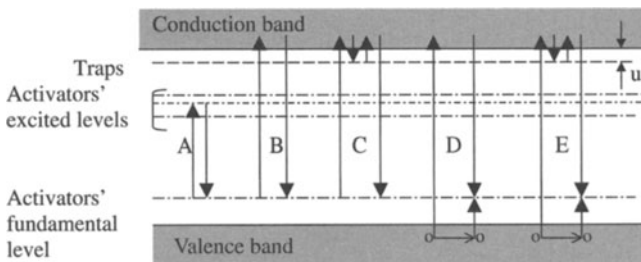


**Figure IX-14.** Energy levels in a semiconductor (II-VI) activated by transition metals or rare earths.



Table IX.1

	$\lambda$ (nm)	E (eV)
ZnS (blende)	341	3.64
ZnS (wurtzite)	335	3.70
CdS (wurtzite)	510	2.43
ZnSe (blende)	477	2.60
CdSe (wurtzite)	711.5	1.74
ZnTe (blende)	578	2.15
CdTe (wurtzite)	871	1.42

which can therefore no longer act as recombination centres, or excitation of carriers simply to be trapped non-radiatively at extinction centres.

### 3 Characteristics of inorganic phosphors from groups II–VI [cur 60]

Groups II–VI have a forbidden band of energy  $E_G$  which is close to that of photons in the visible range. The materials most widely used are ZnS (which as zinc blende in Europe or sphalerite in the USA is of a cubic structure, or as wurtzite is of a hexagonal structure) and CdS. Table IX.1 below gives the values of  $E_G$  and the wavelength of corresponding photons for the principal mixtures used.

The emission band to band transitions observed for these phosphors actually appear unrealistic, however, it is the introduction of luminescent centres, as mentioned above typically based on copper or manganese, which permit a circumnavigation of the problem.

In Figure IX-15 there is shown the relative position of energy levels associated with copper luminescent centres introduced either into ZnS or CdS. In both cases there are two principal emission bands. In the case of ZnS(Cu) there is one in the green at 523 nm and one in the blue at 445 nm.

In classical terms, photoluminescence occurs when centre excitation (by UV light) results in the generation of valence band holes, into which there is then a fall of electrons from luminescent centres (see Figure IX-16-a).

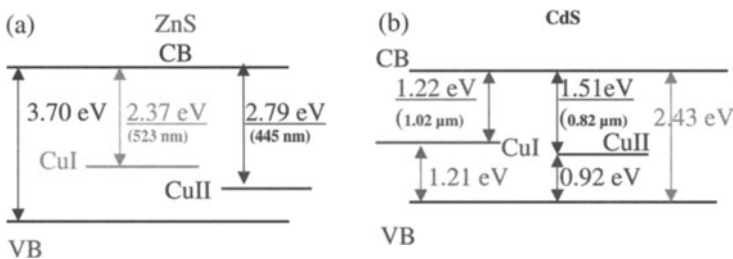
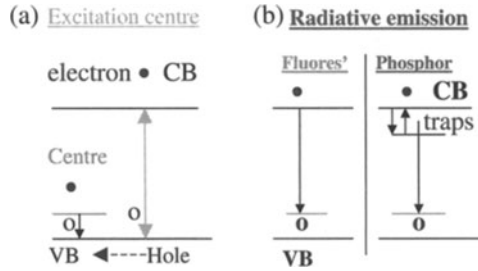


Figure IX-15. Energy levels in: (a) ZnS(Cu); and (b) CdS(Cu).



**Figure IX-16.** (a) centre excitation; and (b) radiative emission.

Radiative emission though corresponds to the recombination of conduction band electrons (from group II–VI elements) with holes localised at luminous centres (through process D indicated in Figure IX-14). If the transition occurs directly, without passing *via* traps situated just below the valence band, then the emission occurs as fluorescence, however, if electrons relax on passing through trap levels, then the emission occurs as phosphorescence, as shown in Figure IX-16-b.

Phosphors based on ZnS are not easy dope so that they are of n or p type, [page 79 of mom 95] and this sort of material cannot be used in a pn type LED.

#### 4 Electroluminescent thin film displays: how they work with alternating current

A general abbreviation often used in this area is ACTFEL standing for ‘A.C. supplies in a Thin Film Electroluminescent displays’ [bre 99].

Typically, thin film electroluminescent displays are based on an insulator—semiconductor—insulator structure, as detailed in Figure IX-17-a.

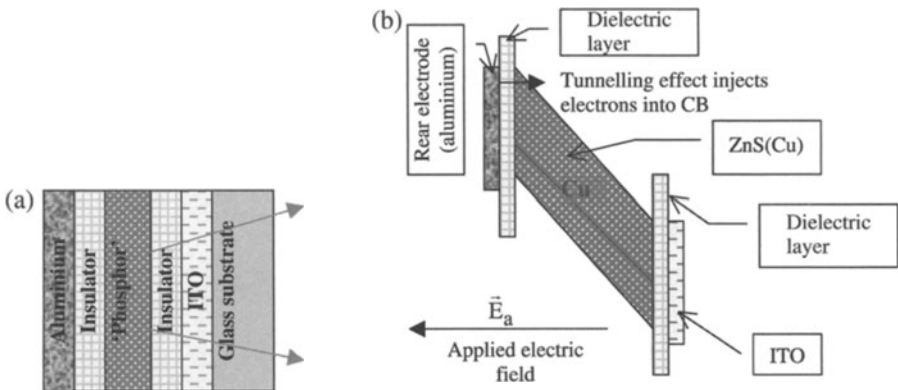


**Figure IX-17.** (a) The different layers in an ACTFEL screen; (b) Band positioning on application of an intense electric field.

The active 'phosphor' layer ( $\text{ZnS}(\text{Cu})$ ), which is about 700 nm thick, is set between two transparent dielectric layers, themselves each about 400 nm thick. The latter layers are in contact with electrodes, one aluminium, the other transparent ITO deposited on a glass substrate. This structure resembles that of capacitors in series, and permits the generation of a relatively high tension at the active  $\text{ZnS}(\text{Cu})$  layer from a low tension at the electrodes by using the low capacities of the thin dielectric layers.

On application of a strong electric field ( $E_a$ ) the high degree of band 'bending' of the active layer allows electrons, which would otherwise be trapped at interface states, to pass through to the conduction band by tunnelling effects (Figure IX-17-b). Electrons cross the active layer by collecting energy along their pathway of distance  $l$ . With  $W = e E_a l$ , and starting at the threshold energy, these electrons can transfer by collision a high enough amount of energy to excite the luminescent centres with a return to equilibrium through luminous radiation.

Given that the concentration of centres is rather low, of the order of  $10^{18} \text{ cm}^{-3}$ , and that of the phosphor hosts is of the order of  $10^{23} \text{ cm}^{-3}$ , the actual available surface for generating impact excitations is very low. Accordingly, only a small proportion of the injected electrons result in the excitation of a centre while most reach the opposing electrode to give rise to a space charge which can affect following charge injections into the component. The application of an alternating current, which continually reverses the sense of the applied tension, can use these electrons to again excite the luminous centres in the reverse direction (these electrons accumulate with electrons newly injected through tunnel effects from levels localised around the second electrode).

The overall brilliance of these screens remains relatively low, principally because the source of the electrons, the semiconductor-insulator interface, has at any single moment a relatively low concentration of electrons and leading to a low availability of electrons for impacts with luminous centres. However, the screens are relatively robust and are widely used as monochrome displays in military applications. In addition, different colours can be prepared. On using manganese ions ( $\text{Mn}^{2+}$ ), introduced by way with zinc sulfide ( $\text{Mn}^{2+} : \text{ZnS}$ ), a yellow emission at 585 nm can be obtained, a result of the d-d transitions with the breakdown of d-orbitals by crystal potentials. Other colours can be generated from f-f orbital transitions (due to incomplete internal, atomic 4f layers) in rare earths. For example, red can be obtained with europium [ $\text{Eu}^{2+} : \text{CaS}$ ], green with terbium [ $\text{Tb}^{2+} : \text{ZnS}$ ] and blue with thulium [ $\text{Tm}^{3+} : \text{F}^- \text{ZnS}$ ] (see also Chapter VII, Section II for more details).

## 5 Electroluminescent devices operating under direct current conditions

Here, the structures used are either of the metal-insulator-semiconductor (MIS) or the Schottky barrier type. In both systems, the electron source is a metallic electrode.

The structure shown in Figure IX-18 operates by the passage of electrons through the insulator barrier from the semiconductor valence band (VB)—typically  $\text{CdS}$ —towards a positively polarised metal electrode. The mechanism is equivalent to the

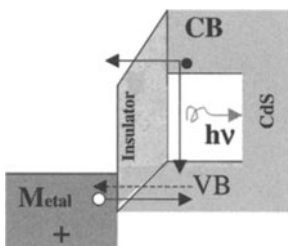


**Figure IX-18.** MIS structure with CdS semiconductor.

injection of holes into the semiconductor VB with the following recombination of VB holes with conduction band (CB) electrons.

This structure does, however, present two inconveniences:

- in the recombination zone, which is placed close to the interface, the interference of defects, which act as trap levels, results in non-radiative recombinations; and
- the efficiency of hole injection is very poor due to the competing flow of electrons through tunnel effects from the semiconductor CB to the metal.

In the case of the Schottky junction, an inverted tension is applied (*i.e.* the metal is negative if the semiconductor transports electrons). Once the tension is strong enough, electrons may be injected through tunnelling effects (barrier triangulation) from the metal to the semiconductor. Thus, a considerable number of electrons can be injected—more than is possible using an alternating tension—and can as carriers collide with luminescent centres such as Mn (transition metal) or rare earths.

These devices can function in both continuous and pulse modes, although in the former mode their lifetimes are shortened by a increase in resistivity, a problem which is reduced by using the pulsed mode. (An alternating mode does not give the same problems as it relies upon the structural capacitance). The quantum yields of these devices in the continuous mode is rather poor ( $\eta \approx 0.1\%$ ) because of:

- the difficulties in obtaining a high enough number of hot carriers to excite the luminous centres;
- a low, effective sectional area of centres for collisions; and
- a limited concentration of luminous centres (from 0.1 to 10 %). Above a certain concentration, however, extinction of luminescence occurs due to the crossed relaxation by transfer of energy between luminescent ions (Chapter VII gives further details).

The main advantage of these systems, over those operating under alternating current, is their low consumption of electricity and their relatively easy construction due to their simple structure.

## VIII Organic (OLED) and polymer (PLED) electroluminescent diodes

### 1 Brief history and résumé

The ability of organic materials, both molecular and macromolecular, to be deposited on virtually any substrate, even flexible ones, has solicited the long running and ongoing research into their use as replacements for inorganic semiconductors in a wide range of applications. For a considerable time, the necessary tension required to produce electroluminescence (the required work voltage) of these organic materials was found to be too high for their general use. An example is that of anthracene which required, because of the thickness of the crystals used, an application of around 100 V to operate [pop 82]. However, in the last 10 years, the emergence of new materials based on molecules such as 8-tris-hydroxyquinoline aluminium ( $\text{Alq}_3$ ) [tan 87] and on  $\pi$ -conjugated polymers such as poly(*para*-phenylene vinylene) (PPV) [bur 90] has got around this problem and has allowed the formation of thin films by evaporation and spin-coating techniques, respectively. More recently, there has been tremendous growth in this technology, stimulated by the economic gains available in the display market. Companies of note are Kodak and Uniax in the States, Cambridge Display Technology (CDT) in Great Britain, Pioneer in Japan, Philips in Holland, Siemens in Germany and Thales and Thomson Multimedia with the CEA and Leti in France.

### 2 The two main developmental routes

There do remain, however, certain problems to overcome before these materials can provide the qualities required for full industrial exploitation. Most important is the fact that, until now, most organic materials have displayed relatively short lifetimes, varying from several hours to several hundred hours, although in some cases several thousand hours. This limitation results just as much from the deterioration of the materials themselves as the degradation in the various interfaces and the electrodes, and depends heavily upon the configuration used in each device [sly 96]. In addition, the material of choice for the emitter has yet to be determined [bar 00], and could be either based on molecules (for example  $\text{Alq}_3$  or more generally speaking  $q_3$  type complexes with group IIIa metals such as Al, Ga or In) or based on polymers (such as PPV and its derivatives, poly(*para*-phenylene) (PPP), polythiophene (PTh) or poly(vinyl carbazole), to name but a few). Each material presents both advantages and disadvantages. Oligomers, polymers made up of just a few monomer units, present an interesting advantage in that the maximum emission wavelength can be altered with chain length, given that with changes in their length, their optical band gap also varies [had 00]. Polymers, meanwhile, generally present a better thermal stability and can be easily processed to give large surface area films, although small molecules can be spread onto large, flexible supports using the 'roll on roll' technique [bur 97]. Materials based on molecules are generally more organised, charge mobilities are higher and function at lower operating tensions. In addition, they are readily purified, resulting in lower numbers of reactions and diffusions at the electrodes.

For the present moment, both technologies based on molecules or on macromolecules remain important in the fabrication of organic electroluminescent diodes. The terminology used for devices depends on the materials used: the term Organic Light Emitting Diodes (OLEDs) is widely used for devices based on small molecules and Polymer Light Emitting Diodes (PLEDs) is used for those based on macromolecules. For the latter, another term although less used is Light Emitting Polymers (LEPs).

### 3 How OLEDs function and their interest

As detailed above, OLEDs have the advantages of low power consumption (requiring operating voltages of only 2 V) and ease of fabrication (easily formed into thin films or layers). In addition to which, relatively high quantum yields have already been obtained. Their theoretical maximum yield is 25 %, however, this figure may be eclipsed by recent methodologies which try to circumnavigate selection rules. Given these qualities, it is not surprising that we are now witnessing an exponential growth in the technology and its market [ole 01].

In the following Chapter X, we shall look in more detail at how these organic LEDs actually work, both in terms of theory and practise. At the most fundamental level though, the origin of the optoelectronic properties of these organic solids has been given in Chapters VI and VII.

In very general terms, the study of photometric characteristics of OLEDs, in particular their quantum yields but also their lifetimes, are guided by an understanding of the underlining mechanisms of charge behaviours and recombinations (radiative or not) within the organic material. In classical terms, an OLED can be schematised as shown in Figure IX-19.

The structure used for an organic diode is very different from that used for an inorganic diode. It is not possible to use organic semiconductors in their doped form, which would permit the fabrication of pn junctions similar to inorganic diodes, as doping agents tend to act as extinction centres, 'killing' radiative luminescence [ham 96 and hay 97]. In organic materials, what does happen is that the low mobility of the charge carriers is exploited, so that when two charges are injected into the emissive

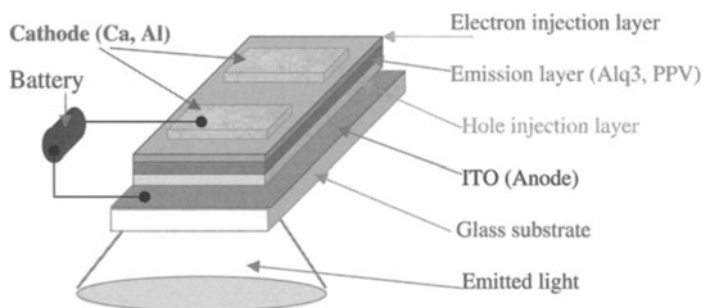


**Figure IX-19.** Typical structure of an electroluminescent organic diode.

layer and come into close proximity, their recombination is inevitable. This is in contrast to inorganic systems in which charge carriers have such a high mobility that recombination centres are required to realise a satisfactory level of recombinations. It is due to the very low mobility of charge carriers in organic materials that there is this gain in a high concentration of optically active recombinations.

It is thus useful to study the how organic diodes function in terms of four successive steps:

- injection of electrons and holes at the cathode and the anode, respectively;
- their transport through one or more organic layers;
- their association to form a exciton quasi-particle; and
- the relaxation of the quasi-particle resulting in luminescence.

As detailed in Chapter X, the models so far defined for each of these steps remain controversial. What is probably true is that each type of material, and each type of structure, follows a different system model. For example, current-voltage characteristics are often studied, and explained, in terms of injection either through Schottky effects or through tunnel effects. They can also be interpreted through the so called 'space charge limited' (SCL) current model. In order to reduce the threshold tension for a particular diode, and depending on the dominant process, we should look more to varying the metal of the electrode and the mobility of charge carriers within the organic layers.

In Chapter X, we shall concentrate on this physical aspect of the functioning of electroluminescent diodes. The chemical and physico-chemical aspects of these devices have already been covered in depth elsewhere [bar 00a, den 00 and kra 98] so will not be covered in any great depth here. We shall finally concentrate on device applications currently being developed, with special regards to the area of display technology.

## Electroluminescent organic diodes

### I Introduction

To have an idea of the vast number of articles published regularly on the subject of electroluminescent organic diodes, it is worth looking at the journal 'Synthetic Metals', in particular issues devoted to the 'ICSM' conference. While a large number of papers are published in this journal, it shows only a small fraction of all the material available. This Chapter can therefore only limit itself to a very condensed view of the subject.

Following on from Chapter 9 where the principle upon which these devices function was presented, this Chapter:

- compares empirically obtained results with those expected from theories detailed in Chapters VI and VII;
- considers the yields obtained with organic light emitting diodes (OLED)s and the strategies used to improve these yields; and
- details the actual and possible future applications of these devices.

This Chapter will not go into discussions on the origins of electroluminescence in organic materials (radiative transitions) as Chapter VII (Section V-4) has already covered an interpretation of the obtained spectra, while Section VI of the same Chapter detailed the nature of excitations (excitons). We have also seen how electron-lattice interactions play a role in these properties, without forgetting the limits of the model, originally proposed for small molecules, when applied to polymers.

For now, we shall just give the simple example, as understood by Burrows *et al.* [bur 96], that electroluminescence in molecular organic light emitting diodes (OLEDs) is due to the generation and recombination of Frenkel excitons within the Alq<sub>3</sub> layer. This was shown by observing luminescence spectra of Alq<sub>3</sub> in solution (in dimethylformamide), which, unchanged from those of solid, vacuum evaporated Alq<sub>3</sub>, indicated that the recombinations were independent of the molecular environment and originated from excitations localised at individual molecules. These excitons come from both electrons and minority holes, which control luminescence intensity, and diffuse through layers which will accept their injection. We shall look at these



layers in more detail later on in this Chapter. The electrons are localised at traps, which are themselves distributed within a gap of average depth  $E_t < E_{\text{LUMO}}$ . These levels come from electrons, which act as polarons initially placed within the LUMO conduction band (CB) and localised (trapped) at molecules with relaxations generating a level with depth  $E_t$ . Indeed, the shift in the spectrum of electroluminescence with respect to that of absorption can be interpreted as a Franck–Condon displacement, due to the change in the conformation of excited molecules, while the width of the electroluminescence spectrum can be attributed to strong exciton-phonon coupling.

## II Comparing electronic injection and transport models with experimental results

### 1 General points: properties and methods applied to their study

#### a Properties

From the first studies performed on organic solids (using anthracene), it was observed that various regimes of behaviour could exist, especially for example with respect to applied tension. Chapter VI gives further details. However, with OLEDs, clean transitions between different regimes are generally rather rare. Experimentally, we tend more to see only slight variations from the slopes predicted by laws detailed in Chapter VI.

Two examples are used in this Section: for the small molecules, a derivative of Alq3; and for the polymers, poly(*para*-phenylene vinylene) (PPV). The structure in which these materials are presented is simplified to anode/organic solid/cathode, in which either Alq3 or PPV is the organic solid acting as a layer into which both holes and electrons are injected and electroluminescence occurs. There have been published proposals for distinct mechanisms for each of the materials under study here, respectively, [bur 96] and [par 94], with following and differing proposals, again respectively, [ioa 98] and [blo 97a, blo 97b and blo 98]. More complicated multi-layer structures are discussed in Section V.

#### b The nature of the electrical measurements and some practical precautions

Given that these materials are relatively resistant, it is worth bearing in mind that any measurements must take account of their relatively long relaxation times, of the order of a millisecond to a second, rather than of nanoseconds or less [kar 97]. In practical terms, we can observe in the first characteristic  $I(V)$  curve that there are peaks in the tension which may appear randomly, only to be unobservable on the second trace. These peaks may be due to the filling, during the first trace, of certain deep traps which, statistically, do not empty themselves—and therefore do not need refilling—so that they effectively disappear from the second  $I(V)$  trace. It is generally the second curve which is shown.

Classically, characterisations are performed by measuring the current flow across a sample to which is applied an increasing tension. The intensity of any electroluminescence is simultaneously recorded (initially with respect to luminance) and the following identification of charge transport mechanisms is made by comparing the empirically obtained  $I(V)$  curve against those predicted by theory. The results, interpretations and discussions issuing from this process are presented in the following paragraphs.

It is worth noting, however, that there are other important electrical characterisations which may be performed:

- time of flight measurements which indicate charge carrier mobility (for example, with PPV, at an applied field of  $10^5 \text{ V cm}^{-1}$ , a mobility  $\mu \approx 10^{-5} \text{ cm}^2 \text{ V}^{-1} \text{ s}^{-1}$  has been observed);
- measurements of thermally stimulated detrapping, using thermally stimulated currents (TSC) or thermoluminescence (TL), which permit studies of the population of traps and their origin or eventual depth. Using these methods, the depth ( $U$ ) of traps in Alq<sub>3</sub> were determined as  $U \approx 0.2 \text{ eV}$  [for 98] and in PPV as  $U = 0.35 \text{ eV}$  for traps in the volume and  $U = 0.68 \text{ eV}$  and  $0.82 \text{ eV}$  for the levels of traps at the interface, whose values depended on the polarisation tension [ngu 01]; and
- dielectric studies which permit measurements of metal-semiconductor barriers for Schottky junctions (using the curve  $1/C^2 = f(V)$ ), or the evolution of relaxation phenomena with temperature and frequency to resolve both real ( $\epsilon'$ ) and imaginary ( $\epsilon''$ ) dielectric permittivities.

Different layers of dielectrics and their interfaces can be represented by equivalent circuits of resistors and capacitors, the values and connections (series or parallel) of which are varied until a near approximation is obtained [jon 83]. For the phenomenon of ideal relaxation, or a Debye dipolar relaxation, for the curve  $\epsilon'' = f(\epsilon')$  we have a semi-circle or flat half-circle (as in the Cole–Cole diagram which corresponds to a distribution of relaxation times), and the presence of a (default) interfacial layer can be characterised by an oblique Cole–Davidson type arc [ngu 01]. While relaxation phenomenon in the volume are dependent on temperature, those due to interfacial layers (next to empty space) exhibit a behaviour practically independent of temperature, as we have already seen in Alq<sub>3</sub>. The same material has also exhibited a Debye dipolar absorption with a relaxation energy ( $U$ ) around  $2.3 \text{ eV}$ , a value associated with the depth of trap levels in the volume of the material [jeo 01b]. Appendix A-10 gives further details.

## 2 Small molecules (Alq<sub>3</sub>)

### a A study of interface barriers in a standard structure of ITO/Alq<sub>3</sub>/Ca

*α Principal points* The simple ITO/Alq<sub>3</sub>/Ca structure simplifies the study of properties of charge injection and transport. The electroluminescent properties, with respect to an electroluminescent diode are, however, relatively limited as although injection, transport and radiative recombinations occur readily in Alq<sub>3</sub>, the same is not

true for the injection and transport of holes, which control the radiative emissions (thus the necessity of a specific layer added to the anode side in device fabrication).

Thermoelectronic or Schottky [cam 99] or Fowler-Nordheim electrode emissions are generally accepted to be responsible for injection at contacts, when the latter are not ohmic. When the height of the apparent barrier is above 0.6 eV, in general, the current within a structure is thought to be governed and thus limited by these electrodes [she 98]. Once the barrier is lower though, the current is only slightly dependent on the electrode emission (as the contact is on principle ohmic) but is heavily dependent on the volume and follows the laws we established in Chapter VI, where at low tensions the ohmic law reigns and at higher tensions the SCL and TCL laws play their roles.

It is interesting to note here how there is a considerable gap between language and reality: an ohmic contact actually results in a non-ohmic conduction law of the type  $I \propto V^m$  (with  $m \geq 2$ ) and is characteristic of TCL or SCL laws, which reign over virtually all values of tension. The SCL law is exceptional in that between the values of around 0 to 1 V, typically, the density of injected carriers remains lower than that of thermally generated carriers (which is such that  $n_0 = N_c \exp[-E_c - E_F/kT]$ ). It is only in this minor domain that ohmic characteristics are retained.

We shall denote the workfunctions of ITO, calcium and Alq3 as  $W_{ITO}$ ,  $W_{Ca}$  and  $W_{Alq3}$ , respectively, and the electron affinity, the potential ionisation energy and the size of the forbidden band of Alq3 as  $\chi_{Alq3}$ ,  $I_{PAIq3}$  and  $E_{GAlq3}$ , respectively. As empirically derived values, we have  $W_{ITO} = 4.6$  eV,  $W_{Ca} = 2.9$  eV,  $\chi_{Alq3} = 3.3$  eV,  $E_{GAlq3} = 2.6$  eV, and thus  $I_{PAIq3} = 5.9$  eV [values for Alq3 obtained from sch 95]. On taking  $W_{Alq3} = \chi_{Alq3} + (E_c - E_F)$ , a value calculated from the expression  $(E_c - E_F) = kT \ln(N_c/n_0)$  using  $N_c = N_{LUMO} = 10^{19} \text{ cm}^{-3}$  and  $n_0 = 10^{11} \text{ cm}^{-3}$  (for Alq3 see [bur 96]), we obtain  $(E_c - E_F) = 0.5$  eV, that is  $W_{Alq3} = 3.8$  eV. Figure X-1 shows the electron levels prior to the application of a tension. Once contact is made with the electrodes, the positions of bands are adjusted by the alignment of Fermi levels, as shown in Figure X-2 for  $V_{\text{applied}} = 0$ . The values of the diffusion potentials at the two interfaces adjust so that  $W_{\text{diff}} = W_{ITO} - W_{Alq3}$  and  $W'_{\text{diff}} = W_{Alq3} - W_{Ca}$ . In general, we assume that for these organic solids the bands are rigid (oblique, thick grey lines in Figure X-2) and correspond to the metal-insulator-metal (MIM) structure in which there is a constant field across the insulator.

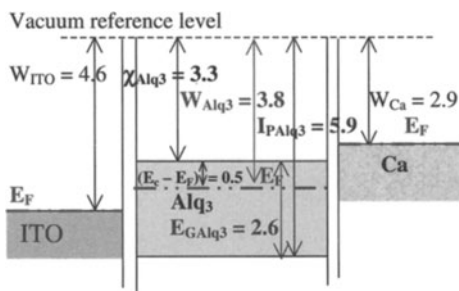


**Figure X-1.** Electron levels prior to application of tension.

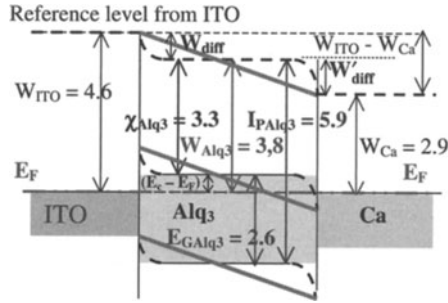


**Figure X-2.** Electron levels after contact made ( $V_{\text{applied}} = 0$ ).

We should note that a constant potential gradient corresponds to a homogeneous distribution of charges within a volume and that band curvature occurs, typically, in solids in which the concentration of carriers is higher than  $10^{17} \text{ cm}^{-3}$  [lei 98, p. 855], and that occurs only for organic solids when they are doped, something not generally applicable to electroluminescent diodes.

*β Electron levels following polarisation* On making contact with electrodes and applying a tension of the flat bands, *i.e.*  $V_{\text{BP}} = (W_{\text{ITO}} - W_{\text{Ca}})/q$ , we arrive at the situation detailed in Figure X-3 in which the tension  $V_{\text{BP}} = [V_{\text{ITO}} - V_{\text{Ca}}] > 0$  is applied at ITO and the potential of Ca remains unchanged. Here, the bands are in a rigid conformation and are horizontal after application of the flat band tension  $V_{\text{BP}}$  (thick, grey lines show the band structure of Alq3 with HOMO and LUMO levels parallel to metal (ITO and Ca) bands and the initial vacuum level).

Once a flat band tension ( $V_{\text{BP}}$ ) and an additional positive tension ( $V_{\text{Ps}}$ ) is applied to the anode (ITO), that is  $V_{\text{appl}} = V_{\text{BP}} + V_{\text{Ps}}$ , the electron levels take up the configuration described in Figure X-4 in which is represented the resulting band movement.

*γ Recapitulation of applied schemes (Figure X-5)* In practical terms, OLEDs are generally fabricated as detailed in Figure X-5-a.

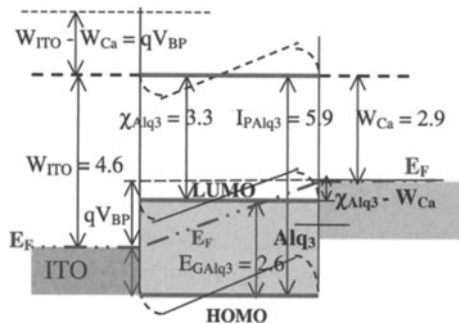


**Figure X-3.** Regime of flat bands.

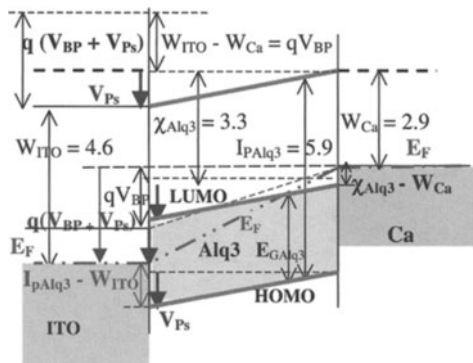


Figure X-4. Band scheme following polarisation  $V_{\text{appl}} = V_{\text{BP}} + V_{\text{Ps}}$ .

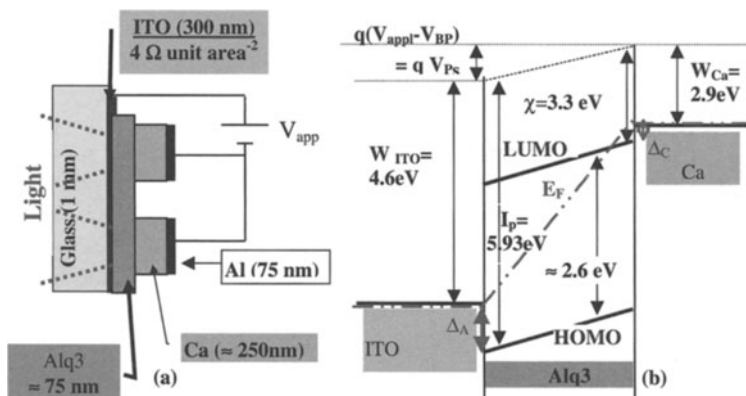


Figure X-5. Practical ITO/Alq3/Ca diode: (a) conception; and (b) band scheme.

Given the results shown in Figure X-4, it was possible to prepare the electronic structure shown in Figure X-5-b for the example system. We can see that the drop in tension which appears of its own accord is in fact what we called  $V_{\text{Ps}}$  (the ‘positive supplementary’ tension applied to the ITO anode), and is equal to the total applied tension minus the flat band tension ( $V_{\text{FB}}$ ). The latter is such that  $V_{\text{BP}} = (W_{\text{ITO}} - W_{\text{Ca}})/q$ . In this example  $V_{\text{BP}} \approx 2$  volts, a non-negligible value in contrast to those generally used of the order of 0 to 15 V.

Important information can be gained with respect to the interfaces, where the barrier at the anode, seen by holes, is equal to  $\Delta_{\text{A}} = I_{\text{pAlq3}} - W_{\text{ITO}}$ , which in this example is  $\Delta_{\text{A}} = 1.3$  eV. Given the widely accepted value  $W_{\text{ITO}} = 4.9$  eV,  $\Delta_{\text{A}}$  can be considered to approximate to 1 eV. Following on from the points noted above at the beginning of this Section, we can imagine that the contact at the anode is not ohmic and risks even being limited by Fowler–Nordheim emissions.

We can note though that at the cathode, there is no barrier to the injection of electrons (the drop in potential energy for electrons being  $\Delta_{\text{C}} = \chi_{\text{Alq3}} - W_{\text{Ca}}$  which

works out as  $\Delta_C = 0.4 \text{ eV}$ ). Indeed the contact can be assumed to ohmic as in the region of this electrode the Fermi level penetrates the degenerated Alq3 LUMO.

## b Experimental behaviour and first interpretations

Studies of  $I(V)$  characteristics have shown that Schottky emissions can give an ideality factor ( $n$ ) of the order 20, a very high value indeed, and an unusually high diode series resistance at  $50 \text{ k}\Omega$ . However, the emission law for tunnelling effects is not completely verified, even at high tensions, and contrary to theory it has been experimentally shown to increase with temperature. In fact, only the TCL law is followed completely within domains which yield electroluminescence (see Figure X-6 for the ITO/Alq3/Ca structure).

The same conclusions as those detailed just above have been reached, qualitatively, for more complicated systems based on ITO/TPD/Alq3/Mg-Ag by Burrows *et al.* [bur 96]. TPD is a material used to reinforce hole injection, and Mg-Ag as the cathode has, like calcium, a low workfunction, but exhibits a slightly lower reactivity [rot 96]. For Burrows *et al.*, interface reactions between the low workfunction electrodes and the electron transport layer (EL) introduce states into the HOMO-LUMO gap and result in ohmic injection at the point of contact. On replacing Mg-Ag with In, which has a higher workfunction, the TCL law is no longer followed and current is not volume limited but controlled by the electrode injecting electrons. More precisely, the ohmic law is followed at low tensions (due to thermally generated carriers of density  $n_0$ ) in thick films, while the SCL law is followed in the same regime for thin films (current varies as  $V^2/d^3$ , so when  $d$  is large, the current is dominated by the simple ohmic law). As the tension increases, the Fermi pseudo-level rises and traps start to fill up. This decrease in the number of empty traps, which now receive few electrons, induces a rapid increase in mobilities and the overall current, resulting in the TCL law being observed ( $I \propto V^{m+1}/d^{2m+1}$ ). At a sufficiently high value of  $V$ , all traps are filled and we should once again find the classic SCL law, although this type of value of  $V$  is rarely obtained without destroying the films.

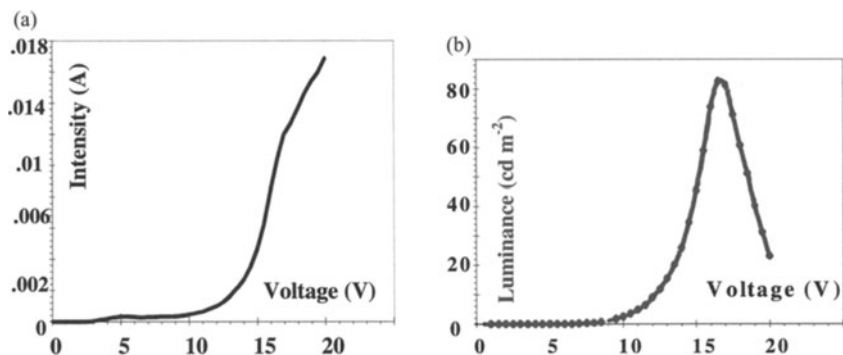


**Figure X-6.** (a)  $I(V)$  characteristics of the ITO/Alq3/Ca structure; (b) Luminescence curve with tension for the ITO/ALq3/Ca structure.

There have been numerous arguments developed as to why the TCL law is observed [bur 94] and [bur 96]:

- when  $m$  is sufficiently high,  $I \propto V/d^2$ , so that when  $I$  is a constant,  $V = f(d^2)$  is a straight line as indicated in Figure X-7-a;
- as  $T_t = E_t/k = mT$ ,  $m$  must increase as  $T$  decreases, again shown in Figure X-7-b;
- additionally,  $m = T_t(1/T)$ , and plotting  $m = f(1/T)$  gives  $T_t = 1780$  K and  $E_t = 0.15$  eV which is a value in agreement with that given by quantum calculations (0.21 eV and detailed in Chapter IV, Section III-3 (see also Figure X-7-c));
- taking the law  $I \propto V^{m+1}/d^{2m+1}$ , it is possible to determine  $N_t = 3 \times 10^{18} \text{ cm}^{-3}$  and  $N_c = 10^{19} \text{ cm}^{-3}$  (also using the formula for  $J_{\text{exp}}$  given in Chapter VI, Section IV-6-b). In addition, from the volume mass, the density of molecular sites can be evaluated to the order of  $2 \times 10^{21} \text{ cm}^{-3}$ . We can conclude that electrons injected into LUMO levels are subsequently strongly localised and with a high proportion of which being held in trap levels, from which they can recombine (radiatively) with holes; nevertheless, their low concentration with respect to the overall number of molecular sites can explain their low quantum yield in Alq3 (around 1 %).

Figure X-7-d gives a general view of the mechanism of electroluminescence.

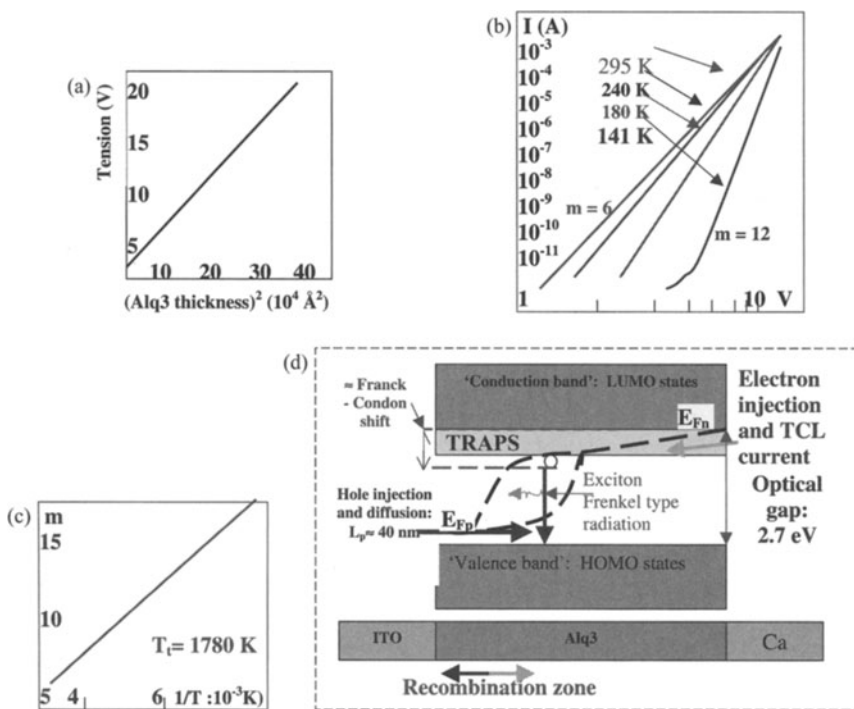


**Figure X-7.** (a) Line  $V = f(d^2)$  in which  $d \equiv$  film thickness. (b)  $I(V)$  curves with varying  $T$ . (c) Line  $m = f(1/T)$  in which the slope gives  $T_t$ , that is  $E_t = kT_t$ . (d) Electroluminescence mechanisms in Alq3.

An ‘academic’ hypothesis of the TCL model operating with the trapping time being longer than the average transit time (for a hop between two molecules in the LUMO) was proposed to answer criticisms concerning electronic transport in the model, which envisages a band structure arising from the solid (see discussion in Chapter VI, Section IV-2-a). The mechanism of transport limited by traps (TCL) simply demands a sufficient delocalisation of charges to establish a thermal equilibrium between free and trapped charges [bur 96]. As we have seen,  $N_t \approx N_c$ , indicating that each electron introduced into the LUMO band will subsequently and automatically be trapped on an Alq3 molecule. A relaxation would follow yielding a polaronic state which would then result in conduction occurring through hopping mechanisms appropriate to these quasi-particles (with reduced mobility, as experimentally confirmed with  $\mu_n \approx 5 \times 10^{-5} \text{ cm}^2 \text{ V}^{-1} \text{ s}^{-1}$ ).

### c Controversial points and proposed improvements [ioa 98]

$\alpha$  *Controversial points* [ioa 98] There are essentially two details which remain under discussion:

- that concerning the actual existence of the band scheme for small molecules, although this argument is not discussed here; and
- that which relates to the hypothesis of invariance of mobility with respect to an electric field, which is used in establishing the SCL and TCL laws. There are the following considerations which can be brought to mind:
  - up until now, because of the low mobilities and short mean free pathways (mfp) observed in organic solids, it was thought that between any 2 collisions the carriers could not gain much energy from an applied field, and that mobilities and transport were governed by temperature (T) through thermal vibrations overcoming barriers and were essentially independent of the applied field (in contrast to inorganics).
  - However, in disordered systems, the general expression for  $\mu$  is empirically obtained and has only been verified through Monte Carlo simulations in terms of position and energy for individual jumps between disordered sites [bäs 93]:

$$\mu = \mu_0 \exp\left(\frac{-\Delta^2}{k^2 T^2}\right) \exp\left(C \left\{ \left[\frac{\sigma}{kT}\right]^2 - \Sigma^2 \right\} E_a^{1/2}\right)$$

in which  $\mu_0$  is the mobility in a zero field,  $\sigma$  and  $\Sigma$  are parameters which characterise, respectively, the energetic (diagonal disorder) and positional (non-diagonal disorder) degrees of disorder [cam 98b] and [shi 98], while  $\sigma$  represents the width of the Gaussian distribution of transport states and  $\Delta = 2\sigma/3$ .

Alternatively, Gill’s empirical law for charge transfer, established using amorphous complexes is also used [gil 72]:

$$\mu(T, E_a) = \mu_0 \exp\left(-\frac{\Delta_0}{kT_{\text{eff}}}\right) \exp\left(G \frac{\sqrt{E_a}}{kT_{\text{eff}}}\right), \quad \text{where } \frac{1}{T_{\text{eff}}} = \frac{1}{T} - \frac{1}{T_0}$$



in which  $\Delta_0$  is the activation energy at zero field,  $T_0$  is the temperature at which straight lines  $\mu = f(1/T)$  with respect to the applied electric field gives an intersection (experimentally, these lines converge at  $1/T_0$ ).

Generally for small molecules, the derived mobility of carriers increases with the applied field. In the presence of energetic disorder, the electric field aids electrons overcome potential barriers due to energy differences between sites, which affect mobilities [ioa 98]. The mobility follows a Poole–Frenkel like law (which works over concentration—see Chapter VI, Section VI) of the form:

$$\mu \propto \mu_0 \exp(\alpha E_a^{1/2})$$

from which variations with temperature can be obtained by placing  $\tau = \tau_0 \exp(-\Delta/kT)$  into  $\mu = q\tau/m$ .

However, in certain materials such as polymers doped with molecules to the order of 5 to 25% by mass, mobilities do decrease above a certain value of the applied field  $E_a$ . As shown in Figure X-8, in qualitative terms, we can suppose that this effect is due to ‘diagonal disorder’ associated with the variable distances between molecules [gre 95]. Under a weak field, there are many available and facile pathways (short distance hops in different directions with respect to the field) which are, nevertheless, removed once a strong field is applied.

$\beta$  *Possible models* The presence of trapping levels has been shown not to be necessary by Conwell’s group, by modelling the characteristics of organic materials [ioa 98]. The group has even supposed that such levels do not exist, because in examples where only electrons have been injected (using the same LiF/Al contacts on either side, which are supposedly ohmic), the I(V) curves are identical whether or not the tension is interrupted during the measurements, indicating negligible electron trapping. We should consider, however, the kinetics of such an experiment—see the preceding Section II-1-b. Experimental characteristics may be verified simply by using Ohm’s law, into which can be included the appropriate law for variations in mobility:  $\mu = \mu_0 \exp(\alpha E_a^{1/2})$  where  $\mu_0$  is the mobility under a weak field and  $\alpha$  a parameter increasing with disorder. This has been found to be true when using  $I = ne \mu_0 [\exp(\alpha E_a^{1/2})] E_a$ , with  $\alpha = 1.3 \times 10^{-2} \text{ cm}^{0.5} \text{ V}^{-0.5}$  and  $\mu_0 = 6.5 \times 10^{-10} \text{ cm}^2 \text{ V}^{-1} \text{ s}^{-1}$ .

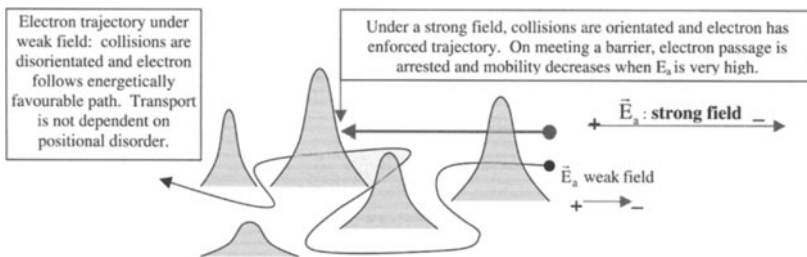


**Figure X-8.** Qualitative description of charge transport in strong and weak fields.

It is important to state though that the presence of trapping levels has been confirmed using a variety of techniques:

- Thermo-Stimulated Luminescence (TSL) [for 98] in which the principal peak was modelled using a distribution of traps with energies between 0.25 eV and 0.15 eV. Two supplementary peaks were observed towards lower energies (around 0.07 eV); and
- Photodipolar absorption [jeo 01b] which results from a thermo-photo-dielectric effect due to:
  - a photonic, preliminary luminescence excitation with electron ‘pumping’ onto trap levels (typically with a Wood lamp emitting light at  $\lambda = 365$  nm);
  - a thermal effect with an initial cooling then heating of the sample; and
  - a dielectric effect by reorientation of dipoles associated with trapped charges using a radio frequency field.

This technique has given rise to traps with depths of approximately  $E_t = 0.2$  eV, and has shown that traps can persist, following excitation with daylight, for around 1 hour.

It seems reasonable enough to assume that effects due to space charges and mobility dependencies on the applied electric field should affect  $J(V)$  characteristics [she 98]. However, if we look closely at these characteristics with respect to TCL representations (which is the most widely respected law), then we can see that they do not follow perfectly straight lines. There is very possibly an improvement which can be made to the TCL law by taking into account mobility dependence on other parameters such as temperature and the electric field.

If we look again at the general expression for current density, ignoring the diffusion term, we have  $J = \rho v = qn\mu E$ , that is,  $J = qn\mu V/d$ . In general, as above discussed, the concentration  $n$  of current limited by space charge are in the form  $n \propto V^m$ . Once only free (untrapped) charges contribute to the space charge, then  $m = 1$  (giving the saturation current  $J_s$  in Mott-Gurney’s law). If charge space is dominated, however, by trapped charges (as can be supposed given the above detailed results) within traps of exponential energy distribution, we now have  $m = T_c/T$  where  $E_t = kT_c$ . As detailed above, we now have  $J \propto V^{m+1}$ , and in addition, if we suppose that mobility ( $\mu$ ) is not actually a constant, the  $J(V)$  law will depend on variations in  $\mu$  and will no longer follow a law based on  $V^{m+1}$ , if  $\mu$  varies with the electric field, that is with  $V/d$  (where there is a break with the TCL law).

The essential problem is to resolve the dominant effect (space charge or mobility) in any specific tension domain. If we can suppose that mobility varies negligibly with respect to  $E_a$ , so that Laplace’s equation may be integrated, we can directly introduce the appropriate mobility law  $\mu(E_a, T)$  into TCL type equations.

### 3 Polymers

#### a Initial models [Par 94]

$\alpha$  Emissions through tunnelling effects (Fowler-Nordheim) In the case of poly(2-methoxy,5-(2'-ethylhexoxy)-*para*-phenylene vinylene), commonly called MEH-PPV,

Parker showed by experiment that carrier injection is controlled by the height of the electrode-polymer barrier. For the demonstration, diodes which gave preferential injection of one charge carrier type over the other (see Figure X-9) were used.

This effect is classically obtained by varying differences between the workfunction of the cathode metal and the electron affinity of the polymer on the one hand, and the workfunction of the anode metal and the ionisation energy of the polymer on the other. In so doing, at the metal-polymer interfaces, one can favour the passage of holes and destroy that of the electrons, as shown in Figure X-9-a, or indeed favour the passage of holes and destroy that of the holes, as in Figure X-9-b.

With MEH-PPV, the best results have been obtained using a calcium cathode and an indium tin oxide (ITO) anode. Experimental curves have shown that the  $I = f(V)$  curves:

- uniquely depend upon the value of the electric field (and not the tensions, as is found for Schottky inorganic structures); and
- are virtually independent of temperature.

This behaviour can be seen as characteristic of tunnelling effect, following the Fowler-Nordheim equation, over a triangular barrier.  $\text{Log}(I/E_a^2) = f(1/E_a)$  is a straight line, and permits a deduction of the barrier heights at the interface between the injecting electrode and the polymer (for ITO see Figure X-9-a, and for Ca see Figure X-9-b). This conforms with the scheme for rigid bands as the bands curves can only be at a minimum given the low carrier density within the polymer, estimated to be of the order of  $10^{14} \text{ cm}^{-3}$  from  $C(V)$  measurements.

$\beta$  *Functioning voltage and yield* Generally speaking, I-V characteristics are essentially determined by the majority carrier, which are in turn determined, be they holes or electrons, by the lowest electrode-polymer barrier, respectively, situated between the anode and the polymer or between the cathode and the polymer. However, the yield of a diode is determined by the minority carriers injected at the highest level of the barrier, a parameter which we will look at in more detail below. Indeed, the

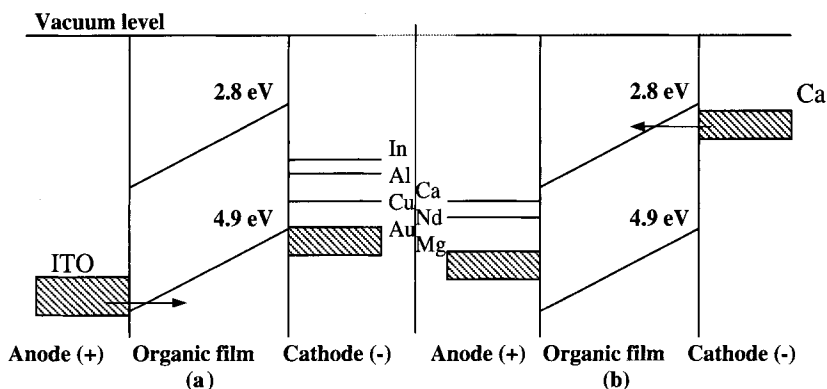
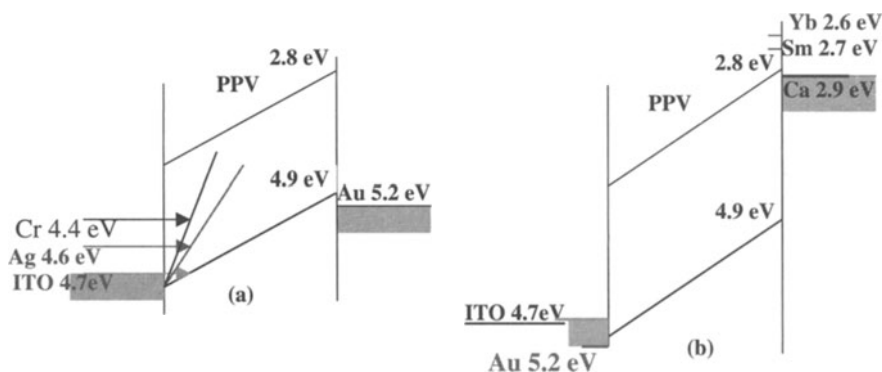


Figure X-9. PLED structure favouring: (a) hole; and (b) electron injection.

yield can be varied by changing the barrier observed by minority carriers, and this can be done without modifying the function voltage (the barrier observed by majority carriers). The inverse is also possible. On going from ITO to Ag and then to Ca, as shown in Figure X-10-a, the anode tension must be increased so that hole injection can be maintained (respectively, 10, 15 and 25 V). The slopes of the bands ensure that tunnelling effects are as large as the workfunction of the metals are low.

There is an optimised yield when the barrier observed by minority carriers is zero, as in Figure X-10-b, *i.e.* the barrier at the cathode is as low as possible. However, the lowest functioning voltage is obtained when a zero (minimum) barrier is observed by the majority carriers (at the anode). Diode optimisation is generally accepted when the chosen electrodes are such that the workfunction of the anode is equal to the ionisation potential of the polymer, and that the workfunction of the cathode is equal to the electron affinity of the polymer. For the system here, using MEH-PPV, the best pair of electrodes are thus ITO for the anode and calcium for the cathode (See Annex A-11, Section II-1 for the description of MEH-PPV). The yield is around 1% for a field of approximately  $3 \times 10^7 \text{ Vm}^{-1}$ . We can remark that the barrier observed by holes is around 0.2 eV, and for electrons is near 0.1 eV, and that the roles of majority and minority carriers has been reversed. It has been shown the yield can be improved when using Ag as an anode, and at the cathode, with Sm (2.7 eV) or Yb (2.6 eV), the operational voltage does not decrease and chemical reactions between the low workfunction metals and the polymer may occur—risking the formation of interfacial barriers.

$\gamma$  *Starting and function tensions* The starting voltage depends only on the band gap of the polymer, and would be equal to this gap if it were not for non-zero barriers at the interfaces (see Figure X-11-b). The tension does not depend on the thickness of the polymer film—as verified by the characteristics shown in Figure X-11-d. The minimum voltage required for the diode to function—that is to produce tunnel effects and emit a visible light—as shown in Figures X-11-c and d, does however depend on film thickness, as the tunnel effect is a current fixed by the field, which has a value



**Figure X-10.** (a) Effects on tunnelling at the barrier due to work functions; and (b) an optimised component.

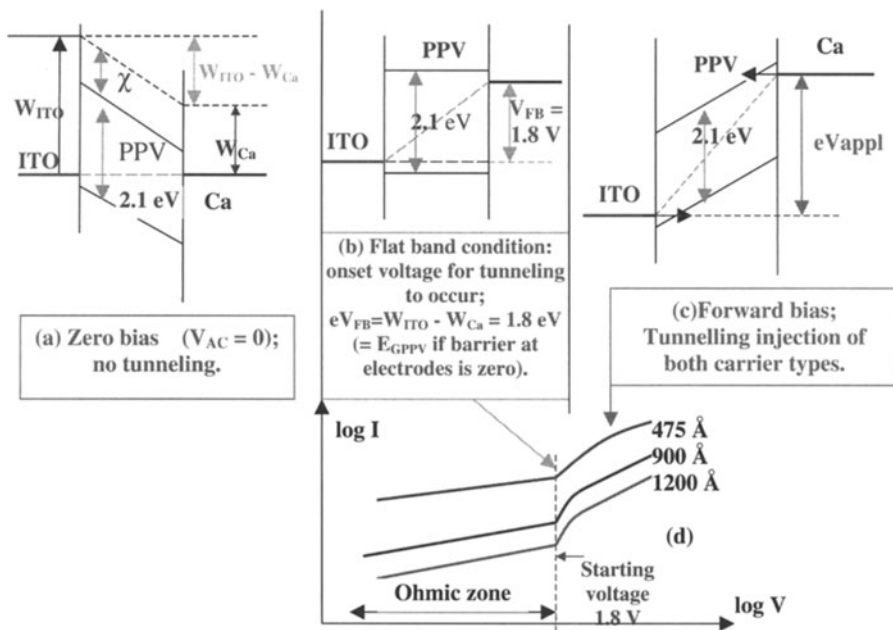


**Figure X-11.** Band structures of ITO / PPV / Ca system: (a) zero bias; (b) at flat band condition; (c) forward bias; and (d) corresponding  $\log I = f(\log V)$  characteristics.

dependent on film thickness. The minimum functional voltage is sensitive to barriers at the electrodes, in contrast to the starting voltage which would vary directly by  $0.1 \text{ eV}$  for a barrier of  $0.1 \text{ eV}$ , as detailed in Figure X-11-b.

### **b The roles of current limited by space charges (SCL), traps (TCL) and double injection (VCC)**

Bradley and his team have shown that for PPV used in the simple set-up ITO/PPV/Al [Cam 97], the Fowler-Nordheim law did not correctly account for experimentally obtained results with respect to temperature, film thickness and the amplitude of  $I(V)$  characteristics. At high tensions, the law observed was of the TCL type, with an exponential distribution of traps of average depth of  $0.15 \text{ eV}$ . At lower tensions, the law followed was space charge limited (SCL), exhibiting a mobility which varied with temperature and field in accordance with the Arrhenius law. The transport through the volume can be seen as a hopping mechanism between states distributed following a Gaussian curve, with deep sites playing the role of traps.

Another study, run simultaneously to that detailed above and following the same idea as that detailed previously [par 94], was carried out in the Philips laboratories [Blo 97a, Blo 97b and Blo 98]. The Fowler-Nordheim law gave rise to currents considerably higher (by several orders) than those found experimentally. Two mechanisms were studied, those of hole and electron transport. Here we will describe each individually.

$\alpha$  *Hole transport* Using the ITO/PPV/Au structure, which favours hole injection only, it was shown that current followed the SCL law, as shown in Figure X-12-a. We have  $J_s = (9/8)\epsilon\mu_p V^2/d^3$ , showing that current is volume and not electrode limited. With  $\epsilon = 3$ , hole mobility could be estimated as  $\mu_p = 5 \cdot 10^{-11} \text{ m}^2 \text{ V}^{-1} \text{ s}^{-1}$ . It should be noted that at high fields, a deviation from the SCL law occurred (experimentally, the current was higher than that given by  $J_s$ , as shown in Figure X-12-b).

As detailed above, because of ‘non-diagonal’ disorder associated with variable distances between molecules, under low fields facile transport pathways are available (short hops in directions at variance with the applied field) which become inaccessible at higher fields. As the field strength increases, the mobility follows a Poole–Frenkel type law (assuming that traps are not responsible for disorder, as there is a quadratic SCL regime without traps unlike the TCL system).

With  $\mu_0$  the mobility under zero field and  $\Delta$  the energy of activation,  $\mu = \mu_0 \exp(-\Delta/kT_0) \exp(\alpha E^{1/2})$ . This gives  $\Delta = 0.48 \text{ eV}$  and  $\mu_0 = 3.5 \times 10^{-3} \text{ m}^2 \text{ V}^{-1} \text{ s}^{-1}$ . The factor  $\alpha$  has been empirically defined with respect to temperature as  $\alpha = G \left( \frac{1}{kT} - \frac{1}{kT_0} \right)$ . The insertion of  $\mu$  into  $J_s$  has been used to obtain an excellent agreement with experimentally obtained  $J(V)$  curves. Here,  $G = 2.7 \times 10^{-5} \text{ eV V}^{0.5} \text{ m}^{-0.5}$  and  $T_0 = 600 \text{ K}$ , values similar to those obtained for poly(*N*-vinyl carbazole) (PVK).

We should note again, however, that to obtain  $J_s$  from the SCL law, we have to suppose that  $\mu$  is a constant with respect to  $x$ , but  $E = E(x)$ , so we have to state that the variation is sufficiently small so as to be able to perform the integration!

$\beta$  *Electron transport* The example used here is that of Ca/PPV/Ca which favours electron transport and is shown in Figure X-13. The current due only to electrons is less than that due only to holes, up to 3 orders at low tensions. Limited by traps, electron current is strongly field dependent, and follows a TCL law, that is  $J \propto V^{1+1}/d^{2+1}$ , in which traps are exponentially distributed. The slope of  $\log J = f(\log V)$  gives  $m$  and  $T_t = 1500 \text{ K}$  and  $N_t = 10^{18} \text{ cm}^{-3}$ .

$\gamma$  *Recombinations* On the basis of bimolecular recombinations, mechanisms involved in recombinations have also been studied [Blo 97a]. The  $I(V)$  characteristics

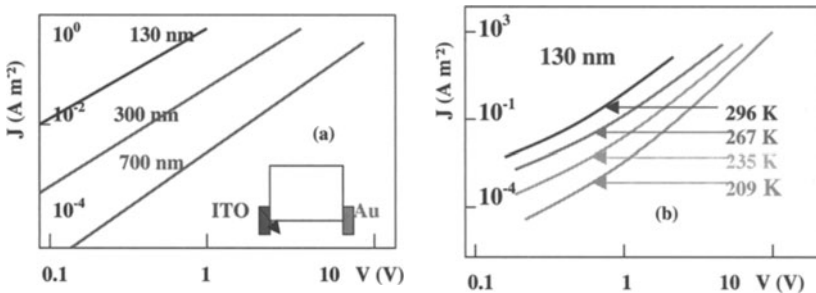


**Figure X-12.** (a) SCL  $I(V)$  curves at  $T_{\text{ambient}}$ ; and (b) deviation from the SCL law at low temperature and under a high field.

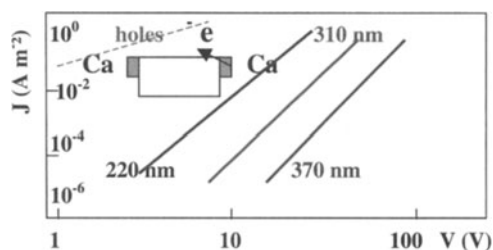


Figure X-13.  $I(V)$  characteristics for electron transport.

give rise to only a slight difference between single hole and double injections. Double injections are hole dominated while electrons are highly trapped. The recombination constant has been estimated to show that only around 5 % are actually radiative, the greater part in PLEDs occurring non-radiatively.

### III Strategies for improving organic LEDs and yields

#### 1 Scheme of above detailed processes

Figure X-14 details the various stages towards electroluminescence [Bra 96].

To give a summary of the different stages, covered above:

- A in which currents {1} (electrons) and {2} (holes) are injected, respectively, giving rise to leak currents {1'} and {2'}. Figure X-14 shows current densities and carrier speeds;

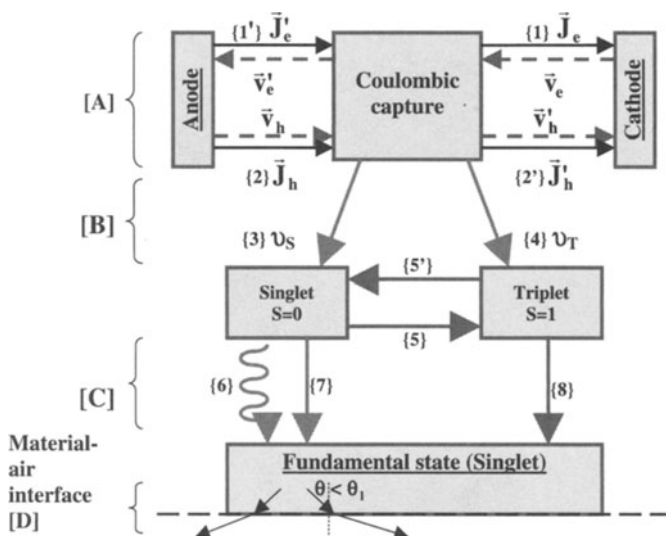


Figure X-14. Basic mechanisms in electroluminescence.

- B in which electron-hole recombinations occur, resulting in the initial formation of excitons in singlet {3} and triplet {4} states;
- C in which excitons are dissipated either through the radiative {6} (singlet  $\rightarrow$  singlet) or non-radiative {7} (singlet  $\rightarrow$  extinction centre) and {8} (triplet  $\rightarrow$  singlet) pathways; and
- D in which there is refraction of the light beam on going from the material to air interface.

## 2 Different types of yields

As detailed in Chapter VIII, in general terms, different types of yields may be defined as:

### a The external quantum yield

This yield, the external quantum yield, is defined by:

$$\eta_{\text{ext}} = \frac{\text{number of photons emitted outside the structure}}{\text{number of injected charges}} = \eta_{\text{EL}}.$$

The external quantum yield can also be thought of as the product of two other yields:  $\eta_{\text{ext}} = \eta_{\text{opt}} \eta_{\text{phint}}$ , where  $\eta_{\text{phint}}$  is the internal quantum yield and  $\eta_{\text{opt}}$  the coefficient given in Chapter VIII to account for refractions at the diode-air interface (step D in Figure X-14). With an organic material with an indice  $n$  greater than that of air, only internal emissions incident to the interface at an angle below the limiting angle  $\theta_1$  can escape towards the exterior. The result is a non-negligible loss, as the factor  $\eta_{\text{opt}} \approx 1/2n^2$  (calculated in Chapter VIII, Section III-2, using Lambert emissions) is of the order of 0.2 when  $n = 1.6$ . External yields are therefore only around 20 % of internal yields. Efforts required to improve this figure are detailed later on.

### b The internal quantum yield

The internal quantum yield can be thought of as the product of three different factors. Each one is with respect to the steps A, B and C, detailed in Figure X-14, and can be singled out in the defining equation for this yield,  $\eta_{\text{phint}} = \gamma \eta_r \phi_f$ , where:

- $\gamma$  is the level of recombination of injected carriers *i.e.*  $\gamma = J_r/J_T$ . In Step A, with  $\vec{J}_T = \vec{J}_h + \vec{J}'_e = \vec{J}_e + \vec{J}'_h$  (total current density) and  $\vec{J}_r = \vec{J}_h - \vec{J}'_h = \vec{J}_e - \vec{J}'_e$  (recombination current density) then  $\gamma = 1$  if there are no leak currents ( $\vec{J}'_e = \vec{J}'_h = 0$ ) and there is an exact equilibrium between the two types of current, *i.e.*  $\vec{J}_e = \vec{J}_h$ . However, for example, if all holes are used up in recombinations,  $\vec{J}'_h = 0$ , then some electrons will traverse the whole structure without recombining giving  $\vec{J}'_e \neq 0$ , and  $\gamma < 1$ ;
- $\eta_r$  is the generated fraction of radiative singlet excitons, as denoted in Step B, due to the probabilities of the spins required to yield electroluminescence from



singlet states ( $S = 0, M_s = 0$ ) and triplets ( $S = 0, M_s = -1, 0, 1$ ).  $\eta_r$  can be directly estimated from  $\eta_r = \nu_S/[\nu_S + \nu_T] = 0.25 = 25\%$ ; and

- $\Phi_f$  is the fluorescence quantum yield (see Step C) and while always below 1, it can reach up to 0.7, the loss being due to inevitable, non-radiative recombinations [7]. The latter are due to singlet excitons recombining, in general, close to the interfaces, or because of the presence of extinction centres such as impurities and non-radiative traps. In addition, bimolecular recombinations do not operate at 100%, even with the low mobility of carriers in organic media.

### c The quantum energy yield

The quantum energy yield is expressed in  $W W^{-1}$  and represents the ratio

$$\eta = \frac{\text{Emitted luminous energy}}{\text{Supplied electrical energy}} = \frac{n_{\text{photons}} h\nu}{n_{\text{charges}} eV} = \eta_{EL} \frac{h\nu}{eV}$$

From the above equation it is evident that for a given emitted wavelength (given  $h\nu$ ), the lower the operational voltage, the higher the energetic yield. This explains the interest in trying to reduce the operating voltage. Typically, organic materials exhibit values of  $h\nu/eV$  of around 0.3.

### d The luminous yield

The luminous yield takes into account the photo-optical response of the human eye, which is defined by the relationship  $\eta_L = \eta \cdot K(\lambda)$  in which  $K(\lambda)$  is constant relating observed and actual scales of energy. At  $\lambda = 555 \text{ nm}$ ,  $K(\lambda) = 683 \text{ lm W}^{-1}$ . This yield is thus expressed in lumen watt<sup>-1</sup>.

## 3 Various possible strategies to improve organic LED performances

Luminance, which depends on the intensity of emitted light, is determined principally by the current density of minority charge carriers and then by the number of these carriers which undergo radiative recombinations with the majority carriers.

The quantum yield, which can be written as the product of the four terms detailed just above  $\eta_{EL} = \eta_{opt} \eta_{\phi} \eta_{int} = \eta_{opt} \gamma \eta_r \Phi_f$ , can be optimised with each of these terms.

The optimisation of these components necessitates:

- the highest number of minority carriers undergoing radiative recombinations. This in turn necessitates the use of efficient electrodes and injection layers for these carriers (with a high injection current or ohmic contact). Given that interfaces tend to favour the presence of defects, which act as extinction centres of luminance, it is judicious to try and displace the recombination zone for the minority carriers towards the bulk of the material. This necessitates the use of a minority carrier transport layer, as the injection layer may not necessarily be good for minority charge transport;

- an improved method for allowing otherwise trapped emitted light to exit the device. Microcavities, structures which diffuse light, can help direct the emissions and improve the otherwise highly detrimental value of  $\eta_{\text{opt}}$ ;
- as high a possible level of injected carrier recombination.  $\gamma = J_r/J_T$  will increase if:
  - $J_r$  is large and, as previously noted, there is as great a current of minority carriers as possible, which in turn demands as low a leak current as possible. The use of layers confining the holes and electrons can respond to this demand;
  - $J_T$  is small and therefore the majority current is not too great with respect to the minority current. The injection of majority charges which do not go on to recombine with minority charges adds nothing beneficial to the optical behaviour of the device, uselessly consumes current and results in a harmful heating effect which reduces its lifetime [tes 98];
- the highest possible level of radiative exciton production possible (*i.e.* a high value of  $\eta_r$ ). This in turn means recovering the highest possible percentage of triplet excitons which result in electron injection. The use of phosphorescent materials and mechanisms which can transfer triplet to singlet states can be envisaged; and
- the fluorescence quantum yield ( $\Phi_f$ ) should be as high as possible. Generally, in the solvated state, this factor can be very high, even near to 1 (for example, laser dyes). However, in the solid state, this value is generally much lower, typically of the order of 0.1 to 0.5. This is due to forbidden dipolar transitions between the fundamental and lowest excited states which appear, either localised on a dimer or as a band in the solid state, following the breakdown of degenerate levels present in the solvated state [sch 00]. Thus well organised and crystalline states should be avoided, as we have already seen in Chapter VII, Section VI-6. There is nevertheless a condition that can be imposed upon the latter remark, and that is that any disorder imposed should not be so great as to limit any gains in transport (injection and that of minority charge carriers) which can arise from the organisation of a system (where charge mobility can be high) and would otherwise improve the fluorescence yield. This is a characteristic of certain types of materials, for example those based on discotic molecules [seg 01]. In addition, as previously mentioned, non-radiative centres should be excluded, by the use of layers free of structural faults or other imperfections.

Another, delicate problem is that of ageing, which results from external effects or from the electrodes. The former may be resolved using encapsulation, while the latter is slightly more difficult but can be resolved using barrier layers, an example of which is PPX deposited *via* VDP (see Chapter VII, Section I-3).

There is no way we could even pretend to detail all the possible strategies that have been devised to answer the above criteria. Instead, we shall limit this Chapter to only the most currently used solutions, especially when we look at actual applications of these devices. Nevertheless, we shall briefly detail why some organic solids are p-type (polymers such as PPV or poly(*para*-phenylene) (PPP)) and why others are n-type (small molecules such as chelates), at least when protected from oxygen.

## IV Adjusting electronic properties of organic solids for electroluminescent applications

### 1 A brief justification of n- and p-type organic conductivity

#### a Small molecules

The best known example is Alq<sub>3</sub>, in which the chelation, or complexation, of the Al<sup>3+</sup> ion with 3 ligands leaves the aluminium reduced in electron density to become effectively an electron acceptor. When assembled with other Alq<sub>3</sub>s, this character results in a facile transport of electrons, and thus Alq<sub>3</sub> is considered an n-type material.

Another example is that of layers of the complex rare earth complex of diphtalocyanine Pc<sub>2</sub>M, where Pc is [C<sub>32</sub>H<sub>16</sub>N<sub>8</sub>]<sup>2-</sup> and M is the rare earth ion. These materials are intrinsically n-type (under vacuum). Scandium diphtalocyanine is paramagnetic, as its outer orbital is but half-filled and has unpaired electrons delocalised over the phthalocyanine macrocycles. The n-type conductivity, under vacuum, can be due to intermolecular transfer of these single electrons. On contact though with oxygen, the gas is chemi-absorbed and forms oxygen- Pc<sub>2</sub>M bonds. The oxygen cannot be removed by the simple application of a vacuum, due to the formation of a charge transfer complex in which the Pc<sub>2</sub>Sc is lacking in electrons and the oxygen gains a negative charge. The positive state of the Pc<sub>2</sub>Sc moves as a hole through diphtalocyanine molecules which surround the negatively ionised oxygen molecule. In effect, these materials change to being p-type once exposed to air, as do many polymers which are subject to a similar mechanism.

#### b Polymers

In general, polymers tend to behave as p-type semiconductors. The origin of this can again be contributed to the presence of oxygen [gre 94, p 58]. We can also add that in the case of PPV, obtained like many other polymers from the thermal conversion of a precursor, that the process used for its preparation can give rise to many pendent bonds. A possible result is therefore the transfer of electrons through the corresponding levels, also possibly generated by thermally diffused oxygen, from levels at the highest point of the polymer valence band. The latter thus generates holes. The generation of this p-type character of polymers can also be evidenced on doping using ion implantation [mol 96].

#### c Adjusting the type of conduction

The type of conduction of a material can be changed by altering the 'backbone' of the organic material, simply by adding on electron donating or accepting groups (see also Chapter XII, Section II-3). For example, PPV can be modified to facilitate:

- the injection of electrons by increasing the electron affinity ( $\chi$ ) of the polymer on adding electron attracting groups, such as cyano (CN), onto its backbone.

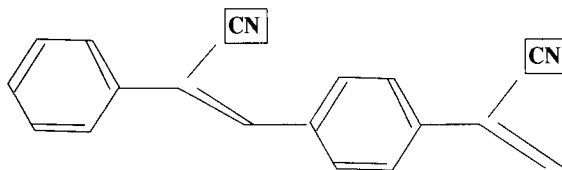


**Figure X-15.** Structure of cyanated poly(*para*-phenylene vinylene) (CN-PPV).

Figure X-15 shows the example of CN-PPV [bra 96]. Even aluminium can be used to replace calcium as the cathode with this material, without altering the yield;

- the injection of holes by stabilising their presence on the polymer by modifying it with electron donors such as alkoxy ( $-OR$ ) or amine ( $-NH_2$ ) groups.

## 2 The problem of equilibrating electron and hole injection currents

As detailed above, the equilibration of electron and hole injection currents is essential in order to generate excitons. If this cannot be done then:

- a large current of electrons or holes can pass through the device without generating excitons, an obligatory step in the process of light emission, thus reducing the yield; and
- there is an initial formation of excitons only to be reduced in the neighbourhood of one or the other of the electrodes (the cathode or the anode if, respectively the majority current is holes or electrons) in a process tied to the presence of default extinction sites of the organic-inorganic interface.

There are two methods by which an equilibrium can be reached (Figure X-16):

- adjust the workfunctions of the metallic electrodes so that the barriers at both organic-inorganic interfaces are close, in a method only valid if the current is determined by injection and not by the bulk. However, this can mean the use of reactive electrodes, which suffer from problems which will be detailed in Section 3 below; and
- modify the organic solid to the workfunction of the metallic electrodes so as to reduce the size of the barriers at the two interfaces. Electron affinity and ionisation potentials are parameters used to choose appropriate materials, although the choice is also governed by the type of transport.

## 3 Choosing materials for electrodes and problems encountered with interfaces

A very simple and conventional structure is illustrated in Figure X-16, into which PPV or Alq3 can be placed.



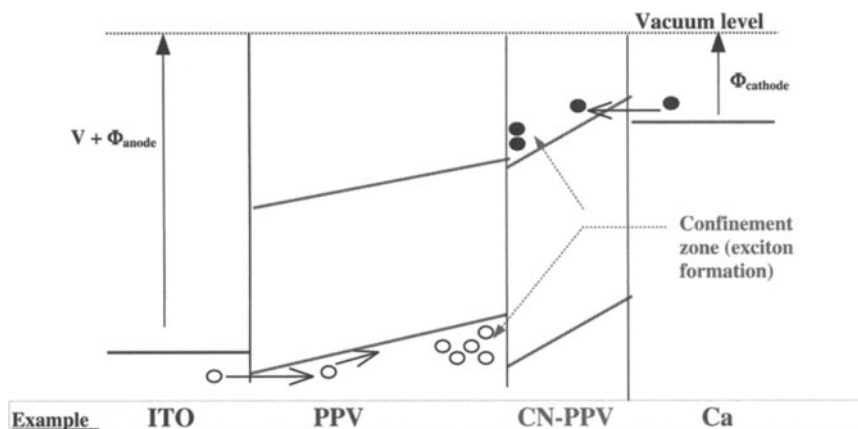


Figure X-17. Confinement zone formation.

#### 4 Confinement layers and their interest

It was very quickly realised that confinement layers were necessary to improve the probabilities of carrier recombinations [fri 92], even though organic materials provide high probabilities due to the relatively low carrier mobilities. The use of this layer though also allowed greater separation of the recombination zone from the electrode interfaces. As shown in Figure X-17, the confinement zone is obtained by choosing materials which at their interfaces form barriers against holes coming from the anode and against electrons coming from the cathode.

### V Examples of organic multi-layer structures: improvements in optoelectronic properties

#### 1 Mono-layer structures and the origin of their poor performance

As an example of a mono-layer structure we will detail ITO/Alq<sub>3</sub>/Ca. Figure X-5 shows that while electrons may be easily injected at the cathode towards the emitting layer, as there is no potential barrier, a similar remark cannot be made for holes. The high potential barrier, around 1 eV, which holes observe at the interface between anode and Alq<sub>3</sub>, reduces any charge injection. This can only be overcome by the application of a high potential, which results in charge transfer, notably, by tunnelling effects. As previously discussed, luminance and electroluminescent yields are strongly dependent on the minority current. With the Alq<sub>3</sub> molecule being n-type, the difficulty found in injecting holes explains to a greater degree the poor luminances obtained with mono-layer structures. To reduce these problems, different types of layers can be used and there are examples of di-layer, tri-layer, and even multi-layer structures.

## 2 The nature of supplementary layers

Independent of the nature of the emitting organic layer (the organic material used original in a mono-layer device), various other layers can be introduced. Generally speaking, these layers can be termed:

- Hole Injection Layer (HIL);
- Hole Transport Layer (HTL);
- Electron Injection Layer (EIL); and
- Electron Transport Layer (ETL).

The following paragraphs detail the way in which these layers function and will exclude descriptions of the operation of chemical groups from which they come, a subject covered elsewhere [bar 00b]. Appendix A-10 does however give the chemical formulae for molecules and polymers from which the layers are formed. HIL and HTL layers are particularly necessary when the emitting layer is made of a small molecule such as Alq<sub>3</sub> which favours electron transport. When the emitting layer favours hole transport, for example with polymers and notably PPV, it seems reasonable that to aid minority carriers, electrons injected at the cathode, EIL and ETL layers should be used. Here, we will study only examples relating to small molecules.

It is worth adding that, as we have seen in Chapter VIII, there are effects associated with different physical treatments of the emitting layer, which can be similar to those obtained using various chemical layers. We shall see in Section 4 that the densification by ion beam assisted deposition of the emitting zone in contact with the anode can augment up to 10 times optoelectronic performances of OLEDs.

## 3 Classic examples of the effects of specific organic layers [tro 01]

### a HIL layer effect

The HIL layer is in contact with the anode. One of its many roles is to perfect the planeness of the interface, reducing effects caused by points which otherwise locally rupture the dielectric field. Another of its roles is to act as a barrier against impurities, notably oxygen, which diffuse from the ITO anode towards the organic emitter. If allowed through, oxygen gives rise to premature ageing of the organic layer and non-radiative centres may be formed.

The most widely known material, which fulfils this role, is poly(3,4-ethylenedioxythiophene) doped with poly(styrene sulfonate) (PEDOT-PSS) and it can be prepared as a film using spin coating. Alternatives, although less efficient, are available in the form of copper phthalocyanines.

In order to study the benefits of using an HIL layer, optimised structures of ITO/Alq<sub>3</sub>/Ca/Al and ITO/PEDOT-PSS/Alq<sub>3</sub>/Ca/Al have been compared. It was found that the monolayer structure had a performance which was considerably improved upon by the bilayer structure. As shown in Figure X-18, the luminance for the former was 49 cd m<sup>-2</sup> (at 18.0 V) while the latter displayed greater than 5000 cd m<sup>-2</sup> (at *c.a.* 9.2 V). The threshold voltage, in the same order, dropped from 8.0 to 4.1 V,

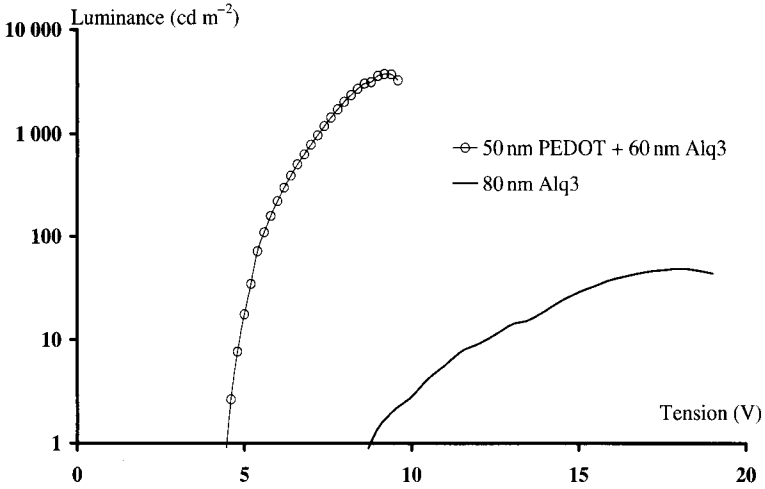


**Figure X-18.**  $L = f(V)$  characteristics for ITO/Alq<sub>3</sub>/Ca/Al and ITO/PEDOT-PSS/Alq<sub>3</sub>/Ca/Al structures.

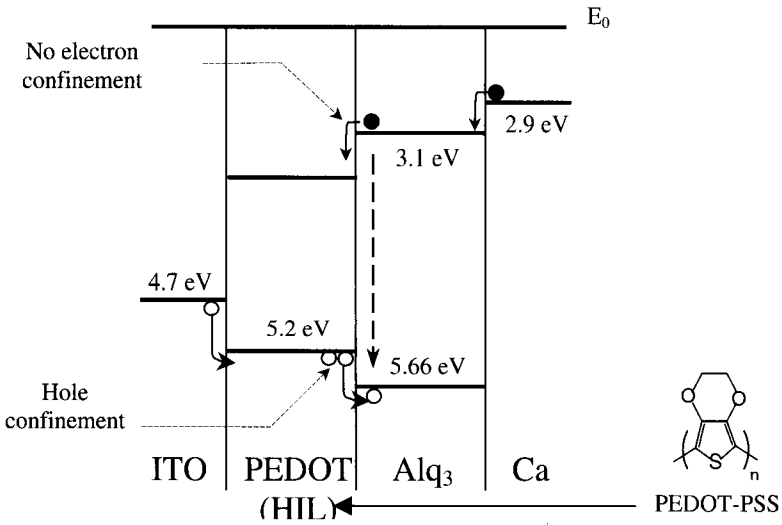


**Figure X-19.** Band scheme of the ITO/PEDOT-PSS/Alq<sub>3</sub>/Ca structure.

while the quantum yield improved from 0.02 to 0.72% (luminance yield increased from 0.02 to 0.99 lm W<sup>-1</sup>).

In Figure X-19 it is evident that the band scheme of the bilayer ITO/PEDOT-PSS/Alq<sub>3</sub>/Ca/Al structure has the PEDOT-PSS HOMO level lying in between that of Alq<sub>3</sub> and the workfunction of the anode Alq<sub>3</sub>, permitting hole injection into the structure. There is also a confinement of holes at the PEDOT-PSS/Alq<sub>3</sub> interface.



## b HTL layer effect

This layer is generally deposited in between the HIL and emitting layers.

The materials used for this layer are either sublimed small molecules such as *N,N'*-diphenyl-*N,N'*-(3-methylphenyl)-1,1'-biphenyl-4,4'-diamine (TPD) or polymers such as PVK, which may be deposited using spin coating. These materials display relatively high hole mobilities ( $\mu_p \approx 10^{-3} \text{ cm}^2 \text{ V}^{-1} \text{ s}^{-1}$ ) and have a HOMO band quite close to the Fermi level of ITO.

In the bilayer structure of ITO/TPD/Alq<sub>3</sub>/Ca, as detailed in Figure X-20, we can see that on the one hand, the intermediary level of the TPD HOMO level aids hole injection into Alq<sub>3</sub>, while on the other, the LUMO level appears as a sizeable potential barrier at the TPD/Alq<sub>3</sub> interface. The latter stops electrons from going from Alq<sub>3</sub> to TPD and confining carriers. Thus at the same time the TPD layer generates more holes and more electrons in the Alq<sub>3</sub> layer, increasing the number of radiative recombinations and improving the luminance from 49 to 9600 cd m<sup>-2</sup>, as shown in Figure X-21.

## c Trilayer structures

Individual studies of the effects of HIL and HTL layers on diodes have demonstrated that:

- the HIL layer allows lower working voltages; and
- the HTL layer permits confinement of electrons and holes at the HTL/Alq<sub>3</sub> interface.

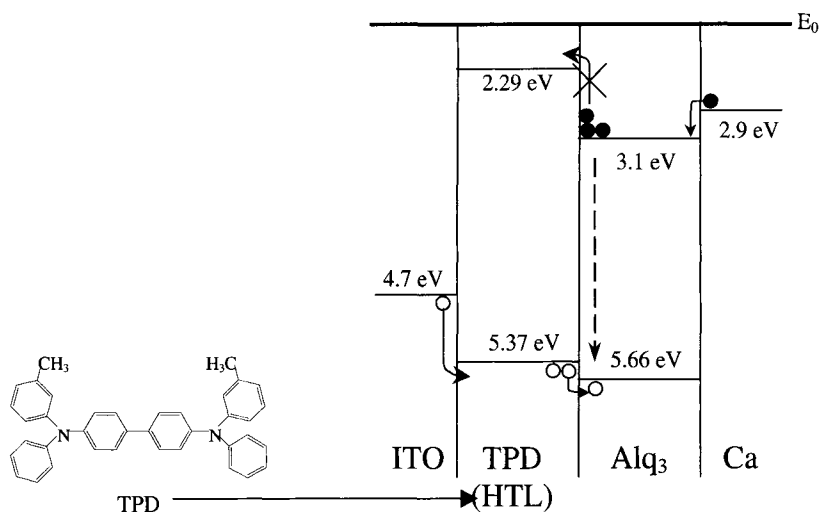
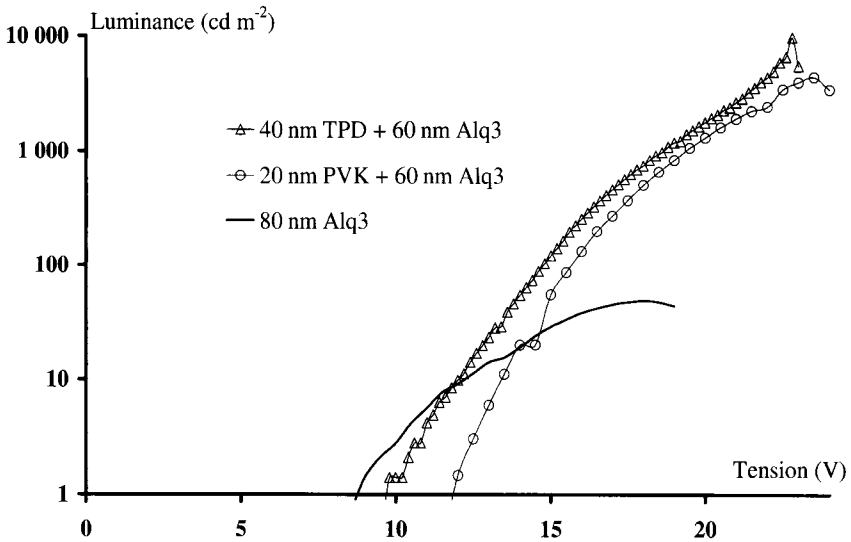
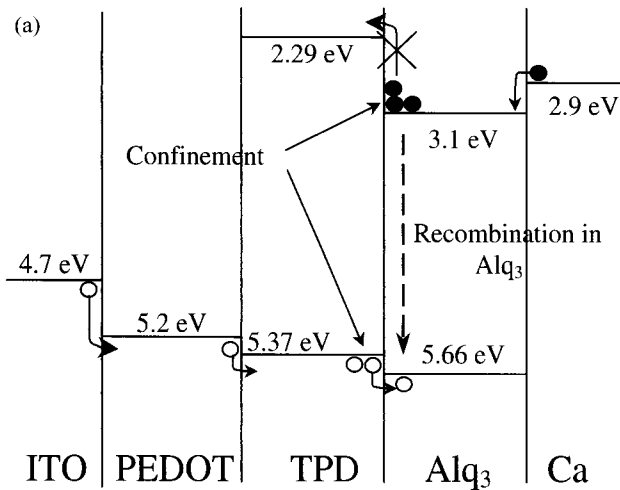


Figure X-20. Band scheme for the ITO/TPD/Alq<sub>3</sub>/Ca structure.



**Figure X-21.**  $L = f(V)$  characteristics for ITO/Alq<sub>3</sub>/Ca/Al, ITO/TPD/Alq<sub>3</sub>/Ca/Al and ITO/PVK/Alq<sub>3</sub>/Ca/Al structures.

Figure X-22-a shows how a structure can be made to combine the effects of both of these layers. The results, shown in Figure X-22-b show that this optimisation can give rise to a luminance of around 22500 cd m<sup>-2</sup> (at 12 V). The working voltage actually used can be optimised by varying the thickness of the various layers [tro 01].



**Figure X-22.** (a) Band scheme of the ITO/PEDOT-PSS/TPD/Alq<sub>3</sub>/Ca/Al (2) structure, (b)  $L = f(V)$  characteristics of bi- and tri-layer structures.

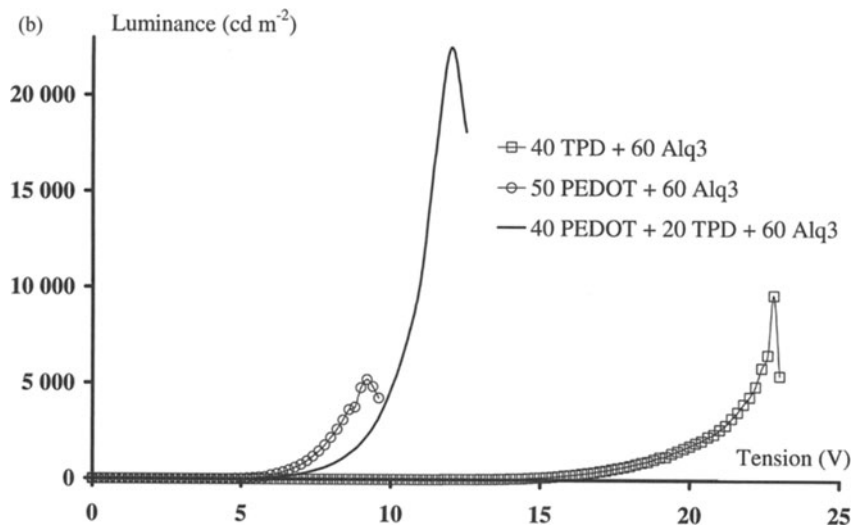


Figure X-22. (Continued)

#### 4 Treatment of the emitting zone in contact with the anode

While physico-chemical treatment of the anode (ITO) using oxygen plasma can lead to an improvement in organic LED performances, we have seen that treatment of the actual emitting zone can also improve the injection and transport of minority carriers leading to an increase, by an order of size, of the luminance and yield of a LED. The effect of this treatment is detailed in Chapter VIII, and here it suffices to present a

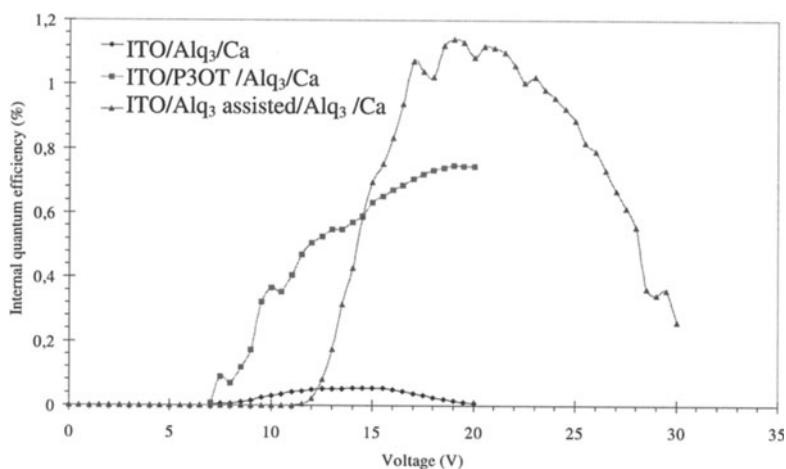


Figure X-23. Quantum yields for mono-layer, chemical bilayer and physical bilayer structures, in order of increasing yield.

comparison of the yields obtained by three different structures in Figure X-23. These three structures are:

- a single layer ITO/Alq<sub>3</sub>/Ca structure;
- a non-optimised 'chemical bilayer' of ITO/P3OT/Alq<sub>3</sub>/Ca, in which P3OT plays the role of the HTL layer, preferentially transporting holes; and
- a 'physical bilayer' of ITO/25 nm Alq<sub>3</sub> deposited using ion assistance/50 nm Alq<sub>3</sub>/Ca, where the assisting beam was of helium ions with energy 100 eV and current density  $j = 50 \text{ nA cm}^{-2}$  and the period of assisted deposition was optimised at  $\Delta t = 100 \text{ s}$ .

The advantage of the physical bilayer is that it requires only one single chemical product to be evaporated, however, the technique does necessitate an ion source and cannot be applied to OLEDs prepared using vacuum sublimation.

## VI Modification of optical properties of organic solids for applications in electroluminescence

### 1 Adjusting the emitted wavelength

There are several ways in which the wavelength of the emitted light can be varied:

- The size of the forbidden band varies with the conjugation length  $n$  of a polymer (or oligomer). When  $n$  is increased, for example in going from an oligomer to a polymer, there is a global evolution in the number of interacting states and thus a decrease in the size of the forbidden band. The result is a shift in emissions to the red. Inversely, the use of oligomers shifts emissions towards the blue. In the case of PPP, an empirical law has been given detailing the absorption peak ( $E_0$ ) [lei 98]:

$$E_0 = \left[ 3.36 + \frac{3.16}{n} \right] \text{ eV},$$

which explicitly shows how, for example, when  $n$  decreases, on using oligophenylenes,  $E_0$  increases;

- when monomer units within a polymer gives rise to weak  $\pi$  interactions (overlaps), for example between phenyl rings, the resulting gap is large. For example, PPP is a good candidate for blue emissions as its gap (emission peak at 465 nm) is greater than that of PPV (peak at 565 nm). The introduction of non-conjugated sequences, which diminish the degree of conjugation, has been used with PPVs to induce a blue shift in the emission. MEH-PPV, PPV modified with alkoxy groups (used by CDT, Cambridge) emits at 605 nm (in the orange–yellow);
- on turning to small molecules, we can see that the most widely used are organometallic complexes, for example based on a central metal ion such as beryllium, magnesium, zinc or gallium and an outer set of ligands which act as

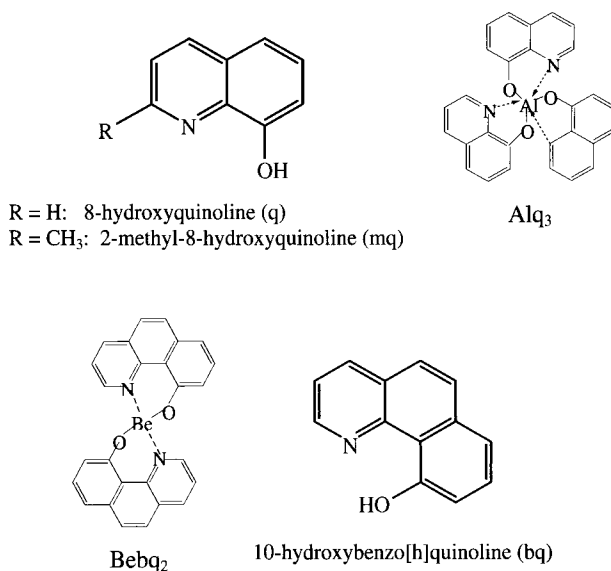


**Figure X-24.** Representations of Alq<sub>3</sub> and Bebq<sub>2</sub> along with the ligands q, mq and b.

emitters (as we have seen in the case of Alq<sub>3</sub>). The emission wavelength for these species is generally towards the green, but can also be modified slightly by using a different metal cation, thus altering bond lengths with the ligands. For example, we have  $\lambda = 530$  nm for Alq<sub>3</sub> and  $\lambda = 517$  nm for Bebq<sub>2</sub>, as shown in Figure X-24. Blue green and even blue colours can be reached by displacing the emitting zone towards TPD, for example.

The central ion can also be a rare earth, giving rise to a change in the emitted wavelength. This is discussed further in Section 4.

- Another strategy consists of grafting small electroluminescent molecules onto polymers [gau 96]. Various possibilities have been explored, using varying concentrations of dye, such as coumarin. Alone, these dyes have a tendency to crystallise, thus losing efficiency. The problem remains though that such structures require high starting tensions and do not appear to be particularly stable.

## 2 Excitation energy transfer mechanisms in films doped with fluorescent or phosphorescent dyes

Studies of host-guest systems, Alq<sub>3</sub> (host) - DCM<sub>2</sub> (2% guest fluorescent dye) and Alq<sub>3</sub> (host - PtOEP (8% guest fluorescent dye), have shown in both cases that excitations are formed directly on the host Alq<sub>3</sub> system [bal 99]. However, the emissions of the guest systems are very strong, and in the former system less than 1% of emissions come from Alq<sub>3</sub>. This indicates a high level of excitation transfer from the host towards the guest.

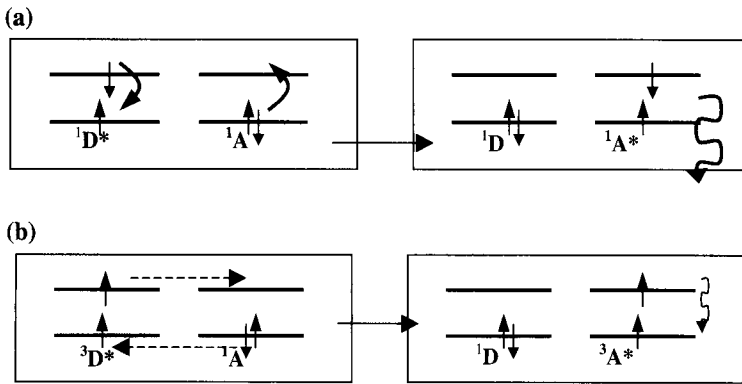


**Figure X-25.** Transfer of excitation energy from a host molecule (D: Alq3) to a fluorescent dye guest molecule (A: DCM<sub>2</sub>). (a) Single host  $\rightarrow$  singlet dye fluorescent transfer;  $^1D^* + ^1A \rightarrow ^1D + ^1A^*$  Both Förster and Dexter transfer possible, but former is more important (b) Triplet host  $\rightarrow$  triplet dye fluorescent transfer;  $^3D^* + ^1A \rightarrow ^1D + ^3A^*$  Only Dexter transfer possible here; with fluorescent dye, phosphorescence is only slightly possible.

Given the results detailed in Chapter VII, Section VI-7 concerning mechanisms of excitation transfer, we can summarise the possible energy transfer processes from the host (D for donor) to the guest (A for acceptor) for a fluorescent dye (Figure X-25) and for a phosphorescent dye (Figure X-26). If the two mechanisms, Förster and Dexter

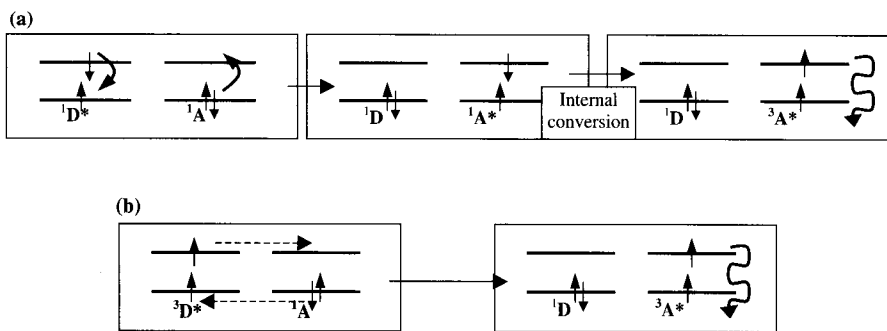


**Figure X-26.** Transfer of excitation energy from the a host molecule (D: Alq3) to a phosphorescing dye guest molecule (A: PtOEP). (a) Singlet host  $\rightarrow$  singlet phosphorescent dye  $\rightarrow$  triplet phosphorescent dye transfer;  $^1D^* + ^1A \rightarrow ^1D + ^1A^* \rightarrow ^1D + ^3A^*$ . Förster and Dexter transfer are both possible, but the former is more probable. The following internal conversion,  $^1A^* \rightarrow ^3A^*$ , relaxes radiatively as A phosphoresces. (b) Triplet host  $\rightarrow$  triplet phosphorescent dye transfer;  $^3D^* + ^1A \rightarrow ^1D + ^3A^*$ . Only the Dexter transfer is possible between D and the phosphorescent doping agent A, which radiates.

transfers, are allowed in a given system, then the Förster transfer normally dominates, due to its ability to act over long distances.

### **3 Circumnavigating selection rules: recuperation of non-radiative triplet excitons**

#### **a The problem**

As detailed in Chapter VII (Section V-3-a), following an injection of electrons, three triplets states appear for each singlet state. In fluorescent materials, only emissions from the latter state occur radiatively, and more or less instantaneously, in a relaxation to the fundamental state, which is generally also a singlet state. Three quarters of excitons occur in the triplet state, which principally undergo non-radiative relaxations, and therefore it is evident that for electroluminescent applications these excitons should be recovered so that they can relax radiatively. Phosphorescent materials can be used to do this. On modifying the (spin) symmetry of a system, the triplet states disappear slowly through radiative recombinations. It is this slow decrease in luminescence which correspond to phosphorescence. While admittedly this method is not highly efficient, the phosphorescence can be improved by the presence of heavy atoms favouring spin-orbit coupling, mixing triplet and singlet states. However, there are almost no useful phosphorescent organic materials, which have, however, given rise to a vast choice in fluorescent materials.

#### **b Initial, poorly efficient solutions: a phosphorescent layer and Dexter transfers**

An initial solution to recovering energy associated in electroluminescence with triplet excitons is the introduction, in an organic LED, of a supplementary layer containing phosphorescent material [bal 00 and sam 00]. However, as we have mentioned, there are very few organic materials which can generate from their triplet excited state a significant phosphorescence. In addition, the slow decline of triplet states in the phosphorescent layer leaves open the possibility of a transfer of these triplet states to triplet states in the fluorescent layer (Alq3), which are non-radiative.

In practise, in a donor-acceptor system, where the fluorescent acceptor directly dopes the phosphorescent donor material, only transfers over short distances can occur. Förster type transfers are unlikely; Dexter transfers occur more readily due to the proximity of acceptor and donor molecules, and excitons hop from one molecule to the closest neighbour simply by overlapping molecular orbitals. The transfer of energy from triplets states (phosphorescent molecule) to singlet states (fluorescent molecule) is highly unlikely, as the mechanism of hopping over short distances conserves symmetry over the donor-acceptor pair, and only transfer from the donor triplet state to the same triplet state on the acceptor can result. Once excitons reach the acceptor triplet state, in terms of radiation efficiency, they are lost as the fluorescent dye can only yield a negligible phosphorescence.

A change in spin orientation, thus assuring a transfer from triplet to singlet states, is only possible if the donor exciton relaxes before reforming at the acceptor, following a random exchange of electrons. This mechanism though remains improbable as the required disassociation of the donor exciton requires a high amount of energy—of the order of 1 eV in molecular systems.

### c Multi-layer systems and Förster transfers

As we have already seen, there remains an alternative transfer mechanism. The Förster transfer is associated with long distances, around 5 nm, and does not require contact between molecules, and permits changes in spin of transferring excitons [bal 00]. Chapter VII, Section VI-7-b gives further details. In addition, in order to transfer excitons from a host material to an excited singlet state on a fluorescent dye, a phosphorescent and organometallic intermediate is required. Thus, both singlet and triplet states from the host material are transferred to the phosphorescent intermediate, which in turn allows transfers to the singlet states of a fluorescent emitter, which in turn works radiatively in an efficient manner. So that these transfers are possible, the exciton observes a reduction in its energy at each step, much like a ball descending a stairway and as schematised in Figure X-27. The phosphorescent dye, in this configuration, stimulates the transfer of energy from the host material, which acts as donor, to the fluorescent dye acceptor. The transfer is in effect step-wise. However, the concomitant non-radiative Dexter transfer (illustrated by crossed out arrows in Figure X-20), which permits the passage from the triplet state of the phosphorescent intermediate to the triplet state of the fluorescent emitter, should be limited if not completely suppressed. A near total suppression can be accomplished by using an emitting layer itself consisting of alternate layers of phosphorescent intermediate and fluorescent emitter both diluted within a host which ensures the sought Förster energy transfer. Once any

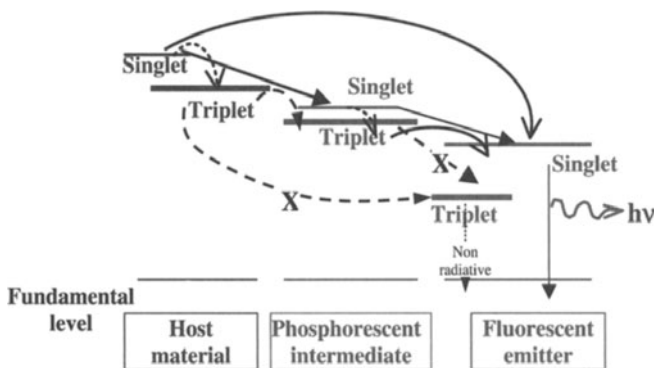


**Figure X-27.** Schematisation of Förster transfer mechanism (full line), where the phosphorescent intermediate stimulates energy transfer from the donor host material to the acceptor fluorescent dye. The internal conversion is detailed as a dotted line, while Dexter type transfers are shown as dashed lines. Dexter transfers—to eliminate—are schematised as dashed lines crossed out. After [bal 00].



fluorescing dye singlet is formed, its radiative fall is immediate. This helps to reduce the total number of excitons in the system at any one moment and, by consequence, the risk that they would transfer towards a triplet state and extinction.

A widely used material for the host electron donor layer is a dicarbazole-biphenyl called CBP. Typically, the phosphorescent intermediate is iridium tris(2-phenylpyridine) otherwise denoted Ir(ppy)<sub>3</sub>, and the fluorescent dye is often DCM2, a red dye. Complete chemical formulae can be found elsewhere [bal 00]. With an optimised structure, which contains a considerable number of transport layers of both holes and electrons, external quantum yields greater than 3% have been found, a multiplication by four of that obtained from the fluorescent dye alone.

Another advantage of this configuration is that it does not rely upon phosphorescent emissions, which permits the application of molecules which are not necessarily phosphorescent as the phosphorescent intermediate [sam 00]. We can also note that the increase in radiative yield decreases the number of phonon descent processes, which in turn diminishes losses due to heating and, accordingly, increases LED lifetimes. There is however a cost, and that is that as the energy transfer descends towards lower and lower levels, and the resulting emissions are mostly in the red, sometimes in the green and with extreme difficulty in the blue. This tends to limit the number of available applications for these systems.

In the fabrication of electrically pumped lasers we can see that this technique can be used to limit losses due to reabsorption of light emitted by triplet excitons. In addition, this by-passing of selection rules can be useful not only to optimise the number of singlet excitons produced but also in order to prepare organic lasing diodes.

## 4 Energy transfer with rare earths and infrared LEDs

### a Ligand-rare earth transfers at the heart of chelates

The name chelate encompasses a group of compounds consisting of multi-dentate ligands attached to a central cation. Co-ordination bonds between the ligands and the cation are formed by the ligands donating electron pairs. As already detailed for the chelate Alq<sub>3</sub>, the standard chelate for electroluminescence, the emission colour is determined by the ligands with a peak at 525 nm. Doping with dyes can induce blue or red emissions. On inserting a hole transport layer at the anode side, luminances as high as 10000 cd m<sup>-2</sup> have been reached with yields of 1.5 lm W<sup>-1</sup>.

Photoluminescence or electroluminescence can be obtained from chelated rare earths, attached to ligands by single or double bonds. Gadolinium yields UV light, while cerium gives rise to the colour blue. Terbium gives green, europium shows red, dysprosium displays yellow and erbium emits in the infrared. Figure X-28 schematises the basic mechanism. Either by photoluminescence or electroluminescence, respectively from incident photons or electron injection, ligand electrons are excited from a fundamental singlet to an excited singlet state from which relaxation results in fluorescence. Triplet states are also occupied due to excitation by electroluminescence. The excited states, whether they be singlet or triplet can go on to transfer energy to energy levels associated with the rare earth 4f orbitals, as long as Crosby's

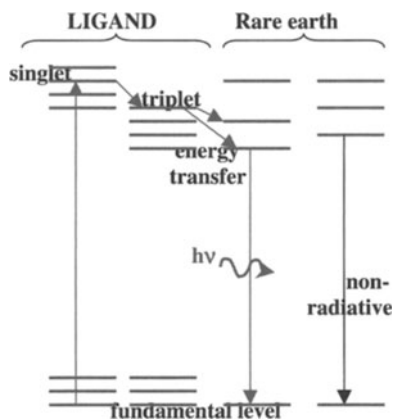


**Figure X-28.** Rare earth ion excitation by organic solids.

rule is respected [Cro 61]. This states that the lowest energy level of a ligand triplet state in the complex should be close to equal or just above the resonance energy level of the rare earth ion. A difference of 0.05 eV is sufficient to ensure a 95% photoluminescence yield. On emitting light or through non-radiative processes, the rare earth ion can then relax to its fundamental state.

It is interesting to remember that when a ligand is excited from its fundamental state, 25% of the resulting states are singlets and 75% are triplets. All this energy can be transferred to the rare earth ion, which means that there is a potential internal quantum yield of 100% [Bel 99].

In these chelate systems, it is the rare earth which is responsible for their lifetimes and the wavelength of the emitted light. The ligand though is responsible for the absorption, the power of the emission and, in practical terms, the ease of handling. ELAM, a company in London, indicates that yields obtained with these systems can be up to 60 to 70 lm W<sup>-1</sup>, which can be compared against that of fluorescent tubes at 100 lm W<sup>-1</sup>. OPSY, a company in Oxford, UK, has announced luminances of 200 cd m<sup>-2</sup> in the red and green, with photoluminescent yields of 80%.

### **b Infrared organic LEDs [Gil 99]**

Following purification, sublimation of a methanol solution of erbium chloride and 8-hydroxyquinoline can give films of erbium tris(8-hydroxyquinoline) (Erq<sub>3</sub>). Er<sup>3+</sup> exhibits a strong luminescence centred at 1.54 μm due to a transition from the first excited <sup>4</sup>I<sub>13/2</sub> state to the fundamental <sup>4</sup>I<sub>15/2</sub> level. Light at this frequency is within the window of transparency of silicon based optical fibres, used in communications. Using the OLED structure glass/ITO/TPD(50 nm)/Erq<sub>3</sub>(60 nm)/Al, photoluminescence around 1525 nm and electroluminescence around 1533 nm was obtained. Secondary emissions were also found and attributed to isomers of Erq<sub>3</sub>. There are certainly difficulties with respect to yields, and only qualitative results have been published (*i.e.* graphs with arbitrary scales). The size of the difference in

energy between radiative recombinations at the ligands, which persist in Erq, and the  $^4I_{13/2} \rightarrow ^4I_{15/2}$  line may explain these results.

## 5 Microcavities

A typical structure is made using a Bragg mirror inserted between a glass substrate and a layer of ITO (98 nm and with  $n = 1.8$ ), onto which a layer of PPV is deposited (160 nm). Aluminium or silver electrodes function as a semi-transparent mirror, as shown in Figure X-29-a.

The photoluminescence spectra, like the electroluminescence spectra exhibit considerable narrowing of the spectral curve (having a width of only around 5 nm half way up) with respect to that of PPV obtained in free space [Tes 96]. The intensity of emissions permitted by the cavity are also increased greatly, and even more so when using silver as the mirror as it allows less losses than aluminium (Figure X-29-b).

## 6 Electron pumping and the laser effect

For the OLEDs so far detailed, the current densities are of the order of 1 to 10  $\text{mA cm}^{-2}$  for luminances of around  $100 \text{ cd m}^{-2}$ . For lasers, higher densities are required, but they are *a priori* limited by low carrier mobilities so that at high injection levels absorption increases. The use of tetracene (4 joined phenyl rings) has allowed relatively high mobilities—at least for an organic solid!—at around  $2 \text{ cm}^2 \text{ V}^{-1} \text{ s}^{-1}$  to be attained. Amplified spontaneous emission by optical pumping was observed in the middle of the 70s [Pop 82] in anthracene and doped tetracene. More recently, a lasing effect by injection has been reported [Schö 00]. For the latter, tetracene was used in a perfect crystalline form in order to banish defaults and impurities otherwise insupportable in optoelectronics. Vapour phase deposition was used to give crystals of around 1 to  $10 \mu\text{m}$  thickness and  $1 \text{ mm}^2$  surface area. Two field effects at the electrodes were used to ensure an equilibrated injection of holes and

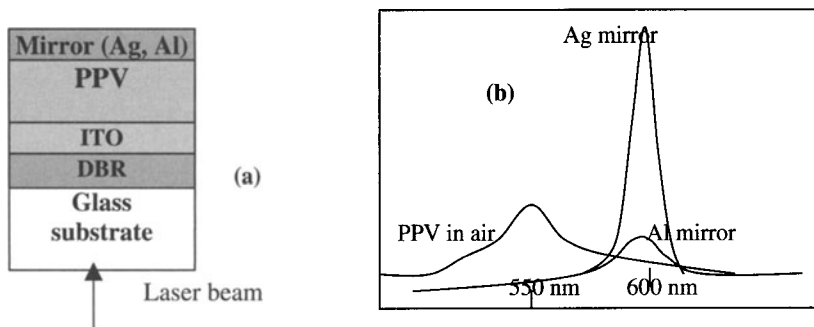


**Figure X-29.** (a) Microcavity structure; and (b) general shape of photoluminescence curves.

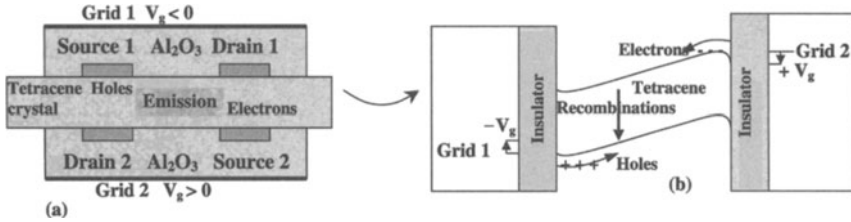


**Figure X-30.** (a) Cross sectional view of structure; and (b) schematisation of grid-source tensions applied to give field effect injections.

electrons (see also this point developed in Section 1-b in this Chapter). Figure X-30 schematises the fabricated structure for this device and shows the two field effect electrodes used to inject charges. To describe the device we will refer to this Figure. Around the crystal there were deposited a source, a drain, a dielectric grid and a grid, with the former two for hole injections made from gold, while aluminium was used to inject electrons. Holes were injected by the application of a negative source-grid at the upside and electrons were injected at the lower side by the application of a positive tension between the source and grid deposited on the lower side. The field effect acts much like a variable doping at the contacts with the crystal, and the concentration of carriers can be varied by adjusting the grid tension. Between drain 1 and source 2, and source 1 and drain 2, a tension was applied (around 5V) to a slice of the crystal allowing electrons and holes to traverse the device, respectively, upwards and downwards. Electroluminescence and amplified stimulated emissions are detected laterally.

In addition, the organic crystal can play the role of waveguide, but the grid dielectric here is too thin at 150 nm to act as a coating. In fact it is air which plays this role, allowing only a multi-modal guide. Cleavage of the crystal faces, which have a reflectivity of 8% can induce a Fabry-Perot type resonance. At a value  $V_g = 50$  V, carrier densities of  $10^{13} \text{ cm}^{-3}$  were estimated using measurements of capacity and variations in tensions and thus conductivities. A potential drop of 5 V held between the high and low points of the structure assure current flow. As a consequence of injection, excitons are formed and light emissions are observed. At a temperature of 5 K, three peaks were observed for a very low pulsed current ( $< 1 \text{ A cm}^{-2}$ ). The peaks were characterised as being due to radiative transitions between first excited and fundamental states and included vibronic levels (0-1, 0-2 . . . transitions). They were separated by 170 eV, a value corresponding to intramolecular vibrations. As shown in Figure X-31, an increase in current density, by increasing the grid-source tension, gave rise to a dominant 0-1 band with a mid-height width reduced to 10 meV at a density of  $30 \text{ A cm}^{-2}$ . At  $j > 500 \text{ A cm}^{-2}$ , a vertical line appeared, of width less than 1 meV. This abrupt narrowing of the spectral line at a threshold current of  $30 \text{ A cm}^{-2}$  is typical of a spontaneously amplified emission with the contributed guidance gain. The second drop at  $j > 500 \text{ A cm}^{-2}$  corresponds to the start of the lasing effect.

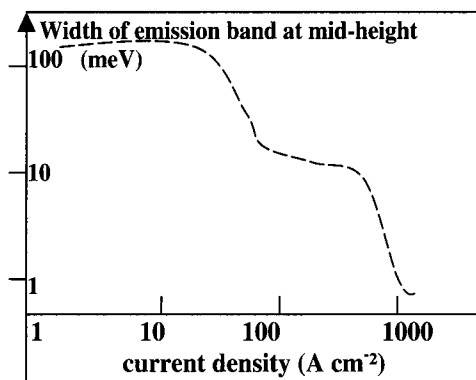


**Figure X-31.** Emission line width at mid-height and at 5 K with respect to the function of pulsed current density (10  $\mu\text{s}$ , 100 Hz).

## VII Applications in the field of displays: flexible screens

### 1 The advantages

One of the potentially most interesting developments, in industrial terms, is the fabrication of flexible displays and screens. It was realised, right from the start of the development of screens with pixels made from OLEDs and PLEDs, that they had numerous advantages. (Recalling the term, pixel comes from the contraction of 'picture-element', while interestingly in French the word 'eldim' would be used, a similar contraction of the words 'élément d'image'.) When compared to liquid crystal displays (LCDs), they have the advantages of giving a wider angle of view (Lambert's emission), a higher luminance (several  $100,000 \text{ cd m}^{-2}$  have been attained), an extremely high commutation speed, a low minimum working voltage around 5 V, low levels of energy consumption and no need for back-lighting. There have been plans to use OLEDs as back-lights and white diodes have been prepared for the lighting market.

We will first say a few words on white diodes, before looking more in depth at the realisation of screens.

### 2 The problem of ageing

Ageing determines the lifetimes of LEDs [Ngu 98 and Miy 97]. The definition used to qualify the lifetime of a device is the time it takes for the luminance to descend to one half of its original value [Si 97]. The measurement can be made using either of two methods. In one the applied tension is kept constant, and in the other the current which traverses the device is retained constant. Figure X-32 shows the results obtained using the latter method. The original luminance is fixed at around  $100 \text{ cd m}^{-2}$ . The tension and the luminance are measured every 30 seconds so that the curves  $L = f(t)$

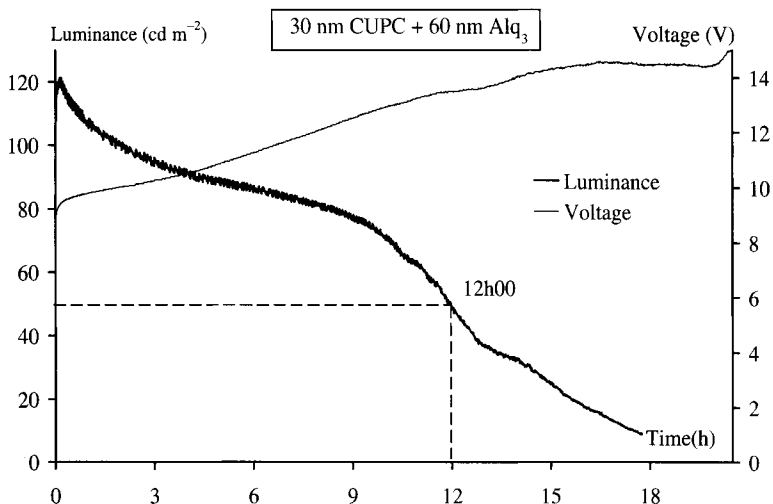


**Figure X-32.**  $L = f(t)$  and  $V = f(t)$  characteristics of the ITO/CuPc/Alq<sub>3</sub>/Ca/Al structure.

and  $V = f(t)$  can be traced. The example structure shown, ITO/30 nm CuPc/60 nm Alq<sub>3</sub>/Ca, has a half-life thus estimated as 12 hours.

Outside of problems due to breakdown, which can result from an inhomogeneous film, migrations from the electrodes towards the layers can occur, stimulated by field effects. As examples we can cite metallic indium which comes from ITO, as does oxygen which can go on to modify chemical groups, most notably those which fluoresce. At the cathode we can blame oxygen and water vapour for the appearance of black points localised about defaults which were there to start with and just go on growing. Another participating fault is no doubt that of crystallisation of active layers due to heating. This is the reason why there have been numerous works published concerning the treatment and improvement of electrodes and interfaces, most notably those of ITO. An example of one treatment is that of subjecting an ITO surface to oxygen plasma for 10 minutes which results in an improvement in its workfunction and this an improvement in hole injection. The roughness and the resistance of the ITO surface are also improved using this method and the overall yields are improved [Kim 99]. Finally it is worth mentioning the unavoidably necessary process of encapsulation of organic LEDs. Different approaches have been used: that of sealing between two glass plates and a ribbon of glue; and encapsulating within a polymer barrier layer such as PPX or one of its chlorinated derivatives deposited using VDP (see Chapter VIII for further details).

In common with all electrical components, organic diodes need to be fabricated *a priori* in a dust free 'white room' so that the lifetime required for industrial applications is attained, which at present is of the order of 10,000 hours. Indeed, on an industrial scale, the fabrication of specific layered devices requires the connection of individual chambers each operating specifically to a certain layer. At the present moment, each company will have without doubt its own proper techniques.

### 3 The specific case of white diodes

Uniax, within the EEC, has fabricated PLEDs for lighting purposes which have photon to electron yields between 2 and 3% operating at 3 to 4 lm W<sup>-1</sup> at a low applied voltage. The luminance is better than that obtained from incandescent or fluorescent lamps. As ever though, the problem remains lifetimes, mostly due to heat. In a pulsed mode, luminances close to 100,000 cd m<sup>-2</sup> have been reached. If initial yields of 25% can be attained, not an entirely unrealistic value, then this area awaits considerable development.

Figure X-33 schematises the ‘intelligent’ layering of emissive layers with each emitting in the visible region. The ordering of the layers is made with respect to the type of injected carriers and the direction of emission, towards the emission window, so that successive absorptions do not occur. In effect, the layer nearest to the window should have the largest band gap [Jol 97 and Miy 97].

### 4 The structure of organic screens

One of the advantages of organic LEDs is their very short communication time. Inversely, that also means that their remanence is very short lived. So, in the case of multiplexing, where sweeping of each line of pixels is required (as in passive matrices) and so the screen gives an acceptable average luminance (from around 100 to 200 cd m<sup>-2</sup> for a television), the luminance at any one moment needs to be very high (n times the number of lines swept, for a screen with n lines). The lifetimes of LEDs functioning under such conditions is therefore well reduced.

The use of active matrices therefore becomes inevitable. They also offer a gain in resolution. This change in direction is also justified by the fact that OLEDs are particularly well suited to individual addressing, which can be performed *via* a polycrystalline silicon FET, although organic semiconductors can claim also to be perfect candidates as materials for the commanding transistors [bur 91 and hor 00]. In Figures X-34-a and -b, respectively, are shown a schematisation of a MIS field effect transistor (MISFET), which has a semiconducting channel made from PPV implanted with iodine ions ( $E = 30$  keV,  $D = 4 \times 10^{10}$  ions cm<sup>-2</sup>) and its characteristics. This transistor operates in the accumulation phase, with the gate voltage being negative with respect to the p-type semiconductor finally obtained [Pic 95].

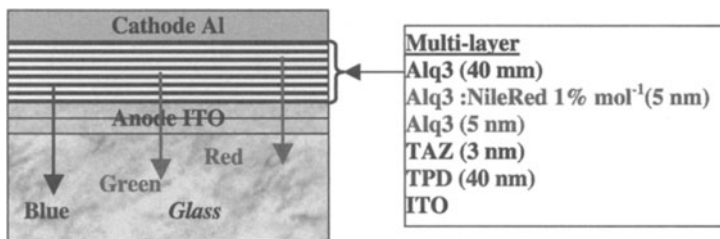
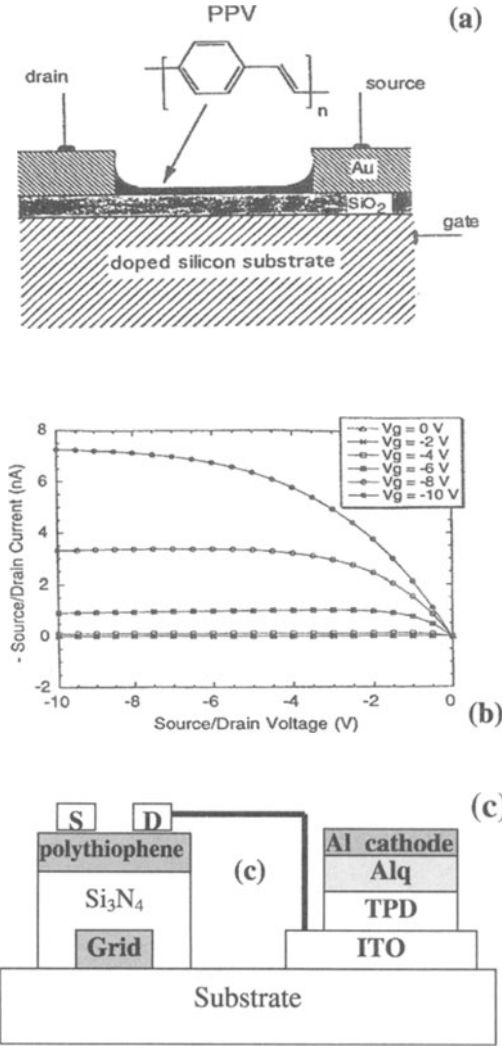


Figure X-33. Schematisation of a white LED with the required order of layers.



**Figure X-34.** (a) Configuration used in a polymer based MISFET transistor (after [pic 95]); (b)  $I_{ds} = f(V_{ds})$  characteristics following  $V_{gs}$  for a MISFET with an iodine implanted PPV semiconductor channel; and (c) schematisation of a completely organic pixel.

Figure X-34-c shows the general constitution of a completely organic pixel from a monolithic integrated polymer FET and an organic LED [Bao 99]. The ITO, placed against the substrate, makes the LED anode while a photographically imposed layer of gold defines the gate electrode of the FET. The insulator for the gate is a layer of Si<sub>3</sub>N<sub>4</sub> which is about 180 nm thick. The semiconductor, poly(3-hexylthiophene) (P3HT) is a regio-regular polymer helping give it a high charge mobility at around  $0.002 \text{ cm}^2 \text{ V}^{-1} \text{ s}^{-1}$ . Above this is the drain and the source and the channel is about



5  $\mu\text{m}$  long and 1 mm wide. The drain is joined to the anode of the LED, which is of a classical bilayer structure and has an external yield of about 0.4%. The maximum current through the LED is  $50 \mu\text{A cm}^{-2}$  (equivalent to a current density of  $72 \text{ mA cm}^{-2}$ ). The luminance of such a pixel has been estimated at  $2300 \text{ cd m}^{-2}$ , a value well above the  $100 \text{ cd m}^{-2}$  necessary for display applications. An all polymer pixel has also been described, in which PPV replaces Alq3 and polyimide replaces  $\text{Si}_3\text{N}_4$  as the dielectric grid.

As for the deposition techniques used, we can say that small molecules are deposited using evaporation under vacuum and polymers are spread using spin-coating. The technique of ink-jet deposition which has appeared is particularly adapted to polymers, while there are also techniques based on 'roll-on-roll' for small molecules [Bur 97]. It is interesting to consider that while colour screens require the three colours red, green and blue (RGB), the necessary materials have been identified (although need some improvement [den 00]), and that all is required is juxtaposition of the three types of pixels using techniques particular to organic solids, which are not that removed from those currently used in microelectronics [Bar 00a and Bar 00b].

## 5 A description of the fabrication processes used for organic RGB pixels

Research into improving OLEDs lifetimes to greater than 10,000 hours with initial luminances of more than  $300 \text{ cd m}^{-2}$  also stimulated a development in the technology surrounding their use, specifically, in flat screens.

To fabricate the RGB pixels, various technologies were tested, particularly to try and avoid etching based techniques:

- development of white diodes which emitted through RGB filters;
- use of blue diodes (*i.e.* at the highest energy required) which excited phosphors emitting in the green and red; and
- adjustments, using micro-cavities, of emissions from a wide band organic emitter.

However, for the above systems, the power emitted was limited, and the use of three individual layers for each colour was found to be indispensable. This required the fabrication of sub-pixels using etching techniques:

- 'wet' technology using solvents, either acids or water, which nevertheless generate problems associated with the induced degradation of the active organic materials;
- 'dry' technology in which pixels are obtained using plasma etching, which *a priori*, presents no specific problems due to degradation.

In order to obtain high resolution screens, anodes and cathodes necessarily should be made to a precise geometric form, and this in accordance with the structure of the pixels on the screen which are either deposited in a matrix of points or as segments. The ITO anode is the most facile to prepare, using either 'dry' or 'wet' etching techniques being done before any organic layer is deposited. For the cathodes though, which demand an extremely high degree of geometric precision, their fabrication requires extreme care. In reality, the materials used for the cathodes (Al-Li or Mg-Ag

for examples), can be deposited directly onto an organic layer using ‘wet’ etching, however, when the organic layer is one which is fragile and sensitive to thermal or solvent induced effects, then particular steps must be taken. The literature proposes various routes, depending on whether small molecules or polymers are involved, and below we shall look at some of the possible methods.

**a For layers from sublimed molecular materials: use of a T-form cathode separator [Nag 97]**

The technology should allow for the fabrication of OLED devices which have dimensions around  $1\ \mu\text{m}$ . The technique involving T-form cathode separators was used by Pioneer to realise their first commercially available screens. The separator between pixels, sized around  $30\ \mu\text{m}$ , was prepared prior to depositing the organic layers and the metallic cathode.

Practically speaking, the cathode is fabricated around the T-form separators in three steps, as shown in Figure X-35. The cathode separator is shaped in conical form and has a retracted base—as shown in Figure X-35-a. It can be obtained using a negative working photo-polymer—the irradiated part of which resists etching development—by relying on the cumulated exposure with depth. The photo-polymer, deposited by spin-coating, exhibits properties similar to those of a photo-resin

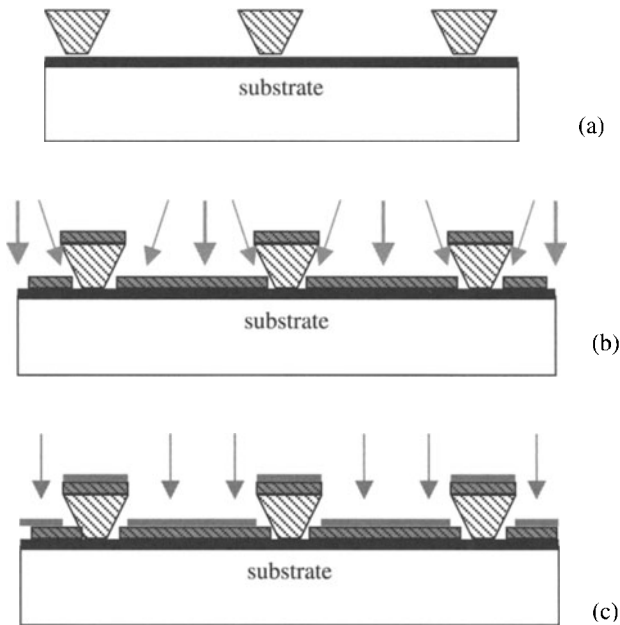


**Figure X-35.** The three stages in diode fabrication *via* a T-form cathode separator: (a) elaboration of the cathode separator; (b) evaporation of organic materials at an oblique angle with respect to substrate; and (c) evaporation of the metal cathode at a angle perpendicular to the surface.

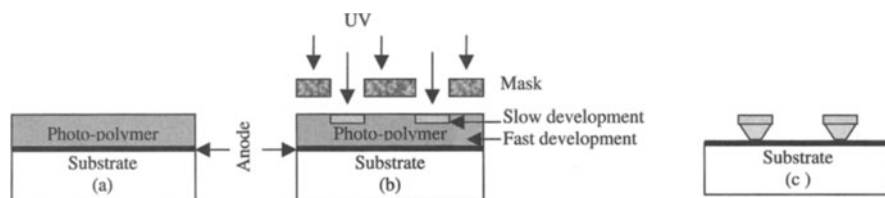


**Figure X-36.** Realisation of the phase given in Figure X-35a: (a) spreading the photo-polymer; (b) selective exposure through mask; and (c) development.

with additional properties in development speeds and exposure time. As shown in Figure X-36, a longer exposure time can result in a more noticeable removal of material.

The T-form of the separator can also be obtained using a double polyimide/SiO<sub>2</sub> layer deposited on the anode (polyimide on the anode then SiO<sub>2</sub> on the polyimide). The SiO<sub>2</sub> layer is etched using a dry technique (to yield an anisotropic form with vertical walls) of selective exposure through a mask (photolithography). The polyimide, which is not sensitive to light, is then etched using a 'wet' process (thus isotropically) as a sub-etching, thus giving rise to the vertical 'leg' of the T.

Organic layers are then evaporated, obliquely, onto the surface, as shown in Figure X-35-b, and surround the foot of the cathode separator. The metal layers are then finally evaporated perpendicularly to the substrate, schematised in Figure X-35-c, in such a way as to never touch the bases of the separators. Adjacent cathodes are thus electrically isolated from one another.

While the T-form separators were prepared with dimensions of 30 μm × 30 μm [Nag 97], with present day photolithographic processes, dimensions as low as 10 μm × 10 μm may be reached. A passive matrix screen was prepared 256 × 64 points with pixels sized around 340 μm × 340 μm. The geometrical placement of cathodes can be rectilinear or curved, another advantage with respect to various fabrication methods.

## b Integrating three RGB polymer LEDs

The technology used for fabricating screens must be able to integrate sub-pixels. Polymer based orange, green and blue pixels have been prepared by sequential sampling of three polymer films on the same glass substrate covered with ITO, over which an insulating layer had been placed. The polymer films were deposited using spin-coating and then covered by a metal electrode, itself deposited by evaporation under vacuum. The last layer served as a self-alignment mask for when the films were subjected to plasma etching to expose adjacent polymer sub-layers [Wu 96]. Thus it is not the organic layer which defines the dimensions of each pixel or sub-pixel (or the LED), but rather it is the electrode (here the cathode metal or, otherwise the ITO anode). The structure is schematised in Figure X-37. It should be noted though that the unprotected sides of the polymer layers deposited first can be attacked by chemical agents,

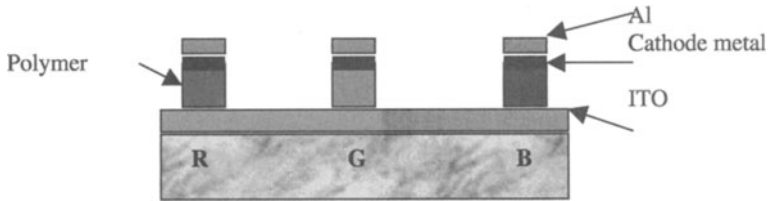


**Figure X-37.** Set-up of three sub-pixels with cathode defined.

for example the solvent of the second polymer layer, which may be required for a different colour. Other than possibly forming geometrical deformations, this process can also result in degradations and electrical short-circuits.

In order to limit and even completely stop these problems, the structure can be modified so as to protect the side of the polymer layer. Figure X-38 shows that in order to do this, an insulating layer is deposited onto the ITO layer, and a window which allows access to the ITO layer is opened at the insulating layer, which defines the active zone.

In practical terms, the insulating film is made of a nitride of silicon deposited by PECVD at 250 °C and has a thickness of around 100 nm. The active window is obtained in the  $\text{SiN}_x$  using standard photolithographic etching processes. For the first set of sub-pixels, the polymer film (orange following the particular reported case) is spread over the whole surface of the screen and the cathode metal (Al included) for this layer of sub-pixels is deposited by evaporation under vacuum ( $\approx 10^{-6}$  torr) through a mask. The structure is then exposed to oxygen plasma which etches away resins and isolated organic material but leaves intact zones below the Al. This plasma etching is in some senses self-aligning and does not require a supplementary masking stage. In addition, its use negates the risks of overexposure of the organic films to solvents that would otherwise be encountered in a 'wet' process.

An additional layer of Al can be deposited through a mask to seal the device, as shown in Figure X-39. This takes the sides of the organic layers out of harms way from organic solvents, air and humidity. We can also note that this technology can be extended to small molecules.

The following green polymer layer can then be deposited to gain the second pixel. The above detailed stages, up to the sealing layer, are then repeated.

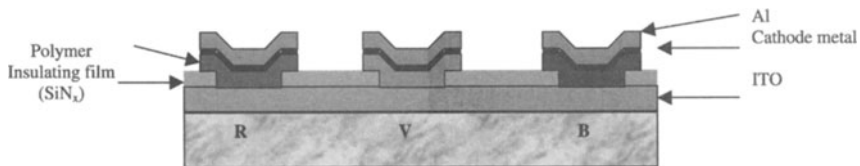


**Figure X-38.** RGB structures prepared to protect pixel edges.

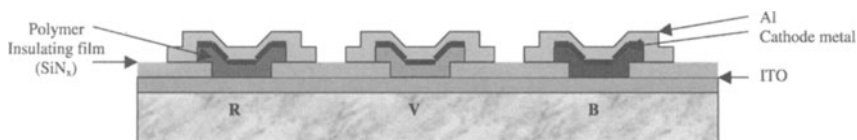


**Figure X-39.** Sealing sub-pixels with a layer of aluminium.

With mechanically aligned films, typically, dimensions for the active zone are  $2 \times 2 \text{ mm}^2$  and the metallic contacts are  $4 \times 4 \text{ mm}^2$ . The zones of the metallic contact go beyond that of the active material giving some space between the side of the system and the electronically useful zone. This configuration has been tested with success under a dry nitrogen atmosphere, without loss of characteristics. This technique may be extended to pixels of smaller sizes (hundred of microns), to fabricate high-resolution screens, using classic photolithographic technologies. Excepting the transfer of samples from the etching chamber, all preparation steps should *a priori* be effected within a glove box under a dry nitrogen atmosphere.

The technology described above has been used with success, and without altering optoelectronic characteristics, to prepare an integrated structure with PVK as the hole transporter, doped PVK as the emitting layers, layers of Alq3 or PBD to transport electrons and the following various dyes:

- PVK/Alq3/nile red for red (orange) sub-pixels;
- PVK/Alq3/coumarin-6 for green sub-pixels;
- PVK/PBD/coumarin-47 for the blue sub-pixels.

### c Ink-jet technology [Bha 98]

The technique of polymer spin-coating presents, in fact, a considerably number of disadvantages with respect to preparing pixelated screens. Normally, nearly 99% of the polymer solution is wasted and it is difficult, if not impossible, to prepare lateral faces. Deposition using ink-jets could therefore appear to be an excellent substitute method, with only less than 2% of solution lost. This technology also allows treatment of large surfaces, is compatible with the indispensable addressing of (coloured) pixels and is relatively cheap to operate. Certain precautions are necessary, however, to ensure a regular deposition of polymer solution. The use of dilute polymer solutions was evaluated, with deceptive results with respect to the quality of the components. Eventually a hybrid technology was adopted which uses an absorbent, intermediate layer, which can be made of a host polymer, and has a thickness of around 100 nm. The intermediate layer exhibits three principal characteristics:

- it smoothes out bumps and dips which can be generated by the ink-jet;
- it acts as a sponge, virtually fixing the polymer solution; and
- if it is formed of a semiconductor with a large band gap, then a multi-colour emission can be obtained by energy transfer when the ink-jet deposited material has a smaller band gap.

In order to fabricate colour screens, red, green and blue polymers are used and the intermediate layer can be an electron injecting layer. Inversely, good results can be obtained by using the ink-jet process for the charge injecting layer and with a luminescent polymer for the intermediate layer. The emitting zone is thus defined by the charge injection layer deposited directly by the ink-jet printer.

Figure X-40 shows a cross-sectional scheme of a system with the hole injection layer deposited using an ink-jet printer. A commercial printer was used with an aqueous solution of PEDOT [bha 98]. The active polymer, MEH-PPV, was deposited using spin-coating and serves also as the absorbing, intermediate layer (120 nm thick obtained from a 1% solution of MEH-PPV spun at 2500 turns per minute). At 5 V, the 'logo sandwich' ITO/PEDOT/MEH-PPV/Ca gave rise to a luminance of  $200 \text{ cd m}^{-2}$  with a contrast close to 800 (the luminance ratio of emitting and dark zones). Given the ease of controlling the ink-jet printer and its depositions, a practically infinite range of logos can be made and writing, in particular, can be computer generated. In addition to variations in colour, different grey levels can be attained by changing the superficial concentration or size of the deposited spots. Typically, plots of sizes between 180 and 400  $\mu\text{m}$  were possible in the original experiments. For monochrome screens, dimensions of the order of 100  $\mu\text{m}$  suffice. Ink-jet technology is thus well placed to be used in the fabrication of screens and this is without having to define pixel positions by overlapping lined anodes and cathodes in columns, for example.

As another example, we can cite the bicolour screen [Cha 98] which was fabricated by directly spin-coating an intermediate layer onto ITO, and then ink-jet printing was used to deposit a polymer that had a lower band gap and was capable of diffusing through the intermediate layer. The intermediate layer was made from a polymer with a large band gap, was soluble in water and emitted in the blue part of the visible spectrum. The material that was ink-jet deposited was also water soluble but emitted red-orange light. On absorption, there was a transfer of energy from the former to the latter, and red-orange photoluminescence or electroluminescence could be obtained from the ink-jet pattern, as detailed in Figure X-41.

A tricolour prototype has been presented by CDT-Seiko-Epson, as shown in Figure X-42. Its structure was based around series of pillars, formed from strips of polyimide (Figure X-42-a) deposited onto ITO and placed so as to leave spaces to receive ink-jet deposited drops of solution. After adapting the wettability of the

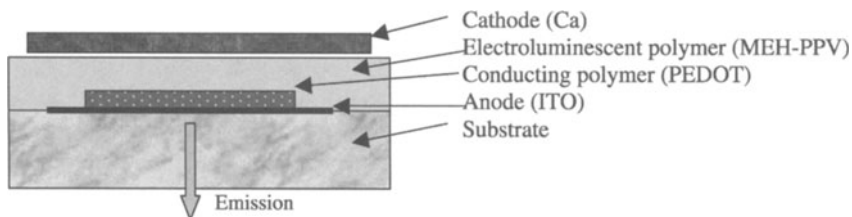


**Figure X-40.** Pixel with an emitting zone defined by the charge injection layer (here, PEDOT deposited by ink-jet process).

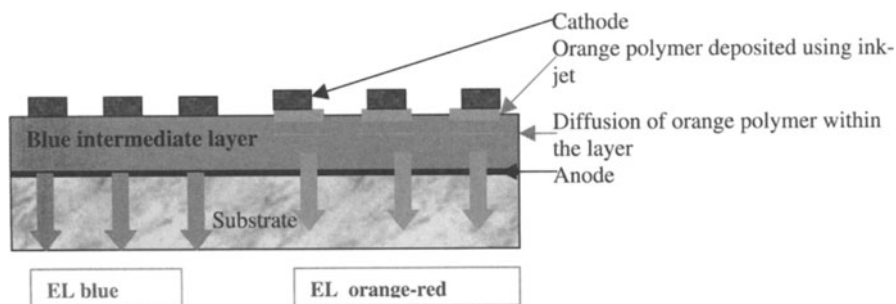


**Figure X-41.** Bi-coloured pixels obtained following excitation of a polymer by another with a larger gap.

polyimide by  $O_2$  and then  $CF_4$  plasma treatments, into each pixel caisson, constituted from three sub-pixels, were placed in the following order:

- PEDOT by spin-coating into the base of the caisson;
- a red emitter and a green emitter by ink-jet printing into respective sub-pixels, as shown in Figure X-42-c;
- a blue emitting polymer by spin coating, as in Figure X-42-d; and
- a cathode (Ca then Al) as in Figure X-42-e.

## 6 Emerging organic-based technologies: flexible electronic ‘pages’

As often occurs in the course of scientific development, the electronic-ink (e-ink) technologies were developed in parallel to that of the electroluminescent (EL) organic screens. Given that most people prefer reading ink deposited on paper, it is not unimaginable to think that ‘e-ink’ systems will replace EL screens, at least with respect to certain needs.

A group at the University of Gröningen proposed the use of e-ink systems in the preparation of flexible screens, which might be used as electronic pages [ber 01a]. We could call these ‘e-pages’. This technology could be adapted to the fabrication of screens operating either by transmission or by reflection, and uses as base a thick plastic film covered with micro-holes each 10 to 20  $\mu\text{m}$  in diameter. The holes resemble pixels once they are filled either with a light emitter or by an electrophorescing ink. For the latter, a coloured solution which contains white particulates is used. After sealing the pixels, applied electrodes can control the movement of these particles, directing them either towards the surface or the base of the plastic film and thus changing their appearance from white to coloured. The German ‘start-up’ company, Papyron, which developed this technology is in competition though with an American technology, developed notably by E Ink Corporation) which is based on capsules. The capsules, again between electrodes, are about 100  $\mu\text{m}$  in diameter and are filled with a dye and a white, negatively charged chip. On applying a positive tension to the upper surface electrode, a capsule appears white as the chip is attracted towards

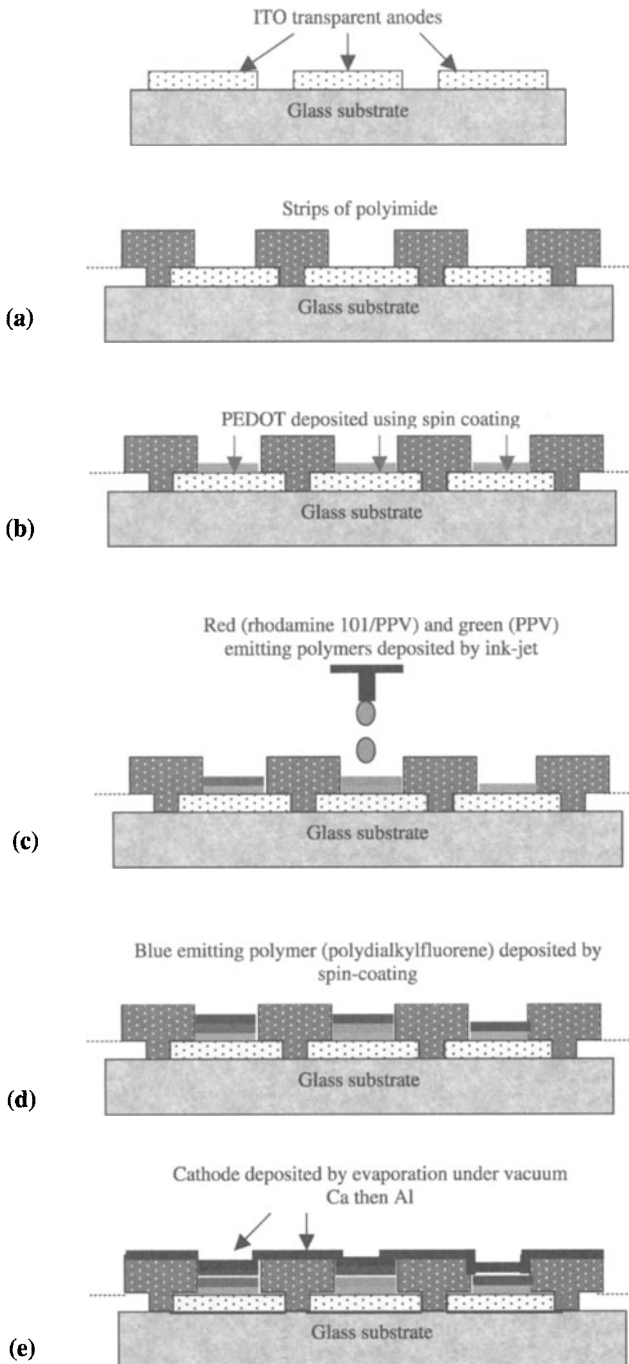


**Figure X-42.** Steps in the realisation of a tri-colour prototype developed by CDT-Seiko-Epson.



the screen. According to agreements made between E Ink Corporation and Philips (from the journal *Opto Laser Europe*, vol 5, page 84, 2001) the ink can be activated using electronic controls delivered *via* an active matrix developed by Philips.

Papyron insists that its technology exhibits numerous advantages over that of E Ink. Papyron states that its system allows a wider angle of view due to its pixels being flat rather than curving inwards and that its system allows a simpler fabrication of colour screens by filling different holes with different colours, an objective which can be realised using ink-jet technology. Thus, each pixel can be individually and electronically controlled using plastic transistors or other variants such as poly-crystalline silicon based transistors. For more stable displays, a liquid which exhibits wide variations in viscosity with changes in temperature can be used to facilitate image displays, as once the image is formed at a temperature high enough to allow easy movement of coloured particles, then the image can be 'fixed' by decreasing the temperature of the pixels, an operation which can be controlled by laser, for example.

For the present time, most companies concentrate their efforts on developing systems which can be fabricated using 'roll-on-roll' techniques. A research group in Limoges, France, is currently studying the formation of micro-holes through ionic columns due to field effects, in a system probably well adapted to automatic control of the depth of micro-holes for pixel fabrication. Xerox at Pali Alto have invented a technology called Gyricon which may compete in the same domain [ber 01b]. This procedure uses a thin plastic film into which is randomly inserted small pearls. The opposite hemispheres of these pearls are oppositely charged and are black on one side and white on the other. Depending on the charge applied, the spheres present a black or white surface. A continuous application of charge is not required; the spheres do not rotate back to a certain position; their power consumption is thus relatively low. Given that this sort of technology is not sensitive to air or humidity, it can be easily transferred to large surfaces. However, the time required for each sphere to change shade is relatively long and the integration of colour (using the three primary colours) in the system is hard to envisage, so this technique may not be useful for video applications. Nevertheless, such a system is sufficiently effective to enable rechargeable electronic books, a possible market worth over US\$10 billion.

Other possible techniques have been evaluated, notably by Lucent which developed a polymer based 25" screen using transistors fabricated through embossing processes.

## VIII The prospective and actual production at 2002

Most of the following information has come from issues of *Opto Laser Europe* at the end of 2001 and details the actual commercial and industrial situations at this time.

The market for flat screens is worth several billions of US dollars, and concerns both e-ink technologies, which necessitate external light sources, and emitting screens based in particular on organic electroluminescence, which do not. The market estimated for the year 2000 was US\$24 million, a 100% increase on 1999, while the

year 2005 is expected to encompass a market worth US\$3.3 billion. An explosion in this market is predicted for the period 2006 to 2010.

The main aims for those economically involved in this market concern the fabrication of screens which are lightweight, flexible and exhibit high luminance, contrast, wide angle of view, have low energy consumptions, and last but not least, cost little to make. The target market includes applications such as portable telephones, digital cameras, televisions – which can be hung up on walls or rolled up, tables which can act as displays, programmable and therefore rechargeable books and even wallpaper!

Pioneer, with a licence from Eastman Kodak, commercialised, in September 1997, the first organic screen, which was destined for an auto-radio facade. It was based on Alq<sub>3</sub> and had dimensions of 9.5 × 2.1 cm, and consumed 0.5 W. LG-LCD in Korea announced the fabrication of a  $\frac{1}{4}$  VGA screen functioning at 5 V and displaying a contrast of 100:1. The screen was green and had a luminance of at least 200 cd m<sup>-2</sup>. Uniax fabricated small screens for portable telephones which emitted orange light at 610 nm, operated at 10 V and required only 1 mA per pixel to yield a luminance of 200 cd m<sup>-2</sup>. This screen was based on small molecules, much like the first colour screen introduced by Pioneer for a portable Motorola telephone. In May 2000, Sanyo Electric associated with Kodak presented an active matrix screen of 5.5" consisting of 240 × 320 pixels. The American company Universal Display Corporation (UDC), risen from Princeton and South California universities, subsequently also developed screens based on small molecules.

On turning to technology based on polymers, a highly involved company is Cambridge Display Technologies (CDT), which grew from the Cavendish Laboratory at the University of Cambridge, in which macromolecular electroluminescence was discovered. The firm Covion has announced an annual production of 40,000 litres of conjugated polymers, destined to be used by CDT and by Philips, the latter having a factory in Heerlen (The Netherlands) producing screens based on light emitting polymers (LEP)s for portable telephones. In March 2000, CDT and Seiko announced the realisation of a R-G-B screen based on polymers deposited using ink-jet methods. The fabrication, however, posed more problems than initially supposed, with incompatibilities arising between the polymer inks and the ink-jet deposition procedure. Collaboration with Seiko Epson brought about the presentation of a colour prototype in May 2000 and then again in May 2001 at San Jose as part of the Society for Information Display's conference there. Lifetimes greater than 50,000 hours have been attained using adapted encapsulation procedures. CDT has agreements with the Japanese firm Tokki for vapour phase physical deposition procedures and encapsulation, according OLE in July and August 2001. A pilot line worth US\$25 million was built in Godmanchester with the aim of fabricating 5 million screen units per year. The effective production was planned for the start of 2002 with 'roll-on-roll' procedures taking the place of ink-jet methods.

At the University of Arizona, the ink-jet method was applied to screen fabrication and yields of 0.9% were obtained. Sony though announced the fabrication of a 13" diagonal screen with 800 × 600 pixels (SVGA), R-G-B colour and a peak luminance of 300 cd m<sup>-2</sup>, the device controlled by an active matrix formed from polycrystalline silicon.

CDT's polymer technology has also been developed by Hewlett-Packard and Philips. The latter company has, in Heerlen, developed a pilot line for PLEDs on a glass substrate, as the flexible films were found to not entirely fulfil the role of barrier against humidity and oxygen. Philips consider that in addition to their higher luminance and wider viewing angle, organic LEDs are preferable to liquid crystal displays because of their shorter response times. By mid-2001 it was planned to realise a monochrome display for portable phones of size  $65 \times 100$  mm and capable of displaying video images. Nevertheless, DuPont in the USA has announced a plan to develop and fabricate plastic substrates for polymer based screens on active matrixes with Philips and Alien Technology, another British 'start-up' company. DuPont have also planned, in co-ordination with other new companies, to develop more classical technologies using active matrixes on glass in China and the Philippines. The German company Osram, bought up licences from CDT and Uniax (a company started by A. Heeger and subsequently bought by DuPont) and has installed a PLED pilot line in San José (USA) and planned to start production in Malaysia during 2002.

Japanese firms are not sitting back. Sony announced the prototype of the largest OLED screen, Toshiba planned to be selling in the market place polymer based screens by April 2002 and Tohoku-Pioneer and Sharp began an association to invest 424 million Euros into the production of organic EL screens. NEC and the Korean company Samsung, meanwhile, also formed an alliance to invest over a 5 year period 472 million Euros for the production of similar screens in South Korea from the Autumn of 2001 onwards.

In England, outside of CDT, there is another relatively young company called Opsys based in Oxford which seems to be going through considerable expansion, with at the time of writing this book, 25 employees and 15 University researchers financed. The company first worked on organometallic luminescent materials, including transition metals and rare earths, and then on macromolecular materials such as dendrimers. At the same time, the company expanded in different areas, notably being the first in Europe to take up licences to exploit Kodak's small molecules. Opsys has also been developing new small molecules with greater stabilities and yields than those of Kodak, and, according to the Director, the absence of the necessary competencies within Europe have meant that they have had to go to Fremont (USA) to produce their screens. From 2002 onwards Opsys planned to fabricate their 1" to 5" diagonal screens, with active matrixes and back-lighting for portable devices. Larger screens, with appropriate licensing have been planned. The technology of the present time—based on the evaporation of small molecules—allows for little flexibility (for example with respect to changing substrate size), and it is planned that it will be changed at some point to a technology such as ink-jet or spin-coating based on polymers. The company does not see the choice between small or macro-molecules being one of chemistry or even optoelectronics, but more to do with problems associated with fabrication and costs. In addition, it seems that Opsys has already at its disposition a new class of polymers which do not fall under the umbrella of CDT's patents.

## IX Conclusion

The industrial competition is wide open and the diversity of competitors currently operating is without doubt justified by the existence of such an enormous, and financially consequent, market. The market goes beyond that reached by liquid crystals and is planned to be used not only in conventional systems such as screens but also in a wide range of other devices, for example aeroplanes, cars, display panels, electronic books and in teaching systems. While the field of organic electroluminescent diodes remains young (for the most part being developed in the last 10 years), it is already vast and the number of annual publications on the subject is considerable. We can remark that a decade of intense research has actually given rise to a new source of light which is now ready to enter our everyday lives. Organic solids, largely studied during the 20th century with relatively few actual practical applications have now found in the form of electroluminescent diodes an enormous field of applications, a field which should continue to grow.

In this Chapter, we have tried to present the essence of current knowledge. However, it would be highly pretentious to imagine that we have covered everything. As a useful indicator of the results of ongoing research, it is worth mentioning the reference [tro 01] which was prepared in collaboration with Thales and concerns the preparation of an OLED emitting blue-green light.

A four layer structure, shown in Figure X-43, combines a hole injection layer (HIL) made of PEDOT, an emitting hole transport layer (TNATA), a hole blocking layer (HBL) made of BCP and an electron transport layer (ETL) made of Bebq<sub>2</sub>, which has been shown to be more efficient than Alq<sub>3</sub>. These molecules and their chemical formulae are further detailed in Appendix A-11. The structure ITO/PEDOT/TNATA/BCP/Bebq<sub>2</sub>/Ca, emitting in the blue-green at 508 nm gives rise to a luminance of the order of 12980 cd m<sup>-2</sup> operating at 11.2 V (Figure X-44). In the green though a greater luminance, more than 20,000 cd m<sup>-2</sup>, was obtained using a tri-layer structure detailed in Figure X-22-b.

To conclude, these results show that luminances obtainable with OLEDs can be particularly high and can satisfy the demands of a wide range of applications.

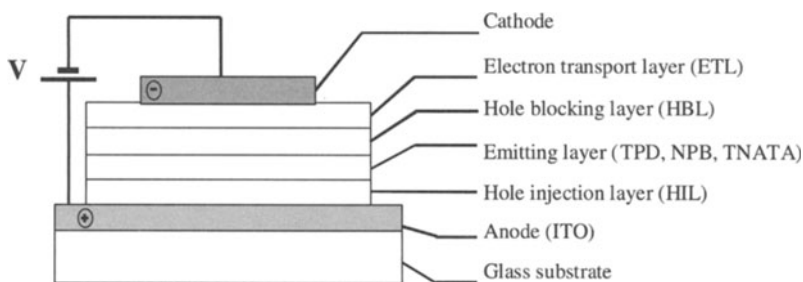


**Figure X-43.** OLED obtained from a four layer structure.

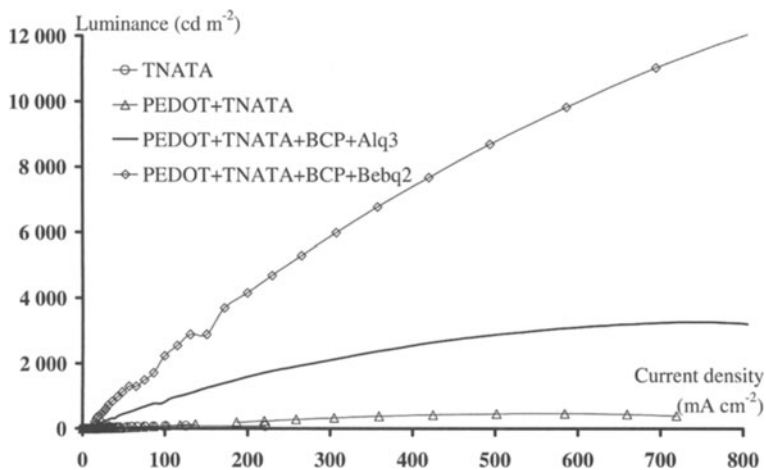


**Figure X-44.**  $L = f(J)$  curves for various structure based on TNATA, including, notably, the structure ITO/PEDOT/TNATA/BCP/Bebq<sub>2</sub>/Ca.



As an example is shown the prototype screen for a portable telephone fabricated by the British firm OpsyS using small organic molecular technology, a technology in which Kodak Eastman holds numerous patents. The screen has diagonal size of 1.24", is 1.8 mm thick and exhibits a luminance of 40  $\text{cd m}^{-2}$ . It consists of  $128 \times 64$  pixels (image from Displays Europe, February 2002).

## X Actual state-of-the-art and prospectives

During the Society for Information Display (SID) meeting in Baltimore, USA, in May 2003, two firms claimed to have built the largest OLEDs yet. IDTech demonstrated a 50 cm diagonal display driven by "super amorphous technology", a technology with a cost much lower than this incurred with polycrystalline transistors. It had previously been thought that amorphous silicon was incapable of delivering sufficient current to

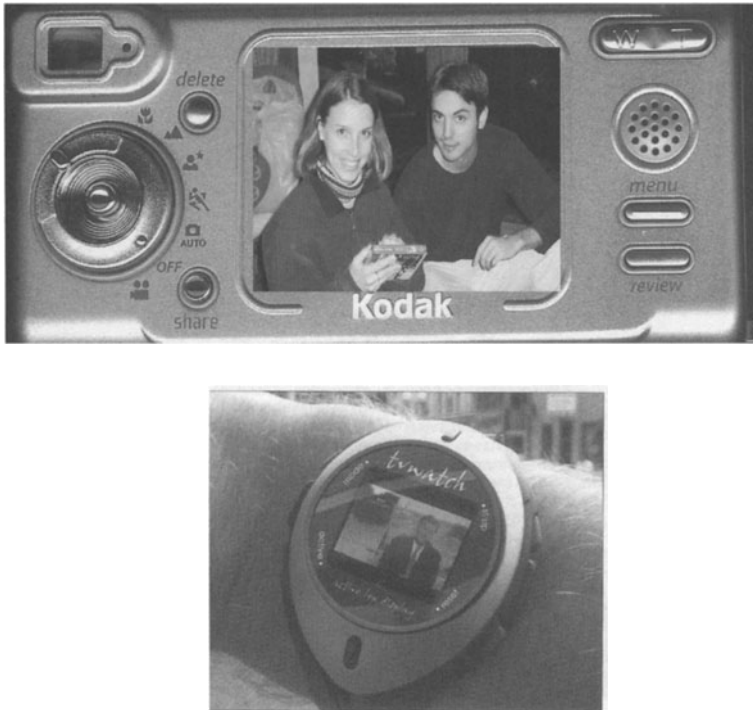


**Figure X-45.** (a): Kodak camera EasyShare LS 633; and (b) CDT concept for a TV watch using its light-emitting technology.

drive OLED pixels, but IDTech claims that its display consumes half the power of a typical high-end LCD, and offers better colour saturation and a wider viewing angle. It has a resolution of  $1280 \times 768$  pixels and draws  $25 \text{ W}$  of power at  $300 \text{ cd m}^{-2}$ . Sony exhibited a substantially bigger active-matrix OLED display at  $60 \text{ cm}$ . It was comprised of four seamlessly joined pieces (displays) using a new tiling technology. The Sony display, at  $1024 \times 768$  pixels, had a slightly lower resolution than the IDTech screen. Both companies say that their developments could lead to OLED displays being used in televisions. Furthermore, Kodak and its manufacturing partner Sanyo showed a  $15 \text{ inch}$  OLED screen which will be commercialised in three to four years [Ole 03-b].

The first commercialised large scale OLED display ( $2.2 \text{ inch}$  diagonal) was inserted into the Kodak Easyshare LS633 camera (Figure X-45-a) sold with a price tag of around  $\text{€}450$ . The display, with a viewing angle of  $165^\circ$  has a resolution of  $512 \times 218$  pixels and a power consumption of around  $300 \text{ mW}$ . It was developed by SK display, a joint venture between Sanyo Electric and Kodak. SK will initially produce around  $100,000$  two-inch OLED displays each month, and hope to boost this value to  $1 \text{ million}$  at the end of 2003 [Ole 03-a]. Meanwhile, Phillips Electronics hopes to sell more than  $100,000$  electric shavers incorporating a small monochrome

OLED display in 2003. Phillips have already exhibited a 1.4 inch passive-matrix monochrome PLED at SID 2002, held in May 2002 at Boston, USA.

Cambridge Display Technology (CDT) of the UK and the Japanese firm Seiko-Epson developed in a joint company, Polyink, an inkjet printing technology based on light emitting polymers. They have fabricated a TV watch, shown in Figure X-45-b, and commercialisation is in progress. However, an opportunity for CDT to buy up Litrex, a Californian company which also manufactures industrial inkjet equipment, may lead to new directions being taken.

It should be mentioned that displays made by Pioneer for car stereos and cell phones have been on the market for sometime already.

Research into OLEDs has given—apologies for the pun—a vision of what may be possible in the future. Flexible displays could one day depict an electronic newspaper or, as curved screens, furnish the automobile or plane cockpit of tomorrow. ‘Electronic ink’ is an alternative way to produce soft electronic newspaper and the E ink company of Cambridge, Massachusetts, USA, has demonstrated the world’s thinnest active-matrix display (0.3 mm thick). The construction combines a thin, shatterproof steel foil transistor substrate with E ink’s paper-like electronic-ink display material coated onto a plastic sheet.

In 2003 the OLED display market is valued at around \$500 million, and according to various market analysts (DisplaySearch, Stanford Resources, iSuppli), may reach \$3 billion (€2.7 bn) in 2007 or 2009 [OLE 03-a or Sie 03].

## Organic photovoltaic devices

### I Principles and history of organic based photovoltaics

#### 1 General points: the photovoltaic effect

##### a The photoelectric process

In general terms, photoelectronic processes correspond to those engaged in the absorption or emission of light by a material. Solids can be subject to various effects, such as photo-conduction (conduction once the material is illuminated) or the photovoltaic effect (generation of a tension by illumination), and these effects are directly tied to transport mechanisms. Here we shall concern ourselves expressively with the second process.

Within a photovoltaic system, we can see that following exposure to a ray of light, charge carriers can be generated by:

- electron band to band transitions (valence band to conduction band);
- electron transitions from localised states in the forbidden band up to the conduction band, or from the valence band to empty localised states in the band gap; and
- the generation of excitons following their dissociation or their ionisation.

The first process can be found in inorganic crystalline solids, the second in inorganic amorphous solids, and the third, most commonly, in organic solids.

Whatever the process though, the photovoltaic process consists of 3 steps which are:

- photogeneration of charges, by one of the three mechanisms above;
- the separation of those charges and their transport (and eventual multiplication) to the physical limits (terminals) of the device; and
- the realisation of an electrically active contact that can give rise to a signal which can be analysed either as a phototension with the circuit open, or as a photo-current with the circuit closed.



## b Various configurations used for collecting photogenerated charges

For a photovoltaic device to operate, the second step mentioned just above is essential and can be caused by several different effects [Kao 81]:

$\alpha$  *The volume or mass photovoltaic effect* This effect can arise from the diffusion of charge carriers subject to a non-equilibrated regime, with holes and electrons each having different mobilities. This effect was first observed in 1932 in diamond, and then later in zinc sulfide, and is often called the Dember effect. It could be discerned at the limits of materials which were under an intense light. Submitting anthracene to light with wavelength  $\lambda = 365$  nm, equal to its fundamental absorption, yields a phototension around 0.2 V. The negative 'pole' can be found on the side exposed to light, as holes have a greater mobility than electrons, and therefore the former move more readily away from the exposed side.

$\beta$  *The surface photovoltaic effect* This effect appears at the interface between a metal and a semiconductor and leads to the formation of a potential barrier (a Schottky barrier as detailed in Figure XI-1). When a metal (M) is placed in contact with a p-type semiconductor ( $SC_p$ ), and the metal has a work function ( $W_M$ ) which is less than that of the semiconductor ( $W_{SC_p}$ ) i.e.  $W_{SC_p} > W_M$ , then the equilibration of Fermi levels occurs *via* the passage of electrons from the metal to the semiconductor. In the semiconductor, the same electrons recombine with holes and then acceptor ions ( $A^-$ ), negatively charged, are no longer stabilised by neighbouring holes. The result is the appearance of a negative space charge due to a certain density ( $N_a$ ) of acceptors. Given the low value of  $N_a$ , the space charge actually goes quite deeply into the semiconductor and the diffusion of electrons from the metal to the semiconductor stops when the internal field, generated by the space charge directed from the metal to semiconductor, equilibrates the diffusion current. The metal takes on a positive charge near the interface and then holes there observe a barrier  $\Delta W = \chi + E_G - W_M$ , where  $\chi$  and  $E_G$  are the electronic affinity and the gap of the semiconductor respectively. On the semiconductor side of the interface, holes moving towards the metal observe

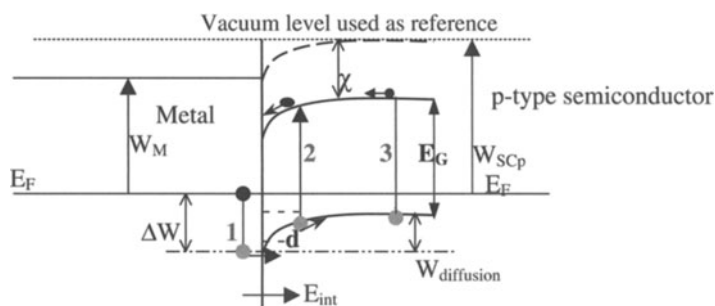


**Figure XI-1.** Representation of the mechanisms giving rise to a phototension in a Schottky junction (metal/p-type semiconductor) with  $W_{SC_p} > W_M$ .

the barrier  $W_{\text{diff}} = W_{\text{SCp}} - W_{\text{M}}$ . At equilibrium, the modulus of the current of holes going through  $\Delta W$  is equal to that going through  $W_{\text{diff}}$ . The space charge zone is not a great conductor; it is resistive due to the lattice  $A^-$  ions being relatively immobile. Thus, it is also the seat of any drop or rise in tension if we negatively or positively polarise the semiconductor. If a negative tension is applied to the p-type semiconductor, the current of holes going from the semiconductor to the metal is blocked by a barrier which is raised to  $W_{\text{diff}} + |qV^-|$ . If a positive tension is applied to the p-type semiconductor, then the barrier is reduced to  $W_{\text{diff}} - |qV^+|$  and the current of holes from the semiconductor to the metal is reinforced. In effect, we have a rectifying contact which permits the passage of strong currents going from semiconductor to metal and blocks those from metal to semiconductor.

Turning now back to the photovoltaic system, there are three possible effects in the structure of Figure XI-1, in which there is an interface between a p-type semiconductor and a metal where the workfunction of the former is greater than that of the latter (again,  $W_{\text{SCp}} > W_{\text{M}}$ ):

- the absorption of light by the metal with the associated generation of a hole of energy that can overcome the barrier  $\Delta W$ , only when the light is such that  $h\nu > \Delta W$ , at the M/SC interface. With a sufficient amount of energy, the generated holes can penetrate into the semiconductor and form a phototension at the barrier;
- with an incident ray of light with  $h\nu > E_{\text{G}}$ , an electron-hole pair is created in the hole depleted zone  $d$ . The intense electric field, which dominates this zone, of  $E_{\text{int}}$  generated on the equilibration of metal and semiconductor Fermi levels, in the direction left to the right of the Figure, efficiently separates photogenerated carriers. The result is a phototension between the metallic electrode and the semiconductor volume; and
- when the incident wave has a low energy, and a long wave, the optical absorption coefficient is small and in effect there is a poor formation of electron-hole pairs, as  $h\nu$  is not greater than  $E_{\text{G}}$ . Such waves can penetrate quite deeply into the material and can generate, within the semiconductor volume, electron-hole pairs. In addition, minority carriers can be formed, created at a distance from the depleted zone around their diffusion length ( $L_{\text{m}}$ ), to diffuse towards the junction where they are controlled by the field  $E_{\text{int}}$ . They can then contribute to the phototension at the barrier limits.

Generally speaking the first process is relatively unimportant, and is associated with photoemissions with an intensity of light dependent on the thickness of the metallic film. When  $h\nu > E_{\text{G}}$ , the second and third processes are the most important. Once the photons have an energy much greater than  $E_{\text{G}}$ , the absorption coefficient is very high and any rays are, practically speaking, absorbed near the interface. A decrease in the photoresponse is thus due to strong recombinations that occur close to the surface, where there are normally a high concentration of defaults.

Photovoltaic effects like those described above have been observed in anthracene [Kil 71], tetracene, chlorophyll and phthalocyanine [Gho 74]. We shall detail the photovoltaic effects revealed from these materials in the immediately following Subsection 2.

*γ* The photovoltaic effect produced by an internal field at a hetero- or pn junction  
 As in the case above, the internal electric field across a space charge zone propels in opposite directions the photogenerated charge carriers, resulting in the formation of a phototension. There are now standard texts which well detail the theories associated with devices, essentially made from inorganics, based on these effects (photovoltaic cells) such as Section 9.2.4 of [Mat 98]. In organic materials, most photovoltaic effects are obtained using Schottky pn-junctions, which require two types of semiconductor. In Section 2 we will cite the example of phthalocyanine/perylene. Here the former component, p-type, is a highly coloured chemical, historically derived from the conversion of disubstituted benzene derivatives. The second, n-type, is a polycyclic hydrocarbon with the chemical formula  $C_{20}H_{12}$  and is used in the preparation of dyes.

To give an overview, the development of solar photovoltaic systems has up until now been essentially shouldered on inorganic semiconductors, in particular polycrystalline silicon. While the maximum yields approach 24%, the cost of fabrication of the raw materials have limited commercial developments. Alternatives using microcrystalline or amorphous silicon have been widely studied and maximum yields have neared 15%. Nevertheless costs remain a problem due to processes based on the use of highly polluting materials, leaving them to compete poorly with other energy sources. In parallel, the use of organic semiconductors, developed during the 1970s and 80s [Sim 85] was also envisaged as a possible route. In the following Sub-sections 2 to 4 we will show the more notable results, before going on in Section II to describe  $\pi$ -conjugated polymers and organic systems based on specific structures under going development at the present time, notable interpenetrating materials.

## 2 Initial attempts using organic materials: the phthalocyanines

While the first results were hardly very encouraging, with yields of the order of  $10^{-2}$  to  $10^{-3}\%$ , significant results, around 1%, were realised in 1978 using merocyanine [Mor 78]. The considerable problem of instability associated with organics put considerable break on their development. This was in part resolved though by using phthalocyanines (Pc). Indeed, this material has found commercial success as a photoconductor in photocopiers or printers (Xerography). Their chemical structure, shown with the example of CuPc in Figure XI-2, is close to that of chlorophyll [Keo 98], indicating that real possibilities do exist for the conversion of solar energy. Two classical configurations have been explored with this material: Schottky and pn-junctions. In both cases, the Pc layer on being submitted to light rays is used to generate electron-hole pairs. Their separation by an internal tension, which governs the limits of the junction, can give rise to a photocurrent in an external circuit.

As shown in Figure XI-3, the Schottky junction is typically prepared with a sandwich structure. The p-type semiconductor, phthalocyanine (see also Chapter X, Section IV-1-a), is placed between an electrode that ensures an ohmic contact (Au or ITO, which have high work functions) and a second, rectifying electrode which permits the passage of current from the p-type semiconductor towards the latter metal (Al or In, which have low work functions).

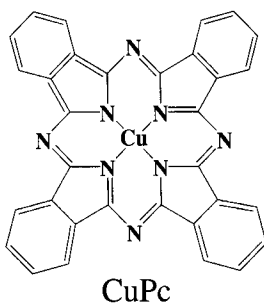


**Figure XI-2.** Structure of the CuPc molecule.

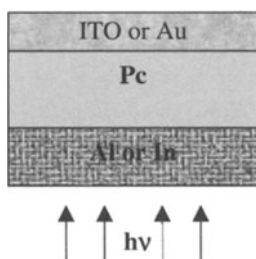


**Figure XI-3.** Configuration, under light, of a Schottky Pc/Al or In junction.

The rectifying effect, detailed in Figure XI-4, can only be efficient if the phthalocyanine layer exhibits a negative space charge and is truly p-type. If the layer is deposited under air it shows strong rectifying properties (Figure XI-4-a), however, if deposited under vacuum the same properties are only weakly exhibited

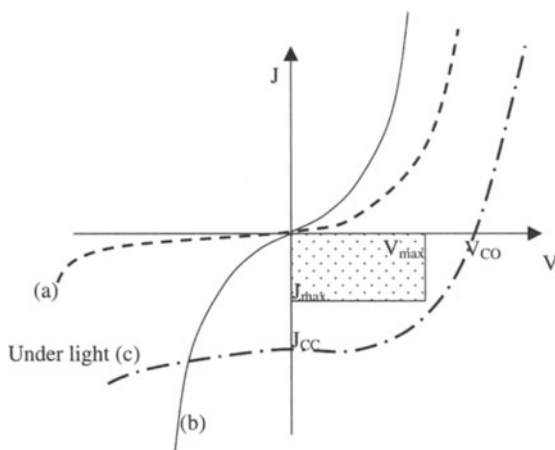


**Figure XI-4.** The (a) rectifying or (b) non-rectifying behaviour with respect to deposition conditions used with CuPc; and (c) the resulting  $J(V)$  curve obtained on exposure to light.

(Figure XI-4-b). In general, the degree of contamination by oxygen is highly variable, making it difficult to compare results from different laboratories. However, the characteristic curve obtained under light, as in Figure XI-4-c, can be used to determine the open circuit tension ( $V_{CO}$ ) (the photovoltaic regime) and the short circuit current ( $J_{CC}$ ).

The maximum electrical power ( $P_{max}$ ) is such that  $P_{max} = V_{max} J_{max} = J_{CC} V_{CO} F$ . The factor  $F$ , called the fill factor, depends on the series resistance of the device.  $V_{max}$  and  $J_{max}$  are defined in Figure XI-4. The yield of the system, generally expressed as a percentage, is the ratio of maximum electrical power to the power of the total incident light.

Using this Schottky configuration, yields of 1% were finally attained using materials based on a spacer group (X) and non-metallic phthalocyanines (X-H<sub>2</sub>Pc) and lighting through an indium electrode. The poor transparency of the electrode resulted in a global efficiency of only 0.2 to 0.3%. Lighting the device from the side of the transparent electrode (ITO) did not improve the result due to the Pc layer filtering light, which otherwise would have reached the space charge zone situated near the indium electrode.

The use of pn-junctions should, in part, help overcome the problem associated with absorption due to the metallic electrode, used as a rectifying contact. This is because the space charge now appears at the interface between the n- and p-type semiconductors. Structures based on n-type perylene and p-type Pc, schematised in Figure XI-5, have been experimented with. Better performances than those observed with Schottky structures were obtained, due to a higher degree of light transmission to the space charge zone. Excitons which diffused up to the interface between the two semiconductors were thus ionised and the electrons and holes could be collected. With devices sufficiently thin, a fill factor of 0.65 can be obtained. Tang, using this method [tan 86], realised conversions of the order of 0.4 to 1%. However, a higher value is required for the system to be viable at an industrial level.

### 3 Solar cells based on pentacene doped with iodine [Schö 00b]

In order to dope pentacene with iodine, the pentacene is introduced into a hexane or acetonitrile solution of iodine and left there for 72 h. This process gives rise

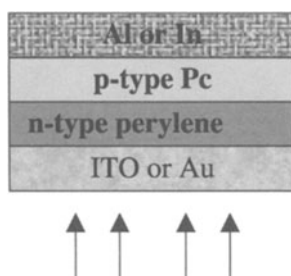
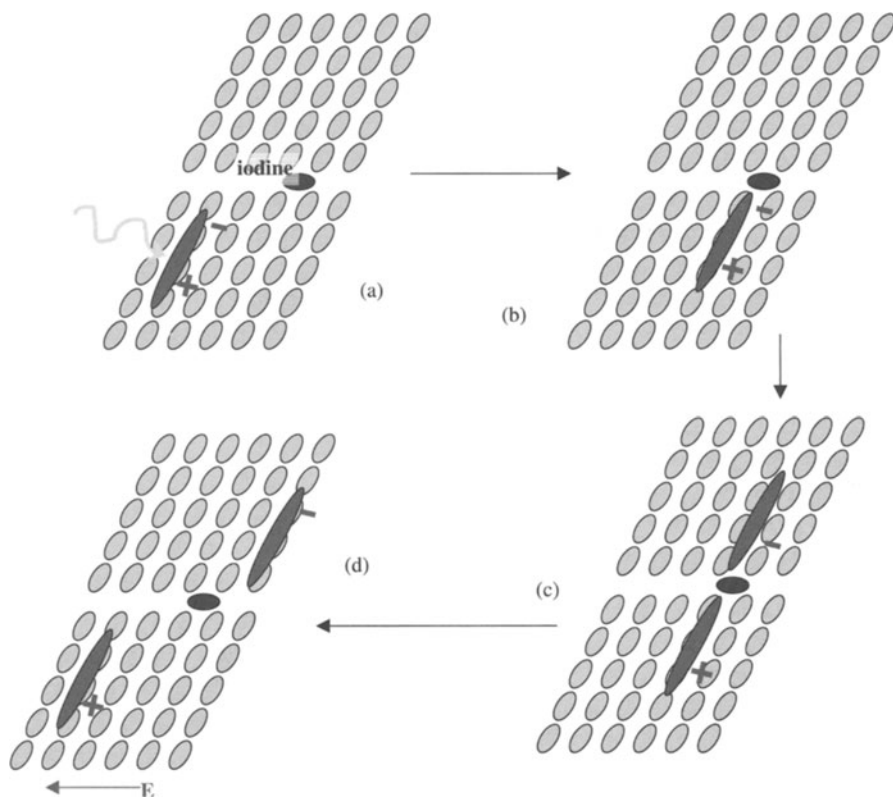


Figure XI-5. Organic pn-junction under light.

to a good p-type semiconductor. The iodine molecules are incorporated between layers of pentacene molecules and the resulting charge concentration can vary from  $10^7$  to  $10^{18} \text{ cm}^{-3}$ . The iodine enables a high charge mobility (comparable to naphthalene and anthracene at  $1$  to  $2 \text{ cm}^2 \text{ V}^{-1} \text{ s}^{-1}$ ) and good electrical conductivity, in addition to the efficient separation of charges. Useful also is the displacement of the absorption spectrum (threshold at  $1.4 \text{ eV}$ ) towards that of the solar spectrum.

The increase over several orders of size of the quantum yield of this system, which can reach from  $1.9$  to  $2.4\%$ , can be reasoned by the following mechanism:

- the incident photon is absorbed by the active zone where an exciton is formed (Figure XI-6-a);
- the exciton diffuses into the neighbourhood of an iodine dopant molecule to generate an excited state at the pentacene-iodine-pentacene complex level (Figure XI-6-b);



**Figure XI-6.** Charge photogeneration in the pentacene-iodine system: (a) photogeneration of an exciton; (b) diffusion of the exciton near to the iodine; (c) transfer of negative charge towards the iodine and dissociation of the exciton; and (d) separation of positive and negative charges under the field (E) effect.

- the negative charge of the exciton is partially transferred towards the doping molecule (Figure XI-6-c) and thus aids in the dissociation of the exciton; and
- the hole and electron are finally separated and the charges carriers are collected, with the help of an electric field, to yield the photocurrent. (The electric field which gives rise to the collection of these charges is an internal field generated by a Schottky junction or a heterojunction).

The lifetimes of such devices remain controversial and it is for this reason that any results announced should be viewed with some caution.

Cells with dimensions 5 by 5 mm have been made using the structure ITO/iodine doped pentacene (50  $\mu\text{m}$  thick)/Mg or Al and have yielded  $V_{\text{CO}} = 995 \text{ mV}$ ,  $J_{\text{CC}} = 4.5 \text{ mA cm}^{-2}$ , and a fill factor (ff) of 0.45.

#### 4 The general principle of Graetzel and current organic solar cells

In general terms, and as we have already seen in some examples, the heart of a solar cell consists of a semiconductor which normally absorbs photons and thus passes electrons from valence to conduction bands. This requires that the photons have at least a minimum energy and that excess energy is lost, even if this means that in the best materials 50% of the available energy is wasted. It is for this reason that the size of the forbidden band ( $E_{\text{G}}$ ) must be well adapted to the incident light. Excess photon energy, with respect to  $E_{\text{G}}$ , results in the thermal excitation of photoelectrons towards the LUMO band minimum (with, for example, an excitation of lattice vibration energy).

In the natural world, green plants which use solar energy are *a priori* subject to the same problem. Graetzel [Gra 91] was inspired to transfer the solution that they provided to photovoltaic systems. In plants, light is recovered by chlorophyll molecules which exhibit an absorption band well adapted to the solar emission spectrum. In effect, few photons are not used. Once the solar energy is absorbed, it is transferred *via* a protein complex in which a separation of charges gives rise to chemical reactions. These reactions convert carbon dioxide and water into hydrocarbons and oxygen. In terms of photovoltaic systems, the principal idea applied during the 1970s came from the same logic. In order to limit losses, the processes of light absorption and conversion to electrons were separated. Initially therefore, the structures were based on a layer of absorbent dye molecules deposited on a SC surface. Once the dye molecules were excited, they liberated, or rather transferred, an electron to the SC conduction band. This completely removed the dependence of photon absorption with respect to the SC absorption spectrum.

The problems that are now faced are:

- the efficiency of electron-hole pair (exciton) disassociation; and
- the efficiency of charge transfer towards the SC and the following collection of charges at the electrodes.

In practical terms, the slow transfer of charges from the dye required that this layer be extremely thin. If not, numerous recombinations could occur. The available material

for absorption is thus reduced and the number of electrons that can be generated becomes limited.

So, rather than using a specifically semiconducting material, such as crystalline  $\text{TiO}_2$ , Graetzel prepared a porous material from a large number of colloidal  $\text{TiO}_2$  particles and impregnated it with dye molecules. The particles, which were hardly 20 nm across, were in effect inserted within a dye layer of about 1 micron. The effective specific surface area of the dye using this technique hence became very large indeed.

Now standardised, the Graetzel cell is made up of a liquid electrolyte sandwiched between two transparent electrodes. The instability of the system, due to evaporation of the electrolyte, however, does demand a low operating temperature range, something which has tended to limit their widespread use.

Poly(*para*-phenylene vinylene) (PPV) and its derivatives are, at present, materials widely under investigation for insertion in porous  $\text{TiO}_2$  matrices. A problem remains in the macromolecular size of the PPVs, especially important now that the  $\text{TiO}_2$  is prepared on a rotating disc from a very fine powder. At the Universities in Santa Barbara and Cambridge, principally, research has now centred on the use of buckminster fullerene ( $\text{C}_{60}$ ) in place of  $\text{TiO}_2$  in composites with PPV. Here a PPV chain is grafted onto  $\text{C}_{60}$ , and we will look at these materials now in more depth.

## II $\pi$ -Conjugated materials under development for the conversion of solar energy

There are many envisaged advantages to making polymer ('plastic') based photovoltaic systems. They include their ease of fabrication and manipulation, their flexibility and low weight and their low cost, all of which are good reasons to imagine their facile integration into buildings. These expectations have done much to push research rapidly forward over the last few years.

### 1 Metal-Insulator-Metal structures

On using the structure of organic LEDs as a basis, the classic metal-insulator-metal (MIM) structure was envisaged as a possible route to the preparation of photodetectors. Organic LEDs were, incidentally, the first optoelectronic devices made using  $\pi$ -conjugated polymers.

As shown in Figure XI-7, once a contact is made, then the alignment of Fermi levels adjusts band positions. Without an applied tension, *i.e.*  $V = 0$ , there is a swing in the polymer bands so that, still without the application of the external field, there appears an external field  $E_{\text{int}} = -\text{grad } V_{\text{int}} \neq 0$ . The difference in internal potential is due to the energy difference  $\Delta W_{\text{int}} = W_{\text{anode}} - W_{\text{cathode}}$ , *i.e.* the difference in work functions of the anode and cathode metals.

With the inception of a photon an exciton is produced. Under the photovoltaic regime, only the slight difference in internal potential controls—with a low yield—the dissociation of the photogenerated quasi-particle. In practical terms, the generated phototension is not great enough to be of any use. With the structure ITO/PPV (120 nm



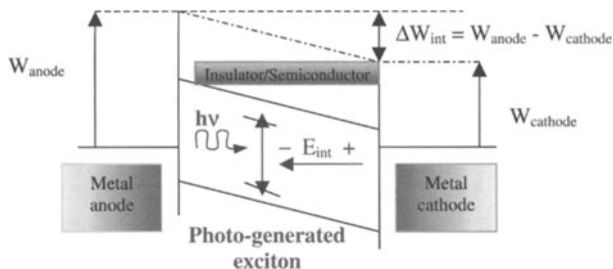


**Figure XI-7.** Photogeneration of charges in a MIM structure.

thick)/Mg, the tension at open circuit is 1.2 V and the short-circuit current is equivalent to a quantum yield of 1% (electrons collected per incident photon). This yield, however, improves drastically once the system is subject to an inverse polarisation (around 10 V) and can permit envisaging this system applicable as a large surface photodetector.

The use of a Schottky structure resulted in only a slight improvement in charge photogeneration.

It is generally acknowledged [Mar 94] that charge photogeneration in the volume of the material occurs through dissociation of exciton singlets under field effects. Instead of traversing the polymer layer, electrons are either trapped or undergo combination with holes, giving rise to a rather unremarkable result.

## 2 How bilayer hetero-structures work and their limits

Following on from the fundamental principles, derived from the photosynthetic systems described in Section I, any improvements in the photophysics of the preceding organic monolayer structures (MIM or Schottky M-SC) necessitate the use of bilayer systems. The use of a donor/acceptor structure would allow the efficient transfer of photo-electrons from a 'donor' semiconductor  $\pi$ -conjugated polymer (p-type semiconductor  $P_{OD}$ ) towards an 'acceptor' material which can either be an n-type  $\pi$ -conjugated polymer (which are rather rare), or an accepting molecule, of which the archetype is  $C_{60}$ .

### a Production and collection of photoinduced charges

The making and harvesting of photoinduced charges follows the processes given below:

- the incident light generates electron-hole pairs at the p-type donor polymer ( $P_{OD}$ ) due to electron transitions from  $\pi$  HOMO to  $\pi^*$  LUMO bands;
- the created pair is separated close to the acceptor, and electrons generated in the  $P_{OD}$  LUMO band are accepted on energetically favourable terms into the acceptor LUMO band. As Figures XI-8 (which shows the flat band condition) and XI-10

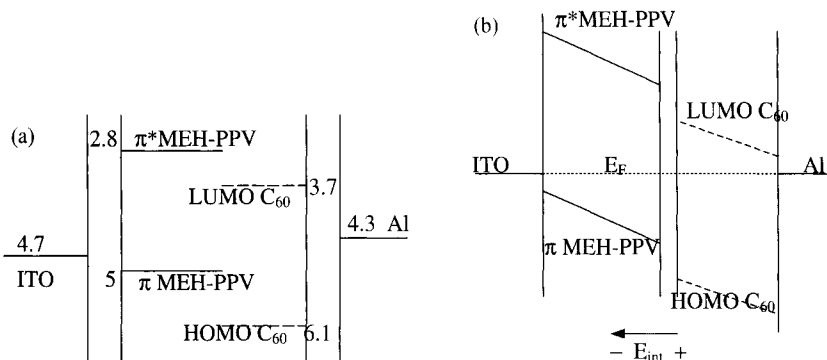


**Figure XI-8.** (a) Flat band regime of MEH-PPV/ $C_{60}$  system; (b) Energy levels in the MEH-PPV/ $C_{60}$  system in the short circuit state.

indicates, this is due to the acceptor LUMO being of a lower energy than that of the  $Po_D$  LUMO;

- the separated charges are propelled in opposing directions due to the internal field—to be collected—and as schematised in Figure XI-8-b.

## b Transport of photoinduced charges to the electrodes

In order to transport charges up to the electrodes, the photovoltaic system exploits the relative conductivities of holes and electrons with respect to the constituent donor and acceptor molecules in the composite.

*$\alpha$  Transport in the p-type donor polymer* Once the donor p-type  $\pi$ -conjugated semiconductor polymer ( $Po_D$ ) is excited by incident light, the first process it undergoes is the transfer of electrons from the bonding  $\pi$ -orbital to the antibonding  $\pi^*$ -orbital. Once the excited electron is transferred to an acceptor molecule, in this example  $C_{60}$ , then a polaronic state, associated with a positive polaron, appears on the  $Po_D$  chain. What we are observing here, in a sense, is a localised photodoping. The polarons have transport mechanisms detailed in Chapter IV.

*$\beta$  Transport in the n-type acceptor  $C_{60}$*  Once an electron is transferred to the  $C_{60}$  from the  $Po_D$ , it can benefit from the n-type semiconductor character which  $C_{60}$  exhibits to be transported throughout the  $C_{60}$  phase. Chapter III gives more relevant details.

*$\gamma$  Overall result* The rapid transfer of a photoinduced electron from  $Po_D$  to  $C_{60}$  permits reinforcement of the generated charges at  $Po_D$  and assures the separation of photogenerated charges—by enhancing their stability through a polaronic effect. It is thus possible to obtain a heterojunction with a rectification factor of the order of  $10^4$  for a bilayer structure based on poly(2-methoxy-5(2'-ethyl-hexyloxy)-p-phenylenevinylene) (MEH-PPV) and  $C_{60}$ , as schematised in Figure XI-8-b. In addition to which, it is possible to yield either a photocurrent or a photovoltage.

### c Properties and practical limits of donor–acceptor bilayer systems

The photophysics of bilayer systems have been studied in depth by C.J. Brabec and N.S. Saricifti [bra 01a]. Notably, it was shown that the time required for a decrease in the luminescence of MEH-PPV ( $\tau = 550$  s) was reduced by more than one order by the presence of  $C_{60}$ . This ‘quenching’ of luminescence by  $C_{60}$  seems to be a general phenomena for all  $\pi$ -conjugated non-degenerate polymers. In particular, it indicates that the transfer of a photoinduced electron occurs during an interval sufficiently short to limit any radiative relaxations of the excited, conjugated polymer.

However, a bilayer system must present some limits in performance, as even though the system has a high optical absorption coefficient ( $\approx 10^5 \text{ cm}^{-1}$ ), the absorption zone is considerably greater than the exciton diffusion length. As the exciton can only dissociate in a volume close to its zone of existence (the region at the interface between the donor polymer and the  $C_{60}$  and no further from the  $C_{60}$  than the short exciton diffusion length), all photoexcitations generated outside of this zone are condemned to undergo recombinations without generating efficiently separated photo-carriers. They cannot, for example, participate in the formation of a photocurrent. Also, the photovoltaic effect arises only from photons absorbed with this thin layer. An improvement in this situation can be made by introducing layers with high levels of optical absorptions or, alternatively, by using crystalline semiconductors of a high level of purity which allow longer exciton diffusion lengths.

Another approach to improving this system involves using elaborate thin films constituted of intimate mixtures of both the conjugated polymer and  $C_{60}$ . There is thus a large surface area for absorption which is always close to a  $P_{OD}$  and  $C_{60}$  interface, where the dissociation of an exciton can be assured [Hut 01]. Figure XI-9

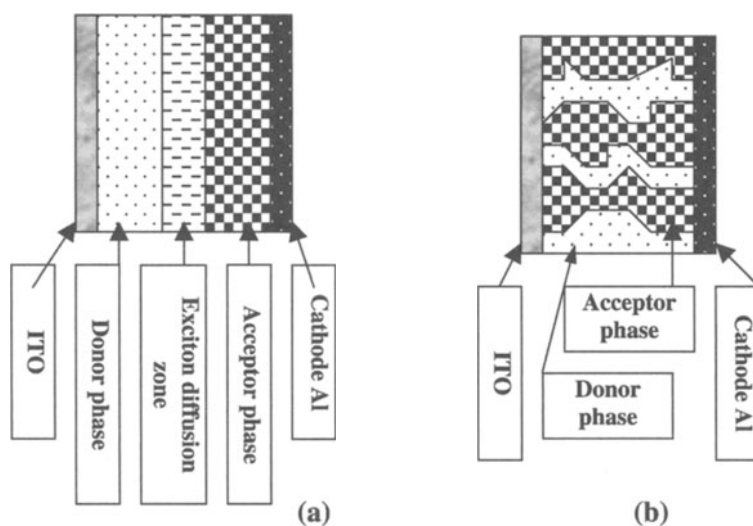


**Figure XI-9.** Schematisation of (a) a bilayer structure; and (b) an interpenetrating structure.

gives two representations corresponding to a classic bilayer device (Figure XI-9-a) and a device made using a composite of two interpenetrating phases (Figure XI-9-b).

### 3 Volume heterojunctions

#### a Principle

At each donor-acceptor element constituting the composite, the same mechanism is reproduced. That is, the creation of the exciton, its disassociation and the transfer of an electron from the donor to the acceptor, and the eventual separation—in opposite directions—of the hole in the donor phase and the electron in the acceptor phase under the influence of the internal field generated by the asymmetric electrodes. This process is detailed Figure XI-10.

As the zone of interaction between the donor and the acceptor are not reduced to a simple plane (as found in the bilayer system in Figure XI-9-a), these composite devices present a zone for the absorption of light which is sufficiently thick while at the same time maintaining the process of dissociation and separation of charge carriers in the volume of the layer. Outside of this, the transport mechanisms are the same as those exhibited by the bilayer device, and the mechanism used in the physical transfer of charges is the same as that schematised in Figure XI-11.

It is for these reasons that an interpenetrating composite can exhibit high (close to 100%) efficiencies in charge generation. It can be thought of as interpenetrating latticework of donor/acceptor heterojunctions, allowing efficient separation of photogenerated charges throughout its volume *via* the two n- and p-type phases. In effect, the photoactive layer is one mass heterojunction. The two intermixed materials of different gaps give rise to zones of sub-systems with levels where electrons are transferred between donors and acceptors.

The ideal situation is that the acceptor is placed at a distance less than the diffusion length of the exciton so that the separation of the photogenerated pair, or in other terms the dissociation of the exciton, is facilitated.

#### b The results

Under solar light, efficiencies have reached 3% [Brab 01a]. The composition and morphology of the film is, however, a critical factor. Rather than obtaining composites which are completely homogeneous, the films are rather disorganised, with isles forming of each component material. The size of these aggregates depends on the solvent used to prepare the film. As an example we can cite the use of chlorobenzene and toluene, the former giving rise to smaller aggregations. This effect acts directly upon the performances of the device as the smaller the size of the aggregates, the greater the specific interface zone available for dissociation of excitons.

We should also remember that the donor-acceptor matrices should interpenetrate to a sufficient degree, so that the transport of the two charge carriers is assured. A high concentration of C<sub>60</sub> can increase both the yield of photo-carriers and their lifetimes, resulting in a global increase in photo-current.

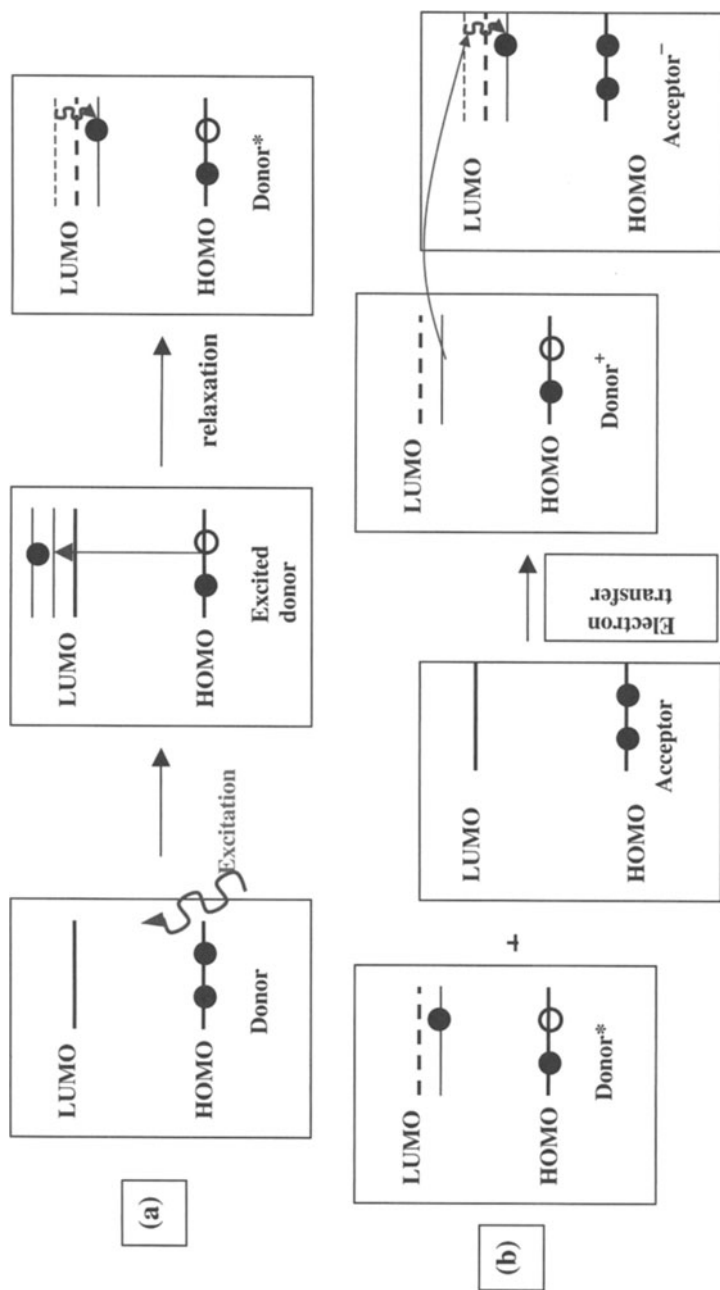


**Figure XI-10.** Schematisation of: (a) the formation of an exciton at an irradiated donor; and (b) transfer of an electron from an excited donor to an acceptor. In effect, a hole or electron carrier are formed, respectively, from the donor and from the acceptor.

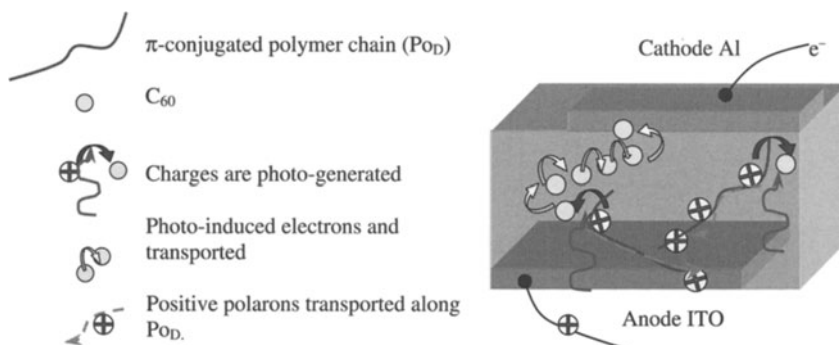


**Figure XI-11.** Schematisation of the physical process within a composite of  $P_{OD}$  and  $C_{60}$ .

Outside of the system based on MEH-PPV/ $C_{60}$ , the research teams of A. Heeger at Santa Barbara [Yu 95] and R.H. Friend at Cambridge [Hal 95] successfully experimented, independently, with a composite based entirely on polymers. The system used was based on MEH-PPV and CN-PPV, the former acting as the donor and the latter, a cyanide derivative of MEH-PPV, acting as the acceptor. CN-PPV exhibits a high electron affinity due to the presence of  $-C \equiv N$  groups substituted on its backbone (which have a character discussed and detailed, respectively, in Chapter X, Section IV-1-c and Appendix 1-10). As shown in Figure XI-8-a, and much like  $C_{60}$ , the LUMO of CN-PPV is below that of MEH-PPV. More recent studies have resulted in even higher efficiencies by gradating the stoichiometries of the different components in the layers, facilitating conduction of electrons and holes in the volume of the heterojunction [Bra 01b].

### c Using $\pi$ -conjugated polymers grafted onto $C_{60}$

One way of reinforcing the contact between donor and acceptor molecules, and overcoming phase separation, is to directly graft the donor chain directly onto the acceptor. Thus, a bicontinuous medium is obtained. There are two notable examples:

- grafting poly(*para*-phenylene) onto  $C_{60}$  (a route chosen by E. Mignard *et al*) [Mig 01]; and
- grafting oligo(*para*-phenylene vinylene) (OPV) onto  $C_{60}$  [Nie 99].

Using the structure ITO/ $C_{60}$ -OPV/Al allowed both the generation of electrons and holes and also their collection at opposing electrodes. On exposure to light, using the oligomer tri(*para*-phenylene vinylene) (3PV) an open circuit tension of 0.46 V was obtained, roughly equivalent to the difference in work functions of the ITO and Al. Under short-circuit conditions, the photo-current was found to be  $10 \mu A cm^{-2}$  and the fill factor 0.3.

The rather poor yield, nevertheless more than two orders greater than that of a layer of 3PV alone without the  $C_{60}$ , could be explained by considering that the transfer of photoinduced electrons (Figure XI-12, level I) between the 3PV and  $C_{60}$

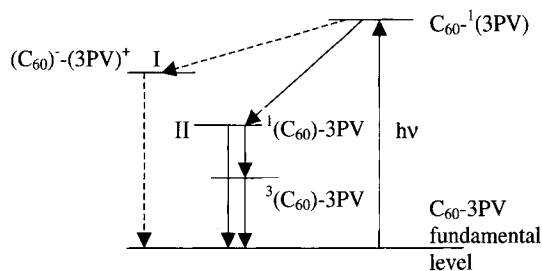


**Figure XI-12.** Schematisation of the energy levels involved in the relaxation of  $C_{60}$ -3PV (after J.F. Nierengarten, G. Hadziioannou, *Materials Today*, 4, (2001), 16).

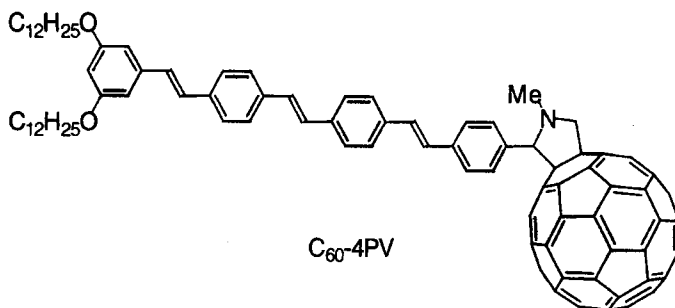


**Figure XI-13.** Representation of the compound  $C_{60}$ -4PV.

molecules was in competition with an energy transfer to the lowest energy singlet state of  $C_{60}$  (Figure XI-12, level II). A better result was obtained using 4PV in the structure shown in Figure XI-13, indicating the relationship between structures and characteristics. These results do highlight the route towards other developments based on, for example, new derivatives of  $C_{60}$  [Nie 01].

### III Additional informations about photovoltaic cells and organic components

#### 1 Discussion about mechanisms leading to the generation of charge carriers in organics

The making and harvesting of photoinduced charges follows the processes given below where donor and acceptor materials exhibit an interface which induces charge separation.

Figure XI-14 details the various processes of varying efficiencies ( $\eta$ ), which are:

- (1) photon absorption ( $\eta_A$ ). The incident light generates electron-hole pairs at the p-type donor material ( $PO_D$ ) due to electron transitions from  $\pi$  HOMO to  $\pi^*$  LUMO bands.  $\eta_A$  depends on the value of the optical absorption coefficient and on the thickness of the donor material;

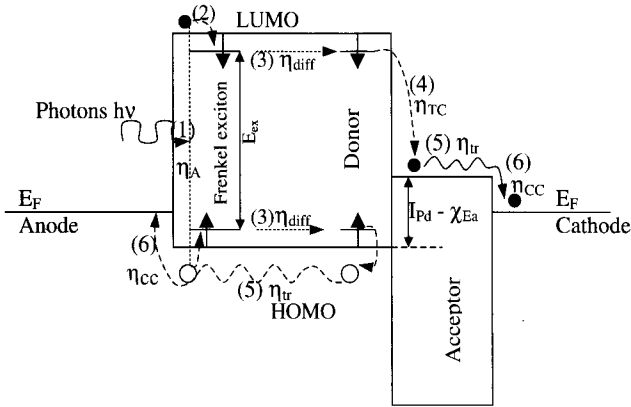


**Figure XI-14.** Mechanisms of photocarrier generation in organics.

- (2) generation of excitons. The generation of an electron-hole pair, by photoexcitation, results in an excited but neutral state with a limited, finite lifetime. This state is termed an exciton and consists of an electron and a hole paired by excited energy states ( $E_{ex}$ ) within the limits of permitted bands (LUMO and HOMO bands, respectively). The occupation of these excited states, the LUMO by the electron, the HOMO by the hole, is termed a non-recombined exciton generally observed in organic materials;
- (3) exciton diffusion ( $\eta_{diff}$ ). This quasi-particle diffuses inside the donor material as long as recombination processes (of the hole–electron pair which make up the exciton) do not take place. The Förster (long range) or Dexter (between adjacent molecules) transfers can take place between an excited molecule (considered as excitation donor) and a molecule that receives the excitation (excitation acceptor).  $\eta_{diff} < 1$  because various recombinations can occur in the thick donor material;
- (4) hole – electron separation (exciton dissociation) ( $\eta_{TC}$ ). If the diffusion length is sufficiently long so that the exciton meets an internal field, hole and electron separation occurs. The internal field may be obtained at a donor-acceptor interface, provided the LUMO level of the acceptor is lower than the excitonic state located at the bottom of the conduction band of the donor. More precisely, Figure XI-14 indicated that the condition which must be fulfilled is  $E_{ex} > I_{pd} - \chi_{Ea}$ , where  $E_{ex}$  is the bounding energy of the exciton,  $I_{pd}$  is the ionisation energy of the acceptor, and  $\chi_{Ea}$  is the electronic affinity of the acceptor. As this condition is generally verified,  $\eta_{TC} \approx 1$ ;
- (5) carrier transport towards the electrodes ( $\eta_{tr}$ ). This transport involves the classic mechanism for hopping processes in organic materials. Traps can reduce the mobility. If carriers are not infinitely trapped (as for example in lattice defects such as dislocations), we can consider that  $\eta_{tr} = 1$ ; and
- (6) charge collection at the respective electrodes ( $\eta_{CC}$ ). For this to occur,  $(E_F)_{cathode} < (E_{LUMO})_{acceptor}$  and  $(E_F)_{anode} > (E_{HOMO})_{donor}$ . When fulfilled,  $\eta_{CC} \approx 1$ .



## 2 Electric circuit based on an irradiated pn-junction; photovoltaic parameters

For this study, we will consider a pn-junction with an ohmic metallic contact.

### a Current inside the junction under short-circuit conditions and in the dark

The Fermi levels are aligned on the same horizontal line and the barrier which prevents the major carrier flowing is  $qV_{b0} = W_{sP} - W_{sN}$ , where  $W_{sP}$  and  $W_{sN}$  are the work functions of the p- and n-type semiconductors (Figure XI-15-a). If we denote with the index 0 the currents in the dark, the resulting electron and hole currents are, respectively:

$\vec{j}_{0n} = \vec{J}_{0nN} + \vec{j}_{0nP} = 0$  (moduli of the majority and minority electron currents are equal); and  $\vec{j}_{0p} = \vec{J}_{0pP} + \vec{j}_{0pN} = 0$  (moduli of the majority and minority hole currents are equal).

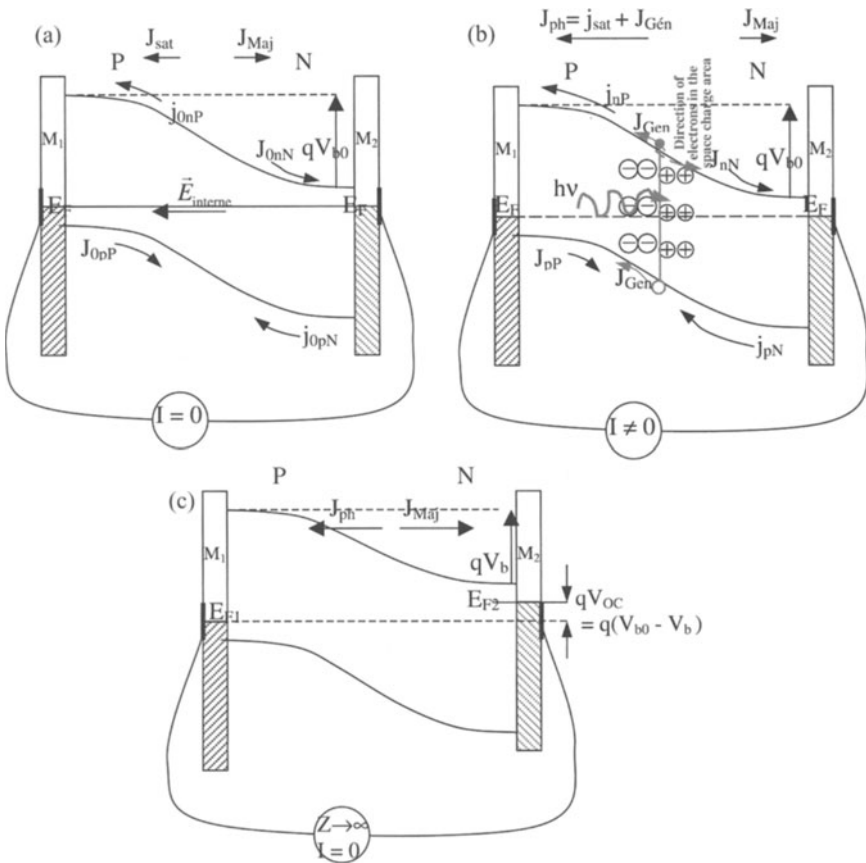


**Figure XI-15.** Current densities in a pn-junction (a) under short-circuit conditions and in the dark; (b) under short-circuit conditions and under irradiation; and (c) in open circuit and under irradiation.

The resulting current is of course zero:

$\vec{j}_0 = \vec{j}_{0n} + \vec{j}_{0p} = 0$ , and we can write:  $\vec{j}_0 = (\vec{j}_{0nN} + \vec{j}_{0pP}) + (\vec{j}_{0nP} + \vec{j}_{0pN}) = \vec{J}_{Maj} + \vec{j}_s$ , with  $(\vec{j}_{0nN} + \vec{j}_{0pP}) = \vec{J}_{Maj}$  (current of majority carriers) and  $(\vec{j}_{0nP} + \vec{j}_{0pN}) = \vec{j}_s$  (saturation current).

### b Current inside junction in short-circuit and under irradiation

Under short-circuit conditions, the Fermi levels remain aligned, but in the irradiated areas the Fermi levels become the *quasi* Fermi levels as shown in Figure XI-15-b. We then have  $\vec{J}_{Maj} = \vec{j}_{nN} + \vec{j}_{pP} \approx \vec{j}_{0nN} + \vec{j}_{0pP}$  because the irradiation does not drastically modify the density of the majority carriers. Conversely though, the minority carrier densities are strongly modified in the n- and p-regions because of the irradiation which generates the hole-electron pairs. The minority electron and hole currents are thus  $j_{nP} \gg j_{0nP}$  and  $j_{pN} \gg j_{0pN}$  and the resulting current is practically generated only by minority carriers as in  $\vec{j}_s = \vec{j}_{nP} + \vec{j}_{pN}$ .

Inside the space charge area there is some recombination of electrons and holes to give a recombination current which we will neglect. In addition, hole-electron pairs are also generated in the space charge area and giving a current going from the n to the p region which is denoted  $J_{Gen}$  in Figure 24-b. As a result, the irradiation produces a reverse current (going from the n to the p zone) and we can write:  $\vec{J}_{ph} = \vec{j}_{sat} + \vec{J}_{Gen}$ .

### c Junction in open-circuit and under irradiation (Figure XI-15-c)

This situation can be obtained when the junction is connected to an electrometer/voltmeter of high impedance ( $Z_{electrometer} \rightarrow \infty$ ).

The Fermi levels move closer to one another as the metallic electrodes are not directly connected by means of a short-circuit and a voltage appears across electrodes. Because the circuit is open, the current density is zero and  $\vec{J} = \vec{J}_{Maj} + \vec{j}_{sat} + \vec{J}_{Gen} = 0$ , where  $\vec{j}_{sat} + \vec{J}_{Gen} = \vec{J}_{ph}$  is the same reverse current as that calculated above in §IV,2,b. The resulting current being zero, the majority current must now be increased so that  $|\vec{J}_{Maj}| = |\vec{j}_{sat} + \vec{J}_{Gen}| = |\vec{J}_{ph}|$ . In fact, if the majority current is increased, then that means that the barrier which prevented the flow of the majority carriers is reduced from its initial value of  $qV_{b0}$  to  $qV_b$ , which verifies  $qV_b < qV_{b0}$ . So that the barrier observed by majority carriers becomes  $qV_b$  (for example, barrier to electrons on the metal ( $M_2$ ) side), the Fermi level must be raised on the same side by a value  $qV_{b0} - qV_b = qV_{OC}$ , and thus  $V_{OC} = V_{b0} - V_b$  is the voltage which appears at the contacts in the open-circuit configuration. The n region which is initially positive with respect to the p region with a value  $V_{b0}$ , becomes less positive under irradiation (with a value  $V_b < V_{b0}$ ).

What is important is to underline that, contrary to what is often stated, the voltage in an open, irradiated circuit is not equal to the voltage difference between the surfaces

of n and p regions and  $(W_{sP} - W_{sN})/q = V_{b0}$ . This value is the bias voltage which has given, not without some error, the name photovoltaic.

As demonstrated above, the value for  $V_{OC}$  is given by the variation in the potential bias between its value without and with irradiation and it is only when  $V_b \rightarrow 0$  that we have  $V_{OC} \approx V_{b0}$ .  $V_{b0} = (W_{sP} - W_{sN})/q$  is thus the maximum value that can be reached by  $V_{OC}$ , the open-circuit voltage for an irradiated pn-junction.

**d Electrical characteristics**

If the non-irradiated junction is biased with a voltage  $V$ , the current of the minority carriers is unchanged at  $j_s$ , while the majority current is exponentially reinforced to become  $J_{Maj} = j_s \exp\left(\frac{qV}{kT}\right)$ . The resulting current density is thus:

$$J = j_s \left[ \exp\left(\frac{qV}{kT}\right) - 1 \right].$$

When the junction is irradiated, the current density becomes:

$$J = j_s \left[ \exp\left(\frac{qV}{kT}\right) - 1 \right] - J_{ph}, \tag{1}$$

and we have the characteristics shown in Figure 25-a. Under irradiation, the curve no longer goes through the origin. The irradiated biased junction can thus work as:

- a rectifier with a forward bias  $V > V_{OC}$  in the first quadrant;
- a photodiode with a reverse bias in the 3<sup>rd</sup> quadrant where  $V \ll 0$  and  $|V| \gg \frac{kT}{q}$ ,  $J = -(j_s + J_{ph})$  that is to say with  $j_s \ll J_{ph}$ ,  $J \approx -J_{ph}$ . The measured current is approximately proportional to the irradiation and when  $V \rightarrow 0$ ,  $I \rightarrow I_{CC} \approx -I_{ph}$  (short-circuit current); and
- a photovoltaic cell without external bias, but with a current flowing through a load resistance  $R_L$  in the 4th quadrant so that the photovoltaic function is not reduced to the open circuit only. In this 4th quadrant, the product of  $VI$  is negative so that power (and electrical energy) can be produced by the device. With  $I' = -I$ , the curve  $I'(V)$  can be depicted for the general case in the first quadrant (see Figure XI-16-b) where the optimised (maximum) power ( $P_{max}$ ) fits the values  $I' = I'_m$  and  $V = V_m$  so that  $P_{max} = V_m I_m$ .

The fill factor (FF) is then defined as the ratio of  $P_{max}$  to  $V_{OC} \times I_{CC}$  and can be written  $FF = \frac{P_{max}}{V_{OC} \times I_{CC}}$ .

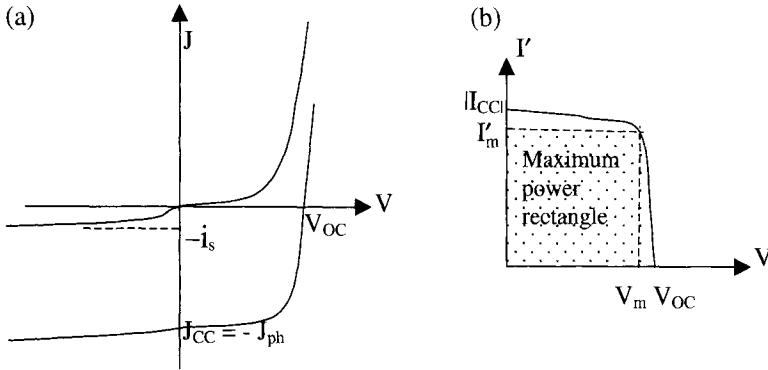


**Figure XI-16.** (a)  $J(V)$  characteristics; and (b)  $I'(V)$  characteristics with the maximum power rectangle.

Furthermore, the open-circuit voltage ( $V_{OC}$ ) can be directly deduced from relation (1), where  $J = 0$ , so that we have:

$$V_{OC} = \frac{kT}{q} \text{Log} \left( \frac{J_{ph}}{J_S} + 1 \right) = \frac{kT}{q} \text{Log} \left( \frac{I_{ph}}{I_S} + 1 \right). \quad (2)$$

### e Photovoltaic parameters

The internal quantum efficiency (IQE), is defined by  $\text{IQE} = \eta_{\text{diff}} \times \eta_{\text{TC}} \times \eta_{\text{tr}} \times \eta_{\text{CC}}$ , while the external quantum efficiency (EQE), is given by  $\text{EQE} = \eta_A \times \text{IQE}$ . In effect, the EQE, obtained by the multiplication of all the efficiencies, represents the ratio between the number of generated electrons to the number of incident photons. This coefficient, also named the Incident Photon-to-Current Efficiency (IPCE) represents the ratio between:

- the measured photocurrent expressed as the number of collected electrons in the unit time and per unit area:  $\frac{I_{CC}/S}{e} = \frac{J_{CC}}{e}$ , where  $J_{CC} = I_{CC}/S$  is the current density in  $\text{A cm}^{-2}$ ;
- to the intensity of the incoming monochromatic light expressed as the number of incoming photons (of  $\lambda$  wavelength) per unit time and area:  $\frac{\phi_e/S}{hc/\lambda} = \frac{E_e}{hc/\lambda}$ ;  $\phi_e$  is the incident energetic flux (expressed in Watt) and  $E_e$  is the illumination defined by  $E_e = \phi_e/S$  (in  $\text{W/cm}^2$ ). Thus, we have:

$$\text{EQE} = \frac{I_{CC}}{\phi_e} \times \frac{hc}{e\lambda} = \frac{J_{CC}}{E_e} \times \frac{hc}{e\lambda}.$$

With  $\lambda$  expressed in  $\mu\text{m}$ , numerically,  $\text{EQE} = 1.24 \frac{J_{CC}}{\lambda \times E_e}$ .

Finally, the external power conversion efficiency  $\eta$  is defined as the ratio of the maximum electric power  $P_{\text{max}}$  to the energetic flux  $\phi_e = E_e \times S$  i.e.  $\eta = \frac{P_{\text{max}}}{\phi_e} = \frac{\text{FF} \times I_{CC} \times V_{OC}}{\phi_e}$ . This yield is the maximum value for the theoretical yield, and to optimise this yield we have to optimise each of the three factors in the numerator. In practice,

the yield is diminished by two factors: the effect of the series and shunt resistances and the effect of reflection at the surface of the cell.

### 3 Circuit equivalent to a solar cell

#### a Equivalent circuit for an ideal solar cell

As  $I = I_S \left[ \exp\left(\frac{qV}{kT}\right) - 1 \right] - I_{ph}$ , the biased and irradiated pn-junction can be seen as a current source  $I_{ph}$  (a reverse current proportional to the incident light) in parallel with a diode in the dark which delivers the current  $i = I_S \left[ \exp\left(\frac{qV}{kT}\right) - 1 \right]$ . We thus obtain the equivalent circuit for an ideal solar cell, outlined in Figure XI-17, which consists of an ideal diode and a current source in parallel.

If the junction is connected to a load resistance ( $R_L$ ), the voltage ( $V$ ) is the result of the ohmic fall of the current through  $R_L$  (in open circuit,  $R_L \rightarrow \infty$  and  $V \rightarrow V_{OC}$ ). The orientation of  $I_{ph}$  towards  $R_L$  produces a  $V$  which induces a forward bias across the junction so that the current ( $i$ ) is a forward current in the direction opposite to  $I_{ph}$ . Alternatively, we can consider that the direction of the photocurrent in the load resistance induces a voltage across the junction which generates the  $i$  forward current in the direction opposite to  $I_{ph}$ , so that in the external circuit we do not observe the entire  $I_{ph}$  photocurrent, but only  $I' = I_{ph} - i$ .

#### b Equivalent circuit for a real solar cell

When the contact resistances (electrode resistivity and metal-materials interfaces) and the ohmic losses (due to the bulk resistivity of the materials) generate a non-negligible resistance in relation to the load resistance, we must include in the equivalent circuit a series resistance ( $r_s$ ), as detailed in Figure XI-18. If we denote  $V_j$  the voltage across the junction, the voltage  $V$  across the cell is reduced to  $V = V_j - r_s I'$ , and in the first quadrant we have:

$$I' = I_{ph} - I_S \left[ \exp\left(\frac{qV_j}{kT}\right) - 1 \right] = I_{ph} - I_S \left[ \exp\left(\frac{q[V + r_s I']}{kT}\right) - 1 \right].$$

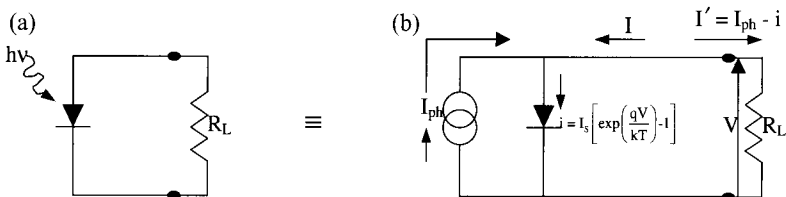


**Figure XI-17.** Electrical circuit of (a) ideal irradiated pn-junction connected with a load resistance  $R_L$ ; and (b) equivalent circuit.

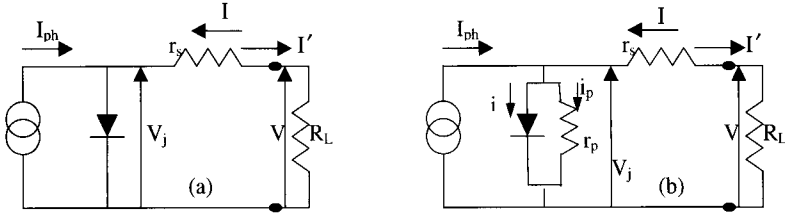


**Figure XI-18.** Equivalent circuit for real irradiated pn-junction with (a) series ( $r_s$ ) resistance; and (b) with series ( $r_s$ ) and shunt ( $r_p$ ) resistances.

Furthermore, when leakage currents (which include shunt currents through short-circuits) arise across the cell, we can take into account this component by introducing a parallel resistance ( $r_p$ ) such that  $r_p \rightarrow \infty$  when leakage current  $i_p \approx 0$ . We then have:

$$I' = I_{ph} - i - i_p = I_{ph} - I_S \left[ \exp\left(\frac{qV_j}{kT}\right) - 1 \right] - \frac{V_j}{r_p}$$

Replacing  $V_j$  by  $V_j = V + r_s I'$  we have:

$$I' = I_{ph} - I_S \left[ \exp\left(\frac{q(V + r_s I')}{kT}\right) - 1 \right] - \frac{V + r_s I'}{r_p}. \quad (3)$$

While for the ideal cell in the external circuit we do not find the total photocurrent ( $I_{ph}$ ) but only  $I' = I_{ph} - i$ , in a real cell the same reduction is more pronounced. This is because the shunt resistor  $r_p$  introduces the linkage current  $i_p$  leading to  $I' = I_{ph} - i - i_p$ . Simultaneously, series resistor consumes the voltage  $r_s I'$ .

In ideal cells, we have  $r_s = 0$  and  $r_p \rightarrow \infty$ : so, the departures from these values give an evaluation of the imperfections of the diode; considering that  $r_s$  always presents a small value and that  $r_s \ll r_p$ , we can then estimate the values  $r_s$  and  $r_p$ : by differentiation of expression deduced from (3):

$$f(I', V) = I_{ph} - I_S \left[ \exp\left(\frac{q(V + r_s I')}{kT}\right) - 1 \right] - \frac{V + r_s I'}{r_p} - I' = 0,$$

we have:  $\frac{dV}{dI'} = -\frac{f'_{I'}}{f'_V}$ , that leads to (with  $u_T = kT/q \approx 0.024$  V):

$$\left[ \frac{dV}{dI'} \right]_{I'=0} \approx -r_s - \frac{r_p}{1 + \frac{I_S r_p}{u_T} \exp\left(\frac{V}{u_T}\right)} \approx -r_s$$

(because when  $I' = 0$ ,  $V = V_{OC} \gg u_T$ )

$$\left[ \frac{dV}{dI'} \right]_{V=0} \approx -r_s - \frac{r_p}{1 + \frac{I_S r_p}{u_T} \exp\left(\frac{r_s I'}{kT}\right)} \approx -r_s - r_p \approx -r_p.$$

(as  $r_s$  is small)

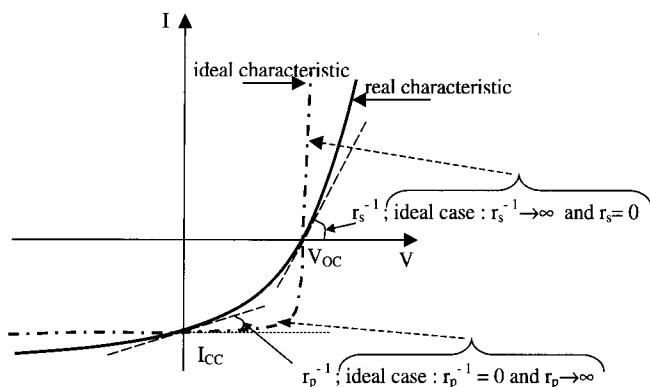


**Figure XI-19.** Reverse values of series resistance ( $r_s^{-1}$ ) and shunt resistance ( $r_p^{-1}$ ) linked with the characteristics slope at  $V = V_{OC}$  and at  $V = 0$ , respectively.

With  $I = -I'$ , we also have  $r_s^{-1} = \left[ \frac{dI}{dV} \right]_{I=0}$  and  $r_p^{-1} = \left[ \frac{dI}{dV} \right]_{V=0}$ . The slopes of the characteristic  $I(V)$  under irradiation, calculated for  $I = 0$  (at open circuit) and in  $V = 0$  (at short circuit) give the inverse values of the series resistance  $r_s$  and of the shunt resistance  $r_p$ , respectively (see Figure XI-19). If  $r_s$  increases, the slope of the characteristic decreases in the first quadrant and  $I_{CC}$  also decreases. If  $r_p$  decreases, the slope increases in the fourth quadrant, and  $V_{OC}$  then decreases.

*Note:* To take into account a more general behaviour of the current inside the real junction (recombination current in the space charge area), eqn (1) must be written in the form:  $J = j_s \left[ \exp\left(\frac{qV_j}{nkT}\right) - 1 \right] - J_{ph}$ , where  $n$  is the "ideality factor" ( $n = 1$  in the ideal case). The relationship between  $V_{OC}$  and  $I_{ph}$  expressed in eqn (2) obtained when  $r_s = 0$  and  $r_p \rightarrow \infty$ , is thus changed to  $V_{OC} = \frac{nkT}{q} \text{Log} \left( \frac{I_{ph}}{I_s} + 1 \right)$ . Eqn (3) is also modified and becomes

$$I \left( 1 + \frac{r_s}{r_p} \right) - \frac{V}{r_p} = I_s \left[ \exp \left( \frac{q}{nkT} (V - r_s I) \right) - 1 \right] - I_{ph}.$$

#### 4 Possible limits

It can be thought that a power conversion efficiency as high as 10% can be reached with organic solar cells ([Nun 02] and [Peu 03]). Given that

$$\begin{aligned} \eta &= \frac{FF \times I_{CC} \times V_{OC}}{\phi_e} = FF \times V_{OC} \times \frac{J_{CC}}{E_e} \\ &= FF \times V_{OC} \times \frac{e}{h\nu} \times EQE, \end{aligned}$$

then (cf. § IV, 2-e):

$$\begin{aligned}\eta &= FF \times \frac{eV_{OC}}{hv} \times \eta_A \times IQE \\ &= FF \times \frac{eV_{OC}}{hv} \times \eta_A \times \eta_{diff} \times \eta_{TC} \times \eta_{tr} \times \eta_{CC}.\end{aligned}$$

As  $\eta_{TC}$ ,  $\eta_{tr}$  and  $\eta_{CC}$  are all close to 1 (see §IV,1), we can consider the power conversion efficiency ( $\eta$ ) as being essentially the product of 4 terms as in  $\eta = FF \times (qV_{OC}/hv) \times \eta_A \times \eta_{diff}$ . With small series and shunt resistances ( $r_s < 50 \Omega$  and  $r_p > 25 k\Omega$ ), and  $FF \approx 1$  (see §IV, 3), we have for the power conversion efficiency,  $\eta = \frac{eV_{OC}}{hv} \times \eta_A \times \eta_{diff}$ . With  $\frac{eV_{OC}}{hv} \approx \frac{0.5 eV}{2 eV} = 0.25$ ,  $\eta_A = 0.5$  and  $\eta_{diff} \approx 1$ , a value we can hope to achieve with appropriate systems [Nun 02], we finally have  $\eta \approx 10\%$ .

So, with at least 3% power conversion efficiency already demonstrated, and with improvements to reach 10% in the years to come, “plastic solar cells” may significantly contribute to future energy needs.

## 5 Examples; routes under study and the role of various parameters

### a Recent results

As recent results we should mention Brabec’s cell based on PPV and fullerene derivatives: at Siemens, he claims an efficiency around 5% [Bra 04]. Conversely to this wet route, dry deposition with small molecules can also be realised; so, with the structure ITO/PEDOT/CuPc – C60/Ca+Al, we obtained as photovoltaic parameters (Figure XI-20):  $V_{co} = 0.45 V$ ,  $J_{cc} = 0.768 \text{ mA cm}^{-2}$ ,  $\eta \approx 1.8\%$  with

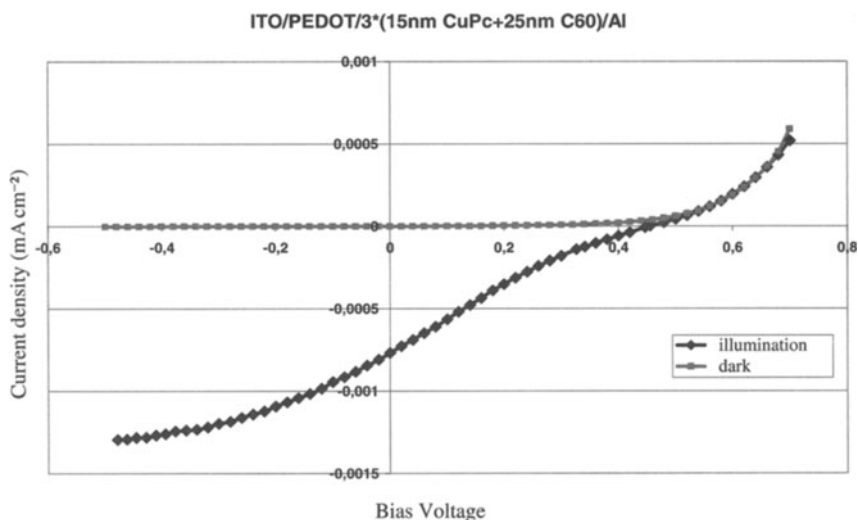


Figure XI-20. I(V) characteristic of ITO/PEDOT/CuPc – C60/Ca+Al.



$4 \text{ mW cm}^{-2}$  as luminous flux. As we can see on the  $I(V)$  characteristic, an important series resistance drastically disturb the measurements; an electron transport layer at the cathode interface could improve the results.

With pure CuPc as an acceptor layer and a BCP layer acting as a blocking layer in relation to exciton diffusion at the cathode interface, J.M. Nunzi [Tro 03] obtained very encouraging results with an interpenetrating network made of ITO/PEDOT:PSS/CuPc:C<sub>60</sub> (1:1) (40 nm)/BCP (8 nm)/Al (60 nm) with annealing of CuPc:C<sub>60</sub> at 150 °C under argon atmosphere for 20 min. Under irradiation of  $100 \text{ mW cm}^{-2}$ , the optoelectronic parameters are as following:  $V_{oc} = 0.50 \text{ V}$ ,  $J_{sc} = 11.5 \text{ mA cm}^{-2}$ ,  $FF = 0.37$  and  $\eta = 2.14\%$ .

## b Improving the photovoltaic properties of materials

It could go *via* the implication of several different technological routes. Here we can cite five examples:

- *Adapting the band gap of materials to solar light*  
this step is possible using the various, available, synthetic routes to  $\pi$ -conjugated polymers with differing band gaps [Ronc 98];
- *Orientation of chromophores to generate an internal field*  
An alternative method to effect photodissociation throughout the whole volume of a film was proposed by C. Sentein *et al.* [Sen 97]. The proposed route implicates the creation of an internal field due to the orientation of chromophore molecules by the continuous application of an external field, in a technique otherwise known as 'poling'. This provokes in the photovoltaic device an effect of rectification which would stimulate photodissociation. This effect has been shown to improve a mono-layer device, based on non-optimised polythiophene used initially for photovoltaic conversion, by a factor of 40 [Sic 00];
- *Improving deposition techniques to increase absorption capacities [Fic 00]*  
The octamer octathiophene ( $\alpha$ -8T), shown in Figure XI-21, was examined by C. Videlot and D. Fichou. They found that its properties varied greatly with respect to its orientation once deposited on a substrate. A pn-junction, in which the  $\alpha$ -8T acted as the p-type semiconductor and a derivative of perylene was used as the n-type semiconductor, was used in the system ITO/ $\alpha$ -8T/perylene derivative/Al. Between 400 and 600 nm, a photo-current ( $I_{PC}$ ) was generated when the system was illuminated from the ITO side with polarised light. It was found that the current increased by a factor of ten when the  $\alpha$ -8T molecules went from being perpendicularly aligned to being aligned in parallel with the substrate. This effect was attributed not only to an improvement in the transport properties of the  $\alpha$ -8T,

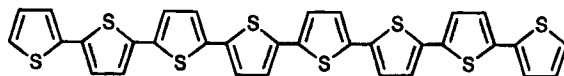


Figure XI-21. Representation of  $\alpha$ -8T.

but also to a better coupling between the molecules and the incident light, an effect which improved their optical absorption;

- *Improving charge transport*

Following the disassociation of photogenerated charges, the problem of their transport to the electrodes, as we have seen, needs to be tackled. Given the low mobility of charges in organic solids, possible solutions may exist in the use of ordered phases based, for example, on liquid crystals. Furthering this idea, the mobility of electrons being again low in polymers, an eventual solution may rest in the use of mixed organic/inorganic systems, in which the transport of the electron may be assured through the inorganic phase. Doping effect of n or p layers is also studied, as well with molecular materials (dyes) as with the ion beam implantation technique we have previously developed [Mol 98] to realize organic devices (diodes or transistors);

- *Optimising the morphology of interpenetrating systems* The optimisation of photogenerated charge separation requires, on the scale of exciton diffusion lengths, a perfect homogeneity of the donor-acceptor system. A solvent free method, using the co-evaporation of p-type oligomers and n-type molecules could reasonably result in such a structure; the vacuum quality is a critical parameter really. It has also been remarked that the use of composites which exhibit concentration gradients, with donors and acceptors on opposite sides of a structure, should improve the collection of positive and negative charges at the respective electrodes.

## 6 Conclusion

At the present moment there is a considerable push in research into the field of organic photovoltaics and it is with some excitement that more results are expected in the near future. On bringing together the various possible techniques, which are not necessarily exclusive to one another, the short term aim is realise structures which display efficiencies of the order of 5%–6% and have lifetimes of around 5000 hours. Activities based on organic photovoltaics should be possible on an industrial scale. And given the recently published results, researchers could well be there in the next few years.

## XII

---

# The origin of non-linear optical properties of $\pi$ -conjugated materials and electro-optical modulators

## I Introduction: basic equations for electro-optical effects

### 1 Context

Whilst this book is mostly concerned with coupling electron transport properties with emission and optical absorption properties, this Chapter deals specifically with the effect of an electric field ( $E$ ), whether static or variable, on the optical properties of an organic material. In particular we will look at the effect of electrical fields on the indices of materials, and the changes in the intensity or phase of an optical wave propagated through a polarised organic medium. The assembly of polymer based electro-optical modulators is then introduced. First of all though, as a general overview, we shall detail the generally observed laws.

### 2 Basic equations used in non-linear optics [Sal 91]

#### a Standard equations

In general terms, a material subject to a static or low frequency electric field undergoes certain deformations. These typically result from either ionic movements in mineral based composites or from electron displacements in organic media (following electronic and molecular orbital deformations). Under the effect of an external electric field, as shown in Figure XII-1, the change in polarisation induces a modification of the optical indice of the material at a given frequency. There are two main types of effect that can be observed:

- when the indice varies proportionally to the strength of the applied field the electro-optical effect is called the Pockels effect; or
- when the indice varies with the square of the applied field then the effect is called the Kerr electro-optical effect.

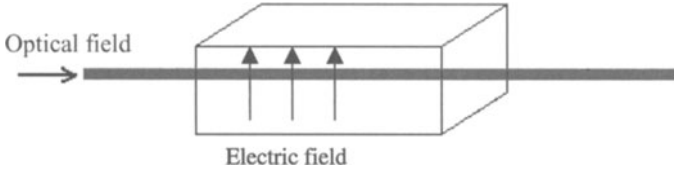


**Figure XII-1.** Coupling an electric field with an optical field traversing an electro-optical material.

On following the hypothesis that the variation in the indice is small with respect to the applied field, we can use a Taylor type development around values of the indice for when  $E = 0$ . Using the notation thus:

$$n(E = 0) = n(0) = n, \quad a_1 = \left. \frac{dn}{dE} \right|_{E=0}, \quad a_2 = \left. \frac{d^2n}{dE^2} \right|_{E=0},$$

gives:

$$n(E) = n + a_1 E + \frac{1}{2} a_2 E^2 + \dots \quad (1)$$

For the reasons of notation which will become apparent in Section b:

$$\left. \begin{aligned} r &= -\frac{2a_1}{n^3} \\ s &= -\frac{a_2}{n^3} \end{aligned} \right\}$$

are the electro-optical coefficients which are such that:

$$n(E) = n - \frac{1}{2} r n^3 E - \frac{1}{2} s n^3 E^2 + \dots \quad (2)$$

Typically, the 2nd and 3rd order terms are small, by several orders, with respect to  $n$ .

### b The form of electrical impermeability

The term electrical impermeability is particularly useful when describing anisotropic media (for example, following ellipsoidal indices). It is defined by  $\eta = 1/\epsilon_r = 1/n^2$ .

As on one side  $\eta = \frac{1}{n^2}$ , that is  $\frac{d\eta}{dn} = -\frac{2}{n^3}$ , and on the other there is

$$\Delta n = n(E) - n = -\frac{1}{2} r n^3 E - \frac{1}{2} s n^3 E^2,$$

we can write

$$\Delta \eta = \left( \frac{d\eta}{dn} \right) \Delta n = \left( -\frac{2}{n^3} \right) \left( -\frac{1}{2} r n^3 E - \frac{1}{2} s n^3 E^2 + \dots \right) = rE + sE^2.$$

With  $\Delta\eta = \eta(E) - \eta$ ,

$$\eta(E) = \eta + rE + sE^2 + \dots \quad (3)$$

(The coefficients  $r$  and  $s$  are defined beforehand to arrive at this simple relationship for  $\Delta\eta$ , which introduces the simple coefficients  $r$  or  $s$  in front of  $E$  or  $E^2$ ).

### c Pockels effect and order of size

In many materials the term relating to the 2nd order Kerr effect is small with respect to that of the 1st order Pockels effect. In effect:

$$n(E) \approx n - \frac{1}{2}rE^2. \quad (4)$$

Typically,  $r \approx 10^{-12}$  to  $10^{-10} \text{ m V}^{-1}$ , that is from 1 to 100 pm  $\text{V}^{-1}$ .

If  $E = 10^6 \text{ V m}^{-1}$ , then the term  $\frac{1}{2}rE^2$  is of the order of  $10^{-6}$  to  $10^{-4}$ , a very small variation in the indice with respect to the effect  $E$  (the usual minerals considered are  $\text{KH}_2\text{PO}_4$ ,  $\text{LiNbO}_3$ ,  $\text{LiTaO}_3$  and  $\text{CdTe}$ ).

## II The principle of phase modulators and organic materials

### 1 Phase modulator

Phase modulation means that information, based on either  $V(t)$  or  $\vec{E}(t)$ , can be transferred using an optical signal by modifying the phase of this optical wave. An alternative method is with an amplitude modulator which varies the intensity of the optical wave by using parallel monochromatic luminous beams, *i.e.* a laser beam.

When an optical beam traverses a Pockels cell of a certain length ( $L$ ) subject to an electric field ( $E$ ), as detailed in Figure XII-2, the wave undergoes a shift in phase:

$$\varphi = n(E)k_0L = \frac{2\pi}{\lambda_0}n(E)L, \quad (5)$$

where  $\lambda_0$  is the wavelength of the light in a vacuum.

The introduction of eqn (5) into eqn (4) yields:

$$\varphi = \frac{2\pi}{\lambda_0}nL - \frac{2\pi}{\lambda_0}L\frac{1}{2}rE^2 = \varphi_0 - \pi\frac{rE^2L}{\lambda_0}, \quad (6)$$

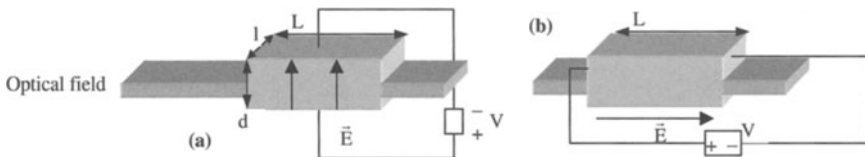


**Figure XII-2.** Pockels cell under: (a) transversal ( $E = V/d$ ); or (b) longitudinal polarisation ( $E = V/L$ ).

with  $\varphi_0 = \frac{2\pi nL}{\lambda_0}$  ( $\varphi_0$  representing the shift in phase at  $V = 0$ , *i.e.* at zero applied tension).

The variation in  $\varphi$  (the shift in phase in the presence of a polarising field  $E$ ) with respect to the polarisation tension ( $V$ ) is shown in Figure XII-3. From the Figure we can define the ‘half-wave tension’ as an applied tension at which point results in a shift of  $\pi$  from an unaffected wave. This can be written as  $\varphi_0 - (\varphi)_{V=\text{half-wave tension}} = \pi$ .

In the transversal cell, shown in Figure XII-2-a, the half-wave tension is denoted as  $V_\pi$ , (and accordingly  $\varphi_0 - (\varphi)_{V=V_\pi} = \pi$ ). In addition, in this system  $E = (V/d)_{V=V_\pi} = V_\pi/d$ . The value introduced into eqn (6) can give eqn (7) in the form

$$\varphi_0 - (\varphi)_{V=V_\pi} = \pi = \frac{\pi n^3 V_\pi L}{\lambda_0 d} \tag{7}$$

Accordingly, we can deduce eqn (8):

$$V_\pi = \frac{\lambda_0 d}{n^3 L} \tag{8}$$

For a longitudinal Pockels cell, as in Figure XII-2-b, the field is now of the form  $E = V/L$  and the half-wave voltage, which is commonly denoted by  $V_{P,\pi}^1$ , becomes  $V_{P,\pi}^1 = \frac{\lambda_0}{n^3}$ . We can now use eqn (6) again in the form

$$\varphi = \varphi_0 - \pi \frac{V}{V_\pi} \text{ (transversal cell), or } \varphi = \varphi_0 - \pi \frac{V}{V_{P,\pi}^1} \text{ (longitudinal cell)} \tag{6'}$$

Thus the shift in phase changes linearly with the applied tension. This we can use to modulate the wave traversing the cell.

Generally, the value of  $V_{P,\pi}^1$  can be of the order of 1 to several kV for longitudinal modulators. Transversal modulators permit a lowering of the value of  $V_\pi$  through variation of the ratio  $\frac{d}{L}$  ( $d$  can be several microns and  $L$  can be around 1 cm), so that  $V_\pi \approx 1$  to 100 V.

*Comment* If the applied field ( $E = E(t)$ ) varies greatly during the transit time ( $T$ ) of the optical wave, then obviously the optical wave will be subject to a varying value of  $E$  during its passage through the modulator. The field  $E(t)$  which can be used is the

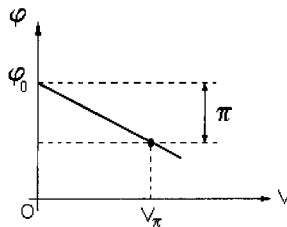


**Figure XII-3.** Variation in dephasing( $\varphi$ ) as a function of the applied polarising tension ( $V$ ), and the definition of  $V_\pi$  (transversal cell).

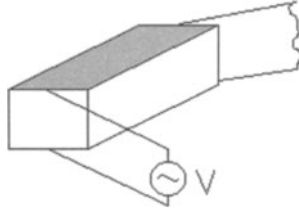


**Figure XII-4.** Positioning of electrodes with respect to the transmission in a transverse modulator.

average field  $\bar{E}$  during the two instant  $t$  and  $t + T$ . The size of the modulation band is generally taken as being equal to  $1/T$ .

In order to limit this problem, the tension ( $V$ ) can be applied at the side of the entrance of the optical guide so as act directly on the transmission axis. This is schematised in Figure XII-4. Modulation up to several GHz is possible using this technique.

## 2 The advantages of organic materials

Other than the advantage that organic materials have in being easily shaped, they do present other advantages specific to this field:

### a Advantages over inorganic materials

As the inorganic materials used are normally ionic in nature, the displacement of these charges is slower relative to the movement of electrons alone, especially electrons delocalised in organic media. Ionic polarisation is relatively slow especially when compared to the response times of organic materials, and in particular  $\pi$ -conjugated polymers, which can be extremely fast (of the order of femtoseconds).

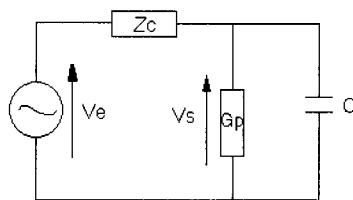
### b Advantages due to the low dielectric permittivity of organic materials ( $\epsilon_r \approx 2$ )

Figure XII-5 schematises the circuit used to control a Pockels type cell. The generator provides an excitation at low frequencies which is applied to the cell and acts, no less, as a condenser. Its losses are shown in the scheme by the parallel conductance  $G_p$ . The response time,  $\tau = RC$ , is small if  $C$  is small. This is favoured in organic materials as their permittivity ( $\epsilon_r$ ) is also relatively small ( $\epsilon_r \approx 2$ ).

In addition, we have:

$$\frac{V_s}{V_e} = \frac{1}{1 + Z(G_p + j\omega C)} \approx \frac{1}{1 + j\omega ZC} \quad (\text{with } G_p \ll \omega C).$$

The modulator acts as a low frequency filter, with a cut-off frequency ( $f_c$ ) at  $f_c = \frac{1}{2\pi ZC}$ . As  $C = \frac{\epsilon_0 \epsilon_r S}{d} = \frac{\epsilon_0 \epsilon_r l L}{d}$  (denoting  $S = [l \times L]$  as the available surface of



**Figure XII-5.** Schematisation of a Pockels cell control unit.

capacitance, see also Figure XII-2), we can see straight away that with organic materials that have a low value of  $\epsilon_r$ ,  $C$  is also small given that the cut-off frequency is high.

*Comment* On introducing  $V_\pi$ , which insures the phase shift by  $\pi$  and is such that  $V_\pi = \frac{\lambda_0 d}{n^3 r}$ , we arrive at:  $\frac{f_c \lambda_0}{V_\pi} = \frac{n^3 r}{2\pi Z l \epsilon_0 \epsilon_r} = \text{constant}$ , for a given system.

For any given system in which  $f_c$  increase,  $V_\pi$  also increases (along with consumption). And the ratio  $f_c \lambda_0 / V_\pi$  defines the figure of merit of the modulator.

### c The state of the art

Y. Shi at the TACAN Corporation, along with his colleagues at the Universities of Southern California (Department of Chemistry and the Centre of Photonic Technologies) and Washington, has shown that by controlling the form of the organic chromophores it is possible to obtain electro-optical modulators having half-wave tensions lower than 1 V ( $V_\pi \approx 0.8$  V with  $V_\pi L \approx 2.2$  V cm) [Shi 00]. The results also showed a large increase in gain (inversely proportional to  $V_\pi^2$ ). And the considerable decrease in parasite signals allowed the operation frequency to be increased to 100 GHz, equivalent to a transfer of data of  $100 \text{ Gbits s}^{-1}$ . The decrease in  $V_\pi$  was realised by increasing the concentration of chromophores while simultaneously limiting electrostatic interactions (which reduce the electro-optical effect). This was made possible by inserting chromophore molecules containing bulky groups that contributed to steric effects. Other materials, notably those with octapolar charge distributions, have been used in attaining 'giant' non-linear effects [Med 95].

### 3 Examples of organic donor-acceptor non-linear optical systems

Two principal effects are responsible for electronic displacements in molecules [Mer 95]:

- the induction effect which gives rise to a preferential attraction for electrons shared by atoms having  $\sigma$ -bonds (in a range of electronegativities range based on the capacity of atoms to attract electrons); and
- a mesomeric effect which brings into play  $\pi$ -electrons or doublets of unshared electrons situated in p-orbitals. These charges can move from one bond to another and are not localised to the extent of electrons in  $\sigma$ -bonds.



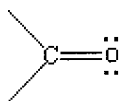
### a The induction effect

Briefly put, when two atoms are bonded by a  $\sigma$ -bond, the more electronegative atom tends to attract the electrons in the bond towards itself giving rise to a dipolar moment. In addition, the polarisation effect can be transmitted along a chain of covalent in an effect which diminishes with distance (and typically disappears beyond the third bond). The inductive effect is represented by the symbol  $+\rightarrow$  with the arrow directed towards the negative end of the dipole, and in the opposite direction to the sign  $-\rightarrow + : \delta\vec{\mu}$ .

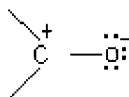
### b The mesomeric effect

The structure of a molecule, in reality, is in between the two limited formulas which are both unable to describe the partition of electrons, given that  $\pi$ -electrons are more mobile than  $\sigma$ -electrons.

*Example: the isolated double bond* The carbonyl group is normally represented by:



Nevertheless, O is much more electronegative than C, and can attract electrons more powerfully. The following representation is therefore also plausible:



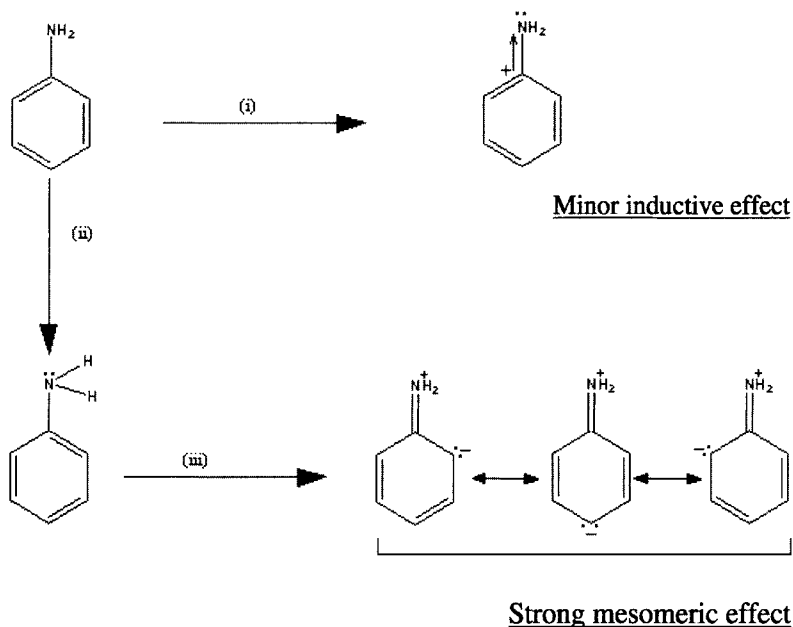
The  $\pi$ -electrons are delocalised towards O and, in effect, this situation can only be written using both of the proposed forms. These two forms are called mesomers and are both intermediate with respect to reality.

### c Competition between induction and mesomeric effects and the example of substitution on benzene rings

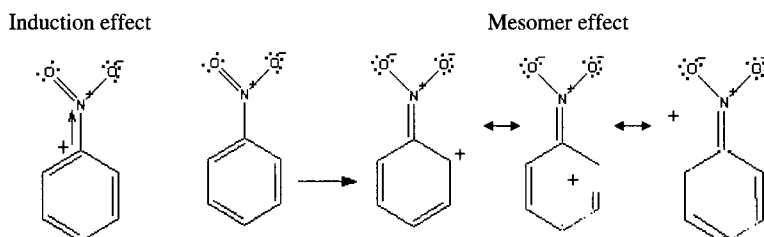
$\alpha$  *Influence of an electron donor:  $-\text{NH}_2$ , resonating with the benzene ring* The chemical representation schematises specific effects:

- (i) a weak induction effect [N ( $5e^-$ ) is more electronegative than C];
- (ii) a strong mesomeric effect through the conjugation of the N free pair of electrons with the benzene ring; and
- (iii) the pair of electrons on N(:) tend to delocalise towards the ring.

**Result** The electron cloud is delocalised towards the cycle and, in effect, the  $-N(:)H_2$  group acts as a donor.



$\beta$  *The influence of an electron attracting group:  $NO_2$*  In the case of  $NO_2$  there is no free electron pair ready to delocalise towards the benzene ring. With O being more negative than N, O tries to saturate itself with electrons moving them from the ring. In effect,  $NO_2$  is an attracting (or acceptor) group.



#### 4 General structure of molecules used in non-linear optics [opt 93]

As will become apparent when looking at the materials in more real terms, organic molecules which allow intermolecular charge transfer can give rise to a particularly high hyperpolarisability. These molecules are termed 'push-pull' molecules. They consist of donor and acceptor groups linked by a conjugated system, otherwise termed a 'spacer' (S) or a transmitter, as shown in Figure XII-6.

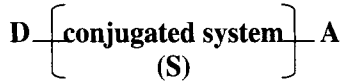


Figure XII-6. Donor-spacer-acceptor system.

### III The molecular optical diode

Here we will show that molecular optical diodes can in fact give a rectifying effect. Light polarised in one direction can pass, while light polarised in the opposite direction is ‘blocked’. An analogue is, of course, a rectifying pn-junction, which rectifies by exploiting effects due to a passing current and the excitation developed by an electric field.

In molecular optics, the created electronic response is  $\vec{P}_E = n d\vec{\mu} \left( = \frac{d\vec{\mu}}{d\tau} \right)$  in which  $n$  is the density of electrical charges and  $d\vec{\mu} = qd\vec{l}$  is the dipole formed on displacing by  $d\vec{l}$  an electric charge from its centre of gravity due to the passage of an optical wave.

*Comment* In linear optics, the polarisation is tied to the optical indice by the relationship  $\vec{P} = \epsilon_0(\epsilon'_r - 1)\vec{E}$ , with  $\epsilon'_r = n^2$  for non-absorbing media. In absorbing media,  $\epsilon^*_r = n^{*2}$ .

#### 1 The centrosymmetric molecule

The centrosymmetric molecule contains electrons which are highly polarisable. A good example is that of delocalised  $\pi$ -electrons, as found in benzene ( $C_6H_6$ ).  $d\vec{\mu} = qd\vec{l}$  represents the dipole moment.

$$-q \xrightarrow{d\vec{l}} +q$$

Additionally, in one dimension, moving a charge ( $q$ ) by a distance  $d\vec{l}$  superimposes on the system a dipole moment of  $d\vec{\mu} = qd\vec{l}$ , as detailed in Appendix A-9, Section III. Similarly, moving a charge  $-e$  by  $-d\vec{l}$  is the same as applying a dipole moment  $d\vec{\mu} = ed\vec{l}$ , as shown in Figure XII-7. In addition, if we move electrons under an

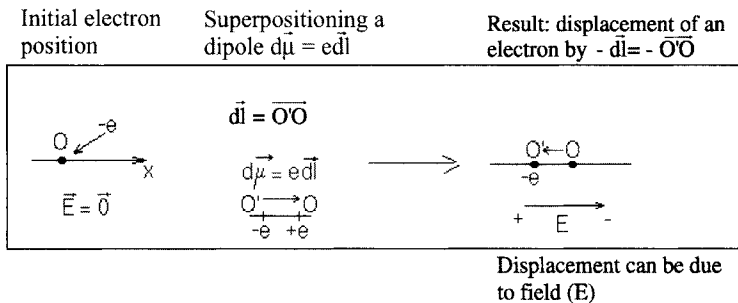
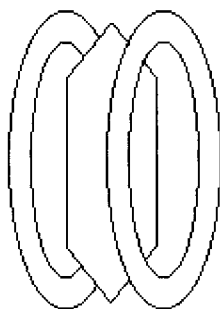


Figure XII-7. The equivalence of charge displacement, polarisation generation and *vice-versa*.



**Figure XII-8.** Representation of the electron clouds in an unpolarised benzene molecule.

electric field ( $\vec{E}$ ), with direction  $-\vec{d}\vec{l}$ , that implies the application of  $d\vec{\mu} = e\vec{d}\vec{l}$  and thus a polarisation  $\vec{P} = nd\vec{\mu}$  is generated in the opposite direction, depending on  $d\vec{l}$ .

If  $\vec{E} = 0$ , the benzene molecule electron cloud has the form described in Figure XII-8.

We can now consider the same benzene molecule under an electric field ( $E$ ), as in Figure XII-9.

With respect to the axis of time, successive lobes due to the function  $\vec{P}$  remain symmetric. There is no 'rectifying' effect observed at this size of optical field ( $\vec{E}$ ), whether it be a weak field in which case  $\vec{P}$  is directly proportional to  $\vec{E}$  as  $\vec{P} = \epsilon_0(\epsilon_r - 1)\vec{E}$ , or whether it be a strong field in which case the polarisation stays as a unpaired function (with successive + and - lobes) and a non-linear effect is introduced simply by the unpaired harmonics at the level of  $\vec{P}$ .

## 2 Non-centrosymmetric molecules

Now we can look at the same benzene molecule which has, however, been modified by the addition of electron donor (D) and acceptor (A) groups so that it has become non-centrosymmetric. This modification results in the displacement of the electron cloud towards the attracting, acceptor group. Any effect exerted by an optical field will be exacerbated by orientating the optical field so that it displaces electrons towards A. Inversely, its effect would be minimised by orientating the field so that it tends to move electrons towards D. Figure XII-10 schematises these two, opposing effects.

As detailed in Figure XII-11, Fourier analysis of the resulting polarisation wave shows that it contains, that for non-centrosymmetric molecules, a fundamental, a second harmonic and a continuous component. In a one-dimensional medium and when the optical wave is  $\vec{E} = \vec{E}^\omega$ , the terms for the polarisation wave should thus be written in the form:

$$\vec{P} = \vec{P}_0 + \chi_{a1}\vec{E}^\omega + \chi_{a2}\vec{E}^\omega\vec{E}^\omega$$

wherein  $\chi_a$  is the absolute dielectric susceptibility and such that  $\chi_a = \epsilon_0\chi_r$ . Here  $\chi_r = (\epsilon_r - 1)$  is the relative susceptibility, hereon denoted simply by  $\chi$ .

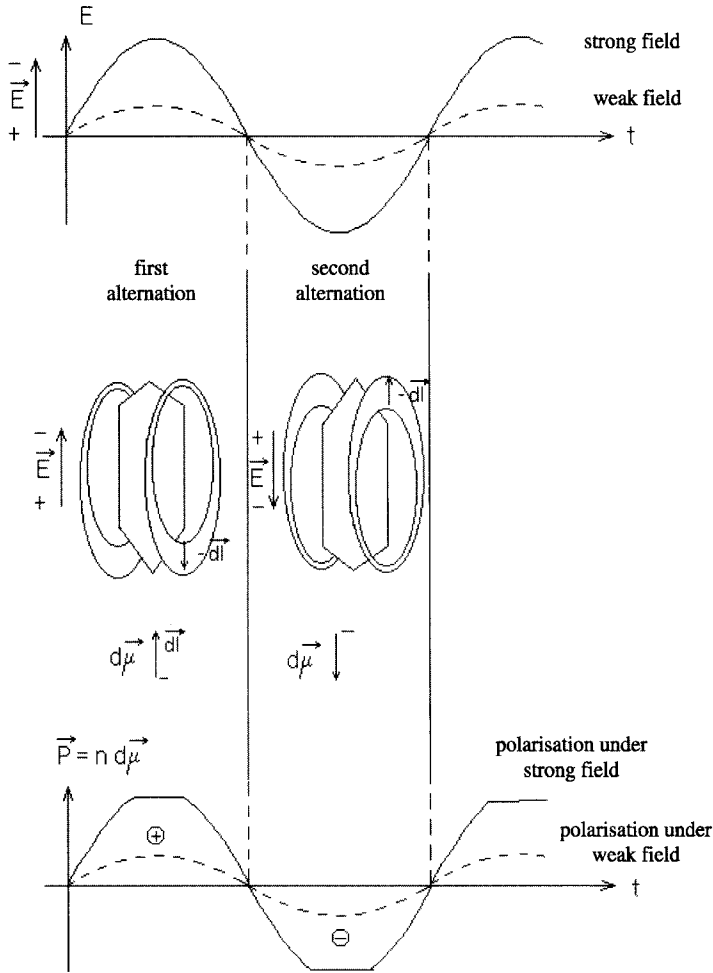


**Figure XII-9.** Polarisation by strong and weak fields of a centrosymmetric molecule.

### 3 Conclusion

The second order non-linear polarisation ( $P^{(2)}$ ) is proportional to the square of  $E$  (the term  $E^2$  introduces  $\cos^2 \omega t = \frac{1+\cos 2\omega t}{2}$ ). It is only with a non-centrosymmetric molecule that either  $\chi_2$  or  $\chi_{a2}$  can be zero. In addition to the phenomenological evidence described above, we can also perform a direct demonstration of this effect [yar 89].

If a molecule is symmetric, then changing from  $\vec{E}$  to  $-\vec{E}$  is effectively the same as moving charges in an exactly similar but symmetrically direction, so:

$$P^{(2)}(\vec{E}) = -P^{(2)}(-\vec{E}) \tag{1}$$

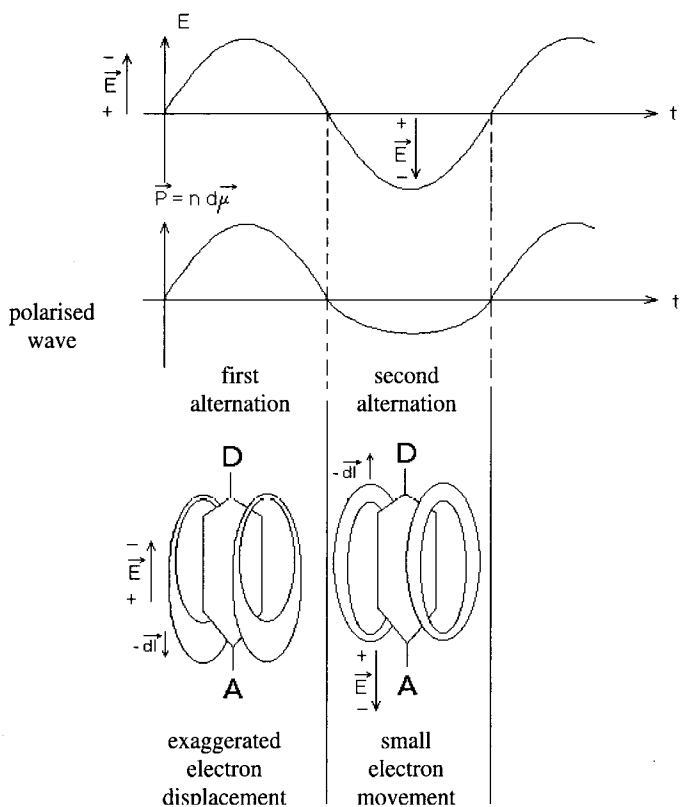


Figure XII-10. Polarisation of a non-centrosymmetric molecule.

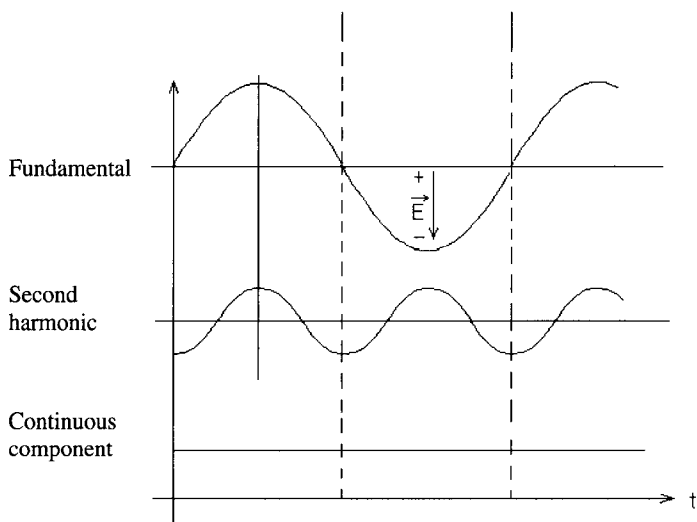


Figure XII-11. Resolution of polarisation wave for a non-centrosymmetric molecule.

Additionally, the definition of  $P^{(2)}$  gives:

$$\left. \begin{aligned} P^{(2)}(\vec{E}) &= \chi_{a2} \vec{E} \cdot \vec{E} \\ P^{(2)}(-\vec{E}) &= \chi_{a2} (-\vec{E}) \cdot (-\vec{E}) \end{aligned} \right\} \Rightarrow P^{(2)}(\vec{E}) = P^{(2)}(-\vec{E}) \quad (2)$$

And finally:

$$\left. \begin{aligned} \text{from eqn (1): } \chi_{a2} \vec{E} \cdot \vec{E} &= -\chi_{a2} (-\vec{E}) \cdot (-\vec{E}) \\ \text{and from eqn (2): } \chi_{a2} \vec{E} \cdot \vec{E} &= \chi_{a2} (-\vec{E}) \cdot (-\vec{E}) \end{aligned} \right\} \Rightarrow \chi_{a2} = -\chi_{a2}, \text{ that is } \chi_{a2} = 0.$$

## IV Phenomenological study of the Pockels effect in donor-spacer-acceptor systems

Here we shall describe a molecular system containing  $\pi$ -electrons and establish, directly, the relationship between modifications of the function indice with respect to the applied field, otherwise known as the Pockels effect. The establishment of the same type of equation, using more conventional methods, is detailed in Appendix A-11.

We will use an optical wave ( $E^\omega$ ) which propagates in the Oz direction and is polarised in the Ox direction. Figure XII-12 indicates how the electrodes are placed about the active medium.

### 1 Basic configuration

#### a Molecular system with prior orientation of $\pi$ -orbitals in the direction Ox

A static polarisation field ( $E_S$ ) is applied using 'poling', that is to say the field is applied during a descent in temperature of an electro-optical material from its glass transition temperature ( $T_g$ ) to ambient temperature ( $T$ ) to give the result shown in Figure XII-13-a.

#### b For systems also containing a D-A pair

Here we are considering the system surrounded by the dashed line in Figure XII-13. The electronic cloud is deformed and the centre of gravity for the charges is moved

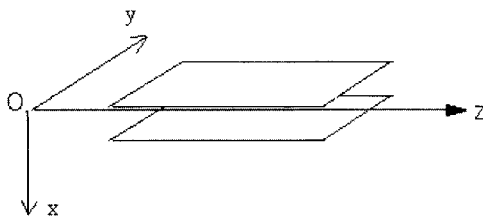


**Figure XII-12.** Configuration of an active medium placed between electrodes parallel to the plane  $yOz$  and traversed by an optical field polarised with respect to the  $Ox$  direction.

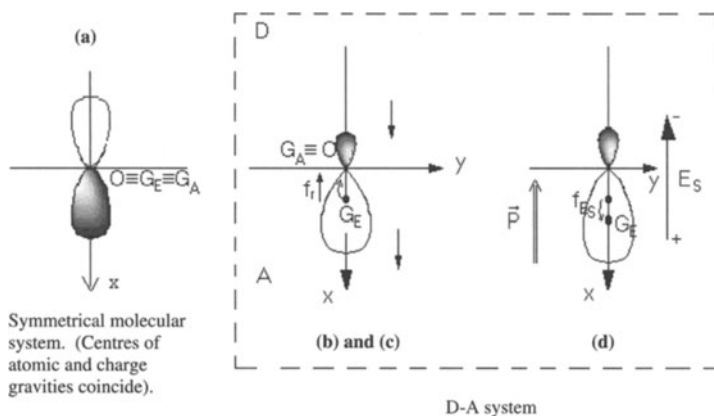


**Figure XII-13.** The position of the centre of gravity of electronic charges ( $G_E$ ) for: (a) a symmetrical molecule; (b) a non-centrosymmetrical molecule whether or not (c) in the presence of an optical field directed towards  $Ox$ ; and (d) the same as (c) excepting that the field is directed towards  $-Ox$ .

by  $x > 0$  so that  $OG_E = x$ . The greater the donor-acceptor character of the additional groups, and in effect the greater the size of the electron cloud, the higher the value reached by  $x$  (Figure XII-13-b).

### c In the presence of an optical field

The ions which are attached to atoms within the solid material and in effect it is only the electronic cloud which moves, in a manner similar to that shown in Figure XII-13-b, once the system is under the influence of an optical field. The movement of the electron cloud is with respect to its centre of gravity, already moved by the D-A pair. With  $G_E$  displaced under the effect of both the D-A pair and the optical field by a distance  $x$  we thus have  $f_r = -kx$  (Figure XII-13-c, identical to Figure XII-13-b).

### d The effect of a static electric field ( $E_s$ ) applied in the direction $-Ox$

Here we consider the situation presented in Figure XII-13-d. The electric field goes against the return force  $f_r$  and has a tendency to displace  $G_E$  towards  $x > 0$ . This displacement occurs as strongly as the charged electron cloud is large due to coupling strength. In effect, as we have seen in Sub-section b just above, the value of  $x$  tends to be high. We can therefore write that the force generated by  $E_s$  is in the form  $f_{ES} = +Dx$ ; the force  $f_{ES}$  increases proportionally with  $E_s$ .

### e Result of combined forces

The result of the forces ( $f_R$ ) with respect to  $Ox$  of forces  $f_r$  and  $f_{ES}$  is thus in the form  $f_R = f_r + f_{ES} = -kx + Dx$ .



With  $k = m\omega_0^2$  and  $D = m\delta^2$  (which is such that  $\delta^2 \propto E_S$ , as  $D \propto E_S$ ):

$$f_R = -m(\omega_0^2 - \delta^2)x. \quad (1)$$

*Comment 1* If the resulting displacement  $x$  is, in effect, as large as  $E_S$  and thus also  $D(D \propto x)$ , the term  $Dx = \delta^2x$  varies similarly to  $x^2$ , that is as an inharmonic term.

*Comment 2* With an optical wave polarised in the direction  $Oy$ , the fundamental relationship for the dynamics of the system can also be written for the direction  $Oy$ . Here the field  $E_s$  is put into terms of  $Oy$  and this effect may be greater than that in the direction  $Ox$  given the anisotropy of molecular orbitals (see Comment 2 at the end of this Chapter, Section IV-4).

## 2 Fundamental equation for a dynamic system

Here we will assume that in the permanent regime under study frictional forces ( $f_t = -m\Gamma\dot{x}$ ) are negligible due to  $\Gamma \ll |\omega - \omega_0|$  (the further from the resonance point we go ( $\omega - \omega_0$ ) the more  $\Gamma$  tends to zero).

Therefore, the fundamental dynamic relationship for an electron with respect to  $Ox$  is:

$$m\ddot{x} = -m(\omega_0^2 - \delta^2)x + qE^\omega. \quad (2)$$

Only the  $qE^\omega$  component contributes to the Coulombic force. The effect due to the static field ( $E_s$ ) was taken into account within the term  $m\delta^2x$ , which is included as part of the return force ( $f_r$ ) as the electronic effect of  $E_s$  was considered as a modification, or rather perturbation, of the return force.

With  $E^\omega = E_0 \cos \omega t$ , the solution under a forced regime  $x = x_0 \cos \omega t (= x_0 e^{i\omega t})$  that is  $\ddot{x} = -\omega^2 x$  gives us:

$$([\omega_0^2 - \delta^2] - \omega^2)x = -\frac{eE^\omega}{m}$$

## 3 Expressions for polarisability and susceptibility

With  $N$  as the electron density, a polarisation of  $\vec{P}$  caused by the displacement of electrons by a distance  $x$  along  $Ox$  can be determined using  $\vec{P} = -Ne \times \vec{u}_x$  and  $\omega_p^2 = \frac{Ne^2}{\epsilon_0 m}$  in

$$\vec{P} = \epsilon_0 \frac{\omega_p^2}{[\omega_0^2 - \delta^2] - \omega^2} \vec{E}^\omega = \epsilon_0 \chi \vec{E}^\omega. \quad (3)$$

Typically, we set

$$\chi_\omega = \frac{\omega_p^2}{\omega_0^2 - \omega^2}. \quad (4)$$

This is the term which appears in a linear polarisation of a system not subject to an additional static polarisation ( $E_s$ ). In this case, we have  $f_{ES} = 0$  and the term in  $\delta^2$

disappears. The eventual expressions of the polarisation ( $\vec{P}^{(\omega)}$ ) is thus in the form:

$$\vec{P}^{(\omega)} = \epsilon_0 \frac{\omega_p^2}{\omega_0^2 - \omega^2} \vec{E}^\omega = \epsilon_0 \chi_\omega \vec{E}^\omega.$$

On assuming that  $\delta$  is small with respect to  $|\omega - \omega_0|$ , placing it outside of the resonance zones. And on using eqn (3) then with eqn (4):

$$\chi = \frac{\omega_p^2}{\omega_0^2 - \omega^2 - \delta^2} = \frac{\omega_p^2}{(\omega_0^2 - \omega^2) \left(1 - \frac{\delta^2}{\omega_0^2 - \omega^2}\right)} \approx \chi_\omega \left(1 + \frac{\delta^2}{\omega_0^2 - \omega^2}\right) \quad (5)$$

#### 4 Expression for the indice—and the insertion of the electro-optical coefficient $r$

With  $\epsilon_r = n_x^2 = 1 + \chi$ , we have as a relationship for the indice in Ox and in the presence of  $E_S$ :

$$\begin{aligned} n_x &= \sqrt{1 + \chi} \approx \left(1 + \chi_\omega + \frac{\chi_\omega \delta^2}{\omega_0^2 - \omega^2}\right)^{1/2} \\ &= \left\{ (1 + \chi_\omega) \left[ 1 + \frac{\chi_\omega \delta^2}{(\omega_0^2 - \omega^2)(1 + \chi_\omega)} \right] \right\}^{1/2} \\ &= (1 + \chi_\omega)^{1/2} \left[ 1 + \frac{\chi_\omega \delta^2}{(\omega_0^2 - \omega^2)(1 + \chi_\omega)} \right]^{1/2}. \end{aligned}$$

On introducing  $n_\omega = \sqrt{1 + \chi_\omega}$ , the indice in Ox and without  $E_S$  gives

$$n_x \approx n_\omega \left(1 + \frac{1}{2} \frac{\chi_\omega \delta^2}{(\omega_0^2 - \omega^2) n_\omega^2}\right) = n_\omega + \frac{\chi_\omega \delta^2}{2n_\omega(\omega_0^2 - \omega^2)}. \quad (6)$$

Finally:

$$\Delta n = n_x - n_\omega = \frac{\chi_\omega \delta^2}{2n_\omega(\omega_0^2 - \omega^2)} \quad (7)$$

With  $\chi_\omega = \frac{\omega_p^2}{\omega_0^2 - \omega^2}$ , or rather  $\frac{1}{\omega_0^2 - \omega^2} = \frac{\chi_\omega}{\omega_p^2}$ , we have  $\Delta n = n_x - n_\omega = \frac{\chi_\omega^2 \delta^2}{2n_\omega \omega_p^2}$ .

As  $n_\omega = \sqrt{1 + \chi_\omega} \Leftrightarrow \chi_\omega = n_\omega^2 - 1$ , we can write

$$\Delta n = \frac{(n_\omega^2 - 1)^2}{2n_\omega} \left(\frac{\delta}{\omega_p}\right)^2 \quad (8)$$

As indicated above,  $\delta^2 \propto E_S = aE_S$ , so that to a first approximation—neglecting 1 in front of  $n_\omega^2$  (given that with the presence of chromophores the medium is, intrinsically,

highly polar so that its permittivity ( $\epsilon_r = n_\omega^2$ ) can be relatively high by even 3 or 4 orders)—we have:

$$\Delta n \approx \frac{n_\omega^4}{2n_\omega \omega_p^2} a E_S, \quad \text{in which } \Delta n \text{ is in the form}$$

$$\Delta n = \frac{1}{2} r m^3 E_S \quad (9)$$

in which  $r \equiv r_p \approx \frac{a}{\omega_p^2}$  and is the electro-optical coefficient, and  $n_\omega \equiv n$  by notation, an indice following the direction of the polarisation of the optical wave and measured in the absence of the polarising field  $E_S$ .  $\Delta n$  is proportional to  $E_S$ , and eqn (9) is identical to eqn (4) and well characterises the Pockels effect.

*Comment 1* There is another, possible way to represent the Pockels effect:

as  $d\left(\frac{1}{x^2}\right) = d(x^{-2}) = -2x^{-3}dx$ , we can write

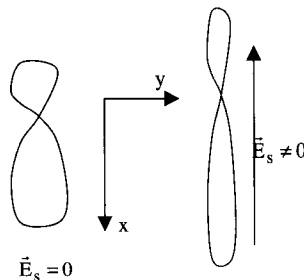
$$\Delta\left(\frac{1}{n^2}\right) = \left|d\left(\frac{1}{n^2}\right)\right| = 2n^{-3}\Delta n = 2\frac{\Delta n}{n^3} \quad \text{and on using eqn (9) leaves}$$

$$\Delta\left(\frac{1}{n^2}\right) = rE_S. \quad (10)$$

Here we recover the classical expression used to define the electro-optical effect, which was evolved from the ellipsoidal deformation of indices at a low frequency electric field (linear variation within the electric field of coefficients  $\left[\frac{1}{n^2}\right]_i$  from an ellipsoid of indices).

*Comment 2* Variations in the indice due to the application of  $E_S$  can themselves be variable. This depends on the orientation of the static field  $E_S$  with respect to the direction of polarisation of the incident optical wave and anisotropic effects can appear. However, in reality it can be advantageous to polarise the wave in the direction Oy perpendicular to  $E_S$  (which follows Ox).

The deformation of orbitals by  $E_S$ , only for the propagation of the same wave but polarised in the direction Ox, can have a greater effect on propagation along Oz than along Oy. In the adjacent scheme, we can see that the p-orbital retains the same elongated form in Ox (admittedly slightly longer in the presence of  $E_S$ ), but is also much 'skinnier' in the presence of  $E_S$ .



## V Organic electro-optical modulators and their basic design

### 1 The principal types of electro-optical modulators

An electro-optical material can be used as a polarised wave phase or amplitude modulator depending on the design geometry chosen.

#### a Phase modulator

The phase modulator demands the more simple structure. It consists of a modulator arm constructed from a simple optical guide, onto which the incident wave falls. The modulation is performed by applying a transversal tension, which induces a phase delay ( $\Delta\phi$ ) dependent on the frequency of the electric field. The information contained in the latter frequency is then 'written' on to the optical wave in the form of a phase modulation, as detailed in Figure XII-14. The electrodes, which can be placed in either of two positions, used to apply E are not shown in the Figure for the sake of clarity. One position corresponds to a sandwich structure, in which the organic material is held in between the two contacts shown in the Figure. The alternative is to make the electrodes coplanar, that is to deposit the contacts on individual parts of the same surface of the organic material. The latter design gives rise to field lines which interact—to a lesser extent—with the electro-optical material. The often introduced overlap figure (T) between optical and electrical fields actually decreases and in turn  $V_\pi$  increases. The latter can be written in an equation more widely applicable than eqn (8):

$$V_\pi = \lambda_0 \frac{1}{r n^3} \frac{d}{TL} \quad (8')$$

#### b Amplitude modulator

Phase shifting alone does not change the intensity of the optical wave subject to modification. However, here, the modification of the intensity of an optical wave is possible by using, for example, a Mach-Zehnder amplitude modulator. This device can be inserted into an arm of an interferometer.

As shown in Figure XII-15, the amplitude of the incident wave ( $I_i$ ) is equally shared into two waves, each with intensity  $\frac{1}{2}I_i$ , down two arms neither of which have been subject to an electrical field E. The form of the modification induced by E on

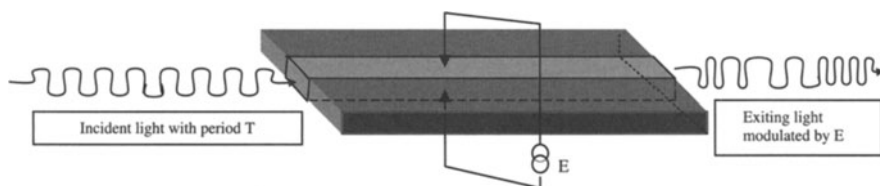
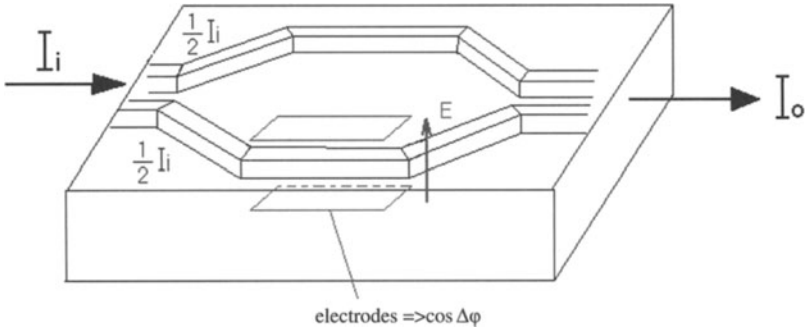


Figure XII-14. Schematisation of a phase modulator.



**Figure XII-15.** Schematisation of a Mach-Zehnder type amplitude modulator.

one of the arms is  $\frac{1}{2}I_i \cos \Delta\varphi$  in which  $\Delta\varphi$  is the degree of dephasing with respect to the non-modulated wave in the unaffected arm.

The exit intensity is therefore:

$I_0 = \frac{1}{2}I_i + \frac{1}{2}I_i \cos \Delta\varphi = I_i \cos^2 \frac{\Delta\varphi}{2}$ , with  $\Delta\varphi = |\varphi - \varphi_0| = \pi \frac{V}{V_\pi}$  (eqn (6') from Section II-1). When  $\cos^2 x = \frac{1+\cos 2x}{2}$  and  $\cos 2x \approx 1 - \frac{4x^2}{2}$ , that is

$$\cos^2 x \approx \frac{1}{2} \left( 1 + 1 - \frac{4x^2}{2} \right) = 1 - x^2, \quad \text{and} \quad x = \frac{\Delta\varphi}{2},$$

we can obtain:

$$I_0 = I_i \left[ 1 - \frac{\Delta\varphi^2}{4} \right] = I_i \left[ 1 - \frac{\pi^2}{4V_\pi^2} V^2 \right] = I_i - KI_i V^2,$$

or in other terms,  $\frac{I_0}{I_i} = 1 - KV^2$ .

If  $V = V_0 \cos \omega t$ , then  $V^2 \propto \cos^2 \omega t \propto \cos 2\omega t$ , and thus  $\frac{I_0}{I_i} \propto C_1 - C_2 \cos 2\omega t$ . The intensity  $I_0$  is thus modulated by a frequency  $2\omega$ .

## 2 Figures of merit

As already described in Section II-2-c, the half-wave tension, in the form  $V_\pi = \lambda_0 \frac{1}{r n^3} \frac{d}{L}$  for a transversal polarising modulator, should be as low as possible (in principle around 1 V).  $V_\pi$  is often used to characterise the performance of a modulator.

Given the expression for  $V_\pi$ , in order to decrease this parameter it is in our interest to decrease the coefficient  $\frac{d}{L}$  and in effect increase within reason the length of the modulator arms.  $d$  is normally around several microns and  $L \approx 3$  cm. In addition, the factor  $r n^3$  needs to be as large as possible to decrease  $V_\pi$ , and can thus also be taken as a figure of merit as in  $FM = r n^3$ , and is expressed in  $\text{pm V}^{-1}$ .

Figure XII-16 shows the figure of merit as a function of the wavelength of the optical field for several different materials (from [Bos 95]).

Figure XII-17 shows the general configuration of optimised stilbene and benzene in addition to values of  $r$  and  $n$  at given wavelengths of light.  $D$  and  $A$ , respectively,

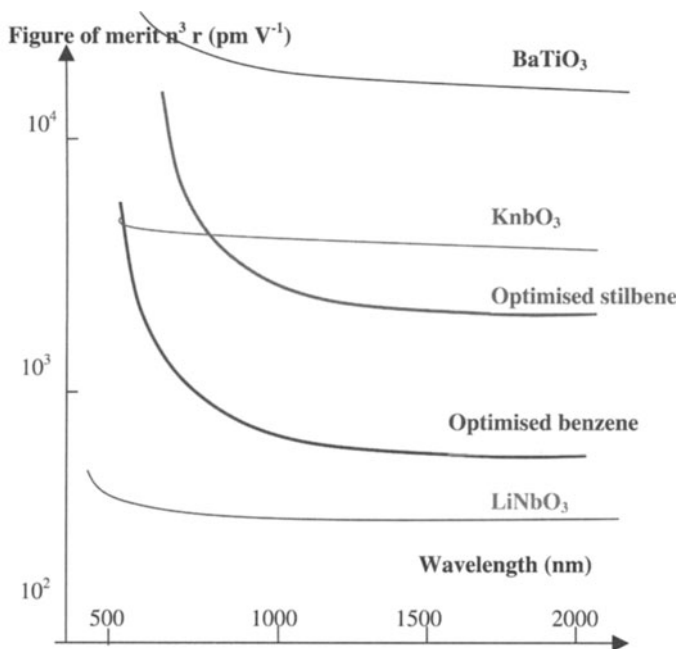


Figure XII-16. Figure of merit  $MF = n^3r$  ( $\text{pm V}^{-1}$ ) as a function of  $\lambda$  (nm).

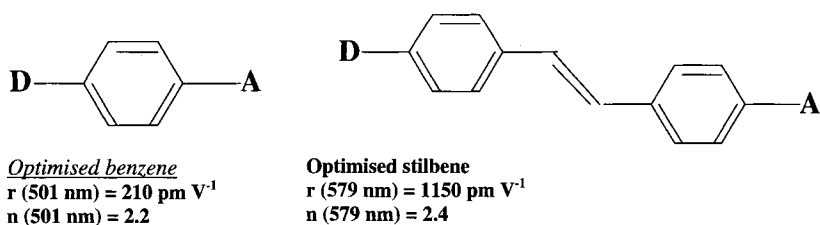


Figure XII-17. Configuration of optimised benzene and stilbene with example values for  $r$  and  $n$ .

Acceptor A	Donor D			
	CH <sub>3</sub>	OCH <sub>3</sub>	NH <sub>2</sub>	N(CH <sub>3</sub> ) <sub>3</sub>
CN	12	20	56	60
NO <sub>2</sub>	35	67	197	218

Figure XII-18. Values of  $\beta$  ( $10^{-4} \text{ m V}^{-1}$ ) for D-C<sub>6</sub>H<sub>6</sub>-A with varying donors and acceptors A ( $\lambda = 1064 \text{ nm}$ ) (from [bos 95]).

donor and acceptor groups exhibit efficiencies in the following orders: D, N(CH)<sub>3</sub> > NH<sub>2</sub> > OCH<sub>3</sub> > OH; and A, NO > NO<sub>2</sub> > CHO > CN.

The second order molecular polarisabilities ( $\beta$ ), expressed in  $10^{-4}$  m V<sup>-1</sup>, are given in Figure XII-18 for various *para*-substituted benzenes.  $\beta$ , which is also called first order hyperpolarisability, is defined by the relationship:

$$p = \mu_0 + \epsilon_0([\alpha]E_1^\omega + [\beta]E_1^\omega E_1^\omega + [\gamma]E_1^\omega E_1^\omega E_1^\omega + \dots)$$

in which  $\mu_0$  is the dipole moment of the fundamental state, without deformations and therefore without contributions from the various first [ $\alpha$ ], second [ $\beta$ ], third [ $\gamma$ ] and so on orders of polarisabilities. [ $\alpha$ ], [ $\beta$ ] and [ $\gamma$ ] are tensors in effect and  $E_1^\omega$  is the field localised at each molecule.

Macroscopic polarisation follows the form (see also Section III-2):

$$\vec{P} = \vec{P}_0 + [\chi_{a1}]\vec{E}^\omega + [\chi_{a2}]\vec{E}^\omega\vec{E}^\omega + [\chi_{a3}]\vec{E}^\omega\vec{E}^\omega\vec{E}^\omega + \dots$$

Once molecules are organised in systems with centres of inversion, resulting in centrosymmetric dispositions, strong, microscopic non-linear effects (high value of  $\beta$ ) become ineffective at the macroscopic level ( $\chi_{a2}$  is small).

### 3 The various organic systems available for use in electro-optical modulators

#### a Benefits and losses with organic media

As already mentioned in Section II, polymers exhibit several attractive qualities with respect to their use in electro-optical devices such as their low cost, their ease of synthesis and manipulation (using spin-coating techniques for example) in addition to their interesting physical characteristics, which include their low functioning voltage and dielectric permittivity ( $\epsilon_r$  or the order of 2 to 4), the latter of which makes it possible to envisage a good adaptation to the response times between the electrical excitation and the optical wave.

Certain inconveniences found with these materials should, however, not be ignored. They include the elimination of the isotropic character in organic (amorphous) media, most notably in polymers ( $\pi$ -conjugated included) which tend to form centro-symmetrical systems in which non-linear second order effects also tend towards zero. In addition, in order to activate the non-linear properties, 'poling' microscopic aggregates with an electric field is necessary.

Any alignment of such aggregates breaks down the centro-symmetry. The material does, however, retain a certain instability due to the ability of thermal effects to agitate and disorientate any aligned aggregates. The stabilisation of centro-symmetry is the main cause of problems at an industrial level, especially when the materials otherwise exhibit high chemical resistance, and a reasonably low sensitivity to humidity and to oxidation of  $\pi$ -bonds. For the present moment, one of these materials used in organic modulators is polyimide [Gar 99].

## b The different systems

Most crystalline organic materials are centro-symmetric and thus useless with respect to second order effects. Non-linear moieties are thus often used incorporated into an amorphous polymer, which is vitrified directly following preparation into a film. The electro-optical performances are conditioned by the concentration of the chromophores (non-linear  $D - \pi - A$  moieties) used which can be inserted into the final material. Different systems, using this technique, can be prepared:

- 'guest-host' systems, as shown in Figure XII-19-a, are prepared from a mixture of an optically active medium mixed with a polymer (which necessitates solvents such as toluene or chloroform). Solubility parameters control the final chromophore concentration;
- systems prepared by grafting chromophores onto the back bone of a polymer, as detailed in Figure XII-19-b; and
- covalent systems obtained *via* the formation of covalent bonds between chromophores and polymers chains, as shown in Figure XII-19-c.

A step common to the use of these systems is that once prepared the chromophores must be aligned so that the material loses as much as possible its amorphous character and improves its electro-optical efficiency. The effect of this procedure is shown in Figure XII-20-a and -b for guest-host and polymer grafted systems. In order to

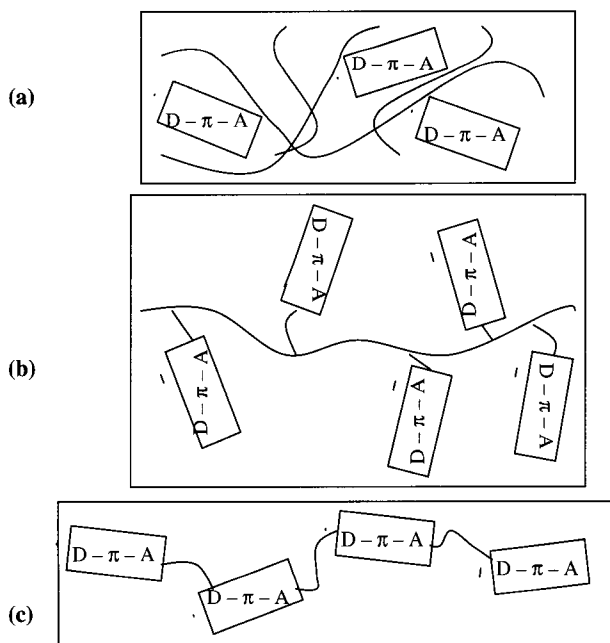


**Figure XII-19.** Different possible systems: (a) 'guest- host'; (b) chromophore grafted to back bone chain; and (c) chromophore inserted into polymer chain.



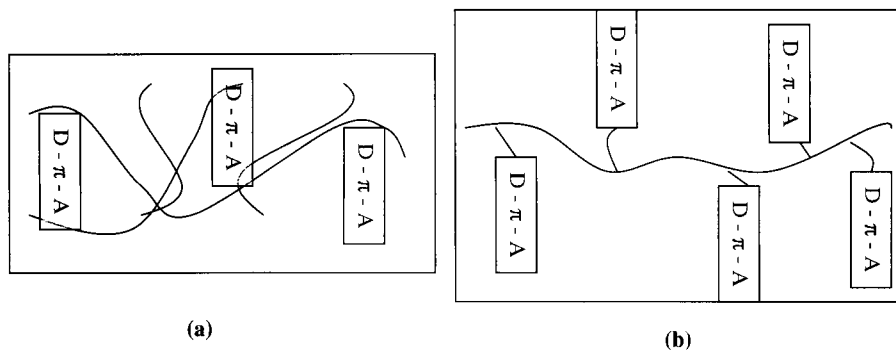


**Figure XII-20.** (a) 'Guest-host' and (b) grafted systems, after chromophore orientation by 'poling'.

get around this stage, or to stabilise the orientation obtained by using this method, mesogens (polymer mesogens) can be used which orientate themselves in a given direction (in the liquid crystal state). In theory though it seems that this latter method may not give satisfying electro-optical performances.

## VI Techniques such as etching and polyimide polymer structural characteristics

### 1 Paired materials: polyimide/DR1

As a material for a polymer matrix, polyimide presents numerous advantages including its low optical losses, low water permeability, low refraction indice (1.56 at 1.3  $\mu\text{m}$ ) and dielectric constant ( $\approx 3.2$  to 3.5) and good thermal stability ( $T_g = 290^\circ\text{C}$ ).

The method used for obtaining films has been well established. In the case of polyimide 6FDA/ODA (otherwise known as PI 2566 and supplied by DuPont) which is detailed in Figure XII-21, an adherence promoter is used first of all (VM 651 promoter spread at 2500 rpm for 30 s), then an initial layer of PI 2566 is spread at 500 rpm for 5 s, and then finally the PI 2566 is spread at 200 rpm for 30 s. Following this step is an annealing step at  $120^\circ\text{C}$  for 30 min on a heating plate and then a second heating stage at  $300^\circ\text{C}$  in an oven for at least 1 h.

Turning to one-dimensional chromophores, a good example and representative molecule is Disperse Red One (generally called DR1) (Figure XII-22), a well known

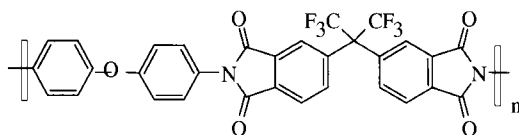


**Figure XII-21.** The monomer unit structure of polyimide 6FDA-ODA (PI 2566, DuPont).

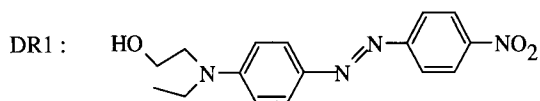


**Figure XII-22.** The structure of DR1.

nitroazobenzene based dye. It has been well characterised and widely used for the last decade.

## 2 Device dimensions—resorting to lithography

### a The dimensions

$\alpha$  *Intensity modulator* Figure XII-23 shows the commonly used Mach-Zehnder configuration for an amplitude modulator. The sizes, shown in the Figure, have been determined with respect to both guiding conditions (mono-mode) and the need to produce a significant electro-optical effect. Assuring the length of the component (to obtain the required effect and reduce  $V_\pi$ ), while retaining a guide depth of around 1 micron (to verify guiding conditions) complicates the experimental preparation of such a device. Lithographic masks are used which have to work well at very different scales: of the order of microelectronics and of the order of several centimetres. The technology used for motifs results in poor quality preparations.

$\beta$  *Phase modulator* The simplest device to prepare is that based on a single arm, as it consists of an optical guide sandwiched between two electrodes. In order to obtain a good electro-optical signal and to have appropriate guiding conditions, the dimensions of the device can resemble those shown above for the amplitude modulator. A simplified component can be obtained by using a cladding material to cover over the device made from a polymer which rests in contact with air. This type of guide can be particularly useful in determining losses due to the polymer (such as polyimide, polyimide/DR1 *etc.*). The geometrical form of the guiding conditions were determined by Petermann [Pet 91 and Pet 96]. With the expression

$$H = (h/\lambda)\sqrt{n_1^2 - n_2^2} \geq 1,$$

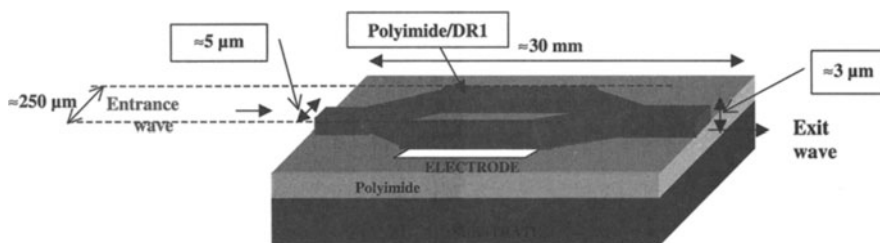


**Figure XII-23.** Dimensions of a Mach-Zehnder amplitude modulator.

the mono-mode guiding condition is

$$R = \frac{w}{h} \leq 0.3 + \frac{t/h}{\sqrt{1 - (t/h)^2}}$$

Definitions of parameters for these equations are detailed in Figure XII-24.

For polyimide using the parameters detailed above, we have  $H = 1.49$  (which holds well to the condition  $H \geq 1$ ) and  $R = w/h = 1.25$ , a value below that derived from  $0.3 + \frac{t/h}{\sqrt{1 - (t/h)^2}} = 1.44$ .

The distribution of field lines, obtained equally well from calculations or experiment, is shown in Figure XII-25-a. What is particularly interesting is the way in which the lines are well confined within the rib guide. Figure XII-25-b shows the critical evolution of the ratio  $w/h$  with respect to  $h$  for different values of the coefficient  $r = t/h$  for a ribbon guide.

A mono-modal regime is reached when  $(w/h) = 1$  for  $r = 0.5$ . For polyimide, when  $r = 0.75$  and  $(w/h) = 1.25$  the mono-modal regime is attained.

### 3 Etching

Once the dimensions of the devices have been determined, they can be prepared by photolithography (see Chapter VIII, Section II-2) using masks of an appropriate size and quality. Given the research already gone into preparing etched surfaces exhibiting vertical walls, in principle it should be possible to use dry etching techniques to attain an excellent level of anisotropy. The speed at which the etching can be done depends on the rate of pulverisation, which in itself depends on two component parts. One is physical and is based on the inert ions used such as argon, and the other component is chemical and is based on reactive reagents, for example oxygen ions used for polymer etching. Appendix A-9 details the principal mechanisms and characteristic parameters used. As described therein, the etching of polymers (polyimides) by ion beams used for microelectronics must be performed using parameters close to those used in plasma etching (RIE etching).

Figure XII-26 indicates (for polyimide PI 2566) the rate of etching speeds with respect to the energy ( $E$ ) of the incident ion beam ( $3 \text{ keV} \leq E \leq 6 \text{ keV}$ ). With a current density  $J = 0.4 \text{ mA cm}^{-2}$ , and a liquid nitrogen trap set close to the sample so as to

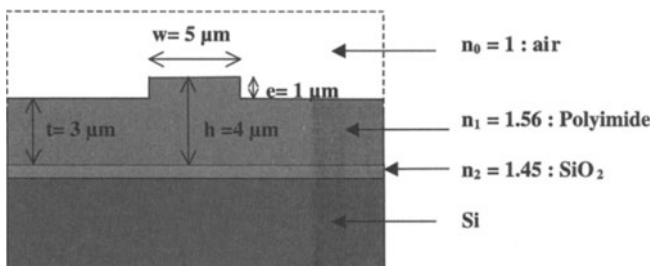


**Figure XII-24.** Parameters used in the Petermann conditions (mono-mode guide).

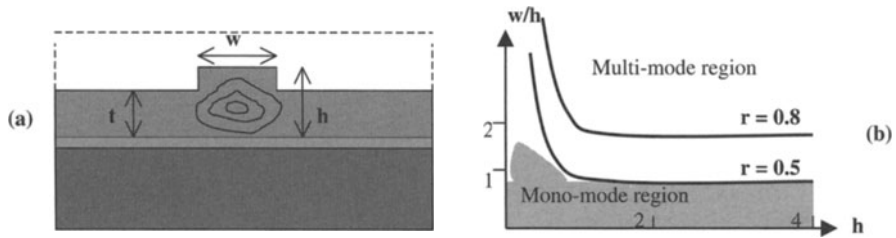


**Figure XII-25.** (a) Distribution of field lines in a rib shaped guide; and (b) mono- and multi-mode regions.

cool the sample, limit its degradation, trap excess reagents and condense reaction products, a comparison of etching speeds has been performed for various ion beams (see also with Figure XII-16 in which the characteristics of the techniques used are shown), including:

- dry etching using  $\text{Ar}^+$  ions;
- Reactive Ion Beam Etching (RIBE) using  $\text{O}^+$  ions without a trap;
- Ion Beam Assisted Etching (IBAE) using  $\text{Ar}^+$  ion beam with a flux of molecular oxygen; and
- IBAE with a beam of  $\text{O}^+$  ions and a flux of molecular oxygen.

As we can see in Figure XII-26:

- the difference between dry etching and RIBE etching is as great as the energy  $E$  is small; and
- there is a step between the optimised energy for RIBE etching ( $E \approx 3 \text{ keV}$ ) and the energy used for the optimised IBAE process ( $E \approx 6 \text{ keV}$ ). This difference can be accounted for by the energy of  $\text{O}^+$  ions which generate reactive species ( $\text{O}^\bullet$ ) by colliding with the oxygen flux. The energy transmitted through collisions

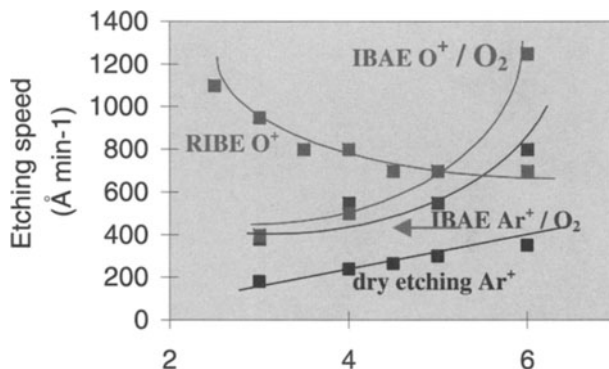


**Figure XII-26.** Etching speeds compared using different techniques.

between  $O^+$  and  $O$  is of the order of 3 keV (taking into account the kinetic transfer coefficient  $\gamma = 1/2$ ), in precise equivalence with the energy of  $O^+$  ions used to optimise  $O^+$  RIBE etching.

Finally, the optimised parameters obtained were:

- RIBE  $O^+$  etching:  $E = 2.5$  keV (with  $J = 0.4$  mA cm $^{-2}$  and realised using a similar method [Mou 00]); and
- IBAE  $O^+$  etching:  $E = 6$  keV (with  $J = 0.4$  mA cm $^{-2}$  realised also for an ion beam current density).

#### 4 Examples of polymer based structures [Cor 01]

##### a Polyimide guide (as passive material) and characterisation of optical losses

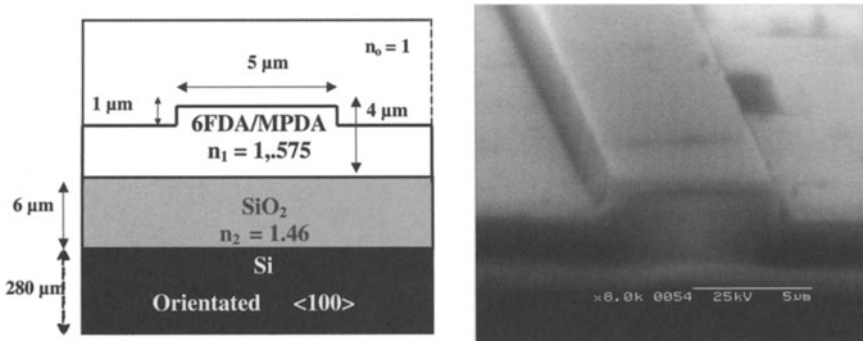


Figure XII-27. Geometrical structure of electron microscopic image of a polyimide guide.

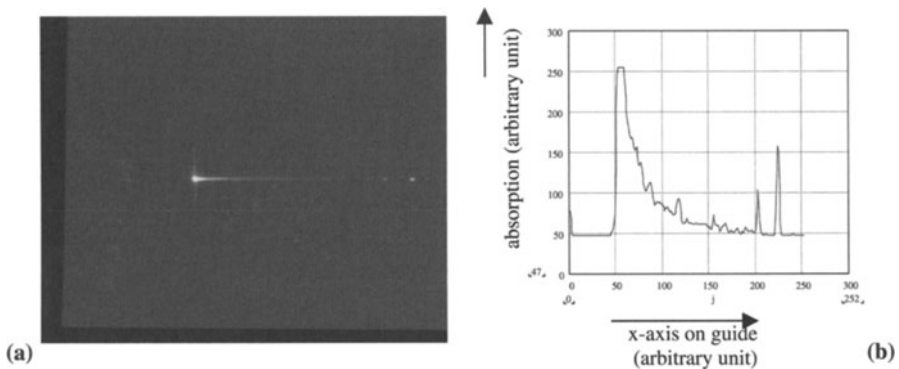
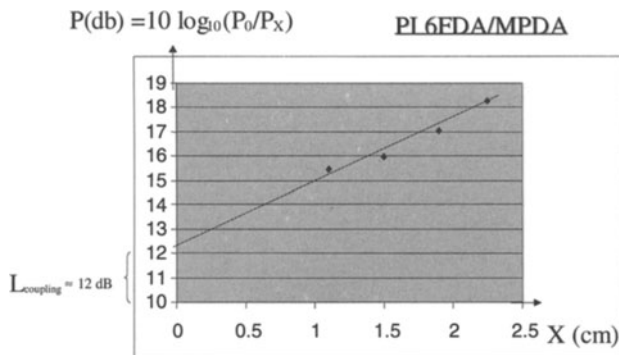
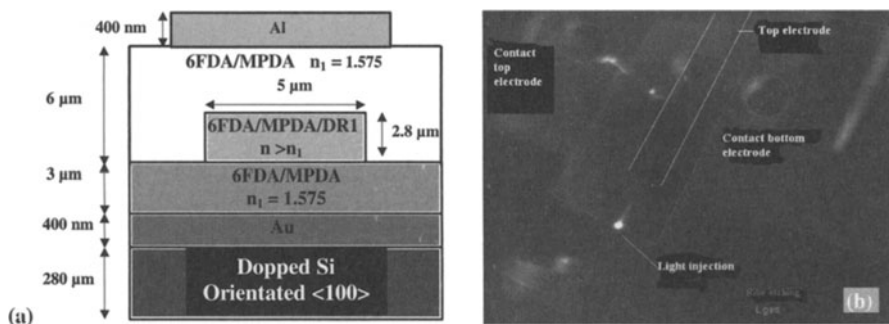


Figure XII-28. (a) Appearance of transversally diffused light; and (b) the corresponding absorption of the optical signal along the guide length.



**Figure XII-29.** Measuring propagation losses using the 'cut-back' method ( $L_{\text{Propagation}} \approx 2 \text{ dB cm}^{-1}$ ).

### b Modulator structure with polyimide/DR1 as the electro-optical material



**Figure XII-30.** (a) Scaled representation of a polyimide/DR1 phase modulator; and (b) light injected into the same phase modulator equipped with electrodes.

## VII Conclusion

Using electro-optical materials such as lithium niobate ( $\text{LiNbO}_3$ ) [Pap 85], the method by which modulators worked was well understood from the beginning of the 1980s. However, the rapid development of active organic materials during the last decade or so indicates that completely organic modulators will be soon available. These hold the promise of being relatively cheap to fabricate and could be used in fibre optic networks either directly with the user or through a Hertzian process. Their exceptionally fast response times, originating from the electronic processes involved, will probably be required in response to the demand placed on communication systems, a demand

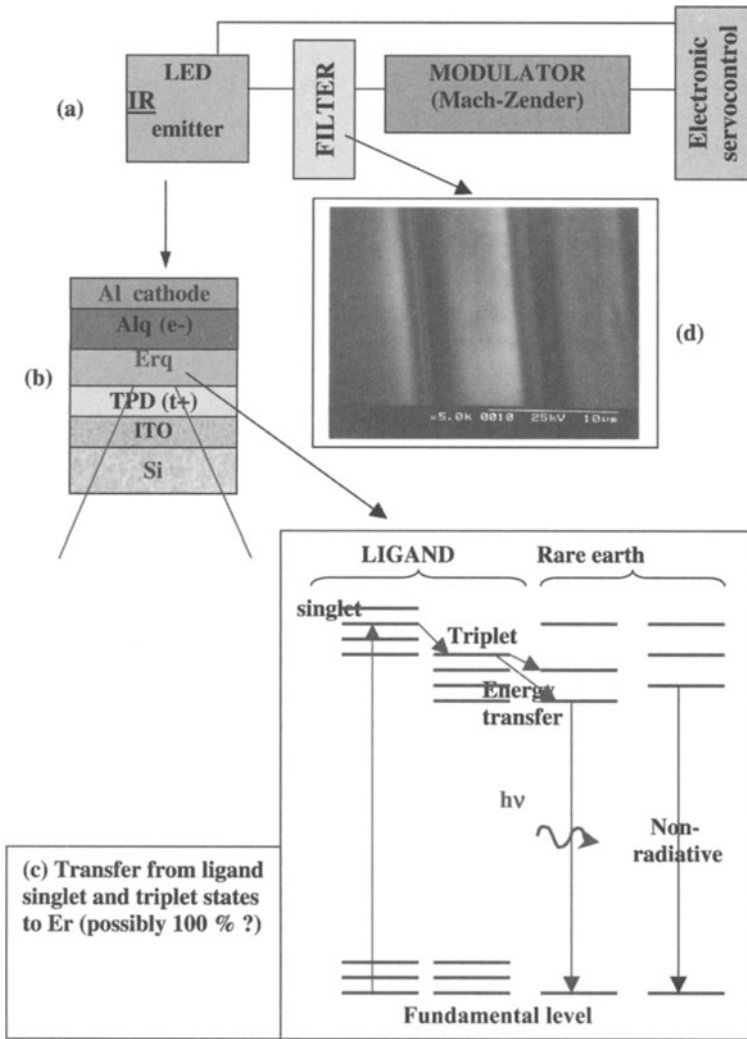


**Figure XII-31.** Future prospects: (a) schematisation of an all-organic electro-optical device; (b) schematisation of an emitter; (c) principal of erbium emission; and (d) photolithography of polyimide which may permit network fabrication.

necessitating a doubling in optical telecommunication networks every 18 months in a process nicknamed ‘Moore’s optical law’ [Tou 01].

Figure XII-13 shows the possible structure of an all organic device [Umop 99]. The emitter could be fabricated using the layering shown in Figure XII-13-b and using the current knowledge detailed in Chapter X. The transfer of singlet and triplet states from the ligand q to erbium could be highly efficient, as detailed in Figure XII-13-c. The filter, within a network, could be fabricated using a focalised ion beam (FIB) machine,

giving 1.5  $\mu\text{m}$  mono-mode guides with polyimide derivatives. Figure XII-13-d shows a photo of the derivative 6FDA-ODA as a pertinent example.

The electronic servocontrol needs to be constructed taking into account the behaviour of the polymer based electro-optical modulator. In simple terms, experiments are devised in order to model derivatives and their characteristic behaviours and any secondary opposing reactions. In order to measure the dephasing attained at a given applied and continuous tension, a triangular and periodic signal can be directed at one arm of a Mach–Zehnder device. Then the modulated sinusoidal exit signal is recorded and once again another triangular tension is applied but this time with the continuous component. The recorded signal, again sinusoidal can be compared with the previous signal and the difference in the two accorded to the continuous component.

We can finally say that the actual progress made recently will allow the fabrication of such devices without any major obstacles. As we have already mentioned, one problem does remain and that is the stability of organic materials. The continuous improvement in their qualities should, however, allow the emergence of devices very early in the 21st century.



# Appendices

## Atomic and molecular orbitals

### Introduction

This appendix proposes a relatively simple construction of atomic and molecular orbitals for a covalently bound solid. And is aimed at readers relatively well versed in physical electronics. An example is made of the hybridisation of carbon orbitals.

## I Atomic and molecular orbitals

### 1 Atomic s- and p-orbitals

Speaking approximately and with respect to atomic orbitals, we can imagine that each electron within an atom moves in a spherically symmetrical symmetry. This is the result of a potential from the nucleus which varies with  $1/r$ , represents the overall effect of all other electrons and is, to a first approximation, spherical.

The electronic state is represented by the wave function ( $\Psi_{n,l,m}$ ) which is dependent on the three quantum numbers  $n$ ,  $l$  and  $m$ . The energy level depends only on  $n$  and  $l$  while the degree of degeneration is equal to the number of values taken on by  $m$ .

When  $l = 0$ , the atomic orbitals are called s-orbitals and the wavefunctions vary only with  $n$ , as in  $\Psi_{n,0,m} = R_{(r)}\Theta_{(0)}\Phi_{(0)} = R_{n,0}\Theta_{0,0}\Phi_0$ , in which  $\Theta_{0,0} = \frac{\sqrt{2}}{2}$  and  $\Phi_0 = \frac{1}{\sqrt{2\pi}}$ . These wavefunctions do not depend on  $\theta$  nor on  $\varphi$ . Only  $R_{(r)}$  takes on different values as the principal quantum number  $n$  varies. The s-orbital therefore takes on the spherical symmetry shown in Figure 1.

When  $l = 1$ ,  $m = -1, 0, 1$  and the orbitals are called p-orbitals:

$$m = 0: \Theta_{1,0} = (\sqrt{6}/2) \cos \theta \text{ and } \Phi_0 = 1/\sqrt{2\pi}$$

$$m = 1: \Theta_{1,1} = (\sqrt{3}/2) \sin \theta \text{ and } \Phi_1 = (1/\sqrt{\pi}) \cos \varphi$$

$$m = -1: \Theta_{1,-1} = (\sqrt{3}/2) \sin \theta \text{ and } \Phi_{-1} = (1/\sqrt{\pi}) \sin \varphi$$

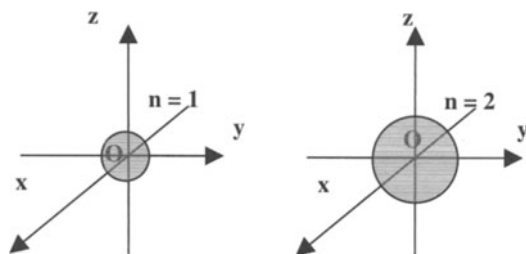


Figure 1. s-Orbitals.

If  $R(r)$  represents the function  $R_{n,1}$ , as  $n$  varies, invariably the wavefunctions for the three preceding p-states are of the form:

$$(I) : \Psi_0 = \frac{1}{2} \sqrt{\frac{3}{\pi}} R(r) \cos \theta \quad (II) : \Psi_1 = \frac{1}{2} \sqrt{\frac{3}{\pi}} R(r) \sin \theta \cos \varphi$$

$$(III) : \Psi_{-1} = \frac{1}{2} \sqrt{\frac{3}{\pi}} R(r) \sin \theta \sin \varphi$$

If we set  $R(r) = R(r_f)$  so that  $r_f$  has a value defined by the relationship  $\int_0^{r_f} |R(r)|^2 r^2 dr = 95\%$  (which indicates that the probability of an electron being within a sphere of radius  $r_f$  is equal to 95%), then we can say that the three equations represent the orbitals in a conventional manner.

*Comment* It is worth noting the placing of points  $M$  as defined by  $\Psi = OM$  in Figure 2.

As an example, we'll use the relatively simple relationship

$$\Psi_0 = \frac{1}{2} \sqrt{\frac{3}{2}} R(r) \cos \theta = \|\overrightarrow{OM}\| = OM.$$

Here  $D$  is at the origin of the  $Oz$  axis, where  $\cos \theta = 1$ , and therefore  $OD = \frac{1}{2} \sqrt{\frac{3}{2}} R(r)$ . Now  $OM = OD \cos \theta$ . If  $\theta \in [0, \pi/2]$ ,  $OM > 0$ . The  $M$  points are now placed with a varying  $\theta$  in a sphere above the plane  $(xOy)$ .

If  $\theta \in [\pi/2, \pi]$ ,  $\cos \theta < 0$ , then the  $M$  points are in a sphere below  $(xOy)$ .

The signs of the orbitals  $\Psi_0$ ,  $\Psi_1$  and  $\Psi_{-1}$  can be obtained directly from the signs taken by the variables  $x$ ,  $y$ ,  $z$ . To do this, we can use the relationship between spherical

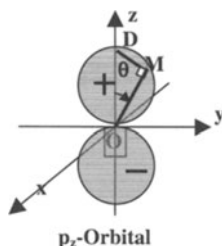
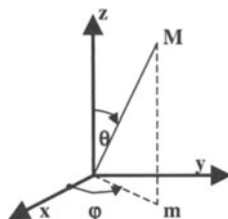


Figure 2. Shape of the  $p_z$ -orbital. The + and - signs concern  $\Psi_0$  which follows  $\cos \theta$ .



**Figure 3.** Axes normally used for spherical co-ordinates.

co-ordinates and the Cartesian co-ordinates indicated in Figure 3:

$$\begin{cases} \frac{x}{r} = \sin \theta \cos \varphi \\ \frac{y}{r} = \sin \theta \sin \varphi \\ \frac{z}{r} = \cos \theta \end{cases}$$

So for example, if  $\cos \theta < 0$ , then  $z < 0$  and  $\Psi_0 < 0$ .

For  $f(r) = \frac{1}{2} \frac{R(r)}{r} \sqrt{\frac{3}{\pi}} > 0$  (with  $r \approx r_f$ ), the functions  $\Psi_0$ ,  $\Psi_1$  and  $\Psi_{-1}$  can thus be written in the following way:

$$\Psi_1 = X = x f(r) = \Psi_{px} \quad (\Psi_{px} > 0 \text{ or } < 0 \text{ depending if } x > 0 \text{ or } x < 0)$$

$$\Psi_{-1} = Y = y f(r) = \Psi_{py} \quad (\Psi_{py} > 0 \text{ or } < 0 \text{ depending if } y > 0 \text{ or } y < 0)$$

$$\Psi_0 = Z = z f(r) = \Psi_{pz} \quad (\Psi_{pz} > 0 \text{ or } < 0 \text{ depending if } z > 0 \text{ or } z < 0)$$

We can at last schematise in Figure 4 the *s*- and *p*-orbitals using  $r$  fixed to the value  $r_f$  (which is such that  $\int_0^{r_f} r^2 |R(r)|^2 dr = 95\%$ ):

To conclude, the *s*-orbitals are non-directional, unlike the *p*-orbitals.

*Comment* The orbitals we have shown so far concern only one electron per orbital. They are the orbitals which we will go on to use when constructing molecular orbitals from the sharing of one electron per atom in covalent bonding. However, if we were

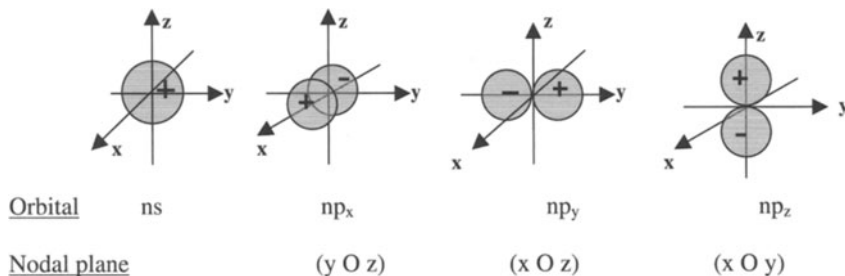


**Figure 4.** The *ns* and *np* orbitals. Note: the nodal plane is the plane in which there is zero probability of finding an electron.

to consider atomic orbitals which contained more than one electron, or  $i$  electrons, then the orbitals will take on the form  $\Psi = \Pi_i \Psi_i$  in which  $\Psi_i$  are the wavefunctions for each electron. Prior to being anti-symmetric (Pauli), these  $\Psi$  functions are used in the Slater determinate form.

## 2 Molecular orbitals

### a The example of the simplest molecular system $H_2^+$

In the simplest scenario we ignore the possible overlapping between adjacent orbitals, which would otherwise have to be taken into account using the supplementary condition  $\partial E / \partial k = 0$  in which energy is minimised following a variation method. With the two nuclei in our system placed—and fixed—at  $\vec{R}_1$  and  $\vec{R}_2$  and the shared electron at  $\vec{r}$ , as shown in Figure 5, we have the Hamiltonian for the system

$$H = -\frac{\hbar^2}{2m} \Delta - \frac{e^2}{4\pi\epsilon_0(|\vec{r} - \vec{R}_1|)} - \frac{e^2}{4\pi\epsilon_0(|\vec{r} - \vec{R}_2|)}.$$

If  $\varphi(r) = A \exp(-r/a_0)$  is the wavefunction for the fundamental state for a hydrogen atom, the solution for the system  $H_2^+$  can be used on assuming that the electron is localised preferentially on one of the two nuclei:

- if the electron is localised on the nucleus (1), then  $\varphi(r) \rightarrow \varphi(|\vec{AD}|) = \varphi(|\vec{r} - \vec{R}_1|) = \varphi_1$ ; or
- if the electron is localised on the nucleus (2), then  $\varphi(r) \rightarrow \varphi(|\vec{BD}|) = \varphi(|\vec{r} - \vec{R}_2|) = \varphi_2$ .

If the electron is localised in between the two nuclei, then the solution has to come from a mixture of the two preceding states. We can therefore look for a wavefunction  $\varphi$  of the  $H_2^+$  molecular ion in the form  $\varphi = c_1 \varphi_1 + c_2 \varphi_2$ . If the electron is localised on nucleus (1), then  $c_1 \rightarrow 1$  and  $c_2 = 0$ . If the electron is localised on nucleus (2),  $c_1 = 0$  and  $c_2 \rightarrow 1$ .

As this equation must satisfy the demand for proper values, then:

$$H|\varphi\rangle = E|\varphi\rangle, \text{ or rather } H|c_1\varphi_1 + c_2\varphi_2\rangle = E|c_1\varphi_1 + c_2\varphi_2\rangle.$$

On multiplying the left of the equation by  $\langle\varphi_1|$ :

$$c_1 \langle\varphi_1|H|\varphi_1\rangle + c_2 \langle\varphi_1|H|\varphi_2\rangle = E c_1 \langle\varphi_1|\varphi_1\rangle + E c_2 \langle\varphi_1|\varphi_2\rangle.$$

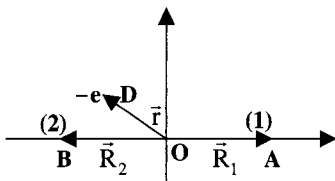


Figure 5. Layout of ions and the electron in  $H_2^+$ .

On using the simplifying assumption of negligible overlapping, *i.e.*  $S = \langle \varphi_1 | \varphi_2 \rangle = 0$ , we can place  $H_{11} = \langle \varphi_1 | H | \varphi_1 \rangle$  and  $H_{12} = \langle \varphi_1 | H | \varphi_2 \rangle$  and then obtain:

$$c_1 H_{11} + c_2 H_{12} = E c_1.$$

Similarly, on multiplying the left hand side of the same equation with  $r\langle \varphi_2 |$ , and with

$$H_{ij} = \langle \varphi_i | H | \varphi_j \rangle, \quad \text{we obtain } c_1 H_{21} + c_2 H_{22} = E c_2.$$

Thus there is a system of two equations in which there are two unknowns ( $c_1$  and  $c_2$ ), which can be written:

$$c_1 (H_{11} - E) + c_2 H_{12} = 0 \quad (\text{IV}); \text{ and}$$

$$c_1 H_{21} + c_2 (H_{22} - E) = 0. \quad (\text{V})$$

In addition:

- we know that the wavefunctions  $\varphi_1$  and  $\varphi_2$  are real, so can write

$$H_{12} = \langle \varphi_1 | H | \varphi_2 \rangle = \langle \varphi_2 | H | \varphi_1 \rangle = H_{21} = -\beta \text{ (with } \beta > 0); \text{ and}$$

- the problem (and thus also the Hamiltonian) remain invariant by permutation of the nuclei A (indice 1) and B (indice 2), so that  $H_{11} = H_{22} = -\alpha$ .

As the system of the two eqns (IV) and (V) contain two unknowns, the solution is admittedly non-trivial as its determinant is zero. Using our notations, we obtain the equation  $(\alpha + E)^2 - \beta^2 = 0$ , which gives rise to two solutions for the energy  $(\alpha + E) = \pm\beta$  that can be written using the form:

$E_L = -\alpha - \beta$  (the lowest energy corresponding to a bonding level as  $\alpha$  and  $\beta$  are positive); and  $E_A = -\alpha + \beta$  (the highest and therefore least stable energy, corresponding to the anti-bonding level). In passing, we can just note that  $E_A - E_L = 2\beta$ .

On inserting  $E_A$  into eqns (IV) and (V), we obtain  $(c_1 + c_2)\beta = 0$ , that is  $c_1 = -c_2 = c_A$ .

In the same manner, on placing  $E_L$  into eqns (IV) and (V), we discern  $(-c_1 + c_2)\beta = 0$ , that is to say  $c_1 = c_2 = c_L$ .

The wavefunction of the  $H_2^+$  system will allow us two solutions which can be written in the following way:

$$\Psi_L = c_L(\varphi_1 + \varphi_2); \text{ and}$$

$$\Psi_A = c_A(\varphi_1 - \varphi_2).$$

The normalisation condition for these two functions  $\Psi_L$  and  $\Psi_A$  is  $\langle \Psi_L | \Psi_L \rangle = \langle \Psi_A | \Psi_A \rangle = 1$  and allows determination of  $c_L = c_A = (1/\sqrt{2})$ . We thus finally obtain

$$\Psi_L = \frac{1}{\sqrt{2}}(\varphi_1 + \varphi_2)$$

$$\Psi_A = \frac{1}{\sqrt{2}}(\varphi_1 - \varphi_2)$$

As shown in Figure 6, a schematisation of these wavefunctions is quite possible. It is of interest to see that for the bonding solution, the electrons displays a very high probability of being between the two nuclei so that the strong electrostatic attraction between the electron and nuclei (1) and (2) bonds the entire system. However, we can see in the anti-bonding system that the electron displays a high probability of being on the outside of one of the other nuclei so that the strong electrostatic repulsion between nuclei (1) and (2) is destabilising.

*Comment* With  $S = \langle \varphi_1 | \varphi_2 \rangle \neq 0$ , a similar, longer calculation results in:

$\Psi_L = \frac{\varphi_1 + \varphi_2}{\sqrt{2(1+S)}}$	$E_L = -\frac{\alpha + \beta}{1+S}$
$\Psi_A = \frac{\varphi_1 - \varphi_2}{\sqrt{2(1-S)}}$	$E_A = -\frac{\alpha - \beta}{1-S}$

## b The molecule $H_2$

In  $H_2$  there are two electrons which we can assume are placed at the same potential as the electron in the previous example of  $H_2^+$ , as to a first approximation we can neglect the interaction potential between the two electrons.

Each of the two electrons has available to it two orbitals ( $\Psi_L$  and  $\Psi_A$ ). The system with the lowest energy would be with both electrons each in a bonding orbital. In this

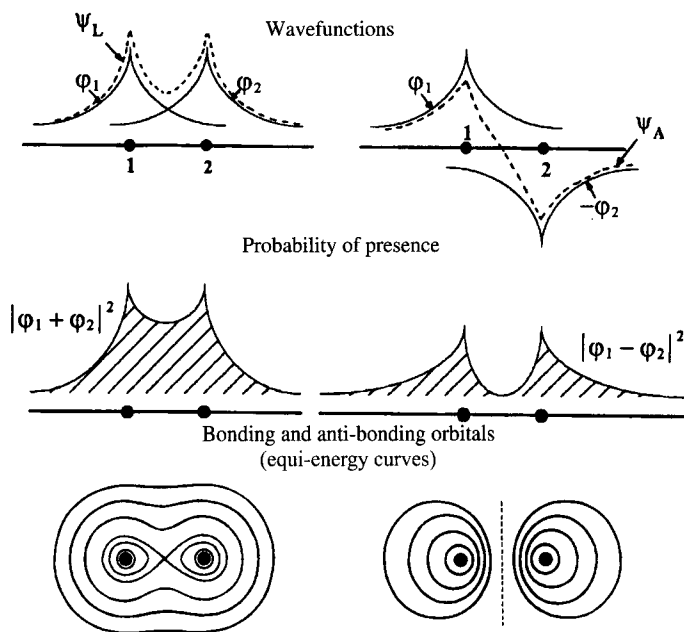


**Figure 6.** Wavefunctions and orbitals in  $H_2^+$ : left and right, respectively, bonding and anti-bonding orbitals.

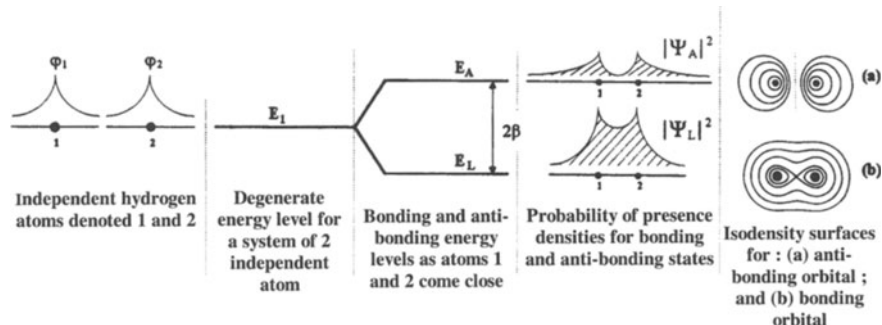


Figure 7. Energy and electronic states in  $H_2$ .

state, with the electrons localised around the position between the two nuclei, the system energy would be minimised as the electrons would benefit from an attracting potential (negative potential energy) due to the overlapping of Coulombic potentials developed by the positively charged nuclei. This charge localisation (and the maximum electronic density between two nuclei) is the very basis of the concept of covalent bonding.

When looking at the overall system, the combination of two hydrogen atoms resembles the melting of one into the other with the final result of an increased local probable electron density in between the two nuclei. The bonding state is again realised using a linear additive combination of the individual orbitals of each atom, as shown schematically in Figure 7.

The wavefunction can be written, generally speaking for both bonding and anti-bonding states, as  $\Psi = c_1\phi_1 + c_2\phi_2$  and results from the linear combination of atomic orbitals (LCAO).

*Comment* While the function  $\Psi_L$  is symmetric, the function  $\Psi_A$  is antisymmetric.

- on the  $E_L$  level, the spins are anti-parallel so as to distinguish the two electrons (undistinguished from the point of view of the orbitals as  $\Psi_L$  remains unchanged if they are permuted) so  $S = 0$  (singlet states);
- on the  $E_A$  level, the spins can be parallel as they are distinguished at the level of the orbital ( $\Psi_A$  changes sign if the two electrons are permuted) so  $S = 0$  or 1 (singlet or triplet states).

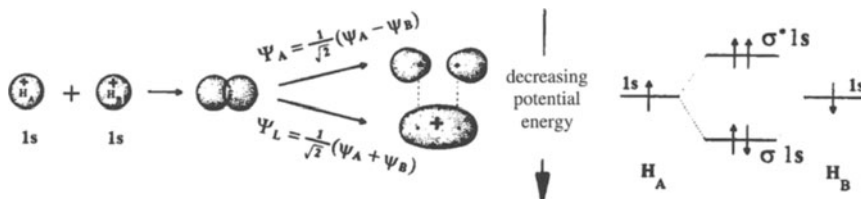


Figure 8.  $1s$   $\sigma$ - and  $\sigma^*$ -orbitals.



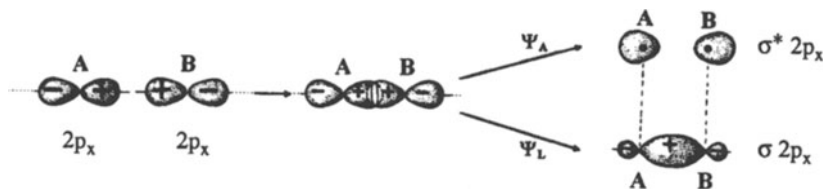


Figure 9.  $2p$   $\sigma$ - and  $\sigma^*$ -orbitals.

### 3 $\sigma$ - and $\pi$ -bonds

#### a $\sigma$ -bonds

Sigma ( $\sigma$ ) bonds are those which have as axis of symmetry the straight line in between the two covalently bonded atoms.

For example, from a pair of s-orbitals we can derive the ( $\sigma$ -orbitals shown in Figure 8.

If the axis Ox is that on which the two atoms (A and B) are placed, the  $2p$  orbitals will have the combination shown in Figure 9.

$$\text{With } \Psi_L = \frac{1}{\sqrt{2}}(\Psi_{A2p_x} + \Psi_{B2p_x}) \text{ and } \Psi_A = \frac{1}{\sqrt{2}}(\Psi_{A2p_x} - \Psi_{B2p_x}).$$

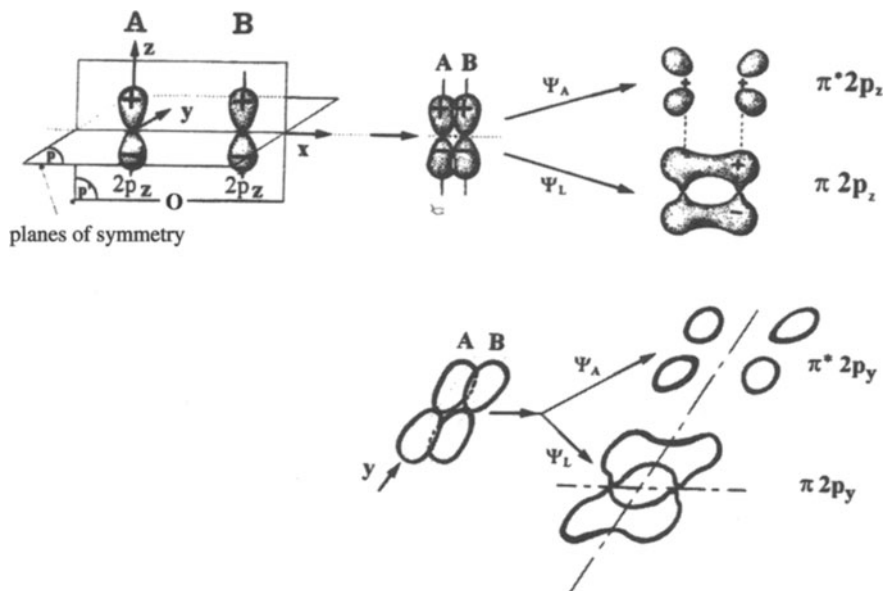


Figure 10.  $\pi 2p_z$ -,  $\pi^* 2p_z$ -,  $\pi 2p_y$ -, and  $\pi^* 2p_y$ -orbitals.

## b $\pi$ -bonds

$\pi$  bonds are molecular orbitals which have a plan of symmetry which passes through the straight line Ox joining the atoms and is perpendicular to the direction Oy for  $\pi 2p_z$ -orbitals or the direction Oz for  $\pi 2p_y$ -orbitals, as shown in Figure 10.

## II The covalent bond and its hybridisation

### 1 Hybridisation of atomic orbitals

#### a What is hybridisation?

Imagine a carbon atom with the atomic configuration  $1s^2 2s^2 2p^2$ . While it should behave like a divalent element, as in  $\text{CO}_2$ , the same configuration does not explain how  $\text{CH}_4$  comes to exist in its tetrahedral  $sp^3$  state, how  $\text{CH}_2 = \text{CH}_2$  exists in its triangular hybrid  $sp^3$  state nor how  $\text{C}_2\text{H}_2$  presents a diagonal  $sp^1$  hybridisation.

These structures can be interpreted on realising that when two carbon atoms are 'united', the valence states of each carbon atom (2s and 2p) are in effect presented as one s and three p orbitals. This first excited configuration ( $1s^2 2s^1 2p^3$ ) is favoured if the energy levels of its constituent orbitals are lowered on its formation, and this is what happens when they are 'mixed', or rather, hybridised.

The general form of molecular orbitals derived from the process of hybridisation can be written using quite self-evident notations (here carbon atoms A and B are identified by 1 and 2, respectively):

$$|\Psi\rangle = A_1|2s\rangle_1 + A_2|2p_x\rangle_1 + A_3|2p_y\rangle_1 + A_4|2p_z\rangle_1 \\ + B_1|2s\rangle_2 + B_2|2p_x\rangle_2 + B_3|2p_y\rangle_2 + B_4|2p_z\rangle_2 = |\Psi_1\rangle + |\Psi_2\rangle.$$

#### b Different degrees of hybridisation

There are indeed different levels of hybridisation—different levels of coupling of each of the various and involved orbitals.

*Diagonal  $sp^1$  hybridisation* This sort of hybridisation, involving for example s- and  $p_x$  orbitals gives:

$$|\Psi\rangle = A_1|2s\rangle_1 + A_2|2p_x\rangle_1 + B_1|2s\rangle_2 + B_2|2p_x\rangle_2 \\ = |\Psi_1\rangle + |\Psi_2\rangle,$$

in which  $|\Psi_1\rangle$  and  $|\Psi_2\rangle$  correspond each to 2 possible orbitals to give a total of 2 bonding  $\sigma_1$ -orbitals and 2 anti-bonding  $\sigma_a^*$ -orbitals. So  $|\Psi_1\rangle$  can thus correspond to  $|\Psi_{11}\rangle = a_1|2s\rangle_1 \pm a_2|2p_x\rangle_1$  or to  $|\Psi_{1a}\rangle = a'_1|2s\rangle_1 \pm a'_2|2p_x\rangle_1$  and in both cases the + and - give the signs of each of the pairs of hybrid orbitals.

The resulting  $\pi$ -orbitals are obtained with respect to both Oy and Oz, as shown in Figure 11.

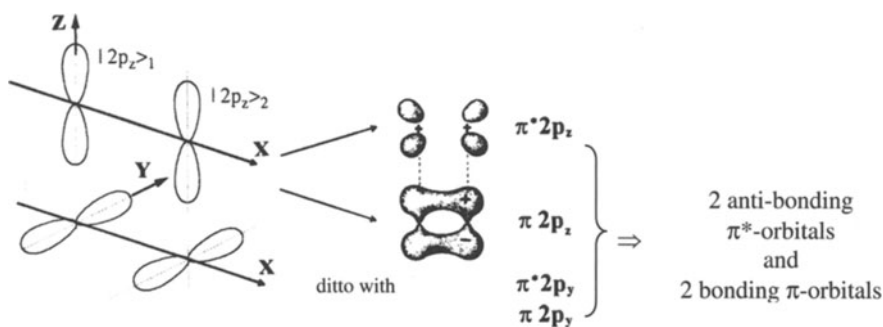


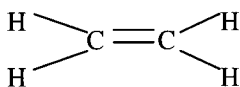
Figure 11.  $\pi^*$  and  $\pi$ -orbitals.

*Triangular  $sp^2$  hybridisation* The system couples only the states  $|2s\rangle$ ,  $|2p_x\rangle$  and  $|2p_y\rangle$  while leaving the state  $|2p_z\rangle$  outside of this linear coupling. The coupling can thus be written:

$$\Psi = A_1|2s\rangle_1 + A_2|2p_x\rangle_1 + A_3|2p_y\rangle_1 \\ + B_1|2s\rangle_2 + B_2|2p_x\rangle_2 + B_3|2p_y\rangle_2 = |\Psi_1\rangle + |\Psi_2\rangle$$

The three hybrid orbitals have their axes in the same plane and are generally denoted  $2sp_a^2$ ,  $2sp_b^2$  and  $2sp_c^2$ . In a plane perpendicular to these is the fourth orbital,  $2p_z$ , which gives rise to the  $\pi$ -orbital.

For the molecule  $C_2H_4$  below, the orbitals are schematised in Figure 12.



The angles between the three hybrid  $\sigma$ -orbitals, which originate from the same carbon atom, must be  $120^\circ$ . A calculation performed in the same manner as that shown in the following Section 2 (for the  $sp^3$  hybridisation), allows a determination of the three

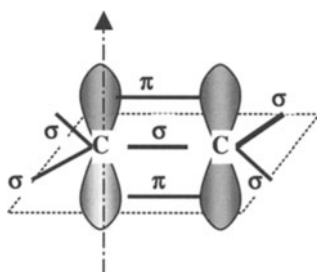


Figure 12. Orbitals in the molecule  $C_2H_4$ .

hybrid orbitals with respect to the  $sp^2$  hybridisation:

$$h_1 = \frac{1}{3^{1/2}} \left( |s\rangle + 2^{1/2} |p_x\rangle \right), h_2 = \frac{1}{3^{1/2}} \left( |s\rangle - \frac{|p_x\rangle}{2^{1/2}} + \frac{3^{1/2}}{2^{1/2}} |p_y\rangle \right),$$

$$h_3 = \frac{1}{3^{1/2}} \left( |s\rangle - \frac{|p_x\rangle}{2^{1/2}} - \frac{3^{1/2}}{2^{1/2}} |p_y\rangle \right).$$

*sp<sup>3</sup> Tetragonal hybridisation* This state draws on all states without exclusion through a hybridisation which corresponds to the structure of diamond and is further detailed below.

## 2 $sp^3$ Hybridisation

### a Rotational symmetry of the orbitals

The normalised wavefunctions for the s- and p-states (with  $r \approx r_f$ ) of the valence electrons in carbon ( $n = 2$ ) result from initial calculations (see Section 1-1):

$$|s\rangle = R_{n,0}(r)\Theta_{0,0}\Phi_0 = h_{(r_f)} = S \quad (n = 2, l = 0, m = 0)$$

$$|p_z\rangle = \varphi_0 = \frac{1}{2}\sqrt{\frac{3}{\pi}}R(r_f)\cos\theta = g(r)\cos\theta$$

$$= zf(r) = Z = \varphi_{2p_z} \quad (n = 2, l = 1, m = 0)$$

$$|p_x\rangle = \varphi_1 = \frac{1}{2}\sqrt{\frac{3}{\pi}}R(r_f)\sin\theta\cos\varphi$$

$$= g(r)\sin\theta\cos\varphi = xf(r) = X = \varphi_{2p_x} \quad (n = 2, l = 1, m = 1)$$

$$|p_y\rangle = \varphi_{-1} = \frac{1}{2}\sqrt{\frac{3}{\pi}}R(r_f)\sin\theta\sin\varphi$$

$$= g(r)\sin\theta\sin\varphi = yf(r) = Y = \varphi_{2p_y} \quad (n = 2, l = 1, m = -1)$$

(the functions  $f(r)$  and  $g(r)$  are related simply by  $g(r) = rf(r)$ ).

The four proper functions, S, X, Y and Z constitute the orthonormalised basis for a space in four dimensions. On considering the carbon hybrid state  $sp^3$  in which none of the four orbitals (X, Y, Z and S) play a specific role, the proper functions of this new state can be developed using the preceding basis, although we now have four more functions to deal with given the number of dimensions in the system;

$$\begin{cases} \Psi_1 = \alpha_1 S + a_1 X + b_1 Y + c_1 Z \\ \Psi_2 = \alpha_2 S + a_2 X + b_2 Y + c_2 Z \\ \Psi_3 = \alpha_3 S + a_3 X + b_3 Y + c_3 Z \\ \Psi_4 = \alpha_4 S + a_4 X + b_4 Y + c_4 Z \end{cases}$$

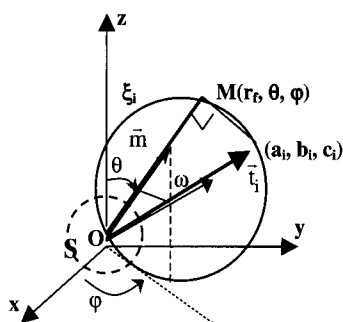


Figure 13. Representation of  $\Psi_i$ .

$|\Psi_1\rangle$ ,  $|\Psi_2\rangle$ ,  $|\Psi_3\rangle$  and  $|\Psi_4\rangle$  are the hybrid orbitals which correspond to the excitation  $1s^2 2s^2 2p^2 \rightarrow 1s^2 2t^4$ . This is only possible if the reached energetic states are equal to the gain in energy required by the atomic excitation.

Here  $\vec{m}$  is the unit vector going in the direction and the point M has the spherical co-ordinates  $r_f$ ,  $\theta$  and  $\varphi$ . In Cartesian co-ordinates  $\vec{e}_x$ ,  $\vec{e}_y$  and  $\vec{e}_z$  are the unit vectors for the axes Ox, Oy, Oz, and the respective components of  $\vec{OM}$  are  $x = r_f \sin \theta \cdot \cos \varphi$ ,  $y = r_f \sin \theta \cdot \sin \varphi$  and  $z = r_f \cos \theta$  as shown in Figure 13.

The components of  $\vec{m}$ , a unit vector equal to  $|\vec{r}| = 1$ , with respect the system of axes Ox, Oy and Oz are thus:

$$\vec{m} \begin{cases} \sin \theta \cos \varphi = \vec{m} \cdot \vec{e}_x \\ \sin \theta \sin \varphi = \vec{m} \cdot \vec{e}_y \\ \cos \theta = \vec{m} \cdot \vec{e}_z \end{cases}$$

Given the form of X, Y and Z, detailed at the beginning of this Section, we can write:

$$\begin{cases} X = g(r) \cdot \vec{e}_x \cdot \vec{m} \\ Y = g(r) \cdot \vec{e}_y \cdot \vec{m} \\ Z = g(r) \cdot \vec{e}_z \cdot \vec{m} \end{cases}$$

We can now write (with  $i = 1, 2, 3, 4$ ):  $\Psi_i = \alpha_i S + g(r) (a_i \vec{e}_x + b_i \vec{e}_y + c_i \vec{e}_z) \cdot \vec{m}$ .

On introducing the vector  $\vec{t}_i = a_i \vec{e}_x + b_i \vec{e}_y + c_i \vec{e}_z$ , which thus has components  $a_i$ ,  $b_i$ , and  $c_i$  in the system based on the axes Ox, Oy, Oz.

Each function  $\Psi_i$  can now be written as:  $\Psi_i = \alpha_i S + g(r) \vec{t}_i \cdot \vec{m}$ .

With  $|\vec{m}| = 1$ ,  $|\vec{t}_i| = \sqrt{a_i^2 + b_i^2 + c_i^2}$  and on setting  $\omega = (\vec{t}_i, \vec{m})$ , we have

$$\Psi_i = \alpha_i S + g(r) \sqrt{a_i^2 + b_i^2 + c_i^2} \cos \omega.$$

We can state that  $\Psi_i = \alpha_i S + \xi_i$ , in which the orbital  $\xi_i$  thus introduced exhibits the form  $\xi_i = a_i X + b_i Y + c_i Z = g(r) \vec{t}_i \cdot \vec{m}$ .

Once  $\zeta_i$  is normalised co-linearly to  $\xi_i$ , and by consequence verifies:  $\langle \zeta_i | \zeta_i \rangle = 1$  and  $\xi_i = \lambda_i \zeta_i$ .

$\zeta_i$  thus takes on the form

$$\zeta_i = \frac{\xi_i}{\lambda_i} = \frac{1}{\lambda_i}(a_i X + b_i Y + c_i Z) = (a'_i X + b'_i Y + c'_i Z)$$

$$= \frac{1}{\lambda_i} \mathbf{g}(r) \vec{t}_i \cdot \vec{m} = \mathbf{g}(r) \frac{\vec{t}_i}{\lambda_i} \cdot \vec{m} = \mathbf{g}(r) \vec{t}'_i \cdot \vec{m}, \text{ with } \vec{t}'_i = \frac{\vec{t}_i}{\lambda_i} \begin{cases} \frac{a_i}{\lambda_i} = a'_i \\ \frac{b_i}{\lambda_i} = b'_i \\ \frac{c_i}{\lambda_i} = c'_i \end{cases}$$

As  $\langle \zeta_i | \zeta_i \rangle = 1 = a'^2_i + b'^2_i + c'^2_i = |\vec{t}'_i|^2$ , we can say that

$$\zeta_i = \mathbf{g}(r) \vec{t}'_i \cdot \vec{m} = \mathbf{g}(r) \cos(\vec{t}'_i, \vec{m}) = \overrightarrow{OD} \cdot \vec{m}, \text{ in which } \overrightarrow{OD} = \mathbf{g}(r) \vec{t}'_i.$$

Using  $\omega = (\vec{t}'_i, \vec{m})$ , now  $\zeta_i = OD \cos \omega$ , the position of points  $M'$  are such that  $\zeta_i = OM'$  is a sphere with diameter  $|\overrightarrow{OD}| = \mathbf{g}(r)$  and is directed following the unit vector  $\vec{t}'_i$ .

Figure 14 shows, in the plane of the paper, a representation close to that which allowed us to determine the  $p_z$  orbitals.

Similarly, the  $M$  points are placed so that  $OM = \xi_i = \lambda_i \zeta_i$  giving rise to a sphere of radius  $\lambda_i OD$ .

As in Figure 13, we finally reach the hybrid orbital  $\Psi_i$  through the addition of the  $S$  orbital (which has a spherical symmetry around  $O$ , as shown in the Figure) with the orbital  $\xi_i = \lambda_i \zeta_i$ , and is also equivalent to a rotation about  $\vec{t}'_i$  or about  $\vec{t}_i (= \lambda_i \vec{t}'_i)$ .

## b The angle between the direction of equivalent hybrid orbitals

It is possible to determine the expression for the angle between the directions for two orbitals of the  $\xi_i$  (or  $\zeta_i$ ) type in rotation (so that the  $\Psi_1$  and  $\Psi_2$  orbitals are equivalent).

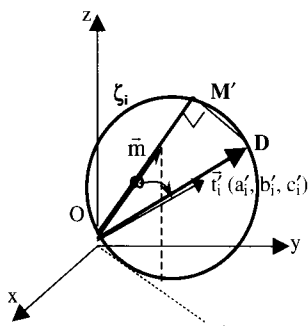


Figure 14. Representation of  $\zeta_i$

If we take the indice of the two orbitals under consideration using eqns (1) and (2), we can write, for example,

$$\begin{aligned}\Psi_1 &= \alpha_1 S + \xi_1 \\ &= \alpha_1 S + \lambda_1 \zeta_1 = \alpha_1 (S + \mu_1 \zeta_1) \text{ with } \lambda_1 = \alpha_1 \mu_1; \\ \Psi_2 &= \alpha_2 S + \xi_2 \\ &= \alpha_2 S + \lambda_2 \zeta_2 = \alpha_2 (S + \mu_2 \zeta_2) \text{ with } \lambda_2 = \alpha_2 \mu_2.\end{aligned}$$

The orthogonal addition of  $\Psi_1$  and  $\Psi_2$  gives:

$$\begin{aligned}\langle \Psi_1 | \Psi_2 \rangle &= \alpha_1 \alpha_2 \langle S + \mu_1 \zeta_1 | S + \mu_2 \zeta_2 \rangle \\ &= \alpha_1 \alpha_2 [1 + \mu_1 \mu_2 \langle \zeta_1 | \zeta_2 \rangle] = 0\end{aligned}$$

(with the functions  $S$  and  $\zeta_i$  orthonormal with respect to one another).

With  $\alpha_1$  and  $\alpha_2$  unequal to zero, we can say that we should have  $1 + \mu_1 \mu_2 \cos \alpha_{12} = 0$ , in which  $\alpha_{12} = (\vec{t}'_1, \vec{t}'_2)$  represents the angle between the two directions given by the rotational axes of the two normalised wavefunctions  $\zeta_1$  and  $\zeta_2$ .

The interchangeability of orbitals applied to the orbitals  $\Psi_1$  and  $\Psi_2$  in effect impose that  $\mu_1 = \mu_2$  ( $\Psi_1$  and  $\Psi_2$  orbitals, as for  $S$  orbitals, are equivalent as the parenthesis has the same coefficient of 1, and so we should have  $\mu_1 = \mu_2 = \mu$  so that  $\Psi_1 \equiv \Psi_2$ ).

Finally, we can state the orbitals  $\Psi_1$  and  $\Psi_2$  are equivalent if  $\cos \alpha_{12} = -\frac{1}{\mu^2}$ .

### c Wavefunctions in the $sp^3$ hybridisation

Here we now have a carbon atom at the centre of a tetrahedral with orbitals about axes that join the centre to the extremities of the tetrahedron, as shown in Figure 15. The lines of the axes have angles between them which can be calculated, for example, using the  $\vec{t}'_1$  and  $\vec{t}'_2$  components.

As  $|\vec{t}'_1| = 1$  and the carbon is at the centre of a tetrahedron, we should be able to write that  $a'_{12} + b'_{12} + c'_{12} = 1$  and  $a'_1 = b'_1 = c'_1$ , and in other terms that  $a'_1 = b'_1 = c'_1 = \frac{1}{\sqrt{3}}$ . Similarly, for  $\vec{t}'_2$ , and in taking into account its geometrical position,  $a'_2 = c'_2 = \frac{1}{\sqrt{3}}$  and  $b'_2 = -\frac{1}{\sqrt{3}}$ .

From this we now have  $\cos \alpha_{12} = \vec{t}'_1 \cdot \vec{t}'_2 = -\frac{1}{3}$ , that is  $\alpha_{12} = 109^\circ 28'$  and  $-\frac{1}{\mu^2} = -\frac{1}{3}$ , which is the same as writing  $\mu = \sqrt{3}$ .

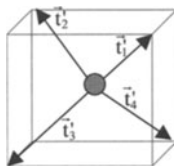


Figure 15.  $sp^3$  Hybridisation.

Using  $\Psi_1 = \alpha_1(S + \mu_1 \zeta_1)$ , we can say that  $\Psi_1 = \alpha_1(S + \sqrt{3}\zeta_1)$ , and the normalisation condition for  $\Psi_1$  brings us to a value for  $\alpha_1$ :

$$\langle \Psi_1 | \Psi_1 \rangle = 1 = \alpha_1^2 [1 + (\sqrt{3})^2] = 4\alpha_1^2, \text{ which is } \alpha_1 = \frac{1}{2}.$$

Finally,

$$\Psi_1 = \frac{1}{2}(S + \sqrt{3}\zeta_1) = \frac{1}{2}[S + (a'_1 X + b'_1 Y + c'_1 Z)\sqrt{3}],$$

in which  $(a'_1, b'_1, c'_1)$  are the director cosinus:  $a'_1 = b'_1 = c'_1 = \frac{1}{\sqrt{3}}$ , to yield:

$$\Psi_1 = \frac{1}{2} \left( S + \sqrt{3} \left( \frac{1}{\sqrt{3}} \varphi_{2p_x} + \frac{1}{\sqrt{3}} \varphi_{2p_y} + \frac{1}{\sqrt{3}} \varphi_{2p_z} \right) \right).$$

We obtain:

$$\begin{cases} \Psi_1 = \frac{1}{2}(S + \varphi_{2p_x} + \varphi_{2p_y} + \varphi_{2p_z}) = \frac{1}{2}(S + X + Y + Z) \\ \Psi_2 = \frac{1}{2}(S - \varphi_{2p_x} - \varphi_{2p_y} + \varphi_{2p_z}) = \frac{1}{2}(S - X - Y + Z) \\ \Psi_3 = \frac{1}{2}(S + \varphi_{2p_x} - \varphi_{2p_y} - \varphi_{2p_z}) = \frac{1}{2}(S + X - Y - Z) \\ \Psi_4 = \frac{1}{2}(S - \varphi_{2p_x} + \varphi_{2p_y} - \varphi_{2p_z}) = \frac{1}{2}(S - X + Y - Z) \end{cases}$$



## Representation of states in a chain of atoms

### I A chain of atoms exhibiting $\sigma$ -orbital overlapping

#### 1 $\sigma$ -orbitals and a compliment to the example of 8 atoms in a chain

A chain of 8 atoms ( $N = 8$ ) was detailed in practical terms in Chapter I, Section VII. Each atoms presented was considered as having the  $s$  state. The energy levels are shown in Figure I-24 and the representative functions for the lowest lying band bonding states (of the function  $\Psi_{k_4}$ ) and the highest band antibonding states (of the function  $\Psi_{k_0}$ ) are shown explicitly in Figures I-22 and I-23, respectively. Figures 1-a and 1-b describe the forms of these functions as an *aide-mémoire*.

In addition, between  $k = k_0$  and  $k = k_4$  there are the intermediate states, which are represented the real parts of the wavefunctions  $\Psi'_{k_1}$  and  $\Psi'_{k_2}$  for  $k = k_1$  in Figure 2 and for  $k = k_2$  in Figure 3, with

$$\Psi'_{k_p}(x) = R(\Psi_{k_p}(x)) = c'_0 \sum_{t=0}^8 \cos(k_p t a) \psi_0(x - t a).$$

Here,

$$c'_0 = \sqrt{\frac{2}{N}}, k_p = 2\pi \frac{p}{Na} \quad \text{and} \quad \Psi_0(x - t a) = C e^{-\alpha x}.$$

— For  $p = 1$ , we have:

$$k_1 = \frac{\pi}{4a} \quad \text{and} \quad \lambda_1 = \frac{2\pi}{k_1} = 8a.$$

The successive values for  $t$ ,  $k_1 t a = \frac{\pi}{4} t$ , and  $\cos \frac{\pi}{4} t$  are listed in the table below.

$t$	0 $\equiv$ 8	1	2	3	4	5	6	7
$k_1 t a = \frac{\pi}{4} t$	0	$\frac{\pi}{4}$	$\frac{\pi}{2}$	$\frac{3\pi}{4}$	$\pi$	$\frac{5\pi}{4}$	$\frac{3\pi}{2}$	$\frac{7\pi}{4}$
$\cos \frac{\pi}{4} t$	1	$\frac{\sqrt{2}}{2} = 0.707$	0	-0.707	-1	-0.707	0	0.707

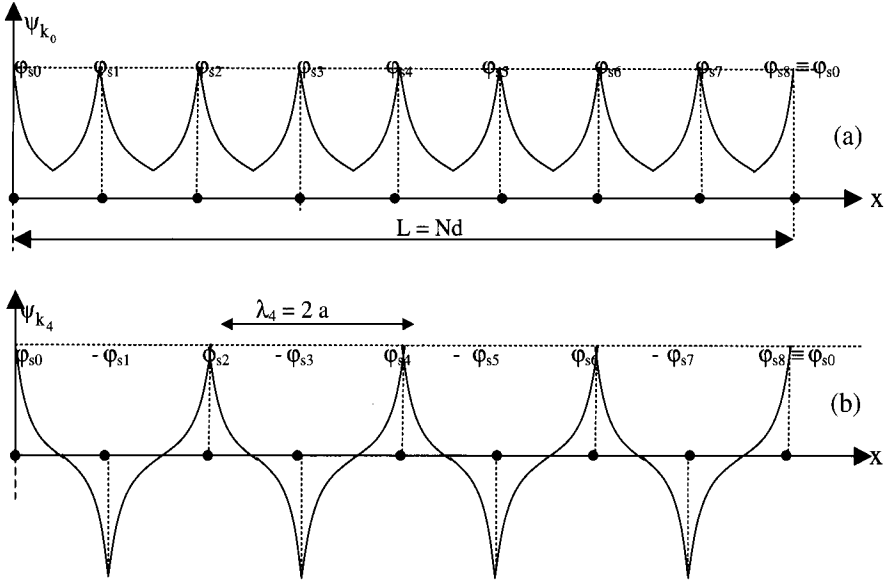


**Figure 1.** (a) Representation of  $\Psi_{k_0} = \varphi_{s1} + \varphi_{s2} + \varphi_{s3} + \varphi_{s4} + \varphi_{s5} + \varphi_{s6} + \varphi_{s7}$ ; and (b) representation of  $\Psi_{k_4} = \varphi_{s0} - \varphi_{s1} + \varphi_{s2} - \varphi_{s3} + \varphi_{s4} - \varphi_{s5} + \varphi_{s6} - \varphi_{s7} + \varphi_{s8} \equiv \varphi_{s0}$ .

From this we can deduce, to an approximation of  $c'_0$ , the expression for  $\Psi'_{k_1}$ :

$$\Psi'_{k_1} = \varphi_{s0 \equiv 8} + 0,707 \cdot \varphi_{s1} + 0 \cdot \varphi_{s2} - 0,707 \cdot \varphi_{s3} - \varphi_{s4} - 0,707 \cdot \varphi_{s5} + 0 \cdot \varphi_{s6} + 0,707 \cdot \varphi_{s7}$$

We can thus see that when  $k = k_1$ , the nodal points start to appear in the wavefunction as shown in Figure 2.

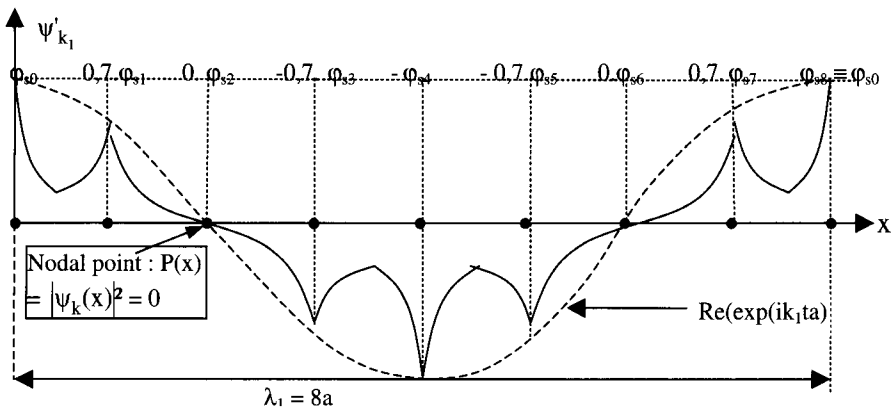


**Figure 2.** Representation of  $\Psi'_{k_1}$  with  $\Psi'_{k_1} = \text{Re}(\Psi_{k_1}) = \varphi_{s0 \equiv 8} + 0,707 \cdot \varphi_{s1} + 0 \cdot \varphi_{s2} - 0,707 \cdot \varphi_{s3} - \varphi_{s4} - 0,707 \cdot \varphi_{s5} + 0 \cdot \varphi_{s6} + 0,707 \cdot \varphi_{s7}$ .

— For  $p = 2$ , we have

$$k_2 = \frac{\pi}{2a}, \quad \text{and} \quad \lambda_2 = \frac{2\pi}{\frac{\pi}{2a}} = 4a$$

The successive values of  $t$ ,  $k_1 t a = \frac{\pi}{2} t$ , and  $\cos \frac{\pi}{2} t$  are shown in the table below:

$t$	$0 \equiv 8$	1	2	3	4	5	6	7
$k_1 t a = \frac{\pi}{2} t$	$0 \equiv 4\pi$	$\frac{\pi}{2}$	$\pi$	$\frac{3\pi}{2}$	$2\pi$	$\frac{5\pi}{2}$	$3\pi$	$\frac{7\pi}{2}$
$\cos \frac{\pi}{2} t$	1	0	-1	0	1	0	-1	0

Here we can state that at the centre of the band, for  $k = k_2$ , the states are neither bonding nor antibonding, as shown in Figure 3.

### 2 General representation of states in a chain of overlapping $\sigma$ s-orbitals

When we have positive s-orbitals (a lone, single atom with an s state—see Appendix 1-4, Figure 4) and a chain as in Chapter I, Section VII, we have from Chapter I, eqn (20)

- $\beta_s = \langle \Psi_0(x - ta) | W(x - sa) | \Psi_0(x - sa) \rangle = \langle \Psi_t | W | \Psi_s \rangle < 0$ , as  $\Psi_t$  and  $\Psi_s$  have the same positive sign (from the orbital of the lone  $n^{\circ}t$  or  $n^{\circ}s$  atoms) while  $W < 0$ .

From an energetic point of view, the result with  $E$  given by eqn (22) of Chapter 1 that  $E_s = E_{0s} - \alpha_s - 2\beta_s \cos ka$ , and the energy is, as in the lower half of Figure 4 for s-orbitals:

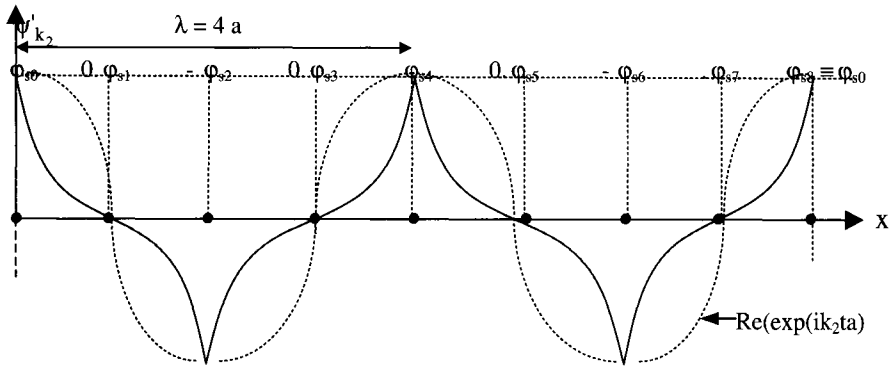


**Figure 3.** Representation of  $\Psi'_{k_2}$  with  $\Psi'_{k_2} = \text{Re}(\Psi_{k_2}) = \varphi_{s0} \equiv \varphi_{s8} + 0 \cdot \varphi_{s1} - \varphi_{s2} + 0 \cdot \varphi_{s3} + \varphi_{s4} + 0 \cdot \varphi_{s5} - \varphi_{s6} + 0 \cdot \varphi_{s7}$ .

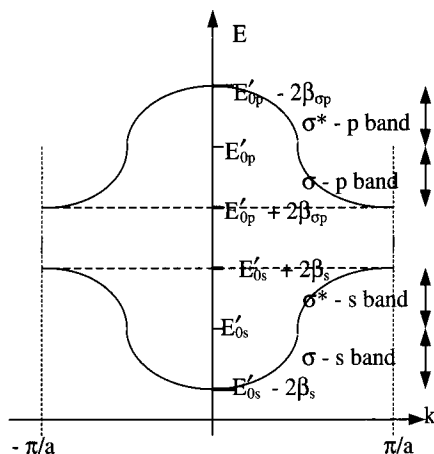


**Figure 4.**  $E = f(k)$  curves for the  $\sigma$  overlapping of s and p orbitals.

- lowered at the lowest part of the band as  $-\beta_s$  is always negative and  $\cos ka > 0$  ( $-\pi/2 \leq ka \leq \pi/2$  at the bottom of the band) and we have a bonding state ( $\sigma$ -s band);
- increased at the highest part of the band as  $-\beta_s$  is always negative and  $\cos ka < 0$  ( $\pi/2 \leq ka \leq \pi$  at the top of the band) and we have an antibonding state ( $\sigma^*$ -s band).

This result can again be found by taking into account the phase term associated with each wavefunction for each atom in the chain:

- two adjacent and bonding s-orbitals are in phase ( $k = 0$  as in Figure 1-a) and have the same sign. The geometrical form and the orbital and its sign can also be shown graphically, as in Figure 5-a. The interaction (coupling) of the two states gives rise to a decrease in the energy (the  $\sigma$ -s band); however,
- the antibonding states are associated with adjacent orbitals which have opposite phases (when  $k = \pm\pi/a$ ) and also therefore opposing signs, as in Figure 1-b. This situation is represented in Figure 5-b in which the geometric form of the orbitals along with their signs are shown. The energy resulting from their interaction is increased (in an unfavourable state) and the result is the ( $\sigma^*$ -s band shown in Figure 4.

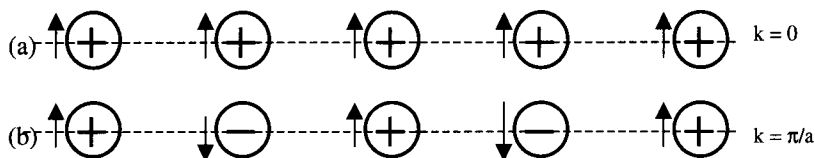


**Figure 5.** Distribution of: (a)  $\sigma$ -s bonding orbitals; and (b)  $\sigma^*$ -s antibonding orbitals (arrows indicate phase terms).

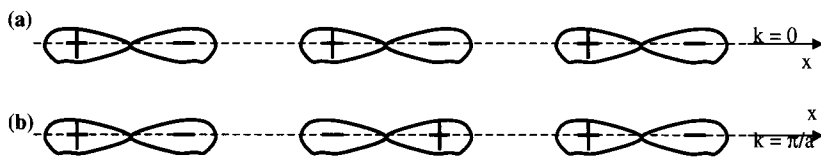


**Figure 6.** Distribution of: (a) antibonding  $\sigma^*$ -p orbitals; and (b) bonding  $\sigma$ -p orbitals (arrows indicate phase terms).

### 3 General representation of states in a chain of overlapping $\sigma$ p-orbitals

For the p-orbitals, once again we can use  $-\beta_{\sigma p} = \langle \Psi_0(x - ta) | W(x - sa) | \Psi_0(x - sa) \rangle = \langle \Psi_t | W | \Psi_s \rangle$  where  $W < 0$ . Now the functions  $\Psi_t$  and  $\Psi_s$  represent p-orbitals, which have the form shown in Figure 6. Noticeably each has adjacent positive and negative lobes so that  $-\beta_{\sigma p}$  is positive (see the upper half of Figure 4 which details  $\sigma$ -p orbitals). We can note that:

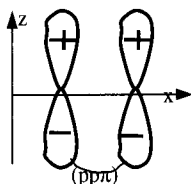
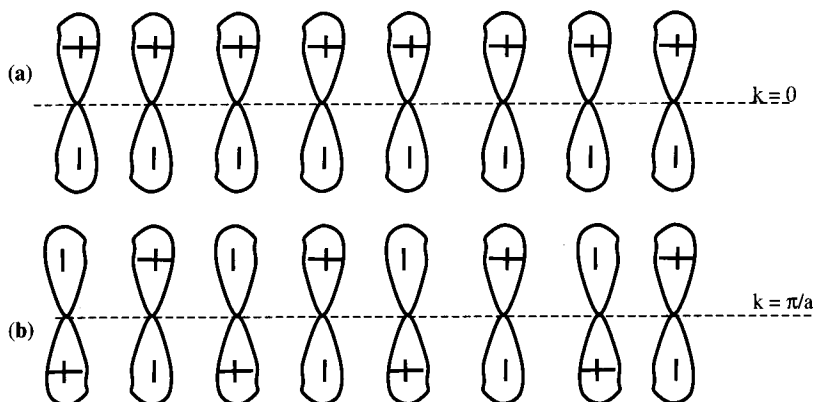
- when  $-\pi/2 \leq ka \leq \pi/2$ ,  $\cos ka > 0$  and the energy is increased by  $E'_{0p} = E_{0p} - \alpha_p$ ;
- when  $\pi/2 \leq ka \leq \pi$  and  $-\pi \leq ka \leq -\pi/2$ , we have  $\cos ka < 0$  and the energy decreases by  $E'_{0p} = E_{0p} - \alpha_p$ .

The same result can be found:

- when  $k = 0$ , the wavefunctions are distributed in phase (following Floquet's calculations, the term  $\cos k_p sa$  is equal to 1) and they can be geometrically represented as shown in Figure 6-a (using as example the  $p_x$ -orbitals). A positive lobe interacts with a negative lobe to produce an antibonding state with the appropriate increase in energy ( $\sigma^*$ -p band shown in Figure 4). This behaviour is in opposition to that of the s band in the same k region; or
- when  $k = \pm\pi/a$ , the phase factors alternate ( $\cos k_p sa$  equals, alternatively, +1 and -1) so that the geometric representation is that shown in Figure 6-b and corresponds to the interactions between lobes of the same sign. The result is a decrease in the energy for what is a  $\sigma$ -p bonding state as detailed in Figure 4.

## II $\pi$ Type overlapping of p-orbitals in a chain of atoms: $\pi$ -p- and $\pi^*$ -p-orbitals

The  $p_z$ -orbitals bonded to each other by a  $\pi$ -bond give rise to a  $\pi$ -p type orbital, as shown in Figure 7. The resonance integral,  $-\beta_{\pi p}$ , involves both the overlapping of the two positive and the two negative lobes. With  $W < 0$ ,  $-\beta_{\pi p}$  is now negative (as for  $-\beta_s$ ) giving a behaviour similar to that of ( $\sigma$ -s-bonds. Figure 8-a and -b show, respectively, the geometrical representations of the lowest energy bonding and highest energy anti-bonding orbitals.

Figure 7. The  $\pi$ -p-orbital.Figure 8. Distribution of (a)  $\pi$ -p-orbitals and (b)  $\pi^*$ -p-antibonding orbitals.

### III $\sigma$ -s- and $\sigma$ -p-bonds in chains of atoms

In general terms, and as we have seen in Chapter I, with  $k = \pi/a$  a stationary wave system can easily arise. The wavefunctions and the presence probabilities take up solutions of the type (Figure I-5) in which:

- the electron charges are essentially spread in the neighbourhood around the lattice nodes, so that  $\Psi^+ \propto \cos(\pi x/a)$  and  $P^+ = \cos^2(\pi x/a)$ ; and
- the charges are essentially about the mid-point between lattice nodes, so that  $\Psi^- \propto \sin(\pi x/a)$  and  $P^- = \sin^2(\pi x/a)$ .

Given the geometrical shape of the atomic s- and p-orbitals and their corresponding electron distributions:

- the electron charges associated with s-orbitals are concentrated about the atomic nodes with probability  $P^+$ ; and
- the concentration of electrons associated with  $p_x$ -orbitals, mid-way between atomic nodes, can be expressed as the probability  $P^-$ .

In terms of energy the two orbitals and their associated electron concentrations are separated by a gap of  $E_G$  which is precisely defined by  $k = \pi/a$ .

In addition, as the waves ( $\Psi^+$ ) associated with the s-states tend to concentrate electrons in the neighbourhood of the centre of the atoms, the electrostatic interaction energy effectively lowers the energy of the electrons, which are more stable than

those associated with the progressive wave (in  $\exp(ikx)$ ) which delocalises any sort of electron.

Conversely, the  $\Psi^-$  wave associated with the p-states concentrates electrons at the mid-point between atoms (that is the further point from the centre of the atoms involved) and minimises as much as possible the electrostatic interaction energy. The result is that the electron charges are less stable than those associated with a progressive wave (in  $\exp(ikx)$  delocalising all electrons) of the s-states  $\Psi^+$  wave.

Thus, in this particular example, an energy gap can appear in a 1-dimensional system with the simultaneous existence of at least two orbitals (here s and p). Figure 4 can be compared with Figure I-12.

## IV Comments

### 1 The Bloch function

In Chapter I it was shown how with a zero order approximation (an electron placed in a flat-bottomed well) an electronic wavefunction can be written:

$$\Psi_k(x) = \Psi^0 = e^{ikx} \quad (\text{to the order of a normalisation constant}).$$

However, for a semi-free electron (placed within a potential well with a bottom perturbed by electrostatic interactions with atomic nuclei situated at lattice nodes and undergoing a periodic perturbation  $w(x) = w_0 \cos \frac{2\pi}{a}x$ ) we need to find a wavefunction for the perturbed state of the type  $\Psi_k(x) = \Psi^0 u(x) = e^{ikx} u(x)$ , in which  $u(x)$  is the unknown function. With a potential perturbation of  $w(x)$ , the Hamiltonian can be written as

$$H = -\hbar^2 \frac{d}{dx^2} + w(x),$$

and is conserved on undergoing the translational operator  $T_a$ , which transforms  $x$  into  $x + a$ . This can be expressed in

$$T_a H = -\hbar^2 \frac{d}{d(x+a)^2} + w(x+a) = -\hbar^2 \frac{d}{dx^2} + w(x) = H.$$

$H$  remains invariant with respect to the effect of  $T_a$ , and commutes with  $T_a$ :  $[H, T_a] = 0$ . We can thus find the same proper system of functions for  $T_a$  and for  $H$ , in a process which is followed up in most standard text books on quantum mechanics.

In order to find the form of the proper functions of  $T_a$  which can also be taken as the proper function of  $H$ , we can use the following equation which they verify:

$$T_a \Psi_k(x) = c_{k,a} \Psi_k(x).$$

The product from the application of these functions is  $T_a \circ T_{-a}$ , and involves successive translations with modules  $-a$  and then  $a$  so that the operator  $T_a \circ T_{-a}$  changes

as though it has the identity I. Thus:

$$(T_a \circ T_{-a})(\Psi_k(x)) = c_{k,a}c_{k,-a}\Psi_k(x) = I(\Psi_k(x)) = \Psi_k(x).$$

From this we can deduce that  $c_{k,a}c_{k,-a} = 1$ , that is  $c_{k,a} = e^{ika}$ , and the equation for the proper values becomes:

$$T_a \Psi_k(x) = e^{ika}\Psi_k(x) = e^{ika}e^{ikx}u(x) \quad (1)$$

From outside we have the definition of the operator  $T_a$  which transforms  $x$  to  $x + a$ , and allows the expression:

$$T_a \Psi_k(x) = \Psi_k(x + a) = e^{ik(x+a)}u(x + a). \quad (2)$$

On comparing, eqns (1) and (2) we can extract  $u(x) = u(x + a)$ . So, the proper function  $\Psi_k(x) = e^{ikx}u(x)$ , which describes the state of a semi-free electron—which has the form under analysis—is such that  $u(x) = u(x + a)$ . This proper function,  $\Psi_k(x) = e^{ikx}u(x)$  with  $u(x) = u(x + a)$  is called the Bloch function.

## 2 Expression for the effective mass ( $m^*$ )

By definition,  $m^* = \frac{F_{\text{ext}}}{\gamma}$ , in which  $\gamma = \frac{dv_g}{dt}$  and  $v_g$ , in the dualistic theory, is given by the velocity of the package of the wave group as

$$v_g = \frac{d\omega}{dk},$$

so with

$$E = \hbar\omega, \quad v_g = \frac{1dE}{\hbar dk},$$

and

$$\gamma = \frac{1d}{\hbar dt} \left( \frac{dE}{dk} \right) = \frac{1d^2E}{\hbar dk^2 dt}.$$

In addition the exterior work force ( $F_{\text{ext}} = qE_{\text{ext}}$  for an external field  $E_{\text{ext}}$  applied on a charge  $q$ ) is such that  $dE = F_{\text{ext}}dr = F_{\text{ext}}v_g dt$ , so

$$F_{\text{ext}} = \frac{1dE}{v_g dt} = \frac{1dE}{v_g dk dt} = \frac{\hbar}{\frac{dE}{dk}} \frac{dE}{dk dt} = \hbar \frac{dk}{dt}.$$

Calculating the ratio

$$\frac{F_{\text{ext}}}{\gamma} = m^* \text{ gives } m^* = \frac{\hbar^2}{\frac{d^2E}{dk^2}}.$$

For a free electron,  $E = \frac{\hbar^2 k^2}{2m}$ , and we find again  $m = m^*$  as  $F_{\text{int}} = 0$ , so that

$$F_{\text{ext}} = F_{\text{Total}} = m\gamma = m^*\gamma.$$



## Electronic and optical properties of fullerene-C60 in the solid (film) state

### I Electronic properties of fullerene-C60: the band scheme as indicated by the Local Density Approximation Method [Tro 92 and 96]

Figure 1 schematises the first Brillouin zone of the cubic face centred (cfc) system of fullerene-60 ( $C_{60}$ ).

Table 1 goes on to detail the energies of states at the centre ( $\Gamma$ ) of the Brillouin zone and have been calculated using the density function in the Local Density Approximation (LDA) [Tro 92]. In Figures 2-a and -b the theoretical state densities are compared against empirically obtained photoemission or inverse photoemission spectra, respectively.

In Figure 2-a, the theoretically obtained spectra of the density of full states, compared against photoemission spectra, and the highest energy peak arising from a valence band results from the  $\pi_5$ -states. These states are derived from the HOMO  $h_u$

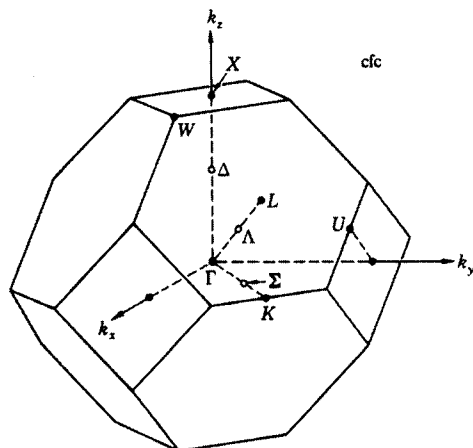


Figure 1. Brillouin zone for a cfc structure.

**Table 1.** Electronic state energies for  $C_{60}$  at the Brillouin zone point  $\Gamma$ .

Energy (eV)	Label	Energy (eV)	Label	Energy (eV)	Label
-18.766	$\sigma_0$ -a <sub>g</sub>	-7.109	$\sigma_7$ -t <sub>u</sub>	-0.965	$\pi_4$ -t <sub>g</sub>
-18.146	$\sigma_1$ -t <sub>u</sub>	-6.533	$\sigma_7$ -t <sub>u</sub>	-0.225	$\pi_5$ -e <sub>u</sub>
-17.262	$\sigma_2$ -t <sub>g</sub>	-5.829	$\sigma_7$ -a <sub>u</sub>	0.000	$\pi_5$ -t <sub>u</sub>
-17.221	$\sigma_2$ -e <sub>g</sub>	-5.802	$\sigma_7$ -t <sub>u</sub>	1.710	$\pi_5$ -t <sub>u</sub>
-16.098	$\sigma_3$ -t <sub>u</sub>	-5.563	$\pi_1$ -t <sub>u</sub>	2.372	$\pi_6$ -t <sub>g</sub>
-15.381	$\sigma_3$ -a <sub>u</sub>	-5.389	$\pi_2$ -t <sub>g</sub>	3.469	$\pi_5$ -t <sub>u</sub>
-15.326	$\sigma_3$ -t <sub>u</sub>	-5.371	$\sigma_8$ -e <sub>g</sub>	4.052	$\pi_6$ -e <sub>g</sub>
-14.137	$\sigma_4$ -e <sub>g</sub>	-5.257	$\sigma_8$ -t <sub>g</sub>	4.103	$\pi_6$ -t <sub>g</sub>
-13.983	$\sigma_4$ -t <sub>g</sub>	-5.004	$\pi_2$ -e <sub>g</sub>	4.217	$C_0$ -a <sub>g</sub>
-13.585	$\sigma_4$ -a <sub>g</sub>	-4.946	$\sigma_8$ -a <sub>g</sub>	4.971	$\pi_7$ -e <sub>u</sub>
-13.542	$\sigma_4$ -t <sub>g</sub>	-4.929	$\sigma_8$ -t <sub>g</sub>	5.149	$\pi_6$ -a <sub>g</sub>
-12.021	$\sigma_5$ -e <sub>u</sub>	-4.587	$\sigma_8$ -t <sub>g</sub>	5.515	$\pi_7$ -t <sub>u</sub>
-11.993	$\sigma_5$ -t <sub>u</sub>	-4.109	$\sigma_9$ -t <sub>u</sub>	5.878	$\sigma_9$ -a <sub>u</sub>
-11.873	$\sigma_5$ -t <sub>u</sub>	-4.089	$\sigma_9$ -a <sub>u</sub>	6.240	$\pi_6$ -t <sub>g</sub>
-10.917	$\sigma_5$ -t <sub>u</sub>	-3.597	$\pi_3$ -a <sub>u</sub>	6.423	$\sigma_9$ -t <sub>u</sub>
-9.830	$\sigma_6$ -t <sub>g</sub>	-3.452	$\pi_3$ -t <sub>u</sub>	6.495	$O_0$ -a <sub>g</sub>
-9.752	$\sigma_6$ -e <sub>g</sub>	-3.189	$\sigma_8$ -e <sub>g</sub>	6.974	$T_{0A}$ -a <sub>u</sub>
-9.564	$\sigma_6$ -t <sub>g</sub>	-3.120	$\sigma_8$ -t <sub>g</sub>	7.212	$T_{0B}$ -a <sub>g</sub>
-9.423	$\sigma_6$ -a <sub>g</sub>	-2.766	$\sigma_9$ -e <sub>u</sub>	7.430	$C_1$ -t <sub>u</sub>
-8.252	$\sigma_6$ -a <sub>g</sub>	-2.755	$\sigma_9$ -t <sub>u</sub>	7.454	$\sigma_{10}$ -t <sub>g</sub>
-8.128	$\sigma_6$ -t <sub>g</sub>	-2.628	$\pi_3$ -t <sub>u</sub>	7.815	$\sigma_9$ -t <sub>u</sub>
-7.368	$\sigma_7$ -e <sub>u</sub>	-1.850	$\pi_4$ -e <sub>g</sub>	8.298	$C_2$ -t <sub>g</sub>
-7.271	$\sigma_7$ -t <sub>u</sub>	-1.615	$\pi_4$ -a <sub>g</sub>	8.318	$\sigma_{10}$ -e <sub>g</sub>
-7.114	$\pi_0$ -a <sub>g</sub>	-1.084	$\pi_4$ -t <sub>g</sub>	8.754	$O_1$ -t <sub>u</sub>

level of the molecule, which is however broken down on the interior of the tetrahedral crystal to give 5 bands with symmetries t<sub>u</sub> and e<sub>u</sub>. Yet this dispersion of bands does not permit their resolution and the breakdown can only be discerned at the point  $\Gamma$  (see Table 1). In the same Figure 2-a, the band of  $\pi_4$ -states derived from the molecular states g<sub>g</sub> and h<sub>g</sub>. On increasing the energy of the bond, there is the first appearance of  $\sigma$  and  $\pi$  character mixtures.

In Figure 2-b, the theoretical spectral state densities calculated for empty states are compared against inverse photoemission spectra. The conduction band, here called 'A', is formed from  $\pi_5$  states, which are derived from LUMO states exhibiting T<sub>1u</sub> symmetry. There follows this the band 'B' formed from  $\pi_6$ -states and appears at an energy lower at the point  $\Gamma$  than in the state density spectrum.

On dissecting the various contributions which go up to make the 'C' band, it is possible to see that the first non-molecular state is at 4.217 eV. This state and its wavefunction are localised about the centre of the molecules and, characterised by L = 0, is denoted C<sub>0</sub>.

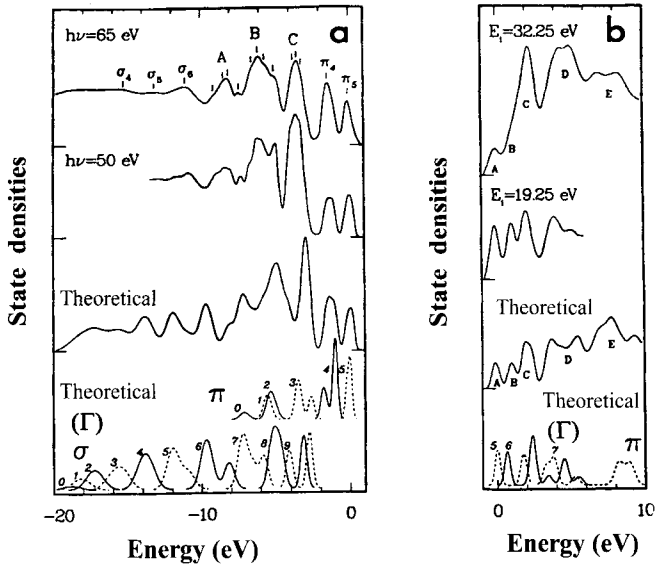


**Figure 2.** (a) Calculated state density functions for the valence band and empirical photoemission spectra. The lower 2 plots show density distributions for  $\sigma$  and  $\pi$  at  $\Gamma$ d of the Brillouin zone (bands numbered in terms of L); and (b) the lower conduction band function densities compared against two experimentally obtained inverse photoemission spectra.

Using the self-consistent field theory it was shown that there are relatively flat regions at the centre of the  $C_{60}$  sphere and in the tetrahedral and octahedral interstitial sites of a fcc lattice. The wavefunctions localised around these sites appear with energies between 4.8 and 5.3 eV above the conduction band and are called  $O_0$ ,  $T_{0A}$  and  $T_{0B}$ , with the latter two names being, respectively, for bonds and antibonds around a tetrahedral site.

The D and E peaks are due to simultaneous contributions from both molecular and non-molecular states; in effect they have reached the stage of delocalised states.

We can see that with these results the derived peaks are distinct, considerably more so than those observed for graphite and diamond and would tend to indicate the molecular nature of solid  $C_{60}$ . As already discussed in Chapter III, we can safely say that Hückel's method results in a good approximation.

To end this Section, we have shown the structure of the  $C_{60}$  crystal bands along the  $\Delta$  senses in Figure 3. They are defined by the points  $\Gamma$  and X from the Brillouin zone and Z defined by X and W, as shown in Figure 1. Figure 3 shows energies close to the fundamental gap and shows the highest group of valence bands and the two lowest groups of conduction bands. The direct gap is here determined as 1.2 eV at the point X, although this method tends to underestimate the actual value.

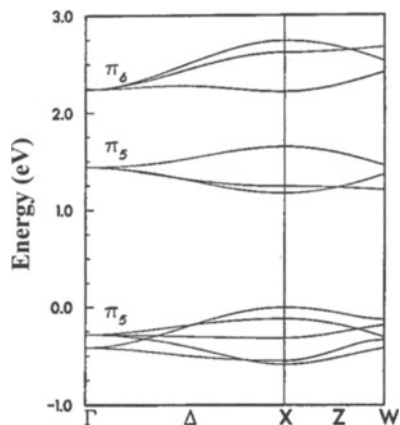


**Figure 3.** Band structure of  $C_{60}$  in a cfc structure along the  $\Delta$  and  $Z$  directions.

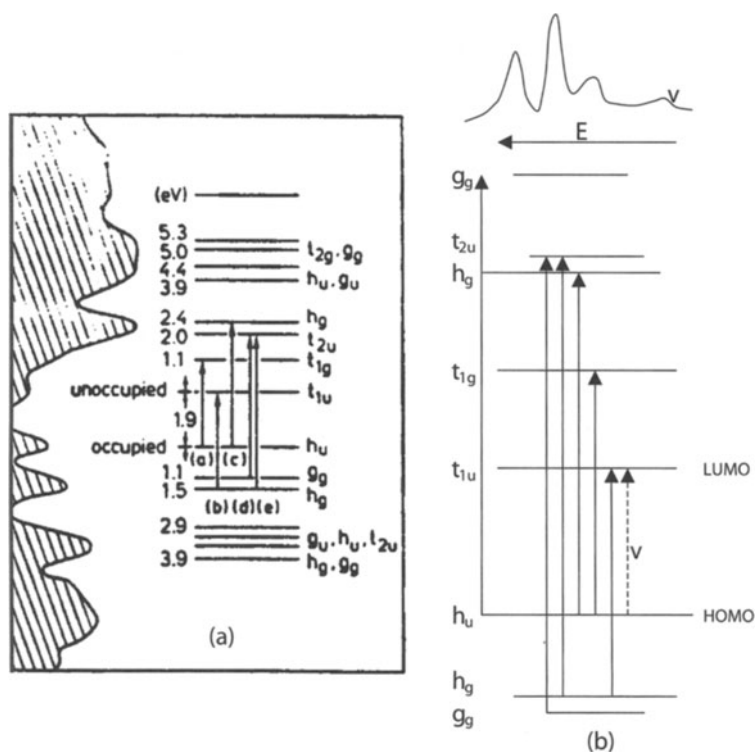


**Figure 4.** (a) The relationship between the experimentally derived state densities in the solid and the molecular orbitals levels along with permitted transitions [Law 92]; and (b) permitted transitions derived from the energy levels of molecular orbitals. The  $\nu$  band is forbidden for reason of symmetry, however, it is not excluded from electron-phonon coupling effects and appears weakly in the spectrum [Kel 92].

## II Optical properties and observed transitions

It has been observed that the absorption spectra derived from solid C<sub>60</sub> were very close to those of C<sub>60</sub> in the molecular state, a result which indicated that C<sub>60</sub> displays only very few interactions between molecules in the solid state [Kel 92]. The eventual similarity of spectra derived from solid and solution state C<sub>60</sub> allowed an attribution of the solid phase bands, along with help from known optical transitions associated with the energy diagram of molecular orbitals as shown in Figure 4-a. Even though the  $h_u \rightarrow t_{1u}$  transition is forbidden, (as it accords  $\Delta L = 0$  and not  $\Delta L = \pm 1$ —see Figure III-13 where the  $h_u$  and  $t_{1u}$  levels both correspond to  $L = 5$ ), it is nevertheless just observable (Figure 4-b). This is due to vibronic coupling which modifies the selection rule (see Chapter VII on optical properties for further details). And accordingly a rather weak band at 550 nm (2.50 eV) was attributed to this transition [Law 92] with an energy rather elevated when compared to alternative estimations (from 1.5 to 1.9 eV). Figure 4-a permits the deduction of the energy of additional transitions which are  $h_u \rightarrow t_{1g}$ ,  $h_g \rightarrow t_{1u}$ ,  $h_u \rightarrow h_g$ ,  $g_g \rightarrow t_{2u}$ , and  $h_g \rightarrow t_{2u}$ , each of which has, respectively, an energy of 3.0, 3.4, 4.3, 5.0 and 5.4 eV. These values coincide quite closely to those experimentally derived [Kel 92].

# General theory of conductivity for a regular lattice: the Kubo – Greenwood equation for conductivity in delocalised states and expressions for mobility

## I Electron transport effected by an external force and its study

### 1 Effect of force on electron movement and reasoning within reciprocal space

Here we take as example a square plane crystal with sides (L) defined by  $L = na$ . The Brillouin first zone and the dispersion curve ( $E(k)$ ) exhibit the forms represented in Figure 1.

The first band is assumed to be partially occupied by electrons in a symmetrical manner so that  $E(k) = E(-k)$ . At the point of thermal equilibrium, the velocity of an electron can be given by:

$$\vec{v} = \frac{1}{\hbar} \vec{\text{grad}}_k E. \tag{1}$$

As all the carrier velocities cancel each other out (orthogonal in the circle  $E = \text{constant}$  as in Figure 1-a) the total result is zero and there is no charge transport.

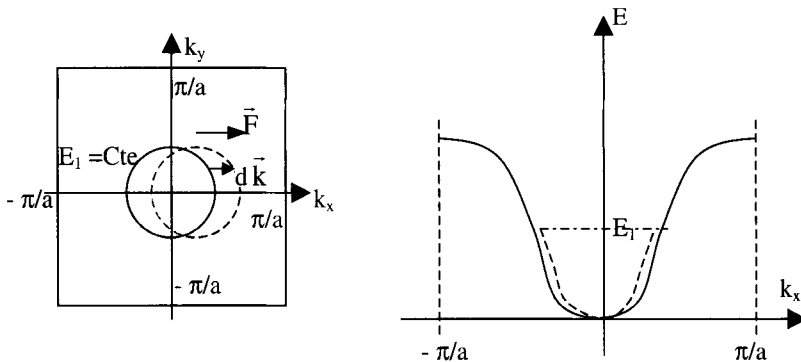


**Figure 1.** Representation of a reciprocal lattice with: (a) the Brillouin zone and an equi-energy surface; and (b) the dispersion curve  $E = f(k_x)$ .

*Comment* Eqn (1) can be justified by the following: the velocity of an electron can be represented by the velocity of the group associated with the wave packet, which describes the wave-like character of an electron:

$$v_g = \frac{\partial \omega}{\partial k}; \quad \text{with } E = \hbar \omega \implies v_g = \frac{1}{\hbar} \frac{\partial E}{\partial k},$$

to give in 3-D:

$$\vec{v}_g = \frac{1}{\hbar} \overrightarrow{\text{grad}}_k E = \vec{v} \quad (\text{simplified notation}).$$

If an external force ( $\vec{F}$ ) is applied for a certain time ( $dt$ ) on an electron which has a velocity  $\vec{v}$ , then the resulting change in energy is expressed by  $dE = \vec{F} \cdot \vec{v} \cdot dt$ . Following eqn (1) we have:  $dE = \vec{F} \cdot \left( \frac{1}{\hbar} \overrightarrow{\text{grad}}_k E \right) dt$ .

Additionally, in 3-dimensions

$$dE(k_x, k_y, k_z) = \frac{\partial E}{\partial k_x} \cdot dk_x + \frac{\partial E}{\partial k_y} \cdot dk_y + \frac{\partial E}{\partial k_z} \cdot dk_z = \overrightarrow{\text{grad}}_k E \cdot \vec{dk}$$

By identifying between the two last equations,

$$\vec{F} = \hbar \frac{d\vec{k}}{dt}. \quad (2)$$

Eqn (2) shows how  $\vec{F}$  and  $d\vec{k}$  are colinear and results from the effect of a force displacing an electronic population in the Brillouin zone parallel to  $\vec{F}$  (dashed circle in Figure 1), and the distribution symmetry is perturbed (as  $E(-k) \neq E(k)$ ). The resulting speed of the electrons is non-zero and charge transport is initiated.

## 2 Boltzmann's transport equation

At the thermodynamic equilibrium, the probability that an electron with a wave vector  $\vec{k}$  will be in the reciprocal space is given by the Fermi–Dirac function:

$$f_0(\vec{k}) = \frac{1}{1 + e^{(E(\vec{k}) - E_F)/kT}} \quad (3)$$

This function changes in the presence of an external force:

$$f(\vec{k}, \vec{r}, t) = f_0(\vec{k}) + f_1(\vec{k}, \vec{r}, t) \quad (4)$$

Most generally, this function depends not only on  $\vec{k}$  but also on the geometrical position ( $\vec{r}$ ) of an electron, when the force induces a local inhomogeneity in temperature or concentration, and also on the time ( $t$ ), if the permanent regime is not reached.

During an interval of time  $dt$ , the variation in  $f$  is equal to the sum of variations caused by the applied force (interactions with the exterior) along with a contribution

due to collisions (internal interactions). This gives:

$$\frac{df}{dt} = \left(\frac{df}{dt}\right)_{\text{applied force}} + \left(\frac{df}{dt}\right)_{\text{collisions}}$$

And with

$$\begin{aligned} (df)_{\text{forces}} &= (f)_{\text{instant } t-dt} - (f)_{\text{instant } t} = -[(f)_{\text{instant } t} - (f)_{\text{instant } t-dt}] \\ &= - \left\{ f(\vec{k}, \vec{r}) - f\left(\vec{k} - \frac{d\vec{k}}{dt} dt, \vec{r} - \frac{d\vec{r}}{dt} dt\right) \right\} = -\frac{\partial f}{\partial \vec{k}} d\vec{k} - \frac{\partial f}{\partial \vec{r}} d\vec{r}, \end{aligned}$$

during the interval  $[t - dt, t]$  we have:

$$\left(\frac{df}{dt}\right)_{\text{forces}} = -\frac{\partial f}{\partial \vec{k}} \frac{d\vec{k}}{dt} - \frac{\partial f}{\partial \vec{r}} \frac{d\vec{r}}{dt},$$

and in 3-dimensions:

$$\left(\frac{df}{dt}\right)_{\text{forces}} = -\vec{\text{grad}}_{\vec{k}} f \cdot \frac{d\vec{k}}{dt} - \vec{\text{grad}}_{\vec{r}} f \cdot \frac{d\vec{r}}{dt}$$

On introducing the last expression into eqn (2) and given that  $\vec{v} = \frac{d\vec{r}}{dt}$ , we find:

$$\left(\frac{df}{dt}\right)_{\text{Applied force}}(\vec{r}, \vec{k}) = -\hbar^{-1} \vec{F} \cdot \vec{\text{grad}}_{\vec{k}} f - \vec{v} \cdot \vec{\text{grad}}_{\vec{r}} f$$

With respect to the collisions, the contribution is in the following form (system with a relaxation time):

$$\left(\frac{df}{dt}\right)_{\text{collisions}} = -\frac{f - f_0}{\tau}, \tau \text{ being the relaxation time.}$$

Under a permanent regime,  $\frac{df}{dt}$  is zero and we find Boltzmann's equation (in which we have replaced  $f$  by  $f_0$  for all  $\text{grad}_{\vec{k}} f$  and  $\text{grad}_{\vec{r}} f$ , in a legitimate act as  $f_1 \ll f_0$  and the perturbation is weak and therefore negligible with respect to the value at the equilibrium state).

$$\hbar^{-1} \vec{F} \cdot \vec{\text{grad}}_{\vec{k}} f_0 + \vec{v} \cdot \vec{\text{grad}}_{\vec{r}} f_0 + \frac{f_1}{\tau} = 0 \quad (\text{Boltzmann's equation}). \quad (5)$$

If we assume that the crystal we have is homogeneous, then  $\vec{\text{grad}}_{\vec{r}} f_0 = 0$ , and eqn (5) becomes

$$\hbar^{-1} \vec{F} \cdot \vec{\text{grad}}_{\vec{k}} f_0 + \frac{f_1}{\tau} = 0, \text{ or even } f_1 = -\tau \hbar^{-1} \vec{F} \cdot \vec{\text{grad}}_{\vec{k}} f_0 \quad (5')$$

On taking the latest expression and inserting it into eqn (4)  $f = f_0 + f_1$ , and on using eqn (1) for velocity  $\vec{v} = \frac{1}{\hbar} \vec{\text{grad}}_{\vec{k}} E$ , we can write that  $\vec{\text{grad}}_{\vec{k}} f_0 = \frac{\partial f_0}{\partial E} \vec{\text{grad}}_{\vec{k}} E = \hbar \frac{\partial f_0}{\partial E} \vec{v}$ , to finally obtain

$$f = f_0 - \tau \cdot \vec{F} \cdot \vec{v} \cdot \frac{\partial f_0}{\partial E} \quad (6)$$



## II State density function, carrier flux and current density in the reciprocal space

### 1 General expressions for fluxes of particles

The flux of charge carriers generated by an applied force ( $\vec{F}$ ) is consistent with respect to the product of the concentration ( $c$ ) of charge carriers of a certain charge ( $q$ ) and their displacement velocity ( $\vec{v}_d$ ). This is because the flux represents the quantity of charge which traverses a unit surface in a unit time. So we can write for the average over all carriers that  $\langle \vec{\Phi} \rangle = \langle cq\vec{v}_d \rangle$ .

In reciprocal space, the carrier concentration is expressed by  $c = \int_{\mathbf{k}} N(\mathbf{k})f(\mathbf{k})d^3\mathbf{k}$ , in which  $N(\mathbf{k})$  is the state density function and represents the number of possible states for carriers in a unit volume in reciprocal space when they are in a unit volume in direct space. We can thus write that

$$\vec{\Phi} = \int_{\mathbf{k}} N(\mathbf{k})f(\mathbf{k})q(\mathbf{k})\vec{v}(\mathbf{k})d^3\mathbf{k}. \quad (7)$$

### 2 Expressions for the state density function

#### a Initial comment on the expression for charge carrier concentration

From the expression we have just given for the state density function  $N(\mathbf{k})$  in reciprocal space, we can directly note the carrier concentration by:

$$n = \int_{\mathbf{k}} N(\mathbf{k})f(\mathbf{k})d^3\mathbf{k}, \text{ so with } f \approx f_0, n \approx \int_{\mathbf{k}} N(\mathbf{k})f_0(\mathbf{k})d^3\mathbf{k}. \quad (8)$$

#### b Form of the state density function in $\mathbf{k}$ space

In order to evaluate  $N(\mathbf{k})$ , we can use a simple cubic lattice with sides of length  $L$ . Here the conditions on the periodic limits (the Born-Von Karman conditions) are written, for example, in the  $x$  direction so that  $\psi(x) = \psi(x + L)$  and are applied to the Bloch wavefunctions, as in:  $\Psi(x) = e^{ikx}u(x) = \psi(x + L) = e^{ik(x+L)}u(x + L)$  [with  $u(x + L) = u(x)$  as  $L$  is written as  $L = na$  in which  $a$  is the crystal periodicity]. This gives us the relationship  $e^{ikL} = 1$  which fixes the form of  $k$ , which has to be such that  $k = n\frac{2\pi}{L}$  (where  $n$  can be either positive or negative).

In the direction  $k_x$ , one cell (the space in which we can place a state without having to take spin into account) therefore has the dimensions  $\Delta k_x = \frac{2\pi}{L}$ , which can be written in 3-dimensions, using the usual notations, as  $(\Delta \mathbf{k})^3 = \frac{8\pi^3}{V}$  (with  $V = L^3$ ).

Without taking spin into account, the number of states into which we can possibly place carriers, in a unit of reciprocal space, is equal to  $\frac{1}{(\Delta \mathbf{k})^3} = \frac{V}{8\pi^3}$ .

Once we introduce the spin states, which multiply by two the preceding result, and remember that  $N(\mathbf{k})$  is defined for a unit volume of direct space ( $V = 1$ ), then

we can write definitively the density function of  $N(k)$  states as:

$$N(k) = 2 \left( \frac{V}{8\pi^3} \right)_{V=1} = \frac{1}{4\pi^3}. \tag{9}$$

**c State density function in energy space**

The titled function we shall denote as  $N(E)$ , although sometimes it is called  $Z(E)$ , and it such that  $N(E)dE$  represents the number of states distributed in energy space between  $E$  and  $E + dE$ , the whole still being in respect of the direct unit volume in space ( $V = 1$ ).

Supposing that the electron effective mass ( $m^*$ ) is invariable whatever the value of  $k$ , and that variations in  $k$  are isotropic in the space of wavefunctions, then we can write (in approximation of the effective mass) that  $E = \frac{\hbar^2 k^2}{2m^*}$ , taken with  $p = \hbar k = m^* v$ ,  $E = \frac{1}{2} m^* v^2$  (and thus with  $v = \frac{\hbar k}{m^*}$ ).

In  $k$  space, as shown in Figure 2, the surface equienergy  $E = cte$ , and is a sphere of radius  $k = \frac{\sqrt{2m^*E}}{\hbar}$ . In the same way the surface of the equienergy  $E + dE$  is a sphere with radius

$$k + dk = \frac{\sqrt{2m^*(E + dE)}}{\hbar} \left( \text{as } E + dE = \frac{\hbar^2(k + dk)^2}{2m^*} \right).$$

In terms of the state density function, the density of the states  $N(E)dE$  corresponds to the density of states spread throughout the  $k$  space in between the spheres of radius  $k$  (for  $E = \text{constant}$ ) and  $k + dk$  (where  $E + dE = \text{constant}$ ). As the volume held between these two spheres, and shown as the greyed zone in Figure 2, is equal to  $d^3k = 4\pi k^2 dk$ , we can write that

$$N(E)dE = N(k)d^3k. \tag{10}$$

With

$$d^3k = 4\pi \frac{(2m^*E)^{1/2}}{\hbar} \cdot \frac{m^* dE}{\hbar^2},$$

we have:

$$N(k)d^3k = \frac{1}{4\pi^3} d^3k = \frac{4\pi(2m^*)^{3/2} E^{1/2}}{\hbar^3} dE = N(E) \cdot dE.$$

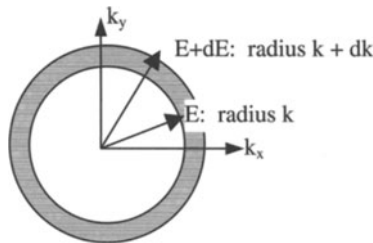


**Figure 2.** Representation of equi-energy spaces within reciprocal space.

From this we deduce that

$$N(E) = \frac{4\pi(2m^*)^{3/2}E^{1/2}}{\hbar^3}. \quad (11)$$

### 3 Expression for flux

In general terms, eqn (7) describes the carrier flux and is an expression in which we can now introduce the value of  $N(k)$  given by eqn (9). Additionally, the statistical distribution function ( $f$ ) is such that  $f(k) = f_0(k) + f_1(k)$  and with the velocities being zero at the point of thermodynamic equilibrium it is only  $f_1(k)$  which contributes to the expression for the carrier flux, which can thus be written:

$$\vec{\Phi} = \frac{1}{4\pi^3} \int q(k)f_1(k)\vec{v}(k)d^3k. \quad (7')$$

### 4 Expression for current density in reciprocal space

For a force due to an applied electric field we can assume that the electric field ( $E_x$ ) is applied parallel to the axis  $k_x$  in reciprocal space in order to simplify the expressions used.

With the force being exerted on a charge  $q$  being  $\vec{F}(x) = q\vec{E}_x$ , eqn (6) becomes

$$f = f_0 - q\tau E_x v_x \frac{\partial f_0}{\partial E}. \quad (6')$$

On writing

$$f_0 = \left[ 1 + \exp\left(\frac{E - E_F}{kT}\right) \right]^{-1} = [u(E)]^{-1} \text{ and posing } v = \left(\frac{E - E_F}{kT}\right),$$

the derivative with respect to  $E$  in the expression for  $f_0$  gives:

$$\begin{aligned} \frac{\partial f_0}{\partial E} &= -[u(E)]^{-2} u' = -f_0^2 u', \text{ with } u' = [1 + \exp(v)]' \\ &= [\exp(v)]' = v' \exp(v) = \frac{1}{kT} \exp(v). \end{aligned}$$

$$\text{As } 1 + \exp v = \frac{1}{f_0}, \text{ so } \exp(v) = \frac{1 - f_0}{f_0}, \text{ we have } u' = \frac{1}{kT} \frac{1 - f_0}{f_0}$$

and finally:

$$\frac{\partial f_0}{\partial E} = -\frac{f_0^2}{kT} \frac{1 - f_0}{f_0} = -\frac{f_0}{kT} (1 - f_0) \quad (12)$$

We then find that eqn (6) gives  $f = f_0 + f_0 \frac{q\tau}{kT} E_x v_x (1 - f_0)$ , in which  $f - f_0 = f_1 = \frac{q\tau}{kT} E_x v_x f_0 (1 - f_0)$ .

On assuming that the field  $E_x$  is constant and uniform, the result gained from eqn (7') for the flux, now the current density ( $J_x$ ) is such that:

$$J_x = \frac{q^2 E_x}{4\pi^3 k_B T} \int \tau v_x^2 f_0 (1 - f_0) d^3 k. \quad (13)$$

(Here the Boltzmann constant is denoted  $k_B$  in order to distinguish it from the wavenumber  $k$  which defines the reciprocal lattice and is such that, for a cubic 3-dimensional system,  $k = \sqrt{k_x^2 + k_y^2 + k_z^2}$ .)

### III Different expressions for the current density and relaxation times and forms of conductivities and mobilities

#### 1 Usual expression for current density in energy space

Eqn (13) which gives the current density can be rewritten as a function of energy by using eqn (10), which is such that  $N(E)dE = \frac{1}{4\pi^3} d^3 k$ . Eqns (7) and (13) thus give:

$$J_x = q^2 E_x \int \frac{\tau v_x^2}{kT} f_0 (1 - f_0) N(E) dE. \quad (14)$$

When considering both an isotropic diffusion and the approximation for the effective mass then  $E = \frac{m^* v^2}{2}$  and  $v_x^2 = v_y^2 = v_z^2$ , (in which  $v_x^2 = \frac{v^2}{3}$ ), so that  $v_x^2 = \frac{2E}{3m^*}$ . Inserting this value for  $v_x^2$  into eqn (14) in addition to eqn (11) for  $N(E)$ , and on setting  $A = \frac{2\pi}{\hbar^3} (2m^*)^{3/2}$  we now have

$$J_x = \frac{2}{3} \frac{q^2 E_x}{4\pi^3 m^* kT} \int \tau(E) E f_0 (1 - f_0) A E^{1/2} dE. \quad (14')$$

In addition, from eqn (8) we have  $n \approx \int_k N(k) f_0(k) d^3 k$ , that is:

$$n = \frac{1}{4\pi^3} \int f_0 4\pi k^2 dk = \frac{1}{4\pi^3} \int f_0 \frac{2\pi}{\hbar^3} (2m^*)^{2/3} E^{1/2} dE = \frac{A}{4\pi^3} \int f_0 E^{1/2} dE,$$

in which

$$A = \frac{4\pi^3 n}{\int f_0 E^{1/2} dE}. \quad (8')$$

Introducing eqn (8') into eqn (14') results in

$$J_x = \frac{2}{3} \frac{n q^2 E_x}{m^* kT} \frac{\int_0^{E_{\max}} \tau(E) E^{3/2} f_0 (1 - f_0) dE}{\int_0^{E_{\max}} E^{1/2} f_0 dE}. \quad (15)$$

## 2 Studies using various examples

### a When $\tau$ is a constant *i.e.* $\tau(E) = \tau$

$\tau$  can be given by the integral I of a numerator which is limited:

$I = \int_0^{E_{\max}} E^{3/2} f_0 (1 - f_0) dE$ . On using eqn (12):

$$I = -kT \int_0^{E_{\max}} E^{3/2} \frac{\partial f_0}{\partial E} dE = -kT \left\{ \left[ f_0 E^{3/2} \right]_0^{E_{\max}} - \int_0^{E_{\max}} \frac{3}{2} E^{1/2} f_0 dE \right\}.$$

The first term in the integration by parts is zero (as  $f_0(E_{\max}) = 0$  when  $E_{\max} \rightarrow \infty$ ), so that  $I = \frac{3}{2} kT \int_0^{E_{\max}} E^{1/2} f_0 dE$ .

Moving this into eqn (15), we find the usual formula

$$J_x = \frac{nq^2 \tau}{m^*} E_x. \quad (16)$$

### b Degenerate semiconductor

*$\alpha$  First order calculation* Here the Fermi-Dirac function goes from 1 to 0 in small intervals (of the order of  $kT$ ) about  $E_F$ . So for  $E < (E_F - kT/2)$  we have  $f_0 \approx 1$ , and for  $E > E_F + kT/2$  we have  $f_0 \approx 0$ .

On placing  $\Phi = \tau(E)E^{3/2}$ , for a numerator for  $J_x$  given by eqn (15) the term B appears which is such that  $B = \frac{1}{kT} \int_0^{E_{\max}} \Phi(E) f_0 (1 - f_0) dE$ . Using eqn (12) and factorising the integral gives:

$$B = - \int_0^{E_F - kT/2} \Phi(E) \frac{\partial f_0}{\partial E} dE - \int_{E_F - kT/2}^{E_F + kT/2} \Phi(E) \frac{\partial f_0}{\partial E} dE - \int_{E_F + kT/2}^{E_{\max}} \Phi(E) \frac{\partial f_0}{\partial E} dE.$$

As  $f_0 \approx 1 =$  a constant between 0 and  $E_F - kT/2$ , the first term is zero, as is also the third term as  $f_0 \approx 0$  between  $E_F + kT/2$  and  $E_{\max}$ .

As between  $E_F - kT/2$  and  $E_F + kT/2$ , we have  $\Phi(E) \approx \text{cte} = \Phi(E_F)$ , we can write

$$\begin{aligned} B &= - \int_{E_F - kT/2}^{E_F + kT/2} \Phi(E) \frac{\partial f_0}{\partial E} dE \approx -\Phi(E_F) \int_{E_F - kT/2}^{E_F + kT/2} \frac{\partial f_0}{\partial E} dE \\ &= -\Phi(E_F) [f_0]_{E_F - kT/2}^{E_F + kT/2} = \Phi(E_F) = \tau(E_F) E_F^{3/2}. \end{aligned}$$

Calculating the denominator means determining

$$\int_0^{E_{\max}} E^{1/2} f_0 dE \approx \int_0^{E_F} E^{1/2} dE = \frac{2}{3} E_F^{3/2}. \quad (17)$$

On introducing the last two results into eqn (15) we have:

$$J_x = \frac{nq^2 \tau(E_F)}{m^*} E_x. \quad (18)$$

β *The more general form* Eqn (15) can be written in the form

$$J_x = \frac{nq^2 E_x}{m^*} \frac{2}{3} \frac{1}{kT} \frac{\int_0^{E_{\max}} \tau(E) E^{3/2} f_0 (1 - f_0) dE}{\int_0^{E_{\max}} E^{1/2} f_0 dE},$$

so that with eqns (12) and (17) we now have

$$J_x = \frac{nq^2 E_x}{m^*} \left[ -E_F^{-3/2} \int_0^\infty \tau(E) E^{3/2} \frac{\partial f_0}{\partial E} dE \right].$$

By consequence

$$J_x = \frac{nq^2 \bar{\tau}}{m^*} E_x, \quad (19)$$

with

$$\bar{\tau} = -E_F^{-3/2} \int_0^\infty \tau(E) E^{3/2} \frac{\partial f_0}{\partial E} dE. \quad (20)$$

### c Non-degenerate semiconductor

Here  $E - E_F \gg 2kT$ , so that  $\exp([E - E_F]/kT) \gg 1$ . And

$$f_0 = \frac{1}{1 + \exp([E - E_F]/kT)} \approx \frac{1}{\exp([E - E_F]/kT)} = A \exp\left(-\frac{E}{kT}\right)$$

in the Boltzmann distribution.

As  $f_0 \ll 1$ , we have  $f_0(1 - f_0) \approx f_0$ , and eqn (15) gives:

$$J_x = \frac{2}{3} \frac{nq^2 E_x}{m^* kT} \frac{\int_0^\infty \tau(E) E^{3/2} \exp\left(-\frac{E}{kT}\right) dE \int_0^\infty E^{3/2} \exp\left(-\frac{E}{kT}\right) dE}{\int_0^\infty E^{3/2} \exp\left(-\frac{E}{kT}\right) dE \int_0^\infty E^{1/2} \exp\left(-\frac{E}{kT}\right) dE}.$$

With

$$\langle E \rangle = \frac{\int_0^\infty E^{3/2} \exp\left(-\frac{E}{kT}\right) dE}{\int_0^\infty E^{1/2} \exp\left(-\frac{E}{kT}\right) dE} = \frac{3}{2} kT \quad \text{and}$$

$$\langle \tau \rangle = \frac{\int_0^\infty \tau(E) E^{3/2} \exp\left(-\frac{E}{kT}\right) dE}{\int_0^\infty E^{3/2} \exp\left(-\frac{E}{kT}\right) dE},$$

we finally have:

$$J_x = \frac{nq^2}{m^*} \langle \tau \rangle E_x. \quad (21)$$

(We can note that the weighting factor is  $E\mathcal{N}(E)$ , with  $\mathcal{N}(E) = N(E)f_0 \approx E^{1/2} \exp(-\frac{E}{kT})$ , and not  $\mathcal{N}(E)$  as we might initially think).

### 3 Expressions for mobility\*

As a preliminary step we can note that mobility ( $\mu$ ) is classically defined by one of the two relations  $|v| = \mu E_x$ , or  $\sigma = qn\mu$ .

**a When the relaxation temperature ( $\tau(E)$ ) is constant i.e.  $\tau(E) = \tau$**

Eqn (16) written as  $J_x = \frac{nq^2\tau}{m^*}E_x$  allows us to write  $\sigma = \frac{nq^2\tau}{m^*}$ , so that

$$\mu = \frac{q\tau}{m^*}. \quad (22)$$

**b For a degenerate semiconductor**

$\alpha$  *First order calculation* Eqn (18) written

$$J_x = \frac{nq^2\tau(E_F)}{m^*}E_x, \text{ yields } \sigma = \frac{nq^2\tau(E_F)}{m^*}, \text{ so that } \mu = \frac{q\tau(E_F)}{m^*}. \quad (23)$$

$\beta$  *The more general form* With

$$\bar{\tau} = -E_F^{-3/2} \int_0^\infty \tau(E)E^{3/2} \frac{\partial f_0}{\partial E} dE, \text{ eqn (19) written } J_x = \frac{nq^2\bar{\tau}}{m^*}E_x,$$

gives

$$\sigma = \frac{nq^2\bar{\tau}}{m^*} \quad \text{and} \quad \mu = \frac{q\bar{\tau}}{m^*}. \quad (24)$$

**c Non-degenerate semiconductor**

Here, eqn (21) written

$$J_x = \frac{nq^2}{m^*} \langle \tau \rangle E_x, \quad \text{with} \quad \langle \tau \rangle = \frac{\int_0^\infty \tau(E)E^{3/2} \exp\left(-\frac{E}{kT}\right) dE}{\int_0^\infty E^{3/2} \exp\left(-\frac{E}{kT}\right) dE},$$

is such that  $\sigma = \frac{nq^2}{m^*} \langle \tau \rangle$ , so

$$\mu = \frac{q}{m^*} \langle \tau \rangle. \quad (25)$$

#### 4 The Kubo – Greenwood expression for conductivity

##### a General case

We have already realised eqn (14) for current density, that is

$$J_x = q^2 E_x \int_E \frac{\tau v_x^2}{kT} f_0(1 - f_0) N(E) dE.$$

So that conductivity is in the form

$$\sigma = q^2 \int_E \frac{\tau v_x^2}{kT} f_0(1 - f_0) N(E) dE. \quad (26)$$

Eqn (26) can be rewritten to give

$$\sigma = q \int_E \mu(E) f_0(1 - f_0) N(E) dE, \quad (27)$$

with

$$\mu(E) = \frac{q\tau(E)v_x^2}{kT} \quad (28)$$

in the Kubo–Greenwood expression for conductivity initially found in general physical theory.

Following on from eqn (12), we can also write

$$\sigma = - \int_E \sigma_E \frac{\partial f_0(E)}{\partial E} dE, \quad (29)$$

with

$$\sigma_E = q kT N(E) \mu(E). \quad (30)$$

##### b Isotropic diffusions and with an approximation of the effective mass

$$\left( v_x^2 = \frac{v^2}{3} = \frac{2E}{3m^*} \right)$$

The introduction of  $v_x^2$  into eqn (14) gives

$$\begin{aligned} \sigma &= q \int_E q \frac{2\tau E}{3kTm^*} f_0(1 - f_0) N(E) dE, \quad \text{so with } \bar{E} = \frac{3}{2}kT, \\ \sigma &= q \int_E \frac{q\tau E}{m^* \bar{E}} f_0(1 - f_0) N(E) dE. \end{aligned} \quad (31)$$

We once again find eqn (27) of the Kubo–Greenwood expression in

$$\sigma = q \int_E \mu(E) f_0(1 - f_0) N(E) dE,$$

but here with

$$\mu(E) = \frac{q\tau}{m^*} \frac{E}{\bar{E}}. \quad (32)$$



## IV Complementary comments

### 1 Concerning the approximation of the effective mass and isotropic diffusions

#### a Basic expressions

If the band structure is known we can express  $E(\mathbf{k})$  as a Taylor series, as in

$$E(\mathbf{k}) = E(0) + \mathbf{k} \left[ \frac{\partial E}{\partial \mathbf{k}} \right]_{\mathbf{k}=0} + \frac{1}{2} \mathbf{k}^2 \left[ \frac{\partial^2 E}{\partial \mathbf{k}^2} \right]_{\mathbf{k}=0} + \dots$$

Once the band exhibits a minimum at

$$\mathbf{k} = 0, \left[ \frac{\partial E}{\partial \mathbf{k}} \right]_{\mathbf{k}=0} = 0 \quad \text{and} \quad E(\mathbf{k}) = E(0) + \frac{\hbar^2 \mathbf{k}^2}{2m^*},$$

with

$$\frac{1}{m^*} = \frac{1}{\hbar^2} \frac{\partial^2 E(\mathbf{k})}{\partial \mathbf{k}^2}.$$

On introducing the crystal moment,  $\hbar \mathbf{k} = m^* \mathbf{v}$ , we have for a parabolic band which is such that  $E(\mathbf{k}) - E(0) = \frac{\hbar^2 \mathbf{k}^2}{2m^*}$  (which also takes into account the origin of the energies for electrons in  $E(0) = E_C$  (lowest conduction band),  $E(\mathbf{k}) = \frac{\hbar^2 \mathbf{k}^2}{2m^*}$ ) and  $E = \frac{1}{2} m^* v^2$ . As we have already seen, for isotropic diffusions, we therefore derive  $\langle v_x^2 \rangle = \langle v_y^2 \rangle = \langle v_z^2 \rangle = \frac{v^2}{3}$ , so that on using the effective mass approximation we have  $\langle v_x^2 \rangle = \frac{2E}{3m^*}$ .

#### b Additional remarks concerning the approximation of the effective mass [Lun 00]

When an electron moves through a device, it is subject to both a periodic potential of the crystal ( $V_C$ ) and an internal or applied tension ( $V_{IA}$ ) caused by impurities due to donors, acceptors, super-lattice effects and so on. Typically,  $V_{IA}$  varies little in space with respect to  $V_C$ . Electrons evidently see both  $V_C$  and  $V_{IA}$ .

If we assume the collisions between electrons and the lattice to be negligible, then the electronic wavefunctions must accord to

$$\left[ -\frac{\hbar^2}{2m} \frac{\partial^2}{\partial x^2} + V_C + V_{IA} \right] \Psi(x, t) = i\hbar \frac{\partial \Psi}{\partial t}. \quad (33)$$

In the absence of  $V_{IA}$ , the solutions of eqn (33) are the well known Bloch functions.

The question which must now be asked is with what condition is it possible to express the solutions for the complete problem as expressed in eqn (33), and, without an evident solution, do this with the help of the known forms of the simplified problem. The response is that it is possible using carriers situated at the lowest point ( $\mathbf{k} = 0$ )

in a parabolic band (which exhibit energy bands with a minimum at  $k = 0$ ) for which we can write  $\Psi(x, t) = F(x, t) \cdot u_{k=0}$ , in which  $F(x, t)$  is such that

$$\left[ -\frac{\hbar^2}{2m^*} \frac{\partial^2}{\partial x^2} + V_{IA} \right] F(x, t) = i\hbar \frac{\partial F}{\partial t}. \quad (34)$$

The function  $\Psi$  is thus the product of a function envelop and varies slowly due to the presence of  $V_{IA}$  in the equation, and also a function  $u_{k0}(r)$  which is periodic and varies rapidly with the Bloch function calculated from  $k = 0$ .

The advantage of this type of solution is that the complicated crystal potential effects ( $V_C$ ) can be written into a single value for the effective mass, hence the name the effective mass approximation. Nevertheless, writing eqn (34) did necessitate that  $V_{IA}$  varied sufficiently slowly with respect to  $V_C$ . In effect the potential wells associated with  $V_{IA}$  should not be too steep implicating a low level of internal disorder and tension, and a sufficiently low frequency and tension in the applied field.

## 2 General laws for changes in mobility with temperature

### a Semiconducting system (non-degenerate)

We have seen that generally speaking  $\tau$  is dependent on the energy of the charge carriers in  $\tau = \tau(E)$ . The classical law for the evolution of  $\tau$  is  $\tau = AE^{-s}$ , in which  $s$  depends on the type of collision encountered.

With eqn (21) which expresses  $\langle \tau \rangle$ , following [smi 61], the calculation can give

$$\langle \tau \rangle \propto A(kT)^{-s}. \quad (35)$$

In more precise terms, we can put  $\tau$  into the general formula  $\tau(E) = \tau_0 \left( \frac{E}{kT} \right)^r$ , in which  $\tau_0$  is a parameter dependent on the nature of the interaction and the temperature of the lattice. When collisions do occur:

- on the lattice (collisions with phonons), when the temperature is sufficiently high, we have  $r = -1/2$ , and  $\tau_0$  is proportional to  $T^{-1/2}$ . We then have  $\tau_{res} = aE^{-1/2}T^{-1}$ , so that:

$$\langle \tau_{res} \rangle \propto T^{-3/2} \text{ as much as } \mu_{res} \propto T^{-3/2}; \quad (36)$$

- on ionised impurities, then  $r = 3/2$  and  $\tau_0 \propto T^{3/2}$ , and  $\tau_{ii} = bE^{3/2}$ , so that:

$$\langle \tau_{ii} \rangle \propto T^{3/2} \text{ much as } \mu_{ii} \propto T^{3/2}; \quad (37)$$

and

- on neutral impurities, then  $r \approx 0$ ,  $\tau \propto T^0$ , and  $\tau \approx \text{constant}$ .

If we consider that neutral impurities are negligible, then here we also have  $\frac{1}{\tau} = \frac{1}{\tau_{res}} + \frac{1}{\tau_{ii}}$ , which can also be equal to  $\frac{1}{\mu} = \frac{1}{\mu_{res}} + \frac{1}{\mu_{imp}}$ . Depending on the temperature regime:

- $\frac{1}{\mu} \approx \frac{1}{\mu_{res}}$  and  $\mu \approx \mu_{res} \propto T^{-3/2}$  at higher temperatures ( $T^{3/2} \gg T^{-3/2}$ ); and
- $\frac{1}{\mu} \approx \frac{1}{\mu_{ii}}$  and  $\mu \approx \mu_{ii} \propto T^{3/2}$  at lower temperatures ( $T^{3/2} \ll T^{-3/2}$ ).

**b metallic conduction (cf. example given by [moo 93])**

Metallic systems involve transport by electrons which are considered to be practically free and diffused by phonons and impurities, of which:

- the frequency of electron-phonon collisions ( $W_{\text{ph}}$ ), at a temperature higher than the Debye temperature, is proportional to the number of phonons ( $N_{\text{ph}}$ ), which is such that  $N_{\text{ph}} \propto T$ . Thus  $W_{\text{ph}} = \frac{1}{\tau_{\text{ph}}} \approx N_{\text{ph}} \propto T$ . With  $\sigma \propto \tau$ , the law of change of conductivity ( $\sigma_{\text{ph}}$ ) as a function of temperature is  $\sigma_{\text{ph}} \propto T^{-1}$ , and also  $\rho_{\text{ph}} \propto T$ ;
- if the concentration of impurities ( $N_{\text{imp}}$ ) remains independent of  $T$ , the frequency of collisions between carriers and impurities is  $W_{\text{imp}} = \frac{1}{\tau_{\text{imp}}} \propto N_{\text{imp}}$ , so that  $\rho_{\text{imp}} \propto \frac{1}{\tau_{\text{imp}}} = \rho_0$  (constant).

If we assume that the two collision mechanisms are independent from one another, then we have as a total number of collisions  $W = W_{\text{ph}} + W_{\text{imp}}$ , in which the average time between collisions (equally electron-phonon and electron-impurity) is  $\frac{1}{\tau} = \frac{1}{\tau_{\text{ph}}} + \frac{1}{\tau_{\text{imp}}}$ . The upshot is that the resistivity ( $\rho$ ) is such that  $\rho \propto \frac{1}{\tau} = \frac{1}{\tau_{\text{ph}}} + \frac{1}{\tau_{\text{imp}}}$ , and can be written, following Matthiesen's law:

$$\rho = \rho_{\text{ph}} + \rho_0 = \rho_0(1 + \alpha T). \quad (38)$$

Eqn (38) is useful at temperatures close to ambient.

## **General theory of conductivity in localised states: generalisation of the Kubo–Greenwood formula, thermally activated mobility, and localised and degenerate state bands**

Even if the application of transport equations, usually obtained for ordered media in which it is a simple matter to define a reciprocal lattice—see Appendix A-4—is ‘fanatically’ classical, we shall now record how a general Kubo–Greenwood type expression can be used to describe hopping transport mechanisms between localised states. We will indicate an expression for mobility and detail a new distribution function form which may be used in accordance with whether or not the Fermi level can be found in the band of localised degenerate or non-degenerate states.

### **I Expression for current intensity associated with hopping transport of a given charge placed on a specific energy level**

#### **1 Transcribing transport phenomena into equations**

We will consider that the transport here is of a given charge ( $q$ ) which is initially placed on a certain energy level ( $E$ ) (occupied with the probability  $f(E) = f_0$  which, very generally speaking, is the Fermi–Dirac function). The transport is through hopping over a potential barrier of height  $U$  and situated between two sites A and B, each pair of sites for the moment having a given energy  $E$ .

In the absence of an applied electric field, as in Figure 1-a, the probabilities of occupation ( $f_0$ ) are identical for the two sites. Per unit time, transition probabilities from A to B and from B to A above the potential barrier  $U$  are also equivalent. We can therefore write  $P_{AB} = P_0 \exp\left(-\frac{U}{kT}\right) = P_{BA}$  in which  $P_0$  is the transition probability per second from A to B or from B to A with zero barrier and can be written as  $P_0 = \frac{\omega_0}{2\pi} = \frac{1}{\tau_0}$  (as is the frequency of oscillation between two sites unaffected by barrier or external field). Once a barrier is set up, but still there is no external field, we have therefore

$$P_{AB} = P_{BA} = \frac{1}{\tau_0} e^{-\frac{U}{kT}} = \frac{1}{\tau},$$

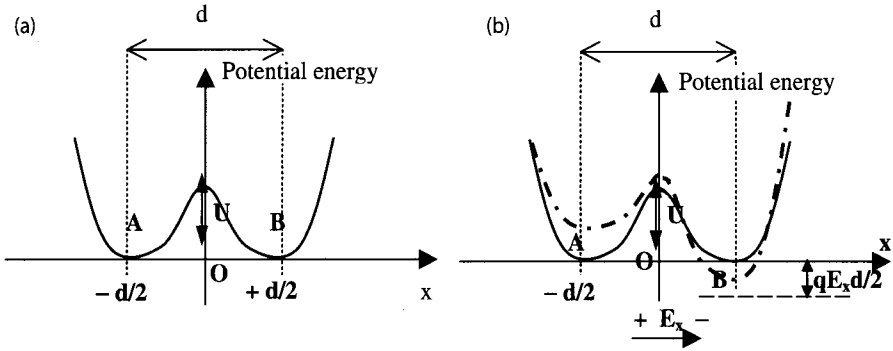


**Figure 1.** (a) A and B sites separated by a barrier over which hop carriers; and (b) the modification of potential energies following application in Ox of an electric field ( $E_x$ ).

or rather

$$\tau = \tau_0 e^{\frac{U}{kT}}. \tag{1}$$

In the presence of an applied electric field  $E_x$  which is directed with respect to Ox, as shown in Figure 1-b, the potential energy  $W = qV$  for a charge  $q$  is reduced at B and increased at A (when  $q > 0$ ). With  $E_x = -dV/dx$ , and supposing that  $E_x$  is uniform with respect to Ox, on taking the origin of the potentials in terms of  $O(V(O) = 0)$  we have:

$$V(A) - V(O) = \int_O^A dV = \int_A^O E_x dx = E_x(0 - x_A) = E_x \frac{d}{2} = V(A).$$

$$V(B) - V(O) = \int_O^B dV = \int_B^O E_x dx = E_x(0 - x_B) = -E_x \frac{d}{2} = V(B).$$

For a charge  $q$  situated at A or B, the modification in energy due to the application of  $E_x$  is, respectively,  $W(A) = qE_x d/2$  or  $W(B) = -qE_x d/2$ . It is noticeable that the energy increased by  $(qE_x d/2)$  at A and decreased by the same quantity at B. Here we finally have an asymmetry with the A wells increased in height and the B wells pulled down.

At A the barrier to overcome is reduced and becomes:  $U_A = U - qE_x d/2$ . At B the barrier is increased and can be written as  $U_B = U + qE_x d/2$ .

Consequently, in the presence of an electric field the transition probabilities,  $P_{AB}$  and  $P_{BA}$ , are no longer equivalent and become:

$$P_{AB} = P_0 \exp\left(-\frac{U - qE_x d/2}{kT}\right) = \frac{1}{\tau} e^{+\frac{qE_x d/2}{kT}} \approx \frac{1}{\tau} \left[1 + \frac{qE_x d/2}{kT}\right]$$

$$P_{BA} = P_0 \exp\left(-\frac{U + qE_x d/2}{kT}\right) = \frac{1}{\tau} e^{-\frac{qE_x d/2}{kT}} \approx \frac{1}{\tau} \left[1 - \frac{qE_x d/2}{kT}\right]$$

## 2 Calculating the current intensity due to hopping mechanisms

The current due to transport of a charge  $q$  between A and B,  $I_C$ , is the resultant of charge transport from A to B and from B to A, *i.e.*  $I_C = I_{A \rightarrow B} + I_{B \rightarrow A}$ . It is the total charge moving per second in both these directions. If  $f_0$  is the probability of site occupation at equilibrium and if  $(1 - f_0)$  is, inversely, the probability of non-occupation, the quantity of charge moving from A to B can be written as  $|I_{A \rightarrow B}| = qf_0(1 - f_0)P_{AB}$ . Similarly,  $|I_{B \rightarrow A}| = qf_0(1 - f_0)P_{BA}$ .

As the currents  $I_{AB}$  and  $I_{BA}$  are in opposing directions, the resultant can be obtained:

$$I_C = |I_{A \rightarrow B}| - |I_{B \rightarrow A}| = qf_0(1 - f_0)[P_{AB} - P_{BA}],$$

which gives:

$$\begin{aligned} I_C &= qf_0(1 - f_0) \frac{1}{\tau} \left[ e^{+\frac{qE_x d/2}{kT}} - e^{-\frac{qE_x d/2}{kT}} \right] \\ &= qf_0(1 - f_0) \frac{1}{\tau} 2 \sinh \left( \frac{qE_x d/2}{kT} \right) \approx qf_0(1 - f_0) \frac{1}{\tau} 2 \left[ \frac{qE_x d}{2kT} \right], \end{aligned}$$

or rather:

$$I_C \approx f_0(1 - f_0) \frac{1}{\tau} \left[ \frac{qE_x d}{kT} \right]. \quad (2)$$

## II Expression for current density and thermally activated mobility

### 1 Expression for current density relative to transport at a particular energy level

The state density function for an energy level  $E$  being  $N(E)$  (number of states per unit volume of material) with in the volume  $V$  of a unit section is  $V = [S \times d]_{(S=1)} = d$ , and the number of states with energy  $E$  is thus  $N(E)d$ . This is the number of individual charges ( $q$ ) situated at sites with energy  $E$  (with  $\tau = \tau(E)$  for carriers leaving the sites).

If we take a unit section between two sites A and B separated by the distance  $d$ , the current passing through this section thus becomes a current density with the value:

$$\begin{aligned} J(E) &= I_C N(E)d = \frac{2q}{\tau(E)} f_0(1 - f_0) \sinh \left( \frac{qE_x d/2}{kT} \right) N(E)d \\ &\approx \frac{q}{\tau(E)} f_0(1 - f_0) \left[ \frac{qE_x d}{kT} \right] N(E)d, \end{aligned}$$

which yields:

$$J(E) \approx q^2 E_x \frac{d^2}{\tau(E) kT} f_0(1 - f_0) N(E). \quad (3)$$

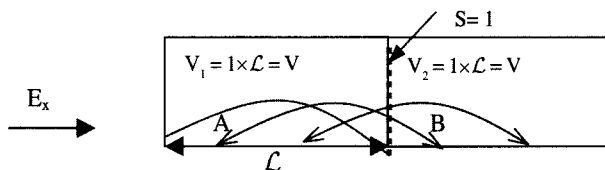


**Figure 2.** Schematisation of all possible hops through the section  $S = 1$  giving rise to the current  $J(E)$ .

## 2 Generalisation of the form of Kubo–Greenwood conductivity

In order to assimilate all the possible hops—shown in Figure 2—through the section  $S$ , the length  $d$  must be placed in to terms of the mean free pathway ( $\mathcal{L}$ ) the mean distance between two hops. In addition the current density, which involves all carriers from a volume  $V$  traversing the section  $S$  in both senses whatever their initial energy ( $E$ ), can be written as:

$$J = q^2 E_x \int \frac{\mathcal{L}^2}{\tau(E)} \frac{1}{kT} f_0(1 - f_0) N(E) dE \quad (4)$$

Again using the definition of conductivity ( $\sigma$ ) as that given by the relationship  $J = \sigma E_x$  can be used to give a Kubo–Greenwood type equation:

$$\sigma = q \int \mu(E) f_0(1 - f_0) N(E) dE, \quad (5)$$

$$\text{with } \mu(E) = q \frac{\mathcal{L}^2}{\tau(E)} \frac{1}{kT}. \quad (6)$$

### Comment

With  $\mathcal{L} = v_x \tau(E)$ , and with the help of eqn (4), we can go directly to:

$$\sigma = q \int_E \frac{q v_x^2 \tau(E)}{kT} f_0(1 - f_0) N(E) dE,$$

a form of  $\sigma$  deduced from the Boltmann transport equation shown as eqn (14) in Appendix A-4. We can thus be content to use eqn (14), Appendix A-4, in which  $\mathcal{L} = v_x \tau(E)$  is introduced and from which we can directly obtain eqn (4). However, such a path tends to hide the physical reality of the problem which we have detailed in this Appendix.

## 3 Thermally activated mobility

Following on from eqn (1), we have  $\tau = \tau_0 \exp\left(\frac{U}{kT}\right)$ , and on placing  $\mu_0 = \frac{q\mathcal{L}^2}{\tau_0 kT}$ , eqn (6) gives:

$$\mu = \mu_0 \exp\left(-\frac{U}{kT}\right) \quad (7)$$

This equation shows us that the mobility is thermally activated.

*Comment*

From eqn (6), we can write that

$$\mu(E) = q \frac{\mathcal{L}^2}{\tau(E)} \frac{1}{kT} = \frac{q}{kT} \frac{\mathcal{L}^2}{\tau}.$$

On posing

$$D = \frac{\mathcal{L}^2}{\tau}, \tag{8}$$

which has as dimensions a diffusion constant, we find Einstein's relation:

$$D = \frac{kT}{q} \mu. \tag{9}$$

While the study of transport with respect to the direction of the electric field does not *a priori* require the introduction of the coefficient 1/6, we can have the isotropic diffusion

$$D = \frac{1}{6} P \mathcal{L}^2, \quad \text{with } P = \frac{1}{\tau}. \tag{10}$$

### III Approximations for localised and degenerate states

Here the calculations for conductivity can be performed using the Kubo–Greenwood relationship *i.e.*  $\sigma = q \int \mu(E) f_0(1 - f_0) N(E) dE$ , but require, in general, the following approximations:

- as the states are neighbours at the level  $E = E_F$ , we assume that  $N(E) \approx \text{constant} = N(E_F)$ ; and
- $\mu = \mu_0 \exp\left(-\frac{U}{kT}\right) = \text{constant}$  with respect to  $E$ , as in  $\mu(E) = \mu(E_F)$ .

The calculation for  $\sigma$  requires therefore the evaluation of

$$\sigma = q \mu_0 \exp\left(-\frac{U}{kT}\right) N(E_F) \int f_0(1 - f_0) dE.$$

We must therefore go on to evaluate  $\int f_0(1 - f_0) dE$ . This can be done using eqn (12) of Appendix A-4, so  $f_0(1 - f_0) = -kT \frac{\partial f_0}{\partial E}$ . Figure 3-a represents the Fermi function and Figure 3-b the function  $-\frac{\partial f_0}{\partial E}$ .

At not too high a value of  $T$ , ( $T \approx T_1 = 300 \text{ K}$ ), the above schematic representation shows that  $\frac{\partial f_0}{\partial E}$  behaves similarly to a delta function, so that

$$\int kT \left( \frac{\partial f_0}{\partial E} \right) dE \approx kT.$$

Thus:

$$\int f_0(1 - f_0) dE \approx kT.$$

When a high number of defaults result in deep localised states within the gap, we find that  $(E_C - E_F) \gg kT$ , and carriers cannot be thermally excited into



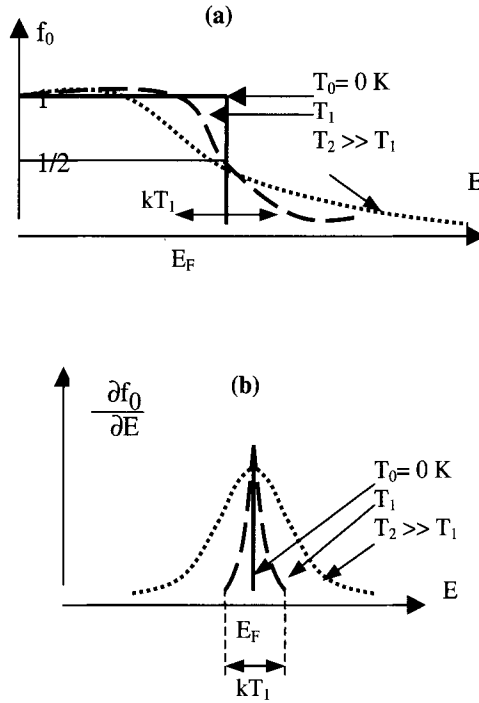


**Figure 3.** Representations of: (a) the Fermi function; and (b) the function  $\frac{\partial f_0}{\partial E}$ .

the conduction band. These carriers remain localised around  $E_F$  in a degenerate band of states. The transport process in the neighbourhood of  $E_F$  is realised by bringing into play a density of charge carriers given by  $n = \int N(E)f_0(1 - f_0)dE \approx N(E_F) \int f_0(1 - f_0)dE \approx kTN(E_F)$ .

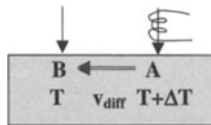
The conductivity is thus in the form  $\sigma = q kTN(E_F)\mu_0 \exp\left(-\frac{U}{kT}\right)$  and is thermally activated by the form of the mobility.

## Expressions for thermoelectric power in solids: conducting polymers

### I Definition and reasons for use

#### 1 Definition

Under the effect of a temperature gradient, there is a diffusion of carriers from hot to cold points which is associated either with a concentration gradient as in the case of semiconductors, or a velocity gradient of carriers in the case of metals. The result is an excess charge and, in effect, the birth of an internal electric field ( $E$ ). The resulting current is the sum of two parts:  $\vec{j} = \sigma \vec{E} + M \overrightarrow{\text{grad}T}$



At equilibrium the current is zero and the internal field is such that:

$$\vec{E} = S \overrightarrow{\text{grad}T}, \text{ so } S = -\frac{\text{grad}V}{\text{grad}T} = -\frac{V_A - V_B}{T_A - T_B} = -\frac{\Delta V}{\Delta T}$$

in which, by definition,  $S$  is the Seebeck coefficient.

#### 2 Reasons for use

The parameter, called thermoelectric power (TEP) is:

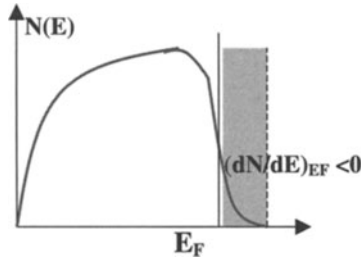
- an intrinsic property of a material and is independent of the geometrical dimensions and insensitive to faults such as cracks, in contrast to other properties such as conductivity; and
- essential to distinguish metals from insulators and understand which carrier is in the majority in a particular material.

## II TEP of metals ( $E_F$ within a band of delocalised states)

A rigorous calculation must be performed within the context of the Boltzmann transport equation:

$$S_m = -\frac{\pi^2}{3} \frac{k}{q} kT \left\{ \frac{d \ln \sigma(E)}{dE} \right\}, \quad \text{with } \sigma(E) \propto N(E).$$

For a metal close to the Fermi level, we have  $(d \ln \sigma/dE) < 0$  and therefore  $S_m > 0$ .



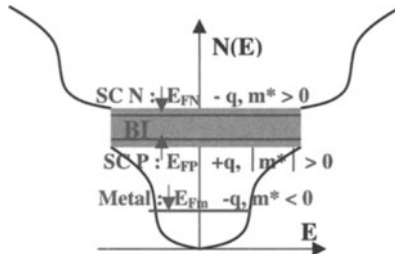
On developing the calculation with  $\sigma(E) \propto aE^l$  and  $[d \ln \sigma(E)/dE]_{E_F} \approx 1/E_F$  we have the following equation:

$$S_m \approx \frac{k}{q} \frac{\pi^2}{3} \frac{kT}{E_F} \approx \text{several } \mu\text{V/K}.$$

Thus  $S_m$  has a low positive value and  $S_m = f(T)$  is linear with  $S_m \rightarrow 0$  with temperature.

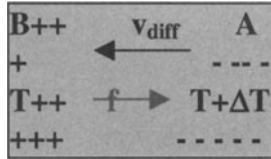
Qualitatively speaking, we can say that with a good metal the thermal gradient does not practically ‘destroy’ the equipotential at its surface and that  $\Delta V \approx 0$ , so  $S$  is very small.

## III TEP of semiconductors (SC) ( $E_F$ in the gap)



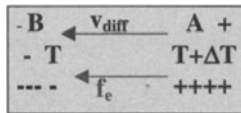
### 1 Preliminary remark

In a metal the diffusion of hot electrons of charge  $-q$ , takes place above  $E_F$  and therefore the effective negative mass is such that the associated force is directly opposite to the diffusion velocity:  $\Rightarrow V_A < 0$  and  $V_A - V_B < 0$ , which gives  $S_m > 0$ , as we have already seen. For SCs, the carriers ( $-q$ ) have  $m^* > 0$ , so, only in p-type SCs, we have carriers with  $+q$  and  $m^* > 0$ . In order to determine the force applied on the carriers, ( $+q$  or  $-q$ ), we can use  $\vec{f} = m^* \vec{\gamma}$  with  $\vec{\gamma} // \vec{v}$  and  $m^* > 0$  or  $< 0$ ).



### 2 An ideal n-type semiconductor

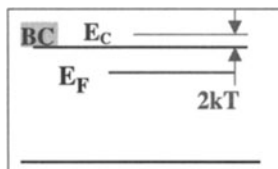
Locally around A, the concentration of carries increases with the effect of  $\Delta T$  ( $n \propto T^{3/2} \exp(-[E_c - E_F]/kT)$ ). The result is that electrons diffuse from A towards B ( $m_e^* > 0 \Rightarrow f_e // v$ ) where a charge  $< 0$  appears. And leaves a charge  $> 0$  at A. We can thus write that  $V_A - V_B > 0$  and  $T_A - T_B > 0$ , so that  $S_N < 0$ .



More quantitatively, without going through the rigorous treatment of the transport equation) we have  $S = \frac{\Pi}{T}$  (Kelvin's 1st relationship), where  $\Pi$  is Pelletier's coefficient. For electrons, with the energy transported per unit charge and by taking the potential origin as  $E_F$ , and then with

$$\text{Energy} = P_{\text{potential}} + E_{\text{kinetic}}, E_{\text{potential}} = E_C - E_F,$$

$$E_{\text{kinetic}} \approx 2kT : \Pi = \frac{E_C - E_F + 2kT}{-q}$$



Finally:

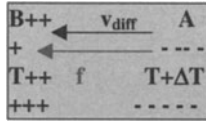
$$S_N = -\frac{k}{q} \left[ \frac{E_C - E_F}{kT} + B \right], \quad \text{with here } B = 2$$

Thus  $S_N < 0$  and typically goes in value from a hundred or so  $\mu\text{VK}^{-1}$  to more than several  $\text{mV K}^{-1}$ .

### 3 An ideal n-type semiconductor

The diffusion of holes ( $+q, m_t^* > 0$ ) with  $f_t/v$  results in charging B positively (while leaving a negative charge at A). So we have  $V_A - V_B < 0$  and  $T_A - T_B > 0$ , and that  $S_P > 0$ . Thus:

$$S_P = \frac{k}{q} \left[ \frac{E_F - E_V}{kT} + B \right], \quad \text{here with } B = 2$$



### 4 Comment on amorphous semi-conductors

for which  $E_C - E_F = \Delta E - \alpha T$ . For a n-type semiconductor, for example,

$$S_N = -\frac{k}{q} \left[ \frac{\Delta E}{kT} - \frac{\alpha}{k} + B \right]$$

while  $S = f(1/T)$  and  $\ln \sigma = f(1/T)$  exhibit the same slope. The ordinate at the origin for  $S = f(1/T)$  yields  $\alpha$ .

### 5 A non-ideal amorphous semiconductor with $E_F$ below its states in the band tails

Here the carriers have a thermally activated mobility in the band tails and  $\mu = \mu_0 \exp(-U/kT)$ . The form of the tail band is such that

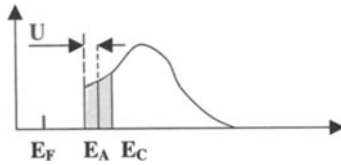
$$N(E) = \frac{N(E_C)}{(E_C - E_A)^s} (E - E_A)^s$$

and calculating S within Boltzmann restrictions gives

$$S = -\frac{k}{q} \left[ \frac{E_A - E_F}{kT} + \frac{C_s}{C_{s+1}} \right]$$

$$(\sigma \approx \sigma_0 C_s \left( \frac{kT}{E_C - E_A} \right)^s \exp \left( -\frac{E_A - E_F + U}{kT} \right))$$

as discussed in Chapter V, Section IV-1).



**Conclusion** The slope of  $\ln \sigma = f(1/T)$  is larger than  $S = f(1/T)$  by an amount  $U$ , and is characteristic of this transport mechanism within tail band localised states (in the absence of localised states in the band tails, the two slopes are identical).

## IV TEP under a polaronic regime

We will distinguish between high and intermediate temperatures in a manner similar to that used for conductivity.

### 1 High temperature regime

Here,  $S$  can also be deduced using Kelvin's 1st relationship,  $S = \Pi/T$  in which Pelletier's coefficient (energy transported per unit charge) is such that we can suppose that the polaron does not transport the vibrational energy  $\Pi = \frac{E_0}{-q}$  ( $E_0$  is the energy which characterises the thermal generation of carriers and  $E_0 = E_P - E_F$ ). From which we can deduce that in the high temperature regime,  $S = -\frac{k}{q} \left( \frac{E_0}{kT} \right)$ .

### 2 Intermediate temperature regime

The regime implicates a VRH transport mechanism and, as we shall see in the following Section,  $S$  follows a law of the form  $S/T = f(T^{-1/4})$ .

### 3 Other regimes

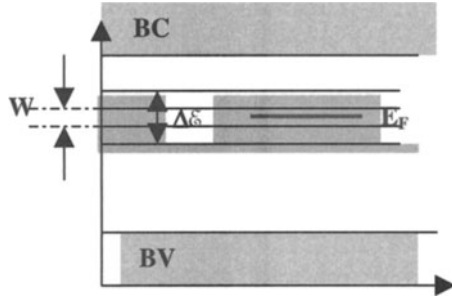
It has been found that for amorphous semiconductors,  $S \approx Cte$  with respect to  $T$ . Nagels proposed that with the concentration of polarons being constant with  $T$ ,  $S$  follows Heikes law which is of the form  $S \approx -(k/q) \ln([N - n]/n)$ , in which  $N$  is the number of sites and  $n$  is the number of carriers.

## V The TEP for a high density of localised states around $E_F$

### 1 Initial hypothesis

If  $E_F$  were to 'dive' into a band with a high density of (localised) states, it has been supposed that the expression used for a metallic system for the TEP would still be

valid by Cutler and Mott. In reality, however, experimental results have shown that  $S \neq 0$  as  $T \rightarrow 0$  in complete discord with the hypothesis.



In fact Nagels has shown [Nag 85] that in the low temperature domain we can write:

$$S = -\frac{\pi^2 k}{3 q} KT \left\{ \frac{d(\ln \sigma(E))}{dE} \right\}_{E=E_F}$$

and that  $\sigma(E)$  is expressed as a function of  $N(E)$  for which we assume that close to  $E_F$  there is a linear variation such that  $N(E) = N(E_F)[1 + \gamma(E - E_F)]$  with  $\gamma W \ll 1$ , in which  $W$  is the height of the hop.

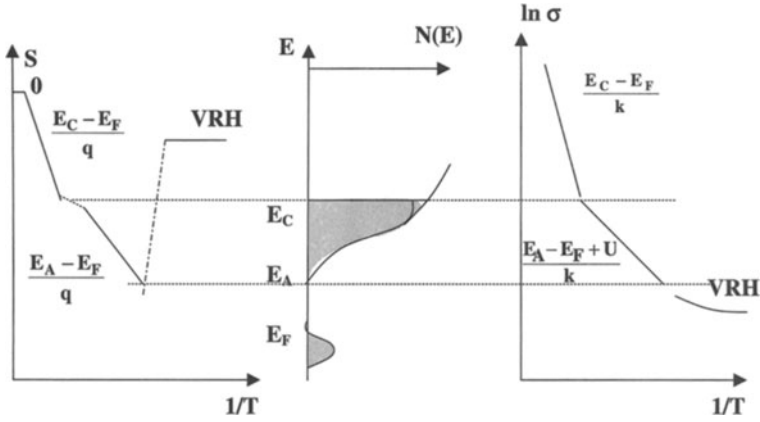
**2 The result in VRH**

Here we follow the work of Nagels in J. Non Cryst Sol. (1983) and consider the VRH condition with respect to the optimisation of both the hopping distance and the hopping height ( $W(E)$ ), the calculation of  $S$ , with  $\gamma = (1/N(E_F))[dN(E)/dE]_{E=E_F}$ , gives:

$$\frac{S}{T} = -\frac{\pi^2 k^2 \gamma}{12q} \left( \frac{T_0}{T} \right)^{1/4}$$

*Comment* The advantage of the above calculation with respect to other possible routes is that it brings in the factor  $\gamma$  which takes into account variations in  $N(E)$  near to  $E_F$  and does this independently of the origin of the states in the gap disorder, polarons etc.).

## VI General representation



## VII Real behaviour

### 1 General laws

#### a Different levels of conduction participate in parallel

The law is derived from the general equation itself generated from the Boltzmann formalisation, and is such that

$$S = -\frac{M}{\sigma} = -\frac{\sum_i M_i}{\sigma} = -\frac{\sum_i \sigma_i \frac{M_i}{\sigma_i}}{\sigma} = \frac{\sum_i \sigma_i S_i}{\sigma}.$$

As an example, we can cite the conduction by both electrons and holes in

$$S = \frac{\sigma_e S_e + \sigma_h S_h}{\sigma_e + \sigma_h},$$

and that in an intrinsic semiconductor we have

$$S_{int} = \frac{k}{|e|} \frac{\mu^+ - \mu^-}{\mu^+ + \mu^-} \left( \frac{E_g}{2kT} + B \right).$$

#### b Differing domains in series

Kaiser proposed [Kai 89] that during a drop in temperature, is remain proportional to the thermal resistance ( $W_i$ ) of each domain, so that from  $S = -\Delta V / \Delta T = -(\Delta V_1 +$



$\Delta V_2)/\Delta T = (\Delta T_1/\Delta T)S_1 + (\Delta T_2/\Delta T)S_2$  we can deduce that  $S = (W_1/W)S_1 + (W_2/W)S_2$ , with  $W$  being the total resistance.



## 2 Behaviour as a function of doping levels

### a Highly doped conducting polymers

In addition to the metallic component in  $S$ , it has been observed that at low temperatures there is a distortion of which Kaiser brought into account by using a non-linear component  $\lambda^*(T)T$  associated with effects on the carriers due to phonons. The resulting equation is therefore:

$$S = XT + \lambda^*(T)T$$

### b Moderately doped conducting polymers

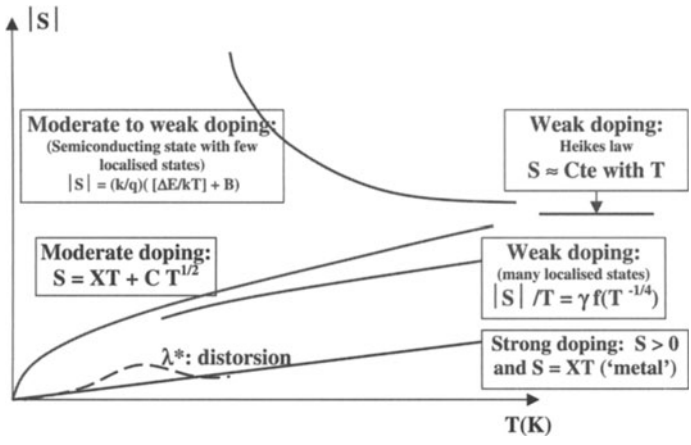
Here there are two ways of looking at the scenario:

- $E_F$  is more or less outside of the extended states and the system tends towards a semiconductor character  $\Rightarrow S/T \propto -\gamma(T_0/T)^x$  (see also Section  $\gamma$ ) or the system is an ideal semiconductor in which case exhibits a slope  $[E_C - E_F]/q$  with  $1/T$ ; and
- that we have a heterogeneous structure (Kaiser, Phys Rev 1989), with conducting fibres separated by barriers and we have  $S = (W_1/W)S_1 + (W_2/W)S_2 = XT + CT^{1/2}$ . The first term in this equation characterises the (metallic) transport along the fibres while the second term, for inter-barrier hops, follows a VRH type law with respect to  $T^{1/2}$  de type proposed by Mott. If the barriers are thin and conduct heat better than electricity, we can simplify things by assuming  $W_1 \gg W_2$  and that  $S \approx XT$  (see also Section a).

### c Poorly doped conducting polymers

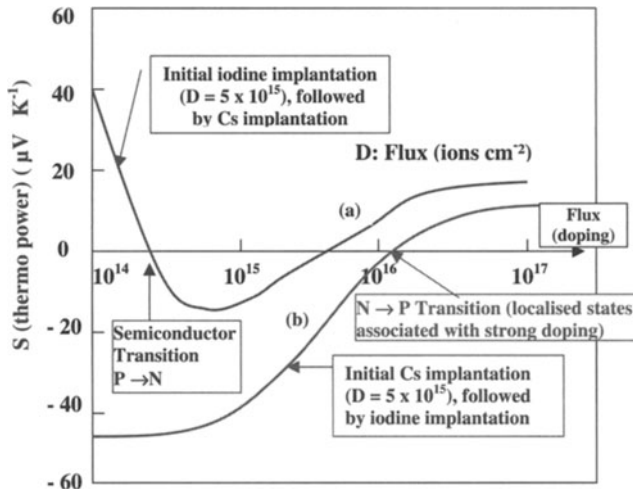
( $E_F$  is placed within a quite large gap that has few states and the material is close in character to an insulator). Whether looking at polaronic states or states tied to localised defaults, at low and intermediate temperatures, in principle they both follow a VRH law in the form  $S/T \propto f[T^{-1/4}]$ . Indeed, under certain conditions, such as in the impurity band, Heikes law can be envisaged so that  $S \approx -(k/q) \ln([N - n]/n)$  is reasonably constant or decreases only slightly with  $T$ .

### 3 Representational graph



### 4 An example result

An useful example is that with reversible doping—performed with ion implantation at 30 keV in poly(*para*-phenylene)—followed with respect to the changing positive and negative value of  $S$  [Mol 98]. In the Figure below, the curve (a) shows the variations of a sample initially made p-type using iodine and then doped to n-type by an increasing flux of n-type alkaline ions. Curve (b) shows the effects due to a sample undergoing initial n-type doping with alkaline ions and then a subsequent implantation with an increasing flux of halogen ions.



## Stages leading to emission and injection laws at interfaces

### I Thermoelectric emission and the Dushman – Richardson law

With  $W_s \gg kT$ , we have  $E - E_F \gg kT$  and the Fermi function tends towards the Boltzmann function:

$$f(E) \approx \exp(-[E - E_F]/kT) = \exp\left(\left[E_F - \frac{\hbar^2 k^2}{2m}\right] / kT\right).$$

So that an electron is emitted in Oz—simply through thermal agitation—and without taking into account a reflection coefficient, the equation  $[(E)_{\text{selon Oz}} - E_F] \geq W_s$  must be true, as schematised in Figure 1. Given that the energy is uniquely kinetic than the emission condition is thus

$$[E]_{\text{in Oz}} = \frac{\hbar^2 k_z^2}{2m} \geq E_F + W_s = \frac{\hbar^2 k_{z0}^2}{2m}. \quad (1)$$

We will define the number of electrons as  $dn$  in the reciprocal space volume  $d^3k$ . The latter is divided into elementary cells so that  $\Delta k_x \Delta k_y \Delta k_z = \Delta k^3$  and  $\Delta k^3 = \frac{8\pi^3}{V}$ . On reasoning that  $V = 1$  ( $dn$  will be a density) and the possibility of placing two electrons per elementary cell (due to electron spin), we have:

$$dn = 2 \times [\text{number of cells in } d^3k] \times f(E[k]) = 2 \frac{d^3k}{8\pi^3} f(E).$$

The elementary current density ( $dJ_z$ ) emitted in the direction Oz and effective for  $dn$  electrons is therefore

$$dJ_z = d\rho v_z = e dn v_z = e dn \frac{\hbar^2 k_z}{m} = e \frac{d^3k}{4\pi^3} \exp(E_F/kT) \exp(-E/kT) \frac{\hbar k_z}{m}.$$

The emitted current density can be obtained by adding over all electrons which have a vector  $\vec{k}$  with a component  $k_z$  which complies with the already established condition eqn (1):

$$\frac{\hbar^2 k_z^2}{2m} \geq E_F + W_s = \frac{\hbar^2 k_{z0}^2}{2m},$$

whatever the other components  $k_x$  and  $k_y$ .

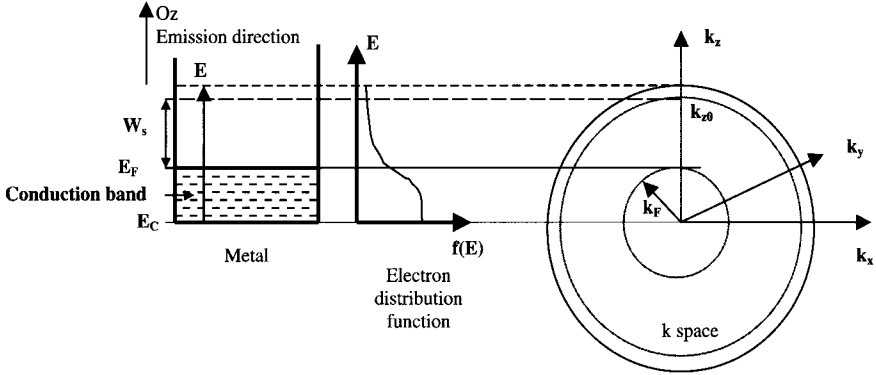


**Figure 1.** Schematisation of the thermoelectric emission condition.

Therefore:

$$|J| = \iiint |dJ_z| = \frac{e\hbar}{4\pi^3 m} e^{E_F/kT} \int_{-\infty}^{+\infty} e^{-\frac{\hbar^2 k_x^2}{2mkT}} dk_x \times \int_{-\infty}^{+\infty} e^{-\frac{\hbar^2 k_y^2}{2mkT}} dk_y \int_{k_{z0}}^{+\infty} e^{-\frac{\hbar^2 k_z^2}{2mkT}} k_z dk_z.$$

With  $k_{z0} = \frac{2m(E_F+W_s)}{\hbar^2}$ , on calculating by way of the well known results for integrals

$$\int_{-\infty}^{+\infty} e^{-\alpha x^2} dx = \sqrt{\frac{\pi}{\alpha}} \quad \text{and} \quad \int_{z_0}^{+\infty} ze^{-\alpha z} dz = \frac{1}{2\alpha} e^{-\alpha z_0^2},$$

we arrive at the desired equation:

$$J = J_T = \frac{4\pi emk^2}{h^3} T^2 e^{-\frac{W_s}{kT}} = AT^2 e^{-\frac{W_s}{kT}}. \tag{2}$$

Exactly speaking, a reflection coefficient R should be introduced to take into account any possible reflection during emission.

An example of this calculation can be given with tungsten ( $W_s = 4.5\text{ eV}$ ). With  $A = 1.2 \times 10^6 \text{ A m}^{-2} \text{ K}$  and  $\frac{W_s}{kT} \approx 19$  at  $T = 2700 \text{ K}$ , the calculation gives  $J = 2.2 \text{ A cm}^{-2}$ .

## II Schottky injection (field effect emissions)

Here we have an increase in the thermoelectronic emission due to the lowering of the barrier ( $W_s$  in thermoelectronic emission) due to the electric field effect applied at the metal (electrode) interface.

### 1 The potential barrier at the atomic scale

On the atomic scale at a metal-vacuum or dielectric interface, the potential barrier observed by an electron extracted from the metal is not an abrupt step (see Figure 2-a). In effect, an electron situated at  $z > 0$  in an insulator is not completely free and to distance itself from the metal it must overcome the attractive force exerted by the latter material due to the image charge ( $+q$ ) which the electron induces in the metallic electrode (see Figure 2-b). For an electron ( $-q$ ) on the  $z$  abscissa, its image (hole  $+q$ ) is at a distance  $2z$ .

The force which is therefore exerted on the electron, which is in an insulator that exhibits absolute permittivity  $\epsilon$ , is thus

$$\vec{F} = -\frac{q^2}{4\pi\epsilon(2z)^2} = -\frac{q^2}{16\pi\epsilon z^2} = -\vec{\text{grad}} W_e,$$

in which  $W_e$  is the electrostatic energy. In 1-dimension,

$$W_e(z) - W_e(\infty) = W_e(z) = -\int_{\infty}^z Fdz = \int_{\infty}^z \frac{q^2}{16\pi\epsilon z^2} = -\frac{q^2}{16\pi\epsilon z}$$

(with the origins of energy at infinity).

*Comment* The above representation is only acceptable when the distance  $z$  is large with respect to the interatomic distances. When  $z \rightarrow 0$ ,  $W_e(x)$  is brought towards the potential energy level at the bottom of the conduction band ( $E_C$ ). When  $z = 0$ , we join the energy of the electrons to  $E_C$ .

### 2 Emission conditions: Schottky emission law and the decrease in the potential barrier by field effect

#### a Without an applied field

Here the condition  $(E)_{in Oz} \geq E_F + W_s$  must be fulfilled (in the  $Oz$  axis) using the metal side as the origin of potentials in the lowest conduction band (in  $E_C$ ). With the

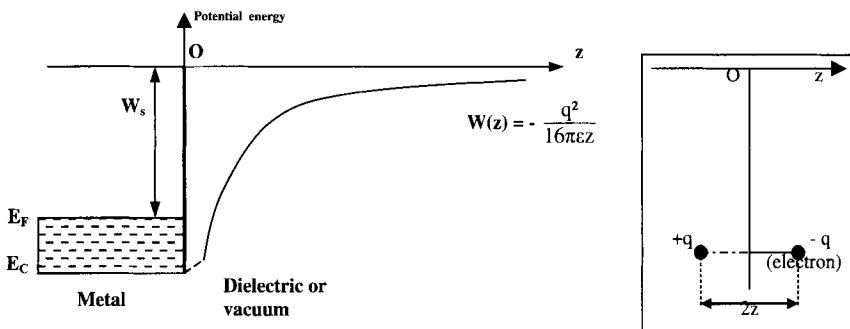


**Figure 2.** Graphical representations of: (a) an electrode potential as seen by an electron at the atomic scale; and (b) the charge image ( $+q$ ) of an electron.

energy of electrons exiting being solely kinetic energy, we should be able to apply condition (1) which can also be written as  $\frac{1}{2}mv_z^2 \geq E_F + W_s$ .

**b In the presence of an electric field**

The field is applied so that the metal has a negative potential (cathode) and the part external to the metal is positive.

We have

$$\vec{F} = -\vec{\text{grad}} W_e = -q\vec{E}_a, \text{ and } W_e(x) = -\int_0^z qE_a dz = -qE_a z.$$

Thus, the total potential energy of an electron situated at a distance  $z$  from the surface becomes:

$$W_{\text{Total}} = -qE_a z - \frac{q^2}{16\pi\epsilon z}.$$

The resulting curve presents a maximum in  $z_m$ , which is such that

$$\left(\frac{\partial W_{\text{Total}}}{\partial z}\right)_{z=z_m} = 0, \text{ and } z_m = \left(\frac{q}{16\pi\epsilon E_a}\right)^{1/2}.$$

The result is that

$$W_{\text{Total}}(z_m) = -\frac{q}{2} \left(\frac{qE_a}{\pi\epsilon}\right)^{1/2}.$$

The work function is reduced by an amount  $\Delta W_s = |W_{\text{Total}}(z_m)|$ , a value not more than  $W'_s = W_s - q\sqrt{\frac{qE_a}{4\pi\epsilon}}$  (see Figure 3).

The emission condition (1) now becomes the condition (1'):  $\frac{1}{2}mv_z^2 \geq E_F + W'_s$ .

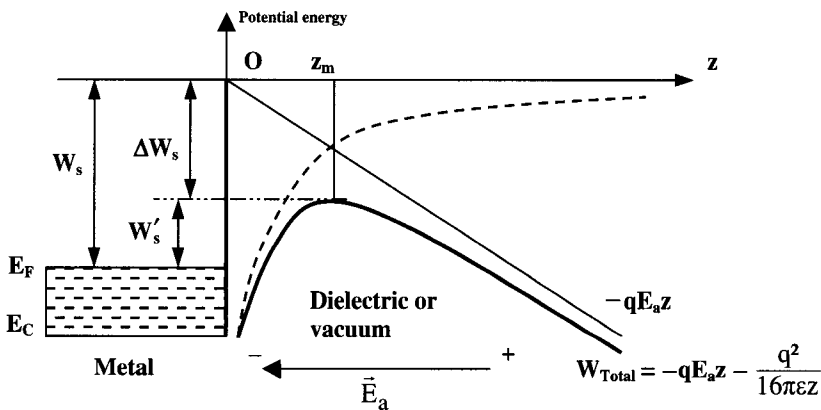


**Figure 3.** Energy diagram describing effects due to application of an electric field.

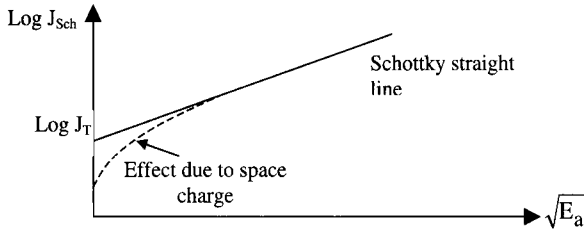


Figure 4. Representation of  $\text{Log } J_{\text{Sch}} = f(\sqrt{E_a})$ .

Eqn (2) for current density is still usable, as long as  $W_s$  is replaced by  $W'_s$ . In the presence of an electric field the emitted current density thus becomes

$$J = J_{\text{Sch}} = AT^2 \exp \left( - \left[ \frac{W_s - q\sqrt{\frac{qE_a}{4\pi\epsilon}}}{kT} \right] \right). \quad (3)$$

For a given value of  $T$ ,  $\text{Log } J_{\text{Sch}} = f(\sqrt{E_a})$  is a straight line. Nevertheless, in practical terms, we can observe at low values of  $E$  a deviation from the linear law and this is due to the appearance of space charge close to the emitting surface (see Figure 4).

**b Comment using numerical example**

With  $E_a = 10^4 \text{ V m}^{-1}$ , we have (Figure 3)  $z_m \approx 0.2 \mu\text{m}$ , while with  $E_a = 10^{19} \text{ V m}^{-1}$ , we find  $z_m \approx 0.7 \text{ nm}$ . The height of the potential barrier is reduced in the first case by  $\Delta W_s = 4 \times 10^{-3} \text{ eV}$ , and by  $\Delta W_s = 1.2 \text{ eV}$  in the second. In a strong field,  $\Delta W_s \approx W_s$  and the height of the barrier to overcome is extremely low, so that breakdowns can occur under high fields ( $W_s[\text{Cs}] = 1.8 \text{ eV}$ ;  $W_s[\text{Th}] = 3.35 \text{ eV}$  and  $W_s[\text{W}] = 4.5 \text{ eV}$ ).

**III Injection through tunnelling effect and the Fowler–Nordheim equation**

**1 The problem**

As the applied electric field increases, the height of the barrier observed by electrons close to the Fermi level actually decreases. This in turn greatly facilitates the passage of electrons over the barrier (field emission due to a Schottky effect). In fact, another mechanism appears once the field is increased. As shown in the qualitative example just above, as  $E_a$  increases  $z_m$  decreases; also we can perceive a qualitative decrease in the barrier. If the barrier decreases sufficiently then the probability of electron presence, initially close to that of the barrier (in terms of  $z$  is equal to 0), turns to being non-zero at the other side of the barrier. This is due to the wave like character

of electrons, which is accounted for in the probability of presence at the point  $z$  being written as  $P(z) = |\psi(z)|^2$ . The barrier transparency can be calculated for simple cases.

Before going in to the calculations, we can remark that if  $E_a$  increases, then the effect due to the force image—which is predominant in a weak field and in Schottky emissions (close to  $z = z_m$ )—diminishes when we are at a sufficiently high value of  $z$ . This can be a point, for example, in the region of  $z \approx z_F$  (defined in Figure 5 in which  $z_F$  corresponds to the point at which  $E = E_F$ ). On the side of the insulator, the potential energy there is simply approximated to using the field effect of the electric field so  $W(z) = -q E_a z_F$ , in which  $z_F$  is the size  $L$  (such that  $z_F = L$ ) of the barrier seen by electrons situated at  $E = E_F$ . Thus  $q E_a L = W_S$ , that is

$$L = \frac{W_S}{qE_a} \tag{4}$$

In effect, the higher the value of  $E_a$ , the more narrow the barrier.

In the case of tungsten, we can use  $W_S = 4.5 \text{ eV}$  and  $E_a = 4.5 \times 10^9 \text{ V m}^{-1}$  to calculate that  $L = 1 \text{ nm}$ . At high enough field strengths, the barrier becomes sufficiently narrow to present a non-negligible transparency to electrons free in the metallic electrode.

**2 Form of the transparency (T) of a triangular barrier**

The transparency ( $T$ ) of a barrier is usually defined by:

$$T = \frac{\text{Flux of transmitted particles}}{\text{Flux of incident particles}},$$

in which the flux represents the number of particles which traverse an unit surface area per unit time. The flux can this be represented by the product of the probability of

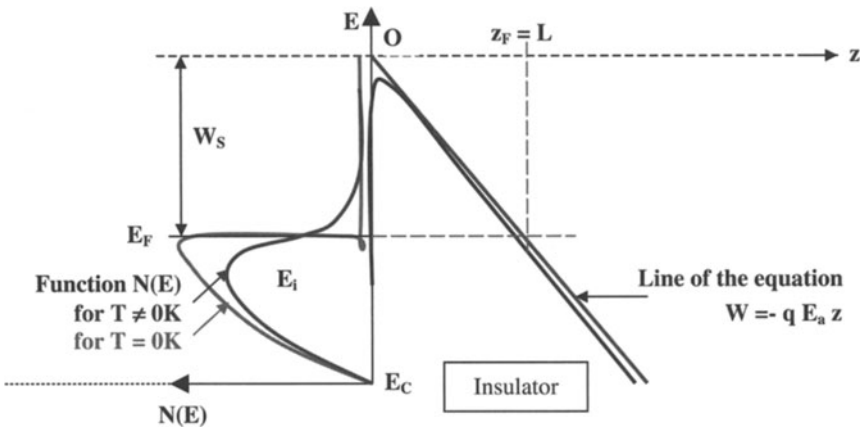


**Figure 5.** Diagram of potential energies for tunnel effect emissions.



presence per volume with a unit section and a length  $v$  (if  $v$  denotes particle velocity) (see Figure 6).

It is possible to write eqn (5) for a barrier of length  $L$  by assuming that the initial velocity of free electrons in the metal ( $v_i$ ) and their velocity after traversing the barrier ( $v_t$ ) are such that  $v_i \approx v_t$ :

$$T = \frac{v_t |\psi_{\text{transmis}}|^2}{v_i |\psi_{\text{incident}}|^2} \approx \frac{|\psi_t|^2}{|\psi_i|^2} = \frac{|\psi(L)|^2}{|\psi(0)|^2}. \quad (5)$$

In this problem, it is reasonable to think that the most important part of the injected current, following the application of a field, will come from electrons which have an energy close to the Fermi level as the distribution function  $N(E)$  has a maximum  $E \approx E_F$ .

Thus the expression for  $T$  of the barrier is given by eqn (5) in which  $L$  is the size of the barrier observed by electrons for  $E = E_F$  (Figure 5). In order to calculate the size of the barrier more precisely, we shall have to look at the origin of the energy at the  $E_F$  level by treating a classical rectangular barrier with quantum mechanics (see Figure 7).

We shall look at electrons with an energy  $E_i$  just above  $E_F$  and denote their velocity  $v$  when  $z < 0$  and  $v'$  when the electrons are at  $z > 0$ .

Generally, the conservation of energy for an electron placed initially at the level  $E_i$  (neighbour to  $E_F$ ) and then at  $A$  after having traversed the barrier can be written, using the notations detailed in Figure 7, as:

$$E_i = \frac{1}{2} m v^2 = \frac{1}{2} m v'^2 + U(z)$$

from which can be deduced  $m^2 v'^2 = p'^2 = 2m(E_i - U(z))$ , so that with  $k'^2 = \frac{p'^2}{\hbar^2}$  we have  $k'^2 = \frac{2m(E_i - U(z))}{\hbar^2}$ . For  $E_i < U(z)$ ,  $k'(z)$  is imaginary and

$$k'(z) = j \left[ \frac{2m(U(z) - E_i)}{\hbar^2} \right]^{1/2}.$$

The wavefunction, in the form  $e^{jkz}$  for free electrons and with a real  $k$ , takes on the form  $\psi(z) = e^{j \int_0^z k'(z) dz}$ .

$$T \text{ can be written therefore as } T \propto \frac{|\psi(L)|^2}{|\psi(0)|^2} = e^{-2 \int_0^L \left( \frac{2m}{\hbar^2} \right)^{1/2} [U(z) - E_i]^{1/2} dz},$$

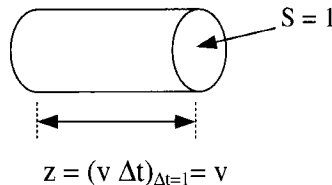


**Figure 6.** Geometric parameters required to define flux.

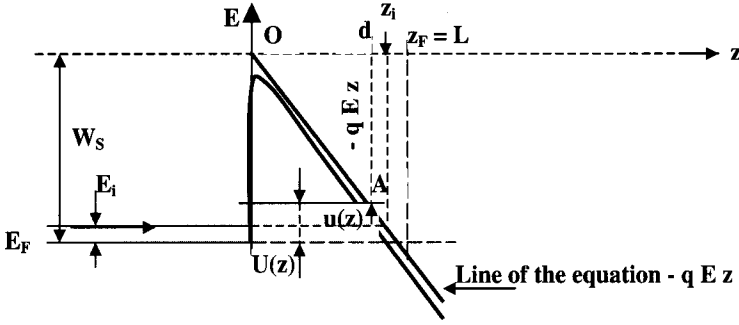


Figure 7. Representation of a triangular barrier.

and definitively

$$T = f(E, W_s) \exp \left\{ -2 \left[ \frac{2m}{\hbar^2} \right]^{1/2} \int_0^L [U(z) - E_i]^{1/2} dz \right\}. \quad (6)$$

### 3 The Fowler–Nordheim equation

In the relationship (6) for  $T$ , the term to integrate,  $[U(z) - E_i]$ , is such that:  $[U(z) - E_i] = W_s - qE_a z - E_i = u(z)$ , so that  $u'(z) = -qE$ .

Thus

$$\begin{aligned} \int_0^L [U(z) - E_i]^{1/2} dx &= \int_0^L [u(z)]^{1/2} dz = -\frac{1}{qE} \int_0^L [u(z)]^{1/2} du(z) \\ &= -\frac{1}{qE} \frac{2}{3} \left( u(z)^{3/2} \right)_0^L, \end{aligned}$$

and on taking into account eqn (4):

$$\begin{aligned} \int_0^L [U(z) - E_i]^{1/2} dx &= -\frac{1}{qE} \frac{2}{3} \left\{ \left[ W_s - qE_a \frac{W_s}{qE_a} - E_i \right]^{3/2} - [W_s - E_i]^{3/2} \right\} \\ &\approx \frac{2}{3} \frac{1}{qE} W_s^{3/2}, \text{ as } E_i \ll W_s \end{aligned}$$

(and notably at  $T = 0$  K). Finally:

$$T = f(E, W_s) \exp \left[ -2 \left( \frac{2m}{\hbar^2} \right)^{1/2} \frac{2}{3} \frac{1}{qE_a} W_s^{3/2} \right]. \quad (7)$$

As  $L = \frac{W_s}{qE_a}$ , we can see that ( $T \approx 0$  K) the transmission coefficient is an exponential function of the size of the barrier. Only electrons very close to  $E_F$  can leave with a non-negligible probability.

When  $T \neq 0$ , electrons situated just above  $E_F$  are privileged as even though they are few in number the actual barrier they have to cross is thinner.

The Fowler–Nordheim calculation performed at 0 K does nevertheless take into account all electrons. In using the fact that the current density contribution from levels situated in the interval  $[E_i, E_i + dE_i]$  is in the form  $dJ = q N(E_i)T(E_i) dE_i$ , the sum over all the  $E_i$  states results in a current density of the form:

$$J = \frac{q^3 E_a^2}{8\pi h W_s} \exp \left[ -\frac{4}{3} \left( \frac{2m}{\hbar^2} \right)^{1/2} \frac{W_s^{3/2}}{qE_a} \right].$$

(Note that  $N(E_i) dE_i$  is the number of electrons hitting the unit surface area per unit time with an energy between  $E_i$  and  $E_i + dE_i$ ).

Numerically speaking we can use this equation as in:

$$J(\text{Am}^{-2}) = 1.54 \times 10^{-10} \frac{E_a^2}{W_s} \exp \left( -6.83 \times 10^9 \frac{W_s^{3/2}}{E_a} \right).$$

The above relation shows that the current density emitted for this process is negligible at  $E_a < 10^8 \text{ V m}^{-1}$ , and that it increases rapidly at higher field strengths.

$\text{Ln}(\frac{J}{V^2}) = f(\frac{1}{V})$  or  $\text{Ln}(\frac{J}{E_a^2}) = f(\frac{1}{E_a})$  are the lines drawn for these types of emissions and linear behaviour over a decade of  $1/V$  can permit determination of  $W_s$ .

*Comment* The obtained equations relate to emissions into vacuum (barrier  $W_s$  seen by electrons coming from the metal). When an emission is into an insulator the barrier to overcome for the electrons coming from the metal is just  $W_B = (W_s - \chi)$ , where  $\chi$  is the electron affinity of the insulator or semiconductor.  $W_B$  can be substituted for  $W_s$  in the equations (see the Fowler–Nordheim equation in Section III-4 of Chapter VI).

## Energy levels and permitted transitions (and selection rules) in isolated atoms

This Appendix gives a brief, but ultimately essential description of the construction of energy levels in an atom which appear under the effects of successive perturbations, going from the most to the least intense.

### I Spherical atoms with an external electron

Typically the titled scenario resembles that of hydrogen atoms, but it can also be applied as a first approximation to the more general problem of describing an atom with more than one electron (through the potential, observed by an electron, being approximated as a symmetrical sphere).

#### 1 Energy levels and electron configuration [Cag 71]

Given the symmetry of the system under study, the energy levels can be obtained by assuming that each electron moves, to a first approximation, within a potential sphere which originates from the nucleus potential and the spherical potential which globally represents the effects due to all other electrons. The states of the electron orbitals (without therefore taking into account spin) are written using an electron orbital wavefunction ( $\psi_{n,l,m_l} = R_{n,l}\theta_{l,m_l}\phi_{m_l}$ ) which depends of three quantum numbers. They are:  $n$ , characteristic of the layer;  $l$ , characteristic of the sub-layer and the kinetic orbital momentum  $\vec{l}$ , which is such that  $|\vec{l}| = \hbar\sqrt{l(l+1)}$ ; and  $m_l$ , characteristic of the projection  $l_z$  of the kinetic orbital momentum along the axis  $Oz$  which is such that  $l_z = \hbar m_l$ , while  $m_l$  takes on  $(2l+1)$  values:  $m_l = -l, -l+1 \dots (l-1), l$ .

The movement of an electron about itself brings into play the spin kinetic moment ( $\vec{s}$ ), which is such that  $|\vec{s}| = \hbar\sqrt{s(s+1)}$  where  $s = 1/2$ . Here it is worth realising that the electron is a fermion and therefore the wavefunction is antisymmetric while the spin is one half (see the symmetry postulation in [p 1374, Cohen 73]). The projection of  $s_z$  on the  $Oz$  axis of the spin kinetic moment is  $s_z = \hbar m_s$  in which  $m_s$  takes on  $(2s+1)$  values, so here  $m_s = -\frac{1}{2}, +\frac{1}{2}$ .

In addition, the invariability of the Hamiltonian of the system during a rotation shows that the energy levels ( $E$ ) of a spherical system depends only on the two quantum numbers  $n$  and  $l$  so that  $E = E(n, l)$ . This can mean that the system is highly degenerate and at a given energy level  $E(n, l)$ , we can associate  $[2l + 1][2s + 1]$  electronic states represented through electronic wavefunctions ( $\psi(n, l, m_l, m_s)$ ), using Dirac notation,  $|n, l, m_l, m_s\rangle$  from orbital and spin wavefunctions.

In order to know the total energy of an atom, we need to sum over all the energies relating to each of its electrons. This requires an understanding of the spread of electrons with respect to layers and sub-layers, as defined by the quantum number  $n$  and  $l$ , respectively. In other words, the atomic configuration of the atom must be known. To denote this, each layer is symbolised by a number equal to the principal quantum number ( $n$ ) following by a letter which represents the value of the quantum number  $l$  (for  $l = 0, 1, 2, 3 \dots$  the letters are, respectively, s, p, d, f...). When several electrons are in the same sub-layer, we just write the symbol denoting the sub-layer once, and then add an indice indicating the number of electrons in that sub-layer. As an example, we can write the configuration of sodium, which has 11 electrons in all, as  $1s^2 2s^2 2p^6 3s$ .

The filling up of layers with electrons occurs in a specific order defined by Klechkowski's rule, which states that it follows the increasing order  $(n + l)$ . For a value given which is the same as  $(n + l)$ , then it is the value which corresponds to the lowest value of  $n$  which is filled first, as shown in Figure 1.

## 2 Selection rules

In this Section we finally have to consider the conservation of kinetic momentum and how, for a lone atom with one electron, there is a radiative transition. this occurs when the variations in quantum numbers of the energy levels involved concord with:

- $\Delta n =$  any integer (as the principal quantum number is not tied to kinetic moment and governs only the energy level); and
- $\Delta l = 1$  (as in, for example, the transition from the p-state [ $l = 1$ ] to the s-state [ $l = 0$ ] is radiative, as for the transition  $d \rightarrow p$ , however, the transition  $d \rightarrow s$  is forbidden and is therefore impossible with photon emission).

$l$	$n$	1	2	3	4	5
0		s	s	s	s	s
1			p	p	p	p
2				d	d	d

Figure 1. Filling up layers following Klechkowski's rule.

## II An atom with more than one peripheral electron

In addition the electron configuration ( $\gamma$ ), which uses only the  $n$  and  $l$  quantum numbers to represent energy levels and only includes a global, symmetrical, spherical potential representation of electron interactions, we need to take into account successively:

- the exact electrostatic interactions between electrons which introduce into the Hamiltonian of the system a perturbation operator  $H_{ee}$ , which raises the degeneration of the system; and
- weaker perturbation terms which progressively raise the remaining degeneration in the energy levels. The nature of the perturbation terms which must be successively introduced depends on the type of atom under study—whether it be heavy or light, with the limit generally around the mercury atom ( $Z = 80$ ), along with its environment, for example whether or not it has been inserted into a matrix. The latter effect has been discussed with respect to atoms with incomplete inner layers in Chapter VII, Section II.

### 1 First effect produced from the perturbation $H_{ee}$ due to exact electronic interactions

The Hamiltonian of the system is only invariant when there is a simultaneous rotation of all electrons. This can be associated with an orbital resulting kinetic momentum operator and a spin resulting kinetic momentum operator. We can show, relatively simply [Cag 71, Mol 81], that the energy levels from an electron configuration ( $\gamma$ ), under the influence of a perturbation  $H_{ee}$ , correspond to energy levels ( $E$ ) in the form  $E = E(\gamma, L, S)$ . For an atom with two peripheral electrons, respectively characterised by quantum numbers  $l_1$  and  $s_1$  for one, and  $l_2$  and  $s_2$  for the other,  $L$  and  $S$  are such that they vary by whole values in the Clebsch-Gordan series, so that  $L = l_1 - l_2 \dots \dots l_1 + l_2$  and  $S = s_1 - s_2 \dots \dots s_1 + s_2$ .

The electron states are, for their part, written using a wavefunction in the form  $|\gamma, L, S, M_L, M_S\rangle$ , in which  $M_L = -L, (-L + 1), \dots + L$  and  $M_S = -S, (-S + 1), \dots, +S$ , so that the energy levels are degenerated  $(2L + 1)(2S + 1)$  times.

The fundamental state is thus determined from Hund's rule which indicates that the lowest energy terms that for which:

- $S$  is the maximum (because from Pauli's principle, taking on the maximum spin implicates a distinction between states by their orbital states which must thus be different and minimises electrostatic interactions by distancing electrons); and
- $L$  is a maximum after taking into account the above condition.

The spectral terms, which relate to the different states, are thus denoted by an approximation  $n^{2S+1}T$ , where  $T$  is one of the letters  $S, P, D$  or  $F$  for which  $L$  takes on respectively to signify one of the values  $0, 1, 2, 3 \dots$ . If we take  $\text{Cr}^{+++}$  as an example, it has the configuration  $3d^3$ , and we find:

$$— S_{\max} = 3 \times \frac{1}{2} = \frac{3}{2}$$

— As  $l = 2$  (sub-layer d), we have  $m_l = -2, -1, 0, 1, 2$  and  $(\sum m_l)_{\max} = (M_L)_{\max} = 2 + 1 + 0 = 3$ , wherein  $L_{\max} = 3$ .

By consequence, the fundamental state of  $\text{Cr}^{+++}$  is  $3^4F$  (denoted simply as  $^4F$ ).

## 2 Perturbation involving the coupling energy between different magnetic moments exactly tied to kinetic moments

Two different cases can be distinguished:

### a when the spin orbit interaction energy is weak (typically for atoms with masses below that of mercury)

In this case we use *Russel-Saunders* coupling, which is generally considered to not be significant until we have coupled it up with, on one side, all the orbital kinetic moments and, on the other, the total spin kinetic moments. It is only after this that the two kinetic moments interact through the intermediate of spin orbit coupling.  $\vec{L}$  and  $\vec{S}$  represent the resultant of this total coupling. The perturbation Hamiltonian due to the spin-orbit coupling is in the form  $H_{S.O.} = \lambda(L, S)\vec{L}\cdot\vec{S}$  in which  $\lambda(L, S)$  is positive in the first half of the layer. With  $J = L + S \dots L - S$ , there is a rise on the degeneration of the energy levels which is given by the proper values of the perturbation Hamiltonian  $H_{S.O.}$ :

$$\Delta E = \frac{\lambda(L, S)\hbar^2}{2} [J(J + 1) - L(L + 1) - S(S + 1)].$$

The spectral terms are thus denoted  $n^{2S+1}T_J$ , in which T corresponds, as above indicated, to the letters S, P, D and F which as values of L are, respectively, 0, 1, 2, 3... The upper left indice gives the number of possible orientations of the resulting spin, and is called the multiplicity of the term (doublet, triplet and so on), however, one needs to be prudent in using this notation. If  $S < L$ , then J takes on  $2S + 1$  and the number of values for J is given by the upper left indice, however, if  $S > L$ , then J cannot be negative and can only take  $2L + 1$  values and therefore there are only  $2L + 1$  permitted levels.

In the case of Russel-Saunders coupling (also termed L – S coupling), the schematic representation of increments in degeneration of energy levels under the influence of increasingly small perturbations are shown in Figure 3. For example, from the level  $L'S'$  degenerated  $[2L' + 1][2S' + 1]$  times (resulting from exact electron interactions, also called electron correlations) the spin orbit coupling is partially raises the degeneration so that  $J'$  takes on  $[2L' + 1]$  or  $[2S' + 1]$  values (denoted as the values  $J'_1, J'_2, J'_3$  in Figure 2).

### b Heavy atoms—*jj coupling*

When the spin and orbital kinetic moments of each electron are coupled in the first step (with the resultant kinetic moment  $j_i$  for the  $i$ th electron again obtained from

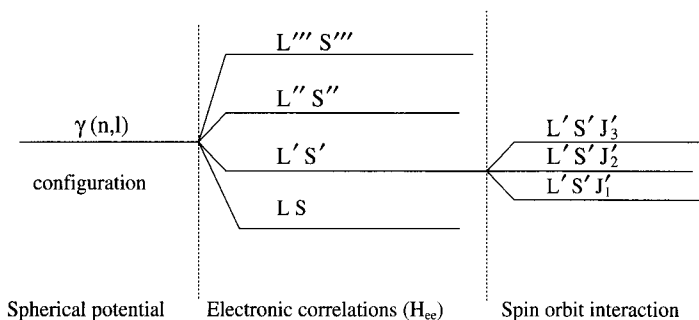


**Figure 2.** Levels of degeneration in L – S coupling.

terms of the Clebsch-Gordan series), the resultant kinetic moments of each electron are then coupled between each other (*jj* coupling) to yield a global moment  $J$ . For an atom with 2 electrons with kinetic moments  $j_1$  and  $j_2$ ,  $J$  takes on the values  $J = |j_1 - j_2|, \dots, j_1 + j_2$ .

### 3 Selection rules

There are two final cases to consider:

#### a Russel–Saunders coupling for light atoms with several electrons

The emission or absorption of light, which requires a variation by one unit of the kinetic moment, can happen when (selection rules):

- $\Delta S = 0$  and the optical wave does not affect the internal movement of the electrons;
- $\Delta L = \pm 1, 0$  with  $\Delta l = \pm 1$  ( $l$  is the kinetic moment of an electron which undergoes the transition, while  $L$  is the kinetic moment of the atom);
- $\Delta J = \pm 1, 0$ , however, the transition  $J = 0 \rightarrow 0$  is forbidden.

#### b *jj*-Coupling for heavy atoms with several electrons

The Russel–Saunders coupling selection rules are not applicable to heavy atoms with several electrons as the  $S$  and  $L$  quantum numbers no longer have any physical significance, as the effective *jj* coupling suppresses the coupling of orbital moments to give  $L$ , along with the coupling of spin kinetic moments which give  $S$ . In this eventuality, transitions between singlet and triplet states  $S = 0 \rightarrow S = 1$ , where  $\Delta S \neq 0$ , become possible (*jj* coupling for heavy atoms). However, the condition  $\Delta J = \pm 1, 0$  with the forbidden transition  $J = 0 \rightarrow 0$ , remains [page 372, Cag 71].



## Etching polymers with ion beams: characteristics and results

### I Level of pulverisation (Y)

#### 1 Definition

$$Y = \left( \frac{\text{Mean number of atoms ejected from target}}{\text{number of incident ions}} \right)_{\text{for a given } \Delta t}$$

In effect  $Y = f(E, J, \theta, M1, M2)$ , in which  $M2, E, J$  and  $\theta$  are, respectively, the mass of the target atom, the energy of the incident ions ( $M1$ ), the incident ionic current density and the angle between the incident ion beam and the normal to the target surface.

With:

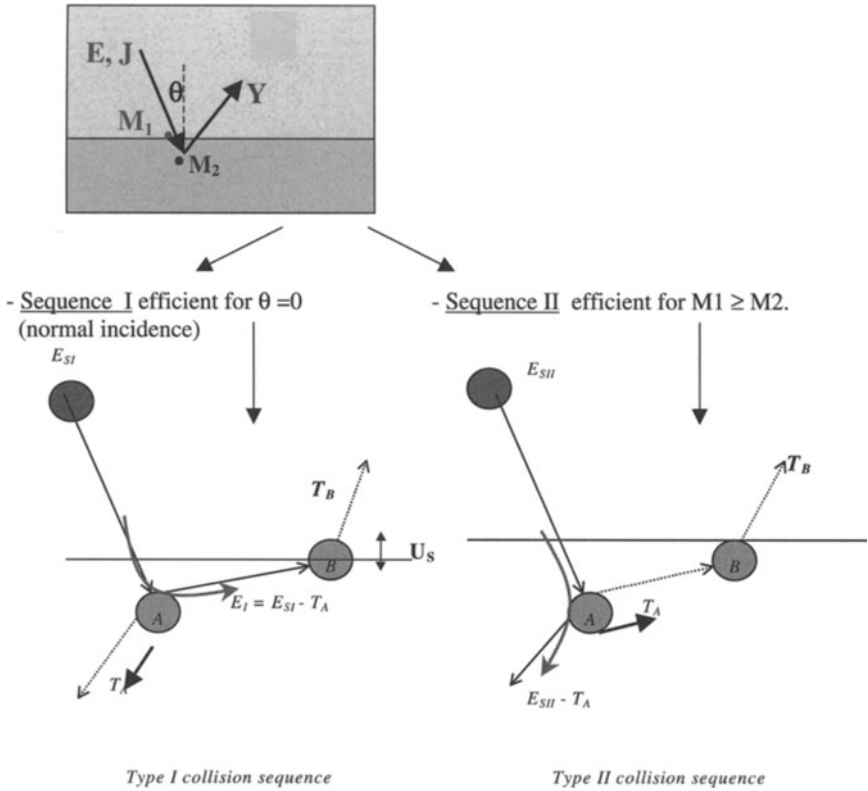
- the energy transmitted to B during a sequence of collisions ( $T_B$ );
- the energy of the surface bond ( $U_s$ ) reasonably estimated to be equal to the sublimation of the target, so around 5 to 10 eV,

the condition for ejecting an atom from the target is that  $T_B \geq U_s$ .

There are two possible sequences:

For the threshold energy, either  $E_{SI}$  for sequence I or  $E_{SII}$  for sequence II, and with the energy of displacement as  $E_d$ , and

$$\gamma = \frac{2M_1M_2}{(M_1 + M_2)^2},$$



it is possible to write that

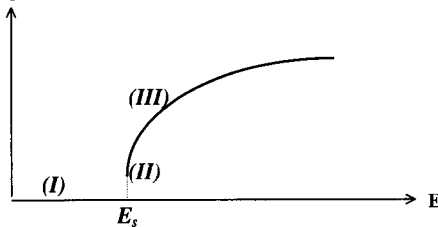
$$E_{SI} = \frac{U_S}{\frac{1}{2} (1 - \frac{1}{2}\gamma)}$$

and

$$E_{SII} = \frac{2}{\gamma} (2U_S + E_d)$$

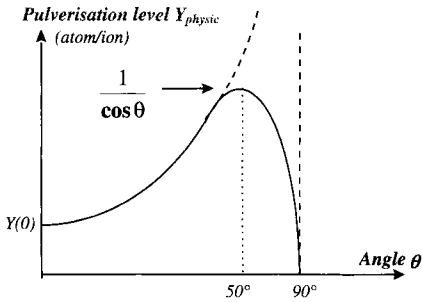
**2 The result  $Y_{\text{physical}} = f(E)$ : 3 zones**

$Y$  (pulverised atoms/incident ions)



I: below threshold ( $T_B \leq U_S$ );  
 II:  $E \approx E_s$  and threshold energy fixed by sequence type I or II ( $T_B \geq U_S$ ); and  
 III: when  $E > E_s$ , rapid increase in  $Y$ , then a saturation plateau (reached rapidly if mass  $M_1$  and  $M_2$  are greatly different).

**Analytical forms ( $Y_{\text{physical}}$ ):**



*Thomson:*

$$Y \propto \frac{N^{2/3}}{U_S} \frac{1}{1 + \frac{M_2}{M_1} \cos \theta}$$

(N: target atomic density)

*Sigmund:*  $Y(E, U_S) \propto S_N(E)/U_S$

$$Y(\theta) \propto \frac{1}{\cos^n \theta}$$

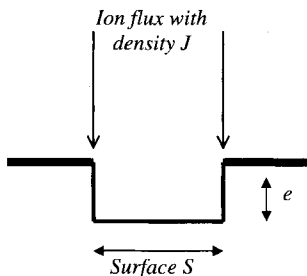
*Result* if  $M_1 \uparrow, Y \uparrow$ ; if  $\theta \uparrow, Y \uparrow$ :  
well verified when  $\theta < 60^\circ$ .

**3 Level of chemical pulverisation**

- When using RIBE or IBAE, we can write:  $Y_{\text{total}} = Y_{\text{physical}} + Y_{\text{chemical}}$
- If the projectile (P) forms with the target (T) a compound ( $T_aP_b$ ) which is volatile, then in general, we observe that  $Y_{\text{chemical}} \leq \frac{a}{b}$  and the sign  $\leq$  takes into account the reflection of particles and the re-pulverisation of implanted atoms;
- If P and T form a non-volatile compound  $T_aP_b$ , we observe a decrease in the velocity of attack on the target, so that  $Y_{\text{chemical}} \cong -\frac{b}{(a+b)} Y_{\text{physical}}$ ;
- When  $0.25 < E < 2.5$  keV, we tend to observe  $Y_{\text{chemical}} > \sqrt{E}$ ;
- It has been observed that  $Y_{\text{chemical}} \propto \cos \theta$ , so if  $\theta$  increases then  $Y_{\text{chemical}}$  decreases.

**II The relationship between etching speed and degree of pulverisation**

**1 At normal incidence**



If N is the atomic density of the target and the volume eroded is equal to  $S \times e$  (see Figure to left) then the number of atoms pulverised is  $N \times S \times e$ .

During time  $\Delta t$ , the number of ions incident to the surface S is equal to the flow of ions (D) multiplied by S.

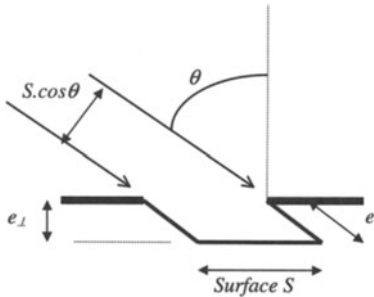
With  $D = \frac{J\Delta t}{q}$  in which q is the charge on mono-charged ions,

$$Y = \frac{NSE}{SJ\Delta t/q} = \frac{Nq}{J} \frac{e}{\Delta t} = \frac{Nq}{J} V.$$

With  $V = \frac{e}{\Delta t}$  we have the etching speed.

In addition, it is possible to write  $V = \frac{1}{Nq} YJ \propto YJ$ .

**2 At oblique incidence**



The number of atoms pulverised is equal to  $N \times S \times e \times \cos \theta$ .

During time  $\Delta t$ , the number of ions incident to the surface at S is equal to D multiplied by  $S \times \cos \theta$ .

The result is again  $Y = \frac{Nq}{J} \frac{e}{\Delta t}$ .

By defining

$$V(\theta) = \frac{e_{\perp}}{\Delta t} = \frac{e \cdot \cos \theta}{\Delta t},$$

we have:

$$Y(\theta) = \frac{Nq}{J} \frac{V(\theta)}{\cos}$$

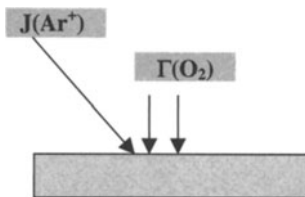
and we can also write:

$$V(\theta) = \frac{1}{Nq} Y(\theta) J \cos \theta \propto YJ.$$

Finally, we can always apply  $V \propto YJ$  when dealing with:

- non-reactive dry etching  $Y = Y_{\text{physical}}$ ;
- RIBE or IBAE in which  $Y = Y_{\text{total}} = Y_{\text{physical}} + Y_{\text{chemical}}$ .

**III Speed of reactive etching (IBAE  $\text{Ar}^+/\text{O}_2$  or  $\text{O}^+/\text{O}_2$ )**



Degree of resurfacing (or fraction of absorbed surface):  $\theta = \frac{N}{N^*}$ , in which N is the surface concentration of absorbed molecules and  $N^*$  is the surface concentration of absorption centres.

$\Gamma$  is the flux of  $\text{O}_2$  and J is the flux of incident ions, so the flux of O particles absorbed is  $2\Gamma\eta(1 - \theta)$  in which  $\eta$  is the probability of absorption for a molecule which hits an absorption centre.

The degree of O atoms pulverised consists of 2 terms:

- O atoms which have not reacted and is written  $\alpha\theta J$ , in which  $\alpha$  is the level of pulverisation of O atoms which have not reacted and  $\theta$  the degree of absorbed surface;
- O atoms which have reacted and is written  $\beta\theta J$ , in which  $\beta$  is the degree of reacted O atoms pulverised.

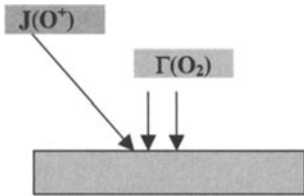
At equilibrium, the number of absorbed O atoms equals the number of pulverised O atoms and:  $2\Gamma\eta(1 - \theta) - (\alpha \cdot \theta \cdot J + \beta \cdot \theta \cdot J) = 0$ , so

$$\theta = \frac{1}{1 + \frac{\alpha + \beta}{2\eta} \left(\frac{J}{\Gamma}\right)} \quad \text{if } J \ll \Gamma, \theta = 1.$$

The etching speed is the sum of 2 components. One is physical and the other is chemical, each taking on the form  $Y \times J$  in which J is the flux of incident ions. For a unit surface ( $S = 1$ ) of a given substrate,  $\theta S = \theta$  takes on the chemical pulverisation while  $(1 - \theta)S = (1 - \theta)$  takes on the physical pulverisation.

Thus:

$$V \propto Y_{\text{chemical}}\theta J + Y_{\text{physical}}(1 - \theta)J$$



If the current of ions under study is  $O^+$ , we have to take into account the  $O^+$  ions which attach themselves to the outer atom layers to yield reaction products. If  $\gamma$  is the probability of an  $O^+$  ion being fixed (implantation does not bring into play a  $\theta$ -type coefficient for the absorbed surface), the contribution from the  $O^+$  ion beam to the resurfacing of the target with oxygen is  $2\gamma J$ .

The equilibrium equation becomes  $2\gamma J + 2\Gamma\eta(1 - \theta) - (\alpha \cdot \theta \cdot J + \beta \cdot \theta \cdot J) = 0$ .  
With

$$\Omega = \frac{\gamma}{\eta} \quad \text{and} \quad \Phi = \frac{\alpha + \beta}{2\eta},$$

we have

$$\theta = \frac{1 + \Omega \frac{J}{\Gamma}}{1 + \Phi \frac{J}{\Gamma}}$$

and retain:

$$V \propto Y_{\text{chemical}}\theta J + Y_{\text{physical}}(1 - \theta)J$$

If the reaction products are of the form  $XO_n$  (in which, for polymers X is principally carbon), the probability of desorption being  $\beta$  (through pulverisation), and the number of O atoms which carry away X atoms is  $1/n$ , then the level of pulverisation of X atoms is:  $Y_{\text{chemical}} = \beta/n$ .

From V we can deduce  $Y_{\text{chemical}}$ , if  $Y_{\text{physical}}$  is determined using an additional method, such as, for example, TRIM or empirically using a beam of  $Ar^+$  ions.

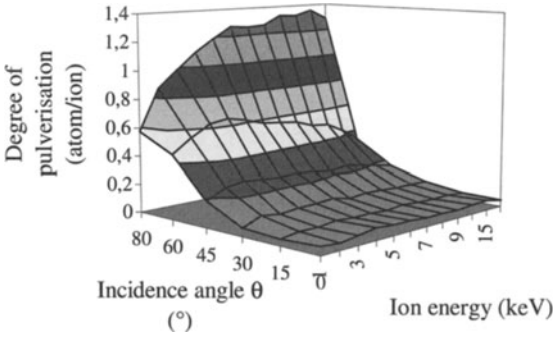
### IV Preliminary modelling of $Y_{\text{physical}}$ for PI 2566 (a polyimide commercialised by Dupont and dedicated to microelectronics)

For its use in microelectronics, PI2566 has a chemical formula which tends to favour etching, and can be used as an example to indicate typical etching parameters.

#### 1 Levels of carbon pulverisation using $O^+$ ions

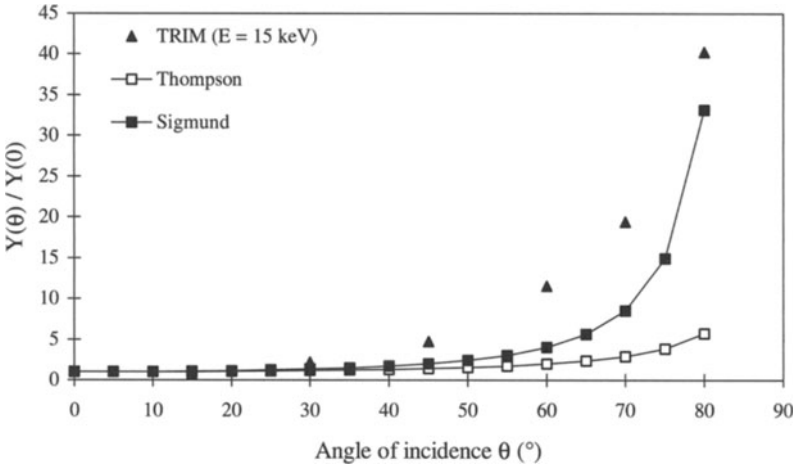
Here the calculation is made on the basis of the surface bond strength ( $U_S$ ) being 7.4 eV and with 2000 shots:

- the chemical effects are not taken into account, so here are only cascading collisions or rather, physical effects;
- the level of pulverisation is at a maximum when  $E \approx 11$  keV and  $\theta = 80^\circ$  ( $Y_{\text{max}} \approx 1.36$  atoms C/ion  $O^+$ ).



#### 2 Comparing simulations of $Y_{\text{physical}}(\theta) = f(\theta)$ and the Thompson and Sigmund models

The various models show good agreement with TRIM obtained results.



## V Results from etching of polyimides

### 1 Self-supporting polyimide: the UPILEX

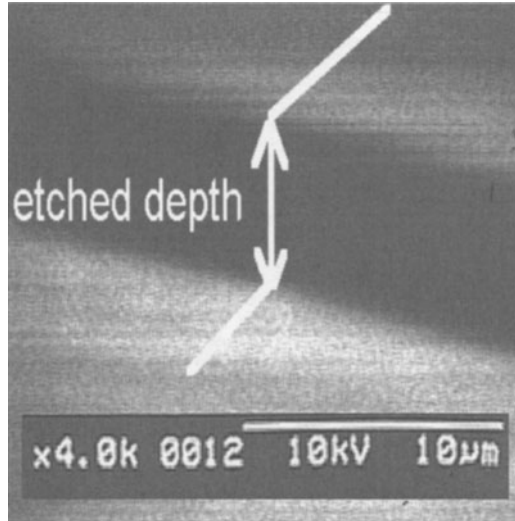
This material presents high losses in optical absorption most likely due to added plastifying agents.

#### a Etching conditions

The accelerating base energy was configured with the following optimised, and rather critical, parameters: (oxygen ions)  $E = 30 \text{ keV}$ ,  $D = 10^{17} \text{ ions cm}^{-2}$ ,  $J = 2 \text{ } \mu\text{A cm}^{-2}$ .

#### b Result

A reasonably good result was obtained in that an etching with depth  $4 \text{ } \mu\text{m}$  was realised.



#### c Nature of the etching

With  $\text{O}^+$  ions, there is no orientation effect from the beam (Sigmund or Thomson type laws are unverified for  $Y_{\text{physical}}$ ). With  $\text{Ar}^+$  ions, and the same ion beam parameters, etching to  $100 \text{ nm}$  only is possible. If  $D \geq 10^{17} \text{ ions cm}^{-2}$ , for  $\text{O}^+$ , the depth of the etching decreases and the polymer changes its appearance (due to a repeated depositing phenomenon).

## d Conclusion

Reactive etching due to oxygen chemical effects is extremely sensitive to the flow rate and can even greatly influence the structure of the polymer, determining whether or not etching can take place. This test material, developed for its electrical properties, is not particularly well suited to optical applications, due to its high absorbency. With fluorinated polyimides (for example Dupont's PI 2566), which are well suited to etching, more satisfying results were obtained (see Chapter XII, Section V).

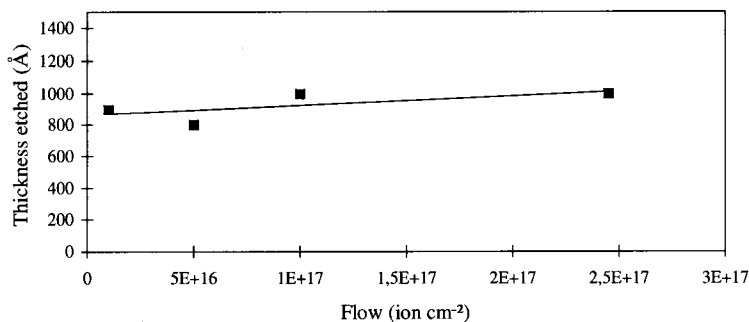
## 2 A study of the etching of PI 2566

### a Results from etching under accelerating conditions

The parameters used come from those optimised for Upilex.

*Nature of the ions*  $O^+$  was used with  $E = 30 \text{ keV}$ ,  $J = 2 \mu \text{ A cm}^{-2}$ , and the flow ( $D$ ) was varied. In contrast to Upilex, the depth of the etching was insensitive (more or less constant) and remained relatively poor at  $e \approx 90 \text{ nm}$ .

*Observation* At  $D > 2 \times 10^{17} \text{ ions cm}^{-2}$ , the polyimide was degraded and could not be measured. Bubbles appeared due to strong local heating.

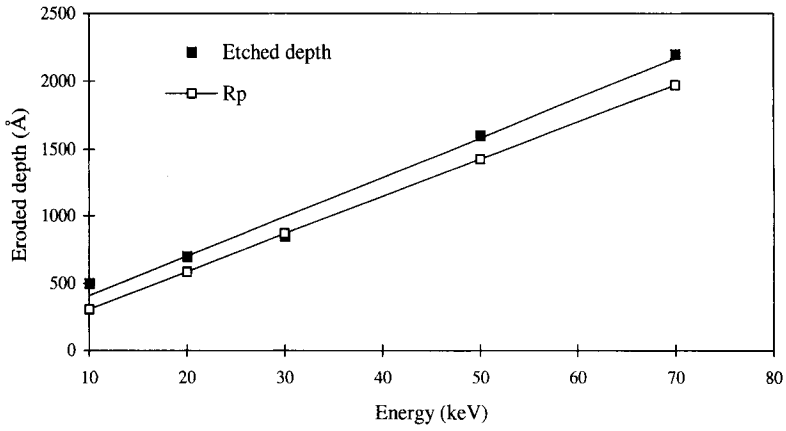


### b Why?

With  $O^+$  ions, and also with  $Ar^+$  or  $He^+$  ions, a study of the effect of energy shows that  $e \approx R_p$  (see Figure below). In addition, under the ion beam the polyimide is very fragile and there is a formation, from the start of the irradiation (at  $E > 10 \text{ keV}$ ) of a hard layer with  $e \approx R_p$  (due to  $C = C$  and  $C = O$  bond ruptures and in consequence reticulation and contraction of the polyimide leading to  $e = Cte$ ) which:

- limits (blocks) physical pulverisation ( $e \approx \text{constant}$  while  $D$  increases); and
- decreases the reactive polymer component in the polymer, which becomes just a thick carbonised layer.





### c Conclusion

These results indicate the importance of keeping close to the RIE parameters (with an increase in  $J$  and a decrease in  $E$  which is of the order of only a few keV). Results obtained using parameters close to the RIE are detailed in Chapter XII, Section V.

## **An *aide-mémoire* on dielectrics: a model for double potential well and its application in determining the depth of trap levels**

### **I Definitions of various dielectric permittivities [And 66] and the classification of different dielectric phenomena [Fre 60]**

#### **1 Absolute permittivity**

Generally, absolute permittivity ( $\epsilon$ ) of an isotropic, dielectric material is defined as a quotient of an electrical induction formed by an electric field, so  $\epsilon = \frac{D}{E}$ . If we consider a charge ( $Q$ ) caused by a potential difference ( $V$ ) between the arms of a flat capacitor with surfaces  $S$  placed at a known distance ( $d$ ) apart, the preceding ratio can be formed as:

$$\epsilon = \frac{\sigma_{\text{real}}}{E} = \frac{Q/S}{V/d} = \frac{Cd}{S},$$

in which  $C$  is the capacitance. By consequence, in the meter, kilogram and second (MKS) system, the absolute permittivity can be expressed in  $F\ m^{-1}$ . If the system under study is a vacuum, then the vacuum permittivity ( $\epsilon_0$ ) is  $\epsilon_0 = \frac{1}{36\pi} 10^{-9} F\ m^{-1}$  under MKS conditions, while in a centimeter, gram and second (cgs) system,  $\epsilon_0 = 1$ .

#### **2 Relative permittivity**

It is often practical to introduce the term relative permittivity ( $\epsilon_r$ ), which is also simply called, in an abuse of terms, permittivity. It is defined by the relationship  $\epsilon = \epsilon_r \epsilon_0$  in which  $\epsilon_r$  is a number without dimension and equal in the ues system to absolute permittivity (or the dielectric constant), which explains the often encountered confusion between these two parameters.

When an alternating tension ( $V = V_0 e^{j\omega t}$ ) is applied to the flat condenser, which has a capacity  $C_0$  when with an empty dielectric, the current which flows between the two plates on inserting a perfect dielectric (does not exhibit a leakage current) with permittivity  $\epsilon_r$  can be written as

$$I^* = \frac{dQ}{dt}. \text{ With } Q = CV = \epsilon_r C_0 V_0 e^{j\omega t} \text{ we have } I^* = j\omega \epsilon_r C_0 V.$$

### 3 Complex relative permittivity

As usual, in reality, the dielectrics in use are not perfect. They exhibit various sorts of currents, which we shall not detail for the moment, but give rise to a variety of similar effects. (Suffice to say that the effects of ‘free’ or ‘bonded’ carriers can give rise to heating effects or dielectric ‘losses’). Such a current flow is entirely due to the dielectric material and we can characterise it with an imaginary component of the relative permittivity in the expression  $\epsilon_r^* = \epsilon_r' - j\epsilon_r''$ . In order to simplify the notation, the indices ‘r’ are often left out, and the reader is left to understand whether the system under study is working in relative or absolute permittivities.

The intensity of the current thus becomes:

$$I^* = \omega\epsilon_r''C_0V + j\omega\epsilon_r'C_0V = I_R + jI_C$$

The second term corresponds to a dephasing of  $\frac{\pi}{2}$  between the tension and the purely capacitor based current.  $\epsilon_r'$  Characterises therefore the capacitor (insulator) part of the dielectric. The first term, relating to the fact that V and the intensity are in phase, corresponds to the resistive quality of the dielectric and is thus characterised by  $\epsilon_r''$ .

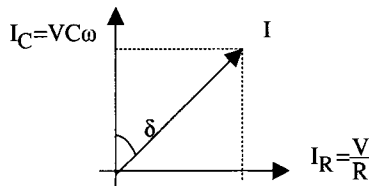
The power dissipated by the Joule effect is thus written:

$$P_J = \frac{1}{2}V_0I_0 = \frac{1}{2}C_0\epsilon_r''\omega V_0^2;$$

and the quantity  $\epsilon_r''$  is called the dielectric absorption as it intervenes in the expression for the conversion of electrical energy to heat in the medium, thus absorbed by the dielectric and lost to the electrical circuit.

$$\text{The quantity } \tan \delta = \frac{|i_R|}{|i_C|} = \frac{\omega\epsilon_r''C_0V}{\omega\epsilon_r'C_0V} = \frac{\epsilon_r''}{\epsilon_r'}$$

is the (dielectric) loss tangent and allows a definition of the loss angle ( $\delta$ ), which translates the dephasing between the resulting current and the ‘ideal capacitor’ part ( $I_C$ ) of the current.



The quantity  $Q = \frac{1}{\tan \delta}$  is a quality factor of the capacitor and is as large as  $\tan \delta$  is small.

### 4 Limited permittivities

$\epsilon_s$  is defined as the limiting (occasionally relative) permittivity obtained at low frequencies (the indice ‘r’ is removed by convention). At zero frequency we have a static field and  $\epsilon_\infty$  is the (relative) limiting permittivity at very high frequencies (infinite frequency).

## 5 Dielectric conductivity

On taking the expressions  $E = V/d$  and  $C_0 = \epsilon_0 S/d$  into  $I^*$ ,

$$I^* = \omega \epsilon_r'' \epsilon_0 \frac{S}{d} Ed + j \omega \epsilon_r' \epsilon_0 \frac{S}{d} Ed.$$

With  $J = \sigma E$  and  $I = \iint J \, dS = JS$ , we can go on to the complex relation:

$$\sigma^* = \frac{J}{E} = \frac{I^*}{ES} = \omega \epsilon_0 \epsilon_r'' + j \omega \epsilon_0 \epsilon_r'.$$

The real component for conductivity, called here the dielectric conductivity, is thus  $\sigma_d = \omega \epsilon_0 \epsilon_r''$ .

## 6 Classification of divers dielectric phenomena [Fre 60]

As already noted, the introduction of an imaginary term ( $\epsilon''$ ) into the dielectric permittivity, to take into account the existence of a current in phase with the applied tension, makes no presumptions about the origin of this current, whether how it is conducted or what losses may occur. In fact, there are numerous possible origins of this dielectric absorption and we can class them, schematically, with respect to the frequency or temperature domain in which they appear:

- I absorption due to free carriers, for example, thermally generated carriers in the permitted band which exhibit a very low density ion insulators due to the limiting large forbidden band in these materials, or ions which permit ionic conduction at low frequencies;
- II the Maxwell–Wagner effect, due to charge accumulation in the discontinuities of the dielectric, found most notably in powders;
- III the dipolar Debye absorption which is caused by bonded tied carriers and electrical dipoles;
- IV anomalies in  $\epsilon'$  and  $\epsilon''$  due to orientations of foreign molecules such as water at the solid surface;
- V anomalies in  $\epsilon'$  and  $\epsilon''$  tied with changes in phase; and
- VI absorption due to resonance.

Finally we present the Freymann representation [Fre 60] in Figure 1 below. Here the parameters of frequency and temperature are coupled. For a classical representation of  $\epsilon'$  and  $\epsilon''$  with respect to frequency only, we can turn to a textbook on electromagnetism, for example [May 96] or [Per 96].

Phenomenon I is due to a leak current resulting only from free charges, the number of which can be increased introducing impurities (such as ZnS, CdS doped with copper in analogy with semiconductors) into the dielectric. This results in an insertion of trap levels into the large forbidden band of the dielectric. Under a sufficiently high field, their electrons can attain a sufficiently high enough energy to collide with the lattice and provoke ionisations of the atoms. The upshot of this is that electrons are

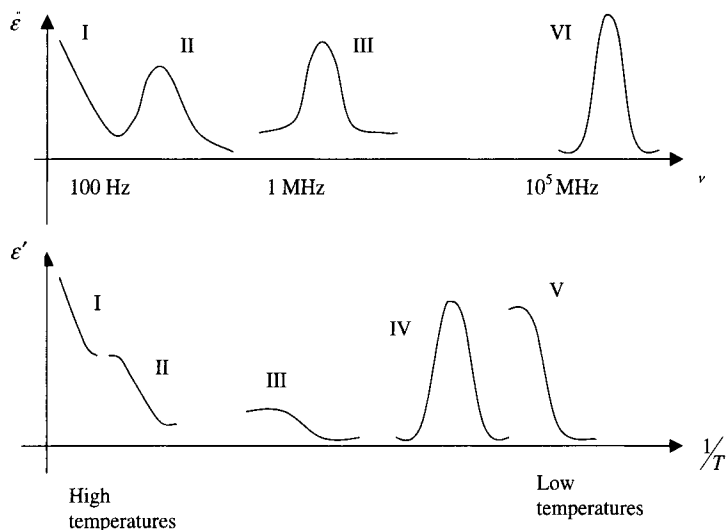


**Figure 1.** Representation of  $\epsilon'$  and  $\epsilon''$  as a function of  $1/T$ .

advantageously ejected into the conduction band to produce what is commonly known as a intrinsic breakdown of the dielectric.

Phenomenon II is due to an accumulation of charges, such as electrons, in discontinuous regions within the dielectric. We can treat this problem as though studying a condenser made of several dielectric layers.

Phenomenon III, otherwise known as a Debye dipolar absorption (DDA) generally results from the presence of neighbouring + and - charges (dipoles) which are linked so as to be indissoluble, and act as pairs of tied carriers. The phenomenon is due to dielectric relaxations associated with the orientation of these dipoles once submitted to an electric field. The orientation occurs after a certain delay, characterised by a relaxation time. The dipoles exhibit a dephasing due to the inertia of their orientation with respect to viscous brushing against the rest of the material. We shall show in the following Section 2 how the hopping of a single charge over a potential barrier can be analysed following this sort of relaxation.

Phenomenon IV can relate to a surface conductivity of the insulator, caused by 'semiconductors' such as dust, soilings and so on deposited on the insulator. This can also include surface humidity—impure water is a conductor with an extremely elevated dielectric constant of around 80. It is for this reason that the surface of a dielectric must be carefully cleaned prior to being studied. A usual methodology is to use alcohol first, to remove the humidity, and then a non-polar solvent such as benzene or toluene to remove the polar molecules, which could otherwise disturb the characterisation. And then of course, to work, if possible, in a dry atmosphere.

Phenomenon V relates to an evolution in  $\epsilon'$  with changes in the dielectric density, caused by changes in phase, and above all, when the dielectric is a polar material, a degree of blocking of the dipoles in a new phase, for example when going from

the liquid to solid state. This mechanism can be accompanied by dipole ‘frictions’ between the dipoles and their environments giving rise to a heating effect in the dielectric which can be comparable to that due to a current.

Phenomenon VI can be explained by considering that the charges of a dipole are elastically tied to an equilibrium position (in the simplest cases they can be compared to harmonic oscillators). Following the suppression of a field which displaced these dipoles from their equilibrium positions, they return to the equilibrium with a series of oscillations which display an amplitude which decreases as quickly as the breaking forces are strong. This model directly permits the possibility of an absorption due to resonance, which has a maximum at a characteristic alternating field frequency.

## II Relaxation of a charge occupying two position separated by a potential barrier: dielectric model for double potential wells and its application to trap levels

### 1 *Aide-mémoire* (see also Chapter IX, Section VII-2)

The existence of trap levels in solids was demonstrated during the study of optical processes in semiconductors of groups II–VI. As an example we can take the spread of electronic levels in an inorganic phosphor such as ZnS(Cu), shown in Figure 2 and resembling that in Figure IX-14.

Phosphorescence is due to a radiative emission which occurs with a delay after the initial luminous excitation, which excites electrons towards the conduction band (CB). The delay is caused by the passage of the same electrons, excited into the CB, through intermediates levels, called traps, in the forbidden band (FB). The relaxation from these traps is not instantaneous, thus the delay in the luminous emission and the persistence of phosphorescence, and occurs with a probability given by the Mott, Randall and Wilkins law, which states  $p = v_0 \exp(-U/kT)$ , where  $v_0$  is a constant for a group of traps. We can write  $\tau = 1/p$  to detail the average trapping lifetime [Cur 60]. In contrast, fluorescence, caused by an instantaneous emission, results from an electron which does not pass through these intermediate trap levels.

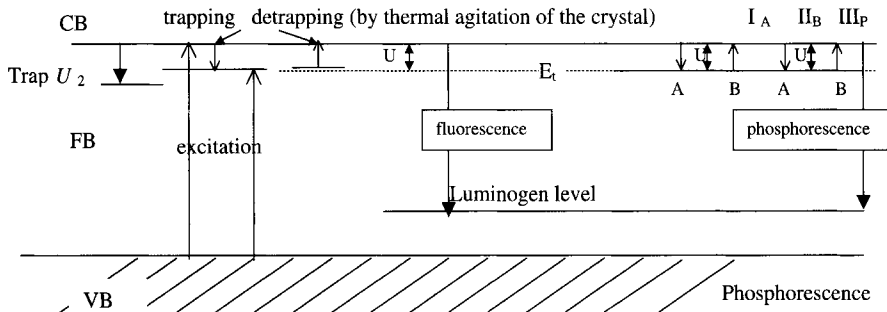


Figure 2.

Physically speaking we can characterise phosphorescence with respect to a thermal energy ( $kT$ )—loaned by phonons—which is involved in the transit of electrons trapped at an energy level A (the transition  $I_A$ ) towards another position with energy B by overcoming a potential barrier of height  $U$  (the transition  $II_B$ ). The barrier corresponds to a trapping level  $E_t$  with respect to the lowest part of the conduction band. Together, the transitions  $I_A$ ,  $II_B$ , and eventually,  $III_P$ , make up the mechanism of phosphorescence. In addition, different trapping levels can exist, so we can have  $U$ ,  $U_2$  and so on.

## 2 Transportation in a dielectric with trapping levels, and the effect of an electric field on transitions between trap levels

### a In the absence of an electric field

Here we shall look at an electron with two possible equilibrium positions (A and B) separated by a distance  $a$  and a barrier  $U$  (assumed to be considerably greater than  $kT$ ). The electron has as much chance of being found in A as in B, and the overall situation can be represented by a model of two potential wells separated by  $U$ , as in Figure 2-a.

The probability per unit time for the electron to hop from A to B (and reciprocally from B to A) is given by  $P_0 \exp(-U/kT)$ , where  $P_0$  represents the same probability when the barrier is zero (*i.e.* when  $U = 0$ ). At equilibrium, with  $N$  electrons per unit volume, all electrons of this type are equally spread between the two sites and the mean polarisation, due to these electrons, is zero.

### b When an electric field ( $\vec{E}$ ) is applied in the sense AB (dielectrical measurements)

The potential energies  $U_A$  and  $U_B$  of an electron (of charge  $-q$ ) differ by the quantity  $U_A - U_B = qaE$ . Given the orientation of the field, we have  $V_A < V_B$ , and by consequence (with  $U = -qV$ )  $U_A$  is above  $U_B$  by a quantity  $qaE$ , if the origin of the potential is taken as being at B (as in Figure 3-b). The symmetry of the system is thus broken, implicating a probability of presence of the electron being higher at B

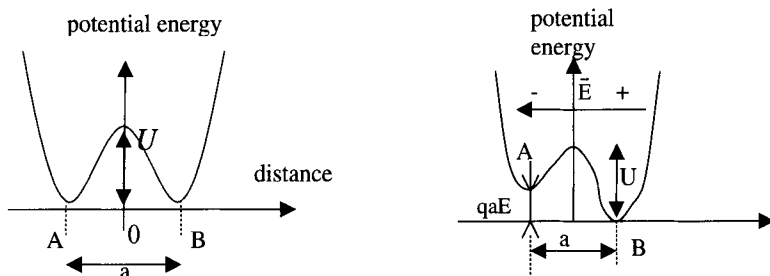


Figure 3.

than at A, if we take into account the Boltzmann function which is proportional to  $\exp(-U/kT)$ .

### c Expression for probability of transfer between wells

*α Calculation of transition probabilities* Initially we assume that the electrons oscillate (with their thermal energy) about their equilibria positions with a frequency  $\omega_0/2\pi$ . In the absence of a barrier, the probability that an electron will transfer from A to B or from B to A, in one second, is thus  $\omega_0/2\pi = P_0$ . With a barrier of height  $(U - qaE)$  on the A side and  $U$  on the B side, and in the presence of an electric field, these transition probabilities, respectively,  $P_{AB}$  and  $P_{BA}$ , become:

$$P_{AB} = \frac{\omega_0}{2\pi} \exp\left(-\frac{U - qaE}{kT}\right) \quad \text{and} \quad P_{BA} = \frac{\omega_0}{2\pi} \exp\left(-\frac{U}{kT}\right). \quad (1')$$

If we suppose that  $qaE \ll kT$ , which typically is true for dielectric measurements taken under weak fields around  $1 \text{ V cm}^{-1}$ ), we can go on to write:

$$P_{AB} = \frac{\omega_0}{2\pi} e^{-U/kT} \left(1 + \frac{qaE}{kT}\right) = P_{BA} \left(1 + \frac{qaE}{kT}\right). \quad (1)$$

*β Variation in the number of particles in the A and B states at an instant t* If at the instant  $t$  there are  $N_A$  electrons in A and  $N_B$  electrons in B, then there are  $N_A P_{AB}$  electrons which undergo the transition  $A \rightarrow B$  and  $N_B P_{BA}$  electrons which undergo the transition  $B \rightarrow A$ , so that:

$$\frac{dN_A}{dt} = -N_A P_{AB} + N_B P_{BA} \quad \text{and} \quad \frac{dN_B}{dt} = N_A P_{AB} - N_B P_{BA}. \quad (2')$$

On taking the difference between the above two equations and given that  $N = N_A + N_B$  is a constant and equal to the total number of electrons, then

$$\frac{d(N_B - N_A)}{dt} = -(P_{BA} + P_{AB})(N_B - N_A) + (P_{AB} - P_{BA})N. \quad (2)$$

On using eqn (1),

$$P_{AB} + P_{BA} \approx 2P_{BA} \left(1 + \frac{qaE}{2kT}\right) \approx 2P_{BA} \quad (3)$$

and

$$P_{AB} - P_{BA} \approx \frac{qaE}{kT} P_{BA}. \quad (4)$$

Moving eqns (3) and (4) into eqn (2) yields:

$$\frac{d(N_B - N_A)}{dt} = -2P_{BA}(N_B - N_A) + 2P_{BA} \frac{qaE}{2kT} N.$$

The integration of this differential equation, without a second member yields:

$$N_B - N_A = C \exp(-2P_{BA}t).$$



And moving this into the differential equation, while varying the constant C, gives:

$$C = \frac{qaE}{2kT} N \exp(2P_{BA}t) + K$$

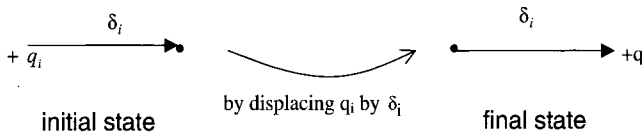
By using the limiting conditions which are that at  $t = 0, N_A = N_B = N/2$ , determines that  $K = -\frac{qaE}{2kT}N$ , from which can be derived that:

$$N_B - N_A = \frac{N}{2} \frac{qaE}{kT} (1 - \exp[-2P_{BA}t]). \tag{5}$$

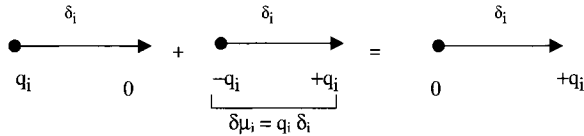
### 3 Expression for the polarisation at an instant t following the displacement of electrons

#### a General case for displacement $\delta_i$ in a system of $q_i$ charges at a concentration $n_i$

Moving the charge  $q_i$  by  $\delta_i$  is the same as superimposing a dipole  $\delta\mu_i = q_i\delta_i$  on the initial state. Schematically:



To arrive at the final state from the initial, it suffices to superimpose on the latter a dipole  $\delta\mu_i = q_i\delta_i$ , as shown in the scheme below:



Similarly we can consider that the displacement of the charge  $q_i$  by  $\delta_i$  is the same as applying a dipole  $\delta\mu_i = q_i\delta_i$ . The polarisation (dipole moment per unit volume) associated with the displacement of charges  $q_i$  by  $\delta_i$  is the same as applying a dipole moment per unit volume equal to  $P_i = n_iq_i\delta_i$ , where  $n_i$  is the number of charges  $q_i$  per unit volume.

If there are other (i) types of charges ( $q_i$ ) present, then the polarisation is thus

$$P = \sum_i P_i = \sum_i n_iq_i\delta_i.$$

#### b Polarisation due to the displacement of N electrons—per unit volume—shared over a pair of wells with initial potential depth of U

The two wells are separated by a distance a and, at an initial instant  $t = 0$ , are equivalent so that  $N_A = N_B = N/2$ . Under the influence of a field E, the electronic charges

(-q) are displaced by a distance +a for those in A and a distance -a for those in b, so:

$$\begin{aligned} P &= \sum_i n_i q_i \delta_i = N_A(-q)(+a) + N_B(-q)(-a) \\ &= N_B qa - N_A qa = qa(N_B - N_A) \end{aligned} \quad (6)$$

Finally, on moving eqn (5) for  $(N_B - N_A)$  into (6) we acquire:

$$P = \frac{N q^2 a^2 E}{2 kT} (1 - \exp[-2P_{BA}t]). \quad (7)$$

#### 4 Practical determination of potential well depths

##### a Basic formula

Following on from eqn (7), if  $t \rightarrow \infty$ ,  $P \rightarrow P_s$  (static polarisation) we have:

$$P_s = \frac{N q^2 a^2 E}{2 kT}. \quad (7')$$

The term  $\exp(-2P_{BA}t)$  from eqn (7) describes the transitory regime of electrons trapped in potential wells and delayed (dephased) with respect to the applied field. As this varies exponentially with time, the relaxation of the system can be characterised by a macroscopic relaxation function:  $Y(t) = \exp(-t/\tau)$ .

The model for two potential wells thus can be seen in terms of a relaxation, much like that found in Debye's theory, which yields similar equations for dielectrics (Debye's equations). The equivalence of the two terms obtained from the two well model and in Debye's theory (where  $Y(t) = \exp(-t/\tau)$  as has been detailed elsewhere [Jeo 01]), yields:

$$\exp(-2P_{BA}t) = \exp\left(-\frac{t}{\tau}\right), \quad \text{with } \tau = \frac{1}{2P_{BA}}.$$

With  $P_{BA}$  given by eqn (1'), we can deduce:

$$\tau = \frac{\pi}{\omega_0} e^{U/kT} = \tau_0 e^{U/kT} \quad (8)$$

*Comment* The term  $\tau_0 = \pi/\omega_0$  represents the duration of a single oscillation, as in the example  $A \rightarrow B \rightarrow A$ . In addition, as  $U \gg kT$ , we can find  $\tau \gg \tau_0$ .

The representation of the Debye curves shows us that  $\epsilon''$  goes through a maximum at a frequency  $\nu_c$  which is such that  $\omega_c \tau = 1$ . Taking into account eqn (8) for  $\tau$ , we thus have:

$$1 = 2\pi \nu_c \tau_0 e^{U/kT}, \quad \text{so that } \nu_c = \frac{1}{2\pi \tau_0} e^{-U/kT}.$$

In practical terms, the above formula is used in the form:

$$\text{Log } \nu_c = -\frac{U}{kT} - \text{Log } 2\pi \tau_0. \quad (9)$$

## b Empirical characterisation

Theoretically and as shown in Figure 4, we should obtain a straight line if we trace the logarithm of the critical frequency against inverse temperature. The slope of which should allow us to calculate the height of the potential barrier and the ordinance at the origin should yield the value of  $\tau_0$ . In practical terms, we can arrive at the values for  $\tau_0$  and, above all,  $U$ , as we have done below with the example of Alq3.

The law is in the form  $\nu_c = A \exp(-U/kT)$ , so that  $\text{Log } \nu_c = -U/kT + \text{Log } A$ .

For  $1/T = 0$ , we have  $\text{Log } \nu_c = \text{Log } A$ . The ordinance at the origin gives  $\text{Log } A$ , from which  $A = 1/2\pi\tau_0$ .

In addition, when  $T = T_0$  we have  $\text{Log } \nu_c = 0$ , so that  $1/T_0 = k/U \text{Log } A$  which permits a calculation for  $U$  using  $U = kT_0 \text{Log } A$ .  $U$  is in eV with  $k = 8.64 \times 10^{-5} \text{ eV K}^{-1} \text{ molecule}^{-1}$ .

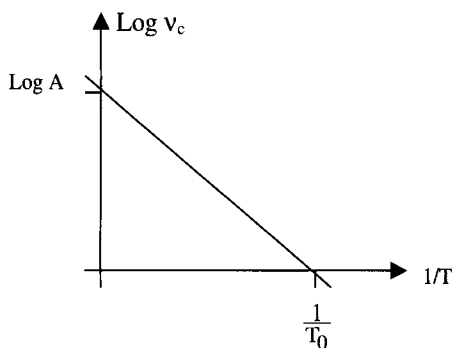


Figure 4.

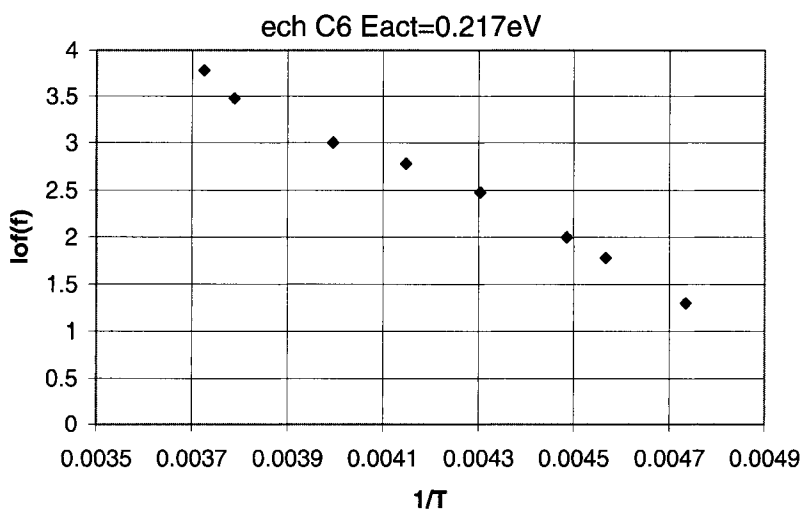


Figure 5.

**c Experimental representation using Alq3 [Jeo 01b]**

The result of empirical observations is shown in Figure 5, from which  $U = 0.217$  eV. This value is in good agreement with quantum chemistry calculations and thermoluminescence measurements.

## A-11

---

# The principal small molecules and polymers used in organic optoelectronics

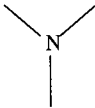
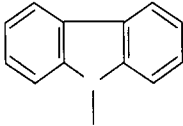
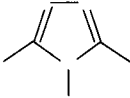
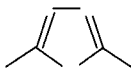
## I Chemical groups and electron transport

As indicated in Chapter X, a particular chemical group can be associated with a certain type of electron transport. As examples, the amine and carbazole functions favour p-type (hole) transport, while oxadiazole and triazole functions tend to favour n-type (electron) transport. Table I details their structures and characteristics. In general, metal based complexes act as electrons transporters.

## II Examples of polymers used for their electroluminescence

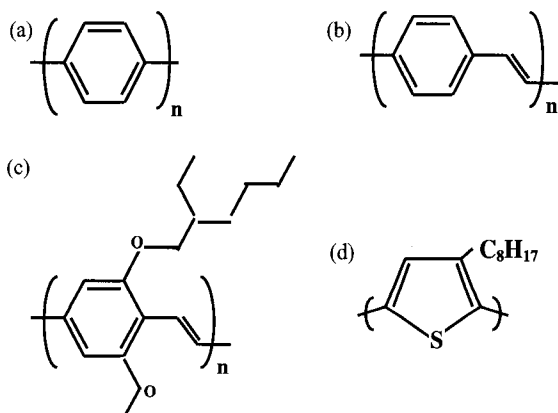
### 1 The principal emitting polymers

**Table 1.** Functional groups and their favoured electrical transport

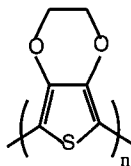
	Amine	Carbazole	Triazole	Oxadiazole
Functional group				
Conduction type	p	p	n	n
Example	TPD			PBD

**Table 2.** The principal polymer based emitters (note abbreviations are widely used)

Material	$\lambda_{\max}$ (nm)
fluorinated polyquinoline (PQ)	450
poly( <i>para</i> -phenylene) (PPP)	465
polyalkylfluorene	470
poly(3-cyclohexylthiophene) (PCHT)	555
poly( <i>para</i> -phenylene vinylene) (PPV)	565
poly[2-methoxy,5-(2'-ethyl-hexoxy)-1,4-phenylene vinylene] (MEH-PPV)	605
poly(3-octylthiophene) (P3OT)	690
poly(3-alkylthiophene) (P3AT)	690

**Figure 1.** (a) PPP monomer unit (the polymer emits in the blue part of the visible spectrum); (b) PPV monomer unit (exhibits yellow emission); (c) MEH-PPV monomer units (emission is yellow-orange); and (d) P3OT monomer unit (emits red light).

## 2 'The' polymer for hole injection layers (HIL)

**Figure 2.** The repeat unit of poly(3,4-ethylenedioxythiophene), which is often mixed with poly(styrene sulfonate), abbreviated commonly as PEDOT-PSS, to give an injection layer(HIL).

### 3 Example of a polymer used in hole transport layers (HTL)

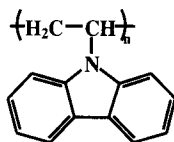


Figure 3. The repeat unit of poly(*N*-vinyl carbazole) (PVK).

### 4 Example of a polymer used in electron transport layer (ETL)

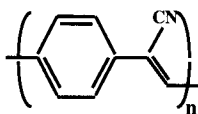
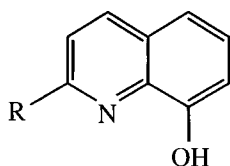


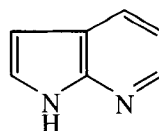
Figure 4. Repeat unit of CN-PPV.

## III Small molecules

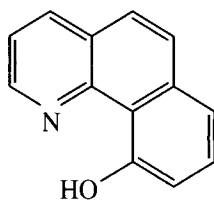
### 1 The principal green light emitting ligands



R = H : 8-hydroxyquinoline (q)  
R = CH<sub>3</sub> : 2-methyl-8-hydroxyquinoline (mq)



7-azaindole



10-hydroxybenzo[h]quinoline (Bq)

Figure 5. The structure of the principal ligands.

## 2 Principal electron transporting small molecules emitting green light

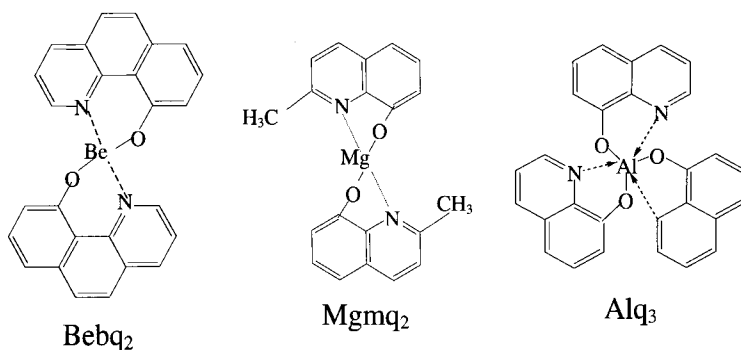


**Figure 6.** Structures of the molecules: beryllium bis(10-hydroxybenzo(h)quinolate) (Bebq<sub>2</sub>) ( $\lambda_{\text{photoluminescence}} = 529 \text{ nm}$ ); magnesium bis(2-methyl-8-hydroxyquinolate) (Mgmq<sub>2</sub>) ( $\lambda_{\text{photoluminescence}} = 487 \text{ nm}$ ); and aluminium tris(8-hydroxyquinolate) (Alq<sub>3</sub>) ( $\lambda_{\text{photoluminescence}} = 504 \text{ nm}$ ).

## 3 Example electron transporting small molecules emitting blue light

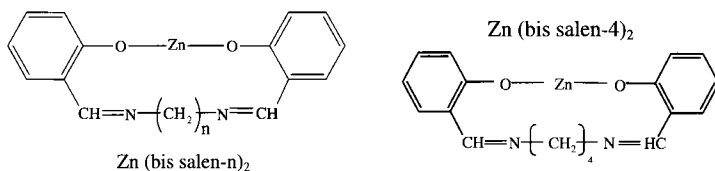


**Figure 7.** Structures of Zn (bis salen-n)<sub>2</sub> and the particular case of zinc bis(2-hydroxyylate-benzylideneamino) butane (Zn (bis salen-4)<sub>2</sub>), which displays  $\lambda_{\text{photoluminescence}} = 460 \text{ nm}$ .

## 4 Example small molecules which emit red light

Small molecules which emit red light are principally based on europium octahedral complexes in which ligands (L) derived from  $\beta$ -diketone or aminopyrazine saturate the co-ordination sphere of the lanthanide (M) along with phenanthroline,



or two electron donating molecules such as triphenylphosphine oxide or dibenzyl sulfoxide.

## 5 Examples of small molecules which serve principally as hole injection layers (HIL)

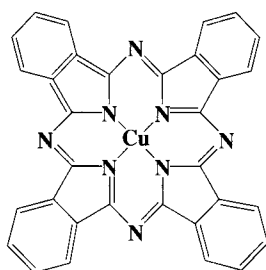


**Figure 8.** Structure of copper phthalocyanine (CuPc).

## 6 Examples of small molecules serving principally in hole transport layers (HTL)

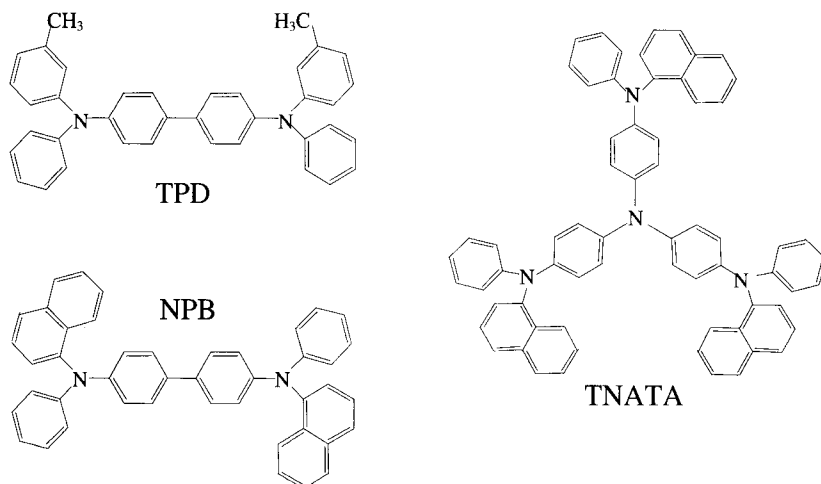


**Figure 9.** Structures of the molecules: *N,N'*-diphenyl-*N,N'*-(3-methylphenyl)-1,1'-biphenyl-4,4'-diamine (TPD); 4,4-bis[*N*-(1-naphthyl)-*N*-phenylamino]biphenyl (NPB); and 4,4',4''-tris[*N*-(1-naphthyl)-*N*-phenylamino]triphenylamine (TNATA).

**7 Example of a small molecule serving principally to confine holes in 'hole blocking layers' (HBL)**

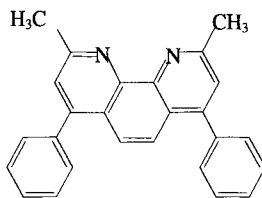


**Figure 10.** Structure of bathocupuroine (BCP).

## Mechanical generation of the second harmonic and the Pockels effect

### I Mechanical generation of the second harmonic (in 1-dimension)

#### 1 Preliminary remark: the effect of an intense optical field ( $E^\omega$ )

Non-linear effects occur when the force (with  $E = E^\omega$ ) returning displaced electrons towards their equilibrium position is no longer of the form  $f_r = -kx = -m\omega^2x$ . It is the Coulombic force developed by nuclei, which is exerted between nuclei and electrons, that gives this returning force. Typically, these internal electric fields are of the order of  $10^8$  to  $10^9$  V cm<sup>-1</sup>, while the optical field developed from several MW cm<sup>-2</sup> is only of the order of  $10^4$  V cm<sup>-1</sup>.

When the optical field is no longer negligible with respect to the internal field, for example on the use of a laser, the returning force must be rewritten in the form  $f_r = -kx + dx^2 = -m\omega^2x + m\delta^2x$ , and is thus privileged by an inharmonic potential ( $W$ , although commonly denoted by  $V$ ):

$$F = -\overrightarrow{\text{grad}} W = -\overrightarrow{\text{grad}} V \implies V = \frac{1}{2}kx^2 - \frac{1}{3}dx^3.$$

#### 2 Placing the problem into equations

The inharmonic potential, which takes on the form  $V(x) = \frac{1}{2}kx^2 - \frac{1}{3}dx^3$ , along with the corresponding returning force  $f_r = -kx + dx^2$  are schematised in Figure 1.

The response of the system, in terms of displacements, due to an optical excitation (electrical field  $E^\omega = E_0 \cos \omega t$ ) is governed by the fundamental dynamic law for which a displacement  $x(t)$  is formulated with respect to the various harmonic components.

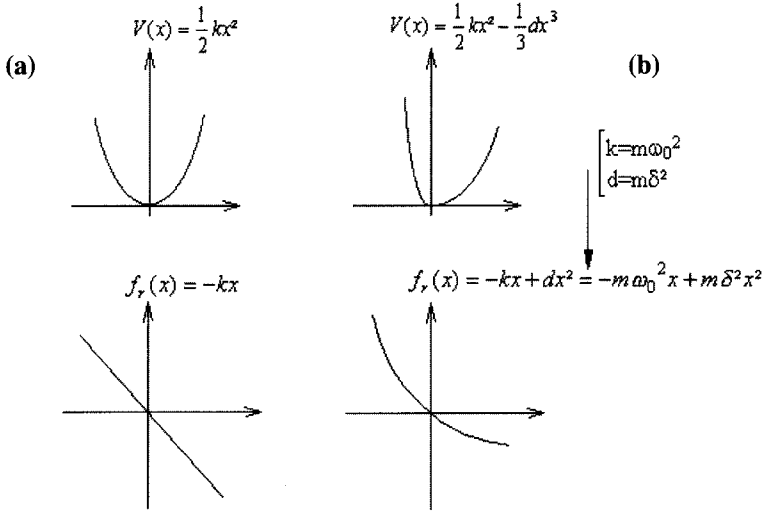


**Figure 1.** Representations of: (a) harmonic potentials; and (b) inharmonic potentials, each shown with their corresponding forces.

With the system being non-linear, we have to be prudent in using our habitual imaginary notation ( $E^\omega = \text{Re}(E_0 e^{j\omega t})$ ), and have to work always with real functions. On denoting the conjugated complex by  $cc$ , we have

$$E^\omega = E \cos \omega t = \frac{E}{2} (e^{j\omega t} + cc).$$

When we study the movement of electrons in a material using classical forms (in the linear regime with a returning force  $f_r = -kx$ ), we can bring in all the applied forces in the system, which include the Coulombic force  $f_c = q\bar{E}^\omega$ , in which  $q$  is the charge under study ( $q = -e$  for electrons), the friction force ( $f_t$ ), which is such that  $f_t = -m\Gamma v_x = -m\Gamma \dot{x}$ , and the returning force  $f_r = -kx$  (see, for example, Chapter 4 of [May 96]).

The same route can be used in non-linear regimes, although we must take on board the new expression for  $f_r$ , as in  $f_r = -kx + dx^2 = -m\omega_0^2 x + m\delta^2 x^2$ .

The fundamental equation for the dynamics with respect to  $x$  can thus be written as:  $m\ddot{x} = \sum F = f_r + f_t + f_c$ , so as to give, on simplifying with  $m$ :

$$\ddot{x} + \Gamma \dot{x} + \omega_0^2 x - \delta^2 x^2 = \frac{qE}{2} (e^{j\omega t} + cc). \tag{1}$$

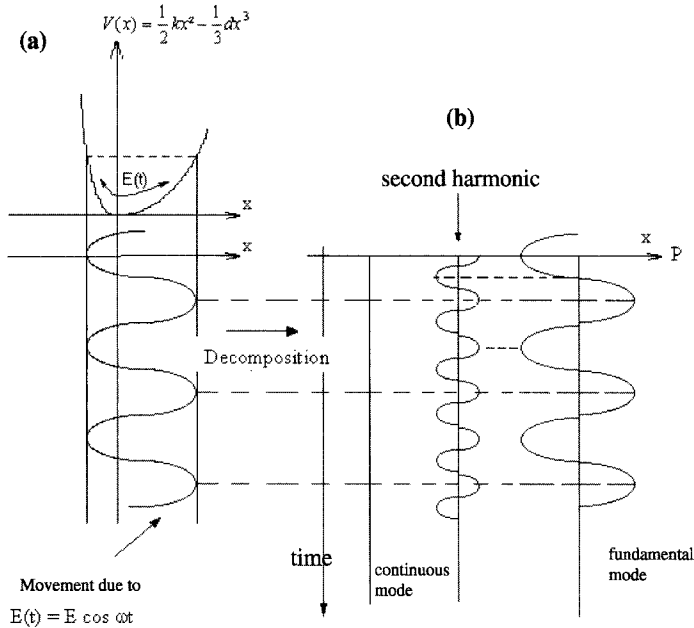


**Figure 2.** Displacement of a charge placed in an inharmonic potential (a) and its decomposition (b).

Under a permanent regime,  $x$  is thus sort after in a form which displays its development with respect to the harmonic components:

$$x(t) = \frac{1}{2} \left( x_0 + x_1 e^{i\omega t} + x_2 e^{i2\omega t} + \dots + cc \right). \quad (2)$$

To simplify the calculation we can take  $x_0 = 0$  (even if the term exists: see Chapter XII, Section III, studies therein).

The resolution of the problem is sadly through long, laborious calculations, which involve inserting eqn (2) for  $x(t)$  into eqn (1). The result is the startlingly long equation (3):

$$\begin{aligned} & -\frac{\omega^2}{2} \left( x_1 e^{i\omega t} + cc \right) - 2\omega^2 \left( x_2 e^{i\omega t} + cc \right) + \frac{i\omega\Gamma}{2} \left( x_1 e^{i\omega t} + cc \right) + i\omega\Gamma \left( x_2 e^{i\omega t} + cc \right) \\ & + \frac{\omega_0^2}{2} \left( x_1 e^{i2\omega t} + cc \right) + \frac{\omega_0^2}{2} \left( x_2 e^{i\omega t} + cc \right) + \frac{\omega_0^2}{2} \left( x_2 e^{i2\omega t} + cc \right) \\ & - \frac{\delta^2}{4} \left( x_1^2 e^{2i\omega t} + 2x_1 x_2^* e^{-i\omega t} + x_1 x_1^* + x_2 x_2^* + 2x_1 x_2 e^{3i\omega t} + x_2^2 e^{4i\omega t} + cc \right) \\ & = \frac{qE}{2m} \left( e^{i\omega t} + cc \right) \end{aligned} \quad (3)$$

### 3 Solving the problem

#### a First order terms (linear approximation)

Identifying the coefficient to the  $e^{i\omega t}$  terms in eqn (3) gives

$$x_1 = \frac{qE}{m} \frac{1}{(\omega_0^2 - \omega^2) + i\omega\Gamma} \approx \frac{qE}{2\omega m} \frac{1}{(\omega_0 - \omega) + i(\Gamma/2)}. \quad (4)$$

↑  
if resonating at  $\omega_0 = \omega$

The linear polarisation for a displacement  $x_1(t)$  of the charge  $q$  is thus

$$P^{(1)}(t) = Nqx_1(t) = Nq \frac{x_1}{2} (e^{i\omega t} + cc).$$

By identifying with

$$P^{(1)}(t) = \frac{P_0}{2} (\chi_1^{(\omega)} E e^{i\omega t} + cc),$$

we obtain

$$\chi_1^{(\omega)} = \frac{Nq}{m\epsilon_0} \frac{1}{(\omega_0^2 - \omega^2) + i\omega\Gamma} \quad (5)$$

(here of course we find again the expression for the dielectric susceptibility of a linear medium; see eqns (4–36) in [May 96]).

#### b Second order terms

In the same way as for the linear system, the identification of the coefficients for  $e^{i2\omega t}$  allows us to determine  $x_2$ , which is such that

$$x_2 \left( -4\omega^2 + 2i\omega\Gamma + \omega_0^2 \right) = \frac{\delta^2}{2} x_1^2.$$

We can thus see that it is the term in  $x_1^2$  (term  $dx^2$  in the relation  $f_r = -m\omega_0^2 x + m\delta^2 x^2 = -kx + dx^2$ ) which generates (forces) the movement in  $2\omega$ . On moving eqn (4) for  $x_1$  into our latter equation, we arrive at:

$$x_2 = \frac{q^2 \delta^2 E^2}{2m^2} \frac{1}{[(\omega_0^2 - \omega^2) + i\omega\Gamma]^2 [(\omega_0^2 - 4\omega^2) + 2i\omega\Gamma]}. \quad (6)$$

The second order susceptibility appears within the second order term of the polarisation, which is written by analogy to the linear polarisation as

$$P^{(2)}(t) = \frac{\epsilon_0}{2} \left[ \chi_2^{(2\omega)} E^2 e^{i2\omega t} + cc \right] = Nq \frac{x_2}{2} (e^{i2\omega t} + cc).$$

From which we can therefore deduce  $\chi_2^{(2\omega)}$ :

$$\chi_2^{(2\omega)} = \frac{Nq^3\delta^2}{2m^2\epsilon_0} \frac{1}{[(\omega_0^2 - \omega^2) + i\omega\Gamma]^2 [(\omega_0^2 - 4\omega^2) + 2i\omega\Gamma]}. \quad (7)$$

In a similar manner to  $\chi_1^{(\omega)}$ ,  $\chi_2^{(2\omega)}$  presents both real and imaginary parts but does, however, have a denominator which exhibits double resonance, as in  $\omega = \omega_0$  and  $\omega = \frac{\omega_0}{2}$ .

*Comment 1* Here the charge under consideration is that of an electron, i.e.  $q = -e$ , and thus  $q^3 = -e^3$ . We can thus rewrite eqn (7):

$$\chi_2^{(2\omega)} = -\frac{Ne^3\delta^2}{2m^2\epsilon_0} \frac{1}{[(\omega_0^2 - \omega^2) + i\omega\Gamma]^2 [(\omega_0^2 - 4\omega^2) + 2i\omega\Gamma]}. \quad (7')$$

*Comment 2* In addition, we can establish the following relationship between linear and non-linear susceptibilities, respectively,  $\chi_1^{(\omega)}$  and  $\chi_2^{(2\omega)}$ :

$$\frac{\chi_2^{(2\omega)}}{[\chi_1^{(\omega)}]^2 \chi_1^{(2\omega)} \epsilon_0^2} = \frac{m\delta^2}{2N^2q^3} = \xi^{(2\omega)}$$

The parameter  $\xi^{(2\omega)}$ , called Miller's paramter, is in fact practically identical for all materials:  $\xi^{(2\omega)} \cong 3$  to  $8 \times 10^9$  SI for InAs, GaSb, GaAs, CdTe, ZnTe and ZnSe.

*Comment 3* In this Section we have looked at the problem in one dimension only. If instead of considering an incident wave with only one component, we imagine that it presents three components, then the second order polarisation will have components  $P_x$ ,  $P_y$  and  $P_z$ , which generally can be obtained by using all possible quadratic components of  $E_x$ ,  $E_y$  and  $E_z$ , as in:

$$\begin{bmatrix} P_x \\ P_y \\ P_z \end{bmatrix} = \epsilon_0 \chi_2^{\equiv(2\omega)} \begin{bmatrix} E_x^2 \\ E_y^2 \\ E_z^2 \\ E_z E_y \\ E_z E_x \\ E_x E_y \end{bmatrix}, \text{ in which } \chi_2^{\equiv(2\omega)} \text{ is thus a tensor.}$$

## II Excitation using two pulses and the Pockels effect

### 1 Excitation from two pulses

While studying the mechanical generation of the second harmonic, we have shown, in a classical manner, that an excitation due to a photon ( $E^\omega$ ) can generate movements

with frequencies of  $\omega$  (movement  $x_1(t)$ ) and of  $2\omega$  (movement  $x_2(t)$ ). Respectively, photon emissions from charges which move through  $x_1$  (at a frequency  $\omega$ ) and through  $x_2$  (at a frequency  $2\omega$ ) do so by emitting dipolar rays at the frequencies  $\omega$  and  $2\omega$ .

We can thus generalise this emission mechanism for an excitation in a system of two photons with pulsations  $\omega'$  and  $\omega''$ . We should allow for the emission detailed the Figure 3:

For a system excited with a pulsation  $\omega$ , we can use the classic eqn (7) for the second order (relative) susceptibility as follows:

for an excitation pulse at  $\omega_i$ , given  $D(\omega_i) = \omega_0^2 - \omega_i^2 + i\omega_i\Gamma$ , eqn (7) becomes:

$$\chi_2^{(2\omega_i)} = \frac{Nq^3\delta^2}{2m^2\epsilon_0} \frac{1}{D^2(\omega_i)D(2\omega_i)}; \tag{8}$$

and, similarly, for a two wave excitation pulsating at  $\omega'$  and  $\omega''$ , the pulsation harmonic ( $\omega_T = \omega' + \omega''$ ) is associated with a second order susceptibility in the form:

$$\chi_2^{(\omega'+\omega'')} = \frac{Nq^3\delta^2}{2m^2\epsilon_0} \frac{1}{D(\omega')D(\omega'')D(\omega' + \omega'')} \tag{9}$$

### 2 The Pockels Effect

A particular case which draws interest is when there is an incident optical wave (with pulsation  $\omega' = \omega$ ) and a second wave at low frequency. At the limit zero, for a static field ( $\omega'' = 0$ ), the preceding eqn (9) becomes:

$$\chi_2^{(\omega+0)} = \frac{Nq^3\delta^2}{2m^2\epsilon_0} \frac{1}{D(0)D(\omega)D(\omega)} \tag{10}$$

This second order susceptibility depends only on the optical pulsation  $\omega$ . Nevertheless, a reduction to the single, varying polarisation term is inexact, as we shall see.

If we write the expression for the polarisation using the more usual development (see Chapter XII, Section III-2), we have  $P(t) = P_0 + \chi_{a1}E(t) + \chi_{a2}E^2(t) + \dots$ , in which here  $E(t) = E_{(0)} + E_{(\omega)}e^{j\omega t} + cc$  and where  $\chi_a$  is the absolute susceptibility, we can see that the dependence of the susceptibilities with two pulses

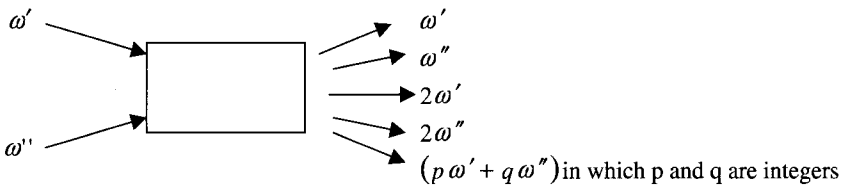


Figure 3. Possible emissions from a system excited by pulses at  $\omega'$  and  $\omega''$



(static and optical) involves some complications in the calculation. In fact, we end up writing that (with relative susceptibilities to the 1st and 2nd order of  $\chi_1$  and  $\chi_2$ )

$$P(t) = \varepsilon_0 \left\{ \chi_1 \left[ E_{(0)} + E_{(\omega)} e^{j\omega t} + cc \right] + \chi_2 \left[ E_{(0)} + E_{(\omega)} e^{j\omega t} + cc \right]^2 + \dots \right\} \quad (11)$$

We can quickly see that this description is completely ambiguous as, for example, the first term ( $\chi_1$ ) carries both the static term ( $E_{(0)}$ ) and the optical term ( $E_{(\omega)} e^{j\omega t}$ ). If we continue with the calculation, even given the previous remarks (and thus  $\chi_1 = \chi_1(0)$  or  $\chi_1 = \chi_1(\omega) \equiv \chi_1^{(\omega)}$  by notation) while limiting ourselves to the static term and the pulsation term  $\omega$ , we have:

$$\begin{aligned} P(t) &= \varepsilon_0 \left\{ \left[ \chi_1(0) E_{(0)} + \chi_1(\omega) E_{(\omega)} e^{j\omega t} \right] + \left[ \chi_2(0) E_{(0)}^2 + 2\chi_2(0 + \omega) \right. \right. \\ &\quad \left. \left. \times E_{(0)} E_{(\omega)} e^{j\omega t} \right] \right\} + \dots \\ &= \left\{ \varepsilon_0 \left[ \chi_1(0) + \chi_2(0) E_{(0)} \right] E_{(0)} \right\} + \left\{ \varepsilon_0 \left[ \chi_1(\omega) + 2\chi_2(0 + \omega) E_{(0)} \right] \right. \\ &\quad \left. \times E_{(\omega)} e^{j\omega t} \right\} + \dots, \end{aligned}$$

which gives a polarisation of the form:

$$P(t) = P_0 + P_{0+\omega}(t). \quad (12)$$

We can see here that the polarisation varying in  $\omega$  (the term  $P_{0+\omega}(t)$ ) depends on  $\omega_2(0 + \omega)$  and also on  $\chi_1(\omega)$ . A polarisation with frequency  $\omega$  is thus in the presence of  $E_{(0)}$ , so:

$$P_{0+\omega}(t) = \varepsilon_0 \left[ \chi_1(\omega) + 2\chi_2(0 + \omega) E_{(0)} \right] E_{(\omega)} e^{j\omega t}. \quad (13)$$

The indice  $0 + \omega$  for  $P_{0+\omega}(t)$  indicates that the polarisation is independent of  $\omega$  in the presence of the static wave  $E_{(0)}$  and the optical wave  $E_{(\omega)}$ . This polarisation is a linear function of  $E_{(\omega)} e^{j\omega t}$  although it is calculated in the presence of the static field  $E_{(0)}$ .

Additionally, in the absence of the static field  $E_{(0)}$ , we have as polarisation due to the pulse  $\omega$ ,  $P_{\omega}(t) = \varepsilon_0 (\varepsilon_{r(\omega)} - 1) E_{(\omega)} e^{j\omega t}$ . With  $(\varepsilon_{r(\omega)} - 1) = \chi_1(\omega) = n^2 - 1$ , in which  $n = n(E_{(0)} = 0) = n_{\omega}$  using the notations detailed in Chapter XII (Section IV-5) we can write  $P_{\omega}(t) = \varepsilon_0 (n^2 - 1) E_{(\omega)} e^{j\omega t} = \chi_1(\omega) E_{(\omega)} e^{j\omega t}$ .

If we now consider the expression which takes on this polarisation in the presence of a static field  $E_{(0)}$ , this supplementary polarisation changes the indice to the form  $n + \Delta n$ , and we find that

$$\begin{aligned} P(t) &= \varepsilon_0 \left[ (n + \Delta n)^2 - 1 \right] \left[ E_{(0)} + E_{(\omega)} e^{j\omega t} \right] \\ &= \varepsilon_0 \left[ (n + \Delta n)^2 - 1 \right] E_{(0)} + \varepsilon_0 \left[ (n + \Delta n)^2 - 1 \right] E_{(\omega)} e^{j\omega t} \\ &= P_0 + P_{0+\omega}(t) \end{aligned}$$

so that:

$$P_{0+\omega}(t) = \varepsilon_0 \left[ (n + \Delta n)^2 - 1 \right] E_{(\omega)} e^{j\omega t}. \quad (14)$$

By identification of  $P_{0+\omega}(t)$  in eqns (13) and (14), we obtain:

$[(n + \Delta n)^2 - 1] = [\chi_1(\omega) + 2\chi_2(0 + \omega)E_{(0)}]$ , so that with  $\chi_1(\omega) = n^2 - 1$  and  $[(n + \Delta n)^2 - 1] \approx n^2 + 2n\Delta n - 1$ . This gives us  $2n\Delta n = 2\chi_2(0 + \omega)E_{(0)}$ . And this we arrive at the definitive equation

$$\Delta n = \frac{\chi_2(0 + \omega)}{n} E_{(0)}. \quad (15)$$

The variations in the indice appear to be proportional to the applied field  $E_{(0)}$ . However, this qualitatively exact result for the dependence of  $\Delta n$  on  $E_{(0)}$  is very imprecise with respect to the function in  $n$  due to the presence of the term  $\chi_2(\omega + 0)$ , itself coming from the rather ambiguous eqn (11).

A more phenomenological and alternative method, which takes account of the dependence of the optical indice on the static polarisation field—in organic media—is proposed in Chapter XII, Section 5.

We can though go on to exploit eqn (11) by remarking that from eqn (5):

$$\chi_1(\omega) = \frac{Nq^2}{m\epsilon_0} \frac{1}{D(\omega)}$$

and that  $D(0) = \omega_0^2 = \text{Cte}$ , and from which, after eqn (11),

$$\chi_2^{(\omega+0)} = \frac{Nq^2\delta^2}{2m^2\epsilon_0} \underbrace{\frac{m^2\epsilon_0^2}{Nq^4} \chi_1^2(\omega)}_{\frac{1}{D(\omega)D_\omega}} \underbrace{\frac{1}{\omega_0^2}}_{\frac{1}{D(0)}}$$

(which resembles Miller's relationship)

$$= \frac{\delta^2\epsilon_0}{2\omega_0^2 Nq^2} \chi_1^2(\omega),$$

If with  $\chi_1^2(\omega) = (\epsilon_r - 1)^2 = (n^2 - 1)^2 \approx n^4$  (and assuming 1 to be negligible with respect to  $n^2$ ), we have  $\chi_2^{(\omega+0)} \propto n^4$ .

If we move this law into eqn (15), we find:

$$\Delta n \propto \frac{n^4}{n} E_{(0)},$$

that is

$$\Delta n = \frac{1}{2} r n^3 E_s$$

where  $E_{(0)} = E_s$ , and  $r$  is a coefficient of proportionality.

*Comment* It is worth noting that  $\chi^{(2\omega)}$  comes from the term of  $\chi_1^2$  (resulting from the term for  $dx^2$  from the inharmonic force  $f = -kx + dx^2$ ) so as to relate to the pulsation  $2\omega$ .

$\chi_2^{(\omega+0)}$  corresponds to a pulsation of  $\omega$ . We have shown in Chapter XII, Section IV, that we do not have to return explicitly to the inharmonic term, thus simplifying greatly our calculations.

---

## Bibliography

- [And 58] P.W. Anderson, 'Absence of diffusion in certain random lattices', *Phys. Rev.* B109, (1958), 1492.
- [And 66] J. Anderson, *Les diélectriques*, Dunod, 1966.
- [And 92] J.J. André, 'Physique élémentaire du transport dans les milieux organiques; applications aux polymères conducteurs'; Vol. 9 (Propriétés électriques des polymères et applications) from the series 'Initiation à la chimie et la physicochimie macromoléculaires' published by GFP (Groupe Français d'Etudes et d'Applications des Polymères), 67083 Strasbourg.
- [Ant 98] R. Antony, 'Réalisation et caractérisations optoélectroniques de diodes électroluminescentes à base de polymères électroactifs et de matériaux moléculaires déposés avec l'assistance d'un faisceau d'ions', PhD, Université de Limoges, June 1998.
- [Ant 00] R. Antony, A. Moliton, B. Ratier, 'Effect of various ions on organic light-emitting diodes obtained by ion-beam-assisted deposition', *Appl. Phys.* B71, (2000), 33–41.
- [Arn 91] P. Arnaud, *Cours de chimie physique*, Dunod, 1991.
- [Ash 76] N.W. Ashcroft and N.D. Mermin, 'Solid state physics', HRW International editions, Saunders College publishing, 1976.
- [Ath 96] L. Athouël, G. Froyer, M.T. Riou, M. Schott, 'Structural studies of paraxexiphenyl thin films: importance of the deposition parameters', *Thin Solid Films*, 274, 1996, 35.
- [Atk 00] P.W. Atkins, 'Physical Chemistry', De Boeck University, 2000.
- [bal 99] M.A. Baldo, D.F. O'Brien, M.E. Thomson, S.R. Forrest, 'Excitonic singlet-triplet ratio in a semiconducting organic thin film', *Phys. Rev. B*, 66(20), 1999, 14422.
- [Bal 00] M.A. Baldo, M.E. Thomson, S.R. Forrest, 'High-efficiency fluorescent organic light-emitting devices using a phosphorescent sensitizer', *Nature*, 403, (2000), 750.
- [Bao 99] Z. Bao, J.A. Rogers, A. Dodabalapur *et al.*, 'Polymer light emitting diodes: new materials and devices', *Optical Materials*, 12 (1999) 177.
- [Bar 00a] P. Le Barny, C.M. Bouché, G. Vériot, 'Matériaux organiques électroluminescents', *Techniques de l'ingénieur*, E1-830 (2000), p. 1–24.
- [Bar 00b] P. Le Barny *et al.*, 'Application of organic electroluminescent materials in visualisation', *C.R. Acad. Sci. Paris*, t.1, Series IV, (2000), 493.
- [Bäs 93] H. Bäessler, 'Charge transport in disordered organic photoconductors, a Monte Carlo simulation study', *Phys. Stat. Sol.* B175, (1993), 15–56.
- [Bel 99] J. Bell 'Organic groups excite rare-earth emissions'. *Opto & Laser Europe*, 60, (1999), 21.

- [Ber 68] D.J. Berets, D.S. Smith, *Trans. Faraday Soc.*, 64, (1968), 823. One can also consult: Liang-Tsé, M. Jozefowicz, R. Buvet, 'Conductivité électronique des composés macromoléculaires conjugués', in 'Chimie Macromoléculaire', vol I, p. 570, Ed. G. Champetier, Hermann, Paris, 1970.
- [Ber 01a] R. Van den Berg, OLE, 'Flexible display is suitable for mass production', 85, June 2001, p. 7.
- [Ber 01b] R. Van den Berg, 'The future looks bright for flexible organic displays', OLE mars 2001, 82, (2001), 29–31.
- [Bha 98] J. Bharathan, Y. Yang, "Polymer electroluminescent devices processed by inkjet printing: polymer light-emitting logo", *Appl. Phys. Lett.*, 72(21), 1998, 2660–2662.
- [Bla 67] A. Blanc – Lapierre, *Mécanique statistique*, Masson, 1967.
- [Blo 97a] P.W.M. Blom, M.J. de Jong, C.T. Liedenbaum, J.J. Vleggar, 'Device characteristics of polymer light-emitting diodes', *Synth. Metals*, 85 (1997) 1287.
- [Blo 97b] P.W.M. Blom, M.J. de Jong, M.G. van Munster, 'Electric field and temperature dependence of the hole mobility in PPV', *Phys Rev B* 55(2), (1997), R656.
- [Blo 98] P.W.M. Blom, M.J. de Jong, 'Electrical characterization of polymer light-emitting diodes', *IEEE J. in Quantum Electronics*, 4(1), (1998), 1077.
- [Bos 95] Ch. Bosshard, K. Sutter, Ph. Prête, J. Hullinger, M. Flörsheimer, P. Kaatz, P. Günter, 'Organic Nonlinear Optical Materials', Gordon and Breach, 1995.
- [Bra 96] D.D.C. Bradley, 'Electroluminescent polymers: materials, physics and device engineering', *Current opinion in Solid State & Materials science*, 1, 1996, 789.
- [Bra 01a] C.J. Brabec, N.S. Sariciftci, J.C. Hummelen, 'Plastic solar cells', *Adv. Funct. Mater.*, 11,1, (2001), 15.
- [Bra 01b] C.J. Brabec, N.S. Sariciftci, 'Recent developments in conjugated polymer based plastic solar cells', in *Electroactive Materials*, Ed. J.O. Besenhard, W. Sitte, F. Stelzer, H. Gamsjäger, Springer, Wien, 2001.
- [Bra 04] A. Boulben 'Les cellules solaires organiques atteignent 5% de rendement', *L'Usine nouvelle*, N°2901: 37 (22 janvier 2004).
- [Bre 99] K.V. Brennan, *The physics of semiconductors with applications to optoelectronic devices*, Cambridge University Press, (1999).
- [Bré 82a] J.L. Brédas, R.R. Chance, R. Silbey, G. Nicolas and P. Durand, *J. Chem. Phys.*, 77, (1982), 371.
- [Bré 82b] J.L. Brédas, R.R. Chance, R. Silbey, 'Comparative theoretical study of the doping of conjugated polymers: polarons in polyacetylene and poly(*para*-phenylene)', *Phys. Rev. B*, 26(10), (1982), 5843.
- [Bro 01] D.J. Broer, J.A. Van Haaren, C.W. Bastiaansen, 'Progress in information displays based on functional polymers', *European Polymer federation, special issue*, June 2001, p. 34–43.
- [brou 01] B. Brousse, 'Caractérisations de films de polyimide fluoré obtenus par VDP en vue de la réalisation de guides optiques', *Rapport de stage DEA. Université de Limoges*, 2001.
- [Bul 01] V. Bulovic, M.A. Baldo, S.R. Forrest, 'Excitons and energy transfer in doped luminescent molecular organic materials', Ch 11 in *Organic Electronic Materials*, Ed. R. Farchioni and G. Grosso, Springer series in Materials Science, Springer, Berlin, 2001
- [Bur 90] J.H. Burroughes, D.D.C. Bradley, A.R. Brown, R.N. Marks, K.D. Mackay, R.H. Friend, P.L. Burn, A.B. Holmes, 'Light-emitting diodes based on conjugated polymers', *Nature*, 347, (1990), 539–541.
- [Bur 91] Burroughes J.H. & R.H. Friend, 'The Semiconductor Device Physics', in *Conjugated Polymers*, Ed. J.L. Brédas & R. Silbey, Kluwer, 1991, p. 555–622.
- [Bur 94] P.E. Burrows & S.R. Forrest, 'Electroluminescence from trap-limited current transport in vacuum deposited light emitting devices', *Appl. Phys. Lett.*, 64(17), 1994, 2285–2287.

- [Bur 96] P.E. Burrows *et al.*, 'Relationship between electroluminescence and current transport in organic heterojunction light-emitting devices', *J. Appl. Phys.*, 79, 1996, p. 7991–8006.
- [Bur 97] P.E. Burrows, S.R. Forrest, M.E. Thomson, "Prospects and application for organic light-emitting devices", *Current Opinion in solid state & materials science*, vol 2, 1997, p.236–243.
- [Bus 94] M.N. Bussac, L. Zuppiroli, 'Stability of transverse bipolarons in conducting polymers', *Phys. Rev. B*, 49(9), (1994), 5876.
- [Cag 71] B. Cagnac, J.C. Pebay-Peyroula, *Physique atomique*, Dunod, 1971.
- [Cam 98] A.J. Campbell, D.D.C. Bradley, D.G. Lidzey, 'Space-charge limited conduction with traps in PPV light emitting diodes', *J. Appl. Phys.*, 82(12), (1997), 6326.
- [Cam 98b] A.J. Campbell, M.S. Weaver, D.G. Lidzey, D.D.C. Bradley, E. Werner, W. Brütting, M. Schwoerer, 'Conduction and trapping in electroluminescent polymer', *Proceeding conf. SPIE, San Diego*, vol 3476, 1998, p. 98–110.
- [Cam 99] I.H. Campbell and D.L. Smith, 'Shottky energy barrier and charge injection in metal/Al/metal structure', *Appl. Phys. Lett.*, 74(4), 1999, 561.
- [Car 84] E. Cartier, 'Des écrans plats à cristaux liquides pour les terminaux', *Electronique industrielle*, 78, (1984), 99.
- [Cha 98] S.C. Chang *et al.*, 'Dual-color polymer light emitting pixels processed by hybrid inkjet printing', *Appl. Phys. Lett.*, 73(18), 1998, 2561.
- [Com 85] P.G. Le Comber, W.E. Spear, 'Doped Amorphous Semiconductors', in *Amorphous Semiconductors*, Ed. M.H. Brodsky, Springer, Berlin, 1985, p. 251.
- [Coh 73] C. Cohen Tannoudji, B. Diu, F. Laloë, 'Mécanique quantique', Herman, 1973.
- [Col 98] B. Colombeau, Contract report, France Télécom, 1998.
- [Con 97] E.M. Conwell, 'Transport in conducting polymers', in *Handbook of Organic Conductive Molecules and Polymers*, Ed. Hari Singh Nalwa, J. Wiley, Vol 4, Ch 1, 1997.
- [Cor 01] C. Cornic, B. Lucas, A. Moliton, B. Colombeau, R. Mercier, 'Elaboration and characterization of 6FDA/MPDA polyimide-based optical waveguide', *Synth. Metals*, paper R/P 44 (2001).
- [Cox 87] P.A. Cox, 'The electronic structure and chemistry of solids', Oxford University Press, Oxford, 1987.
- [Cro 61] G.A. Crosby, R.E. Whan, R.M. Alire, 'Intramolecular Energy Transfer in Rare Earth Chelates. Role of the triplet State', *J. Chem. Phys.*, 34(3), (1961), 743.
- [Cuo 89] J.J. Cuomo, S.M. Rosnagel, H.R. Kaufman, 'Handbook of ion beam processing technology', Noyes Publication, (1989).
- [Cur 56] M. Curie and D. Curie, 'Questions actuelles en luminescence cristalline, Ed. revue d'optique théorique et instrumentale', Paris, (1956).
- [Cur 60] D. Curie, 'Luminescence cristalline', Dunod, (1960), p.160.
- [Den 00] V. Dentan, M. Vergnolle, H. Facoetti, G. Vériot, 'Progress in molecular electroluminescent materials', *C.R. Acad. Sci. Paris*, t.1, Series IV, (2000), 425.
- [Dep 83] S. Depp and W. Howard, 'Les écrans plats,' *Science*, 187, (1993), 78.
- [Des 91] F. Desvigne, *Rayonnements optiques. Radiométrie – Photométrie*. Masson. Paris, 1991.
- [Ebel 92] K.J. Ebeling, 'Integrated optoelectronics', Springer, 1992.
- [Ell 90] S.R. Elliott, 'Physics of amorphous materials', Second edition, Longman, 1990.
- [Ell 98] S.R. Elliott, 'The physics and chemistry of solids', J. Wiley, 1998.
- [Emi 86] D. Emin, 'Basic issue of electronic transport in insulating polymers', *Handbook of Conducting Polymers*, T.A. Skotheim Ed., M. Dekker, Vol.2, Ch 26, 1986.
- [Fav 01] J.L. Fave and M. Schott, personal communication.
- [Fic 00] D. Fichou, 'Structural order in conjugated oligothiophenes and its implications on opto-electronic devices', *J. Mater. Chem.*, 10, (2000), 571.

- [Fis 88] G. Fishman, 'Energie et fonction d'onde des semiconducteurs', Monographie de physique, Les éditions de Physique, 91944-Les Ulis, (1988).
- [För 65] Th. Förster, 'Delocalized Excitation and Excitation Transfer', in 'Modern Quantum Chemistry', Ed. O. Sinanoglu, Part. III: Action of light and organic crystals, Academic Press, 1965.
- [For 98] E.W. Forsythe, D.C. Morton, C.W. Tang, and Y. Gao, 'Trap states in Alq<sub>3</sub> using thermally stimulated luminescence', Proceeding conf. SPIE, San Diego, vol 3476, 1998, p. 123-130.
- [Fre 60] R. Freymann and M. Soutif, 'La spectroscopie hertzienne', Dunod, 1960.
- [Fri 70] H. Fritzsche. 'Les semiconducteurs amorphes', La recherche, novembre 1970.
- [Fri 85] S. Fridrikhov and S. Movnine, 'Bases physiques de la technique électronique', Ed. Mir, Moscou (1985).
- [Fri 92] R.H. Friend, D.D.C. Bradley, A. Holmes, 'Polymer LEDs', Physics world, Nov. 1992, p. 42-44.
- [Fri 98] R.H. Friend, N.C. Greenham, 'Electroluminescence in conjugated polymers', in Handbook of conducting polymers, Dekker, Ch 29, 1998.
- [Gar 99] F. Garnier, J. Zyss, 'Molecular Photonics for Optical Telecommunications: Materials, Physics, and Device Technology', Proceedings MRS 1998, Symposia 88, Elsevier 1999.
- [Gau 96] E. Gautier, J.M. Nunzi, C. Sentein, A. Lorin, P. Raimond, 'Blue light-emitting diodes with doped polymers', Synth. Met., 81, (1996), 197-200.
- [Ger 97] M. Gerl and J.P. Issi, 'Physique des matériaux', Presses polytechniques et universitaires romandes, 1997.
- [Gho 74] A.K. Ghosh, D.L. Morel, T. Feng, R.F. Shaw, C.A. Rowe, 'Photovoltaic and rectification properties of Al/Mg-phthalocyanine/Ag Schottky barrier cells', J. Appl. Phys., 45 (1974), 230.
- [Gil 72] W.D. Gill, 'Drift mobilities in amorphous charge-transfer complex of trinitrofluorene and poly(n-vinylcarbazole)', J. Appl. Phys., 43(12), (1972), 5033.
- [Gil 99] W.P. Gillin and R.J. Curry, 'Erbium (III) tris(8-hydroxyquinoline) (ErQ): a potential material for silicon compatible 1.5  $\mu\text{m}$  emitters', Appl. Phys. Lett. 74, (1999), 798.
- [Gom 93] P. Gomes da Costa, R.G. Dandrea, E.M. Conwell, 'First-principles calculation of the three-dimensional band structure of PPV', Phys. Rev., 47(4), (1993), 1800.
- [Gra 91] B. O'Reagan and M. Graetzel, 'A low cost, high efficiency solar cell based on dye-sensitized colloidal TiO<sub>2</sub> films', Nature, vol. 353, 24 Oct. 1991.
- [Gre 73] G.N. Greaves, 'Small polaron conduction in V<sub>2</sub>O<sub>5</sub>-P<sub>2</sub>O<sub>5</sub> glasses', J. Non-crystal. Solids, 11, (1973), 427.
- [Gre 94] N.C. Greenham, R.H. Friend, D.D.C. Bradley, 'Angular dependence of the emission from a conjugated polymer light-emitting diode: implication for efficiency calculations', Adv. Materials, 6, (1994), 491.
- [Gre 95] N.C. Greenham, R.H. Friend, 'Semiconductor Device Physics of Conjugated Polymers', ed. H. Ehrenreich, Academic Press, (1995).
- [Had 86] R.C. Haddon, L.E. Brus, K. Raghavachari, 'Electronic structure and bonding in Icosahedral C<sub>60</sub>', Chem. Phys. Lett., 125(5,6), (1986), 459.
- [Had 00] G. Hadziioannou, P.F. van Hutten, Semiconducting Polymers, ch 16: 'A model oligomer approach to semiconducting polymers', Wiley VCH (2000).
- [Hal 95] J.J. Hall *et al.*, Nature 376 (1995)498.
- [Ham 96] P.J. Hamer, K. Pichler, M.G. Harisson, R.H. Friend, B. Ratier, A. Moliton, S.C. Moratti, A.B. Holmes, 'Optical studies of chemical doping achieved by ion implantation in PPV', Phil. Mag B, 73(2), (1996), 367-382.
- [Ham 97] Y. Hamada, 'Chelate Metal Complexes as organic electroluminescent materials', in 'Organic Electroluminescent materials and devices', Ed. S. Miyata, Gordon, Ch9, 1997.

- [Hay 87] S. Hayachi, K. Kaneto, K. Yoshino, 'Quenching of photoluminescence in polythiophene films by electrochemical doping', *Solid State Comm.*, 61(4), (1987), 249–251.
- [Hee 88] A.J. Heeger, S. Kivelson, J.R. Schrieffer, W.P. Su, 'Solitons in conducting polymers', *Reviews of Modern Physics*, 60, (1988), 781.
- [Hel 67] W. Helfrich, 'Space-charge-limited and volume-controlled currents in organic solids', in 'Physics and chemistry of organic solid state', Wiley 3, 1967, 1–65.
- [Hol 59] T. Holstein, 'Studies of Polaron Motion', *Annals of Physics*, 8, (1959), 325.
- [Hor 00] G. Horowitz, 'Physics of organic Field-Effect Transistor', in *Semiconducting Polymers*, Ed. Hadziioannou G., van Hutten P.F., Wiley VCH, Ch 14, (2000).
- [hut 01] P.F. van Hutten, G. Hadziioannou, 'The role of interfaces in photovoltaic devices', in 'Molecular Materials and functional polymers', Ed. W. J. Blau, P. Lianos, U. Schubert, Springer, 2001, p. 129.
- [Ioa 98] A. Ioannidis, E. Forsythe, Y. Gao, M.W. Wu, E.M. Conwell, 'Current-voltage characteristic of organic light emitting diodes', *Apl. Phys. Lett.*, 72, 1998, 3038.
- [Iof 60] A.F. Ioffe, A.R. Regel, 'Non crystalline, amorphous and liquid electronic semiconductors', *Progress in Semiconductors*, vol.4, Heywood and Co LTD, London, 1960.
- [Jjol 97] P. Jolinat, 'Etude et réalisation de diodes électroluminescentes organiques; réalisation de diodes blanches'. PhD, Université P. Sabatier, Toulouse, December 1997.
- [Jon 83] A.K. Jonsher, 'Dielectric relaxation in solids', Chaisea Dielectric Press, London 1983.
- [Jon 99] C. Jones, 'The evolution of liquid-crystal displays', *Opto & Laser Europe*, 69, (1999), 41.
- [Jeo 01] Y.S. Jeong, B. Ratier, A. Moliton, L. Guyard, 'UV-Visible and infrared characterization of poly(p-xylylene) films for waveguide applications and OLED encapsulation', *Synth. Metals*, 9135 (2001), 1–5.
- [Jeo 01b] Y.S. Jeong, D. Troadec, A. Moliton, B. Ratier, R. Antony, 'Dielectric studies of Alq<sub>3</sub> and transport mechanisms', *Synth. Metals*, 9136 (2001), 1–6.
- [Kai 89] A.B. Kaiser, 'Thermoelectric power and conductivity of heterogeneous conducting polymers', *Phys. Rev B.*, 2806, B 40(5), 1989.
- [Kao 81] K.C. Kao, W. Hwang, 'Electrical transport in solids', Pergamon Press, 1981.
- [Kar 97] S. Karg, M. Meier, W. Riess, 'Light-emitting diodes based on poly(*para*-phenylene-vinylene): I. Charge-carrier injection and transport', *J. Appl. Phys.* 82, (1997), 1951.
- [Kel 92] M.K. Kelly, P. Etchegoin, D. Fuchs, W. Krätschmer, K. Fostropoulos, 'Optical transitions of C<sub>60</sub> films in the visible and ultraviolet from spectroscopic ellipsometry', *Phys. Rev. B*, 46(8), (1992), 4963.
- [Keo 98] N.B. McKeon, *Phthalocyanines Materials*, Cambridge University Press, 1998.
- [Kil 71] H. Killesreister et H. Bässler, 'Exciton reaction at an anthracene/metal interface : charge transfer', *Chem. Phys. Lett.*, 11, (1971), 411.
- [Kim 98] J.S. Kim, M. Granström, R.H. Friend, N. Johanson, W.R. Salaneck, R. Daik, W.J. Feast, F. Cacialli *et al.*, 'Indium tin oxide treatments for single and double PLEDs', *J. Appl. Phys.* 84(12), (1998), 6859.
- [Kit 96] C. Kittel, 'Introduction to solid state physics', John Wiley and sons, Inc, 1996.
- [Kiv 88] S. Kivelson, A.J. Heeger, 'Intrinsic conductivity of conducting polymers', *Synth. Met.*, 22, (1988), 371.
- [Kra 98] A. Kraft, A.C. Grimsdale, A.B. Holmes, 'Electroluminescent conjugated polymers: Seing polymers in a new light', *Angewandte Chem.*, 37 (1998), 402–428.
- [Law 92] Del R. Lawson, D.L. Feldheim, C.A. Foss, P.K. Dorhout, C.M. Elliott, C.R. Martin, B. Parkinson, 'Near-IR absorption spectra for the Buckminsterfullerene anions: an experimental and theoretical study', *J. Electrochem. Soc.*, 139(7), (1992), L68.

- [Led 95] I. Ledoux, R. Pinsard-Levenson, J. Zyss, 'Matériaux organiques pour les réseaux de communications optiques: de la molécule aux composants'. *L'Echo des recherches*, n° 162, 4<sup>ème</sup> trimestre 1995, p. 35–48.
- [Lei 98] G. Leising, S. Tasch, W. Graupner, 'Fundamentals of electroluminescence in paraphenylene type conjugated polymers and oligomers', *Handbook of conducting polymers*, Dekker, Ch 30, (1998).
- [Lem 95] U. Lemmer *et al.*, 'Aggregate fluorescence in conjugated polymers', *Chem. Phys. Letters*, 240 (1995) 373–378.
- [Lev 68] S.N. Levine, 'Electronique quantique', Masson, 1968.
- [Luc 03] B. Lucas, A. Moliton *et al.*, 'Gravure ionique réactive et applications à la réalisation de modulateurs de phase en polymères' (in press).
- [Lun 00] M. Lundstrom, 'Fundamentals of carrier transport', second edition, Cambridge University Press, 2000.
- [May 96] M. May, A.M. Cazabat, *Optique*, Dunod, 1996.
- [Mar 94] R.N. Marks, J.J.M. Halls, D.D.C. Bradley, R.H. Friend, A.B. Holmes, *J. Phys. Condens. Matter*, 6 (1994) 1379
- [Mat 98] H. Mathieu, 'Physique des semiconducteurs et des composants électroniques', Masson, (1998).
- [Men 93] Reghu Menon, C.O. Yoon, D. Moses, A.J. Heeger, 'Transport in polyaniline near the critical regime of the metal – insulator transition', *Phys Rev B*, 48, 1993, 17685.
- [Men 98] Reghu Menon, C.O. Yoon, D. Moses, A.J. Heeger, 'Metal – Insulator transition in doped conducting polymers', Chapitre 2 du *Handbook of conducting Polymers*, Second edition, Ed. T.A. Skotheim, R.L. Elsenbaumer, J.R.Reynolds, M. Dekker, New York, 1998.
- [Mer 95] J.P. Mercier, P. Godard, 'Chimie organique' Presses polytechniques et universitaires romandes, 1995.
- [Mig 01] E. Mignard, R. C. Hiorns, B François, 'Synthesis and characterisation of star copolymers consisting of fullerene and conjugated polyphenylene', *Macromolecules*, 35(16) 2002, 6132–6141.
- [Mil 60] A. Miller, 'Impurity conduction at low concentrations', E. Abrahams, *Phys. Rev.*, 120 (1960) 745.
- [Miy 97] S. Miyata and S. Nalwa, 'Organic electroluminescent materials and devices', Gordon and Breach (1997)
- [Mol 81] A. Moliton. 'Cours photocopié de physique atomique'. Université de Limoges, (1981).
- [Mol 88] A. Moliton, J.L. Duroux, G. Froyer, 'Aspects théoriques et expérimentaux du dopage physique des polymères électroactifs'. *Ann. Phys. Fr.*, 13, (1988), 261.
- [Mol 91] A. Moliton *et al.*: 'Propriétés électroniques et schémas de bandes dans les semiconducteurs amorphes':  
I 'Concepts fondamentaux', A. Moliton, B. Ratier, *Ann. Phys. Fr.*, 16, (1991), 261.  
II 'Etude des phénomènes de transport', A. Moliton, B. Ratier, *Ann. Phys. Fr.*, 16, (1991), 305.  
III 'Les mécanismes de transport par saut faisant appel aux modèles des paires et à la conduction par polarons', A. Moliton, B. Lucas, *Ann. Phys. Fr.*, 19, (1994), 299–352.
- [Mol 94] A. Moliton, B. Lucas, C. Moreau, R.H. Friend, B. François, 'Ion implantation in conjugated polymers : mechanisms for generation of charge carriers', *Phil. Mag. B*, 69(6), (1994), 1155–1171.
- [Mol 98] A. Moliton, 'Ion implantation doping of electroactive polymers and device fabrication', *Handbook of conducting polymers*, Dekker, Ch 21, (1998).
- [Mol 00] A. Moliton, R. Antony, D. Troadec, B. Ratier, 'Ion beam assisted deposition of organic molecules: a physical way to realize OLED structures', *C.R. Acad. Sci. Paris*, t. I, Series IV, (2000), p. 437–446.



- [Mom 95] B. Mombelli, 'Processus optiques dans les solides', Masson, 1995.
- [Moo 93] E. Mooser, 'Introduction à la physique des solides', Presses polytechniques romandes, 1993.
- [Mor 78] D.L. Morel, A.K. Ghosh, T. Feng, E.L. Stogryn, P.E. Durwin, R.F. Shaw, C. Fishman, *Appl. Phys. Lett.*, 32 (1978), 495–497.
- [Mor 97] C. Moreau, R. Antony, A. Moliton, B. François, 'Sensitive Thermoelectric power and conductivity measurements on implanted PPP films', *Adv. Mat. for Optics and Electronics*, 7, 281, (1997).
- [Mot 71] N.F. Mott, E.A. Davis, 'Electronic processes in non-crystalline materials', Clarendon press, 1971.
- [Mot 79] N.F. Mott, E.A. Davis, 'Electronic processes in non-crystalline materials', Second edition, Clarendon press, 1979.
- [Mot 93] N.F. Mott, 'Conduction in non-crystalline materials', Oxford Science Publications, 1993.
- [Mou 99] C. Moussant, 'Gravure ionique réactive de type RIBE et IBAE. Application à la réalisation de guides optiques polymères'. PhD thesis; l'Université de Limoges, May 1999.
- [Mou 00] C. Moussant, B. Lucas, A. Moliton, 'Etching techniques using a collimated ion beam for the realization of waveguides', *Synth. Metals*, 115 (2000), 29.
- [Mül 89] K.H. Müller, 'Film growth modification by concurrent ion bombardment: theory and simulation', Ch 13 in 'Handbook of Ion Beam Processing Technology', Ed. J.J. Cuomo, S.M. Rossnagel and H.R. Kaufman, Noyes Pub., (1989). See also K.H. Müller, 'Model for ion-assisted thin film densification', *J. Appl. Phys.*, 59(8), 1986, 2803.
- [Nag 85] 'Electronic transfer in amorphous semiconductors', in *Amorphous Semiconductors* (M.H. Brodsky, Ed.), Springer Verlag, Berlin, 1985, Chap. 5.
- [Nag 97] K. Nagayama, T. Yahagi, H. Nakada, T. Tohma, T. Watanabe, K. Yoshida, S. Miyaguchi, 'Micropatterning method for the cathode of the organic electroluminescent device', *Japan J. Appl. Phys.*, 36, (1997), L 15555–L 1557.
- [Ngu 01] T.P. Nguyen, P. Molinie, P. Destruel, 'Organic and polymer-based light-emitting diodes', Chapter 1 of vol. 10, 'Handbook of Advanced Electronic and Photonic Materials and Devices', Ed. H.S. Nalwa, Academic Press, 2001.
- [Ngu 94] Nguyễn Trọng Anh, 'Introduction à la chimie moléculaire', Ellipses, 1994.
- [Nie 99] J.F. Nierengarten, J.F. Eckert, J.F. Nicoud, L. Ouali, V. Krasnikov, G. Hadziioannou, *Chem Commun.* (1999) 617.
- [Nie 01] J.F. Nierengarten, G. Hadziioannou, N. Armaroli, 'Molecular photovoltaic devices', *Materials Today*, 4(2), 2001, 16.
- [Nun 02] J.M. Nunzi, 'Organic photovoltaic materials and devices', *C.R. Physique*, 3 (2002) 523-542.
- [ole 00] *OptoLaserEurope*, vol 79, (nov 2000), 19–23.
- [ole 01] Market report, p. 47, 'Opto et Laser Europe', vol 81, January/February 2001.
- [opt 93] 'Optoélectronique moléculaire', 'Observatoire Français des techniques avancées', Arago 13, Masson, 1993.
- [Pan 71] J.I. Pankove, 'Optical processes in semiconductors', Dover Pub, 1971.
- [Pap 85] M. Papuchon, Y. Bourbin, S. Vatoux, 'Etat de l'art de l'optique intégrée', 'Optique guidée monomode', Masson, 1985, p. 621 references therein.
- [Par 94] I.D. Parker, 'Carrier tunneling and device characteristics in polymer light-emitting diodes', *J. Appl. Phys.*, 75(3), (1994), 1656.
- [Pei 55] R.E. Peierls, 'Quantum theory of solids', Clarendon Press, Oxford, 1955.
- [Per 96] J.P. Perez, R. Carles, R. Fleckinger, 'Electromagnétisme', Masson, 1996.

- [Pet 91] R.A. Soref, J. Schmidtchen, K. Petermann, 'Large single-mode rib waveguides in GeSi-Si and Si-on SiO<sub>2</sub>', IEEE J. Quantum Electronics, 27(8), (1991), 1971, and Electronics Lett., 27, (1991), 1488.
- [Pet 96] G. Fischbeck, R. Moosburger, M. Töpper, K. Petermann, 'Design concept for singlemode polymer waveguides', Electronics Lett., 32(3), (1996), 212.
- [Peu 03] P. Peumans, A. Yakimov, S.R. Forrest, 'Small molecule weight organic thin-film photodetectors and solar cells', J. Appl. Phys., 93(7), 2003, 3693.
- [Pfu 86] P. Pflüger, G. Weiser, Campbell, J. Scott, B. Street, 'Electronic structure and transport in the organic amorphous semiconductor polypyrrole', 'Handbook of conducting polymers', Vol. 2, Ed. T.A. Skotheim, Dekker, Ch 38, (1986).
- [Pic 95] K. Pichler, C.P. Jarrett, R.H. Friend, B. Ratier, A. Moliton, 'Field-effect transistors based on poly(*p*-phenylene vinylene) doped by ion implantation', J. Appl. Phys., 77(7), (1995), 3523.
- [Pop 82] M. Pope, C.E. Swenberg, 'Electronic processes in organic crystals', Clarendon Press, 1982.
- [Qué 88] Y. Quéré, 'Physique des matériaux', Ellipses (Paris), 1988.
- [Ran 45] J.T. Randall and M.H.F. Wilkins, 'Phosphorescence and electrons trap distribution. I- The study of trap distributions', Proc. Roy. Soc., 184A, (1945), 365.
- [Riv 89] J.L. Rivaill, 'Éléments de chimie quantique', InterEditions/Éditions du CNRS (1989).
- [Ron 98] J. Roncali, 'Advances in the molecular design of functional conjugated polymers', Ch. 12 du Handbook of conducting polymers, Dekker, (1998).
- [Rot 96] Rothberg L.J., Lovinger A.J., 'Status of and prospects for electroluminescence', J. Mat. Res., 11(12), 1996, 3174.
- [Sal 91] B.E. Saleh, M.C. Teich, 'Fundamentals of photonics', Wiley, 1991.
- [Sam 00] I.D. Samuel, A. Beeby, 'Sidestepping the selection rules', Nature, 403, 2000, 710.
- [Sap 90] B. Sapoval, C. Hermann, 'Physique des semi-conducteurs', Ellipses, 1990.
- [Sch 94] M. Schott, M. Nechtschein, 'Introduction to conjugated and conducting polymers', in Organic Conductors', Ed. J.P. Farges, M. Dekker, p. 495, (1994).
- [Sch 95] A. Schmidt, M.L. Anderson, N.R. Armstrong, J. Appl. Phys., 'Electronic states of vapor deposited electron and hole transport agents and luminescent materials for light-emitting diodes', 78(9), (1995), 5619.
- [Sch 00] Schott M., 'Introduction to the physics of organic electroluminescence', C.R. Acad. Sci. Paris, t. 1, Series IV, (2000), 381–402.
- [Schö 00] J.H. Schön, Ch. Kloc, A. Dodabalapur, B. Batlogg, 'An organic solid state injection laser', Science, 289, (2000), 599.
- [Schö 00b] J.H. Schön, Ch. Kloc, E. Bucher, B. Batlogg, 'Single crystalline pentacene solar cells', Synth. Met., 115 (2000) 177. See also, J.H. Schön, Ch. Kloc, E. Bucher, B. Batlogg, 'Efficient organic photovoltaic diodes based on doped pentacene', Nature 403, (2000), 408.
- [Seg 01] I. Seguy, 'Réalisation et étude de diodes électroluminescentes organiques à base de molécules discotiques', PhD, Université Paul Sabatier, Toulouse, 2001.
- [Sen 97] C. Sentein, C. Fiorini, A. Lorin, J.M. Nunzi, 'Molecular rectification in oriented polymer structure', Synth. Metals, 91 (1997) 81–82.
- [She 98] J. Shen, F. So., J. Yang, J.H. Xu, V.E. Choong, H.C. Lee, 'Carrier transport in light emitting diodes', Proceeding conf. SPIE, San Diego, vol 3476, 1998, p. 196–201.
- [Shi 132] Y. Shirota, S. Nomura, H. Kageyama, 'Charge transport in amorphous molecular materials', Proceeding conf. SPIE, San Diego, vol 3476, 1998, p. 132–141.
- [Shi 00] Y. Shi *et al.*, 'Low halfwave voltage polymeric electro-optic modulators achieved by controlling chromophore shape', Science, vol. 288, 7 Avril 2000, p. 119–122.

- [Si 97] J. Si and C.W. Tang, 'Doped organic electroluminescent devices with improved stability', *Appl. Phys. Lett.*, 70(13) (1997) 1665
- [Sic 00] L. Sicot, C. Fiorini, C. Sentein, A. Lorin, P. Raimond, J.M. Nunzi, 'Improvement of the photovoltaic properties of polythiophene-based cells', *Solar Energy Materials & Solar Cells*, 63, (2000) 49–60.
- [Sim 85] J. Simon, J.J. Andre, 'Molecular Semiconductors', Ed. J.M. Lehn, Ch. W. Rees, Springer, Berlin, 1985.
- [Sko 86] T.A. Skotheim, 'Handbook of conducting Polymers', M. Dekker, New York, 1986.
- [Sko 98] T.A. Skotheim, R.L. Elsenbaumer, J.R. Reynolds, 'Handbook of conducting Polymers', Second edition, M. Dekker, New York, 1998.
- [Sly 96] S.A. Van Slyke, C.H. Chen, C.W. Tang, 'Organic electroluminescent devices with improved stability', *Appl. Phys. Lett.*, 69(15), 1996, 2160.
- [Smi 90] F.A. Smidt, 'Use of ion beam assisted deposition to modify the microstructure and properties of thin films', *International Materials Reviews*, 35(2), 61 (1990).
- [Smi 61] R.A. Smith, 'Wave mechanics of crystalline solids', Chapman and Hall, 1961.
- [Su 79] W.P. Su, J.R. Schrieffer, A.J. Heeger, 'Solitons in polyacetylene', *Phys. Rev. Lett.*, 42, (1979), 1698.
- [Sut 93] A. Sutton, 'Electronic structure of materials', Clarendon Press, Oxford, 1993.
- [Tah 98] R. Tahar, T. Ban, Y. Ohya, Y. Takahashi, 'In doped oxide films: electrical properties', *J. Appl. Phys.*, 83(5), 1998, 2631.
- [Tan 86] C.W. Tang, 'Two-layer organic photovoltaic cell', *Appl. Phys. Lett.*, 48(1986)183
- [Tan 87] C.W. Tang et S.A. VanSlyke, 'Organic electroluminescent diode', *Appl. Phys. Lett.*, 61, (1987), 913.
- [Tes 96] N. Tessler, G.J. Denton, R.H. Friend, 'Lasing from conjugated polymer microcavities', *Nature*, 382, 1996, 695.
- [Tes 98] N. Tessler, N.T. Harisson, D.S. Thomas, R.H. Friend, 'Current heating in polymer light-emitting diodes', *Appl. Phys. Lett.*, 73(6), (1998), 732–734.
- [Til 00] R. Tilley, 'Colour and the optical properties of materials', Wiley, (2000).
- [Tou 01] E. Toussaere, 'HDR', ENS Cachan, Université of Paris XI, 2001.
- [Tra 00] J.P. Travers, 'Polymères conducteurs: conductivité à diverses échelles', *Bulletin de la S.F.P.*, 124, (May 2000), 8.
- [Tro 92] N. Trouiller, J.L. Martins, 'Structural and electronic properties of C<sub>60</sub>', *Phys Rev. B*, 46(3), (1992), 1754.
- [Tro 96] P. Trouillas, 'Le carbone 60: de l'origine de ses propriétés électroniques et optiques à son comportement sous faisceau d'ions', PhD n° 21-1996, Université de Limoges.
- [Tro 01] D. Troadec, 'Contribution à l'élaboration et à la caractérisation de diodes électroluminescentes organiques', PhD, l'Université de Limoges, November 2001.
- [Tro 03] D. Troadec, J.M. Nunzi, 'Caractérisation optoélectronique de cellules solaires photovoltaïques organiques C<sub>60</sub>/CuPc (P-N) et C<sub>60</sub>:CuPc (co-évaporées)', *Journées Polymères Conducteurs*, A5-6, Dourdans, Sept. 2003.
- [Uet 86] M. Ueta, H. Kanzaki, K. Kobayashi, Y. Toyzawa, E. Hanamura, 'Excitonic Processes in solids', *Solid-State Sciences*, vol. 60, Springer-Verlag, Berlin, 1986.
- [umop 99] A. Moliton, J.P. Moliton, J.M. Dumas, *Compte rendu d'activité du laboratoire UMOP* (1999/2000).
- [Wri 95] J. D. Wright, 'Molecular crystals', Cambridge University Press, 1995.
- [Wu 96] C.C. Wu, J.C. Sturm, R.A. Register, M.E. Thomson, 'Integrated three-color organic light-emitting devices', *Appl. Phys. Lett.* 69(21), 1996, 3117–3119.
- [Wu 97] C.C. Wu, C.I. Wu, J.C. Sturm, A. Kahn, 'Surface modification of ITO by plasma treatment', *Appl. Phys. Lett.*, 70(11), 1997, 1348.

[Yar 89] A. Yariv, 'Quantum Electronics', Third Edition, Wiley, 1989.

[Yu 95] G. Yu, A.J. Heeger, 'Charge separation and photovoltaic conversion in polymer composites with internal donor/acceptor heterojunctions', *J. Appl. Phys.* 78 (1995), 4510.

[Zab 84] A.G. Zabrodskii, K.N. Zinov'eva, 'Low temperature conductivity and metal-insulator transition in compensate n-Ge', *Sov. Phys. JETP*, 59(2), Feb 1984, 425.

[Zup 91] L. Zuppiroli, 'Le fil moléculaire,' Rapport CEA-R-5543, Document service, CEN Saclay.

[Zup 93] L. Zuppiroli, M.N. Bussac, S. Paschen, O. Chauvet, L. Forro, P. Bujard, K. Kai, W. Wernet, 'Hopping in conducting polymers', *Proc. 5th Int. Conf. on hopping and related phenomena*, Ed. C.J. Addkins, A.R. Long, J.A. Mc Innes, Glasgow, 31 August – 3 Sept. 1993, p. 171.

See also, L. Zuppiroli, M.N. Bussac, S. Paschen, O. Chauvet, L. Forro, 'Hopping in disordered polymers', *Phys Rev. B*, 50, 1994, 5196.

---

# Index

- absorption (spectral), 184, 401
- acceptor-donor, 195, 326
- adjusting emissions, 285
- ageing, 294
- aggregates, 194
- Alq3, 61, 69, 94, 259
- amorphous silicon xi
- Anderson localisation, 47
- anodes (OLEDs) 278
- anthracene (narrow band), 109
  
- band**
  - curves, 261
  - forbidden, 6
  - HOMO, 65, 75
  - Hubbart's, 43
  - LUMO, 65, 75
  - scheme, 92, 96
  - structures, 33
- barrier – at interfaces, 259
- benzene (electron structure), 66
- bilayer
  - heterostructure, 324
  - OLED, 280
  - photovoltaic cell, 322
- bipolaron, 82, 86
- Bloch (function), 395
- Boltzmann (transport equation), 404
- bond
  - strong, 4, 9
  - weak, 3, 6
  
- cathodes (OLEDs), 278
- cathode-virtual, 139
- chain
  - of atoms, 12, 26, 389
  - distorted, 20
- characteristics I(V), 264, 271
- charge transfer complex, 45
- chromophore, 177
- coefficients – opto-electric, 341, 356
- conduction-organic (n- or p-type), 276
- conductivity, 99
- conduction by hopping, 112
- configuration
  - curves, 87, 168
  - diagram of, 179
  - electron, 164, 443
- conjugation (molecule/polymer), 62
- contact
  - at electrodes, 259, 268
  - ohmic, 138
  - rectifying, 135
- coupling
  - between atoms, 39
  - between molecular orbitals, 40
  - electron-lattice, 77
  - Frank-Condon, 184, 264
- current
  - bipolar, 157
  - equilibria, 277
  - saturation, with traps, 147
  - space charge limited, 139
  - volume controlled, 154
  
- Davidov (displacement, breakdown), 192**
- defaults (effects of), 90–93
- deposition, 201
  - assisted, 204
  - vapour phase, 202

- Dexter transfer, 197, 288
- dimer, 189
- diodes
  - inorganic, 236
  - molecular optic, 349
  - organic, 253, 257
  - white, 296
- donor-acceptor, 346
- dopants
  - electrical, 126
  - optical, 286
- doping, 87, 126, 431
- Dushman–Richardson law, 136, 433
  
- electric (transport properties), 99, 133
- effective mass, 35, 396
- electro-optic modulator, 358, 368
- electron pumping, 292
- emission
  - electrical (laws), 135
  - optical internal/external, 221
- encapsulation, 203
- etching, 216, 449
  - of ITO, 211
  - of pixels, 298
  - RIBE/IBAE, 366
  - speed, 451–452
- excitation transfer, 286
- exciton, 87, 185
  - charge transfer, 186
  - dissociation, 322
  - Frenkel, 188
  - Wannier, 186
  
- fabrication (techniques), 201
- fill factor, 318, 333
- film, 204
- film growth, 205
- Floquet (theorem), 9
- fluorescence, 182, 194–195
- flux, 406
- Förster (transfer), 196, 289
- Fowler–Nordheim (emission), 137, 437
- fullerenes, 61, 70, 397
  
- gauss (trap distribution), 154
- Graetzel cells, 320
- guides
  - diffusion, 232
  - fabrication, 213
  - losses, 233, 368
  
- half-wave tension, 344
- heterojunction
  - OLEDs, 253
  - volume, 325
- hopping
  - nearest neighbour, 112
  - over variable distance, 113
  - polarons, 116
- Hubbard (band), 43
- hybridisation, 36, 381
- hopping (*see* conduction by hopping)
  
- improving OLEDs, 274
- infra-red OLEDs, 291
- injection (level of), 133
- ink-jet, 305
- ink-jet technology, 302
- interaction
  - dipolar, 196
  - intrachain, 66
  - interchain, 67
- Ioffe–Regel, 48, 51
- irradiation, 94
  
- Jablonsky**, 181–183
  
- Kaiser’s model**, 129
- Kerr effect, 341
- Kubo–Greenwood, 403
  
- laser (effect), 292
- layer
  - confinement, 279, 476
  - emitting, 284, 474
  - injection, 280, 473, 474
  - transport, 282, 473, 474
- layering, 279
- light amplifier, 173
- limits
  - conduction model with delocalised states band, 105–109
  - rigid band theory, 48
- liquid crystal, 239
- localisation (Anderson), 50
- luminance, 220
  - measuring, 230
- luminescence
  - extinction, 248
  
- Mach-Zehnder**, 364
- matrix
  - active, 243
  - doped, 165
  - passive, 243

- merit factor, 359
- merit figure, 360
- microcavities, 292
- Miller and Abrahams, 52
- mobility, 51, 101, 107–108, 412–413
  - in Alq3 265–266
  - in polymers, 271
  - thermally activated, 421
- molecule
  - centrosymmetric, 349
  - non-centrosymmetric, 350
- Mott (localised states), 54
- Mott and Gurney (law), 140
- MIM structure (metal-insulator-metal), 321
- MIS structure (metal-insulator-semiconductor), 252
- multi-layers – *see* layering
  
- OLEDs**, 253, 257
- optical losses, 233, 368
- orbitals – atomic and molecular, 373
  
- page – flexible electronic, 304
- Peirls (transition), 24, 64
- permittivity – dielectric, 459
- phases – interpenetrated, 324
- photodiode (sensitivity), 226
- photovoltaic, 195, 313
- phosphors, 249
- phosphorescence 182, 250
- photoluminescence, 184
- photometry (scaling), 217
- phtalocyanines, 316
- pixels, 298
- Pockels effect, 343
- polaron, 77, 86
- polaron – exciton, 88
- polaron – transverse, 126
- polyacetylene, 64
- polyimide, 363
- polymer
  - degenerate  $-(CH)_x-$ , 64
  - non-degenerate (PPP), 65
- polymerisation in the vapour
  - phase (VDP), 203
- poly(*para*-phenylene) (PPP), 60, 65, 86, 94
- poly(phenylene vinylene) (PPV), 60, 184
- Poole-Frenkel (conduction), 159
- pulverisation time, 449
  
- quantum interferences, 104
  
- rare earths, 164, 169–173
- relaxation, 409
  - energy, 25
  - time, 417
- rules
  - circumnavigating (bending), 288
  - transition, 163, 176, 180, 444, 447
  
- Schottky emission, 136, 434
- screen
  - electroluminescent, 246
  - liquid crystal (LCD), 239
  - micro-points, 245
  - organic, 296
  - plasma, 244
- soliton, 88
- state
  - antibonding, 30, 379
  - bonding, 30, 379
  - densities, 22, 406
  - localised, 41, 50–56
- substrates (preparation), 211
- system
  - degenerate, 103
  - host-guest, 362
  - non-degenerate, 105
  
- thermoelectric power, 423
- transition
  - metal-insulator (Peierls), 24
  - metal-insulator (Anderson), 54
  - Mott–Hubbart, 44–46
  - permitted optical, 180
- transition metals, 166, 171, 177
- transport
  - electron, 74, 99
  - polarons, 116
- transport mechanisms, 99, 127, 133
- traps, 144, 264, 463
  - distribution, 151
  
- yield
  - energetic, 274
  - external quantum, 221, 273
  - fluorescence quantum, 274
  - internal quantum, 221, 273
  - measure of, 226
  - photovoltaic, 333

# Springer Series in OPTICAL SCIENCES

---

## Volume 1

### 1 Solid-State Laser Engineering

By W. Koechner, 5th revised and updated ed. 1999, 472 figs., 55 tabs., XII, 746 pages

## Published titles since volume 80

### 85 Sensing with Terahertz Radiation

By D. Mittleman (Ed.), 2003, 207 figs., 14 tabs., XVI, 337 pages

### 86 Progress in Nano-Electro-Optics I

Basics and Theory of Near-Field Optics

By M. Ohtsu (Ed.), 2003, 118 figs., XIV, 161 pages

### 87 Optical Imaging and Microscopy

Techniques and Advanced Systems

By P. Török, F.-J. Kao (Eds.), 2003, 260 figs., XVII, 395 pages

### 88 Optical Interference Coatings

By N. Kaiser, H.K. Pulker (Eds.), 2003, 203 figs., 50 tabs., XVI, 504 pages

### 89 Progress in Nano-Electro-Optics II

Novel Devices and Atom Manipulation

By M. Ohtsu (Ed.), 2003, 115 figs., XIII, 188 pages

### 90/1 Raman Amplifiers for Telecommunications 1

Physical Principles

By M.N. Islam (Ed.), 2004, 488 figs., XXVIII, 328 pages

### 90/2 Raman Amplifiers for Telecommunications 2

Sub-Systems and Systems

By M.N. Islam (Ed.), 2004, 278 figs., XXVIII, 420 pages

### 91 Optical Super Resolution

By Z. Zalevsky, D. Mendlovic, 2004, 164 figs., XVIII, 232 pages

### 92 UV-Visible Reflection Spectroscopy of Liquids

By J.A. Ráty, K.-E. Peiponen, T. Asakura, 2004, 131 figs., XII, 219 pages

### 93 Fundamentals of Semiconductor Lasers

By T. Numai, 2004, 166 figs., XII, 264 pages

### 94 Photonic Crystals

Physics, Fabrication and Applications

By K. Inoue, K. Ohtaka (Eds.), 2004, 209 figs., XV, 320 pages

### 95 Ultrafast Optics IV

Selected Contributions to the 4th International Conference

on Ultrafast Optics, Vienna, Austria

By F. Krausz, G. Korn, P. Corkum, I.A. Walmsley (Eds.), 2004, 281 figs., XIV, 506 pages

### 96 Progress in Nano-Electro Optics III

Industrial Applications and Dynamics of the Nano-Optical System

By M. Ohtsu (Ed.), 2004, 186 figs., 8 tabs., XIV, 224 pages

### 97 Microoptics

From Technology to Applications

By J. Jahns, K.-H. Brenner, 2004, 303 figs., XI, 335 pages

### 98 X-Ray Optics

High-Resolution-Resolution Applications

By Y. Shvyd'ko, 2004, 181 figs., XIV, 404 pages

### 99 Mono-Cycle Photonics and Optical Scanning Tunneling Microscopy

Route to Femtosecond Ångstrom Technology

By M. Yamashita, H. Shigekawa, R. Morita (Eds.) 2005, 241 figs., XX, 393 pages

### 100 Quantum Interference and Coherence

Theory and Experiments

By Z. Ficek and S. Swain, 2005, 178 figs., XV, 418 pages



# Springer Series in OPTICAL SCIENCES

---

- 101 **Polarization Optics in Telecommunications**  
By J. Damask, 2005, 110 figs., XVI, 528 pages
- 102 **Lidar**  
Range-Resolved Optical Remote Sensing of the Atmosphere  
By C. Weitkamp (Ed.), 161 figs., XX, 416 pages
- 103 **Optical Fiber Fusion Splicing**  
By A.D. Yablon, 2005, 137 figs., XIII, 306 pages
- 104 **Optoelectronics of Molecules and Polymers**  
By A. Moliton, 2005, 229 figs., 592 pages
- 105 **Solid-State Random Lasers**  
By M. Noginov, 2005, 131 figs., XII, 238 pages
- 106 **Coherent Sources of XUV Radiation**  
Soft X-Ray Lasers and High-Order Harmonic Generation  
By P. Jaeglé, 2005, 150 figs., approx. 264 pages
- 107 **Optical Frequency-Modulated Continuous-Wave (FMCW) Interferometry**  
By J. Zheng, 2005, 137 figs., XVIII, 254 pages
- 108 **Laser Resonators and Beam Propagation**  
Fundamentals, Advanced Concepts and Applications  
By N. Hodgson and H. Weber, 2005, 497 figs., approx. 790 pages
- 109 **Progress in Nano-Electro Optics IV**  
Characterization of Nano-Optical Materials and Optical Near-Field Interactions  
By M. Ohtsu (Ed.), 2005, 123 figs., XIV, 206 pages
- 110 **Kramers–Kronig Relations in Optical Materials Research**  
By V. Lucarini, J.J. Saarinen, K.-E. Peiponen, E.M. Vartiainen, 2005,  
37 figs., X, 162 pages
- 111 **Semiconductor Lasers**  
Stability, Instability and Chaos  
By J. Ohtsubo, 2005, 169 figs., XII, 438 pages
- 112 **Photovoltaic Solar Energy Generation**  
By A. Goetzberger and V.U. Hoffmann, 2005, 139 figs., XII, 234 pages
- 113 **Photorefractive Materials and Their Applications 1**  
Basic Effects  
By P. Günter and J.P. Huignard, 2005, 169 figs., approx. XII, 300 pages
- 114 **Photorefractive Materials and Their Applications 2**  
Materials  
By P. Günter and J.P. Huignard, 2005, 100 figs., approx. XII, 300 pages
- 115 **Photorefractive Materials and Their Applications 3**  
Applications  
By P. Günter and J.P. Huignard, 2005, 100 figs., approx. XII, 300 pages
- 116 **Spatial Filtering Velocimetry**  
Fundamentals and Applications  
By Y. Aizu and T. Asakura, 2006, 112 figs., approx. XII, 220 pages